

## ENCLOSURE 2

MFN 10-296

### NEDO-33173-A, Revision 1, Applicability of GE Methods to Expanded Operating Domains

#### Non-Proprietary Information

#### **IMPORTANT NOTICE**

This is a non-proprietary version of NEDC-33173P-A, Revision 1, from which the proprietary information has been removed. Portions of the enclosure that have been removed are indicated by an open and closed bracket as shown here [[ ]].

Note the NRC's Final Safety Evaluation is enclosed in NEDO-33173-A, Revision 1. Portions of the Safety Evaluation that have been removed are indicated with a single square bracket as shown here. [ ]



GE Energy  
Nuclear

3901 Castle Hayne Rd  
Wilmington, NC 28401

NEDO-33173-A  
Revision 1  
DRF 0000-0012-1297  
DRF Section 0000-0123-0447  
Class I  
September 2010

*NON-PROPRIETARY INFORMATION*

## **LICENSING TOPICAL REPORT**

# **Applicability of GE Methods to Expanded Operating Domains**

*Copyright 2010 GE-Hitachi Nuclear Energy Americas LLC*



## INFORMATION NOTICE

This document contains proprietary information of the GE Hitachi Nuclear Energy (GEH) and is furnished in confidence solely for the purpose(s) stated in the transmittal letter. No other use, direct or indirect, of the document or the information it contains is authorized. Furnishing this document does not convey any license, express or implied, to use any patented invention or, except as specified above, any proprietary information of GEH disclosed herein or any right to publish or make copies of the document without prior written permission of GEH.

This is a non-proprietary version of the document NEDC-33173P-A, Revision 1, which has the proprietary information removed. Portions of the document that have been removed are indicated by white space with an open and closed bracket as shown here [[                    ]].

Within the US NRC Safety Evaluation, the proprietary portions of the document that have been removed are indicated by white space with an open and closed bracket as shown here [                    ].

### IMPORTANT NOTICE REGARDING CONTENTS OF THIS REPORT

#### PLEASE READ CAREFULLY

The information contained in this document is furnished for the purpose of obtaining NRC approval of the Applicability of GE Methods to Expanded Operating Domains. The only undertakings of General Electric Company with respect to information in this document are contained in contracts between General Electric Company and participating utilities, and nothing contained in this document shall be construed as changing those contracts. The use of this information by anyone other than that for which it is intended is not authorized; and with respect to **any unauthorized use**, General Electric Company makes no representation or warranty, and assumes no liability as to the completeness, accuracy, or usefulness of the information contained in this document.



NEDO-33173-A, Revision 1  
Non-Proprietary Information  
**UNITED STATES**  
**NUCLEAR REGULATORY COMMISSION**  
WASHINGTON, D.C. 20555-0001

July 21, 2009

**MFN-09-808**

Mr. Jerald G. Head  
General Manager, Regulatory Affairs  
GE Hitachi Nuclear Energy Americas LLC  
P. O. Box 780, M/C A-30  
Wilmington, NC 28401

**SUBJECT: FINAL SAFETY EVALUATION FOR GE HITACHI NUCLEAR ENERGY AMERICAS, LLC LICENSING TOPICAL REPORT NEDC-33173P, "APPLICABILITY OF GE METHODS TO EXPANDED OPERATING DOMAINS" (TAC NO. MD0277)**

Dear Mr. Head:

By letter dated March 14, 2007, the U.S. Nuclear Regulatory Commission (NRC) issued to GE Hitachi Nuclear Energy Americas LLC (GEH, formerly abbreviated GHNE and formerly known as General Electric (GE) Nuclear Energy) the draft safety evaluation (SE) of licensing topical report (LTR) NEDC-33173P, "Applicability of GE Methods to Expanded Operating Domains." By letter dated April 16, 2007, GEH provided comments on the draft SE. The comments provided were dispositioned in an attachment to the final SE issued by letter dated January 17, 2008. By letter dated June 17, 2008, GEH provided proprietary markups of the NRC staff's final SE. Additionally, by e-mail on October 22, 2008, GEH notified NRC of several editorial errors in the final SE.

The NRC staff has reviewed the editorial errors identified by GEH and agrees that the final SE needs to be corrected. Enclosed are a proprietary version of the final SE including revised Pages 24, 37, 38, 51, 55, 113, 118, 119, and 129 and a non-proprietary version of the final SE including revised Pages 24, 37, 38, 51, 55, 113, 118, and 129. The accepted versions of the LTR should incorporate the January 17, 2008, letter without enclosures and this letter with enclosures. The enclosures to this letter supersede those provided with the January 17, 2008, letter.

If you have any questions, please contact Michelle C. Honcharik at (301) 415-1774.

Sincerely,

A handwritten signature in black ink that reads "Thomas B. Blount".

Thomas B. Blount, Deputy Director  
Division of Policy and Rulemaking  
Office of Nuclear Reactor Regulation

Project No. 710

Enclosures:

1. Non-proprietary final SE
2. Proprietary final SE

GEH

Project No. 710

cc:

Mr. James F. Harrison  
GE Hitachi Nuclear Energy Americas LLC  
Vice President - Fuel Licensing  
P.O. Box 780, M/C J-70  
Wilmington, NC 28401-0780  
[james.harrison@ge.com](mailto:james.harrison@ge.com)

Ms. Patricia L. Campbell  
Vice President, Washington Regulatory Affairs  
GE Hitachi Nuclear Energy Americas LLC  
1299 Pennsylvania Avenue, NW  
9th Floor  
Washington, DC 20004  
[patricia.campbell@ge.com](mailto:patricia.campbell@ge.com)

Mr. Andrew A. Lingenfelter  
Vice President, Fuel Engineering  
Global Nuclear Fuel–Americas, LLC  
P.O. Box 780, M/C J-70  
Wilmington, NC 28401-0780  
[Andy.Lingenfelter@gnf.com](mailto:Andy.Lingenfelter@gnf.com)

Mr. James A Ross  
Vice President, Nuclear Licensing  
GE Hitachi Nuclear Energy Americas LLC  
1299 Pennsylvania Ave, NW  
9th Floor  
Washington, DC 20004  
[james2.ross@ge.com](mailto:james2.ross@ge.com)

**FINAL SAFETY EVALUATION BY THE OFFICE OF  
NUCLEAR REACTOR REGULATION**

**LICENSING TOPICAL REPORT NEDC-33173P**

**"APPLICABILITY OF GE METHODS TO EXPANDED  
OPERATING DOMAINS"**

**GE HITACHI NUCLEAR ENERGY**

## TABLE OF CONTENTS

<b>Table of Contents</b> .....	<b>i</b>
<b>List of Figures</b> .....	<b>v</b>
<b>List of Tables</b> .....	<b>vii</b>
<b>Executive Summary</b> .....	<b>viii</b>
<b>1.0 Introduction and Background</b> .....	<b>1</b>
<b>2.0 Applicability of GE Methods and Code to EPU and MELLLA+</b> .....	<b>3</b>
2.1 EPU and Expanded operating domains Core Characteristics .....	3
2.1.1 Key Operating Parameters .....	4
2.1.2 MELLLA+ Core Conditions.....	4
2.1.3 EPU and High-power density Plant Core Tracking Data .....	5
2.2 Topics of Review .....	6
2.2.1 Extrapolation of the Neutronic Methods to High Void Conditions.....	6
2.2.2 Assessment of the 40 Percent Depletion Assumption .....	6
2.2.3 Assessing the Impact of Bypass Voiding .....	7
2.2.4 Assessing the Impact of Neutronic Method Assumptions .....	7
2.2.5 Applicability of the Thermal-Hydraulic Models .....	7
<b>3.0 Extrapolation Of Neutronic Methods to High Void Fractions</b> .....	<b>11</b>
3.1 Assessment.....	11
3.1.1 Assessing Extrapolation of the Neutronic Methods.....	11
3.1.1.1 Neutronic Methods Not Assessed by the NRC Staff for Void Fraction Greater Than 70 Percent.....	12
3.1.2 Confirmatory Lattice Physics Data Comparisons (TGBLA06/HELIOS).....	13
3.1.2.1 $K_{inf}$ Comparisons .....	14
3.1.2.2 Power Distribution Comparisons.....	14
3.1.2.3 Isotopic Comparisons.....	14
3.1.2.4 Confirmatory Analysis Conclusions.....	15
3.1.3 Core-Tracking Data Validation .....	15
3.1.4 Eigenvalue Tracking.....	15
3.1.4.1 Cold Critical Eigenvalue .....	15
3.1.4.2 Hot Critical Eigenvalue.....	16
3.1.5 Assessment of TIP Core Tracking Data .....	17
3.1.5.1 TIP Comparisons with Increased Power Density and Voids .....	19
3.1.5.2 NRC staff Assessment of Reference Plants TIP Core Tracking Data.....	19
3.1.6 TIP Core Tracking Data.....	21
3.1.7 Gamma Scans.....	22
3.1.8 Available Gamma Scan Data .....	23
3.1.9 Assessment Conclusions .....	24
3.2 Interim Approach .....	25
3.2.1 Safety Parameters Influenced by Uncertainties and Margin Evaluation.....	25
3.2.1.1 Impacts of Bias and Uncertainties in Nodal Reactivity.....	25

3.2.1.1.1	Reactivity Prediction Impact .....	25
3.2.1.1.2	Power Peaking and Distribution Impact.....	25
3.2.1.1.3	Void Reactivity Coefficient.....	26
3.2.2	Safety Limit Critical Power Ratio (SLMCPR).....	26
3.2.2.1	Regulatory Requirements and Guidance .....	26
3.2.2.2	Application of Power Distribution Uncertainties .....	27
3.2.3	R-factor.....	29
3.2.4	Operating Limit CPR .....	31
3.2.4.1	Fuel Parameters that Affect OLMCPR .....	32
3.2.4.2	Assessment of Power Distribution Assumptions and Conservatism .....	32
3.2.4.2.1	GE's Axial Power Profile Assessment .....	33
3.2.4.2.2	GE's CR Pattern Assessment.....	34
3.2.4.2.3	NRC staff Assessment.....	35
3.2.4.2.4	TRACG Application for EPU and Operation at Expanded Operating Domains	36
3.2.4.3	Assessment of Void Reactivity Coefficient.....	36
3.2.4.4	Sensitivity Analysis Results.....	37
3.2.4.5	OLMCPR Conclusion .....	38
3.2.5	LOCA Related Nodal Power Limits .....	39
3.2.5.1	LOCA Related Nodal Power Limits .....	39
3.2.5.1.1	ECCS-LOCA Axial Power Distribution Evaluation .....	40
3.2.5.1.2	Plant-Specific Review Process .....	41
3.2.5.1.3	LOCA Conclusions .....	42
3.2.5.2	Approval of the ECCS-LOCA Analytical Models .....	42
3.2.6	Fuel Rod T-M Performance.....	43
3.2.6.1	Power Distribution Uncertainties .....	44
3.2.6.2	Conservative Assumption for Steady-State LHGR Limit .....	44
3.2.6.3	EPU T-M Operating History Data .....	45
3.2.6.4	Monitoring Gd-bearing Nodes .....	46
3.2.6.5	Transient Linear Heat Generation Limit .....	46
3.2.6.5.1	Thermal and Mechanical Overpower Licensing Process.....	47
3.2.6.5.2	Impact of 40 percent Depletion Assumption on Transient LHGR Response 48	
3.2.6.5.3	Qualification Database Supporting the T-M Methodology .....	49
3.2.6.5.4	Assessment of the Qualification Data.....	49
3.2.6.5.5	Internal Rod Pressure Assessment .....	50
3.2.6.5.6	TOP Confirmatory Analyses .....	52
3.2.6.5.7	MOP Confirmatory Analysis.....	56
3.2.6.5.8	Part 21 Evaluation .....	57
3.2.6.5.9	Overall T-M Methodology Conclusion.....	58
3.2.7	Fuel Rod Exposure.....	60
3.2.8	Shutdown Margin .....	61
3.2.8.1	Cold Critical Demonstration .....	61
3.2.8.2	Accuracy of the Prediction of the Strongest Blade .....	62
3.2.8.3	Design Shutdown Margin .....	63
3.2.8.4	Assessment.....	63
3.2.9	Standby Liquid Control System .....	63
<b>4.0</b>	<b>40 Percent Void Fraction Depletion Assumption .....</b>	<b>78</b>
4.1	Assessment of impact on Void Reactivity Coefficient.....	78



4.2	GE Evaluation of Increased Void Coefficient Uncertainty .....	79
4.3	Impact of Void Coefficient Uncertainties on ATWS .....	81
4.4	Void Reactivity Conclusion .....	82
<b>5.0</b>	<b>Bypass and Water Rod Voiding .....</b>	<b>87</b>
5.1	Impact on Neutronic Methods.....	87
5.2	Impact on Steady-State .....	88
5.3	Impact on Transients .....	89
5.4	Bypass and Water Rod Voiding Conclusion.....	89
<b>6.0</b>	<b>Stability .....</b>	<b>91</b>
6.1	Uncertainties That Impact Stability Calculations .....	91
6.1.1	Power Distribution Uncertainties .....	91
6.1.1.1	Bypass and Water Rod Voiding Uncertainties .....	92
6.1.1.2	Cross-section Methodology Uncertainties.....	93
6.2	Errors That Impact Instrumentation Relied Upon By Stability LTS .....	94
6.3	Applicability of Stability LTS .....	96
6.3.1	Enhanced Option 1-A .....	97
6.3.2	Option I-D .....	98
6.3.3	Option II.....	98
6.3.4	Option III.....	99
6.3.5	Option DSS-CD .....	99
<b>7.0</b>	<b>Applicability of Thermal-hydraulic Models .....</b>	<b>102</b>
7.1	GEXL Correlation .....	103
7.2	Void-Quality Correlation .....	103
7.2.1	Extension of the Void-Quality Correlation .....	104
7.2.2	GE Void Fraction Model .....	105
7.2.3	Available Void-Quality Correlation Measurement Database .....	105
7.2.3.1	CISE Database .....	105
7.2.3.2	GE 7x7 Database.....	106
7.2.3.3	ASEA-Atom 8x8 Bundle Data .....	106
7.2.3.4	Simple Geometry Database .....	107
7.2.3.5	Pressure Drop Optimization .....	107
7.2.4	Comparison of Experimental Database to Current Fuel Designs and Operating Conditions and Fuel (10x10 bundle – GE14).....	108
7.2.4.1	Hydraulic Diameter.....	108
7.2.4.2	Pressure.....	109
7.2.4.3	Subcooling Level.....	109
7.2.4.4	Exit Quality .....	109
7.2.4.5	Exit Void Fraction .....	109
7.2.4.6	Reynolds Number .....	109
7.2.4.7	Power Distribution (Axial and Radial).....	110
7.2.4.8	Partial Length Rods.....	111
7.2.5	Comparison of the Findlay-Dix Correlation and Other Drift Flux Models.....	111
7.2.5.1	Key Parameters Discussion .....	112

7.2.5.2	Hydraulic Diameter Ranges and Partial Length Rods.....	112
7.2.5.3	Pressure Ranges .....	113
7.2.5.4	Power Peaking and Distribution .....	113
7.2.5.5	Conclusion of the Comparison to the “World” Data.....	113
7.2.6	GE Assessment.....	114
7.2.6.1	GE Conclusion .....	115
7.2.6.2	The NRC Staff Review of GE’s Assessment.....	115
7.2.7	Void-Quality Correlation Overall Assessment and Conclusion .....	116
7.2.8	TRACG Interfacial Shear Model Qualification .....	120
7.2.9	Void-Quality Correlation Conclusion .....	121
<b>8.0</b>	<b>Licensing Application.....</b>	<b>128</b>
8.1	Overview.....	128
8.2	Mixed Core Applicability .....	129
8.3	Expanded Operating Domain Eigenvalue Tracking.....	130
8.4	TGBLA06 Methodology Upgrades.....	130
8.5	Plant-Specific Application Process .....	132
8.6	Technical Specifications .....	132
<b>9.0</b>	<b>Limitations and Conditions .....</b>	<b>133</b>
<b>10.0</b>	<b>Conclusion .....</b>	<b>138</b>
<b>11.0</b>	<b>References .....</b>	<b>139</b>

## LIST OF FIGURES

Figure 2-1 Maximum Bundle Power vs. Cycle Exposure for EPU Plants and a High-power density 5 percent Uprate Plant.....	7
Figure 2-2 Maximum Power/Flow Ratio vs. Cycle Exposure for EPU Plants and a High-power density 5 percent Uprate Plant.....	8
Figure 2-3 Exit Void Fraction of Maximum Power Bundle vs. Cycle Exposure for EPU Plants and a High-power density 5 percent Uprate Plant .....	8
Figure 2-4 Peak LHGR vs. Cycle Exposure for EPU Plants and a High-power density 5 percent Uprate Plant .....	9
Figure 2-5 Power Flow Map.....	9
Figure 2-6 LHGR operating History for EPU and a High-power density Plant.....	10
Figure 2-7 OLMCPR operating history For EPU and a High-power density Plant (Un-adapted PANACEA Calculation).....	10
Figure 2-8 MAPLHGR Operating History (Unadapted PANACEA Calculation).....	11
Figure 3-1 Cold Critical Eigenvalue Tracking.....	69
Figure 3-2 Hot Critical Eigenvalue Tracking .....	69
Figure 3-3 Hot Critical Eigenvalue Tracking for Plant E.....	70
Figure 3-4 Gamma and Thermal TIP Power Distribution Uncertainties .....	71
Figure 3-5 Four-bundle uncertainty.....	72
Figure 3-6 Axial RMS Uncertainty.....	72
Figure 3-7 Nodal RMS Uncertainty .....	73
Figure 3-8 Axial Void Profile (R-factor Calculation) .....	73
Figure 3-9 Bundle R-factor and Estimated CPR Response.....	74
Figure 3-10 Bundle 2 RIP and Estimated SLMCPR Impact.....	74
Figure 3-11 Lattice 7009 Void Coefficient Comparisons.....	75
Figure 3-12 EPU LHGR Operating History .....	75
Figure 3-13 GE14 Six Weight Percent Gd <sub>2</sub> O <sub>3</sub> -UO <sub>2</sub> LHGR Operating Limit and Analysis Basis	76
Figure 3-14 Six Percent Gd-bearing Rods Operating History for EPU plant.....	76
Figure 3-15 Sensitivity of Cold Critical Eigenvalue to EPU Operation .....	77
Figure 3-16 Difference Between Actual and Projected Cold Critical Eigenvalues .....	77
Figure 4-1 Void coefficient vs. instantaneous Void Fraction for a Range of Historical Void Fractions at an Exposure of 30 GWd/MT .....	83
Figure 4-2 Void Coefficient vs. Instantaneous Void Fraction for a Range of Historical Void Fractions at an Exposure of 60 GWd/MT .....	84
Figure 4-3 Void Coefficient Ratio MNCP / TGBLA06.....	84
Figure 4-4 Typical Void-Quality Relation at High Power-to-Flow Ratio.....	85
Figure 4-5 Reactivity Change for a Small Quality Perturbation ( $\Delta X = 0.001$ ) as a Function of Void Fraction .....	85
Figure 4-6 TRACG Power and Flow Response for MSIVC Event .....	86
Figure 4-7 TRACG Pressure and Relief Valve .....	86
Figure 5-1 Impact of Bypass Voiding on Peak Pin Fission Rate.....	90
Figure 5-2 Impact of Bypass Voiding on Uniformity of Lattice Pin Fission Distribution.....	90
Figure 6-1 NMP2 Instability Event ODYSY Benchmark .....	100
Figure 6-2 Perry Instability Event ODYSY Benchmark .....	101
Figure 6-3 Void Coefficient Ratio MNCP / TGBLA06.....	101
Figure 6-4 Hot Channel Power and Growth Rate with (V33) and without (NV) Void History Correction for Void Coefficient .....	102
Figure 7-1 GEXL14 Application Range.....	124
Figure 7-2 Void Fraction vs. Quality – Data and Calculation .....	124
Figure 7-3 Normalized Radial Power Distribution (8X8 array) – ASEA-713 Experiment .....	125

Figure 7-4 Normalized Radial Power Distribution (8X8 array) – ASEA-813 Experiment .....	125
Figure 7-5 Normalized Power Distribution (10X10 array) - VYNPS Lattice 5168, 40 percent Void, Burnup = 0 .....	126
Figure 7-6 Void Fraction-Quality Relation with Partial Length Rods at Low Flow.....	126
Figure 7-7 Void Fraction-Quality Relation with Partial Length Rods at High Flow.....	127
Figure 7-8 Void Fraction-Quality Relation with Partial Length Rods.....	127
Figure 7-9 Comparison to Findlay-Dix Correlation against Other Drift Flux Models .....	128

## LIST OF TABLES

Table 2-1 Exit Void Fraction.....	5
Table 3-1 Summary of Bundle Average TIP Comparisons, Eight Cycles .....	18
Table 3-2 Axial Power Profile Sensitivity for Limiting Pressurization Events .....	34
Table 3-3 TOP and MOP screening criteria for GE13 and GE14 fuel designs for limiting transients.....	47
Table 3-4 Steady-state Operation at the LHGR Envelope.....	51
Table 3-5 FRAPCON TOP for UO <sub>2</sub> and UGdUO <sub>2</sub> rod .....	53
Table 3-6. Fuel Centerline Temperature Results for GE14 UO <sub>2</sub> and 10 weight percent Gd Rod for Overpower at the Knee of the LHGR Limit Envelope.....	54
Table 3-7 Fuel Melting Temperature as Function of Gadolinium Concentration and Exposure .	55
Table 3-8 Confirmatory FRAPCON MOP (UO <sub>2</sub> rod and UGdUO <sub>2</sub> rods).....	56
Table 3-9 TRACG Impact of High Exposure Void Coefficient Bias.....	65
Table 3-10 GE14 LHGR Limit.....	66
Table 3-11 LHGR Power Distribution Uncertainty Components .....	66
Table 3-12 Internal rod pressure as function of exposure .....	67
Table 3-13 Effect of Early Life LHGR Variation GE14 Six Weight Percent Gd <sub>2</sub> O <sub>3</sub> -UO <sub>2</sub> .....	67
Table 3-14 GSTR Mechanical Qualification Database .....	68
Table 3-15 Key Core Parameters for Reference Plants (from MFN05-029 (Reference 11)).....	68
Table 4-1 Void Coefficient Comparisons between TGBLA06 and MCNP .....	83
Table 5-1 Bypass Void Fractions Calculated for Different Reactor Operating Domains.....	89
Table 6-1 Summary of ODYSY Results for VYNPS High DR Tests .....	100
Table 6-2 Long Term Stability Solution Features.....	100
Table 7-1 Comparison of GE Experimental Database and 10x10 bundle Operating Conditions .....	122
Table 7-2 Void Fraction Correlation Database.....	123
Table 7-3 Comparison between Void-Quality Correlation and Database .....	123
Table 8-1 History of the Changes in TGBLA06A .....	133

## EXECUTIVE SUMMARY

By letter dated February 10, 2006, GE Hitachi Nuclear Energy (GEH, formerly known as General Electric (GE) Nuclear Energy) submitted licensing topical report (LTR) NEDC-33173P, "Applicability of GE Methods to Expanded Operating Domains" to the U.S. Nuclear Regulatory Commission (NRC) staff for review (Reference 1). In LTR NEDC-33173P, GE evaluated the impact of operation at higher void conditions characteristic of an extended power uprate (EPU) and maximum extended load line limit analysis plus (MELLLA+) operation on most of its licensing analytical methods.

### 1.0 EPU/MELLLA+ CORE CONDITIONS

To implement EPU and maintain a 24-month cycle, a higher number of maximum powered bundles are loaded into the core and the power of the average bundle power also increases, leading to a flatter core radial power distribution. Due to the resultant increase in two-phase pressure drop and higher coolant voiding, the flow in the maximum powered bundles decreases. This leads to a higher bundle power-to-flow ratio and a higher exit void fraction. For the proposed MELLLA+ operation, plants will operate at EPU power levels at core flows as low as 80 percent of rated flow. Therefore, the number of bundles operating at higher power-to-flow conditions and consequently higher exit void fractions is expected to increase. Since the maximum powered bundles operate nearest to the thermal limits, for EPU operation the number of maximum powered bundles operating near the thermal limits increases. Depending on the core configuration in terms of size, for some EPU core designs, the power levels of the maximum powered bundle increase relative to the pre-EPU conditions in order to meet the energy needs of EPU operation and long cycle length. There is no regulatory limit on the power level of the maximum powered bundles provided the bundles are operated within the calculated thermal limits and meet the regulatory requirements. However, for operation at EPU and MELLLA+ conditions, the core designs and operation will continue to be constrained by the requirement to meet the thermal limits. Since the high-powered bundle's ability to operate within the thermal limits is analytically determined, it becomes important to ensure that the analytical tools are being applied within the ranges for which it was derived and benchmarked.

#### Review Objective

The overall objectives of the LTR NEDC-33173P review are to confirm the following for operation at EPU and the expanded operating domains:

1. The analytical methods and codes used to perform the design safety analyses will be applied within the applicable NRC-approved validation ranges.
2. The calculational and measurement uncertainties applied to the thermal limit calculations and the models simulating physical phenomena will remain valid for the predicted neutronic and thermal-hydraulic core and fuel conditions during steady-state, transient, and accident conditions.
3. The qualification database supporting analytical models simulating physical phenomena remains valid and applicable to the conditions under which it is applied, including those models and key parameters in which specific uncertainties are not applied.
4. If the NRC-approved analytical methods, models, and codes are extended outside the applicability ranges, the extension of the specific models are demonstrated to be acceptable or additional margin is applied to the affected downstream safety analyses until such time the supporting qualification data is extended.

5. The commitments made by GE to support the approval of LTR NEDC-33173P are acceptable. These commitments are generally related to obtaining additional validation data to benchmark GE's analytical methods in order to extend the validation data to account for the impact of the current fuel design features and operating conditions.

### **Impact on Methods Qualification Databases**

The high void conditions and other characteristics of EPU and MELLLA+ conditions could affect the key assumptions in the analytical methods that impact the safety analyses supporting EPU and MELLLA+ operations or safety features. This LTR review evaluates these effects and the adequacy of the qualification database supporting the analytical methods. The topics of review are as follows:

1. Extension of the neutronic methods to void fractions greater than 70 percent.
2. Generating the lattice physics data based on core average void of 40 percent instead of 70 percent for the instantaneous cases.
3. Reliability of the neutron monitoring instrumentation due to bypass voiding during steady-state and some transients.
4. Assessment of the performance of the void-quality correlation prediction to high void fractions and the applicability of the supporting qualification database.
5. Extension of the qualification data supporting the thermal-mechanical methodology to high exposures.

### **2.0 SUMMARY OF LTR NEDC-33173P APPROACH**

GE addressed these topics and proposed an interim approach. LTR NEDC-33173P parallels and references Entergy Nuclear Operations, Incorporated's interim approach in the Vermont Yankee Nuclear Power Station EPU application (NRC staff approval is Reference 26), including the request for additional information (RAI) responses (References 27, 28, 29, and 30).

The major technical positions in LTR NEDC-33173P and the associated RAI responses are summarized below.

1. LTR NEDC-33173P identifies the key parameters affected by the lattice physics uncertainties and proposes increasing the power distribution uncertainties to account for potential non-conservatism. LTR NEDC-33173P proposes a 0.02 additional margin to the safety limit minimum critical power ratio (SLMCPR). The increased power distribution uncertainty is also accounted for in the steady-state linear heat generation rate (LHGR) limit.
2. LTR NEDC-33173P evaluates conservatism and available margins in the safety analyses. LTR NEDC-33173P concludes that there are sufficient margins and conservatism in the operating limit minimum critical power ratio (OLMCPR), the emergency core cooling system (ECCS) loss-of-coolant accident (LOCA) calculations, LHGR limit, exposure accounting, and shutdown margin.
3. LTR NEDC-33173P evaluates the impact of the 40 percent depletion history assumption on the accuracy of the fuel isotopics generated. Inaccuracies on the predicted isotopics at the high-void-fraction nodes result in a significant bias on void reactivity coefficients. LTR NEDC-33173P quantifies the void reactivity coefficient bias and justifies its impact on the safety analysis, such as transients and stability. LTR NEDC-33173P concludes that impacts on the safety analyses are within the assumed uncertainties, or they are minimal.

4. LTR NEDC-33173P evaluates the occurrence of bypass voiding during steady-state operation and concludes that bypass voiding at the D-level local power range monitor (LPRM) will not exceed 5 percent at nominal conditions. Therefore, the reliability of LPRM measurements during steady-state operation will not be affected.
5. LTR NEDC-33173P and the RAI responses state that some transients may result in higher bypass void fraction levels, but the effect is minimal. LTR NEDC-33173P concludes that the reliability of the response of the neutron monitoring system will only have a minimal effect on the stability long-term solutions (LTSs).
6. LTR NEDC-33173P states that the void-quality correlation is supported by measurement data up to 95 percent void fraction. It proposes that extension of the void-quality correlation to pure steam is acceptable.

### 3.0 NRC STAFF EVALUATION

The NRC staff reviewed the justification provided in LTR NEDC-33173P, the RAI responses, associated referenced documents, and the GE licensing methodology specified in GESTAR II (Reference 38). All of the limitations resulting from the NRC staff review of LTR NEDC-33173P are in Section 9.0, "Limitations and Conditions," of this safety evaluation (SE). Additionally, GE made several commitments related to obtaining additional measurement data to support application of the analytical methods to EPU/MELLLA+ conditions and application of newly developed and improved methodologies to support plant-specific EPU/MELLLA+ applications.

#### Review Summary

The main NRC staff conclusions are as follows:

##### 1. SLMCPR

The neutronic methods are extrapolated to higher void conditions for EPU and MELLLA+ core conditions. However, the available pin and bundle power validation data do not extend to the current fuel and lattice designs as operated. GE has committed to perform and has begun pin and bundle power gamma scan benchmarking to establish the pin and bundle power uncertainties that factor into the safety analyses, including the SLMCPR. As an interim measure:

- a) A 0.02 adder will be included in the cycle-specific SLMCPR value for EPU plants.
- b) A 0.03 adder will be applied to the cycle-specific SLMCPR value for plants implementing EPU/MELLLA+. The additional 0.01 accounts for the impact of the higher void conditions characteristic of MELLLA+ operation.

##### 2. R-factor

The R-factor goes into the SLMCPR calculation and is characterized by within bundle relative pin power-peaking. The current R-factor methodology is generated for each new product line with [

]. The R-factor will be calculated consistent with the lattice axial void conditions.

##### 3. ECCS-LOCA

- a) The ECCS-LOCA calculation will be performed for all statepoints, including the MELLLA+ 55 percent core flow at approximately the original licensed thermal power (OLTP). The higher initial power-to-flow ratio will result in a more limiting peak clad temperature (PCT) value.
- b) The ECCS-LOCA analysis will also be performed with top-peaked power shape, which was demonstrated to be more limiting due the higher initial void conditions.



#### 4. Transient LHGR limit

- a) The transient LHGR limit is not reported in the licensing process and documentation (e.g., Core Operating Limits Report (COLR) and Supplemental Reload Licensing Report (SRLR)). The thermal overpower (TOP) and the mechanical overpower (MOP) will be reported in the SRLR in order to demonstrate that the plant response will meet the overpower acceptance criteria.
- b) EPU/MELLLA+ operating strategy is expected to result in a higher overpower response during pressurization transients relative to pre-EPU conditions, due to the higher core reactivity response associated with the core design necessary in order to meet the EPU and long-cycle length energy requirements. The local pin power-peaking, the bundle powers, the 3D power distributions, and the void reactivity are all factors that contribute to the anticipated operational occurrence (AOO) response. EPU/MELLLA+ operation, including the spectral shift operation at EPU power levels will entail operation outside the current experience base. The transient response and the associated thermal overpower response will be calculated on cycle-specific bases. However, the fuel rod thermal and mechanical overpower response is currently not reported in the COLR or the SRLR or the plant-specific EPU applications. Plant-specific EPU and MELLLA+ applications will include discussion of the plant-specific thermal and mechanical overpower response.
- c) Sensitivity analyses show that the 40 percent depletion assumption results in under-prediction of the thermal overpower response by [ ]. The margin was increased to 10 percent since the sensitivity analyses may not be bounding for all boiling water reactors (BWRs) operating at EPU and MELLLA+ conditions. To account for the impact of the void history bias, plant-specific EPU and MELLLA+ applications using either GE Transient Reactor Analysis Code (TRACG) or ODYN will demonstrate an equivalent to 10 percent margin to the fuel centerline melt and that the 1 percent cladding circumferential plastic strain acceptance criteria due to pellet-cladding mechanical interaction for all of limiting AOO transient events, including equipment out-of-service. Limiting transients in this case, refers to transients where the void reactivity coefficient plays a significant role, such as pressurization events. This margin can be reduced if it is shown that the sensitivity analysis in which the [ ] was derived will bound all BWR EPU and MELLLA+ applications. If the void history bias is incorporated into the coupled neutronic and transient code set, then the additional 10 percent margin to the fuel centerline melt and the 1 percent cladding strain is no longer required.
- d) The qualification data for the internal rod pressure (e.g., up to 20.5 GWd/MTU) and the fuel centerline temperatures (e.g., 30 GWd/MTU) do not extend to the current exposures that the fuel bundles experience. GE committed to perform fission gas inventory and rod exposure gamma scans. There is a restriction associated with this commitment. Appendix F contains associated T-M follow-up RAIs pertaining to the status of the benchmarking data.
- e) In the Economic Simplified Boiling Water Reactor (ESBWR) review, the NRC staff determined that the General Electric Stress and Thermal Analysis of Reactor Rods - Mechanical (GESTR-M) prediction of the fuel centerline temperature becomes non-conservative with exposure. This non-conservatism is not associated with the GESTR-M calculation of the gadolinia (Gd)-bearing rod, which is the bases for the overpower acceptance criteria, since the Gd rod accommodates lower TOP during transients. The NRC staff requested GE to perform a Part 21 evaluation to determine the safety significance of the potential non-conservatism. The associated limitation

states that the conclusions of the NRC staff evaluation of GE's Part 21 report will be applicable to the T-M methodology for EPU and MELLLA+ operation. In addition, the FRAPCON GESTR-M TOP comparisons in Section 3.2.6.5.6 provide the NRC staff assessment of the GESTR-M fuel temperature underprediction. The NRC staff determined that the uncertainties treatment compensates for the UO<sub>2</sub> fuel temperature underprediction. Appendix F provides additional NRC staff follow-up RAIs pertaining to the adequacy of the GESTR-M internal rod pressure calculations and subsequent NRC staff evaluations of GE's Part 21 report.

5. Steady-State Bypass Voiding

The technical specification for the neutron monitoring system (e.g., LPRMs) limits the bypass voiding to 5 percent. For the EPU and MELLLA+ operation, the bypass voiding could be 5 percent or higher at the exit. There is a limitation that the bypass voiding will be limited 5 percent for the LPRM D-level for implementation of EPU and MELLLA+. The steady-state bypass voiding will be reported in the SRLR for every reload.

6. Stability Setpoint Setdown

During some transients, such as recirculation pump trip events, the hot channel bypass voiding could reach a maximum of [ ], depending on the code used. The high in-channel and bypass voids will primarily affect the LPRM neutron detectors by reducing the detector response, assuming the same power in the adjacent fuel bundle. This reduction in detector response is due to a decrease in the moderation caused by the presence of high in-channel voiding at the upper part of the fuel bundle and in the bypass. The in-channel and bypass voids decrease the thermal neutron flux incident on the detectors for the same neutron flux generated in the adjacent fuel. The NRC staff concludes that the instrument calibration error is less than 5 percent for oscillating power range monitor (OPRM) cells and less than 2 percent for average power range monitor (APRM) signals. There is a restriction that requires setdown of the instrumentation to preclude the presence of the high in-channel and bypass voiding for EPU and MELLLA+ conditions.

7. Application of 10 Weight Percent Gd

The overpower limit for the Gd bearing rod, with 10 weight percent Gd, appears to be less than the expected pressurization response for operation at EPU and MELLLA+ conditions. Therefore, there is a limitation that, prior to implementing 10 percent Gd rod for EPU and MELLLA+ bundle designs, the NRC staff needs to review and approve the TOP response of 10 percent weight percent Gd-bearing rod against EPU and MELLLA+ overpower response at the most limiting statepoints, considering the operating flexibilities (e.g., equipment out-of-service).

8. Void-Quality Correlation

In LTR NEDC-33173P and the corresponding RAIs, GE justified extension of the Findlay-Dix correlation to up to pure steam. Historically, the NRC staff had never directly reviewed or approved the correlation and its supporting database. However, the NRC staff had reviewed the application of the void-quality correlation in certain codes.

In this review, the NRC staff evaluated: (1) the qualification database provided in the Findlay-Dix correlation source document (Reference 35); (2) the EPU and MELLLA+ core conditions during steady-state, transient, and accident conditions; (3) the current fuel design geometric features (part-length rods, spacer design changes, and hydraulic diameters); and (4) the current lattice designs as operated (e.g., lattice radial power distribution for controlled and uncontrolled conditions, bundle axial power-peaking). The NRC staff determined that:

- a) Although the supporting data does not cover all of the current operational conditions (e.g., the current radial and axial lattice peaking, the 10x10 bundle design features, such as the part-length rods and new spacer design), the NRC staff finds that, overall, the correlation does not exhibit unexpected behavior and remains relatively predictable. The NRC staff expects that most likely the uncertainty levels are higher than those reported.
- b) The Findlay-Dix validation database is limited in that the database does not appear to cover the full operational and accident parameter space in a way that assures that all local parameter sets are encompassed by the supporting bundle data. Evaluation of the radial within bundle power distribution of the database shows that the validation database is not representative of the current bundle axial or radial power distribution and peaking. This is a deficiency in the database supporting the correlation in relation to the current fuel design as operated. Therefore an additional margin of 0.01 will be applied to the OLMCPR, as discussed in 8.d) below.
- c) The reported accuracy is not well supported and additional measurement data is needed to both validate the correlation and develop the appropriate correlation uncertainty levels.
- d) The conclusion to obtain additional data to validate the impact of non-uniform (e.g., skewed) power distributions is supported by the recommendations made in the initial 1977 LTR NEDE-21565 (Reference 52). The NRC staff believes the weaknesses of the validation database identified in LTR NEDE-21565 are more relevant for the current EPU operating strategy and the proposed expanded operating domain. Specifically, the Findlay-Dix source document recommendations are important in terms of power skewing and countercurrent flows.

Therefore, the NRC staff decided, as an interim measure, the impact of having higher voids than predicted can be accounted for in the impact of the void reactivity coefficient on the transient analyses. The content of LTR NEDC-33173P and the RAI responses did not provide sufficient confidence for the NRC staff to approve the extension of the correlations to new operating domains without interim margin improvement. Since higher uncertainties in the void-quality correlation will result in the existence of higher voids than predicted, the core average voids could be higher assuming that the correlation uncertainties are higher for all lattice levels due to the different power skew, part-length rods, and new design features (e.g., new spacer designs). Higher core average voids will potentially affect the magnitude of the void reactivity coefficient, which is directly proportional to the core average void fraction.

The NRC staff concludes that a 0.01 margin will be applied to the OLMCPR, until the NRC staff reviews and approves a void-quality correlation supplement or revision to LTR NEDC-33173P. The supplement/revision shall provide sufficient assessment of the void-quality correlation prediction as applied to the current fuel geometric and lattice designs as operated under EPU and the proposed high power-to-flow MELLLA+ condition. The supplement/revision shall also include additional measurement data to establish the performance of the correlation and the associated uncertainties. The supplement/revision should address the recommendation in the source document. Note that the NRC staff considers the significance threshold for the critical power ratio (CPR) change for transients to be 0.01. To support the long-term resolution of the qualification of the void-quality correlation, the NRC staff will issue additional RAIs that provide guidance in terms of the NRC staff position and the necessary information needed.

#### 9. MELLLA+ Implementation

LTR NEDC-33006P, Revision 2 (Reference 2), provides the GE safety analysis report for operation at the proposed expanded operating domain (MELLLA+). LTR NEDC-33173P (Reference 1) provides the bases for accepting the application of GE NRC-approved analytical methods and codes to MELLLA+ high power and low flow conditions. The NRC staff SE approving LTR NEDC-33006P, Revision 2, was issued on September 17, 2007 (Reference 56).

#### 10. Use of TRACG for EPU and MELLLA+

Licenses are expected to transition to the TRACG for AOOs and calculation of peak anticipated transient without scram (ATWS) pressure calculations. Some of the sensitivity analyses supporting the methods review are based on TRACG. There are also a number of restrictions associated with the use of GE's methods that apply to TRACG as well. These methodology deficiencies that need to be evaluated for TRACG include: (1) the biases in the void reactivity coefficient associated with the 40 percent depletions assumption; (2) the applicability of the lattices used to develop the void coefficient biases and uncertainties in the response surface in TRACG; (3) the conservatism of the control rod (CR) blade patterns and the associated axial and radial power distribution assumed in TRACG for AOO application relative to the power distributions cores will experience based on the actual plant control rod (CR) patterns; and (4) the adequacy and applicability of the qualification data supporting the coupled PANACEA/TRACG Findlay-Dix correlation and interfacial shear model void fraction calculations.

The NRC staff is currently reviewing a new version of TRACG in LTR NEDE-32906P, Supplement 3, "Migration to TRACG04/PANAC11 from TRACG02/PANAC10," May 2006 (Reference 40). The LTR NEDC-33173P review defers the review and conclusions related to the topics discussed above to the TRACG supplement currently under review. Therefore, there are additional margins such as the 10 percent TOP and MOP margins and the 0.01 OLMCPR adder that have not been applied to the TRACG application. The bases of this approach was to investigate the potential to implement modeling changes in TRACG (e.g., increase in void reactivity biases described in Section 5.0 of TRACG), which has the capability to simulate 3D reactor core model rather than requiring specific margins to be added to plant-specific applications. In addition, it is appropriate to investigate the adequacy of the supporting data in the review of a specific code for application to EPU and MELLLA+. Therefore, any conclusions specified in the NRC staff SE approving Supplement 3 to LTR NEDC-32906P will be applicable as approved.

However, if GE does not adequately address the methodology deficiencies identified in LTR NEDC-33173P in the review of Supplement 3 of NEDE-32906P, the additional margins as described in this SE apply as appropriate.

#### 11. Mixed Core Method Limitations

Plants implementing EPU or MELLLA+ with mixed fuel vendor cores will provide plant-specific justification for extension of GE's analytical methods or codes. The content of the plant-specific application will cover the topics addressed in LTR NEDC-33173P and additional subjects relevant to application of GE's methods to legacy fuel. Alternatively, GE may supplement or revise LTR NEDC-33173P for application to mixed cores.

The NRC staff did not assess the Toshiba, GE Boiling Lattice Analysis Code upgrade (TGBLA06) for use with 11x11 and higher lattices, water crosses, water boxes, or MOX fuels at EPU or MELLLA+ conditions. For any plant-specific applications of TGBLA06 with the

above fuel types, requiring changes to the code, GE needs to provide assessment data similar to that provided for the GE fuels.

#### **4.0 CONCLUSION**

The NRC staff reviewed the application of GE analytical methods and codes to operation at EPU and to the MELLLA+ expanded operating domain. The NRC staff reviewed: (1) the methods to determine if NRC-approved analytical methods were being applied within the approved ranges; (2) the adequacy of the uncertainties applied to the safety analyses; (3) the conservatism in the analytical methods; (4) the margins available; and (5) the adequacy of the available qualifications data. Additional margins were implemented to compensate for uncertainties where the NRC staff found that the extension of the methods to EPU and MELLLA+ operation merited additional benchmarking data.

The review of the LTR NEDC-33173P included a number of commitments by GE to obtain experimental data that, in the long term, will provide additional confidence in the extension of the methods to EPU and expanded operating domain operation. GE also developed new improved neutronic and thermal mechanical methodologies. These methods will be benchmarked against the additional measurement data. In the future, the review and approval of these improved methods will provide adequate bases to remove these interim margin improvements.

Since the GE analytical methods and codes used to perform the safety analyses supporting BWR plants' EPU and MELLLA+ response are described in number of different generic LTRs, the SE approving LTR NEDC-33173P does not address or cover all aspects of the applicable LTRs. The NRC staff approval of LTR NEDC-33173P is limited to those topics or areas covered in: (1) LTR NEDC-33173P; (2) the associated RAI responses; and (3) the NRC staff SE. Therefore, any topics covered in the specific generic LTRs approved in the past but not currently reviewed under this SE are not considered to be part of this approval.

Based on the review performed, the information provided in the RAI responses, the insights from the NRC staff confirmatory analyses, the additional margins included in the methods and the changes in the calculational methodology delineated in the associated limitations, the NRC staff finds that there is reasonable assurance that the application of GE methods to EPU and the expanded operating domain is acceptable. The NRC staff approval is contingent on the conditions and limitations discussed in Section 9.0 of the SE.

## ACRONYMS AND ABBREVIATIONS

TERM	DEFINITION
3D	Three-dimensional
AOO	Anticipated Operational Occurrence
APLHGR	Average Power Linear Heat Generation Rate
APRM	Average Power Range Monitor
ASME	American Society of Mechanical Engineers
ATLAS	GE's 8.6 MW Heat Transfer Loop
ATWS	Anticipated Transient Without Scram
Ba	Barium
BOC	Beginning-of-Cycle
BT	Boiling Transition
Btu/lbm	British thermal unit per pound mass
BWR	Boiling Water Reactor
CF	Core Flow
CFR	<i>Code of Federal Regulations</i>
CHT	Conduction Heat Transfer (a GE task code)
COLR	Core Operating Limits Report
CPPU	Constant Pressure Power Uprate
CPR	Critical Power Ratio
CR	Control Rod
DIVOM	Delta CPR over Initial CPR vs. Oscillation Magnitude
DR	Decay Ratio
DRC	Density Reactivity Change
DSS-CD	Detect and Suppress Solution – Confirmation Density
ECCS	Emergency Core Cooling System
EOC	End-of-Cycle
EOP	Emergency Operating Procedure
EPU	Extended Power Uprate
ESBWR	Economic Simplified Boiling Water Reactor
Gd	Gadolinia
GDC	General Design Criterion
GE	General Electric
GESTAR	GE Standard Application for Reload
GESTR-M	General Electric Stress and Thermal Analysis of Reactor Rods - Mechanical
GEXL	GE Critical Quality Correlation
GNF	Global Nuclear Fuels
GWd/MTU	Giga Watt Days per Metric Ton of Uranium

NEDO-33173-A, Revision 1  
Non-Proprietary Information

GWd/ST	Giga Watt Days per Short Ton
HBB	Hard Bottom Burn
ICPR	Initial Critical Power Ratio
IV	Instantaneous Void
kW/ft	Kilo Watt per foot
kW/l	Kilo Watt per liter
La	Lanthanum
LHGR	Linear Heat Generation Rate
LOCA	Loss-of-Coolant Accident
LPRM	Local Power Range Monitor
LTR	Licensing Topical Report
LTS	Long Term Solution
LVDT	Linear Variable Differential Transformer
MAPLHGR	Maximum Planar LHGR
MAPRAT	Maximum Average Planar Ratio
MCNP	Monte Carlo N Particle Transport Code
MCPR	Minimum Critical Power Ratio
MELLLA+	Maximum Extended Load Limit Analysis Plus
MFLPD	Maximum Fraction of Linear Power Density
Mlbm/hr	Mega pound mass per hour
MLHGR	Maximum Linear Heat Generation Rate
MOC	Middle-of-Cycle
MOP	Mechanical Overpower
MSIV	Main Steam Isolation Valve
MSIVC	Main Steam Isolation Valve Closure
NMP2	Nine Mile Point Unit 2
NRC	US Nuclear Regulatory Commission
ODYN	GE Transient Analysis Code
OLMCPR	Operating Limit MCPR
OLTP	Original Licensed Thermal Power
OPRM	Oscillating Power Range Monitor
PANAC11	GE Three Dimensional BWR Core Simulator
PANACEA	GE Three Dimensional BWR Core Simulator
PBDS	Period Based Detection System
PCT	Peak Clad Temperature
PIRT	Phenomena Identification Ranking Table
psia	Pounds per Square Inch Atmosphere
psig	Pounds per Square Inch Gauge

NEDO-33173-A, Revision 1  
Non-Proprietary Information

RAI	Request for Additional Information
RMS	Root Mean Squared
RPT	Recirculation Pump Trip
SAFDL	Specified Acceptable Fuel Design Limit
SDM	Shutdown Margin
SE	Safety Evaluation
SLCS	Standby Liquid Control System
SLMCPR	Safety Limit Minimum Critical Power Ratio
SLO	Single Recirculation Loop Operation
SRLR	Supplemental Reload Licensing Report
SRP	Standard Review Plan
SRV	Safety Relief Valve
TGBLA	Toshiba, GE Boiling Lattice Analysis
TIP	Traversing In-core Probe
T-M	Thermal-Mechanical
TMOL	Thermal-Mechanical Operating Limit
TOP	Thermal Overpower
TRACG	GE Transient Reactor Analysis Code
TS	Technical Specification
TVA	Tennessee Valley Authority
TVAPS	Transient Varying Axial Power Shape
UB	Underburn
VYNPS	Vermont Yankee Nuclear Power Station



FINAL SAFETY EVALUATION BY THE OFFICE OF NUCLEAR REACTOR REGULATION

LICENSING TOPICAL REPORT NEDC-33171P

“APPLICABILITY OF GE METHODS TO EXPANDED OPERATING DOMAINS”

GENERAL ELECTRIC HITACHI NUCLEAR ENERGY

PROJECT NO. 710

**1.0 INTRODUCTION AND BACKGROUND**

By letter dated February 11, 2006, GE Hitachi Nuclear Energy (GEH, formerly known as General Electric Nuclear Energy) requested U.S. Nuclear Regulatory Commission (NRC) review of licensing topical report (LTR), NEDC-33173P, “Applicability of GE Methods to Expanded Operating Domains” (Reference 1). The purpose of this LTR is to provide the methodology used to demonstrate the adequacy of the GE methods for expanded operating domains. This safety evaluation (SE) provides a generic licensing basis for GE methods applications to operating envelope up to and including extended power uprate (EPU) and maximum extended load line limit analysis plus (MELLLA+).

The NRC reviews and approves fuel vendor analytical methods and codes used to perform safety analyses. Section 5.0 of the boiling water reactor (BWR) Technical Specifications (TSs) specifies that the LTRs document the licensing methodology and codes used to perform the safety analyses supporting the safe operation of BWR plants. In addition, applications involving changes to a plant’s licensed operating conditions shall explicitly specify which NRC-approved methods and codes are used to perform the supporting design-bases safety analyses (e.g., Table 1.1 of the power uprate safety analysis report). Therefore, licensing applications do not, in general, involve review of the analytical methods or codes used to model a plant’s response.

For operation at EPU and MELLLA+, the coupled neutronic and thermal-hydraulic core conditions could extend to higher void conditions outside the current experience base. The NRC staff review verified the following:

1. The analytical methods and codes used to perform the design-bases safety analyses will be applied within the applicable NRC-approved validation ranges.
2. The calculation and measurement uncertainties applied to the thermal limit calculations and the models simulating physical phenomena will remain valid for the predicted neutronic and thermal-hydraulic core and fuel conditions during steady-state, transient, and accident conditions.

3. The qualification database supporting analytical models simulating physical phenomena remains valid and applicable to the conditions under which it is applied, including those models and key parameters in which specific uncertainties are not applied.
4. If the NRC-approved analytical methods and codes are extended outside the applicability ranges, the extension of the specific models are demonstrated to be acceptable or additional margins are applied to the affected downstream safety analyses until such time the supporting qualification data is extended.

The NRC staff reviewed and evaluated the applicability of GE nuclear and thermal-hydraulic methods and codes for operation at EPU and MELLLA+. The NRC staff assessments are based on review of:

1. LTR NEDC-33173P, "Applicability of GE Methods to Expanded Operating Domains," dated February 2006 (Reference 1),
2. LTR NEDC-33006P, Revision 2, "General Electric Boiling Water Reactor Maximum Extended Load Line Limit Analysis Plus," November 2005 (Reference 2),
3. Requests for additional information (RAIs) and commitments (References 3 through 25),
4. Vermont Yankee Nuclear Power Station (VYNPS) Constant Pressure Power Uprate SE (References 26 through 30), and
5. Audits.

The NRC staff concludes that implementation of MELLLA+ will result in operation outside the current experience base. Specifically, for some applications, the maximum powered bundles will operate outside the current operating experience base in terms of key parameters such as bundle power-to-flow ratio and exit void fractions. However, the core designs and operation will continue to be constrained by the requirement to meet the thermal limits.

In order to capture the uncertainties in the neutronic methods for operation at EPU and MELLLA+, GE committed to embark on "on-going benchmarking" program in MFN 06-434 (Reference 8). In the long term such program will benchmark bundles and pins that are operated as close as possible to the MELLLA+ operation through gamma scan, thereby validating the accuracy of the analytical methods and codes for operation at EPU and MELLLA+. As part of the generic method review and formulation of the interim approach, GE presented to the NRC staff: (1) the scope of the planned power distribution and thermal-mechanical (T-M) gamma scans; and (2) the description of the gamma scans process and technique. Reference 31 contains the slides. In Reference 7 of the interim methods review, GE committed to perform the bundle and pin power gamma scans. The commitment letter provided an update of the planned power distribution gamma scan scope only. In RAI 9 response (Reference 25), GE acknowledged the T-M qualification limitation and agreed to perform and submit the thermal mechanical gamma scans needed to benchmark thermal mechanical models for the current fuel designs. Therefore, GE's measurement plan, updating the qualification database supporting the power distribution and T-M models are:

1. fission gas benchmarks for T-M models,
2. rod exposure benchmarks for lifetime integrated rod power,
3. rod-by-rod power-peaking benchmarks, and
4. bundle power allocation benchmarks around instrument positions.

In addition, GE submitted a commitment letter (Reference 14) that presented updated plan for the review and qualification of the void fraction correlations for the current fuel designs and operating strategies as part of the COBRAG code submittal (Reference 14).

Given that the specific measurement data will not be available for some time, the NRC staff review of LTR NEDC-33173P (Reference 1) will:

1. identify the key parameters that are affected by potential errors in the cross-sections important to the downstream safety analyses,
2. account for potential increases in the uncertainties associated with the prediction of the key parameters that are affected, and
3. propose additional margin in the short-term where warranted, in order to ensure that sufficient margins will be available in the affected downstream safety analyses.

The NRC staff review of LTR NEDC-33173P (Reference 1) concludes that these methods may be applied to plants that implement EPU and MELLLA+, given the limitations and conditions in Section 9.0 of this SE. Specifically, this SE imposes an additional 0.02 adder to the cycle-specific safety limit minimum critical power ratio (SLMCPR) for operation with 20 percent power uprate, or a 0.03 SLMCPR adder for plant's approved for implementation of MELLLA+ operation.

LTR NEDC-33173P (Reference 1) refers in generic terms to expanded operating domains. For clarity, MELLLA+ is defined as the expanded power-to-flow operating domain defined in LTR NEDC-33006P, Revision 2, "General Electric Boiling Water Reactor Maximum Extended Load Analysis Plus."

## **2.0 APPLICABILITY OF GE METHODS AND CODE TO EPU AND MELLLA+**

### **2.1 EPU AND EXPANDED OPERATING DOMAINS CORE CHARACTERISTICS**

To implement EPU and maintain a 24-month cycle, a higher number of maximum powered bundles are loaded into the core and the power of the average bundle power increases, leading to a flatter core radial power distribution. Due to an increased two phase pressure drop and higher coolant voiding, the flow in the maximum powered bundles decreases. This leads to a higher bundle power-to-flow ratio and a higher exit void fraction. Since the maximum powered bundles set the thermal limits, EPU operation reduces the margins to the thermal limits. For the proposed MELLLA+ operation, plants will operate at EPU power levels at lower core flow conditions. Therefore, the number of bundles operating at higher power-to-flow conditions and consequently higher exit void fractions will be expected to increase.

There are no direct limits on the operating bundle powers, bundle operating power-to-flow ratio, or void fractions. Instead, the core design and the operating strategy employed are constrained by the thermal limits. The maximum powered bundles must meet the thermal limits so that the technical specification safety limits or the specific fuel design limits are not violated during steady-state, transient, and accident conditions. Since the high-powered bundle's ability to operate within the thermal limits is analytically determined, it becomes important to ensure that the analytical tools are being applied within the ranges for which it was derived and benchmarked. It is for this reason that in this section, the applicability of the analytical methods and codes used to predict EPU and MELLLA+ responses during steady-state, transient, and accident conditions are being investigated.

### 2.1.1 Key Operating Parameters

The core thermal-hydraulic conditions for operation at EPU and MELLLA+ can be measured by review of the following key parameters:

1. **Power of Peak Bundle**  
The bundle power (in MW) is a fundamental direct input to the critical power ratio (CPR) safety parameter calculation, the linear heat generation rate (LHGR), the initial conditions for loss-of-coolant accident (LOCA) response, and the calculation of other intermediate quantities. It represents a local metric of operating conditions and is relevant particularly to the performance of the steady-state nuclear methods.
2. **Coolant Flow for Peak Bundle**  
The active bundle flow (in Mlbm/hr) is also a direct input to the calculation of the CPR safety parameter, as well as other intermediate quantities.
3. **Exit Void Fraction for Peak Power Bundle**  
The void fraction results from the integration of the bundle power and flow, as well as the axial distribution of power deposition along the bundle.
4. **Maximum Channel Exit Void Fraction**  
The peak power bundle (hot channel) may not always coincide with the bundle with the highest channel exit void fraction, since this parameter is based not only on total bundle power, but also on bundle flow.
5. **Core Average Exit Void Fraction**  
The core average exit void fraction is a core-wide metric on the amount of heat being carried by the coolant.
6. **Peak LHGR**  
The peak LHGR (in kW/ft) is a reasonable measure of degree of peaking in the core since it is comprised of the combination of radial, axial, and local (pin) power-peaking. It is also a key design constraint and monitoring parameter.
7. **Peak Nodal or Pin Exposure**  
The nodal and pellet exposures are determined by integration of the energy extracted from the local physical area of the fuel given its original specific mass.

The hot bundles set the steady-state fuel design thermal limits. Therefore, review of these parameters as function of cycle exposure statepoints provide insight into the core conditions of the plant-specific application against current EPU experience base. Figure 2-1 through Figure 2-4 show the key parameters at different exposures for several EPU plants. As depicted by the figures, the limiting bundles would be operating at void fractions above 85 percent. The maximum powered bundles for the non-EPU high-power density BWR (Plant B) are operating within the ranges of EPU plants. However, EPU plants will be operating with cores loaded with a greater number of maximum powered bundles, which will be operating close to the thermal limits. These are the key parameters that influence the plants thermal limit performance and response in the safety analysis.

### 2.1.2 MELLLA+ Core Conditions

For MELLLA+ (see Figure 2-5), the operation at the EPU power levels at core flow as low as 80 percent rated core flow results in higher voids conditions. Table 2-1 compares the hot channel exit voids fraction at the MELLLA+ statepoints and to that at increased core flow. The calculation was preformed using the core simulator (PANACEA11). As shown in Table 2-1, the

exit void fraction at the 55 percent rated core flow statepoint (e.g., Knee) is around [ ]. Depending, on the plant-specific core conditions and the code used to perform the calculations (TRACG versus PANACEA), the hot bundle exit void fraction for MELLLA+ operation during steady-state can be projected to be above 90 percent void fraction. Considering the hot bundle void fractions for all the BWR fleet operating at MELLLA+ conditions, the exit void fraction for the high powered bundles could be projected to be less than 95 percent. As can be seen in Table 2-1, the void fraction for the rated EPU power and core flow is expected to fall within the range of minimum flow and the increased core flow values. The channel operating minimum CPR (MCPR) reflects the actual operating limit for a given bundle power and flow condition.

Therefore, for operation at the MELLLA+ statepoints, BWRs will be operating at higher void fractions than the EPU statepoint. The NRC staff reviewed LTR NEDC-33173P (Reference 1) to determine if the operation at the high void fraction alters key assumptions in the analytical methods and codes. A change in the assumption in the neutronic methods that feed all the downstream codes used to perform the safety analyses may have model uncertainties that are sensitive to void fraction characteristic of MELLLA+ operating conditions.

**Table 2-1 Exit Void Fraction**

Plant / Parameter Hot Channel	Power (%OLTP)/Core Flow (%rated)	Exit Voids
PANACEA 11 (Channel MCPR 1.30)	120/85	[
PANACEA11 (Channel MCPR = 1.48)	120/104.5	
PANACEA 11 (Channel MCPR = 1.37)	93/55	]

It is noted that although the MELLLA+ core conditions are presented in the review LTR NEDC-33173P, evaluation of BWR response for operation at MELLLA+ conditions is covered under LTR NEDC-33006P. Section 9.0 of this SE contains a limitation regarding the implementation of MELLLA+ and the application of LTR NEDC-33173P for MELLLA+ operation. Plant-specific approval and implementation of MELLLA+ operation is contingent upon approval of LTR NEDC-33006P (Reference 2). This SE focused on evaluating the GE analytical methods to the projected high power/low flow MELLLA+ core conditions.

### 2.1.3 EPU and High-power density Plant Core Tracking Data

Evaluation of the operating thermal margins of EPU plants provides additional means to examine the impact of EPU operation. The core simulator monitors the bundle operating conditions and calculates the available thermal margins for compliance with the thermal limits. Sections 3.2.4, 3.2.5, and 3.2.6 of this SE define the specific thermal limits. In response to NRC staff RAI 25 (Reference 11), GE provided a comparison of thermal limits core-tracking for the reference EPU and high-power density plants. The calculation was performed using the steady-state neutronic method (TGBLA/PANACEA). The ratio of the predicted limiting bundle operating thermal limits against the respective TS thermal limit value provides an assessment of the thermal margins available.

The Reference Plants (A through E) are high-power density plants operating at expanded power levels, except for Plant C. Plant B is a high-power density BWR/6, which operates at 5 percent above the original licensed thermal power (OLTP). Only Plants E (BWR/6) and D (BWR/4) are

operating at 20 percent above the OLTP. Plant A (BWR/4) is operating at 12 percent above the OLTP, although it is licensed to operate at EPU power levels.

Figure 2-6 through Figure 2-8 provides the Reference Plant's core-tracking thermal margins. A ratio of 0.9 indicates that the plant is predicted to operate with 10 percent margin to the limit. Core tracking data shows that at some cycle statepoints, the plants operate at the limit.

The RAI response in MFN 04-026 (Reference 5) states that the infrequent thermal margin values greater than 1.0 for maximum fraction of linear power density (MFLPD) and the MAPRAT are not unexpected for states that are close to the limit. The response states that there is not a perfect agreement between the nuclear methods and the plant monitoring measurements. It is reasonable that there are some uncertainties associated with the plant measurement and the nuclear methods coupled thermal-hydraulic and neutronic predictions of the core conditions. However, thermal margins at subsequent cycles for the same plant with the same measurement uncertainties do not appear to result in over-predictions. Therefore, the closer the plants operate near the limit, the more significant the accuracies of the methods and the validation of the uncertainties of the methods become. Note that Plant B, Cycle 9 and Plant E, Cycle 9, core monitoring and offline calculations are based on PANAC10. Current PANAC11 core simulator includes improvements in the nuclear methods. However, since some plant's BWR 3D MONICORE core monitoring systems may rely on PANAC10, assessment of its capability is valid, until all plants transition to TGBLA06/PANAC11.

The LTR NEDC-33173P evaluates the analytical methods used to perform the safety analyses supporting EPU and MELLLA+ conditions. The objective of the evaluation is to demonstrate the following for EPU and MELLLA+ conditions:

1. the NRC-approved methods and codes will be applied within the approved and benchmarked ranges,
2. if the NRC-approved analytical methods and codes are extended outside the applicability ranges, the impact is acceptable, and
3. the uncertainties and biases applied to the safety analyses remain applicable and valid for the EPU and MELLLA+ operation.

## 2.2 TOPICS OF REVIEW

The EPU and MELLLA+ thermal-hydraulic core conditions will affect the following topics:

### 2.2.1 Extrapolation of the Neutronic Methods to High Void Conditions

Assumptions were made in the generation of the lattice physics data that established the neutronic feedback. This review involves evaluating the:

1. impact of extrapolation of the neutronic parameters to void fractions [ ] in the neutronic feedback and
2. impact of assuming core average void fraction of [ ] in generating the R-factors that are used in the SLMCPR.

### 2.2.2 Assessment of the 40 Percent Depletion Assumption

The main effect of the 40 percent depletion history assumption in generating the branch cases of the lattice physics calculation is an increased bias for the void reactivity coefficient. This review involves:

1. quantifying the impact of the 40 percent depletion assumption on void reactivity.
2. review of increased uncertainties on safety analysis, including transients, stability, and anticipated transient without scram (ATWS) events.

### 2.2.3 Assessing the Impact of Bypass Voiding

Reliability of the response and prediction of the instrumentations located in the out-channel regions (i.e., transversing in-core probes (TIPs) and local power range monitors (LPRMs)) is assessed. This review involves evaluating the impact on neutronic methods and the impact on steady-state calculations.

### 2.2.4 Assessing the Impact of Neutronic Method Assumptions

The expected impact of a transient on stability is a transient that is affected by the neutronic methods assumptions. This review involves the evaluation of the impact of these assumptions on the stability long term solutions (LTSs) for bypass voiding and void coefficient bias.

### 2.2.5 Applicability of the Thermal-Hydraulic Models

Applicability of the thermal-hydraulic correlations used to model physical phenomena. This review involves evaluating the GE critical quality correlation (GEXL) and the void-quality correlation.

[

]

**Figure 2-1 Maximum Bundle Power vs. Cycle Exposure for EPU Plants and a High-power density 5 percent Uprate Plant**

[

]

**Figure 2-2 Maximum Power/Flow Ratio vs. Cycle Exposure for EPU Plants and a High-power density 5 percent Uprate Plant**

[

]

**Figure 2-3 Exit Void Fraction of Maximum Power Bundle vs. Cycle Exposure for EPU Plants and a High-power density 5 percent Uprate Plant**



[

]

**Figure 2-4 Peak LHGR vs. Cycle Exposure for EPU Plants and a High-power density 5 percent Uprate Plant**

[

]

**Figure 2-5 Power Flow Map**

[

]

**Figure 2-6 LHGR operating History for EPU and a High-power density Plant**

Note: Plant B, Cycle 9 and Plant E, Cycle 9 core monitoring and offline calculations are based on PANAC10.

[

]

**Figure 2-7 OLMCPR operating history For EPU and a High-power density Plant (Un-adapted PANACEA Calculation)**

Note: Plant B, Cycle 9 and Plant E, Cycle 9 core monitoring and offline calculations are based on PANAC10

[

]

**Figure 2-8 MAPLHGR Operating History (Unadapted PANACEA Calculation)**

Note: Plant B, Cycle 9 and Plant E, Cycle 9 core monitoring and offline calculations are based on PANAC10

**3.0 EXTRAPOLATION OF NEUTRONIC METHODS TO HIGH VOID FRACTIONS**

**3.1 ASSESSMENT**

This section contains assessment of the extension of the neutronic methods to the high void conditions characteristic of EPU and MELLLA+ conditions. The NRC staff evaluates: (1) the NRC-approved validation ranges; (2) the insights from independent code-to-code confirmatory comparisons; (3) the core-tracking data for EPU plants; and (4) the available bundle and pin power gamma scans supporting the power distribution uncertainties currently applied to the safety analyses.

**3.1.1 Assessing Extrapolation of the Neutronic Methods**

The neutronic parameters feed into almost all codes that are used to perform the steady-state, transient, and accident conditions and establish the core operating thermal limits. Therefore, the accuracy of the methods to calculate the neutronic parameters affects the analyses supporting operation at the EPU and MELLLA+ condition. The following sections cover the adequacy of the extrapolation of the neutronic methods outside the NRC-approved applicability ranges. They also discuss the currently available benchmarking data and assess its adequacy for operation at EPU and MELLLA+ conditions.

### 3.1.1.1 Neutronic Methods Not Assessed by the NRC Staff for Void Fraction Greater Than 70 Percent

The GE lattice physics (TGBLA) and core simulator (PANACEA) codes have only been assessed by the NRC staff for void fractions up to 70 percent (Reference 32). Plant-specific EPU data predicts exit void fractions greater than 85 percent. Operation at the EPU power levels with minimum core flow conditions as low as 80 percent rated core flow, which is characteristic of the proposed MELLLA+, would lead to higher exit void fractions. Therefore, the NRC staff reviewed and assessed the extension of the neutronic methods to higher void fractions.

The neutronic methodology employed by GE generates cross-sections and lattice physics parameters at [ ]. The bypass and water rod is assumed to be at saturated liquid conditions. These neutronic data are then parameterized by a quadratic fit as a function of the lattice-average water density, which includes the bypass region and water rods. For nodes operating between [ ], the neutronic data is interpolated. For nodes operating above [ ], the neutronic parameters are obtained by extrapolating the quadratic fit.

In response to NRC staff RAIs, GE submitted Enclosure 3 to MFN 04-026 (Reference 5), which evaluated the extension of the neutronic methods to MELLLA+ conditions. This evaluation was mostly based on code-to-code comparisons to assess the extrapolation errors without additional benchmarking with data. Enclosure 3 to Reference 5 also proposed performing eigenvalue tracking to assess the neutronic methods after implementation of MELLLA+.

In Enclosure 3 to MFN 04-026 (Reference 5), GE examined the extrapolation errors for the historical cases based on a comparison between the Monte Carlo N Particle Transport Code (MCNP) and TGBLA. In its assessment, GE recognized that MCNP is not normally used for lattice depletion and the code was not formally benchmarked. For the historical cases, any MCNP/TGBLA comparison requires the use of the TGBLA isotopics in MCNP. In addition, MCNP does not model the pseudo-fission product and any comparison with TGBLA will require turning off the TGBLA pseudo-fission product model.

For the historical case, GE also investigated the accuracy of the fit to high void technique, using a development code. However, the uncertainties in the lattice physics data as fitted could not be established by comparing it to a developmental code. Therefore, GE used MCNP comparisons.

In addition to the difficulties associated with performing independent code-to-code comparisons, the assessment did not include propagation of the errors associated with the lattice physics code for both the historical and the branch cases to the downstream safety analyses. Independent assessment would require the use of two independent lattice physics and core simulator codes that have been benchmarked against measurement data.

In the MCNP/TGBLA comparisons, GE reported high extrapolation errors in some of the nuclear parameters (e.g., migration area [ ] and flux ratio up to [ ]). Therefore, there is a need to establish the impact of these errors on the core response including axial power profile and pertinent thermal limits. However, propagation of error poses the added difficulty of determining: (1) which key parameter of the cross-sections should be propagated, (2) in which direction should it be propagated, and (3) if individual parameters or several parameters should be propagated per case run. While such propagation of errors are doable, it is time consuming and the outcome may not yield meaningful conclusions to establish accuracy in terms of uncertainties and biases of the analytical methods and codes that are used to support safety analyses of nuclear reactors.

Uncertainties associated with the predictions of the neutronic methods for operation at high void conditions are not limited to the biases associated with the lattice physics data generated by TGBLA or the errors associated with fit/extrapolation techniques employed by PANACEA. They also include the additional inherent errors and biases associated with the neutronic and thermal-hydraulic method employed by PANACEA. These errors need to be quantified as well. Therefore, establishing the accuracy associated with the neutronic method in its predictions of bundle and pin powers, as depleted for the current operating strategies requires obtaining and using actual bundle and pin power measurement data (e.g., gamma scans and heavy isotopic and fission inventory measurement).

Subsequently, the NRC staff focused its evaluation on the available EPU plant data from TIP measurement (see Section 3.1.3, "Core-Tracking Data Validation" of this SE), and benchmark measured data (see Section 3.1.4, "Available Gamma Scan Data" of this SE). In addition, the ORNL staff performed confirmatory lattice physics code-to-code comparisons using HELIOS. It is important to note that the NRC staff confirmatory lattice physics data comparisons do not establish the accuracy and uncertainties associated with GE's coupled lattice physics and core simulator codes (TGBLA/PANACEA), but only serve to confirm consistency between the lattice physics codes results. Specifically, the NRC staff used the lattice physics comparisons to evaluate the acceptability of specific improvements in TGBLA06. Section 3.1.2 "Confirmatory Lattice Physics Data Comparisons (TGBLA06/HELIOS)" of this SE provides a summary of the ORNL staff lattice physics code-to-code comparisons and the evaluation contained in Appendix B provides the conclusions of the lattice physics comparisons.

### 3.1.2 Confirmatory Lattice Physics Data Comparisons (TGBLA06/HELIOS)

Assessment by code-to-code benchmarking of TGBLA06 with other independent codes for lattices and operating conditions typical of EPU and MELLLA+ conditions can reasonably ensure the consistency of the results from the GE lattice physics methods. Code-to-code comparisons are included in MFN 04-026 (Reference 5), comparing TGBLA to MCNP for particular lattices. Given that depletion cannot be performed with MCNP and the code was not coupled independently with depletion code, additional results were obtained with the HELIOS lattice physics code. Additional code-to-code comparisons were also included in the RAI SRXB-66 response in BVY 05-088 (Reference 30) comparing CASMO and TGBLA.

As indicated above, code-to-code comparisons are useful for confirming consistency of results, evaluating numerical and method approximations used in the codes, and identifying code errors. In most cases, it is unknown which code is more accurate, and the code with the higher fidelity methods is typically taken as the reference. However, unless the codes are carefully assessed with measured data, the absolute accuracy, in terms of bias and uncertainty, of the codes cannot be established, because the codes may use common fundamental data (e.g., ENDF/B-VI) and methods that may lead to better agreement than would be observed with comparisons with measurements. Also, without measurement data, the overall applicability of the data and methods to expanding ranges of operating conditions cannot be established.

For this evaluation, comparisons were performed for representative lattices and comparisons of  $K_{inf}$ , peak pin power, plutonium isotopic inventory, and cross-sections, and lattice physics parameters. Example results are presented in Appendix B based on the confirmatory analysis performed with HELIOS for a lattice configuration (enrichment and gadolinium loading) typical of EPU designs. The assessments performed are limited to lattice results computed with lattice physics codes. Since the confirmatory analyses did not include three-dimensional (3D) core simulations, there is no independent assessment of the core axial and radial power-peaking and distributions. Therefore, the comparisons cannot evaluate the GE tools for predicting radial and

axial bundle power profiles within the core. Appendix B contains additional discussions and the associated figures. A summary is provided in the following sections.

#### 3.1.2.1 $K_{inf}$ Comparisons

Comparing lattice  $K_{inf}$  values allow evaluation of the lattice physics methods and data for predicting lattice reactivity versus exposure. This information, along with additional cross-section parameters, is used in the full-core analysis to predict the core eigenvalue and global power distribution. Lattice  $K_{inf}$  values were compared for typical designs as a function of exposure based on calculations with HELIOS and TGBLA06. In summary, the error in  $K_{inf}$  introduced in this extrapolation process has been demonstrated to be small; therefore, a comparison of directly calculated values at 90 percent void fraction is appropriate. Overall, there is excellent agreement in  $K_{inf}$ , with a larger difference for higher void fractions. The level of agreement is not expected to result in any major differences in predicting core eigenvalue and the global bundle power densities. The NRC staff also finds that, while some of the cross-sections do exhibit errors in the extrapolation process, it was found that  $K_{inf}$  was a parameter that did not exhibit significant extrapolation errors.

#### 3.1.2.2 Power Distribution Comparisons

The ORNL staff compared the pin-fission densities computed with TGBLA06 and HELIOS, the root mean squared (RMS) difference, and the peak pin-fission rates. The pin-fission densities are related to the pin power distribution used in calculating the LHGR and R-factors for the SLMCPR limits. Appendix B provides further discussion and related figures showing the comparisons. Based on these code-to-code results, the NRC staff finds that RMS power distribution differences indicate that the RMS differences may exceed the [ ] determined previously. Therefore, this supports the need for increasing the pin power-peaking uncertainty to [ ] as was done for the SLMCPR. Section 3.2.2, "Safety Limit Minimum Critical Power Ratio," of this SE discusses the need for increases in the pin power-peaking uncertainties.

#### 3.1.2.3 Isotopic Comparisons

Isotopic comparisons were performed for key actinides (uranium and plutonium), which are computed using the lattice physics tools. Of particular interest are the comparison of the plutonium compositions as an indication of the prediction of the neutron spectrum and the further investigation of the potential impacts on the void reactivity coefficient and shutdown margin (SDM). The neutron spectrum is highly dependent upon the local void fraction, which has an impact on the neutron moderation. In addition, BWRs can be operated to enhance the plutonium production in the upper part of the core by using a bottom-peaked power distribution with higher void fractions in the core's upper regions. This spectral shift operation results in more energy generation as power distribution becomes more top-peaked near end-of-cycle (EOC), in which the generated plutonium is used. This is particularly relevant for operation at MELLLA+ in which plants can operate at 20 percent above the OLTP at a minimum core flow as low as 80 percent. As a result, the prediction of isotopic compositions can have a substantial impact on the axial power distribution as well. Further discussion and comparisons are provided in Appendix B.

#### 3.1.2.4 Confirmatory Analysis Conclusions

The NRC staff concludes that the code-to-code comparisons provide reasonable assurance that the modified TGBLA06 neutronic methods are acceptable for analyzing the lattices and conditions for EPU and MELLLA+. The differences in the pin-fission rates observed indicate the need for additional measured data to confirm the accuracy of the lattice physics and core simulator prediction. The code-to-code comparisons are insufficient for assessing the uncertainties in the code predictions because of potential commonalities in fundamental data and methods employed as well as general applicability to EPU conditions of interest.

#### 3.1.3 Core-Tracking Data Validation

In addition to code-to-code comparisons, GE uses eigenvalue trending and TIP power distribution (calculated versus measured) comparisons to benchmark the lattice physics code (TGBLA) and the core simulator code (PANACEA) performance. GE receives the plant operating data and performs eigenvalue tracking. In response to RAIs 5, 25, 26, and 27 (Reference 11), GE provided core-tracking data for the Reference Plants. High bundle power-to-flow conditions are characteristic of EPU conditions. The objective was to establish if operation at the high bundle power-to-flow conditions will result in changes in the eigenvalue trending and power distribution uncertainties. Sections 3.1.4 through 3.1.6 present a summary of the observed trending in the core-tracking data and the conclusions of the adequacy of the core follow data in benchmarking the extension of the nuclear methods to EPU and MELLLA+ conditions.

#### 3.1.4 Eigenvalue Tracking

The changes in the performance of the nuclear methods can be assessed globally by evaluating core-tracking data. The plant tracking calculations simulate the behavior of the reactor during operation, using the actual plant operational data (e.g., measured core flow, CR patterns, etc.). The prediction of the 3D simulator includes the accuracy of the cross-sections generated from the lattice physics model, the thermal-hydraulic models, and all other model assumptions that are used to simulate the core response. In predicting the critical state of the core, the simulation of the reactor condition involves the reactor power, total core flow, pressure, inlet conditions, and reactivity control inventory as a function of cycle exposure. Since the actual operating reactor is critical, the calculated keff is compared to 1.0. The deviation of the eigenvalues from 1.0 indicates bias in the nuclear model, including the adequacy of the methods in accounting for the uncertainties in the measured parameters. The cold and hot critical eigenvalue predictions can be evaluated to determine any changes in the biases and uncertainties associated with the nuclear method in simulating global core-wide response. In RAI 25 response (Reference 11), GE provided cold and hot critical eigenvalue tracking database on the Reference Plants (EPU and high-power density plants).

##### 3.1.4.1 Cold Critical Eigenvalue

The design basis eigenvalues are based on the prior history of the particular plant and known trends of the nuclear methods used for design. The measured cold critical eigenvalue is based on the SDM demonstration for the specific plant. The cold critical eigenvalue is predicted using the actual plant critical CR patterns. Since the measured state may be at slightly higher temperatures and for a slightly super-critical state, the cold critical eigenvalue is corrected for temperature and period. The cold critical eigenvalue data provided included distributed CR

patterns (as would occur during normal startup or shutdown) and local criticals where CR(s) are withdrawn in a particular core location.

For the cycles studied for the Reference Plants, the RMS difference between the nuclear design bases and the actual measured critical eigenvalue is [ ]. The calculations were based on TGBLA06/PANACEA 11. An RMS value of [ ] was reported in the initial licensing nuclear methods in LTR NEDC-30130P-A (Reference 32). The differences reflect improvement in the nuclear methods relative to the challenging core designs and operating strategies.

GE also investigated any sensitivity of the cold critical eigenvalues to power density. The RMS differences of the nuclear design bases and the cold critical eigenvalues for Plants B, D, and E were [

]. This indicates the need for continued assessment of the cold critical eigenvalue trending for EPU based on the high-power density plants instead of all historical BWR fleet.

Figure 3-1 presents the variation in the prediction of the cold critical eigenvalue, which results in bias and uncertainty values. However, as can be observed, the deviation of the cold critical eigenvalue from unity in some cases is significant. This difference from unity indicates a bias in the calculational model resulting from unidentified sources. While the GE procedure for determining a design eigenvalue includes an eigenvalue trendline to account for this recurring bias, significant deviation from unity indicates that there is a significant unknown reactivity effect that is not accounted for in the model. However, the study of the EPU plant data shows that the bias of the nuclear methods remain within the current bases of [ ].

The adequacy of the current nuclear methods bias of [ ] and the SDM value of 0.0038 are discussed further in Section 3.2.8, "Shutdown Margin," of this SE.

#### 3.1.4.2 Hot Critical Eigenvalue

GE letter MFN 05-029 (Reference 11) included hot critical eigenvalue tracking of the Reference Plants. Figure 3-2 shows the hot critical eigenvalue data for all the evaluated plants and the trendline showing the bias. In the overall, GE states that overall the RMS difference between the eigenvalue data of the Reference Plants and the trendline is approximately [ ], which remains the same as the reported value in LTR NEDC-30130P-A (Reference 32). Note that LTR NEDC-30130P-A is based on a previous version of GE's nuclear methods.

As can be seen in Figure 3-2, the data is widely dispersed from the trendline. In MFN 05-029 (Reference 11), GE provided discussion and assessment of the deviations seen in Figure 3-2. The evaluation included assessment of individual plant hot critical eigenvalue data in order to determine the bases for the significant deviation. Reference Plants A and E show deviations from the trendline and also implemented EPU since the introduction of two-year cycles and 10x10 fuel. Therefore, GE selected these plants for specific evaluation of the impact of increases in power density, power-to-flow ratio, and void fraction on the hot eigenvalue trending behavior. GE compared the individual cycle data to the trendline and determined that [ ].

Since the exit void fraction is directly related to the power-to-flow ratio (MWt/Mlbm/hr), GE used the power-to-flow ratio as a correlating parameter in assessing changes in the individual plant hot critical eigenvalue with void fraction. Plant A implemented EPU early in the cycle (at 4 GWd/MTU), which corresponds to 37 MWt/Mlbm/hr. Comparisons of the Plant A, Cycle 18, hot critical eigenvalue for bundle power-to-flow ratio less than and greater than 37 MWt/Mlbm/hr showed the decreasing trendline with no significant changes at the transition. This comparison indicates that the higher power-to-flow ratio or higher exit void fraction did not significantly



change the hot critical eigenvalue bias for Plant A, beyond the plant-specific downward trendline with implementation of 12 percent uprate.

Similarly, GE letter MFN 05-029 (Reference 11) provided hot critical eigenvalue trending for Plant E, Cycles 8, 9, and 10 (Figure 3-3). Reference Plant E implemented EPU in Cycle 9, with the power density increasing by 10 percent and the cycle exposure increasing from 11.5 percent to 16.0 percent GWd/MTU. The increased cycle energy was achieved by increasing the GE14 reload batch fraction from 188 to 268 and by increasing the average enrichment from 3.53 to 3.89 weight percent. The power density also increased from 52.5 KW/l to 58 kW/l and the corresponding power-to-flow ratio increase from 27 to 41.42 MWt/MIbm/hr. Therefore, the three cycles for Plant E provide a good example for assessing the changes in the hot eigenvalue behavior for EPU core design and operating strategy.

Figure 3-2, shows the hot critical eigenvalue comparisons for the different cycles. In its assessment of Figure 3-2, GE states that the figure shows very little change in the eigenvalue from Cycle 8 to Cycle 9, in spite of the significant changes in cycle energy, power density, reload batch size, and reload enrichment.

In assessing the eigenvalue deviation early in Cycle 10, GE states that both Cycles 9 and 10 operated at the essentially the same power (approximately 115 percent) and over the same flow range at this power level. Thus, there is no difference in power density and Power/Flow Ratio, and no significant change in exit void fractions. [

]. A reload batch fraction of 312 GE14 fuel bundles with enrichment of 4.21 was loaded in Cycle 10. GE attributed the eigenvalue deviation in Cycle 10 to the loading of high reactivity fuel on the core periphery. Loading of highly reactive bundle in the periphery resulted in higher fast neutron leakage from the core, which could be contributing to the hot eigenvalue differences. GE concludes that while eigenvalue differences exist for Plant E, Cycle 10, the cold critical eigenvalues and 3D power distribution comparisons to the TIP measurements are in good agreement.

Although the Cycle 8 and 9 eigenvalue differences are not marked as Cycle 10, the trendline for Cycle 9 appears to deviate from the downward eigenvalue trendline bias characteristic of GE's nuclear methods. The Cycle 9 hot critical eigenvalue seems to be increasing from 10 to 15 GWd/MTU. Considering the large batch fraction of fresh fuel (268), the upward trendline later in the cycle could be attributed to the modeling the burnup of the gadolinia (Gd) in the fresh GE14 fuel or the modeling of the buildup and burnup of plutonium under the hard spectrum for the EPU operation of a high-power density plant.

For all cycles studied, GE's assessment is reasonable and plausible. However, the eigenvalue deviation in the hot and cold critical eigenvalue indicates the limitation of relying heavily on eigenvalue trending and TIP power distribution uncertainties in the benchmarking of the nuclear methods. The eigenvalue tracking provides an excellent method to trend changes in global quantities but needs to be supported by benchmarking of the nuclear methods against experimental data for assessing the bases for the deviations with implementation of major operating strategy changes.

### 3.1.5 Assessment of TIP Core Tracking Data

BWRs are instrumented with TIPs. The TIP readings provide a means to assess the normalized axial power shape along the length of the bundles surrounding the individual TIP. The core simulator models the response of the instrument to the appropriate particle species (thermal neutrons or gamma rays) at the detector location to produce a simulated signal. For TIP

comparisons, this simulated detector response is compared to the relative strength of the measured signal. For a given TIP string, the measurement is a response to the integrated influence of the surrounding bundles.

Typically, the actual four-bundle peaking uncertainties are derived by averaging the readings from all string nodes across the core for a given exposure. The bundle, axial and nodal TIP uncertainties are in fact weight averages of the nodal TIP string data (e.g., calculated and measured) across the core and for all exposures. In the GE methodology, the [ ] that are applied to the thermal limit [ ] calculations are based on the measured/calculated TIP RMS data for all cores.

The available TIP core follow data include all historical BWR data, thus do not lend itself to investigating any changes in the core average power distribution uncertainties for the high-power density EPU core strategies. In RAI 5, 25, 26, and 29 responses in letter MFN 05-029 (Reference 11), GE compiled core follow TIP comparisons for EPU plants and for a high-power density BWR/6.

All of the Reference Plants (A through E) operated with 24-month cycles, except for Plant C, which operated with a 12-month cycle. The Reference Plants consisted of high-power density plants (from 51.7 to 62.9 kW/l) and different BWR types.

Figure 3-5 through Figure 3-7 show the TIP RMS comparison uncertainties for EPU plants and a high-power density EPU plant at a given cycle statepoint. These figures show the bundle, radial, and axial TIP comparisons for a given plant. The EPU plant TIP comparisons are intended to establish if there are any changes in the [ ]. The bundle RMS uncertainty represents the four-bundle  $\sigma_{P4B}$ . Table 3-1 shows bundle averaged RMS based on the compiled EPU core-tracking data relative to the previous historical data. Table 3-1 also shows the [ ] based on the previous version of GE's neutronic code set. Based on the currently approved power distribution uncertainty treatment, the EPU TIP data confirms that the currently applied average bundle RMS for all the plants [ ] remains applicable for EPU. For MELLLA+ operation, the value of  $\sigma_{P4B}$  would need to be confirmed. This is discussed further in Section 8.4 of this SE. Note that in the GE NRC-approved licensing process, the axial and the radial TIP uncertainties are not directly applied to the safety analyses, because the 3D simulator adapts the TIP axial power distribution of the TIP. The actual thermal limit calculations are performed without adaption, but the monitoring is performed with the adaption feature. However, the current Reference Plant core-tracking study is based on unadapted TGBLA06/PANAC11 calculation, because it is intended to assess the power distribution uncertainty of the neutronic method that feeds into the downstream safety analyses.

**Table 3-1 Summary of Bundle Average TIP Comparisons, Eight Cycles**

Document	Nuclear Model	# of TIP Sets	Weighted RMS Differences
NEDE-32694 (Used in SLMCPR Calculation)	TGBLA04/PANAC10	67	[
NEDE-32773-Rev 1 1999 Amendment	TGBLA06 /PANACEA11	195	
Current EPU DATA	TGBLA06/PANAC11	106	]

### 3.1.5.1 TIP Comparisons with Increased Power Density and Voids

GE also investigated if there are any observable trends in RMS differences as the power density increases and the operating domain is expanded. The core power-to-flow ratio was selected as correlating parameter, because there is a direct relationship between core power-to-flow ratio and the amount of voiding in the core

All of the Reference Plants have gamma TIPs except Plant E, which has thermal neutron TIPs. The sensitivity of these TIP systems are different, therefore the power distribution RMS differences vary. Figure 3-4 depicts the bundle (radial), nodal and axial RMS as the core power-to-flow ratio increases. The radial, nodal, and axial calculated/measured TIP comparisons are derived by combining the actual nodal TIP comparisons (e.g., six-inch node of a string) across the core for given cycle statepoint. Therefore, one value of bundle, nodal, and axial RMS uncertainty corresponds to every reading per cycle exposure.

GE states that the TIP comparisons for both the gamma and thermal TIP data show a slight decrease in the bundle power distribution. This calculated TIP response was performed using unadapted TGBLA06/PANACEA11. Therefore, the core simulator did not adapt the predicted axial power distribution to the measured TIP axial power distribution. As can be seen in Figure 3-4, the nodal and axial RMS differences [

].

Based on the trendline, GE extrapolated the trendlines for the gamma TIP plants to 50 MWt/Mlbm/hr and determined the nodal and axial RMS values of [ ] and bundle RMS of [ ]. GE selected 50 MWt/Mlbm/hr as the limit, because this power-to-flow ratio is expected to bound the plants in the BWR fleet operating at the MELLLA+. For example, operation of the high-power density Plant E at 120 percent power, 85 percent core flow corresponds to 48.4 MWt/Mlbm/hr. It is noted that some plants targeted to reach 80 percent core flow may exceed the 50 MWt/Mlbm/hr limit. This will require additional justification.

Although the [ ], the maximum RMS values throughout the entire cycle for the TIP comparisons were [ ], axial and nodal RMS, respectively. GE notes that this indicates that the power shapes generated by the 3D Simulator are in good agreement with the TIP measurements, even though this cycle has hot eigenvalues that were higher than expected early in the cycle.

In its assessment of the fidelity of the neutronic methods with increased power distribution and voiding, GE states that the global comparison of TIP RMS differences for the eight studied cycles shows good agreement between the TIP measurements and the 3D Simulator. GE acknowledges [

], GE states that the TIP comparison results are within the results previously provided to the NRC (Table 3-1).

### 3.1.5.2 NRC staff Assessment of Reference Plants TIP Core Tracking Data

In SRXB-A-27 RAI response (Reference 27), GE discussed the criteria for acceptance of the power distribution uncertainties obtained from the core-tracking data. Inaccuracy in axial power

distribution may indicate a fundamental problem in the fuel or poison depletion model. In most cases, these effects show up when a significant change is made either in the power density, discharge exposure, or cycle length for a particular plant. Note that the core design changes needed to achieve the energy requirements for operation at EPU at extended cycle length, result in increases in the power density, reload batch fractions and exposure accumulation. The RAI response provides the power distribution uncertainty acceptance criteria based on the RMS difference of all predicted to measured TIP responses as [

] for the nodal RMS difference. Although the axial RMS difference is not included in the licensing process as an applied uncertainty, an average difference of less than [ ] for the Reference BWRs indicate that the axial power distributions are also predicted adequately.

The global RMS value of all the plants, the bundle, axial and nodal power distribution uncertainties meet the power distribution acceptance criteria based on the current NRC-approved methods. As depicted in Figure 3-5 through Figure 3-7, the bundle, axial and nodal RMS difference for Plant E, Cycle 9, remains [ ]. This is attributed to the use of TGBLA04/PANAC10. Plant B Cycle 9, which is also based on TGBLA04/PANAC10, shows some trend [ ]. It is not clear that all BWRs applying GE methods have transitioned to TGBLA06/PANAC11. Review of the cold and hot critical eigenvalue tracking also indicates improvements in the versions of neutronic method employed. Therefore, for EPU/MELLLA+ applications, the NRC staff needs to verify that the nuclear methods are transitioned to TGBLA06/PANAC11 or other NRC-approved neutronic method.

#### **TGBLA/PANAC Version Limitation**

The neutronic methods used to simulate the reactor core response and that feed into the downstream safety analyses supporting operation at EPU/MELLLA+ will apply TGBLA06/PANAC11 or later NRC-approved version of neutronic method.

It is also not apparent that the on-line 3D MONICORE core simulators installed at BWRs using GE core monitoring system have all transitioned to TGBLA06/PANAC11. The axial and nodal power distribution uncertainties do not factor into the safety analyses including the SLMCPR value, because the calculated power distributions are adapted to the measurements. The core simulator [ ] is applied to the SLMCPR calculation; therefore trending outside the RMS value for specific plants employing TGBLA04/PANAC10 is an important consideration. GE usually derives the uncertainty using all historical TIP uncertainty data. However, for those plants using TGBLA04/PANAC10 as can be seen in Figure 3-5, the ( $\sigma_{P4B}$ ) uncertainty is [ ] for those plants using the PANAC10. Therefore, the uncertainty for those particular plants will be higher than employed in the SLMCPR calculation. For those plants using the TGBLA04/PANAC10 core simulator, individual plant core-tracking data will be used to establish [ ]. In the short-term, this will ensure that uncertainty used in the calculation is relevant to the plant core monitoring system performance. This approach will capture the plant-specific trendline and the TGBLA04/PANAC10 nuclear methods performance.

#### **3D Monicore Limitation**

For EPU/MELLLA+ applications, relying on TGBLA04/PANAC10 methods, the bundle RMS difference uncertainty will be established from plant-specific core-tracking data, based on TGBLA04/PANAC10. The use of plant-specific trendline based on the neutronic method employed will capture the actual bundle power uncertainty of the core monitoring system.

In MFN 05-022 (Reference 3) GE had provided a comprehensive evaluation of the changes in the power distribution uncertainties with increase in power density and power-to-flow ratio. The [ ] shows marked differences between the thermal and gamma TIPs, indicating the sensitivity of the thermal TIPs (See Figure 3-4). However, the fact that the Plant E Cycle 10 Axial and Nodal RMS differences are [ ] indicates that deviation cannot solely be attributed to the impact of thermal TIPs sensitivity on the axial and nodal power distribution uncertainties. It is feasible that the use of TGBLA04/PANAC10 attributed to the [ ] with power-to-flow ratio for Cycle 9. In addition, Plant E Cycle 10 data did not extend to the EOC. Therefore, it does not reflect any changes in all of the power distribution with exposure as the Gd depletes for the large batch fraction of the 312 GE14 fuel bundles. Thus, the NRC staff finds that sufficient information is not available to conclude the impact of the thermal TIP sensitivity to the power distribution with increased power-to-flow ratio characteristic of MELLLA+ operation. For future EPU/MELLLA+ applications involving plants with thermal TIPs, the NRC staff should evaluate the plant-specific TIP core-tracking data against compiled EPU Reference Plant core-tracking data. The objective is to determine if the power distribution uncertainties need to be increased for cores with thermal TIPs installed.

#### **Core Thermal Power-to-Total Core Flow Ratio Limitation**

Plant-specific EPU and expanded operating domain applications will confirm that the core thermal power to core flow ratio will not exceed 50 MWt/Mlbm/hr at any statepoint in the allowed operating domain. For plants that exceed the power-to-flow value of 50 MWt/Mlbm/hr, the application will provide power distribution assessment to establish that neutronic methods axial and nodal power distribution uncertainties have not increased.

#### 3.1.6 TIP Core Tracking Data

GE relies heavily on TIP measured/calculated four-bundle power-peaking discussed in Section 3.1.5 of this SE and the code-to-code comparisons (MCNP/TGBLA) to benchmark its neutronic methods. These TIP data do not provide bases to ascertain the accuracy of the bundle-by-bundle prediction, because it assumes that the TIP reading is predominantly due to the four surrounding bundles even in the highly voided top of the fuel bundle. In addition, TIP readings only provide relative bundle powers and it cannot be used to establish the [ ] due to the power allocation within the four bundles surrounding the TIP (e.g.,  $\sigma_{PAL}$ ). TIP data also does not provide a means to validate the pin power uncertainties.

Section 5.2 of the initial TGBLA/PANAC LTR (Reference 32) compared the relative merits of using TIP comparisons (core follow) for validating neutronic code systems, stating, "The TIP signals provide a good picture of the axial power distribution, but do not provide a detailed bundle-by-bundle distribution, because there is only 1 TIP location for every 16 bundles. A more accurate estimate of the reactor power distribution can be obtained just prior to a reactor shutdown by the procedure known as gamma scanning...."

Therefore, even though the TIP signals provide a good picture of the axial power distribution, TIP comparisons do not give a detailed bundle-by-bundle power distribution measurement. Therefore, using the TIP data is not sufficient to determine the uncertainties due to the extension of the neutronic methods to greater than 70 percent or uncertainties associated with individual axial bundle and pin power uncertainties.

Gamma scans provide an alternate method for estimating the reactor power distribution just before reactor shutdown. Most importantly, gamma scan method is completely independent of

the core simulator. Both pins and bundles can be scanned. The gamma scan technique involves removal of the fuel bundles from the reactor core and measuring the gamma ray intensity as a function of axial position in the bundle. Bundles at different exposures and pins can be scanned.

The PANACEA models the operating history of the selected bundles using the neutronic data generated using TGBLA for all the lattices. Therefore, the gamma scan technique captures the accuracy of both the lattice physics codes and the core simulator by comparing the axial measured and calculated power histories just before the reactor shutdown. This comparison quantifies the uncertainty of both the lattice physics and the core simulator in predicting axial bundle and pin power distribution as operated (e.g., depletion at high void condition, control blade history).

The gamma scan benchmarking would provide the bases to validate the neutronic methods prediction of the axial power and distribution of individual bundles and pins.

Therefore, the NRC staff concludes that while the core-tracking data is useful in performing global assessment of the nuclear methods performance, it does not suffice in validating the extension of the neutronic methods to operation at high void conditions for the upper part of the fuel bundle and the corresponding change in the core void distribution. Most importantly, the periodic TIP core follow data is not adequate in establishing the power distribution uncertainties that are important to the thermal limits calculations. The NRC staff focused on evaluating the adequacy and applicability of the current available gamma scan data, supporting the power distribution uncertainties applied to the thermal limits calculations.

The following section describes the gamma scan technique, the available measurement data and the assessment of the adequacy of the available measurement data.

### 3.1.7 Gamma Scans

Gamma scanning is a non-destructive method that is used to determine the relative fission product inventory in nuclear fuel. In gamma scanning, the fuel is removed from the reactor core and the gamma ray intensity is measured as a function of axial position in the bundle

The gamma scan technique measures the 1.596 Mega electron Volt (MeV) gamma ray produced by the decay of lanthanum-140 (La140). The La140 comes from the beta decay of barium-140 (Ba140), a fission product with a half-life of 12.79 days. The La140 has a half-life of 1.68 days, which provides an active mono-energetic gamma source that can be readily measured. Measurement of the La140 activity and correction for the Ba140 decay yields a relative Ba140 concentration as a function of position in the core just prior to shutdown. The Ba140 distribution, in turn, closely follows the actual power distribution. The Ba140 distribution in fuel is characteristic of the fission distribution or integrated power history over the last 5 half-lives or so (approximately 60 days) of reactor operation. Thus the scan results can be used to determine "recent" core power distribution.

The TGBLA and the PANACEA predictions of the nodal relative Ba140 are compared against the measured Ba140. The technique involves: (1) generating the lattice physics data for all of lattice designs using TGBLA, (2) simulating the operating history (e.g., exposure accounting) of the bundles using PANACEA, (3) calculating the estimated nodal relative Ba140 predictions using the power and exposure distributions from approximately the last 60 days of operation, (4) correcting the experimental nodal La140 (Ba140) predictions for decay between shutdown and measurement, (5) correcting the experimental nodal La140 (Ba140) predictions for decay between shutdown and measurement, and (6) comparing the experimental and predicted Ba140 predictions. This benchmarking provides the axial power distribution uncertainties for bundles.

Bundles and pins with different designs (e.g., legacy fuel), exposures, Gd content, and operating power history can be scanned. The gamma scan comparisons can provide assessment of the lattice physics and the core simulators codes in predicting the bundle and pin power distribution with depletion. The integral effects of the neutronic methods modeling of the Gd burnup, fuel isotopic at the highly voided upper portions of the fuel bundles, the control blade history effects, higher enrichment impact, geometric design differences impact (e.g., water cross legacy fuel designs), and burnup can all be indirectly validated through the axial power distribution uncertainties.

### 3.1.8 Available Gamma Scan Data

Comprehensive qualification of GE steady-state neutronic method (TGBLA04/PANAC10) was last performed in 1985. In NEDE-30130PA, (Reference 32) GE qualified their methods for the fuel designs and operating strategies of the time with TIP measured/calculated comparisons (core follow data), gamma scan comparisons, cold critical measurements, and isotopic burnup verifications. The initial TGBLA/PANAC LTR also included measured fissionable nuclide densities (isotopic inventory) and rod exposure measurements.

The gamma scan and isotopic measurements performed in the initial application were based on the following:

1. [ ].
2. [ ].
3. [ ].
4. [ ].

Since the initial qualification of the steady-state neutronic methods in 1985 in NEDE-30130PA (Reference 32), GE has not performed any gamma scans to benchmark the codes' adequacy in predicting the bundle and pin powers for the current fuel designs and for the current operating strategies (depletion at higher void conditions). Submittal approving TGBLA06/PANAC11 (1996) contained code-to-code comparisons with assessment that was limited to 70 percent void fraction.

Changes in fuel design, pin loading/zoning, burnup, and operating strategies (e.g., operation at the 100 percent rod and OLTP compared to the current MELLLA at 120 percent of OLTP) require demonstration of the lattice physics and core simulator codes' capabilities to accurately predict these design features and operating strategy effects. The main differences are as follows.

1. Moderation within bundle (e.g., 14 part-length rods and two water rods).
2. Axial pin and bundle power-peaking changes.
3. Gadolinium concentration and axial zoning.
4. Radial power distribution.
5. Reactivity effects (e.g., higher enrichment).
6. Fuel isotopics depletion and production (hard spectrum in upper part of fuel bundles).

7. Fission gas generated temperature of the fuel and volume available.
8. Geometric and lattice fuel design differences (e.g., water cross in legacy fuel).

Based on the assessment of the differences in the current fuel and core designs and operating strategies in comparisons to the historically available measurement data, the NRC staff concludes that additional gamma scans are necessary to establish the power distribution uncertainties. At issue is not the soundness of the neutronic method, but rather the actual values of uncertainties that are applied to the safety analyses supporting the operation at EPU and MELLLA+.

For example, in the NRC-approved SLMCPR methodology in LTR NEDC-32601P-A (Reference 33) and LTR NEDC-32694P-A (Reference 34), the [ ] and the pin power uncertainty  $\sigma_{Peak}$  are both established using the historical gamma scans and these uncertainties cannot be verified through TIP comparisons. These uncertainties affect the value of the calculated SLMCPR. Therefore, review and approval of the extrapolation of the neutronic methods to higher void conditions characteristic of EPU and MELLLA+ require additional gamma scan benchmarking data.

### 3.1.9 Assessment Conclusions

In RAI 28 of MFN 05-053 (Reference 6), GE committed to perform gamma scan measurements to confirm that the assumptions used in the neutronic method are still appropriate. GE also presented plans for gamma and plenum fission gas scans (Reference 31). The planned measurement data includes:

1. fission gas benchmarks for T-M models,
2. rod exposure benchmarks for lifetime integrated rod power,
3. rod-by-rod power-peaking benchmarks, and
4. bundle power allocation benchmarks around instrument positions.

Operation at the EPU and MELLLA+ will represent operation outside the current operating experience base. Specifically, for some applications, the hot bundle conditions may be outside the current operating experience base in terms of key parameters such as bundle power-to-flow ratio, exit void fractions, and bundle powers. In order to capture the uncertainties in the neutronic methods for operation in MELLLA+, GE committed to begin an on-going benchmarking program. In such a program, bundles and pins that are operated as close as possible to the MELLLA+ operation will be benchmarked through gamma scan, thereby validating the accuracy of the analytical methods and codes for operation at MELLLA+. (Reference 31) outlined GE's plan for performing additional gamma scans data.

Given that the specific measurement data would not be available for some time, the review emphasis shifted to an interim approach, which would:

1. identify the key parameters that are affected by potential errors in the cross-sections important to the downstream safety analyses,
2. account for potential increases in the uncertainties associated with the prediction of the key parameters that are affected, and
3. ensure that there are sufficient margins in the affected downstream safety analyses.



### 3.2 INTERIM APPROACH

The LTR NEDC-33173P (Reference 1) approach seeks to:

1. identify the impact of potentially increased uncertainties and biases in the neutronic methods for operation at EPU and MELLLA+,
2. establish the key parameters and safety analyses that are impacted,
3. evaluate the conservative assumptions and available margins in the safety analyses, and
4. apply additional margins to the impacted safety analyses, if warranted.

In addition, to assess the extension of the neutronic methods, LTR NEDC-33173P (Reference 1) also includes evaluation of the applicability of the thermal-hydraulic correlations and the stability methodology to operation at the EPU and MELLLA+.

This section presents GE's proposed interim approach and the NRC staff review and conclusions. The NRC staff review covers the content of LTR NEDC-33173P (Reference 1), the RAI responses, and additional evaluations provided in MFN 05-005 (Reference 4).

#### 3.2.1 Safety Parameters Influenced by Uncertainties and Margin Evaluation

This section presents the impact of potentially higher uncertainties in the neutronic methods on the key parameters that influence the safety analyses.

##### 3.2.1.1 Impacts of Bias and Uncertainties in Nodal Reactivity

Uncertainties and biases in the macroscopic cross-sections and the neutron flux distribution used to calculate reactivity result in uncertainties and biases in the nodal reactivities. It is difficult to quantify the impact of the errors due to each nuclear parameter individually because only the accumulative error is measurable. Reference 4 describes the potential impacts as discussed below.

###### 3.2.1.1.1 Reactivity Prediction Impact

The core is critical when operating at steady-state. The accumulative error in the cross-sections at any given exposure is measurable as an error in the ability to predict the critical core eigenvalue at that exposure. Thus both the bias and the uncertainty in the calculated eigenvalue can be quantified for a wide range of plant operation by comparing the predicted eigenvalue to the known value of 1.0 for the critical state. The net effect of any particular error in the cross-sections at a nodal level is reflected in the error in predicting the core eigenvalue.

Section 3.2.8, "Shutdown Margin," of this SE reviews the deviation of the predicted core eigenvalue from 1.0 and its impact on the SDM calculation. Section 3.2.8 also evaluates the rod withdrawal error and the cold shutdown requirements under the standby liquid control system (SLCS).

###### 3.2.1.1.2 Power Peaking and Distribution Impact

Local errors in reactivity are more difficult to assess because they are easily masked by a small change in the predicted nodal water density. Localized errors in nodal reactivities can be quantified indirectly in the integral sense by how they impact the power distribution. Practically,

the power and its distribution are of the most interest because the propagation of the reactivity error into a power error impacts the core safety margins in two distinct ways.

The first way that a nodal reactivity error impacts the core safety margins is through its impact on the steady-state power and its distribution. In addition, the error in predicting the nodal power results in an integral error in determining the nodal exposure.

In LTR NEDC-33173P (Reference 1), conservative biases and uncertainties are applied to the power distribution uncertainties for the purposes of determining the licensing parameters. The increased uncertainties can be propagated into the SLMCPR calculations. Section 5.2 of LTR NEDC-33173P (Reference 1) covers the increased power distribution uncertainties in the SLMCPR calculations. The impact of potentially higher uncertainty in the nodal power prediction is evaluated in Sections 5.3, 5.4, and 5.7 of LTR NEDC-33173P (Reference 1).

#### 3.2.1.1.3 Void Reactivity Coefficient

The second way that an error in predicting the nodal reactivity impacts the determination of core safety margins is in how it impacts the transient nodal power responses. The transient power responses in a BWR are dominated by how nodal reactivity changes in response to changes in nodal moderator density. In other words, a nodal reactivity error causes an error in the void coefficient that in turn propagates into an error in the transient nodal power.

The licensing parameter that reflects the transient safety margin is the OLMCPR. The impact of nodal reactivity errors on the calculated OLMCPR is covered in Section 5.3 of LTR NEDC-33173P (Reference 1). In addition, Section 4.0 of this SE evaluates GE's approach in calculating the void reactivity coefficient.

#### 3.2.2 Safety Limit Critical Power Ratio (SLMCPR)

The SLMCPR is a fuel design limit that protects fuel cladding integrity. The SLMCPR limit ensures sufficient margin to transition boiling such that fuel cladding damage due to cladding overheating would not occur. Boiling transition (BT) degrades the heat transfer characteristic leading to cladding overheating. The following section presents a review of the proposed interim approach for the SLMCPR for operation at EPU and MELLLA+.

##### 3.2.2.1 Regulatory Requirements and Guidance

Title 10 of the *Code of Federal Regulations* (10 CFR) establishes the fundamental regulatory requirements with respect to the reactivity control systems. The regulation at 10 CFR Part 50, Appendix A, General Design Criterion (GDC) 10, "Reactor design", states in part, that "the reactor core and associated coolant, control, and protection systems shall be designed with appropriate margin to assure that specified acceptable fuel design limits are not exceeded...."

Section 4.2 of NUREG-0800, The Standard Review Plan (SRP) (Reference 19) specifies the acceptance criteria for the evaluation of the fuel design limits as it related to the thermal limits. SRP Section 4.4 provides guidance on the review of the thermal-hydraulic design in meeting the requirement of GDC 10 and the fuel design criteria established in SRP Section 4.2. For the critical power correlation, there should be a 95 percent probability at 95 percent confidence level, that the hot rod in the core does not experience a departure from nucleate boiling or BT condition during normal operation or anticipated operational occurrences (AOOs), or, for the critical power ratio (CPR) correlations, the MCPR is to be established such that 99.9 percent of the fuel rods in the core would be expected not to experience BT during normal operation or AOOs. SRP Section 4.4 also states that the uncertainties in the values of process parameters,

core design parameters, and calculational methods used in the assessment of the thermal margin should be treated with at least 95 percent probability at a 95 percent confidence level.

### 3.2.2.2 Application of Power Distribution Uncertainties

To meet GDC 10 requirements, the SLMCPR is calculated such that 99.9 percent of the fuel rods do not experience BT during steady-state operation or AOOs. The MCPR is defined as the ratio of the bundle power required to produce onset of transition boiling somewhere in the bundle (critical CP) to the actual operating bundle power. Therefore, the value of the SLMCPR must be greater than 1.0.

The SLMCPR calculation involves statistical treatment that accounts for uncertainties in the measured quantities and key parameters that affect the cores steady-state thermal-hydraulic conditions. The SLMCPR is calculated at different exposures as the core depletes and the base steady-state condition is perturbed in establishing the actual bundle powers that will ensure 99.9 percent of the fuel rods will avoid BT. The power distribution uncertainties are among the significant uncertainties that impact the value of the SLMCPR.

The onset of BT is predicted using CPR correlation derived from full-scale bundle experimental data for each new fuel product line. The uncertainties associated with the CPR correlation are established using separate experimental validation data. The GEXL uncertainties are treated at 95 percent probability at 95 percent confidence level. Section 7.1 of this SE evaluates the applicability ranges of GEXL.

The GE SLMCPR methodology and the associated uncertainty treatments are specified in the NRC-approved GE LTRs NEDC-32601P-A (Reference 33) and NEDC-32694P-A (Reference 34). The technical evaluation report approving the SLMCPR licensing methodology states that the pin and bundle power uncertainties would be confirmed through gamma scan for new fuel designs and operating strategy. Review of the SLMCPR methodology indicates that the [ ] and the peak pin uncertainty  $\sigma_{P_{peak}}$  should have been confirmed through pin and bundle power gamma scans for the GE14 fuel as currently operated for EPU conditions. The SLMCPR calculational uncertainty also includes the [ ]

[ ], which is derived from the TIP data. GE had provided TIP core follow data for EPU plants to reaffirm the [ ]. While these uncertainty components are factored specifically into the GE SLMCPR methodology, the key issue is to confirm the accuracy of the predicted pin and bundle powers for the EPU and MELLLA+ core thermal-hydraulic conditions such that 99.9 percent of the fuel rods avoid BTs. GE has committed to perform gamma scans to confirm the pin and bundle power distribution (see Reference 31).

As an interim measure, LTR NEDC-33173P (Reference 1) proposes [ ]

].

LTR NEDC-33173P (Reference 1) proposes adding a combined value of 0.02 to the core configuration specific SLMCPR values calculated every reload for operation at EPU and MELLLA+. The NRC staff concludes that for plants implementing MELLLA+ operation, a margin of 0.03 will be added to the cycle-specific SLMCPR value. The additional 0.01 value is to account for the fact that operation at lower core flow conditions at rated or EPU power levels are generally more limiting. In addition, operation at MELLLA+ could place the bundle operating conditions outside the current experience base. Note that the 0.03 adder is applicable for operation at all of the EPU/MELLLA+ domain, including the rated conditions.

The NRC staff evaluated the acceptability of the additional 0.02 margin for EPU operation. The NRC staff assessment of the adequacy of the additional 0.02 margin for EPU and 0.03 margin for MELLLA+ follow:

1. In general, an adder of 0.02 or 0.03 to the SLMCPR is a significant value because most plant-specific changes in SLMCPR changes have historically remained within those bounds, considering the SLMCPR methodology changes and generic evaluations of the impact of EPU operation on the SLMCPR. In addition, the 0.02 adder for EPU is also included in the single recirculation loop operation (SLO) SLMCPR methodology.
2. The SLMCPR difference between the EPU statepoint of 120 percent power at the achievable rated core flow and the 120 percent EPU power at the minimum core flow for MELLLA+ is projected to be within the range of 0.01 or slightly higher. Therefore, an additional 0.01, yielding a total SLMCPR adder of 0.03 for operation in MELLLA+ including the rated core flow conditions is a reasonable value.
3. The NRC staff's confirmatory pin power RMS values indicate a value of [ ] uncertainty is a reasonable value. Although, a peak pin RMS of [ ] provides reasonable assurances that the calculated SLMCPR limit is acceptable for EPU and MELLLA+ conditions. Reference 28 contains trending of the local power-peaking in TGBLA/CASMO/4, which indicates that the two codes are, in general, consistent. Both code-to-code lattice physics data comparisons show known TGBLA behavior with Gd burnup. However, with the increased power distribution uncertainties, TGBLA pin power-peaking is reasonably acceptable.
4. The additional 0.03 SLMCPR adder for operation at EPU/MELLLA+ is meant to account for potential changes in the uncertainties due to the higher bundle power-to-flow ratio on both the pin and bundle power. Note that the current SLMCPR methodology will calculate the actual SLMCPR value at the EPU power levels at the minimum core flow. Therefore, the 0.03 will be added to the bounding core design-specific SLMCPR value every reload, providing reasonable assurances on the uncertainties associated with both the pin and bundle powers.
5. Since there are no independent comparisons of coupled lattice physics and core simulator code results, it is difficult to obtain code-to-code insights on the bundle powers for trending purposes. However, the actual 0.02 adder for EPU and 0.03 adder for EPU/MELLLA+ for the cycle-specific SLMCPR value is reasonable in that a 0.01 value added for MELLLA+ is significant in terms of SLMCPR calculation.
6. The confirmatory TGBLA/HELIOS comparisons indicate that the pin power-peaking uncertainty in which a 0.01 SLMCPR adder is derived appears to be within a reasonable range. However, RAI (Reference 3), states that the pin peaking uncertainty could be [ ] that was propagated through the

SLMCPR calculation. However, there is some conservatism in the manner in which the SLMCPR adders were derived by propagating each uncertainty separately into the SLMCPR calculation methodology and the values rounded up. Therefore, the NRC staff accepts the current value of [ ]. However, the NRC staff proposes that the bundle power-to-flow conditions under which the rods selected for gamma scans were operated be scrutinized to ensure that the pin power-peaking uncertainty is derived from spectrally hard conditions expected of MELLLA+ core conditions.

Based on the fact that the additional margin was obtained by a [ ] than currently used in the NRC-approved SLMCPR methodology and that the code-to-code trending did not indicate degraded performance of the corrected TGBLA at high void conditions, the NRC staff accepts a 0.02 adder for EPU and a 0.03 adder for operation at EPU/MELLLA+ as sufficient with reasonable assurance, until GE's neutronic method is confirmed against appropriate measurement data.

**SLMCPR Limitation 1:**

For EPU operation, a 0.02 value shall be added to the cycle-specific SLMCPR value. This adder is applicable to SLO, which is derived from the dual loop SLMCPR value.

**SLMCPR Limitation 2:**

For operation at MELLLA+, including operation at the EPU power levels at the achievable core flow statepoint, a 0.03 value shall be added to the cycle-specific SLMCPR value.

3.2.3 R-factor

The R-factor is a measure of the relative pin power-peaking within a lattice and is a number that is an input into the GEXL correlation. The R-factor characterizes the local within bundle peaking pattern relative to any given rod. It accounts for the effects of the within bundle power distributions and the fuel assembly and channel geometry on the fuel assembly critical power distribution. The uncertainties associated with the R-factor feed into the SLMCPR calculation methodology.

MELLLA+ RAI 31 (Reference 48) requested that the key assumptions in the R-factor methodology be evaluated to ensure that it remains applicable to the EPU/MELLLA+ conditions. Specifically, the RAI requested that the pin power-peaking factors used in the R-factor methodology be evaluated to ensure that it is representative of the pin power-peaking at high void conditions, characteristic of the EPU and proposed operating domain pin peaking. The MELLLA+ RAI 31 (Reference 48) response (Reference 9) states the R-factor is a function of [

].

[

]. The response to RAI 31, GE examined the potential impact of a higher in-channel average void fraction on the R-factor on higher axial bundle averaged void fractions on the R-factor.

In the current methodology, the R-factor methodology assumed a bundle averaged void fraction of [ ]. GE selected six bundles designed for high power density plants, with bundle averaged voids of [ ] and [ ] to assess the impact of higher bundle averaged axial void on the R-factor. For the selected 6 bundles, the R-factors calculated at [ ] core averaged void fraction were compared against the production R-factors calculated at [ ]. Table 31-1 of Reference 9 presented the calculated R-factor for one of the bundles (e.g., bundle 2). The RAI 31 response discussed the R-factor results from the comparisons of the production R-factor and the modified R-factor methodologies. Figure 3-8 shows the bundle averaged void fraction used in the modified R-factor calculations. Changes in the R-factor methodology affect: (1) the SLMCPR and (2) the operating CPR. An increase in the magnitude of the R-factor will decrease the SLMCPR and decrease the operating CPR. Using a general relationship between the decrease in SLMCPR and a decrease of the operating CPR of approximately 1 part in 3, a reduction of core operating limit CPR of 0.01 from an R-factor increase will result in decrease of SLMCPR of approximately 0.0033.

For the 6 selected lattices, Figure 3-9 shows the differences in bundle R-factors calculated at [ ] with exposure and its impact on the operating limit CPR. The relationship between the void fraction and the bundle R-factor depends upon the location within bundle of the limiting R-factor rod. Since each bundle design is unique, it exhibits different response to changes in void fraction. As shown in Figure 3-9, the uncontrolled modified R-factor for bundles increases or decreases with exposure. GE acknowledges that there is no obvious approach that would create a conservative R-factor for all core conditions. [

].

[

].

[

].

Figure 3-9 and Figure 3-10 show the variations in the  $\Delta$ CPR and the SLMCPR with exposure for the selected for the lattice with the modified R-factor methodology. As can be seen from Figure 3-10, the magnitude of the R-factor increases and decreases with [ ], resulting associated changes in the  $\Delta$ CPR and the SLMCPR.

GE acknowledges that the [ ]. However, GE states that based on the current R-factor methodology, [ ] and therefore there is no conclusive evidence that a change in the assumed bundle void conditions is warranted.

The NRC staff evaluated the RAI response and the sensitivity analyses provided. The modified R-factor based on the core average within bundle void fraction does show that both the CPR

and the SLMCPR change with core average void fraction. As discussed above, the  $\Delta$ CPR changes early in the bundle life for core average voids of 70 percent can be approximated as 0.01, which is within the significance level. In addition, for operation at expanded operating domains the exit voids in the maximum powered bundles could be greater than 92. As stated in the RAI response, the impact of the assumed bundle average void is highly dependent on the lattice design. There is no sufficient evidence that the production R-factor methodology calculated for given product line will bound the R-factor performance for specific lattices representing given bundle designs as operated. Therefore, a change in the R-factor methodology is warranted.

The R-factor methodology needs to be updated to reflect the current lattice design and operating void conditions. The NRC staff concludes that the R-factor calculation at a lattice level shall be consistent with the nodal void conditions. However, the change may require modifications of the NRC-approved method specified in LTR NEDC-32505, Revision 1 (Reference 37), which could not be implemented immediately.

In discussion with GE, the NRC staff discovered that similar corrective approach can be achieved through changes in the input such that the axial R-factor lattice calculations will be consistent with the actual lattice-specific void fractions. Instead of performing the R-factor calculation based on the core averaged [ ], the R-factor can be calculated such that the lattices representing different elevation of the fuel bundle will be calculated consistent with the axial lattice void fraction. This approach may result in some lattices experiencing lower R-factor than the production methods, while lattices at higher void conditions may yield higher R-factor with exposure. The corrective R-factor approach will canvas the axial power profiles and exposures so that the exposure and void dependency is accounted for conservatively and consistent with the maximum powered bundle. GE will document the specifics of the proposed interim approach in a letter to NRC. This approach is intended as an interim methodology change.

#### **R-Factor Limitation**

The plant specific R-factor calculation at a bundle level will be consistent with lattice axial void conditions expected for the hot channel operating state. The plant-specific EPU/MELLLA+ application will confirm that the R-factor calculation is consistent with the hot channel axial void conditions.

For the long term, the R-factor methodology needs to be updated and submitted so that the NRC staff can assess whether a core average void of [ ] would be sufficient relative to calculating the R-factor for each lattice design consistent with axial void fraction. The R-factor methodology LTR update needs to incorporate the impact of void fraction and within bundle pin power peaking on the both the controlled and uncontrolled R-factor calculations for the current fuel designs and EPU/MELLLA+ operating strategy.

#### **3.2.4 Operating Limit CPR**

The OLMCPR and the SLMCPR limits ensure that transition boiling would not be encountered resulting in fuel cladding damage due to cladding overheating. BT degrades the heat transfer characteristic leading to cladding overheating. The OLMCPR and the SLMCPR ensure fuel cladding failure would not occur because: (1) the steady-state MCPR limit is established by comparing the predicted rod power level that would result in transition boiling against the actual rod operating power, and (2) the OLMCPR is established by combining the change in the MCPR due to the transient event to the initial SLMCPR value such that rod operating power is limited to

preclude transition boiling. Plants operate above the OLMCPR limits so that if a transient event does occur, the change in the MCPR would assure that the SLMCPR would not be violated. In the standard reload methodology, the limiting transient response is calculated based on the cycle-specific core configuration based on NRC-approved licensing methodology and codes.

Section 2.2.2 of LTR NEDC-33173P (Reference 1) evaluated fuel parameters that affect the OLMCPR calculation and the treatment of uncertainties in the analytical methods and codes used to establish the OLMCPR. The following sections present the justifications provided in LTR NEDC-33173P (Reference 1) and assesses if additional margins are warranted for operation at EPU and MELLLA+.

#### 3.2.4.1 Fuel Parameters that Affect OLMCPR

The local pin power-peaking, the bundle power, the 3D power distributions, and the void reactivity are all factors that contribute to the AOO response. The accuracies of the predictions of these key fuel parameters, the conservatisms assumed in the calculational methodology, and the plant-specific inputs need to be evaluated for EPU and MELLLA+ operation.

Typically, pressurization transient response is dominantly affected by the void reactivity coefficient and the axial power distribution. In terms of power distributions, top-peaked core power profile will reduce the scram reactivity early in the transient and the reduced scram reactivity may increase the transient MCPR change. For the pressurization transients that set the OLMCPR such as turbine trip, a larger void reactivity coefficient increases the initial flux increase. The resulting higher power due to the pressurization will result in re-voiding and the void reactivity coefficient will then aid in the reactor shutdown.

#### 3.2.4.2 Assessment of Power Distribution Assumptions and Conservatism

The core axial power distribution affects the transient response, however the NRC-approved transient methodology does not directly include uncertainties and biases in the axial power shape. GE justifies the reasoning behind this approach, stating that instead of applying uncertainties in the inputs, the transient analyses assumptions are developed in a way that ensures that the axial shape is conservative.

The transient analyses assume [

].

[

]



For operation at MELLLA+, plants generally operate at reduced core flow for the beginning part of the cycle (i.e., spectral hardening) and increased core flow towards the EOC conditions. For EPU operation, most plants are limited in terms of recirculation flow capability and operate with limited core flow window. MELLLA+ operation increases the core flow window as low as 80 percent core flow at EPU power levels.

[

].

NRC staff RAI 7 (Reference 25) asked GE to justify why the conservatism associated with the scram worth and the [ ] assumed in the power history bound the axial power-peaking the plant will experience at different exposure ranges. The RAI also asked that GE include in the assessment the impact of TVAPS, which would result from the scram during power profiles other than top-peaked power shape.

#### 3.2.4.2.1 GE's Axial Power Profile Assessment

The RAI 9 response (Reference 25) states that pressurization events are most limiting at EOC, because the CRs are full withdrawn, which minimizes the scram reactivity. [

].

Table 3-2 (Table 7-1 in Reference 25) provided a comparison of the limiting transient  $\Delta$ CPR result for the [

].

Table 3-2 Axial Power Profile Sensitivity for Limiting Pressurization Events

	HBB Node 4 Axial Peaking	HBB $\Delta$ CPR	UB Node 4 Axial Peaking	UB $\Delta$ CPR
Plant A	[			
Plant B				
Plant C				
Plant D				
Plant E				
Plant F				
Plant G				
Plant H				
Plant I				]

As shown in Table 3-2, the NRC staff finds that at BOC to MOC, [

].

In addition, the sensitivity analysis did not include double hump power shape, in which the TVAPS may be less limiting, but the scram worth would be less compared to the bottom-peaked power shape (UB). Therefore, it appears that if the BOC to MOC yields the limiting transient response relative to MOC to EOC, the axial power shape assumed needs to include both bottom-peaked and double hump early in the cycle. In other words, the axial power shapes assumed in the ODYN/ISCOR/PANCEA/TASC code sets for transient analyses do not seem to be as conservative as stated in LTR NEDC-33173P (Reference 1).

#### 3.2.4.2.2 GE's CR Pattern Assessment

[

].

[

].

[

]

[

].

[

].

[

].

3.2.4.2.3 NRC staff Assessment

In justifying the conservatisms of the exposure dependent CPR response methodology, the RAI response (Reference 9) essentially states that the conservatism due to the assumed [

].

Considering the fact that ODYN models average bundle and the burn assumptions are established to yield limiting core average conditions, the NRC staff accepts the conclusions drawn from the sensitivity analysis. Based on the technical discussion above, the conclusions of the sensitivity analyses, the NRC staff finds that ODYN demonstrates reasonable conservatism and additional margin is not necessary. However, the relative CPR magnitude

attributed to the [ ] in the sensitivity analyses is an important bases for the NRC staff acceptance of the standard ODYN burn strategy for the calculating the exposure dependent CPR. Therefore, the NRC staff notes that these sensitivity analyses may be potential audit items for plant-specific applications.

#### 3.2.4.2.4 TRACG Application for EPU and Operation at Expanded Operating Domains

Considering the CPR response benefit from the use of TRACG instead of ODYN code set, the NRC staff expects most licensees will migrate to TRACG for AOO. For operation at EPU and MELLLA+ conditions, where the pressurization response would be expected to be higher, TRACG, which has the capability to model 3D core conditions, is expected to be more attractive to licensees. Therefore, it is important to evaluate the TRACG AOO methodology for defining the CR patterns and the corresponding axial power shapes modeled in TRACG applications.

Section 7.4.2.7, "High Worth Scram Rods for Pressurization event OLMCPR," of LTR NEDC-32906P (Reference 39), describes the initial conditions used to minimize the worth of the reactivity scram. The "Demonstration Analysis" section covers the bases for application of TRACG for AOO, using sensitivity analyses to establish the initial conditions and assumptions that will be applied on plant-specific bases. Section 8.2, "Initial Conditions and Plant Parameter Review," defines the initial conditions that are demonstrated to have an impact the AOO response. Table 8-9 of LTR NEDC-32906P (Reference 39), "Allowable Operating Range Characterization Basis," lists the key parameters that influence the AOO response. For the axial power shape, the table states that the cases are analyzed at nominal (top-peaked) EOC conditions and at EOC bottom-peaked conditions. For the CR pattern, Table 8-9 of LTR NEDC-32906P (Reference 39) shows that cases are analyzed at MOC with a nominal CR pattern and with a conservative black-white CR pattern.

From the discussion in Section 8-9 of LTR NEDC-32906P (Reference 39), it is not apparent that the bounding axial power shapes or CR patterns assumed ensure that the plant operates with some CR flexibility while ensuring that the assumed axial power shapes bound the power shapes the plant experiences. Therefore, the adequacy of these assumptions in terms of the CR patterns and the corresponding axial power shapes assumed needs to be re-confirmed for operation at EPU and expanded operating domains. Supplement 3 to LTR NEDC-32906P (Reference 40), is currently under NRC staff review. The conservatism of the TRACG methodology in terms of the limiting depletion CR pattern assumed and the exposure dependent power distribution assumed will be addressed in the Reference 40 review. The conclusion of which will apply to EPU and expanded operating domains applications, using TRACG.

#### 3.2.4.3 Assessment of Void Reactivity Coefficient

The reactor core response during transient situations is highly dependent upon the changes in reactivity with changes in void content in the coolant. The impact of the changes in the void content are accounted for in cross-sections and lattice physics parameters in GE nuclear methods cross-section model. This approach involves using the TGBLA06 lattice physics code to perform depletion lattice physics calculations for a particular lattice at 0 percent, 40 percent, and 70 percent void fraction. These "historical" cases are important for capturing the change in the isotopic composition of the fuel with exposure and void fraction.

In addition, instantaneous changes in the void fraction are performed for the 40 percent void history case to capture the change in the cross-sections for the instantaneous void (IV) changes that would occur in transients. [

].

It is feasible that the bases for the 40 percent depletion assumption could stem from the core average 40 percent void fraction for the historical operating strategies (OLTP at the 100 percent rod line). However, for the current operating strategies including EPU and high-power density BWR/6 plants, the core averaged void fraction is 50 percent. For the proposed expanded operating strategy, the core average void fraction would be expected to be greater than 70 percent for operation.

Given that the void reactivity depends particularly on the plutonium content of the fuel, the void reactivity effects for fuel exposure at high void conditions may not be correctly accounted for in the GE nuclear methods primarily impacting the safety analysis calculation. The top part of the fuel bundles would be depleting at void fractions greater than 40 percent and the bottom part of the fuel bundles would be operating at lower void fractions. Figure 4-1, Figure 4-2, and Figure 4-3 show the void reactivity coefficient for 40 percent and 70 percent depletion history. The differences in the isotopic composition with the assumed historical void fraction will result in bias and uncertainties in cross-sections.

Section 5.0 of this SE contains evaluation of GE methodology for parameterization and depletion history assumption for the branch cases. The NRC staff performed confirmatory analyses and evaluates GE's MCNP/TGBLA comparisons that quantifies increased uncertainties and biases in the void reactivity coefficient that affect the transient response discussed.

#### 3.2.4.4 Sensitivity Analysis Results

As shown in Table 2-10 of LTR NEDC-33173P (Reference 1), entitled "TRACG Impact of High Exposure Void Coefficient Bias," the void depletion assumption results in some under-prediction of the transient response. It is important to note that the sensitivity analyses results in Table 2-10 of LTR NEDC-33173P (Reference 1) are not necessarily bounding, but instead provide a general assessment of what the potential impact could be. LTR NEDC-33173P (Reference 1) states that the study found that the use of higher void history results in slightly larger void coefficient and a slightly larger transient impact. LTR NEDC-33173P (Reference 1) adds that the void reactivity coefficient for the part of the core depleting at lower void history provides compensating effect since the void reactivity response will be slight more conservative than the assumed 40 percent void history.

Since ODYN is a 1D transient model, it is not possible to evaluate the impact of an exposure bias. Therefore, GE performed a comparative assessment of the impact of high exposure bias using TRACG. [

]. Currently, a majority of the licensing applications including EPU use ODYN for performing the transient analyses. Since TRACG is approved for AOO applications, GE used TRACG to establish the impact of the exposure dependent bias on the transient response. In the sensitivity analyses, GE performed two TRACG cases: one with high exposure void coefficient bias and one without. The response to RAI 6 (Process) (Reference 24) discusses the sensitivity analyses that established the void reactivity bias with exposure due to the treatment of the void history and extrapolation of cross-section in the higher IV.

The NRC staff conclusions of the transient response sensitivity analyses follow.

1. American Society of Mechanical Engineers (ASME) Overpressure. Since EPU operation increases the peak ASME overpressure response, the NRC staff finds that sufficient

margin and conservatisms are important. GE performed an ASME overpressure main steam isolation valve (MSIV) closure (MSIVC) with a flux scram sensitivity analyses with exposure dependent bias. The analyses showed that accounting for the bias due to the void history impact results in 1 psig under-prediction of the peak pressure.

A 1-psig under-prediction is not significant for plant-specific EPU response showing sufficient margin in the peak (TS dome and vessel) pressure. In addition, considering that for actual operating plants, the reactor will scram earlier (based on 10 percent MSIV valve closure for two valves) than flux scram, a 1-psig under-prediction is also not significant. Additional conservatisms also included in the ASME calculations are: (1) a 102 percent power is assumed in the analysis and (2) the safety and relief valves lift at the upper limit of the valve tolerances. Therefore, the NRC staff concludes that the impact of uncertainties and bias in the void reactivity coefficient for the ASME overpressure response is marginal. However, plant-specific application with a margin a of 5 psig or less warrants NRC staff review attention in terms of key parameters assumed in the analysis.

2. Pressurization Transient MCPR Calculation. [

].

3. Impact of Void History Bias on the Transient LHGR. Table 4.1 of this SE (Table 2-11 of Reference 1) shows that the void history bias results in under-predictions of the thermal and mechanical overpower (MOP) criteria used to establish that the transient LHGR acceptance criteria are met. This is discussed in Section 3.2.6.5, "Transient Linear Heat Generation Limit," of this SE.

#### 3.2.4.5 OLMCPR Conclusion

The NRC staff finds that the sensitivity analyses show that the impact of the void reactivity coefficient due the void history bias is not very significant. For ODYN, the response to SRXB-RAI 68 (Reference 28) also provided relevant update of the ODYN model uncertainty derived from Peach Bottom turbine trip using TBLA06/PANAC11 methods. The analysis used EPU core design to quantify the sensitivity to void coefficient perturbation. A void coefficient perturbation of  $2\sigma$  [

].

Based on the sensitivity analysis provided, the NRC staff concludes that for ODYN the applied uncertainty perturbation is sufficient and the impact of the void history bias on the transient response is acceptable.

### 3.2.5 LOCA Related Nodal Power Limits

For operation at EPU and the expanded operating domains, this section: (1) evaluates that the key assumptions and conservatism in the calculation of the LOCA related thermal limits remain applicable and conservative; (2) evaluates the potential impact of increased uncertainties in the nodal powers on the calculation of the maximum planar LHGR (MAPLHGR); and (3) determines if additional margin is warranted.

The MAPLHGR limit assures adequate protection of the fuel during LOCA event. Section 2.5 of LTR NEDC-33173P (Reference 1) covers the conservatisms in the calculational methodology and codes used to establish the MAPLHGR.

#### 3.2.5.1 LOCA Related Nodal Power Limits

The MAPLHGR is the licensing fuel design parameter that ensures safety margin in the peak clad temperature (PCT) during a postulated LOCA. The value for MAPLHGR is determined so that the maximum PCT will not be exceeded during a LOCA. The LOCA fuel design limit minimizes gross fuel failures due to the severe cladding heatup or fuel fragmentation as result of the quenching of the emergency core cooling system (ECCS) flow. The amount of stored energy in the fuel is proportional to the average kW/ft in each node (bundle-wise) before the scram. Gross cladding failure is prevented by limiting the power level, which would result in PCT of 2200 °F during a design-bases accident such as LOCA. The LOCA MAPLHGR is obtained by averaging the LHGR over each fuel rod in a given plane of a particular fuel bundle and selecting a limiting value as a function of fuel burnup. The PCT is considered to be a function of the average kW/ft of all the rods in a bundle at a given axial location. Amendment 19 to GESTAR approved selecting the MAPLHGR limit based on: (1) the LOCA PCT being below 2200 °F and (2) not exceeding the maximum LHGR (MLHGR).

The NRC-approved LOCA methodology accounts for uncertainties in the bundle power and distribution. Similar to the LHGR, the local pin power-peaking and the bundle powers factor into the generation of the MAPHGR limit. Increased uncertainties in the pin power-peaking and bundle power determine the predicted local nodal powers, which could translate into an under-prediction in the calculated MAPLHGR. Therefore, increases in the uncertainties in the predicted nodal powers for operation at MELLLA+ could impact the MAPLHGR calculation.

In the LOCA scenarios, the PCT depends more on the stored energy than on the instantaneous power change early in the event prior to the scram. Therefore, the PCT is not expected to be sensitive to the void-coefficient. GE also states that the SAFER methodology uses a bounding curve for the reactivity response in the early stages of the accident MFN 05-005 (Reference 4) and this conservatism has been confirmed by recent TRACG LOCA analyses. Note that the NRC staff did not approve TRACG for LOCA calculations, but had accepted the use of TRACG for sensitivity analyses in some circumstances.

The ECCS-LOCA analysis is based on the NRC-approved SAFER/GESTR application methodology documented in Volume III of Reference 41. The analytical methods used to perform the ECCS-LOCA analyses are documented in Volume II of Reference 41.

GE cites the following conservative assumptions in the SAFER/GESTR LOCA methodology in terms of local pin and bundle powers:

1. [ ].

2. In the 10 CFR Part 50, Appendix K calculation, a 2 percent core thermal power uncertainty is applied to the hot rod in order to account for plant core thermal power uncertainty. Note that some plants implemented improved feedwater measurement instrumentations and apply a lower power uncertainty. In the measurement uncertainty uprates, some plants operate at higher powers equivalent to the increased accuracy of the feedwater flow measurement instrumentation. However, for plants that implement EPU's up to 20 percent, additional power measurement uprate due increased accuracy of the feedwater flow measurement uncertainty is not allowed. The EPU is limited to 20 percent above the OLTP. Therefore, the ECCS-LOCA analysis will continue to assume 2 percent above the EPU power level.
3. In order to ensure that the SAFER analysis is bounding for all exposures, the hot rod of the hot bundle is placed at the exposure corresponding to the [ ].
4. The plants' core simulator calculates the margins to the fuel design limits (OLMCPR, SLMCPR, LHGR, and MAPLHGR). As a general practice, plants operated with margins to the MAPLHGR limit for most of the cycle operation.
5. Since the total bundle power is important to the severity of the ECCS-LOCA response, higher bundle power is therefore conservative. The SAFER/GESTR methodology [ ]. In an iterative calculation assuming different OLMCPR and a low the R-factor, the power-peaking is maximized.
6. The full spectrum base ECCS-LOCA analysis is performed during initial implementation of SAFER methodology or transition to GE methodology and fuel. For new fuel introduction, or if new operating conditions are implemented, the limiting areas of the full spectrum base ECCS-LOCA analysis are reanalyzed to assure continued compliance with the 10 CFR 50.46 acceptance criteria for the new fuel or operating conditions. Depending on the specific licensing topical report, full break spectrum analysis may be performed for implementation of new operating strategies. During standard reloads, the assumptions in the ECCS-LOCA analysis-of-record are confirmed to remain applicable in terms of assumed OLMCPR and bundle LGHR and MAPLHGR limits. Therefore, the hot bundle operating power is maximized such that the ECCS-LOCA OLMCPR bounds the OLMCPR calculated from the limiting cycle- and core-specific AOO analyses.
7. To ensure that the ECCS-LOCA results are bounding, the pin power-peaking for the hot rod is also set to a [ ].

GE concludes that the above listed assumptions provide significant conservatisms in the ECCS-LOCA methodology in terms of the accuracy of the assumed local pin and bundle powers as an initial condition.

#### 3.2.5.1.1 ECCS-LOCA Axial Power Distribution Evaluation

Considering the assumed axial power profiles in the SAFER/GESTR methodology, LTR NEDC-33173P (Reference 1) cites the conclusions from recent sensitivity analysis. For large break LOCA, [



] power shape was found to result in more limiting PCT. GE states that large break LOCA usually results in more limiting PCTs.

In terms of axial power distribution, the NRC staff concludes that for small break LOCA, the SAFER/GESTR LOCA analysis should include the mid and top-peaked power distribution for application involving implementation of maximum operating domains. This conclusion is based on the review of EPU applications, which indicate that small break LOCA PCT does increase with EPUs. In addition, the large break ECCS-LOCA PCT is expected to be higher for operation at the minimum core flow conditions at EPU power levels, characteristic of the operation at the higher operating domain. The impact of operation of MELLLA+ on the ECCS-LOCA performance is addressed in MELLLA+ LTR (Reference 2).

The NRC staff confirmatory calculations indicate that the difference in PCT could be up to 200 °F when top-peaked power shape results are compared to mid-peaked power shape results. Plant-specific analyses performed by GE show a difference of approximately [ ]. In these specific applications, even a modest increase in PCT could have a significant impact in the plant's ability to meet the ECCS-LOCA PCT requirements. Therefore, the best alternative approach to resource intensive plant-specific PCT margin evaluation is to amend the SAFER/GESTR licensing methodology.

#### **ECCS-LOCA Limitation 1:**

For applications requesting implementation of EPU or expanded operating domains, including MELLLA+, the small and large break ECCS-LOCA analyses will include top-peaked and mid-peaked power shape in establishing the MAPLHGR and determining the PCT. This limitation is applicable to both the licensing bases PCT and the upper bound PCT. The plant-specific applications will report the limiting small and large break licensing basis and upper bound PCTs.

In addition to the assumptions in pin power-peaking, bundle powers distribution, LTR NEDC-33173P (Reference 1) also discussed the statistical uncertainty treatment in the ECCS-LOCA methodology. The PCT calculations of 10 CFR Part 50, Appendix K, include the conservative modeling assumption. In calculating the upper bound SAFER/GESTR PCT, the nominal PCT is adjusted to account for model uncertainties (at 95 percent probability). The 95 percent probability PCT includes a [ ] applied to the LHGR.

GE adds that the SAFER/GESTR methodology assumes a bounding post-LOCA core power decay and therefore the core kinetics are not modeled. The average and hot bundle void profile is determined by SAFER at the limiting conditions cited above.

Section 2.5 of LTR NEDC-33173P (Reference 1) concludes that the conservatism in the ECCS-LOCA methodology used to determine the MAPLHGR limits adequately consider the effects of the uncertainties in local and bundle powers. These conservatisms provide sufficient and reasonable assurance that those limits provide adequate margin to protect the fuel.

#### 3.2.5.1.2 Plant-Specific Review Process

For EPU and MELLLA+ application, the NRC staff will review the plant-specific ECCS-LOCA response and the available margins to the key parameters in the ECCS-LOCA requirements

(e.g., PCT limit of 2200 °F). The licensing application will include comparisons of the key parameters for each application against the experience (see Section 4.3, "Plants Specific Application Process" of LTR NEDC-33173P (Reference 1)). For those applications, in which the key parameters are outside the experience base in terms of the hot bundle powers or bundle power/flow conditions and/or in those cases in which the margins to the PCT are deemed to have low margins, the NRC staff will audit and review the specific input parameters applied in the ECCS-LOCA analysis. In these cases, the NRC staff can request additional sensitivity analyses in order to obtain additional assurances that ECCS-LOCA assumptions and methodology are acceptable.

The ECCS-LOCA response is sensitive to initial conditions, including the initial power and flow conditions. Most EPU plants operate with a minimum core flow window at the uprated power levels. MELLLA+ operation expands the operating window and allows operation at as low as 80 percent rated core flow at EPU power levels. The expanded operating domain also includes operation at 55 percent rated core flow and about 100 percent OLTP level. MELLLA+ RAI 25b (Reference 5) address the ECCS-LOCA at the limiting statepoints for MELLLA+ operation. Operation at the higher power/ low flow condition, characteristic of the MELLLA+ operation affects the large break ECCS-LOCA response. The specifics of the ECCS-LOCA calculations at the different statepoints in the upper boundary are address in the in the MELLLA+ (Reference 2) review; however, for consistency, the restriction is also covered here. To ensure that the ECCS-LOCA analysis is performed at the limiting statepoint and that the limiting PCT is reported, the follow restriction applies.

#### **ECCS-LOCA Limitation 2**

The ECCS-LOCA will be performed for all statepoints in the upper boundary of the expanded operating domain, including the minimum core flow statepoints, the transition statepoint as defined in Reference 2 and the 55 percent core flow statepoint. The plant-specific application will report the limiting ECCS-LOCA results as well as the rated power and flow results. The SRLR will include both the limiting statepoint ECCS-LOCA results and the rated conditions ECCS-LOCA results.

#### 3.2.5.1.3 LOCA Conclusions

The NRC staff reviewed the conservative assumptions cited in LTR NEDC-33173P (Reference 1). With the exception of the NRC staff concerns covered in the ECCS-LOCA limitations, the NRC staff finds that the conservatisms provide reasonable assurance that potential increases in nodal power uncertainties will not result in significant changes to the calculated PCT, and therefore are acceptable.

#### 3.2.5.2 Approval of the ECCS-LOCA Analytical Models

Section 2.5 of LTR NEDC-33173P (Reference 1) cites LTR NEDC-32950P (Reference 42) as one of the documents that specify the analytical models used to perform the ECCS-LOCA analyses. The ECCS-LOCA analytical model improvements documented in LTR NEDC-32950P (Reference 42) were approved by the NRC in Reference 43. GE will submit an update of LTR NEDC-32950P (Reference 42), which will document the cumulative changes to the ECCS-LOCA analytical models (see MFN-06-424 (Reference 7)). The NRC staff issued a letter to GE, requesting that the LTR include the identified follow-up topics that are relevant to the application of the ECCS-LOCA models to high void conditions. These topics will be addressed separately from NEDC-33173P review.

### 3.2.6 Fuel Rod T-M Performance

This section evaluates that steady-state and transient response of the fuel rods operated under EPU and the expanded operating domain will continue to meet the fuel rod thermal mechanical (T-M) limits. The section also evaluates: (1) the key assumptions in the methodologies used to establish the thermal mechanical limits; (2) assesses potential impact of increased uncertainties in the nodal powers; and (3) determines if additional margin is warranted.

The regulation at 10 CFR Part 50, Appendix A, GDC 10 requires that specified acceptable fuel design limits (SAFDLs) are not exceeded during any condition of normal operation. To demonstrate compliance with GDC-10, fuel rod T-M design limits are established to ensure fuel rod integrity for the core lifetime along the licensed power and flow domain, during normal steady-state operation and in the event of an AOO. The T-M acceptance criteria for new fuel product line are specified in Amendment 22 to the NRC-approved GE licensing methodology GESTAR II. The LHGR is an exposure-dependent limit (in kW/ft) placed on the rod peak pin nodal power that ensures the integrity of the fuel cladding during normal steady-state operation and limits the initial kW/ft during transient thermal overpower (TOP) and mechanical overpower (MOP). The internal rod pressures during steady-state, the maximum fuel temperature, and the cladding strain during transients (i.e., AOOs) all affect the fuel integrity. The fuel T-M design criteria requires, in part, that:

1. Loss of fuel rod mechanical integrity will not occur due to excessive cladding pressure loading.

The fuel rod internal pressure is limited so that the cladding creepout rate due to internal gas pressure during normal operation will not exceed the instantaneous fuel pellet irradiation swelling rate. In establishing the LHGR limit, at each point of the exposure dependent envelope, the fuel rod internal pressure required to cause the cladding to creep outward at rate equal to the pellet irradiation swelling is determined. The calculated internal rod pressures along the LHGR envelope are statistical treated so that there is assurance with 95 percent confidence that the fuel rod cladding creep rate will not exceed the pellet irradiation swelling rate.

2. Loss of fuel rod mechanical integrity will not occur due to fuel melting.

The fuel rod is evaluated to ensure that fuel melting will not occur during normal operation and core-wide AOOs. For every fuel product line, the TOP limit is established to preclude fuel centerline melting. The acceptable TOP during transient event is established by assuming continuous operation at the applicable exposure dependent LHGR envelope followed by instantaneous overpower at selected exposure points in the envelope. The fuel rods loaded in the core must meet the permissible TOP limit that will assure the incipient fuel centerline melt criteria are not exceeded. The TOP limit is determined for both the UO<sub>2</sub> and the (UGd)O<sub>2</sub> bearing pellet rod nodes.

3. Loss of fuel rod mechanical integrity will not occur due to pellet-cladding mechanical interaction.

The fuel rod is evaluated to ensure that the calculated cladding circumferential plastic strain due to pellet-cladding mechanical interaction does not exceed 1 percent during normal operation and AOOs. For every fuel product line, the MOP limit is established to preclude fuel 1 percent diametric strain during an AOO. The acceptable MOP limit during a transient event is established by assuming continuous operation at the applicable exposure-dependent LHGR envelope for each fuel design followed by instantaneous overpower at selected exposure points in the envelope. The fuel rods

loaded in the core must meet the permissible MOP limits during all transient events. The MOP limit is determined for both the UO<sub>2</sub> and the (UGd)O<sub>2</sub> bearing pellet rod nodes.

Therefore, the fuel rods loaded in the core are monitored to ensure that the exposure dependent LHGR (in kW/ft) envelope for each product line is met. The LHGR limit is specified in the TS and/or the core operating limit report. The ratio of the steady-state operating peak nodal kW/ft over the steady-state LHGR limit is referred to as MFLPD. Fuel parameters that affect the local pin powers such as pin power-peaking, void reactivity, and bundle powers all factor into the development of the LHGR limits. Therefore, increases in the power distribution uncertainties affect the prediction and monitoring of the operating LHGR during steady-state operation and transient conditions. Operating experience data shows that fuel rods can operate at or near the LHGR limit at some point in the operating cycle; therefore, the accuracy of the prediction of MLHGR becomes important.

GE has committed to performing gamma scans to benchmark the power distribution uncertainties. In the interim, LTR NEDC-33173P (Reference 1), Section 2.4 provides evaluation of the conservatism in the T-M analyses performed in developing the LHGR limits and the additional margins in the applied power distribution uncertainties.

The LHGR limit is developed for each fuel type (e.g., UO<sub>2</sub> or Gd-bearing rod for different concentrations) and varies with exposure. Table 3-10 shows the exposure-dependent LHGR limit for GE14 UO<sub>2</sub> and a 6 percent Gd-bearing rod changes linearly with burnup. The limit decreases linearly with exposure from 16 GWd/MTU for UO<sub>2</sub> rods and from 13.53 GWd/MTU for the rods with 6 percent Gd concentration. Note that most licensing applications are currently based on Gd concentration of 6 to 7 percent. However, the Gd content can increase to 8 percent and this concentration is expected to be used in the MELLLA+ applications. The T-M confirmatory analyses in Appendix C are based on 8 percent Gd concentration.

#### 3.2.6.1 Power Distribution Uncertainties

[ ] is applied in the development of the LHGR limit. As shown in Table 3-11, increasing the infinite lattice-pin power-peaking [

] based on recent code-to-code core simulator analyses of current lattices. Considering that the applied uncertainty is within the increased power distribution uncertainty, the NRC staff finds that the currently applied power distribution uncertainty is acceptable.

#### 3.2.6.2 Conservative Assumption for Steady-State LHGR Limit

The LHGR limits are developed assuming that the peak power node of the fuel rod operates along the projected power-exposure envelope throughout the lifetime. The fuel rod power shape is alternated from bottom-peaked, middle-peaked, and top-peaked at a selected frequency. The varying axial power shapes account for changes in the axial power shape during steady-state operation and affects the fission gas released from the fuel columns. This "operating history" assumption yields higher internal rod pressures than operating nodes would typically experience.

Sensitivity analyses performed in the VYNPS EPU application (approved by NRC staff in Reference 26) resulted in internal rod pressures of 560 psia for peak node that accumulated the

highest exposure (higher integrated power). The selected rod accumulated the most exposure. In comparison, the best-estimate calculation assuming operation at the LHGR limit envelope resulted in a calculated internal pressure of 1180 psia at EOC. This calculation demonstrates conservatism introduced by the “operating history” assumption in the development of the LHGR limit.

### 3.2.6.3 EPU T-M Operating History Data

Core tracking data (see Figure 2-4) show that the predicted peak node could operate close to the LHGR limit and any potential under-prediction in the operating kW/ft could result in exceeding the limit. However, most licensees operate the plant so that there are margins to the limits. During steady-state operation, the T-M criteria require that loss of fuel rod mechanical integrity will not occur due to excessive cladding pressure loading. As can be seen from the LHGR limit envelope, the LHGR limit decreases with exposure while the internal rod pressure increases with exposure.

In response to RAI 1.1 (Reference 9), GE provided an actual operating LHGR (i.e., MLHGR) of an EPU plant. In the pre-EPU cycle, the plant was loaded with GE13 fuel, which had a higher LHGR limit. The EPU cycle LHGR limit data are based on GE14 fuel. Figure 3-12 shows the margins between the operating LHGR limit for peak nodes at a given exposure against the GE14 LHGR limit as the plant was operated at EPU conditions.

To bound the operation of other EPU plants, the actual operating LHGR for peak nodes (UO<sub>2</sub> rods) at five exposures were increased to the LHGR limit. The objective of the sensitivity analyses was to determine if nodes that operate at the LHGR limit for reasonable duration for different exposures would remain bounded by the “operating history” assumption in terms of diametric strain (internal rod pressure). [

]. Table 3-12 provides the internal rod pressure results corresponding to each exposure case and at EOC. This table gives the nominal values, which do not include the statistical treatment (upper 95 percent confidence level).

As seen from Table 3-12, if a node operates at the LHGR limit for reasonable duration, the resulting internal rod pressure will continue to be bounded by the internal rod pressure based on the “operating history” assumption at that exposure. However, if a UO<sub>2</sub> rod operates at the limit early in the fuel life for reasonable duration [ ]. the margin in terms of internal pressure would be low [ ] for the nominal case. Therefore, it is essential that the fuel cycle operation is designed with a margin to the operating LHGR limit as is usually the case and that the actual CR patterns selected throughout the cycle limit peaking of the fresh fuel rods.

For example, in the Browns Ferry Unit 1 restart cycle, the core is loaded with an atypical number of fresh fuel rods. The data provided by the licensee shows there is a margin in the LHGR as projected to operate the plant at BOC, MOC, and EOC. Note that the BOC data did not necessarily cover the most limiting point early in the cycle for the fresh fuel. In addition, the Browns Ferry Unit 1 startup core consists of GE13 and GE14, which have different limits. The sensitivity analysis is based on GE14, fuel but the T-M performance analysis methodology remains the same.

Considering the margins available in an actual EPU plant operating LHGR limit data and the sensitivity analyses provided, the NRC staff finds that there is reasonable assurance that peak nodes operating at the MLHGR limit will continue to be met and bounded by the steady-state

LHGR limit envelope. However, the margins are expected to be low, requiring additional scrutiny. Section 3.2.6.5 of this SE and Appendix C provide an additional assessment based on confirmatory analyses.

#### 3.2.6.4 Monitoring Gd-bearing Nodes

The LHGR limit for the Gd-bearing fuel rod peak pellet [

].

Figure 3-13 and Figure 3-14 present the actual gadolinium fuel rod local power data as a function of fuel burnup. This data is based on actual operating history of GE14 Gd-bearing rods of an EPU plant. As can be seen from the figure, the operating LHGR limit of the Gd rods remain within the envelope of the LHGR limit for 6 weight percent Gd. As expected, the powers of the Gd rods are low.

Since the operating margin to the LHGR limit for the Gd-bearing rods are not monitored, GE investigated the impact of operation outside the envelope on fuel-mechanical performance during transient and accident conditions. Although the gadolinium fuel rod operating LHGR is not limiting in terms of power-peaking at low exposures, the uncertainty in the predicted operating LHGR for gadolinium rod may be greater at the early life of the Gd rod. GE performed sensitivity analyses to determine whether greater uncertainty in the predicted LHGR early in life may significantly affect the fuel performance at later in life after the gadolinium isotopes transmutation.

In order to quantify the impact of operation outside the early life LHGR envelope, [

]. The bias is decreased in order to reflect the progressive transition to normal unbiased conditions after the transmutation of the gadolinium isotopes and reduction in the uncertainty associated with the prediction of the LHGR limit in the presence of Gd.

Table 3-13 provides the resulting calculated fuel centerline temperature and cladding midplane circumferential stress at selected points. Power History A presents the results corresponding to operation at the normal T-M envelope from early in life through the end. Power History B results correspond to the biased operation early in life and transition to normal T-M after 5 GWd/MTU.

The results show that the minor variation in the actual operating history in early life is not significant, because substantial margin exists in terms of fuel centerline temperature and compressive cladding stress relative to the limiting condition later in life. Therefore, the NRC staff concludes that there is reasonable assurance that the practice of monitoring at the peak LHGR limit for low exposures will not result in a limiting adverse condition.

#### 3.2.6.5 Transient Linear Heat Generation Limit

The number of fuel bundles operating at the peak LHGR envelopes is expected to be higher for plants operating with 24-month cycles at EPU and MELLLA+ conditions. Local pin power-peaking, bundle powers, 3D power distributions, and void reactivity are all factors that contribute to the AOO response. EPU/MELLLA+ operating strategy, including the spectral shift operation

at EPU power levels will entail operation outside the current experience base. Although dependent on the core design and the specifics of the cycle energy needs, EPU/MELLLA+ operating strategy could result in a more limiting transient response relative to pre-EPU operation. Thus, the thermal and mechanical overpower response could be higher. The transient response and the associated overpower responses will be calculated on cycle-specific bases. This section evaluates the plant-specific licensing methodology that ensures that plants meet the TOP and MOP limits, during AOOs for the fuel designs currently loaded in the cores and the proposed EPU/MELLLA+ operating strategy.

### 3.2.6.5.1 Thermal and Mechanical Overpower Licensing Process

Amendment 22 to GESTAR II demonstrates compliance with the transient LHGR limit acceptance criteria based on TOP and MOP limits. Reference 5 provides the TOP and MOP screening criteria for the GE13 and GE14 fuel designs for limiting transients, shown in Table 3-3. Plant-specific applications must show compliance to the TOP and MOP acceptance criteria (e.g., fuel centerline melt and 1 percent diametric strain) based on the limiting transients and allowed equipment out-of-service operation.

**Table 3-3 TOP and MOP screening criteria for GE13 and GE14 fuel designs for limiting transients**

TABLE SBWB-38-1				
TOP (%) GE13	MOP (%) GE13	TOP (%) GE14	MOP (%) GE14	Condition of Applicability
38	38	52	52	Load Rejection/Turbine Trip, No Bypass
37	39	51	51	Feedwater Controller Failure
25	45	29.5	52	Loss of Feedwater Heater
25	45	29.5	52	Slow Recirculation Flow Runout

The NRC staff finds the acceptance criteria is established in Amendment 22 to GESTAR II, but the methodology in which this criteria is met for plant-specific application is not well defined in the NRC-approved licensing documentation. The NRC staff's assessment is largely based on audits and RAI responses. The referenced documentation for the T-M methodology appears to be limited to Reference 45 (e.g., 1984 approval) and Reference 46 (e.g., 1986 approval). If a plant-specific AOO response does not meet the TOP and MOP screening limits, GE performs General Electric Stress and Thermal Analysis of Reactor Rods - Mechanical (GESTR-M) calculations for slow transients. For fast transients, GE performs further evaluations, using a transient heat transfer analysis of anticipated spectrum of transients (CHT). A fast or slow transient is defined by the transient response time relative to the fuel thermal time constant of 5 to 10 seconds.

GE states that the TOP and MOP limits serve as screening criteria only. Therefore, not meeting the TOP and MOP limits - does not imply that a plant's AOO response will exceed the fuel centerline melt and 1 percent diametrical strain acceptance criteria. According to GE, TOP and MOP screening criteria is not included in the NRC-approved licensing process. If a plant-specific transient response exceeds the TOP/MOP screening criteria, detailed analyses will be performed using NRC-approved GESTR-M and CHT codes (References 44 and 47).

Although the transient fuel centerline melt and 1 percent strain limits are SAFDLs that ensure that the fuel integrity limit will be met during an AOO, the current licensing process does not include the TOP and MOP screening criteria or the demonstration that the T-M fuel design limits will be met during an AOO on cycle-specific bases. The NRC staff determined that the transient

overpower limits are not controlled in the plant-specific TSs, core operating limit reports or the SRLR. Therefore, the NRC regulatory process does not monitor the compliance with the TOP and MOP criteria during an AOO. Considering that for EPU and MELLLA+ operation, the plant overpower response may increase and compliance with the fuel centerline melt and 1 percent diametric strain criteria is important, the NRC staff concludes that the plant-specific EPU and MELLLA+ applications must include the plant overpower response. In addition, since the transient response is cycle- and core-specific, the plant T-M response will be provided with the SRLR, or COLR or it will be reported directly to the NRC as an attachment to the SRLR or COLR. RAI 11 response (Reference 49) addresses the inclusions of the TOP and MOP limits in the SRLR.

#### **Transient LHGR Limitation 1**

Plant-specific EPU and MELLLA+ applications will demonstrate and document that during normal operation and core-wide AOOs, the T-M acceptance criteria as specified in Amendment 22 to GESTAR II will be met. Specifically, during an AOO, the licensing application will demonstrate that the: (1) loss of fuel rod mechanical integrity will not occur due to fuel melting and (2) loss of fuel rod mechanical integrity will not occur due to pellet-cladding mechanical interaction. The plant-specific application will demonstrate that the T-M acceptance criteria are met for the both the UO<sub>2</sub> and the limiting GdO<sub>2</sub> rods.

#### **Transient LHGR Limitation 2**

Each EPU and MELLLA+ fuel reload will document the calculation results of the analyses demonstrating compliance to transient T-M acceptance criteria. The plant T-M response will be provided with the SRLR or COLR, or it will be reported directly to the NRC as an attachment to the SRLR or COLR.

#### 3.2.6.5.2 Impact of 40 percent Depletion Assumption on Transient LHGR Response

As discussed in Section 3.2.4.3, "Assessment of Void Reactivity Coefficient," of this SE, the void depletion assumption results in a bias in the void reactivity for the nodes depleting at greater than 40 percent void fraction. NRC staff had performed confirmatory analyses to assess the impact of the 40 percent depletion history and determined that the assumption results error in increasing void reactivity coefficient with exposure. Figure 4-1 and Figure 4-2 show the bias in the void reactivity coefficient due to the 40 percent depletion history for the branch cases. Figure 4-3 also shows GE assessment of the bias on the void reactivity coefficient. Section 2.2.2.2 of LTR NEDC-33173P (Reference 1) presents the results of sensitivity analyses with the bias shown in Figure 4-3 propagated in the safety analyses. Table 3-9 reproduces the results of the sensitivity analyses.

Table 3-9 shows that the 40 percent depletion assumption can result in a under-prediction of 5 percent for the TOP and MOP. As depicted in a plant-specific EPU application, plants may not meet the initial TOP and MOP screening criteria with the allowed equipments out-of-service. In a plant-specific application (Reference 49) a detailed T-M calculation was performed after not meeting the TOP and MOP screening criteria. The detailed T-M calculations demonstrated that there was a 10 percent margin to the TOP and MOP acceptance criteria.

Since the margins to the transient LHGR limits could be low and the conclusions of the sensitivity analyses that established the 5 percent under-prediction in the TOP and MOP may not bound all the BWR fleet, the NRC staff concludes that additional margin greater than 5 percent is warranted. Until such time that GE changes its depletion assumption for the instantaneous cases, plants will demonstrate that there is an equivalent of 10 percent margin in the TOP and MOP response during AOOs. Specifically, plant-specific EPU and MELLLA+



applications will provide confirmation that there is a 10 percent margin to the centerline melt and the 1 percent diametric strain acceptance criteria for the transient LHGR limit calculation.

### **Transient LHGR limit Limitation 3**

To account for the impact of the void history bias, plant-specific EPU and MELLLA+ applications using either TRACG or ODYN will demonstrate an equivalent to 10 percent margin to the fuel centerline melt and the 1 percent cladding circumferential plastic strain acceptance criteria due to pellet-cladding mechanical interaction for all of limiting AOO transient events, including equipment out-of-service. Limiting transients in this case, refers to transients where the void reactivity coefficient plays a significant role (such as pressurization events). If the void history bias is incorporated into the transient model within the code, then the additional 10 percent margin to the fuel centerline melt and the 1 percent cladding circumferential plastic strain is no longer required.

#### 3.2.6.5.3 Qualification Database Supporting the T-M Methodology

In response to RAI 1 (Reference 9), GE presented the qualification database supporting the T-M methodology. Table 3-14 (Table 1.3-1 of the RAI 1 response) provided a summary of the experimental qualification database as compared to the GE14 fuel design characteristics.

The RAI response states that the qualification of the GNF fuel rod T-M performance model (GESTR-M) was performed in a manner to challenge the prediction capability over a wide range of not only duty conditions, but also dimensional conditions and fabrication parameters, to confirm the robustness of the embodied fundamental physical process and mechanism representations. GE added that the range of conditions covered in the experimental qualification database extends beyond the commercial fuel rod conditions, including power uprate conditions. The experimental qualification included comparison of predictions to the following:

- (1) fuel temperatures as obtained by, placement of and continuous measurement by, a fuel thermocouple in the center of the fuel pellet column,
- (2) cladding diametral deformation, as obtained by diametral profilometry performed at various times during normal steady-state operation as well as before and after intentional power ramps,
- (3) cladding axial deformation, as obtained either by continuous on-line LVDT length measurement or periodic conventional length measurements,
- (4) fission gas release, as measured by fuel rod puncture, gas collection, and gas chromatography to determine the amount and composition of released gases, and
- (5) fuel rod internal pressure, as measured continuously by a bellows pressure transducer located in the fuel rod fission gas plenum.

#### 3.2.6.5.4 Assessment of the Qualification Data

The qualification data parametrically cover wide ranges; however some of the qualification data for some of the key parameters does not extend to current conditions. As can be seen from Table 3-14, the fuel centerline temperature data are limited to [ ]. The rod internal pressure data is also limited to [ ]. Much of the old GESTR-M qualification data (data acquired prior to 1984) are atypical of today's fuel designs and do not cover the combination of LHGR at the burnup levels of the LHGR limits achieved for the GE13 and GE14 designs. The inadequacy of the GESTR-M qualification database is apparent even at low

burnups when the GESTR-M best estimate calculational results of  $UO_2$  fuel temperature and rod pressure are compared to those calculated from the new GEH developed fuel performance code, PRIME, and the NRC audit code FRAPCON 3.3 at low to high burnup levels. Both the PRIME and FRAPCON 3.3 fuel performance codes predict higher best estimate  $UO_2$  fuel temperatures and rod pressures (see Table-4 and Section 3.2.6.5.5 below) and both have a much more extensive qualification databases (higher LHGRs at higher burnups) than GESTR-M. These new databases are based on fuel designs much closer to current designs with higher LHGRs at higher burnups that match the LHGR limit curves for these designs. It is noted that the PRIME code was recently submitted to NRC for review but has not been approved at this time.

The internal rod pressures increase with exposure due to increased fission gas release. Therefore, the lack of supporting data for exposures greater than [ ] means that the accuracy of the T-M model is not validated for the current rod lattice designs (e.g., higher enrichment) as operated with higher exposures. The differences between the current fuel designs in terms of geometric configurations such as the fuel column length and part-length rods also need to be benchmarked in terms of the available gas volume, which also affects the internal rod pressures. Qualification data provide the means to establish the adequacy of the uncertainties applied in the calculation of both the steady-state LHGR limits and the calculation of the plant's operating MLHGR response. Therefore, the NRC staff finds that GE needs to expand the database supporting the T-M methodology to the current fuel designs and licensed exposures.

The GE's licensed T-M methodology qualification data was reviewed and approved in MFN 170-84 (Reference 45) and MFN 027-086 (Reference 46) in 1984 and 1986 respectively. The NRC staff audited GE T-M methodology through the vendor inspection program and GE submitted supporting information demonstrating compliance with the inspection findings. However, it is not clear if the code had been specifically updated and reviewed by the NRC staff since the initial approval. Therefore, the NRC staff finds information provided through RAI responses and in LTR NEDC-33173P (Reference 1) is not sufficient to conduct a detailed assessment of GE's T-M methodology.

GE submitted a notification in accordance with 10 CFR Part 21, "Reporting of Defects and Noncompliance," by letter dated January 21, 2007 (Reference 57). Section 3.2.6.5.8 of this SE provides summary of the content of the GE Part 21 report in Reference 57. The NRC staff performed an evaluation in response to a GE Part 21 notification on the GESTR-M T-M methodology. The most recent NRC staff evaluation of the GESTR-M T-M methodology and its qualification database is provided in Appendix F.

#### 3.2.6.5.5 Internal Rod Pressure Assessment

##### Internal Rod Pressure Gamma Scan

The December 2005 presentation slides (Reference 31) provided the scope of planned gamma scans for updating the benchmarking data supporting GE analytical methods also included intention to perform internal rod pressure measurement qualification. In NRC staff RAI 9 response (Reference 25), GE agreed to perform fission gas and exposure gamma scans, although no specific schedule or plan is specified.

##### Internal Rod Pressure Confirmatory Analysis

The NRC staff performed confirmatory analysis using best-estimate FRAPCON code in order to assess independently the internal rod pressure that the GE14 fuel rod will experience.

The rod internal pressure acceptance criterion is that the rate of clad creep-out is less than the fuel thermal swelling rate. In other words, the fuel pellet-to-clad gap does not widen during normal operation. The best estimate rod internal pressure, which would be expected to cause a clad creep-out rate, is approximately 3200 psia.

The confirmatory analyses applied manufacturing tolerances that minimizes the plenum volume and maximizes the fission gas release. The results showed that the UO<sub>2</sub> fuel rod is more limiting than the (UGd)O<sub>2</sub> fuel rod due to less plenum volume and higher rod power. Although the Gd rods exhibit significantly higher operating fuel temperatures ((UGd)O<sub>2</sub> = 3340 °F versus UO<sub>2</sub> = 2989 °F), the extra plenum volume ((UGd)O<sub>2</sub> = 16.6 cm<sup>3</sup> versus UO<sub>2</sub> = 13.8 cm<sup>3</sup>) is able to accommodate the higher fission gas release.

The FRAPCON-3 algorithms are tuned to produce best-estimate predictions. Even though manufacturing tolerances are set at worst case, the modeling uncertainty (which represents the spread in the empirical database) needs to be accounted for. Operating a single rod on the T-M operating limit (TMOL) peak nodal power for its entire lifetime is extremely conservative (as the peak node would migrate to many different fuel rods). This scenario coupled with a 10 percent margin to the fuel centerline melt and the 1 percent cladding circumferential plastic strain acceptance criteria is judged to be more than adequate to accommodate any modeling uncertainty.

Examination of Table C-1 (Appendix C) results show that the worst rod internal pressure experienced is 2656 psia (UO<sub>2</sub>) and 1854 psia (UGdO<sub>2</sub>). As this peak rod internal pressure remains below the pressure, which would cause an outward creep of the fuel cladding, the independent calculations show that the GE14 fuel rod continues to satisfy these design criteria.

#### FRAPCON-GESTR-M Internal Rod Pressure Comparisons

The NRC staff compared FRAPCON UO<sub>2</sub> rod internal rod pressure calculations against GESTR-M. The internal rod pressure calculations provided in Table 3-12 did not include the statistical treatment to account for the uncertainties. The follow-up response to RAI 9d (MFN 06-481, Reference 25) provided GESTR-M internal rod pressure prediction based on the 95 percent confidence level. Table 3-4 below compares the GESTR-M and FRAPCON rod internal pressure for GE14 UO<sub>2</sub> rod. As can be seen in Table 3-4, the GESTR-M internal rod pressure prediction is substantially lower than the FRAPCON prediction. However, using the higher FRAPCON internal rod pressure predictions, there remains sufficient margin to the internal pressure expected to cause clad creep rate of 3200 psia. The lower prediction demonstrates that although the internal rod pressure prediction meets the acceptance criteria, the adequacy of the GESTR-M uncertainty treatment needs to be confirmed through measurement qualification data.

**Table 3-4 Steady-state Operation at the LHGR Envelope**  
 (GESTR-M and FRAPCON Rod Internal Pressure for GE14 UO<sub>2</sub> Rod)

Peak Pellet GWd/MTU	Nominal Pressure Psia	U95% Pressure Psia	Rod Internal Press (psia)	FRAPCON UO <sub>2</sub> and (UGd)O <sub>2</sub> Pressure (psia)			
				Acceptance Criteria Rate)	UO <sub>2</sub> Nom	UO <sub>2</sub> 10%	(UGd)O <sub>2</sub> Nom
7.2	436	[					
22.2	644						
40.8	1109						
55.4	1189						
63.4	1204	]	3200	1986	2656	1558	1854

The rod internal pressure for the (UGd)O<sub>2</sub> (8 percent) calculation for the GESTR-M is not available. However, as seen from the independent confirmatory analyses, the internal rod pressure of the UO<sub>2</sub> rod is more limiting.

Although GE had consistently stated its plan to perform the necessary gamma scans to benchmark its currently licensed T-M methodology, as of this date, GE had not submitted specific schedule outlining when the additional internal rod pressure and exposure accounting qualification data will be submitted to the NRC. Therefore, GE's commitment is documented in this SE as limitation.

#### **LHGR and Exposure Qualification Limitation**

In MFN 06-481, GE committed to submit plenum fission gas and fuel exposure gamma scans as part of the revision to the T-M licensing process. The conclusions of the plenum fission gas and fuel exposure gamma scans of GE 10x10 fuel designs as operated will be submitted for NRC staff review and approval. This revision will be accomplished through Amendment to GESTAR II or in a T-M licensing LTR. PRIME (a newly developed T-M code) has been submitted to the NRC staff for review (Reference 58). Once the PRIME LTR and its application are approved, future license applications for EPU and MELLLA+ referencing LTR NEDC-33173P must utilize the PRIME T-M methods.

In addition, the most recent NRC staff evaluation of the GESTR-M T-M methodology and its qualification database provided in Appendix F includes a requirement to provide additional conservatism in determining the acceptability of the rod internal pressure. This NRC staff evaluation was performed in response to a GE Part 21 evaluation on the GESTR-M T-M methodology. Section 3.2.6.5.8 of this SE provides further information on the GE Part 21 Evaluation and corresponding NRC staff evaluation.

#### **3.2.6.5.6 TOP Confirmatory Analyses**

Since the qualification database did not extend to current exposures for the fuel centerline melt, NRC staff performed the confirmatory overpower analyses using FRAPCON. The calculation is based on single rod overpower initiated from the most limiting exposure of the LHGR envelope in terms of fuel centerline melt. The acceptance criterion for the TOP is the fuel centerline temperature remains below the incipient melting temperature. The calculation used GE14 fuel design for both UO<sub>2</sub> and (UGd)O<sub>2</sub> rods. The Gd-bearing rod calculations assumed 8 weight percent Gd.

The fuel centerline temperature for both the Gd-bearing rod and the UO<sub>2</sub> rod decreases with exposure. The (UGd)O<sub>2</sub> rod centerline melting temperature also decreases with the Gd concentration.

The calculation applied manufacturing tolerances that maximizes fuel temperature (e.g., maximum clad thickness, maximum crud/oxide). The confirmatory calculations results show that the (UGd)O<sub>2</sub> fuel rod is more limiting than the UO<sub>2</sub> fuel rod due to the lower fuel thermal conductivity.

The limiting fuel centerline temperature occurs at overpower from 16 GWd/MTU exposure. Examination of the Table 1 (Appendix C) shows that the UO<sub>2</sub> fuel rod is able to accommodate a 65 percent TOP condition, exhibiting a centerline fuel temperature of [            ]. The (UGd)O<sub>2</sub> fuel rod remains below fuel melt conditions with a 55 percent thermal power at [            ].

The modeling uncertainty related to the fuel temperature prediction increases significantly with burnup. At 16 GWd/MTU (knee in TMOL), the uncertainty is judged to be bounded by a

10 percent margin to the fuel centerline melt and the 1 percent cladding circumferential plastic strain acceptance criteria. Based on high confidence level, the NRC staff determined that GE14 fuel rod design can accommodate a TOP limit of 55 percent UO<sub>2</sub> and 45 percent (UGd)O<sub>2</sub> for the GE14 fuel rod design.

**Table 3-5** below summarizes the FRAPCON results for overpower initiated at 16 GWd/MTU. As can be seen from Table 3-5, a TOP of 55 percent provides a margin of 368 °F, which considering the 10 percent penalty provides sufficient margin. For 8 percent Gd content, Table 3-5 also shows that a TOP of 45 percent provides sufficient margin considering the reduction in the fuel melting temperature at 50 percent overpower.

**Table 3-5 FRAPCON TOP for UO<sub>2</sub> and UGdUO<sub>2</sub> rod**

FRAPCON TOP		
UO <sub>2</sub> : 13.4 kW/ft at 16 GWd/MTU		
Gd: 12.3 kW/ft 16 at GWd/MTU		
Rod Type	Overpower (%)	T centerline (°F)
UO <sub>2</sub>	45	[
UO <sub>2</sub>	55	
UO <sub>2</sub>	60	
UO <sub>2</sub>	65	
8 weight percent Gd	28	
8 weight percent Gd	40	
8 weight percent Gd	50	
8 weight percent Gd	55	]

\* FRAPCON 3.3 calculation/melt temperature

#### FRAPCON-GESTR-M TOP Comparisons

Table 9-2 of MFN 06-481 (Reference 25) provides the fuel centerline melt temperature of GE14 UO<sub>2</sub> rod and a 10 weight percent UGdUO<sub>2</sub> rod. Table 3-6 below provides the steady-state fuel temperature, the nominal overpower temperature, and the overpower fuel temperature based on the 95 percent confidence level. The UO<sub>2</sub> rod temperature calculations are based on 45 percent overpower initiated at the knee of the envelope (16 GWd/MTU). The Gd rod temperature calculations are based on 28 percent overpower initiated from 11.71 kW/ft knee of the 10 percent LHGR limit envelope.

#### UO<sub>2</sub> Rod calculation

For the steady-state temperature of the UO<sub>2</sub> rods at 16 GWd/MTU, the nominal FRAPCON and GESTR-M temperature are relatively close for code-to-code comparisons, differing by 152 °F. The differences become substantial once the 10 percent penalty is included in the FRAPCON calculation, with [ ] for GESTR-M and 3312 °F for FRAPCON. Although the RAI 9 response (Reference 25) did not specifically state, it is probable that the GESTR-M steady-state fuel temperature in Table 9-2 of Reference 25 is nominal value.

As can be seen in Table 3-6 below, the GESTR-M UO<sub>2</sub> overpower temperature with 95 percent [ ] is higher than the FRAPCON temperature calculation with 10 percent margin to the fuel centerline melt and that the 1 percent cladding circumferential plastic strain acceptance criteria (e.g., 4606 °F). Therefore, based on the confirmatory analysis, with the statistical treatment, the GESTR-M UO<sub>2</sub> overpower temperature prediction up to the knee in this case is reasonable and acceptable. The fuel centerline temperature is determined to be limiting at the knee of the envelope, in which case the LHGR envelope limit is reduced with exposure.

Both the FRAPCON and GESTR-M calculations show that the UO<sub>2</sub> rods have the capacity to withstand 45 percent overpower, while avoiding fuel centerline melt at the limiting exposure statepoint.

Table 3-6 below shows both the steady-state and 28 percent overpower fuel temperature for 10 weight percent UGdUO<sub>2</sub> rod temperature. The current BWR reloads are based on less than 7 percent Gd content, therefore the NRC staff confirmatory analysis is based on 8 percent Gd content. While direct one-to-one comparison cannot be made, the higher Gd content is expected to yield higher temperature for the same overpower. For 28 percent overpower, FRAPCON calculated 4175 °F for 8 percent Gd. As can be seen in Table 3-6, GESTR-M calculates a nominal temperature of [ ], which is higher than the FRAPCON 8 percent Gd calculations. The 10 percent Gd rod fuel temperature shows that fuel centerline temperature may not be avoided with 10 percent Gd content. However, the 10 percent Gd calculation is based on non-barrier fuel, which is more conservative. Currently, nonbarrier fuel is no longer loaded in BWRs. Table 3-7 shows changes in the fuel melting temperature with Gd concentration and exposure.

**Table 3-6. Fuel Centerline Temperature Results for GE14 UO<sub>2</sub> and 10 weight percent Gd Rod for Overpower at the Knee of the LHGR Limit Envelope**

GESTR-M Fuel Centerline Temperature					
Rod Type	Overpower (%)	TCenterline At Knee (°F, steady-state)	TOP Nominal T <sub>melt</sub> (°F)	TOP U95% T <sub>melt</sub> (°F)	T <sub>melt</sub> Acceptance Criteria (°F)
UO <sub>2</sub>	45	[			4987
10 weight percent Gd*	28			]	4954

\*13.40 kW/ft and 16.00 GWd/MTU pellet exposure for UO<sub>2</sub>.  
 11.71 kW/ft and 12.93 GWd/MTU pellet exposure for 10 weight percent Gd rod.

**Table 3-7 Fuel Melting Temperature as Function of Gadolinium Concentration and Exposure**

Exposure (GWd/MTU)	Gadolinium Concentration (weight percent)				
	UO2	6%	7%	8%	10%
0	[				
5					
10					
12.93					
15					
16					
20					
25					
30					
35					
40					
45					
50					
55					
60					]

$$T_{melt} = 5080 - 4.68G - 0.0036G^3 - 5.8B$$

Where G is the Gadolinium concentration in weight percent and B is the burnup in GWd/MTU

#### Licensing of 10 Percent UGdUO<sub>2</sub>

It appears that GE has not submitted the T-M LTR for the use of 10 weight percent Gd in licensing applications. Therefore, before applying 10 percent Gd, GE must submit the T-M LTR demonstrating that the fuel centerline melt and 1 percent strain acceptance criteria can be met for overpower conditions expected of EPU and MELLLA+ operation overpower response and other T-M criteria for normal operation and AOOs. The inclusion of 10 weight percent data in RAI 9 response does not mean that through LTR NEDC-33173P, the NRC approved the use of 10 weight percent Gd.

In addition, the NRC staff did not review or approve the use of 10 weight percent Gd for fuel designs for operating reactors. Specifically, TGBLA06 has not been qualified for Gd loadings above 8 weight percent.

#### **Application of 10 Weight Percent Gd Limitation**

Before applying 10 weight percent Gd to licensing applications, including EPU and expanded operating domain, the NRC staff needs to review and approve the T-M LTR demonstrating that the T-M acceptance criteria specified in GESTAR II and Amendment 22 to GESTAR II can be met for steady-state and transient conditions. Specifically, the T-M application must demonstrate that the T-M acceptance criteria can be met for TOP and MOP conditions that bounds the response of plants operating at EPU and expanded operating domains at the most limiting statepoints, considering the operating flexibilities (e.g., equipment out-of-service).

Before the use of 10 weight percent Gd for modern fuel designs, NRC must review and approve TGBLA06 qualification submittal. Where a fuel design refers to a design with Gd-bearing rods adjacent to vanished or water rods, the submittal should include specific information regarding acceptance criteria for the qualification and address any

downstream impacts in terms of the safety analysis. The 10 weight percent Gd qualifications submittal can supplement this report.

TOP Conclusion

Based on the FRAPCON confirmatory analysis and the data provided for the UO<sub>2</sub> rod with 95 percent confidence, there is reasonable assurance that the GESTR-M overpower fuel temperature up to the knee of the GE14 LHGR limit is acceptable. The confirmatory analysis indicates that the UO<sub>2</sub> rod can accommodate a TOP of 55 percent.

The NRC staff concludes the plant-specific application will demonstrate that for both the UO<sub>2</sub> and the UGdUO<sub>2</sub> rods the steady-state and transient overpower response will meet the acceptance criteria. In addition, the adequacy of GESTR-M modeling of the fuel temperature and an associated Part 21 evaluation is discussed further in Section 3.2.6.5.8, "Part 21 Evaluation," of this SE.

3.2.6.5.7 MOP Confirmatory Analysis

The MOP acceptance criterion is that cladding strain be limited to 1 percent plastic strain. Manufacturing tolerances were selected to maximize fuel thermal expansion and clad stress (e.g., minimum clad thickness, maximum fuel pellet diameter, maximum crud/oxide). Based upon comparable strain at lower power levels, the (UGd)O<sub>2</sub> fuel rod is slightly more limiting than the UO<sub>2</sub> fuel rod.

Examination of the Table C-1 (Appendix C) results reveal that the UO<sub>2</sub> fuel rod is able to accommodate 65 percent MOP, with a circumferential permanent strain of 0.67 percent (0.85 percent total). The (UGd)O<sub>2</sub> fuel rod experiences a circumferential permanent strain of 0.66 percent (0.84 percent total) with a 65 percent MOP.

The FRAPCON-3 algorithms are tuned to produce best-estimate predictions. Even though manufacturing tolerances are set at worst case, the modeling uncertainty (which represents the spread in the empirical database) needs to be accounted for. The modeling uncertainty related to predicted fuel swelling and cladding strain is high, especially as burnup increases. The spread in empirical data for power ramp tests may exceed 50 percent. As a result, an uncertainty on the best-estimate FRAPCON cladding strain calculations should be approximately 50 percent. Based upon the calculated strains and a 50 percent uncertainty in the model accuracy, a high confidence MOP for both UO<sub>2</sub> and (UGd)O<sub>2</sub> fuel rods would be 55 percent. Table 3-8 shows that at 55 percent MOP based on 50 percent uncertainty in the model, sufficient margins exists for the 1 percent strain acceptance criteria. No GESTR-M MOP data was available to make equivalent comparisons, however the criteria is expected to be met, since the TOP sets the limit.

**Table 3-8 Confirmatory FRAPCON MOP (UO<sub>2</sub> rod and UGdUO<sub>2</sub> rods)**

<b>FRAPCON MOP</b>		
<b>UO<sub>2</sub>: 13.4 kW/ft at 16 GWd/MTU</b>		
Gd: 12.3 kW/ft 16 at GWd/MTU		
<b>Rod Type</b>	<b>Overpower (%)</b>	<b>Strain<sub>Total</sub> %</b>
UO <sub>2</sub>	45	0.60
UO <sub>2</sub>	55	0.72
UO <sub>2</sub>	65	0.85
8 weight percent Gd	45	0.60
8 weight percent Gd	55	0.72
8 weight percent Gd	65	0.84



### 3.2.6.5.8 Part 21 Evaluation

In a separate ESBWR design certification review, the NRC staff discovered a discrepancy in the GESTR-M T-M calculations, supporting the GE14 fuel designs. Specifically, the NRC staff discovered that the GESTR-M under-predicted the UO<sub>2</sub> fuel temperature calculations in comparison to both FRAPCON-3 and PRIME calculations for high exposures. PRIME is a new T-M code, which GE used for sensitivity analysis in response to ESBWR RAIs. From the review of the ESBWR, the NRC staff attributed the observed differences were primarily due to GESTR-M UO<sub>2</sub> fuel thermal conductivity model, which does not model exposure dependency compared to the other two codes. The concern seems to lie in GESTR-M UO<sub>2</sub> temperature calculation with exposure.

Currently, the same GESTR-M is used in both ESBWR and the operating reactors; therefore the issue was pursued further for operating reactors in general and in this review in particular. The NRC staff asked GE to initiate a Part 21 evaluation to determine the safety significance and adequacy of GESTR-M fuel temperature calculations. NRC staff requested GE to evaluate the overall conservatism of GESTR-M fuel T-M models, specifically the predicted fuel temperatures, against the most up-to-date expanded empirical database (e.g., database used to validate PRIME). As part of the Part 21 evaluation, the NRC staff asked GE to demonstrate the impact of burnup degradation in UO<sub>2</sub> thermal conductivity on the T-M calculations, fuel design analysis and the downstream safety analyses.

On January 21, 2007, GE submitted MFN 07-040 letter, "Part 21 Notification: Adequacy of GE Thermal-Mechanical Methodology, GESTR-M," (Reference 57). The letter provided an assessment of the GESTR-M fuel rod temperature prediction with exposure. It compared both the GESTR-M and PRIME against fuel centerline temperature measurement data. By letter dated January 19, 2007 (Reference 58) GNF submitted a TR for the PRIME Model for Fuel Rod Thermal-Mechanical Performance for NRC staff review and approval. The comparisons show non-conservative exposure dependent bias in the GESTR-M temperature predictions. The Reference 57 letter also identified the key fuel design parameters and safety analyses that will be affected by fuel rod centerline temperature under-prediction and justified the impact. GE's conclusions are as follows:

The primary parameters in fuel thermal-mechanical calculations, fuel design analyses and downstream safety analyses that are impacted by fuel temperature are fuel centerline melting, cladding strain, loss-of-coolant accident (LOCA) response, and fuel rod internal pressure. [

]. Therefore, GESTR-M and its associated statistical methodology are adequate for fuel licensing and design calculations within its qualification domain...

Reference 57 letter also states:

Additionally, GNF has developed a new fuel rod thermal-mechanical model to support high exposure fuel designs ... This model will be submitted to NRC for review and approval, and will be incorporated into the GNF new fuel rod design and licensing process upon approval.

The NRC staff considers this to be a commitment to migrate to PRIME upon NRC staff approval. However, the commitment seems to be limited to new fuel introduction. Therefore the "LHGR and Exposure Qualification" limitation of this SE requires migration and use of PRIME upon NRC staff approval for all future EPU and MELLLA+ applications.

The NRC staff needed to evaluate appropriately the technical merit of GE's Part 21 evaluation. At the time the draft SE for NEDC-33173P was issued to the Advisory Committee for Reactor Safeguards (ACRS), the GE Part 21 was still being evaluated by NRC staff. Therefore, the following limitation associated with the GESTR-M fuel temperature calculation was imposed at the time of issuance of the draft SE, to capture that any conclusions from the NRC staff evaluation of GE's Part 21 report would be applicable to the GESTR-M T-M assessment in this SE.

#### **Part 21 Evaluation of GESTR-M Fuel Temperature Calculation Limitation**

Any conclusions drawn from the NRC staff evaluation of the GE's Part 21 report will be applicable to the GESTR-M T-M assessment of this SE for future license application. GE submitted the T-M Part 21 evaluation, which is currently under NRC staff review. Upon completion of its review, NRC staff will inform GE of its conclusions.

The NRC staff completed its evaluation of GE's Part 21 evaluation (Reference 57), which is provided in Appendix F. The NRC staff evaluation concluded that although the GESTR-M best estimate calculation under-predicts the fuel centerline temperature, the conservative uncertainty treatment compensates for the under-prediction, resulting in bounding 95/95 fuel centerline temperatures. The NRC staff concludes that the GESTR-M fuel temperature calculation with the 95 percent uncertainty treatment is acceptable.

In Appendix F, the NRC staff evaluated the adequacy of GESTR-M methodology and its qualification database to determine the licensing rod internal pressures. Regarding the rod internal pressure calculation, the NRC staff concludes that the adequacy of the GESTR-M uncertainty treatment needs to be confirmed through measurement qualification data and corrected for licensing applications. Therefore the NRC staff position as provided in Appendix F is applicable for GESTR-M rod internal pressure calculations.

In response to the NRC staff concerns, GE now plans to revise the GESTR-M Part 21 evaluation. Preliminary discussions reveal that GE will identify conservative aspects of the rod internal pressure calculation methodology that compensate for the potential non-conservative UO<sub>2</sub> fuel temperature calculation. The revised Part 21 evaluation will conclude that the overall methodology remains conservative and that the proposed 350 psi penalty on P-critical (from Appendix F) is not required. Based upon initial discussions, it appears that GE's goal is achievable. The NRC staff will assess the adequacy of the revised Part 21 evaluation when it becomes available. Until then the NRC staff conclusions in Appendix F remain in effect.

#### **3.2.6.5.9 Overall T-M Methodology Conclusion**

The objective of the interim evaluations of GE's thermal mechanical (T-M) methodology is to: (1) evaluate changes in the fuel T-M performance at EPU and the proposed MELLLA+; (2) assess the conservatisms of the T-M methodology; (3) evaluate the applicability of the experimental qualification database supporting the T-M methodology; (4) establish if there is a need to expand the supporting qualification database in order to achieve additional confidence in the accuracy of the methods; and (5) identify the necessary corrective actions required in the application of the T-M methodology to operation at the EPU and the proposed expanded domains.

The NRC staff concludes that:

1. The core design required in order to achieve a 24-month cycle length and operation at EPU and MELLLA+ could affect the fuel T-M performance, during steady-state and transient conditions. The number of maximum powered bundles operating near the LHGR limit during steady-state increases. In addition, the higher plant response during transients could increase the fuel pellet overpower response, depending on the specifics of the core design utilized to achieve the energy needs for operation at EPU and MELLLA+.
2. The power distribution uncertainties applied and the assumptions in the development of the T-M limits (e.g., operating history assumptions) provide some confidence in the conservatism in the T-M model.
3. Plant-specific EPU and MELLLA+ applications will demonstrate and document that during normal operation and core-wide AOOs, the thermal mechanical acceptance criteria as specified in Amendment 22 to GESTAR II will be met. Specifically, during an AOO, the licensing application will demonstrate that the: (1) loss of fuel rod mechanical integrity will not occur due to fuel melting and (2) loss of fuel rod mechanical integrity will not occur due to pellet-cladding mechanical interaction. NRC-approved methods will be used to perform these analyses. The plant-specific application will demonstrate that the T-M acceptance criteria are met for both the  $UO_2$  and  $GdO_2$  rods, whose T-M performance differ.
4. To account for the impact of the void history bias, plant-specific EPU and MELLLA+ applications will demonstrate 10% margin to requirements for fuel centerline melt and the 1 percent cladding circumferential plastic strain due to pellet-cladding mechanical interaction, for the most limiting AOO transient events, including equipment out of service.
5. The licensing process does not include reporting of the fuel overpower performance, although the fuel design requirements include demonstrating that the SAFDLs should be met during AOOs. Each EPU and MELLLA+ fuel reload will document in the SRLR the calculational results of the analyses to demonstrate compliance to transient thermal mechanical acceptance criteria.
6. NRC staff evaluation of the T-M qualification data indicates that the current database does not extend to the current fuel designs and need to be expanded to the current fuel designs and exposures. GE intends to perform additional scans as presented to the NRC staff (Reference 31), as stated in the initial RAI 28-1 response (Reference 3) and as committed to in RAI 9 response (Reference 25). The NRC staff agreed with this proposal and the NRC staff approval of LTR NEDC-33173P (Reference 1) relies in the long-term on the confirmations of the internal rod pressures and the exposure for the GE14 fuel up to the licensed exposure. The confirmation will also include extension of the fuel temperature data to the current licensed exposures.
7. The conclusions of the plenum fission gas and fuel exposure gamma scans will be submitted for NRC staff review and approval and inclusions in the T-M licensing process. This can be accomplished by supplementing LTR NEDC-33173P (Reference 1), amending GESTAR II, or including it in the benchmarking of the PRIME T-M models.
8. The NRC staff best-estimate analyses with some penalty show that the GE14 fuel can accommodate TOP and MOP values that are within the ranges of the Amendment 22 to GESTAR II TOP and MOP for both the  $UO_2$  and  $(UGd)O_2$  rods. The observed GSTR-M/FRAPCON differences indicate some potential non-conservatism in

GESTR-M fuel temperature calculations, but with statistical treatment the GESTR-M calculation is acceptable up to the limiting envelope knee of [ ] for the UO<sub>2</sub> rod. Regarding the rod internal pressure calculation, the NRC staff concludes that the adequacy of the GESTR-M uncertainty treatment needs to be confirmed through measurement qualification data and corrected for licensing applications. Therefore the NRC staff position as provided in Appendix F is applicable for GESTR-M rod internal pressure calculations.

9. The Gd rod sets the overpower limit. Any increases of the Gd concentration should be scrutinized to ensure that the T-M evaluation is based on overpower conditions characteristic of EPU and expanded operating domains.
10. This review does not approve the use of 10 percent Gd concentration, unless GE demonstrates that the use of the 10 percent Gd was specifically approved through licensing action.

Based on the assessment covered in this section, the insights from the confirmatory analyses, the NRC staff concludes that the application of the current T-M methods to EPU and MELLLA+ are acceptable with compliance to the associated limitations.

### 3.2.7 Fuel Rod Exposure

An exposure limit is applied to the GE fuel designs to ensure that fuel integrity is maintained and that the fuel is not operated beyond the basis supporting the thermal mechanical limits. For the fuel of interest, GE14, the local exposure limit is 70 GWd/MTU (Reference 1). The fuel exposure is directly related to the integrated LHGR over the course of the fuel exposure and is monitored via the plant process computer to ensure that the limit is not exceeded. Therefore, the ability to predict and monitor the exposure is directly related to the ability to monitor the LHGR and is subject to the same biases and uncertainties applied to LHGR.

In Reference 1 and 29, GE stated that near the exposure limit the fuel rod T-M parameter of most interest is the internal rod pressure. In the fuel rod T-M calculation, the fuel rod is assumed to operate on the exposure dependent LHGR curve over its entire lifetime without exceeding the internal rod pressure criteria. Given that the pellet exposure resulting from operation this LHGR curve would greatly exceed the licensed exposure, this evaluated fuel rod internal pressure conservatively bounds the conditions that result in actual operation. The justifications provided are that even if the peak pellet exposure is exceeded, when the monitored condition is at the peak exposure limit, the fuel integrity is not challenged given the level of conservatism assumed in the fuel T-M analysis.

However, the fact still remains that there are no exposure accounting measurements to confirm the accuracy of GE's methods for the current fuel design and operating strategies. In the response to RAI 9 (Reference 25), GE committed to perform the exposure gamma scans as well as the associated fission gas gamma scans. The NRC staff considers the exposure benchmarking important, because a hot rod can accumulate higher exposure early in its core resident life and remain in the core. The NRC staff will track the RAI 9 commitment to ensure that the qualification data is submitted for NRC staff review and approval. The NRC staff should request that GE includes the status of this item in the annual fuel design meeting agenda.

Considering the margins demonstrated in the internal pressure calculation and that the peak pellet exposure is monitored via the process computer, the NRC staff concurs with the GE assessment that in the interim, no additional conservatism in the fuel exposure limited is necessary to maintain the fuel integrity.

### 3.2.8 Shutdown Margin

The regulation at 10 CFR Part 50, Appendix A, GDC 26, “reactivity control system redundancy and capability,” states:

Two independent reactivity control systems of different design principles shall be provided. One of the systems shall use control rods, preferably including a positive means for inserting the rods, and shall be capable of reliably controlling reactivity changes to assure that under conditions of normal operation, including anticipated operational occurrences, and with appropriate margin for malfunctions such as stuck rods, specified acceptable fuel design limits are not exceeded. The second reactivity control system shall be capable of reliably controlling the rate of reactivity changes resulting from planned, normal power changes (including xenon burnout) to assure acceptable fuel design limits are not exceeded. One of the systems shall be capable of holding the reactor core subcritical under cold conditions.

The CR based system uses the control blades and the core designs are developed such that the reactor will be in a subcritical configuration at cold (20 °C), xenon-free conditions with all control blades inserted and the strongest reactivity worth blade fully withdrawn at any point in the cycle. The difference between the effective multiplication factor for this state and unity is known as the SDM. In order to ensure that the system will not be critical the reactor core design must be such that the SDM exceeds the uncertainties and biases that exist in the nuclear analysis methods and in knowledge and variability of the fuel parameters used as input in the SDM calculations.

The SDM is dependent on the prediction of the fuel exposure, isotopic compositions, and reload batch size and enrichment, all of which are impacted at EPU conditions. As will be discussed below, the SDM relies on the calculation of the exposure and isotopic conditions in the core, and therefore, is subject to the accuracy of the neutronics methods, which must be confirmed with measurements. Given the impact of EPU operation on these parameters and little available data for validation of the neutronics methods, an assessment of adequacy of the SDM was performed along with a review of supporting data. The NRC staff evaluated the cold critical demonstration data to establish if there are any changes in the code predictions for the EPU core configurations and operating conditions.

#### 3.2.8.1 Cold Critical Demonstration

An SDM demonstration is performed after each outage to ensure the SDM is met. This demonstration consists of the comparison of the cold critical condition during startup (an in-sequence demonstration) with the calculated criticality at the same CR position to determine the difference in the calculated criticality and the demonstrated criticality. The worth of the strongest CR in this in-sequence test is based on calculations. The SDM requirement for this in-sequence cold critical demonstration is 0.38 percent  $\Delta k/k$  and is given by the following:

$$k_{sro} \leq k_{demo}(1 - 0.0038),$$

where  $k_{demo}$  is the calculated eigenvalue corresponding to the cold critical configuration and  $k_{sro}$  is the calculated eigenvalue for the strongest-rod-out configuration. The 0.0038 value is a two standard deviation value of the combination of uncertainties evaluated to account for reactivity effects associated with fuel manufacturing tolerances, variations in the predictive capability of the neutronics methods, and variations in exposure on the critical configuration.

The accuracy in the prediction of the SDM, therefore, depends on the accuracy of the neutronics methods to predict the distributed criticality (corresponding to  $k_{demo}$ ) and local

criticality (corresponding to  $k_{sro}$ ). A distributed critical configuration is represented by the in-sequence cold critical measurement, where control rods are pulled in a relatively uniform manner in all regions of the core. A local critical configuration is represented by a configuration in which the core becomes critical with a relatively small number of adjacent control blades removed. The local cold critical provides a demonstration of ability to predict the worth of the strongest-rod-out configuration.

The accuracy of the prediction of the cold critical eigenvalues is indicated in Figure 3-16 for five Reference Plants. This figure shows a comparison of the actual and projected cold critical eigenvalues for both local and distributed measurements. The majority of the data is provided for Plant C, which is a small [ ] (see Table 3-15). In most cases the actual eigenvalue is lower than the projected eigenvalue, which is conservative in terms of SDM. Further evaluation of the local criticality measurements for Plant C will be discussed below.

In the response to RAI SBWB-28 (Reference 49) recent cold critical demonstration data was provided for Browns Ferry Units 2 and 3 based on in-sequence measurements. Local critical measurements are not available. The results provided for six measurements indicate that all but one case is within 0.2 percent  $\Delta k/k$ . The remaining case differs by [ ], which exceeds the SDM requirement. However, because of the use of a [ ] design SDM, this case still meets the 0.38 percent  $\Delta k/k$  requirement. However, this reflects the need for additional margin in the SDM calculations to compensate for potentially higher model uncertainties.

The impact of EPU operation was assessed by the review of data provided in request to RAI 2.2 of MFN06-195 (Reference 10), which provides data for three successive cycles (23, 24, and 25) for a plant that began EPU operation in Cycle 25 (see Figure 3-15). However, both Cycles 24 and 25 were designed for EPU operation. The data provided indicates that there is essentially no change in the cold critical prediction based on EPU core designs.

### 3.2.8.2 Accuracy of the Prediction of the Strongest Blade

Since the worth of the strong rod is based solely on calculations and is not directly demonstrated in the in-sequence startup, it is necessary that the accuracy of the prediction of the worth strongest rod be evaluated. Should the worth of the strongest rod be under-predicted by the calculational methodology, the available SDM will be over-predicted and the in-sequence cold critical demonstration will not be sufficient to ensure that the SDM is met.

Local cold critical measurements are performed at some plants and on an infrequent basis. These local cold critical measurements can be used to assess the calculation accuracy of the neutronics methods for the worth of the strongest rod. In MFN 06-195 (Reference 10), data were provided to demonstrate the accuracy of the prediction of both distributed and local critical measurements for high power density plants. The overall standard deviation of prediction of the cold critical eigenvalue was [ ], with the repeatability of the prediction of the cold critical eigenvalue for the same core of [ ]. In response to RAI 2.1 (Reference 10), GE extracted the local critical measurements to allow the assessment of the accuracy of the local cold critical measurements and calculated values. The standard deviation of the differences between the test data and the design basis multiplication factor for these local critical measurements is [ ]

].

### 3.2.8.3 Design Shutdown Margin

In addition to the uncertainties discussed above, GE has historically applied a design margin of [ ] SDM to ensure that the 0.38 percent  $\Delta k/k$  requirement is met. According to Reference 2, this larger design margin is to account for the following factors that affect the prediction of the SDM:

1. [
- 2.
- 3.
- 4.
- 5.
6. ]

GE reports that the largest variation is due to the allowance for operation different from that projected which are related to the flexibility required for operational variations.

### 3.2.8.4 Assessment

The data provided by GE in support of the assessment of the accuracy of the cold critical predictions supports the SDM requirement of 0.38 percent. Given that the in-sequence cold critical demonstration relies on calculation of the worth of the strongest rod, additional review of the prediction accuracy for local critical measurements was performed. Based on the data provided, the accuracy of the local critical predictions, including a [ ], indicates acceptable accuracy of the prediction of local critical states. Per Section 2.3.2 of LTR NEDC-33173P (Reference 1), the normal design SDM is taken as [ ] to ensure that the 0.38 percent margin is met primarily to account for the range of items above. The use of this increased margin is highly recommended and has been shown to be necessary to ensure that the 0.38 percent margin is met.

The review of local critical data indicates that the accuracy of the prediction worth of the strongest rod is acceptable when including [ ]. However, additional data to support the accuracy of the prediction of the worth of the strongest rod is desired. The accuracy of local criticality prediction should also be considered for future significant changes in operating conditions and core designs.

It is recommended that SDM demonstration be included in inspections to ensure that there are no trends in the reduction in SDM with operation at EPU and expanded domains for plant-specific applications of LTR NEDC-33173P (Reference 1).

### 3.2.9 Standby Liquid Control System

The second, independent shutdown system is the SLCS in which soluble boron is introduced into the core to maintain the core in a subcritical condition. The requirement for the SLCS shutdown is provided in the TS, which gives the minimum soluble boron concentration that is to maintain the core in the subcritical condition. Calculations are performed as a function of exposure throughout the cycle to determine the minimum SLCS SDM during the cycle.

The GESTAR methodology specifies that the SLCS analysis be performed at the TS boron value and at the maximum reactivity conditions with no xenon present. In addition, the current

GE process is to assume an [ ]].

There is no demonstration of the SLCS shutdown capability, and therefore the calculational SDM must account for all biases and uncertainties. The determination of uncertainties is based on comparisons of TGBLA with a benchmark MCNP code, the bias and uncertainty in the MCNP code based on borated cold critical experiments, and bias and uncertainty in the assumed cold critical eigenvalue for PANACEA, the core simulator. The roll-up of the biases and uncertainties is on the order of [ ], depending upon the specific methods (code versions) and fuel production line.

The impact of operation at EPU and MELLLA+ on SLCS margins is related to the overall ability of the methods to compute the core reactivity. Such cores may have higher reload batch fractions and the burned fuel may have differing isotopic compositions than non-EPU cores. Since the soluble boron is distributed throughout the core, the SLCS SDM is determined more by core-wide reactivity effects rather than local effects (exposure and isotopic content). Therefore, the assessment of the ability of the nuclear methods to predict the SLCS margin is based on their ability to compute the core reactivity along with the ability to predict soluble boron worth. Based on the results provided for the cold critical demonstration (Section 3.2.8.1 of this SE) and the analysis of the one-rod-out SDM, the biases and uncertainties for the cold critical calculations for EPU core designs are similar to those for non-EPU core designs. The prediction of soluble boron worth is confirmed by the comparison of TGLBA with MCNP code results. The accuracy of lattice physics data generated at different boron conditions will factor into the calculation of the SLCS SDM. However, in this review the NRC staff did not perform code-to-code comparisons to assess TGBLA generated boron libraries.

Based on this assessment above and the additional level of conservatism resulting from the all-rods out assumption, the SLCS calculational procedure remains applicable to EPU and MELLLA+.



**Table 3-9 TRACG Impact of High Exposure Void Coefficient Bias**

[

]

**Table 3-10 GE14 LHGR Limit**

<b>Exposure (GWd/MTU)</b>	<b>LHGR (UO2) kW/ft</b>	<b>Exposure (GWd/MTU)</b>	<b>LHGR (6% Gd)</b>
0.0	[	0	[
16		5	
63		13.53	
70	]	60.625	
		67.067	]

**Table 3-11 LHGR Power Distribution Uncertainty Components**

<b>Component</b>	<b>NEDC- 32601</b>	<b>Revised</b>
Infinite Lattice Pin Power Peaking	[	
Manufacturing Uncertainties		
Gradient Effect Uncertainty		
Channel Bow Uncertainty		
PaI Uncertainty		
TIP Uncertainty		
P4B Uncertainty		
Update Uncertainty		
Total Uncertainty		]

**Table 3-12 Internal rod pressure as function of exposure**

[



]

**Table 3-13 Effect of Early Life LHGR Variation GE14 Six Weight Percent Gd2O3-UO2**

[



]



[

**Figure 3-1 Cold Critical Eigenvalue Tracking**

]

[

**Figure 3-2 Hot Critical Eigenvalue Tracking**

]

[

]

**Figure 3-3 Hot Critical Eigenvalue Tracking for Plant E**

[

]

**Figure 3-4 Gamma and Thermal TIP Power Distribution Uncertainties**

[

**Figure 3-5 Four-bundle uncertainty**

]

Note: Plant B, Cycle 9 and Plant E, Cycle 9 core monitoring and offline calculations are based on PANAC10

[

**Figure 3-6 Axial RMS Uncertainty**

]

Note: Plant B, Cycle 9 and Plant E, Cycle 9 core monitoring and offline calculations are based on PANAC10



[

**Figure 3-7 Nodal RMS Uncertainty**

Note: Plant B, Cycle 9 and Plant E, Cycle 9 core monitoring and offline calculations are based on PANAC10

[

**Figure 3-8 Axial Void Profile (R-factor Calculation)**

]

[

**Figure 3-9 Bundle R-factor and Estimated CPR Response**

]

[

**Figure 3-10 Bundle 2 RIP and Estimated SLMCPR Impact**

]

[

**Figure 3-11 Lattice 7009 Void Coefficient Comparisons**

]

[

**Figure 3-12 EPU LHGR Operating History**

]

[

**Figure 3-13 GE14 Six Weight Percent Gd<sub>2</sub>O<sub>3</sub>-UO<sub>2</sub> LHGR Operating Limit and Analysis Basis**

[

**Figure 3-14 Six Percent Gd-bearing Rods Operating History for EPU plant**

]

[

**Figure 3-15 Sensitivity of Cold Critical Eigenvalue to EPU Operation**

[

**Figure 3-16 Difference Between Actual and Projected Cold Critical Eigenvalues**

]

]

#### 4.0 40 PERCENT VOID FRACTION DEPLETION ASSUMPTION

The reactor core response during transient situations is highly dependent upon the changes in reactivity with changes in void content in the coolant. The impact of changes in the void content is accounted for in cross-sections and lattice physics parameters in GE nuclear methods cross-section model. The NRC staff evaluated GE's neutronic methods to evaluate the impact of void history bias on the void reactivity coefficient.

##### 4.1 ASSESSMENT OF IMPACT ON VOID REACTIVITY COEFFICIENT

The reactor core response during transient situations is highly dependent upon the changes in reactivity with changes in void content in the coolant. The impact is measured by computing a void reactivity coefficient, which is defined as follows:

$$\text{Coolant Void Reactivity Coefficient} = 1/k (dk/d\alpha)$$

In the above equation,  $k$  is the multiplication factor and  $\alpha$  is the void fraction. Since a derivative is involved, the coolant void reactivity coefficient is essentially proportional to the slope of the  $k$  versus void fraction curve. A different shape in the  $K_{inf}$  versus void fraction for a particular lattice would be expected for lattices that have been depleted with different historical void fractions because they will experience a different neutron spectrum resulting in different plutonium content. Therefore, it is expected that the void reactivity coefficient will have some variation with the historical void fraction used in the lattice depletion.

The transient analysis code ODYN performs a one-dimensional analysis of the core using cross-sections that are determined via GE's cross-section model. This approach involves using the TGBLA lattice physics code to perform depletion calculations for a particular lattice at 0 percent, 40 percent, and 70 percent void fraction. These "historical" cases are important for capturing the change in the isotopic composition of the fuel with exposure and void fraction. In addition, instantaneous changes in the void fraction are performed for the [ ] to capture the change in the cross-sections for the IV changes that would occur in transients. [ ]

[ ] used to determine cross-sections at other instantaneous and historical void fractions (the fitting procedure actually uses water density as the independent variable).

Therefore, while ODYN does not specifically use a void reactivity coefficient, the sensitivity study/uncertainty studies performed with ODYN consider a specific value for the uncertainty in the void reactivity coefficient. For example, the analysis performed in response to plant-specific RAI (VYNPS RAI SRXB-A-68; Attachment 1 to Reference 30), assumes a [ ] uncertainty. However, given that the void reactivity coefficient is sensitive to the plutonium content and that [ ]

[ ], an investigation of the potential error in the void reactivity coefficient is warranted. In addition, errors related to the extrapolation [ ]

To assess the potential impact of the [ ] assumption on the void reactivity, the NRC staff requested ORNL to perform confirmatory analyses. ORNL performed confirmatory analyses using the HELIOS code system. The calculations were performed for a lattice with high enrichment, gadolinium loading, and with vanished rods typical of the upper portion of the fuel bundles. The calculations were performed for bundle exposures up to 60 GWd/t and for instantaneous and historical void fractions ranging from 0 to 90 percent.

Comparisons of the void reactivity coefficients for the different void history cases and exposures based on ORNL HELIOS calculations are presented in Figure 4-1 and Figure 4-2. Note that additional instantaneous branch points were calculated at the higher void conditions to resolve the non-linearity of the void coefficient with respect to IV fraction at high fuel exposures. The impacts of the different void histories are evident at the higher void fractions with the increasing differences in the void reactivity profiles with increasing exposure. The difference in the profiles [ ] represents a potential error resulting from GE's methodology. The errors for exposures of about 30 GWd/ST and less are consistent with the [ ] assumed in the ODYN analysis. However, for higher exposures at high void fractions the error increases [ ]. In addition, the deviation of the void reactivity from a linear variation represents an error that results from the quadratic extrapolation used in GE's methodology. As shown in these figures, at high void fractions and high exposures the profile deviates from linear.

The GE approach to cross-section parameterization and fitting [ ] combined with the assumption that the change in cross-sections with instantaneous change in voids is not sensitive to the void history, results in a substantially larger error in the void reactivity coefficient than assumed in the ODYN uncertainty analysis, particularly at high fuel exposures. The NRC staff determined that the impact of these increased errors on the response of the core during a transient needed to be evaluated to ensure that there is no impact on the core transient response.

However, criteria applied to the fuel are also exposure dependent (e.g., LHGR), and therefore it is important to provide a demonstration that the fuel integrity is not compromised in the event of a transient event.

#### 4.2 GE EVALUATION OF INCREASED VOID COEFFICIENT UNCERTAINTY

Section 2.2.2 of LTR NEDC-33173P (Reference 1) covers GE's void reactivity coefficient analyses. Additional expanded discussion is presented in response to NRC staff RAI SRXB-A-RAI 68 (Attachment 1 to Reference 30). GE evaluated the errors in the void coefficient resulting from the cross-section model as described above. The model assumptions that have a significant impact on the void coefficient are:

1. [ ]  
[ ]].
2. The assumption that the void reactivity coefficient determined at a [ ] condition applies to all other void histories. At high exposures the difference in isotopic compositions resulting from differing void histories results in significantly different void reactivity coefficients.

GE considered the cross-section model impacts separately for exposures less than [ ] and greater than [ ]. The calculation and comparison of the void coefficients at exposures of less than [ ] indicated that the void reactivity coefficient errors were within those assumed in the ODYN  $\Delta$ CPR/ICPR uncertainty analysis. The results for exposures greater than [ ] are shown in Figure 4-3 as a ratio of the MCNP to TGBLA06 void coefficients, and are quite similar to the confirmatory results discussed above. These relatively large differences required additional analysis to ensure that they do not result in a significant impact on safety parameters.

To justify the potential under-prediction of void reactivity coefficient in the top portion of the core experiencing the high voids, LTR NEDC-33173P (Reference 1) provided additional assessment of the behavior of the void reactivity. LTR NEDC-33173P (Reference 1) states that typical plot of the void-quality relationship shows that [

]. Small power changes in the lower quality range correspond to a [ ] void fraction change. In general, the void coefficient becomes more negative with increasing core average void fraction. However, in general the net power effect considering the void-quality behavior is that core power response is [

].

GE states that the void coefficient uncertainties and biases also have a [

].

GE adds that Figure 4-5 depicts the relative difference, which was derived from the void and quality values relationship in Figure 4-4 [

]. Figure 4-5 shows the reactivity effect of a small quality perturbation ( $\Delta X = 0.001$ ) using a representative void coefficient over a range of void fraction values.

[

].

[

].

[

].

[

].

[



].

[

].

#### 4.3 IMPACT OF VOID COEFFICIENT UNCERTAINTIES ON ATWS

For an isolation ATWS event, closing the MSIV causes a rapid increase in reactor vessel pressure, which results in core void reduction and an associated power increase. A recirculation pump trip (RPT) is initiated on high pressure and the core flow begins to decrease. When the steam production decreases to the point at which the SRV capacity is sufficient to relieve all of the steam generation, the pressure and core power begin to fall. To reduce further the core power, the vessel water level is lowered, which uncovers the feedwater spargers and reduces the subcooling. Boron injection through the SLCS is initiated if the suppression pool begins to heat up or oscillations are developed.

Typically, the limiting criteria for ATWS events are: (1) the early pressure rise must not result in pressures higher than the ASME Level C criteria for the weakest link in the primary (typically 1500 psi), and (2) the suppression pool temperature must remain low enough to prevent over-pressurization of the containment to the point where it may fail. Criterion 1 is challenged in the early phase of the transient (less than one minute) and Criterion 2 is challenged at the end of the transient (20 to 30 minutes after initiation for stand-pipe BWRs).

The neutronic methodology errors will affect an ATWS through the void reactivity coefficient. An increase of void coefficient magnitude has two competing effects:

1. The initial pressure increase after MSIVC will result in a larger power response, which in turn will increase the pressure further; and
2. The flow reduction after the RPT, results in a larger reduction of core power due to the re-voiding effect.

[

].

[

].

[

].

[

].

[

].

[

].

#### 4.4 VOID REACTIVITY CONCLUSION

[

].

Based on the NRC staff confirmatory analyses, the content of the RAI responses, the assessment and justifications presented in LTR NEDC-33173P (Reference 1), the evaluation of the sensitivity analyses provided, the NRC staff concludes that the GE void history assumption provides reasonable assurance that the impact is not significant and therefore is acceptable, given the limitations below.

##### **Void Reactivity Limitation 1:**

The void reactivity coefficient bias and uncertainties in TRACG for EPU and MELLLA+ must be representative of the lattice designs of the fuel loaded in the core.

##### **Void Reactivity Limitation 2:**

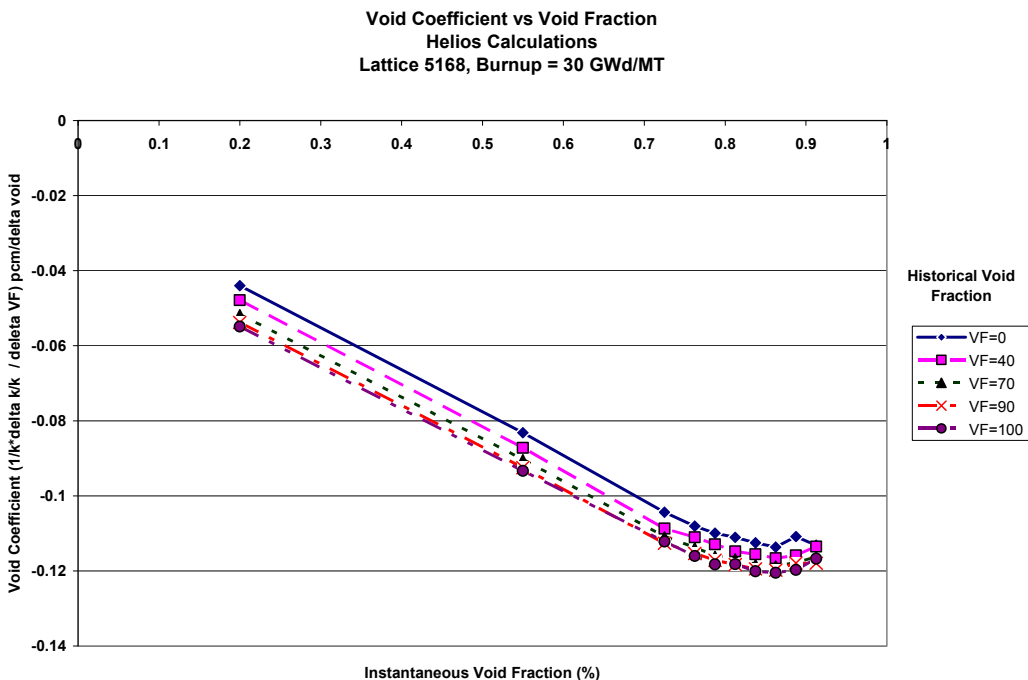
A supplement to TRACG /PANAC11 for AOO is under NRC staff review (Reference 40). TRACG internally models the response surface for the void coefficient biases and uncertainties for known dependencies [

]. Therefore, the void history bias determined through the methods review can be incorporated into the response surface “known” bias or through changes in lattice physics/core simulator methods for establishing the instantaneous cross-sections. Including the bias in the calculations negates the need for ensuring that

plant-specific applications show sufficient margin. For application of TRACG to EPU and MELLLA+ applications, the TRACG methodology must incorporate the void history bias. The manner in which this void history bias is accounted for will be established by the NRC staff SE approving NEDE-32906P, Supplement 3, "Migration to TRACG04/PANAC11 from TRACG02/PANAC10," May 2006 (Reference 40). This limitation applies until the new TRACG/PANAC methodology is approved by the NRC staff.

**Table 4-1 Void Coefficient Comparisons between TGBLA06 and MCNP**

[



]

**Figure 4-1 Void coefficient vs. instantaneous Void Fraction for a Range of Historical Void Fractions at an Exposure of 30 GWd/MT**

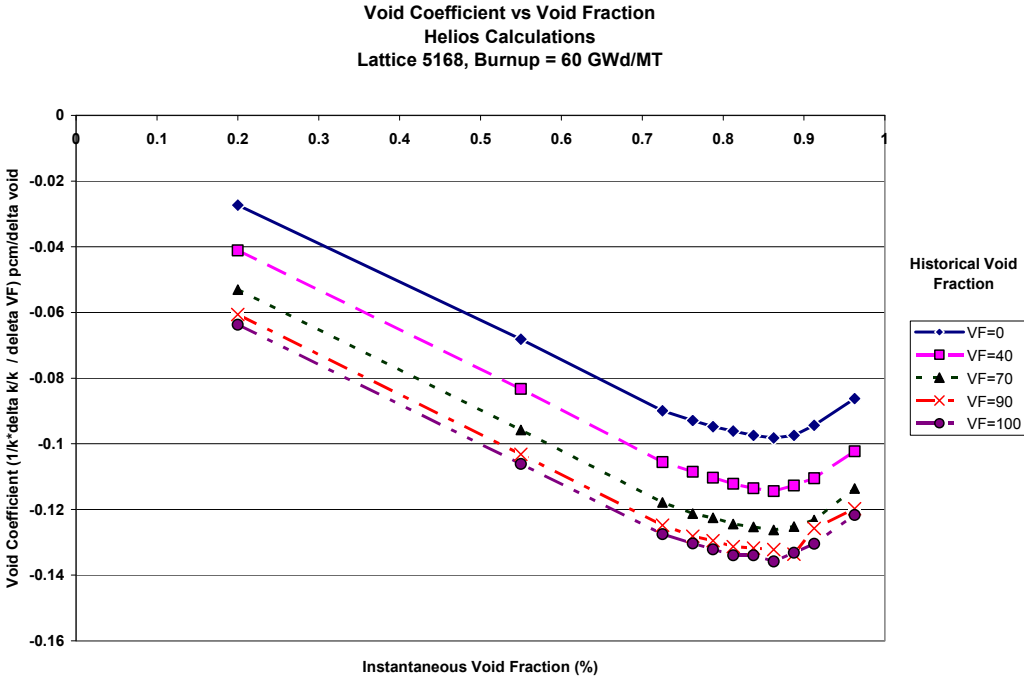


Figure 4-2 Void Coefficient vs. Instantaneous Void Fraction for a Range of Historical Void Fractions at an Exposure of 60 GWd/MT

[

Figure 4-3 Void Coefficient Ratio MNCP / TGBLA06

]

[

**Figure 4-4 Typical Void-Quality Relation at High Power-to-Flow Ratio**

]

[

**Figure 4-5 Reactivity Change for a Small Quality Perturbation ( $\Delta X = 0.001$ ) as a Function of Void Fraction**

]

[

**Figure 4-6 TRACG Power and Flow Response for MSIVC Event**

]

[

**Figure 4-7 TRACG Pressure and Relief Valve**

]

## 5.0 BYPASS AND WATER ROD VOIDING

GE's cross-section methodology relies on a polynomial fit to the lattice physics results at 0 percent, 40 percent, and 70 percent in-channel void assuming no voids in the channel and water rod. The polynomial fit is then performed as function of the lattice-average density, which includes the in-channel, bypass, and water rod. In the response to NRC staff RAIs 3.1 and 3.2 (Reference 24) GE describes this methodology. To obtain the cross-section to be used by ODYSY or TRACG for a given operating condition, first the lattice-average density is computed from the calculated void distribution, and then the polynomial parameters are interpolated or extrapolated. Thus, the bypass and water rod voids are included in the ODYSY and TRACG methodologies, but not in the same way that was considered in the lattice code (TGBLA06), which considers no voids in the bypass or water rod. The substance of the NRC staff review was to determine the impact, if any, on stability calculations. The impact of bypass voids on instrumentation used for stability solutions is described in Section 6.0, "Stability," of this SE.

GE uses four main codes to support stability calculations: ISCOR, PANACEA, ODYSY, and TRACG. Each models the bypass and water rods in a slightly different manner. All codes, except for TRACG, use one average radial node to model the bypass. TRACG uses a minimum of two (one for the periphery channels and one or two for the core center). TRACG uses [ ] while the other codes use the same number as the fuel component (24 to 25). [ ]

[ ]

[ ] There is often confusion when comparing between different reported results because of these different assumptions.

Table 5-1 shows the void fractions calculated using the different models (and their standard assumptions) for a high-power-density plant. These void fractions are calculated at the limiting point in the operating map. As stated above, the differences between the values calculated by the different codes are a function of the code assumptions. This table provides a comparison of bypass boiling levels for OLTP, MELLLA, and MELLLA+. The increase in bypass boiling between OLTP and MELLLA+ is not significant [ ]

[ ] Therefore the impact of bypass boiling on the methodology affects OLTP reactors and plants operating in the MELLLA+ domain.

### 5.1 IMPACT ON NEUTRONIC METHODS

The GE methodology used to account for bypass voiding is provided in the GE response to RAI 3.1a (Reference 10). In this methodology, the cross-section parameterization is based on the use of lattice-averaged water density including the in-channel, bypass, and water rod regions. The lattice physics calculations that are performed with TGBLA assume that no voiding occurs in the bypass and water rods. In the 3D core simulator (PANACEA) and transient simulator (TRACG) the node-average water density is calculated by combining the water

densities in the in-channel, bypass, and water rod regions. This node-average density is used to obtain the representative cross-sections to be used in the calculation.

Should voiding occur in the bypass region, the assumed condition in the lattice physics calculations will be different than the actual conditions.

## 5.2 IMPACT ON STEADY-STATE

An assessment of the accuracy of the use of lattice-averaged water density on  $K_{inf}$ , cross-sections, and peak rod fission density was provided by GE in the response to RAI 3.1b (Reference 10). Calculations were performed for two conditions that have identical node-average water densities, but with and without bypass and water rod voiding. These cases consisted of calculations with a 90 percent in-channel void fraction without water rod voiding and 85 percent in-channel void fraction with a 25 percent water rod and 10 percent bypass voiding. The results provided (lattice  $K_{inf}$ , cross-sections, neutron flux ratios, and the peak fission density) indicate that there is essentially no error introduced by the use of the node-average water density.

Additional results were provided in the response to RAI 3.1b (Reference 10) for the R-factor response with 90 percent in-channel void fraction with no bypass voiding and a 20 percent bypass and water rod void fraction. A comparison of the R-factor response as a function of exposure indicates that there is little impact. GE stated in response to RAI 3.1b (Reference 10), that the R-factor generation process is neither conservative nor non-conservative, when comparing the "production" R-factor based on three void fraction points (0, 40, and 70 percent) without bypass and water rod voiding to the R-factor at 90 percent void fraction with 20 percent bypass.

Confirmatory analysis was performed using the HELIOS code for a typical lattice with a high in-channel void fraction (e.g., 90 percent) and a 30 percent bypass void fraction. For high in-channel void fractions the source of neutrons that drive the fission process are predominately from outside the fuel region because of the limited moderation occurring within the channel. The bypass region, which typically contains water in the liquid phase, has a strong influence on the bundle power distribution. Should voiding occur in the bypass region, the power generation in the bundle is shifted away from the bypass region to the interior regions of the bundle because of the reduction in the moderation in the bypass. This results in a more uniform power distribution improving the R-factor response. In addition, the loss of moderator generally results in a reduction of the lattice  $K_{inf}$  values resulting in a local reduction in the nodal power. Independent analysis performed with HELIOS by ORNL confirmed this behavior based on calculations with an in-channel void fraction of 90 percent and a bypass and water rod void fraction of 30 percent as a bounding value.

Figure 5-1 provides a comparison of the peak relative pin-fission rate for 90 percent in-channel void fraction with and without a 30 percent bypass void fraction. Figure 5-2 provides a similar comparison, but based on an RMS of the difference of the relative pin-fission rates from unity. This later parameter provides an indication of the overall "flatness" of the lattice pin power distribution. The results indicate, as discussed above, that the peak pin-fission rate is reduced and the lattice pin-fission rate distribution is more uniform (flatter) for the case with bypass voiding. Therefore, as far as lattice peaking is concerned, bypass voiding does not have a negative impact. In addition, the 30 percent bypass voiding considered greatly exceeds the maximum value of 5 percent indicated by GE for steady-state operation.



5.3 IMPACT ON TRANSIENTS

The impact of bypass and water rod voiding on stability transients is addressed in Section 6.1.1.1, "Bypass and Water Rod Voiding Uncertainties," of this SE.

5.4 BYPASS AND WATER ROD VOIDING CONCLUSION

The NRC staff, therefore, concludes that the use of the node-average water density for parameterization of the cross-section data is acceptable for a range of the bypass voiding included in analysis provided by GE (10 percent bypass voiding). Furthermore, in response to RAI SBWB-30 (Reference 49), GE stated that specific calculations performed for Browns Ferry Unit 1, Cycles 7 and 8, show that the core will not experience bypass voiding in excess of 5 percent in steady-state operation, which is within the range of the analyzed conditions for the neutronics methods. In addition, independent analysis of bypass voiding in steady-state conditions with high in-channel void fractions demonstrates a reduction in local power and a more uniform power profile resulting in additional margin to thermal limits.

GE is required to confirm on a cycle-specific basis that the 5 percent bypass voiding assumed in its analysis is not exceeded. This requirement also ensures the reliability of the monitoring system, which is also susceptible to errors with high voiding in the bypass region.

Single recirculation loop operation (SLO) is prohibited in MELLLA+ operation unless a plant-specific deviation is requested and evaluated by the NRC staff. SLO operation is however allowed for the currently licensed MELLLA domain. The NRC staff will evaluate on plant-specific presence of greater than 5 percent bypass voiding for the SLO operation, depending on the duration of the operation. In addition, the power/flow conditions of the SLO operation is near or within the Option III armed instability region. The bypass voiding is expected to be less than the value calculated for the natural recirculation statepoint. As a guidance, the NRC staff will assess on plant-specific bases if APRM setdown is needed for SLO operation to satisfy bypass voiding limitations.

**Steady-State 5 Percent Bypass Voiding Limitation:**

The instrumentation specification design bases limit the presence of bypass voiding to 5 percent (LRPM levels). Limiting the bypass voiding to less than 5 percent for long-term steady operation ensures that instrumentation is operated within the specification. For EPU and MELLLA+ operation, the bypass voiding will be evaluated on a cycle-specific basis to confirm that the void fraction remains below 5 percent at all LRPM levels when operating at steady-state conditions within the MELLLA+ upper boundary. The highest calculated bypass voiding at any LRPM level will be provided with the plant-specific SRLR.

**Table 5-1 Bypass Void Fractions Calculated for Different Reactor Operating Domains**

	[				
MELLLA+					
MELLLA					
OLTP					]

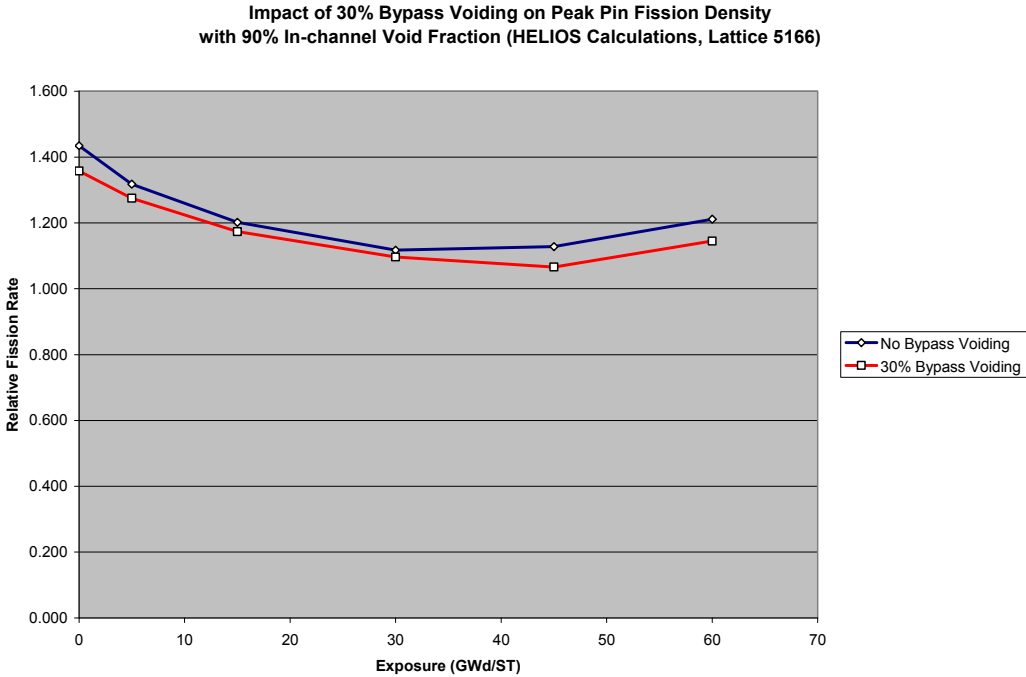


**Figure 5-1 Impact of Bypass Voiding on Peak Pin Fission Rate**

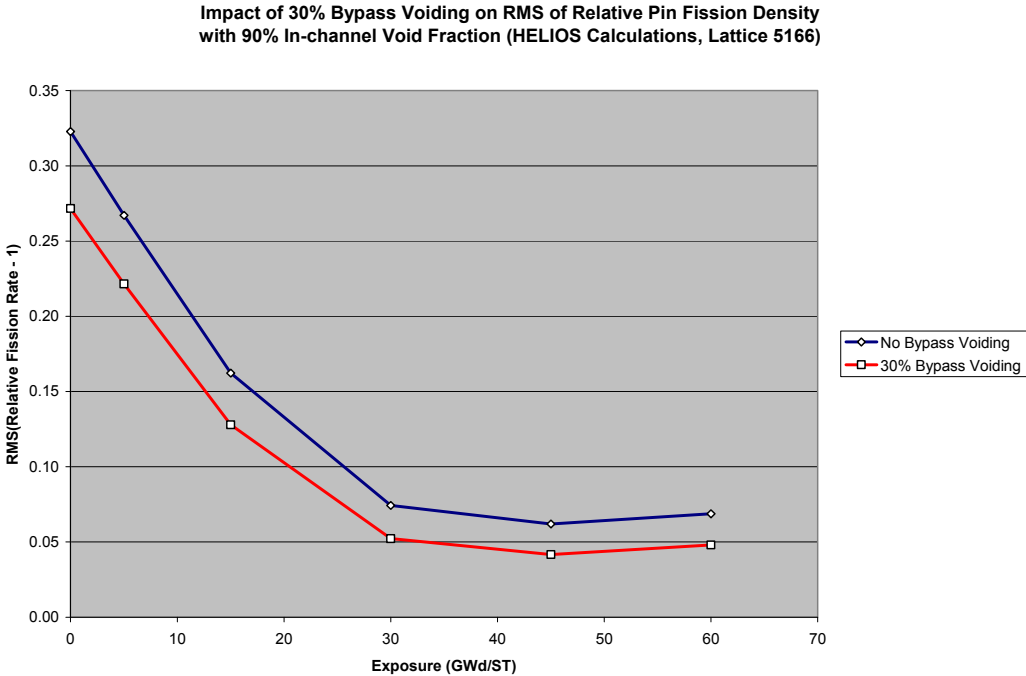


**Figure 5-2 Impact of Bypass Voiding on Uniformity of Lattice Pin Fission Distribution**

## 6.0 STABILITY

This section evaluates the impact that the methodology errors documented in this SE have on reactor stability. This review is based on LTR NEDC-33173P (Reference 1), information provided during audits and conference calls, and the GE responses to NRC staff RAIs.

The impact of the methodology errors on BWR stability can be grouped in two generic categories:

1. errors that impact stability calculations (i.e., power distribution uncertainties that affect the calculated decay ratio (DR)), and
2. errors that impact instrumentation relied upon by stability LTSs (i.e., measurement errors induced by bypass voiding impact both setpoint applicability and the actual measurement of an oscillation should it occur).

### 6.1 UNCERTAINTIES THAT IMPACT STABILITY CALCULATIONS

The main methodology uncertainties that impact stability calculations are:

1. [
- 2.
- 3.

].

#### 6.1.1 Power Distribution Uncertainties

Power distribution uncertainties have a potentially large impact on stability calculations. First, they directly affect the calculated radial and axial power distributions, which are one of the most important parameters that define the stability of a core or channel. Second, they affect the initial conditions of the hot channel, which will affect the MCPR calculations for setpoint and DIVOM (Delta CPR over Initial CPR versus Oscillation Magnitude) calculations.

LTR NEDC-33173P (Reference 1) proposes the following to resolve this error:

1. The GE stability methods have been benchmarked against a variety of plant data. Power distribution uncertainties were included in these benchmarks; therefore, the effect of these uncertainties is included in the uncertainty penalty applied to GE stability methods (i.e., the stability acceptance criterion, which is typically  $\pm 0.2$  in calculated DR).
2. While defining initial conditions for the hot channel for MCPR calculations, the hot channel is placed at OLMCPR limits. The OLMCPR will include a penalty because of these uncertainties (this SE specifies that this uncertainty magnitude be 0.02.); therefore, the uncertainty is captured by the OLMCPR.

In support of item 1, the response to NRC staff RAI 4.1(d) (Reference 24), GE presents the benchmark basis for ODYSY and TRACG. The ODYSY benchmarks database includes the:

1. VYNPS tests (core-wide mode, [                      ]).
2. 1988 LaSalle instability event (core-wide mode, [                      ]).
3. Leibstadt tests (regional mode, [                      ]).

4. KRB-C tests (regional mode, [                    ]).
5. 1991Cofrentes instability event (regional mode, [                    ]).
6. 1995 Laguna Verde instability event (core-wide mode, [                    ]).
7. 2003 Nine Mile Point Unit 2 (NMP-2) instability event (core-wide mode, [                    ]).
8. 2005 Perry instability event (core-wide mode, [                    ]).

The TRACG benchmarks documented in the TRACG qualification report include:

1. 1988 LaSalle instability event (core-wide mode, [                    ]).
2. 1991Cofrentes instability event (regional mode, [                    ]).
3. Leibstadt tests (regional mode, [                    ]).
4. Forsmark tests (core-wide mode, [                    ]).
5. 2003 NMP-2 instability event (core-wide mode, [                    ]).

All these ODYSY and TRACG benchmarks include the uncertainty on the power distribution related to the methodology. These benchmarks and previous NRC staff reviews are the basis for the approved stability acceptance criteria, which define the  $\pm 0.2$  penalty on both core and channel DR. These benchmarks also support the ODYSY regional stability acceptance criteria, which are based on the “dog-bite” correlation that estimates the stability of the regional mode based on the values of the core-wide and channel DRs. Note that, [

].

[

].

#### 6.1.1.1 Bypass and Water Rod Voiding Uncertainties

GE has not performed a detailed evaluation of the effect of bypass boiling on ODYSY or TRACG stability calculations; however, the NRC staff notes that:

1. ODYSY models the bypass channel with [                    ] and feeds back to the core reactivity effects; therefore, at least to first order, ODYSY models the effect on stability of bypass boiling.
2. On the response of NRC RAI 4.1d (Reference 24), GE provides a [

[ ].

].  
Thus, the NRC staff concludes that both ODYSY and TRACG provide a reasonable model of bypass voiding. [

].  
The NRC staff also concurs with GE's evaluation of the impact of bypass voids on ODYSY stability calculations for stability LTSs as presented in the response to NRC RAI 3.2(a)(iii) (Reference 24). This evaluation indicates that [

].  
6.1.1.2 Cross-section Methodology Uncertainties

[ ].  
]. Void reactivity coefficient is one of the primary parameters that affect stability calculations.

[ ].  
] as defined in Figure 6-3. As response to NRC RAI 4.2 (Reference 24), a series of TRACG calculations were performed to demonstrate that [

].

The NRC staff concludes that, when the effective core-average effect on stability of the 40 percent void history assumption error is computed, its effect [ ], and therefore is acceptable.

## 6.2 ERRORS THAT IMPACT INSTRUMENTATION RELIED UPON BY STABILITY LTS

The primary mechanism that impacts the instrumentation readings is bypass boiling. [

].

[

].

LTR NEDC-33173P (Reference 1) evaluates the impact of this effect on instrumentation accuracy and concludes that APRM readings will be approximately 1 percent lower, and [

].

In the response to RAI SBWB-35 (Reference 49), Tennessee Valley Authority (TVA) performed a series of bounding calculations, which included a [

].

[

]. The NRC staff concurs that this effect is negligible, and it is likely to be significantly smaller than this bounding evaluation, and therefore is acceptable.

The NRC staff also evaluated the argument that [

]. Of particular interest

are the following assumptions:

1. [

].

2. [

].

3. [

].

4. [

]. This assessment came about due to comments received from the Advisory Committee on Reactor Safeguards and subsequent NRC staff review of Susquehanna Power Uprate.

5. [

].

The NRC staff evaluation considered: (1) the complications involved in quantifying some of the physical phenomena such as oscillating quality at the LPRM D level; (2) the fact that the some assumptions are conservative while others may not be conservative for the hot channel bypass; and (3) the impact of offsetting any potential OPRM miscalibration error can be reasonably accommodated by setdown.

Therefore, the NRC staff concludes that until such time that additional justification is provided that the OPRM setpoint bias error (miscalibration) will in fact cancel out considering the onset of power oscillation, the OPRM setdown is warranted. It is noted that for the average power range monitors (APRMs), the error cancellation is not relevant because the LPRMs readings feed directly into the APRMs. The averaging of the bias is accounted for in the determination of the APRM bias; however there is no cancellation effect since there is no comparison of peak-over-average signals in initiating APRM scram signal.

Based on this evaluation, the NRC staff concludes that the presence bypass voiding at the low-flow conditions where instabilities are likely can result in calibration errors of less than 5 percent for OPRM cells and less than 2 percent for APRM signals. Each LTS is affected differently by this instrumentation miscalibration error:

1. All solutions that rely on a scram setpoint that applies to the APRM signal need to reduce the scram setpoint by the APRM error (2 percent). These LTSs are Option E1A, Option I-D, and Option II. For all these solutions, the scram setpoint must be set down by the APRM error (2 percent).
2. The limitation below applies only to Option III. As an example, if the OPRM scram setpoint is calculated to be 1.20 (including the 2 percent APRM miscalibration error in the ICPR), it will need to be reduced to 1.19 (a reduction equal to 5 percent of the 20 percent oscillation setpoint). A 2 percent bias applies APRM setpoint to account for the under-prediction of the measured power.
3. The detect and suppress solution – confirmation density (DSS-CD) is a special case, because it does not rely on pre-defined setpoint calculations. The 5 percent OPRM miscalibration error will apply to the DSS-CD oscillatory component, but will not affect the ability of detecting and suppressing the oscillations. Since DSS-CD does not rely on calculated amplitude setpoints, the APRM and OPRM miscalibration errors do not apply.

#### **Stability Setpoints Adjustment Limitation**

The NRC staff concludes that the presence bypass voiding at the low-flow conditions where instabilities are likely can result in calibration errors of less than 5 percent for OPRM cells and less than 2 percent for APRM signals. These calibration errors must be accounted for while determining the setpoints for any detect and suppress long term methodology. The calibration values for the different long-term solutions are specified in the associated sections of this SE, discussing the stability methodology.

### 6.3 APPLICABILITY OF STABILITY LTS

Specific analyses are associated with each of the stability LTSs that have been licensed and implemented in the United States. These LTS include Enhanced Option I-A (Option E1A), Option I-D, Option II, Option III, and DSS-CD.

The methodology errors impact stability LTSs in two generic categories:

1. Errors calculating exclusion regions, and
2. Errors calculating the loss of CPR associated with an unstable power oscillation of given amplitude before they are detected and suppressed.

Table 6-2 presents a summary of the stability LTS features that would be affected by these methodology errors.

As seen in Table 6-2, all solutions have two main features: an exclusion region calculation and/or a detect and suppress feature. The evaluation of the impact of the neutronic methodology errors is different for each feature type.

For exclusion region calculations, the evaluation is based on the following facts.

1. Exclusion regions calculation procedures are well-defined by the approved stability LTS methodology, and they use mostly prescribed power shapes. Therefore, power distribution uncertainties have a small effect on the size of the exclusion regions.
2. The  $\pm 0.2$  uncertainty imposed by the  $DR < 0.8$  criterion captures the possible effect of power distribution uncertainties and cross-section methodology errors (including the effect on void reactivity coefficient).
3. The  $\pm 0.2$  uncertainty level is justified by the ODYSY and TRACG validation database. For these validation analyses, the neutronic methodology included the errors.



For the detect and suppress features, the evaluation is based on the following facts:

1. All detect and suppress features rely on the DIVOM correlation, which defines the reduction in CPR margin for a postulated power oscillation of given amplitude.  
[  
].
2. The effect on setpoints of methodology errors is captured by the ICPR (typically set at the OLMCPR) and the final CPR (which is compared to the SLMCPR). The DIVOM correlation is used to calculate the reduction from the ICPR given the power oscillation amplitude required to scram. Thus, any penalties imposed on the SLMCPR to account for the neutronic methodology uncertainty, will also account for the uncertainty in the detect and suppress setpoint calculations.
3. Instrumentation errors due to neutronic methodology errors have an effect. The main effect on instrumentation errors is bypass voiding. Based on results presented by GE and TVA, the NRC staff has evaluated this error and concluded that under the expected bypass void levels for an EPU plant at natural circulation, the APRM calibration error is of the order of 1 percent lower than 2 percent, and the [  
]. These calibration errors are small when compared to other conservatisms involved in all the detect and suppress stability LTS, but must be included in the calculation of detect and suppress setpoints.

Below, each of the stability LTS is evaluated against the errors identified in Section 5.6.1 and the instrumentation errors identified in Section 5.6.2 of LTR NEDC-33173P (Reference 1).

### 6.3.1 Enhanced Option 1-A

Option E1A is a solution based exclusively on prevention of instabilities. An exclusion region where instabilities are extremely unlikely is defined by cycle-specific calculations based on a well-defined procedure. This exclusion region is enforced automatically by the reactor protection system. Option E1A has no licensing detect and suppress features, but it includes the period based detection system (PBDS) as defense in depth. The PBDS does not provide automatic protection, but it may raise control room alarms. Thus, Option E1A is susceptible to neutronic methodology errors induced by the exclusion region feature.

Power distribution uncertainties have a small effect on the calculated E1A exclusion region, because: (a) the core-wide DR calculation uses a specified Haling distribution, and (b) the hot channel DR calculation uses a procedure-specified axial power shape. Therefore, power distribution uncertainties have only second-order effects on the exclusion region calculations.

The  $\pm 0.2$  uncertainty imposed by the  $DR < 0.8$  criterion captures the possible effect of power distribution uncertainties. This is demonstrated by the ODYSY and TRACG qualification database.

Cross-section methodology errors result in a void reactivity coefficient error of the order of approximately 2 percent, which has only a small effect on DR calculation. Thus, the effect of cross-section methodology errors on exclusion region calculation is small in comparison to other conservatisms built into the solution methodology. This error is also accounted for by the  $\pm 0.2$  uncertainty, as demonstrated by the validation database.

Bypass voiding only affects the defense-in-depth features (i.e., PBDS) of Option E1A. [  
].

The NRC staff concurs with GE's evaluation that power distribution uncertainties and the neutronic methodology errors identified in this SE have a small effect on exclusion region calculations. Instrumentation errors have a minor effect on the defense in depth features of Option E1A (i.e., PBDS). Therefore, the NRC staff concludes that the methodology errors do not affect the licensing basis for LTS Enhanced Option I-A (Option E1A).

### 6.3.2 Option I-D

Option I-D is a mixed solution, where preventive features are mixed with detect and suppress features. Option I-D plants must demonstrate by analysis that they are not susceptible to regional-mode oscillations. An exclusion region is defined using a procedure similar to Option E1A; this region is enforced administratively. In the event the exclusion region is penetrated unintentionally, the flow-biased APRM scram is demonstrated by analysis to provide protection for core-wide oscillations, which are the likely instability mode. Therefore, the Option I-D is susceptible to neutronic methodology errors associated with both the exclusion region and detect and suppress features.

The evaluation for Option I-D exclusion region calculations is similar to the one for Option E1A above. The region-calculation procedures essentially prescribe the power shapes, so the power distribution uncertainties have only a second-order effect. The  $\pm 0.2$  acceptance criterion includes the effects of these uncertainties, as demonstrated by the qualification database. Additionally, [

].

The detect and suppress portion of Option I-D is the flow-biased scram system, which provides protection against core-wide power oscillations. To demonstrate this protection, a plant-specific DIVOM calculation is performed by placing the hot channel at OLMCPR limits and superimposing a power-to-flow oscillation. The DIVOM correlation relates the power oscillation amplitude with the decrease in CPR during the oscillations. This correlation is used to calculate the final MCPR at the moment of scram in the presence of oscillations.

The NRC staff concurs with GE's evaluation that any power distribution errors will be captured by the calculation of the initial OLMCPR and SLMCPR. If these CPR values are defined correctly, the DIVOM correlation is not affected by these uncertainties. Other neutronic methodology errors do not affect the Option I-D detect and suppress calculations, because a postulated oscillation that reaches the scram setpoint is imposed. Errors in DR calculation do not affect this portion of Option I-D. Therefore, the detect and suppress portion of Option I-D is not affected by these errors.

The instrumentation used by the detect and suppress portion of Option I-D is the APRM. APRM errors are only of the order of 1 percent to 2 percent. These errors are small compared to other conservatisms in Option I-D, but should be included in the calculation of the Option I-D flow-biased scram setpoints. Therefore, the NRC staff concludes that the methodology errors do not affect the licensing basis for LTS Option I-D, but they must be included in the setpoint calculations.

### 6.3.3 Option II

Option II is very similar to Option I-D. An administratively enforced region is defined. If upon unintentional entry an oscillation develops, the quadrant-based APRM scram provides protection for both core-wide and regional instability modes.

The evaluation for Option I-D covers all features of Option II. Therefore, the NRC staff concludes that the methodology errors do not affect the licensing basis for LTS Option II as long as these errors are included in the setpoint calculation methodology.

#### 6.3.4 Option III

Option III is a detect and suppress solution, without exclusion region features. A scram is initiated by the OPRM if an oscillation of a pre-defined amplitude and period is detected. A cycle-specific setpoint is calculated using: the DIVOM correlation, a postulated oscillation amplitude, and a series of pre-defined power distributions. Option III is, thus, susceptible to the neutronic methodology errors induced by the detect and suppress features.

The NRC staff concurs with GE's evaluation that any power distribution errors will be captured by the calculation of the initial OLMCPR and SLMCPR. If these CPR values are defined correctly, the DIVOM correlation is not affected by these uncertainties. Other neutronic methodology errors do not affect the Option III calculations, because the postulated oscillation that reaches the scram setpoint is imposed as a boundary condition and not calculated. Errors in DR calculation do not affect the effectiveness of the OPRM scram. Therefore, the detect and suppress features of Option III are not affected by these errors.

The instrumentation used by Option III is the OPRM. [ ]. These errors are small compared to other conservatisms in Option III, but they must be included in the setpoint calculations.

As with the detect and suppress features of Option I-D, the NRC staff concurs with GE's evaluation that the Option III features do not add any errors in addition to those reflected in the OLMCPR and SLMCPR as long as these errors are included in the setpoint calculation methodology.

#### 6.3.5 Option DSS-CD

Option DSS-CD is similar to Option III and it is a detect and suppress solution without exclusion region features. As opposed to Option III, DSS-CD does not compute a cycle-specific setpoint, but uses a generic, small-amplitude setpoint to discriminate the normal occurring noise from unstable oscillations. Option III requires only two OPRM cells to trip the reactor (one on each reactor protection system). DSS-CD requires a relatively large number of OPRM cells to signal a scram; thus the name "confirmation density."

The licensing basis for DSS-CD required a demonstration during the DSS-CD LTR NEDC-33075P (Reference 50) review of margin to CPR violation, which was approved by the NRC in Reference 51. This demonstration was performed with the TRACG code for a number of different postulated conditions. DSS-CD demonstrated significant margin to CPR for all cases studied. The neutronic methodology errors documented in this SE would change the demonstration database of TRACG calculations, but not its conclusion because:

1. The TRACG calculations in LTR NEDC-33075P (Reference 50) use a conservative SLMCPR value of [ ]. The power distribution errors would affect the SLMCPR and OLMCPR values for a cycle-specific calculation, but not these conservative generic calculations, and
2. The TRACG calculations in LTR NEDC-33075P (Reference 50) demonstrated very large CPR margins. [

].

Therefore, the NRC staff concurs with GE's evaluation that the DSS-CD features do not add any errors in addition to those reflected in the OLMCPR and SLMCPR.

**Table 6-1 Summary of ODYSY Results for VYNPS High DR Tests**

Test Point	Power/Flow (% rated)	Test Data		ODYSY Results	
		DR	Frequency	DR	Frequency
[					
					]

**Table 6-2 Long Term Stability Solution Features**

Stability LTS Option	Exclusion Region	Detect & Suppress Features
E1A	Automatic scram	NA
I-D	Administratively enforced	Flow biased APRM scram
II	NA	Quadrant-based APRM scram
III	NA	OPRM scram
DSS-CD	NA	OPRM confirmation density scram
ICA/BSP	ICAs administratively enforced. BSP could be automatic or administrative	NA

[

**Figure 6-1 NMP2 Instability Event ODYSY Benchmark**

]

[

**Figure 6-2 Perry Instability Event ODYSY Benchmark**

]

[

**Figure 6-3 Void Coefficient Ratio MNCP / TGBLA06**

]

[

**Figure 6-4 Hot Channel Power and Growth Rate with (V33) and without (NV) Void History Correction for Void Coefficient**

]

## **7.0 APPLICABILITY OF THERMAL-HYDRAULIC MODELS**

In general, correlations are developed from test data that cover specific ranges of thermal-hydraulic conditions. An independent set of test data is used to validate the performance of the correlations and establish the correlation uncertainties. The key parameters that define the correlation (e.g., thermal-hydraulic and geometric parameters), which the test data is based on, establish the “range of applicability.” Changes in these key parameters could affect the accuracy of the correlation, requiring further evaluation of the performance of the correlation under the condition it is being applied. The NRC approval of licensing methodology requires application of the correlations within the ranges for which it was developed, validated, and approved. Any changes in the correlation’s key “dependence” parameters requires further test data to establish the correlation’s accuracy to the conditions it is being applied, as is the case for the CPR correlation (i.e., GEXL). For new fuel design, involving changes in the fuel T-M design, GE uses new test data to model the features of the new fuel design and to develop a modified GEXL correlation applicable to the new design for the thermal-hydraulic conditions to which it would be applied.

The review in this section entails confirming that for the changes in core thermal-hydraulic conditions of bundles (e.g., higher bundle power-to-flow ratios) and new fuel designs (10x10 fuel designs, with two large water rods and 14 part-length rods), the correlations are being used within the approved applicability ranges for normal steady-state and transient conditions.

## 7.1 GEXL CORRELATION

The GEXL correlation is developed from test data to predict the critical power for a given bundle thermal-hydraulic condition. The GEXL correlation uncertainty factor into the SLMCPR calculation is used to establish the probability of BT. LTR NEDC-33173P (Reference 1) evaluated the applicability of the GEXL correlation for EPU and MELLLA+.

The critical power correlation is developed from full-scale critical power test data for each fuel design. Therefore, the critical power correlation for the current GE14 fuel design was developed from fuel scale tests. The development of GEXL correlation coefficients and constants for a fuel assembly is based on NRC-approved process described in GE licensing methodology, GESTAR II (NEDE-24011-P-A, Reference 32). Specifically, Section 2.8, "Critical Power Correlation," of the NRC staff SE approving Amendment 22 to GESTAR II delineates the acceptance criteria for development of the CPR for new fuel designs and the licensing process for NRC staff review and approval (Reference 32).

GE reports that the critical power correlation experimental data ranges are as follows:

1. Bundle mass fluxes ranges from [            ];
2. Inlet subcooling ranges from the [            ];
3. Pressures range from [            ],
4. LTR NEDC-33173P (Reference 1) states that the experimental data ranges of core flow cover from less than natural circulation to well beyond rated flow and include the flow ranges for EPU and MELLLA+ applications;
5. The bundle power levels of the database range from up to the actual critical power for each set of conditions, which is in the range of [            ] for 10x10 fuel; and
6. The fluid parameter ranges also cover the expected ranges for LOCA and transient events.

Figure 7-1 (Figure 2-1 of LTR NEDC-33173P (Reference 1)) shows the GE14 application range together with the expected range for typical operational transients. In Figure 7-1, the box representing the correlation application range encloses the expected ranges for transients.

For LOCA application, the GEXL correlation is used for the calculation of the early BT during the flow coast down immediately following the break. GE states that this typically occurs when the flow has dropped to 30 to 50 percent of the initial value and the core thermal-hydraulic condition is well within the application range for the GEXL correlation. LTR NEDC-33173P (Reference 1) concludes that the range of bundle powers and hydraulic conditions for the GEXL correlation covers those expected in MELLLA+ and EPU operation.

Since the database appears to cover the ranges of conditions expected for the EPU and MELLLA+, and both the acceptance criteria for the development of the GEXL correlation and the licensing process for submittal of the correlation for NRC staff review and approval are based on NRC-approved process, the NRC staff finds the use of GEXL correlation for EPU and MELLLA+ acceptable.

## 7.2 VOID-QUALITY CORRELATION

The void fraction prediction is determined using an empirically derived void-quality correlation. The Findlay-Dix correlation that was documented in and developed from data presented in the

1977 GE report "BWR Void Fraction Correlation and Data" (NEDE-21565, Reference 52) is used in both the neutronic and the thermal-hydraulic calculations. These affect the safety analyses supporting BWR operation during steady-state, transient and accident conditions. The accuracy of the void-quality correlation affects the predictions of the steady-state power distribution, which establishes the steady-state thermal limits and the initial conditions for the transient and accident analyses. In addition, the void power feedback during transients and accident conditions is also affected by the accuracy of the void-quality correlation. Different code sets used to perform the safety analyses may use different void fraction prediction methods (e.g., TRACG uses shear model); however, the neutronic and thermal-hydraulic calculations rely on the modified Findlay-Dix correlation in determining the void fraction.

This section evaluates applicability of the void-quality correlation to EPU and MELLLA+ core thermal-hydraulic conditions, the current fuel design features, and power distribution and peaking. In LTR NEDC-33173P (Reference 1), and in response to RAIs 5-1, 5-2, and 5-4 (Reference 24), GE discussed the following:

1. Applicability of the void-quality correlation and the corresponding validation ranges to the EPU and MELLLA+ conditions;
2. Performance of the correlation compared to the validation data;
3. Sensitivity of the correlation to part-length rods; and
4. Uncertainty treatment of the void-quality correlation in the major safety analyses.

GE states that the void-quality correlation is based on test data, which covers a broad range of conditions. The void-quality correlation is based on void fraction data [ ], which covers the void fraction range expected for normal steady-state operation and the abnormal operational occurrences that set the OLMCPR. GE asserts that the correlation supports the full range of conditions expected during BWR operation, including constant pressure power uprate (CPPU), EPU, and MELLLA+ conditions. The correlation uncertainty is appropriately accounted for in the SLMCPR. GE concludes that an extrapolation of the void-quality model to void fractions all the way to pure steam flow is justified, and it is not necessary to incorporate additional margin to void fraction uncertainty.

#### 7.2.1 Extension of the Void-Quality Correlation

The NRC staff assessed the applicability of the experimental databases used to derive and validate the correlation to the: (1) core thermal-hydraulic conditions for operation at EPU and MELLLA+; (2) current fuel design geometries (part-length rods, hydraulic diameters, and spacer designs); and (3) current lattice designs (e.g., radial power distribution and peaking). The objective is to determine the performance of the correlation at conditions to which it is being applied and to establish if current validation data is sufficient for extension of the correlation to current fuel, core designs and operating strategies. This evaluation is performed with assistance from ORNL staff.

GE proposes extension of the Findlay-Dix correlation to void fractions of 1.0. Table 7-2 shows the experimental database ranges supporting the correlation. In Table 7-1, the NRC staff expanded on the experimental database used to develop and validate the Findlay-Dix correlation, including the power distribution, peaking, Reynolds number ranges, the hydraulic diameters, etc.



## 7.2.2 GE Void Fraction Model

The GE void fraction model is based on the drift flux model developed by Zuber and Findlay in 1965. Drift flux models have been used to correlate void fraction in a wide variety of geometries, under different sets of parametric conditions, and for a variety of fluids, by developing appropriate correlating parameters. The four major parameters used in the model are:

1. vapor superficial velocity  $j_g$  ( $= G X/\rho_g$  (m/s)), where  
G is the mass flux ( $\text{kg}/\text{m}^2/\text{s}$ ),  
X is the mass quality, and  $\rho_g$  is the vapor density ( $\text{kg}/\text{m}^3$ ),
2. superficial velocity  $j$  ( $=j_g + j_f$  (m/s)), where  
 $j_f$  is the liquid superficial velocity ( $=G(1-X)/\rho_f$  (m/s)), and  $\rho_f$  is the liquid density ( $\text{kg}/\text{m}^3$ ),
3. void distribution coefficient  $C_o$ , and
4. a drift velocity  $V_{gj}$ .

The drift flux equation is:

$$\alpha = j_g / (C_o * j + V_{gj})$$

The coefficient  $C_o$  reflects the void distribution over a flow cross-section. GE has correlated this parameter to the GE database as a function of Reynolds number, fluid properties (pressure), and void fraction. The drift velocity  $V_{gj}$  has also been correlated as a function of the same parameters. The specific form of the  $V_{gj}$  equation GE has developed also depends on flow pattern (bubbly-churn-turbulent or annular) with a transition equation between the two. Similar to the development of Zuber, GE chose to use the property relationship  $(g^* \sigma^* (\rho_l - \rho_g) / \rho)^{1/4}$  as a correlating grouping (along with the Reynolds number, etc.), where  $g$  is the acceleration of gravity (in  $\text{m}/\text{s}^2$ ) and  $\sigma$  is the surface tension (in  $\text{N}/\text{m}$ ). In this case  $\rho$  is  $\rho_l$  for the bubbly-churn-turbulent regime and  $\rho$  is  $\rho_g$  for the annular region.

Basically, the correlation is therefore a function of 4 parameters; mass flux, local pressure (to get fluid properties), local quality, and geometry. The Findlay-Dix correlation itself is therefore similar to other drift flux correlations, except that GE correlated to specific bundle data.

## 7.2.3 Available Void-Quality Correlation Measurement Database

Table 7-2 shows the experimental database ranges supporting the correlation. Table 7-1, compiled by the NRC staff, provides the parameter ranges for the GE 10x10 bundle and the current operating ranges during steady-state and transient conditions. LTR NEDE-21565 (Reference 52) provides discussion of the correlation development and validation. GE referenced NEDE-21565 (Reference 52), but the NRC staff never explicitly reviewed or approved this document. However, discussion of the correlation was included in a number of NRC-approved documents. The NRC staff used the referenced database source document in evaluating the applicability of the correlation validation ranges. The experimental database is described below.

### 7.2.3.1 CISE Database

The CISE data was [ ] taken by using quick closing valves to isolate both the vapor and liquid flows in the bundle. The experiment therefore gives bundle average quality and void fraction. GE considered this data as the most accurate, and states that these data

“...[ ]....” The CISE database covers the entire range of normal operating mass fluxes at a single pressure of [ ]. These data were taken in a bundle with slightly larger hydraulic diameter than the 10x10 bundle. The experiment also used uniform radial and axial power profiles, which differs from the radially-skewed power distribution characteristic of the current lattices with depletion.

#### 7.2.3.2 GE 7x7 Database

The GE 7x7 bundle data were developed using pressure drop information from GE's ATLAS test facility. The experiment had a 3-foot adiabatic section at the end of the bundle where they measured pressure drop. Therefore, this data should provide bundle average exit void fractions. The pressure drop measurement technique is acceptable in this case because the flows were low enough [ ] such that the frictional pressure drop component is small compared to the void effect. The GE 7x7 bundle data were used to specify the extreme low flow conditions of the correlation. The GE 7x7 data were taken at pressures, which range from below steady-state operating conditions [ ] to those that occur during some transients [ ]. This bundle had higher hydraulic diameters than the 10x10 bundle design, and the tests covered the very low mass flux and Reynolds number ranges.

#### 7.2.3.3 ASEA-Atom 8x8 Bundle Data

All of the ASEA void fraction data were taken using gamma densitometry (e.g., multiple beam ray attenuation technique), which gave the local values for the void fraction. As noted in NEDE-21565 (Reference 52), the ASEA-713 data covered a wide range of variables and were used to correlate the void fraction trends. Once the correlation was developed from the GE bundle data [

] series of tests were used to validate (e.g., benchmark) against correlation predictions. Therefore, the ASEA-513 and ASEA-813 databases provide an independent evaluation of the correlation's ability to predict void fraction under conditions somewhat different than those for which it was developed.

The ASEA data covered the majority of the mass flux range (lower range of the tests was slightly above the lower range of expected reactor mass flux under natural circulation conditions  $400 \text{ kg/m}^2/\text{s}$ ), and the entire pressure range except for the ATWS maximum pressure. The maximum quality in the tests was approximately equivalent to the maximum at steady-state operating conditions. The ASEA-513 test series used a [ ] rod bundle test section while both of the ASEA-713 and 813 tests used the same test section geometry, an [ ] bundle.

The ASEA-513 database had uniform radial and axial power distribution. The ASEA-713 series had a symmetric radial distribution, with peaking of 1.24 at the peripheral rods and internal rod peaking of around 0.8. The ASEA-813 series were designed to establish the impact of skewed radial power distribution on the performance of the correlation. Therefore, the ASEA-813 bundles had asymmetric radial peaking, with high peaking range from 1.25 to 1.08 and lower peaking in the 0.89 range.

Table 7-3 (provided by GE in response to RAI 5.2, Reference 24) summarizes the overall uncertainty for each of the database sets, including the ASEA-713 database used to develop the correlation.

#### 7.2.3.4 Simple Geometry Database

The void database included data based on a variety of other geometries – round tubes, rectangular tubes, and annular flow channels. GE also compared these simple geometry data to the Findlay-Dix correlation in NEDE-21565, with indicated errors of [ ] depending on the specific experiment. However, the reported uncertainty components in Table 7-3 did not include the simple geometry uncertainty levels to establish the total void-quality uncertainty. However, the reported hydraulic diameter range given in the RAI 5-2 response (Reference 24) of [ ] includes the simple geometry data as justification that the database covers the lower range of hydraulic diameters.

#### 7.2.3.5 Pressure Drop Optimization

In NEDE-21565, the experimental database was also used to optimize the two-phase pressure drop correlation and its effect on the elevation pressure drop. Based on the newly developed void fraction correlation, GE effectively re-optimized their pressure drop correlation using the new void calculation technique. NEDE-21565 (Reference 52) reports an improvement in pressure drop calculation, with standard deviations (for pressure drop) ranging from about [ ] depending on the data set to which it is compared.

GE reports in the RAI responses in MFN 06-211 (Reference 24) that comparisons have been made to pressure drop data taken in the ATLAS test facility using full-scale test assemblies for all fuel products including the current 10x10 GE14 fuel. This testing covers a wide range of conditions including EPU conditions. For GE14, the bundle pressure drop was predicted with a mean error of [ ] and a standard deviation of [ ]. Since the pressure drop cannot be matched unless the void fraction is accurately predicted (this is increasingly true as the mass flux decreases), these tests serve to confirm the void-quality correlation at low flow rates.

Since the void-quality correlation is incorporated into the pressure drop calculation, and pressure drop measurements are taken by GE for all new bundle geometries, the uncertainties in the void-quality relationship are accounted for in the overall pressure drop uncertainty. The void influence should be covered by the pressure drop uncertainties, as long as the pressure drop database covers the appropriate data ranges. Therefore, the NRC staff finds that the void-quality uncertainty need not be explicitly incorporated in the pressure drop calculation.

Since critical power and two-phase pressure drop testing in the 10x10 bundle geometry have been performed, the NRC staff also notes that these tests could potentially be a source for additional void fraction data that would help verify the void-quality correlation for 10x10 bundle designs under low flow conditions. If testing was performed at sufficiently low flows where frictional pressure drop effects, grid losses, etc., were significantly less than those due to density or elevation effects (such as was done in the GE tests discussed above in Section 7.2.3.2, "GE 7x7 Database"), then pressure drop data in the bundle could be used to back calculate average void fraction information. This data would add some confidence to extending the correlation to this geometry for high bundle power-to-flow conditions. During RPT events, the power-to-flow ratio will be high and the void fraction ranges will also be high, perhaps higher than that in the existing GE database. By using the 10x10 geometry tests at low flow conditions (high power-to-flow conditions) to extract average void fractions, additional confidence may also be gained for predicting void fractions during these events. This possibility depends on whether GE has performed testing using the 10x10 bundle design at flows sufficiently low to permit this analysis.

#### 7.2.4 Comparison of Experimental Database to Current Fuel Designs and Operating Conditions and Fuel (10x10 bundle – GE14)

The comparison of the experimental database to reactor operating conditions was carried out on an individual parameter basis. As discussed above, the drift flux based void fraction model developed by GE uses four major parameters: (1) local pressure (for property evaluation), (2) local quality, (3) mass flux, and (4) geometry. Ideally, the data should be evaluated by comparing this combination of parameters under appropriate operating or transient conditions with the same combination of parameters measured in the experiments. For example, each transient follows a path of parameter values (or a small range of parameter values) that occur in combination (i.e., mass flux, pressure, quality, etc.), and not all parameters exist in every possible combination. The validation database needs to be consistent with those parameter sets. The information provided by GE, did not allow the data (or the pertinent reactor operating conditions) to be parsed in a manner that allowed a comparison of parameters in proper combination. Therefore, the evaluation was carried out by examining only individual parameter ranges.

As shown in Table 7-1, the individual data ranges cover the expected parameter ranges reasonably well; however, some of the 10x10 bundle parameters are outside of the range of the database. Discussion of each parameter range follows.

##### 7.2.4.1 Hydraulic Diameter

As given in response to RAI 5-2 (MFN-06-207 (Reference 9)), the hydraulic diameter range of the current fuel designs ranges are: [

].

Although in the response to RAI 5-2, GE notes that the correlation was compared to data with hydraulic diameters, ranging from [ ] it appears that the lower hydraulic diameter data were taken from rectangular tube experiments (simple geometry data). In addition to geometry differences, the simple geometry data also can not provide equivalent power-peaking or distribution characteristics. In the response to RAI 5-1, a plot of  $Re = 1.1E5$  bundle data is presented from 8x8 bundle tests [ ], and compared to calculations for a 10x10 bundle [ ] at the same Reynolds number. The RAI response states that “Comparing this calculation on the void fraction data used in the development of the Findlay-Dix correlation is not perfectly meaningful as the bundle geometries and the test conditions are not identical.” Although GE uses the simple geometry data as evidence that their correlation can be extended to lower hydraulic diameters, GE did not present any data from that database to justify the extrapolation, while standard deviation values for the simple geometry data presented in NEDE-21565 are significantly higher than those quoted for the rod bundle data.

As a minimum, in order to make the claim that the correlation was benchmarked over this parameter range, GE needs to include the simple geometry data in their correlation uncertainty evaluation. The overall correlation uncertainty in Table 7-3 does not include the uncertainties in the “simplified geometry” data, which, as expected, is significantly higher than that of the bundle data.

GE also noted that even though the hydraulic diameter is out of the bundle database range, the Reynolds number range is still covered. It would provide the NRC staff more confidence in the void-quality correlation if direct comparison to the “simple geometry” data with low hydraulic diameters were made over appropriate void fraction ranges and Reynolds numbers. The applicable Reynolds number ranges for 10x10 bundle geometry are delineated below. Also discussed below, are NRC staff comparisons of the Findlay-Dix correlation at a Reynolds number of 1.1E5 against public domain drift flux correlations developed from an experimental rod bundle database that includes hydraulic diameters as low as [ ].

#### 7.2.4.2 Pressure

The GE bundle database pressure range [ ] covers steady-state operation and some transient pressurization response, with the exception of an ATWS event (10.3 MPa). The GE simple geometry data covers a pressure range of [ ], which is higher than the ATWS peak pressure range (3.1 – 9.7 MPa). This data, however, was not included in either the correlation development or uncertainty assessment. Note that the relevant ASEA-813 validation database with skewed power-peaking is limited to a single pressure of [ ]. Again, the simple geometry database is not included in the overall correlation uncertainty calculation; therefore taking credit for this database does not seem appropriate. GE also did not perform a direct comparison between the simple geometry database and the correlation predictions for the higher pressure range. The data should show the performance of the correlation against the simple geometry database for Reynolds numbers, pressures, and hydraulic diameters of interest (see Table 7-1).

#### 7.2.4.3 Subcooling Level

The correlation was validated against a bundle database with subcooling ranging from [ ], which covers the operating condition subcooling levels, including equipment out-of-service. The overall bundle database (including both development and validation data) includes subcooling levels from [ ].

#### 7.2.4.4 Exit Quality

The steady-state exit quality range is covered by the database.

#### 7.2.4.5 Exit Void Fraction

The NRC staff agrees that as shown in Table 7-1, the void fraction for the bundle data extends to void fractions of 0 percent to [ ] and covers steady-state reactor operating conditions and pressures. However, the quantity of bundle validation data covering high void ranges is limited to a few data sets at [ ].

#### 7.2.4.6 Reynolds Number

Figure 7-2 shows the correlation prediction against the ASEA-813 database for which the correlation was validated, as well as, the ASEA-713 database upon which it was developed. Since the Reynolds number is a function of mass flux, hydraulic diameter, and fluid properties and the fluid properties are a function of pressure, the void-quality correlation can also be reformulated as a function of hydraulic diameter, mass flux, quality, and pressure. Using the

mass flux of typical modern fuel bundle of  $0.8 \text{ Mlbm/hr-ft}^2$ , GE calculated the correlation for a Reynolds number of  $1.1\text{E}5$  for the rodded region (below the part-length rods) of a  $10 \times 10$  bundle. Figure 7-2 provides a qualitative assessment of the correlation for this specific Reynolds number. GE states that there are no trend differences between the validation and the development database.

The database covers the steady-state operating Reynolds number range for the  $10 \times 10$  bundle. However, GE did not systematically provide an assessment of the correlation performance by identifying the sets of parameters (including the Reynolds number) that correspond to steady-state operation and transient conditions and then comparing those parameter sets to those in the database. For instance, Reynolds number ranges were not provided in the RAI responses for either the data sets or the conditions in the reactor for operation at EPU and the proposed higher operating domain. Additionally, information was not sufficient in NEDE-21565 (Reference 35) to determine the Reynolds number ranges for all data sets.

As can be seen in Table 7-1, the upper end of the Reynolds number range for the  $10 \times 10$  fuel designs are bounded by the data when both development data sets (CISE, GE, ASEA-713) and validation sets (ASEA-813, ASEA-513) are included. Not enough information was provided to determine the Reynolds number range for the ASEA-513 validation series.

#### 7.2.4.7 Power Distribution (Axial and Radial)

The GE database includes axial and radial (within bundle) power distributions with peaking of approximately 1.6 and approximately 1.24, respectively. It also includes bundle data with uniform power distributions. The axial peaking in the reactor could reach 2, and the radial peaking could approach a value of 1.45. Evaluation of the radial power distribution of the database shows that the validation database is not representative of the current bundle axial or radial power distribution and peaking. This is a deficiency in the database supporting the correlation in relation to the current fuel design operating conditions. For example, Figure 7-3 shows the radial power-peaking in the ASEA-713 data, while Figure 7-4 shows the radial peaking in the ASEA-813 data. This can be compared to the radial peaking that occurs in the  $10 \times 10$  bundle design under conditions in Figure 7-5 at 0 burnup. Significantly larger radial power-peaking exists in the  $10 \times 10$  bundle design than exists in the GE void fraction database. That, in combination with the conclusions reached in NEDE-21565 (Reference 52), noted below, raise questions regarding the validity of extrapolating the existing void correlation to the new bundle designs.

The impact of the power distributions is not just at high void conditions but they also effect the void distribution throughout the bundle (e.g., an inlet peaked power distribution causes earlier void formation, and exit peaked later, etc.). In the current fuel lattice designs as operated, fuel bundles can experience bottom-peaked, mid-peaked, top-peaked, and double hump. Therefore, the current and proposed bundle power distributions and peaking with depletion to current burnup levels show significantly higher skewing in both radial and axial directions.

As reported in the experimental data assessment in NEDE-21565 (Reference 52):

1. The ASEA-813 database was taken for the purpose of determining the effects of skewed radial peaking. GE has not accounted for the shift in the ASEA-813 and ASEA-513 data. It is uncertain if the differences in the radial peaking caused the shift for the ASEA-813 series.
2. Had the correlation been fitted to the three ASEA bundle databases only, equally weighed, the results would have been as much as 2 percent higher in void fraction.

The recommendations in the 1977 NEDE-21565 (Reference 52) concluded the following:

1. [
- 2.
- 3.

]

The NRC staff believes the weakness of the validation database are more relevant in the current EPU operating strategy and the MELLLA+ conditions, because there could be higher power skews in both the radial and axial directions than existed previously. The current within lattice peaking would be expected to affect the void distribution parameter and the accuracy of the functional trends of the empirical parameters, which were derived from the original GE data. Additionally, the lack of partial length rod data in development or benchmarking of the correlation does not allow the NRC staff to evaluate accurately the present correlation and the uncertainty levels presented.

#### 7.2.4.8 Partial Length Rods

GE presented three plots showing the effect of partial length rods on void fraction (Response to RAI 5.2, Reference 9), which are shown as Figure 7-6 through Figure 7-8. The data in these plots were Japanese data taken from the open literature. The data indicates only a minor change in void fraction between bundles with and without partial length rods. GE noted that the void fraction correlation was not compared to this data because sufficient information about the test apparatus was not available. This limits the usefulness of data since there is no quantitative comparison with Findlay-Dix void that would allow the performance of the Findlay-Dix void-quality correlation to be evaluated for partial length rods.

#### 7.2.5 Comparison of the Findlay-Dix Correlation and Other Drift Flux Models

As can be seen by both Table 7-2 and Figure 7-2, the rod bundle database on which the void-quality correlation was statistically validated does not extend to void fractions of 1.0. Additionally, GE did not provide additional experimental data that incorporate the new fuel design features and power distribution. Also, GE did not use either available public or non-public domain data in rod bundle geometries to support extension of the correlation to the higher void fraction, higher pressures observed during some of the hypothetical transients, lower hydraulic diameter geometries of the new bundle design, or bundle geometry features such as partial length rods.

Therefore, the ORNL staff compared the Findlay-Dix void-quality relationship to other drift flux correlations developed for rod bundle geometry, using Figure 7-2. The objective of this comparison is to assess the overall performance of the correlation rather than to establish the uncertainties associated with correlation prediction for given bundle thermal-hydraulic conditions. Note that this comparison is limited to a single Reynolds number and does not extend to all BWR operating regimes that occur during steady-state, transient, and accident conditions.

The comparison is based on a mass flux value of [ ]. Figure 7-1, which includes the Findlay-Dix correlation and the ASEA-713 and 813 data, is reproduced in Figure 7-9. Three other void fraction correlations are also included in the figure.

Two of these correlations were developed from rod bundle data and taken from a paper by Coddington and Macian of the Paul Scherrer Institute (Reference 53).

The Coddington and Macian database was developed from experiments taken in 9 different rod bundle facilities. The two correlations plotted in Figure 7-9 are: (1) the Inoue correlation (1993) that was developed from Japanese 8x8 data and (2) the Maier and Coddington Correlation developed from the rod bundle data presented in the Coddington and Macian paper. Coddington and Macian note a standard deviation for their correlation of 7.1 percent when compared to the overall database, and a standard deviation of 8.3 percent for the Inoue correlation when compared to the same database.

GE states a standard deviation for the Findlay-Dix correlation of [ ] based on its specific data. This small standard deviation may be possible with very specific experiments using only GE's bundle configurations, while the Coddington and Macian data cover a "world" data set. The correlation, which is labeled "Collier" in Figure 7-9, is a "standard" drift flux based void-quality correlation that is often used and is presented in Collier "Convective Boiling and Condensation" (Reference 54). This correlation was not developed specifically for bundles, and is generally not claimed to be good for all flow patterns. The data was included for a sanity check and is not referenced further.

As can be seen in Figure 7-9, the trends in all of the correlations (GE, Maier and Coddington, and Inoue) are all very similar, and almost identical up to void fractions of 60 percent, with differences between the GE correlation and the Maier and Coddington correlation of about 5 percent and the Inoue correlation of 8 percent at void fractions near 1. Coddington and Macian included comparison of their data to a correlation by Dix; however, this correlation is not the same as the Findlay-Dix model used by GE. Both the Maier and Coddington and Inoue correlations use a drift velocity that is independent of void fraction (or quality), and thus, do not predict a void fraction of 1 at a quality of 1. The GE correlation uses a drift velocity that is proportional to  $(1-\alpha)$  for high void fractions [ ], so it gives a void of 1 at a quality of 1. The Maier and Coddington correlation tends to under-predict void fractions at high quality levels as shown in Figure 15 of the Coddington and Macian paper (Reference 53) (the Inoue correlation may be lower). Therefore, the GE correlation could actually be slightly better under high quality (or void) conditions.

#### 7.2.5.1 Key Parameters Discussion

The key parameter range evaluation of the Findlay-Dix correlation showed that some of the parameters were outside the ranges of current fuel designs. Assessment of the Coddington and Macian "world" data and the correlations representative of that data shown in Figure 7-9 follows.

#### 7.2.5.2 Hydraulic Diameter Ranges and Partial Length Rods

The Coddington and Macian database (which is all bundle data) appears to include hydraulic diameters as low as [ ], with 5 of their 9 data sets having hydraulic diameters [ ]. Thirteen of the fourteen correlations that are included in the database comparisons are based on the drift flux model, and were able to predict all of the data reasonably well. In Figure 7-9, two of the best performing correlations appear to be similar in performance to the Findlay-Dix correlation. This comparison adds some confidence in the acceptability of extending the Findlay-Dix correlation to the lower hydraulic diameter ranges. However, there were no bundles in the database that were identified as having partial length rods.



### 7.2.5.3 Pressure Ranges

The required extension of the Findlay-Dix correlation to pressures beyond the GE bundle database range is not large (from [ ]. The Coddington and Macian “world” database extends to a pressure of 15 MPa with two facilities gathering data at pressures over 10.3 MPa at low mass fluxes. The correlations that Coddington and Macian compared to this data performed well at the high pressures as well as data taken at lower pressures. The Findlay-Dix correlation seems to behave similarly to correlations examined in the Coddington and Macian paper.

### 7.2.5.4 Power Peaking and Distribution

Evaluation of the database benchmarking the Findlay-Dix correlation shows that the axial and radial power distribution and peaking are not consistent with current (or proposed) in-bundle power conditions. Currently, bundles operate with top-, bottom-, and mid-peaked axial power distributions. Also, the radial power distribution characteristics within the bundle differ from the validation database supporting the Findlay-Dix correlation. The quality levels (flow patterns) that occur are still covered by the combination of development and validation databases. The differences in the power distribution and peaking between the experimental data supporting the correlations and the current and proposed core operating conditions makes assessment of the reported correlation uncertainties difficult.

The NRC staff evaluated the Coddington and Macian data in order to establish if relevant local power distributions are covered by this database. The Coddington and Macian database included cosine shaped axial power profiles as well as uniform axial power profiles. The drift flux correlations evaluated by Coddington and Macian seem to predict both uniform and shaped profiles equally well. Although, the details of the power-peaking of the database is not clear, the fact that both the uniform power profile void data as well as the power peaked bundle data can be correlated with the same approach also provides some assurance of the performance of the drift flux correlations.

### 7.2.5.5 Conclusion of the Comparison to the “World” Data

The NRC staff compared the performance of the Findlay-Dix drift flux correlation to other correlations based on multiple bundle experiments with wider parameter ranges than the Findlay-Dix database (a range that does cover higher pressures, lower hydraulic diameters in bundle geometry, and void fractions up to 1.0). This was performed for the set of conditions shown in Figure 7-9. The limited assessment indicates that the Findlay-Dix correlation performs similarly to other drift flux based models. Therefore, the Findlay-Dix correlation is expected to perform similarly at higher void fractions, higher pressures, and smaller hydraulic diameters than are covered in the GE bundle database.

However, the NRC staff cannot predict explicitly from this data the impact of the advanced fuel design features, current operating parameters, and current operating strategies on the performance of the correlation (e.g., axially varying hydraulic diameters, higher power-peaking, the presence of grid spacers, 14 part length rods, 2 large water rods as well as smaller rod diameters combined with differences in the operating ranges). The above comparisons serve as an overall check and cannot be used to establish the accuracy or uncertainty of the GE correlation for application to BWR operation.

## 7.2.6 GE Assessment

LTR NEDC-33173P (Reference 1) justifies the applicability of the current experimental database supporting the correlation, the accuracy of the correlation and the extension of the correlation to void fractions of 100 percent. GE concludes that additional margin is not warranted for application to EPU and MELLLA+. GE's assessment is summarized below.

LTR NEDC-33173P (Reference 1) states that a void fraction of [ ] is relatively high and typical of the conditions where BT will occur in a BWR fuel bundle. Since for plant-specific application the OLMCPR is determined such that BT will not occur, "it is highly unlikely that a void fraction of [ ] will be exceeded (e.g., perhaps momentarily during a transient) by any significant amount.... Some aspects of void fraction and bundle power warrant a brief discussion."

Considering the relationship between the void fraction and the bundle powers, the flow quality is a function of pressure (fluid properties), inlet flow rate and subcooling, and the heat addition rate. For the case of "z" equal to the exit elevation, the integral term essentially represents the channel power. Therefore, the steady-state exit quality is directly proportional to the integrated channel power.

Since BWR fuel bundle is designed and operated such that BT will not occur during steady-state or AOOs, therefore, void fractions that are higher than [ ] will not occur. Figure 2-2 of LTR NEDC-33173P (Reference 1) illustrates this point (see Figure 4-4). Less than half of the quality range ( $X < 0.5$ ) covers up to 90 percent void fraction. GE stated that, "A significant power increase (or a factor of 2 change in quality) is required to drive the void fraction from 90 to 100 percent. It would require a bundle power of approximately [ ] for a bundle at rated flow to reach a void fraction of 0.95 percent, while in reality a high power fuel bundle operates at approximately 7 MW."

The void-quality correlation is based on sound physical principles, particularly for high void fractions, and extrapolation of the measured data to a void fraction of 1.0. Using the Zuber-Findlay expression for two-phase flow, the void fraction  $\alpha$  can be expressed as

$$\alpha = j_g / (C_o * j + V_{gj})$$

Where:

$C_o$  = distribution parameter

$V_{gj}$  = drift velocity

$j_g$  = volumetric flux of steam vapor

$j$  = volumetric flux of the mixture

The drift velocity is the difference in velocity between the vapor and liquid phase. Generally the vapor phase velocity is greater because of buoyant forces. At high quality, the annular flow regime predominates. In the annular flow regime the liquid phase surrounds the fuel rods and channel. As the void fraction increases, the drift velocity decreases, as the buoyant forces become less important. In the GE void-quality correlation, the drift velocity is characterized as

$$V_{gj} \propto (1 - \alpha).$$

This characterization is applied over the entire annular flow region, or for void fractions [ ]. For high void fractions and small values of  $V_{gj}$ , the void fraction is dominated by the ratio of vapor mass flux to total mass flux, determined by a simple mass and energy balance for each node. GE states that the outstanding agreement with the data demonstrated

by Table 7-2 (Table 2-8 of LTR NEDC-33173P (Reference 1)) and the trends shown in Figure 7-6 and Figure 7-7 (Figure 2-2 and Figure 2-3 of LTR NEDC-33173P (Reference 1)) over the entire range shown in the response to SRXB-A-69 (Reference 47) (See Appendix B) and validates this simple model for the drift flux.

#### 7.2.6.1 GE Conclusion

An extrapolation based on this model to void fractions all the way to pure steam flow is justified. In summary, the GE void-quality correlation is based on test data and covers a broad range of conditions. The correlation supports the full range of conditions expected during BWR operation, including CPPU, EPU, and MELLLA+ conditions. The correlation uncertainty is appropriately accounted for in the SLMCPR. It is not necessary to incorporate additional margin for void fraction uncertainty.

#### 7.2.6.2 The NRC Staff Review of GE's Assessment

The GE justifications provided in LTR NEDC-33173P (Reference 1) seem reasonable to a certain degree. Specifically, the NRC staff agrees with GE that:

1. At high void fractions, a high power change is necessary to drive the void fraction from 90 percent to 100 percent during a transient;
2. At steady-state EPU operation, core thermal-hydraulic prediction data indicates bundles operate at powers up to 7 - 8 MW, which is lower than the [ ] that GE states could result in BT for operation with void fraction of [ ]. The current EPU operating experience shows that predicted void fraction ranges are less than 90 percent for the steady-state operation; and
3. For the drift flux correlation, at high void fraction[ ] and low drift velocities, the ratio of the vapor mass flux to total mass flux which is determined by a mass and energy balance is predominant in the void fraction calculations.

However, the NRC staff evaluated GE's assessment and determined that:

1. For a BWR /4 operating at MELLLA+ conditions, RAI 7 (Reference 5) shows that the exit void fraction can be as high as [ ]. Since the specific-plant conditions is not bounding for all MELLLA+ operation plant conditions, the steady-state void fractions can be projected to be greater than [ ] at the lower core flow ranges at EPU power levels. Therefore, for operation at the expanded domains, a void fraction in the greater than the 90 percent range is not limited to "momentary" transient conditions. Instead, bundles can operate with higher exit void conditions as an initial condition. Therefore, for certain plant-specific applications, it is feasible that the void-quality correlation will be extended to close to the 95 percent, during steady-state operation. Meanwhile, it is important to note that the current available operating domain core design's thermal-hydraulic calculations do not indicate significant change in the bundle powers beyond the current EPU bundle powers. The NRC staff does recognize that plants will continue to be constrained to operate within the T-S specified SLMCPR. Therefore, operation with high void conditions will limit the plants' ability to operate with maximum powered bundles operating at high void conditions or high bundle power/flow conditions. Hence, it is not projected that bundles will operate with a high bundle power [ ] or high power/lower core flow conditions, such that BT is not mitigated. It is also feasible that despite the design goals of operation at MELLLA+, plants may be limited in operating at low flow MELLLA+ boundaries by the thermal limits constraints.

- However, it is precisely because of the impact of operation at high void conditions on the SLMCPR response and void reactivity coefficient prediction on the CPR that it becomes important to ensure that the void fraction is not under predicted. Note that bundle powers or bundle power/flow conditions are not directly regulated but compliance with the fuel design limits is required. Thus, higher operating OLMCPR will ensure that plants will operate at lower bundle powers and thus lower corresponding voids fraction such that the SLMCPR is not violated during transient.
2. Although the correlation is dominated by simple mass-energy balance at high void conditions, the available measurement benchmarking does not include or represent fuel design features, bundle powers, peaking, and power and void distribution characteristic of the current operating strategies. Therefore, extension outside of the current operating experience base to MELLLA+ core thermal-hydraulic conditions during steady-state operation based on the currently available measurement data would entail additional extrapolation without the corresponding supporting data. In addition, it does not appear that uncertainties are applied in the void-quality correlation prediction in the codes involved. The underlying assumption is that the impact of the void prediction uncertainties are covered by the overall uncertainty assigned to the power predictions. There are no sensitivity analyses demonstrating the errors in the void prediction to the predicted bundle power levels. TIP calculated versus measured data does not suffice in establishing the sensitivity and uncertainties associated with the within bundle void fractions and the associated predicted bundle powers. The NRC staff could therefore not determine if the bundle power uncertainty applied to the predicted bundle powers would account for an increase in void fraction prediction uncertainty.

Therefore, the NRC staff finds that while the assessment in LTR NEDC-33173P (Reference 1) has merit, it does not provide sufficient bases to conclude that the current available data suffices in the long term for operation at MELLLA+ and this is discussed further below.

#### 7.2.7 Void-Quality Correlation Overall Assessment and Conclusion

In general the performance of the Findlay-Dix correlation does not exhibit any unexpected behavior, and its performance is consistent with other drift flux based correlations that have been developed and compared to a wider range of rod bundle void fraction data.

However, the NRC staff finds that the Findlay-Dix validation database is limited in that it does not extend to the full set of reactor operating conditions for the current and proposed operating strategies. The database does not appear to cover the full operational and accident parameter space in a way that assures that all local parameter sets are encompassed by the supporting bundle data. The quantity of data validating the high void ranges is limited to few data sets.

Moreover, the experimental database benchmarking the Findlay-Dix correlation shows that the axial and radial power distribution and peaking are not consistent with current (or proposed) in-bundle power conditions. Evaluation of the radial within bundle power distribution of the database shows that the validation database is not representative of the current bundle axial or radial power distribution and peaking. This is a deficiency in the database supporting the correlation in relation to the current fuel design operating conditions. The impact of the power distributions is not just at high void conditions, but they also effect the void distribution throughout the bundle (e.g., an inlet peaked power distribution causes earlier void formation, and exit peaked later, etc.). Although the qualities (flow patterns) that will occur are still covered by the combination of development and validation databases, the differences in the power distribution and peaking between the experimental data supporting the correlations and the

current and proposed core operating conditions makes assessment of the reported correlation uncertainties difficult.

The NRC staff also finds that since the void fractions can be close to the [ ] at steady-state for the proposed MELLLA+, extrapolation of the void-quality correlation is not “momentary” during transients as characterized in LTR NEDC-33173P (Reference 1). Operation of all BWRs at the proposed EPU/MELLLA+ could result in bundles operating outside the current experience base in terms of bundle power-to-flow ratio. For EPU operation where plants are limited in terms of available core flow window, the void ranges are expected to remain less than [ ] void fraction during steady-state, but will exceed the [ ] range during some transients and accident conditions. Note that GE states that the void fractions will remain below [ ] for EPU/MELLLA+ operation (See Figure 4-4). The NRC staff does acknowledge that significant power increase is required to drive the void fraction from 90 to 100 percent. However, there is no regulatory limitation on either the bundle powers or the void fractions. The LTR also did not limit the extension of the correlation to [ ] void fraction. Thus, the current experimental database needs to be extended in order to confirm the accuracy of the void-quality correlation for the fuel design features (e.g., 14 part-length rods, impact of the spacer design), bundle powers, power-peaking, and void distributions characteristic of the proposed operating strategies.

The NRC staff also finds that for GE’s analytical methods and codes, uncertainties are not applied to the void-quality correlation prediction. Implicitly, the safety analyses assume that the void-quality correlation is supported by applicable benchmarking data and that the uncertainties associated with it are small. Historically, the NRC staff had also never directly reviewed or approved the correlation and its supporting database. The accuracy of the void-quality correlation affects the coupled neutron and thermal-hydraulic predictions during steady-state, transient, and accident conditions. For most analyses, GE presently applies an uncertainty value directly to the core power. This uncertainty value is used to cover a variety of prediction uncertainties, including the void fraction uncertainty. Some of these uncertainties would impact the power uncertainty in one direction, while others in the opposite direction. Without performing a sensitivity analysis of power to void fraction prediction errors, it is impossible to determine the impact that void fraction uncertainties have on power predictions. GE has not provided this analysis. In a December 14, 2006, meeting, GE did present preliminary bundle gamma scan data and states that gamma scan data provides confirmation of the adequacy of the uncertainty level that they are placing on power. However, GE has not yet submitted the gamma scan results for NRC staff review. Also, the presented scan data did not include the sensitivity of bundle powers gamma scans with voids. Additionally, because gamma scan data can only cover parameters up to normal operating conditions, predictions must be used to extrapolate beyond those conditions. It is therefore important to understand the sensitivity of power to void fraction prediction uncertainty, as well as the uncertainty levels themselves.

Therefore, the NRC staff concludes that the reported accuracy is not well supported and additional measurement data is needed to both validate the correlation and develop the appropriate correlation uncertainty levels. This conclusion is specifically relevant in support of operation at MELLLA+ in which plants would be operating outside the current experience base. It is important to note that the conclusion to obtain additional data to validate the impact of non-uniform (e.g., skewed) power distribution is supported by the recommendations made in the initial 1977 document NEDE-21565 (Reference 52). The NRC staff believes the weaknesses of the validation database identified in NEDE-21565 (Reference 52) are more relevant in the current EPU operating strategy and the proposed expanded operating domain, where there could be higher power skews in both the radial and axial directions than existed previously. Radial power skewing can develop from bundles next to a controlled cell or due to the influence

of an adjacent controlled four-bundle cell. Review of the radial power distribution as bundles deplete with exposure for MELLLA+ lattice designs indicates that the radial power distribution is more peaked early in the cycle and becomes more uniform as the Gd burns up and different pin peak. Therefore, radial power skewing similar to ASEA-813 qualification is most probable early in the cycle and from the influence of a controlled cell. The current within lattice peaking would be expected to affect the void distribution parameter and the accuracy of the functional trends of the empirical parameters, which were derived from the GE database. Additionally, the lack of partial length rod data in development or benchmarking of the correlation does not allow the NRC staff to evaluate accurately the present correlation and the uncertainty levels presented.

The NRC staff considered applying higher uncertainties to the void-quality correlation predictions. Since many of the void-quality correlation applications do not apply uncertainties directly to the void predictions, this would require re-review of all NRC-approved code-sets. In addition, the uncertainties to be applied need to be quantified through sensitivity analyses (perturbation of the voids) for the impact of: (1) the new design features (14 part-length rods); (2) within bundle power-peaking and distribution (lattice loading as operated in the current and proposed operating strategies); and (3) 10x10 fuel and spacer mechanical design. These uncertainties will need to be propagated through all of the steady-state, transient and accident safety analyses to quantify any non-conservative impacts that must be applied to comply with the design bases requirements. Such sensitivity analyses may involve the use of sub-channel codes that had not been approved by NRC. Therefore, the NRC staff believes that a better approach is extension of the experimental validation instead of relying on code perturbations and predictions for qualifying the performance of the correlation for the current and proposed fuel designs and operating strategies.

Although the supporting data does not cover all of the current operational conditions (e.g., the current radial and axial lattice peaking, the 10x10 bundle design features such as the part-length rods and new spacer design), the NRC staff finds that overall the correlation does not exhibit unexpected behavior and remains relatively predictable. However, the NRC staff expects that most likely the uncertainty levels are higher than those reported.

The NRC staff concludes that considering the deficiencies as discussed above, additional relevant experimental data is required to support operation at EPU and MELLLA+. Obtaining experimental data requires time. Therefore, the NRC staff assessed the feasible short-term action plan as discussed below.

As an immediate short-term confirmation for EPU transients, the NRC staff recommends that GE evaluate the use of the bundle pressure drop measurement data taken in the ATLAS facility using 10x10 bundles to back-calculate the void fraction in those tests, comparing those results with predicted void fraction (using Findlay-Dix) for low flow conditions, characteristic of RPT conditions. This data will be relevant to the EPU applications, in which the [ ] void fraction range will be exceeded during transients such as RPT. Similar to the NEDE-21565 (Reference 52) approach, the low flow GE 10x10 pressure drop data could potentially be used to re-establish the functional trends of the empirical parameters. In MFN 06-435 (Reference 14), GE states that during the development of fuel product lines, GE's current practice is to obtain full-scale experimental data for both critical power and pressure drop performance. As part of the requirements to remove the 0.01 penalty on the OLMCPR, GE will provide a report of GE14 pressure drop data and an analysis relating this data to void prediction error. The NRC staff finds that for PANCEA/ODYN/ISCOR/TASC applications, this data will provide additional confidence in the performance of the correlation in the low flow ranges. The objective is to evaluate the axial void fractions calculated from the pressure drop data in order to determine if accuracy of the correlation changes axially at the part-length rods elevation and at the highly voided upper portion of the fuel bundles. The radial and axial power distributions

used in the pressure drop experiments would help to assess the void correlations accuracy. The conclusions of this study will be factored into the acceptability of the void-quality correlation for EPU applications.

In addition, the NRC staff considered short-term margin increase until such time that the qualification database is expanded to include data, which is more representative of current fuel designs. Since higher uncertainties in the void-quality correlation will result in the existence of higher voids than predicted, the core average voids could be higher assuming that the correlation uncertainties are higher for all lattice levels due to the different power skew, part-length rods and new design features (e.g., new spacer designs). Higher core average voids will potentially affect the magnitude of the void reactivity coefficient, which is directly proportional to the core average void fraction.

Appendix E contains an assessment of the impact of void fraction error on the value of the void reactivity coefficient. The results are shown graphically in Figure E-2 in Appendix E. As observed in this figure, the density reactivity change (DRC) error is a function of the void fraction, but it levels to an approximate value of 1.25 percent for void fractions greater than 60 percent, which is the range of interest. Therefore, the NRC staff concludes that a DRC error of 1.25 percent is a reasonable approximation of the error induced by a change in actual void fraction of 1 percent. For example, if the predicted void fraction is 70 percent, but the actual void fraction is 71 percent, the actual DRC is 1.25 percent higher than predicted. An error of the magnitude of the void fraction prediction by 5 percent could be approximated to result in 6.25 percent error in the density reactivity coefficient.

Note that the numbers used in the Appendix E assessments are representative of a BWR/6 plant, but DRC values change with core loading, exposure, operating condition, etc. Therefore, the 1.25 percent error should be considered as an indication for order of magnitude calculation and not a bounding number.

The NRC staff does not believe in changing intermediate parameters such as the void reactivity coefficient, because it may result in an inadvertent non-conservatism in some of the safety analyses. Therefore, the NRC staff decided as an interim measure, the impact of having higher voids than predicted can be accounted for in the impact of the void reactivity coefficient on the transient analyses. In response to RAI 2-6 (Reference 3), GE has stated that the threshold for change in the analysis figure of merit is generally one to two standard deviations. According to NEDE-24154-A, this value is 0.03 for ODYN in terms of the  $\Delta\text{CPR}/\text{ICPR}$ . However, the NRC staff considers the significance threshold for CPR change for transients is 0.01. Therefore, as an interim measure, the NRC staff concludes that until sufficient assessment of the void-quality correlation prediction as applied to the current fuel geometric and lattice designs as operated under EPU and the proposed high power-to-flow MELLLA+ condition is provided, a 0.01 margin will be applied to the OLMCPR. The following limitations will be added until such time that GE expands the experimental database supporting the Findlay-Dix void-quality correlation:

#### **Void-Quality Correlation Limitation 1**

For applications involving PANCEA/ODYN/ISCOR/TASC for operation at EPU and MELLLA+, an additional 0.01 will be added to the OLMCPR, until such time that GE expands the experimental database supporting the Findlay-Dix void-quality correlation to demonstrate the accuracy and performance of the void-quality correlation based on experimental data representative of the current fuel designs and operating conditions during steady-state, transient, and accident conditions.

### 7.2.8 TRACG Interfacial Shear Model Qualification

Most MELLLA+ applications are expected to transition to TRACG. TRACG uses an interfacial shear model in the prediction of the void fractions. Section 3.1 of NEDE-32177PA, "Licensing Topical Report, TRACG Qualification" (Reference 55), covers the adequacy of TRACG in predicting void fraction. FRIGG OF-64 tests simulate a full-scale 64-rod BWR fuel bundle. The test was designed as a full-scale simulation of an Oskarshamn-I fuel assembly, consisting of 64 heated rods placed in a 8x8 array. The test simulated a realistic and somewhat conservative (outlet peaked) BWR heat flux and the TRACG interfacial shear model void fraction prediction is compared against FRIGG OF-64 void fraction data.

Table 3.1-1 of NEDE-32177 (Reference 55) shows the ranges of the FRIGG OF-64 test parameter ranges as follows:

[	
	]

Table 3.1-4 of NEDE-32177 (Reference 55) provides the mean and standard deviation for TRACG Model based on the FRIG OF-64 tests as follows:

Pressure (MPa)	Mean	Standard Deviation
4.8	[	
6.8%		]

NEDE-32177 (Reference 55) concludes that TRACG void fraction predictions agree very well with the OF-64 measurements. While the TRACG shear model agreement with the OF-64 tests appears acceptable, however the qualification range is below the steady-state void conditions for operation at MELLLA+. The pressure ranges are also slightly below the steady-state void ranges for BWRs, and the data does not cover the ranges that BWRs experience during pressurization transients as well as accidents (e.g., ATWS). The impact of the lack of data covering the transients (both pressurization and depressurization) and accidents to the adequacy of the interfacial shear model needs to be assessed.

In addition, TRACG is coupled with neutronic methods (TGBLA/PANCEA) that rely on the Findlay-Dix Correlation in calculating the void fraction. Therefore, the coupled neutronic and thermal-hydraulic models appear to use different methods in calculating the void fraction. For the neutronic methods conclusions reached in the assessment of the Findlay- Dix correlation applies. The adequacy of the TRACG interfacial shear model qualification for application to EPU and MELLLA+ will be covered during the NRC staff review of NEDE-32906P, Supplement 3 (Reference 40). Therefore, any conclusions specified in the NRC staff SE approving Supplement 3 to LTR NEDC-32906P (Reference 40) will be applicable as approved for EPU and MELLLA+ application.

#### **Void-Quality Correlation Limitation 2**

The NRC staff is currently reviewing Supplement 3 to NEDE-32906P, "Migration to TRACG04/PANAC11 from TRACG02/PANAC10," dated May 2006 (Reference 40). The adequacy of the TRACG interfacial shear model qualification for application to EPU and MELLLA+ will be addressed under this review. Any conclusions specified in the NRC staff SE approving Supplement 3 to LTR NEDC-32906P (Reference 40) will be applicable as approved.



#### 7.2.9 Void-Quality Correlation Conclusion

Based on the assessments detailed in this section, the void perturbation studies performed in the past, the ranges of the current supporting database and the relative predictability of the correlation behavior, and the additional margin included in the OLMCPR, the NRC staff concludes that there is a reasonable assurance that the use Findlay-Dix correlation will result in adequate safety margin. The safety findings in Section 7.2, "Void-Quality Correlation," of this SE are contingent on Void-Quality Correlation Limitations 1 and 2.

Table 7-1 Comparison of GE Experimental Database and 10x10 bundle Operating Conditions

	Data used in development and evaluation of the GE correlation						
	Used to develop correlation			Used for correlation comparison			
Data Source	CISE	GE	ASEA-713	Simple Geometry	ASEA-813	ASEA-513	10x10 BWR Bundle (GE14)
Geometry	4X4 Bundle	7x7 Bundle	8x8 Bundle	Round and Rectangular Tube/Annulus	8x8 Bundle	6X6 Bundle	10x10 Bundle
Hydraulic diameter (m)	[						
Pressure (MPa)							
Mass Flux (kg/m <sup>2</sup> /s)							
Inlet Sub-cooling (K)							
Exit Quality							
Void fraction							
Reynolds No.							
Measurement Type							
Axial power distribution							
Radial power distribution							
Quoted std. deviation (%)							]

**Table 7-2 Void Fraction Correlation Database**

[

]

**Table 7-3 Comparison between Void-Quality Correlation and Database**

[

]

[

**Figure 7-1 GEXL14 Application Range**

[

**Figure 7-2 Void Fraction vs. Quality – Data and Calculation**

]

[

]

**Figure 7-3 Normalized Radial Power Distribution (8X8 array) – ASEA-713 Experiment**

[

]

**Figure 7-4 Normalized Radial Power Distribution (8X8 array) – ASEA-813 Experiment**

[

Figure 7-5 Normalized Power Distribution (10X10 array) - VYNPS Lattice 5168, 40 percent Void, Burnup = 0

]

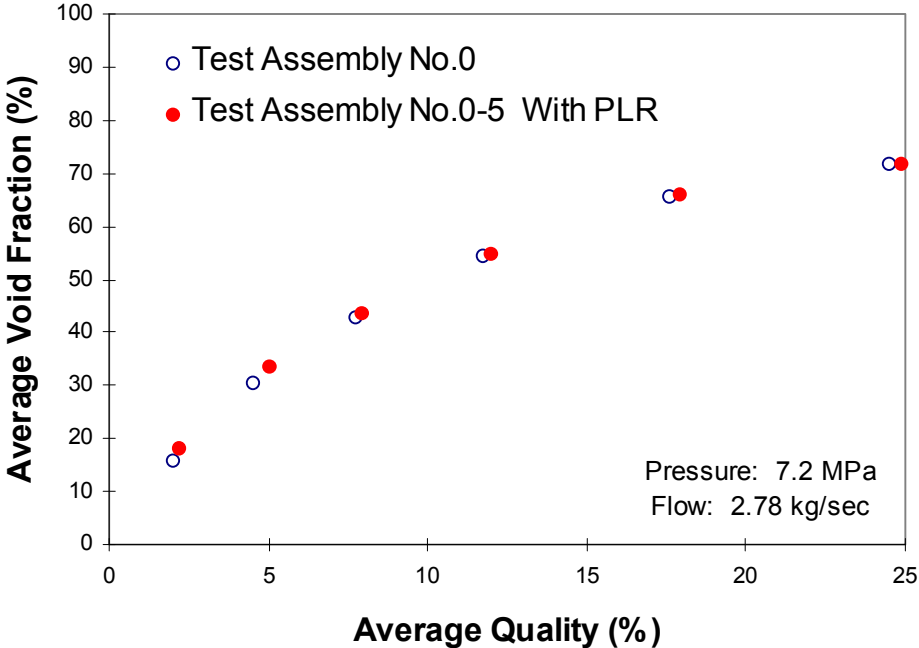


Figure 7-6 Void Fraction-Quality Relation with Partial Length Rods at Low Flow

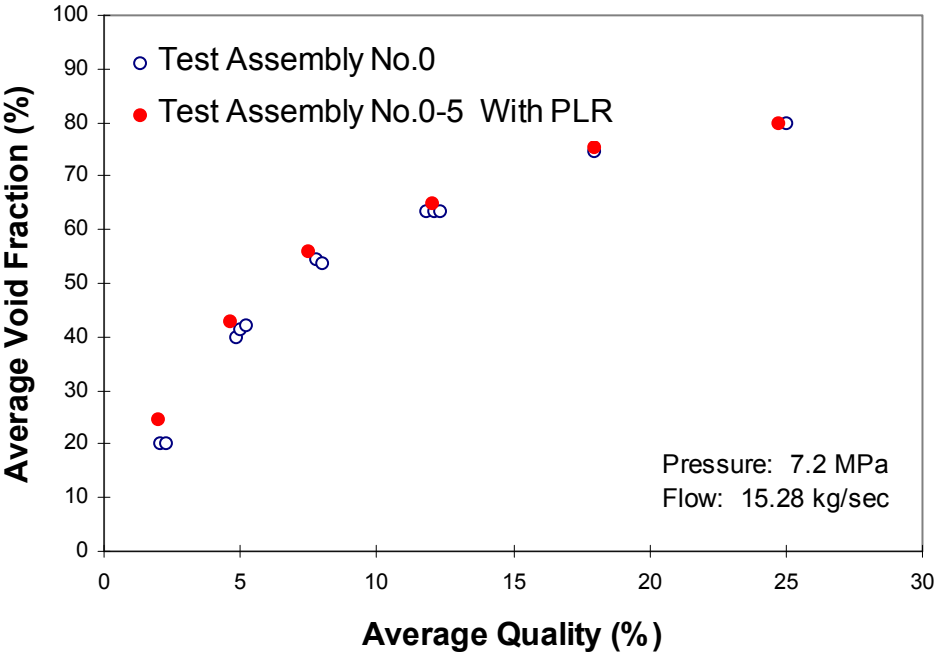


Figure 7-7 Void Fraction-Quality Relation with Partial Length Rods at High Flow

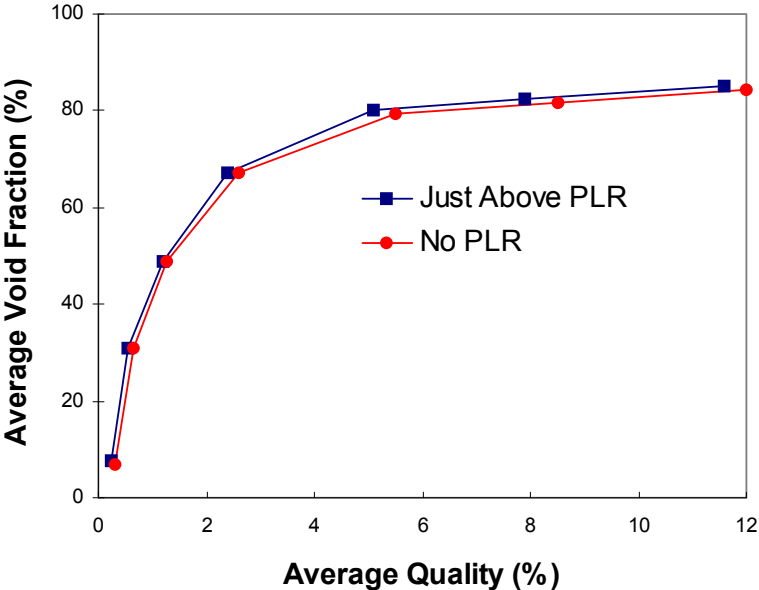


Figure 7-8 Void Fraction-Quality Relation with Partial Length Rods

[

**Figure 7-9 Comparison to Findlay-Dix Correlation against Other Drift Flux Models**

]

## **8.0 LICENSING APPLICATION**

LTR NEDC-33173P (Reference 1) Section 4.0, "Licensing Application," covers its applicability and the specific information that is required to be provided in plant-specific applications.

LTR NEDC-33173P (Reference 1) is applicable for operation at EPU and expanded operating domains, within the MELLLA+ upper boundary. The NRC staff reviewed LTR NEDC-33173P (Reference 1) to ensure that for operation at high power and low flow MELLLA+ conditions, the GE analytical methods and codes that are being applied to demonstrate the safe operation of BWRs are applicable and acceptable. Section 2.1 of this SE provided a summary of the proposed expanded operating domain core conditions.

LTR NEDC-33006P, Revision 2 (Reference 2), provides GE safety analysis report for operation at the proposed expanded operating domains. LTR NEDC-33173P (Reference 1) provides the bases for accepting the application of GE NRC-approved analytical methods and codes to MELLLA+ high power and low flow conditions. The MELLLA+ LTR (Reference 2) was approved by the NRC staff on September 17, 2007 (Reference 56).

### **8.1 OVERVIEW**

The objective of the NRC staff review of LTR NEDC-33173P is to evaluate the applicability of GE's analytical methods to operation at EPU and MELLLA+. Plant-specific applications that reference LTR NEDC-33173P need to comply with Section 9.0, "Limitations and Conditions," of this SE.



MFN 06-434 (Reference 38), the updated response to NRC staff RAI 28-2, specifies the actions required to remove the additional power distribution uncertainties currently applied to GE methods. The NRC staff finds that the approach and actions presented in the Reference 38 commitment letter are acceptable and provide bases for finalizing neutronic methods qualification. The future supplements finalizing LTR NEDC-33173P will also cover the pending generic methods RAIs.

If LTR NEDC-33173P is revised or supplemented, the topics addressed in this SE, associated commitments and the limitations and conditions specified in Section 9.0 should be covered, unless GE demonstrates that the limitations are not needed due to changes in methods or that the additional benchmarking is provided to the NRC staff in another LTR.

## 8.2 MIXED CORE APPLICABILITY

LTR NEDC-33173P (Reference 1) is applicable to current GE BWR fuel product lines licensed with GE's nuclear and safety analysis methods. This approval did not cover the use of GE's methods to legacy fuel designs or mixed cores. Specifically, this review did not evaluate the impact or accuracy of GE's lattice physics (TGBLA06) and core simulator methods (PANAC11) to model legacy fuel designs for operation at EPU and MELLLA+. For example, LTR NEDC-33173P (Reference 1) did not provide lattice physics data demonstrating the uncertainties associated with legacy fuel.

In addition, LTR NEDC-33173P (Reference 1) did not contain margin evaluation of GE methodology for modeling the legacy fuel and establishing the fuel design limits such as the steady-state and transient LHGR and the exposure accounting. Other topics covered in LTR NEDC-33173P (Reference 1) such as the applicability and extension of the void fraction correlation for operation at MELLLA+ were not assessed for legacy fuel. Therefore, plant-specific applications referencing this LTR for operation at EPU and MELLLA+ need to provide plant-specific justifications. Alternatively, GE can supplement or revise LTR NEDC-33173P (Reference 1) with mixed core evaluation for EPU and MELLLA+ applications.

### **Mixed Core Method Limitation 1:**

Plants implementing EPU or MELLLA+ with mixed fuel vendor cores will provide plant-specific justification for extension of GE's analytical methods or codes. The content of the plant-specific application will cover the topics addressed in this SE as well as subjects relevant to application of GE's methods to legacy fuel. Alternatively, GE may supplement or revise LTR NEDC-33173P (Reference 1) for mixed core application.

### **Mixed Core Method Limitation 2:**

For any plant-specific applications of TGBLA06 with fuel type characteristics not covered in this review, GE needs to provide assessment data similar to that provided for the GE fuels.

The Interim Methods review is applicable to all GE lattices up to GE14. Fuel lattice designs, other than GE lattices up to GE14, with the following characteristics are not covered by this review:

- square internal water channels water crosses
- Gd rods simultaneously adjacent to water and vanished rods
- 11x11 lattices
- MOX fuel

The acceptability of the modified epithermal slowing down models in TGBLA06 has not been demonstrated for application to these or other geometries for expanded operating domains.

Significant changes in the Gd rod optical thickness will require an evaluation of the TGBLA06 radial flux and Gd depletion modeling before being applied. Increases in the lattice Gd loading that result in nodal reactivity biases beyond those previously established will require review before the GE methods may be applied.

### 8.3 EXPANDED OPERATING DOMAIN EIGENVALUE TRACKING

In general, GE obtains cycle-specific operating data (e.g., plant measurement data, CR patterns, etc.) and simulates the core conditions as function of exposure, projecting the hot eigenvalue, the cold eigenvalue, and the thermal margins. In MFN 04-026 (Reference 5), GE provided eigenvalue tracking data for EPU plants. To assess and monitor the performance of the nuclear methods for implementation to MELLLA+ conditions, GE will internally perform eigenvalue tracking and evaluate the performance of the nuclear methods for application to the new operating domains. In response, to RAI 5 in MFN 04-026 (Reference 5), GE committed to analyze the operational data for the first plant-specific implementation of MELLLA+ and submit the evaluation for NRC staff review.

#### **MELLLA+ Eigenvalue Tracking Limitation**

In the first plant-specific implementation of MELLLA+, the cycle-specific eigenvalue tracking data will be evaluated and submitted to NRC to establish the performance of nuclear methods under the operation in the new operating domain. The following data will be analyzed:

- Hot critical eigenvalue,
- Cold critical eigenvalue,
- Nodal power distribution (measured and calculated TIP comparison),
- bundle power distribution (measured and calculated TIP comparison),
- Thermal margin,
- Core flow and pressure drop uncertainties, and
- The MIP Criterion (e.g., determine if core and fuel design selected is expected to produce a plant response outside the prior experience base).

Provision of evaluation of the core-tracking data will provide the NRC staff with bases to establish if operation at the expanded operating domain indicates: (1) changes in the performance of nuclear methods outside the EPU experience base; (2) changes in the available thermal margins; (3) need for changes in the uncertainties and NRC-approved criterion used in the SLMCPR methodology; or (4) any anomaly that may require corrective actions.

### 8.4 TGBLA06 METHODOLOGY UPGRADES

Table 8-1 documents the history of changes to the TGBLA06AE5 methodology for versions AE2, AE3, and AE4 for implementation of water-cross feature representative of SVEA fuel.

1. Modification AE2 corrected R-factor output problem, and was approved by NRC in 1999.

2. Modification AE3 corrected a problem in the modeling of controlled water cross fuel model. The NRC staff did not assess this modification, because this modification has no impact on calculations for non-water cross designs, and no information was provided for this review.
3. Modification AE4 incorporated corrections and improvements to several TGBLA06 features.

GE states in MFN 05-029 (Reference 11),

In response to the request for additional analyses of the PANACEA cross-section fitting interpolation/extrapolation process, a “usage range extension” study has been performed to allow examination of 90 percent void depletion uncertainties. [

]. As the impact on the 0, 40, and 70 percent void data is minimal, this weakness does not significantly impact the fitting errors for extrapolation to void fractions higher than 70 percent.

The NRC staff compared the performance of TGBLA06AE5 against HELIOS with lattices with and without vanished rods, and Gd content from 6 percent to 7 percent. From the code-to-code comparisons, as well as the TGBLA06-CASMO4 comparisons provided, the NRC staff finds that the TGBLA06AE5 modifications, including the above Pu-240 modifications, are acceptable for production.

It is important to restate that this SE provides an interim approval for the use of TGBLA06AE5. Actual benchmarking of GE or any other vendor fuel design will be evaluated by the NRC staff once the experimental gamma scan data is provided (Reference 31).

Once the gamma scan validation data is available, the NRC staff will re-evaluate the uncertainties associated with the TGBLA06/PANAC11 methodology. In addition, Supplement 3 to LTR NEDC-32906P (Reference 40) documents the TRACG/PANAC methodology changes and upgrades that are currently under NRC staff review. Any specific limitations arising from that review will be applicable for EPU and MELLLA+ applications.

## 8.5 PLANT-SPECIFIC APPLICATION PROCESS

The core thermal-hydraulic conditions for operation at EPU and MELLLA+ can be gauged by review of: (1) Power of Peak Bundle; (2) Coolant Flow for Peak Bundle; (3) Exit Void Fraction for Peak Power Bundle; (4) Maximum Channel Exit Void Fraction; (5) Core Average Exit Void Fraction; (6) Peak LHGR; and (7) Peak Nodal or Pin Exposure. The hot bundles set the steady-state fuel design thermal limits. Therefore, review of these parameters for cycle exposure statepoints provides insight into the core conditions of the plant-specific application against EPU experience base.

### **Plant-Specific Application Limitation:**

The plant-specific applications will provide prediction of key parameters for cycle exposures for operation at EPU (and MELLLA+ for MELLLA+ applications). The plant-specific prediction of these key parameters will be plotted against the EPU Reference Plant experience base and MELLLA+ operating experience, if available. For evaluation of the margins available in the fuel design limits, plant-specific applications will also provide quarter core map (assuming core symmetry) showing bundle power, bundle operating LHGR, and MCPR for BOC, MOC, and EOC. Since the minimum margins to specific limits may occur at exposures other than the traditional BOC, MOC, and EOC, the data will be provided at these exposures.

## 8.6 TECHNICAL SPECIFICATIONS

Plant-specific TSs reference the NRC-approved licensing methodologies used to perform the design bases safety analyses. Plants implementing LTR NEDC-33173P shall include the LTR in Section 5 of the TS. Alternately, if LTR NEDC-33173P is included in GE's licensing methodology GESTAR II, plants may reference GESTAR II, in lieu of referencing NEDC-33173P directly.

**Table 8-1 History of the Changes in TGBLA06A**

[

]

**9.0 LIMITATIONS AND CONDITIONS**

The NRC staff has concluded that LTR NEDC-33173P (Reference 1) is acceptable with limitations and conditions described below.

1. TGBLA/PANAC Version (Section 3.1.5.2)

The neutronic methods used to simulate the reactor core response and that feed into the downstream safety analyses supporting operation at EPU/MELLLA+ will apply TGBLA06/PANAC11 or later NRC-approved version of neutronic method.

2. 3D Monicore (Section 3.1.5.2)

For EPU/MELLLA+ applications, relying on TGBLA04/PANAC10 methods, the bundle RMS difference uncertainty will be established from plant-specific core-tracking data, based on TGBLA04/PANAC10. The use of plant-specific trendline based on the neutronic method employed will capture the actual bundle power uncertainty of the core monitoring system.

3. Power-to-Flow Ratio (Section 3.1.5.2)

Plant-specific EPU and expanded operating domain applications will confirm that the core thermal power to core flow ratio will not exceed 50 MWt/Mlbm/hr at any statepoint in the allowed operating domain. For plants that exceed the power-to-flow value of 50 MWt/Mlbm/hr, the application will provide power distribution assessment to establish that neutronic methods axial and nodal power distribution uncertainties have not increased.

4. SLMCPR 1 (Section 3.2.2.2):

For EPU operation, a 0.02 value shall be added to the cycle-specific SLMCPR value. This adder is applicable to SLO, which is derived from the dual loop SLMCPR value.

5. SLMCPR 2 (Section 3.2.2.2):

For operation at MELLLA+, including operation at the EPU power levels at the achievable core flow statepoint, a 0.03 value shall be added to the cycle-specific SLMCPR value.

6. R-factor (Section 3.2.3):

The plant specific R-factor calculation at a bundle level will be consistent with lattice axial void conditions expected for the hot channel operating state. The plant-specific EPU/MELLLA+ application will confirm that the R-factor calculation is consistent with the hot channel axial void conditions.

7. ECCS-LOCA 1 (Section 3.2.5.1.1):

For applications requesting implementation of EPU or expanded operating domains, including MELLLA+, the small and large break ECCS-LOCA analyses will include top-peaked and mid-peaked power shape in establishing the MAPLHGR and determining the PCT. This limitation is applicable to both the licensing bases PCT and the upper bound PCT. The plant-specific applications will report the limiting small and large break licensing basis and upper bound PCTs.

8. ECCS-LOCA 2 (Section 3.2.5.1.2):

The ECCS-LOCA will be performed for all statepoints in the upper boundary of the expanded operating domain, including the minimum core flow statepoints, the transition statepoint as defined in Reference 2 and the 55 percent core flow statepoint. The plant-specific application

will report the limiting ECCS-LOCA results as well as the rated power and flow results. The SRLR will include both the limiting statepoint ECCS-LOCA results and the rated conditions ECCS-LOCA results.

9. Transient LHGR 1 (Section 3.2.6.5.1)

Plant-specific EPU and MELLLA+ applications will demonstrate and document that during normal operation and core-wide AOOs, the T-M acceptance criteria as specified in Amendment 22 to GESTAR II will be met. Specifically, during an AOO, the licensing application will demonstrate that the: (1) loss of fuel rod mechanical integrity will not occur due to fuel melting and (2) loss of fuel rod mechanical integrity will not occur due to pellet-cladding mechanical interaction. The plant-specific application will demonstrate that the T-M acceptance criteria are met for the both the UO<sub>2</sub> and the limiting GdO<sub>2</sub> rods.

10. Transient LHGR 2 (Section 3.2.6.5.1)

Each EPU and MELLLA+ fuel reload will document the calculation results of the analyses demonstrating compliance to transient T-M acceptance criteria. The plant T-M response will be provided with the SRLR or COLR, or it will be reported directly to the NRC as an attachment to the SRLR or COLR.

11. Transient LHGR 3 (Section 3.2.6.5.2)

To account for the impact of the void history bias, plant-specific EPU and MELLLA+ applications using either TRACG or ODYN will demonstrate an equivalent to 10 percent margin to the fuel centerline melt and the 1 percent cladding circumferential plastic strain acceptance criteria due to pellet-cladding mechanical interaction for all of limiting AOO transient events, including equipment out-of-service. Limiting transients in this case, refers to transients where the void reactivity coefficient plays a significant role (such as pressurization events). If the void history bias is incorporated into the transient model within the code, then the additional 10 percent margin to the fuel centerline melt and the 1 percent cladding circumferential plastic strain is no longer required.

12. LHGR and Exposure Qualification (Section 3.2.6.5.5)

In MFN 06-481, GE committed to submit plenum fission gas and fuel exposure gamma scans as part of the revision to the T-M licensing process. The conclusions of the plenum fission gas and fuel exposure gamma scans of GE 10x10 fuel designs as operated will be submitted for NRC staff review and approval. This revision will be accomplished through Amendment to GESTAR II or in a T-M licensing LTR. PRIME (a newly developed T-M code) has been submitted to the NRC staff for review (Reference 58). Once the PRIME LTR and its application are approved, future license applications for EPU and MELLLA+ referencing LTR NEDC-33173P must utilize the PRIME T-M methods.

13. Application of 10 Weight Percent Gd (Section 3.2.6.5.6)

Before applying 10 weight percent Gd to licensing applications, including EPU and expanded operating domain, the NRC staff needs to review and approve the T-M LTR demonstrating that the T-M acceptance criteria specified in GESTAR II and Amendment 22 to GESTAR II can be met for steady-state and transient conditions. Specifically, the T-M application must demonstrate that the T-M acceptance criteria can be met for TOP and MOP conditions that

bounds the response of plants operating at EPU and expanded operating domains at the most limiting statepoints, considering the operating flexibilities (e.g., equipment out-of-service). Before the use of 10 weight percent Gd for modern fuel designs, NRC must review and approve TGBLA06 qualification submittal. Where a fuel design refers to a design with Gd-bearing rods adjacent to vanished or water rods, the submittal should include specific information regarding acceptance criteria for the qualification and address any downstream impacts in terms of the safety analysis. The 10 weight percent Gd qualifications submittal can supplement this report.

14. Part 21 Evaluation of GESTR-M Fuel Temperature Calculation (Section 3.2.6.5.8)

Any conclusions drawn from the NRC staff evaluation of the GE's Part 21 report will be applicable to the GESTR-M T-M assessment of this SE for future license application. GE submitted the T-M Part 21 evaluation, which is currently under NRC staff review. Upon completion of its review, NRC staff will inform GE of its conclusions.

15. Void Reactivity 1 (Section 4.4):

The void reactivity coefficient bias and uncertainties in TRACG for EPU and MELLLA+ must be representative of the lattice designs of the fuel loaded in the core.

16. Void Reactivity 2 (Section 4.4):

A supplement to TRACG /PANAC11 for AOO is under NRC staff review (Reference 40). TRACG internally models the response surface for the void coefficient biases and uncertainties for known dependencies due to the relative moderator density and exposure on nodal basis. Therefore, the void history bias determined through the methods review can be incorporated into the response surface "known" bias or through changes in lattice physics/core simulator methods for establishing the instantaneous cross-sections. Including the bias in the calculations negates the need for ensuring that plant-specific applications show sufficient margin. For application of TRACG to EPU and MELLLA+ applications, the TRACG methodology must incorporate the void history bias. The manner in which this void history bias is accounted for will be established by the NRC staff SE approving NEDE-32906P, Supplement 3, "Migration to TRACG04/PANAC11 from TRACG02/PANAC10," May 2006 (Reference 40). This limitation applies until the new TRACG/PANAC methodology is approved by the NRC staff.

17. Steady-State 5 Percent Bypass Voiding (Section 5.4):

The instrumentation specification design bases limit the presence of bypass voiding to 5 percent (LRPM levels). Limiting the bypass voiding to less than 5 percent for long-term steady operation ensures that instrumentation is operated within the specification. For EPU and MELLLA+ operation, the bypass voiding will be evaluated on a cycle-specific basis to confirm that the void fraction remains below 5 percent at all LRPM levels when operating at steady-state conditions within the MELLLA+ upper boundary. The highest calculated bypass voiding at any LRPM level will be provided with the plant-specific SRLR.



18. Stability Setpoints Adjustment (Section 6.2)

The NRC staff concludes that the presence bypass voiding at the low-flow conditions where instabilities are likely can result in calibration errors of less than 5 percent for OPRM cells and less than 2 percent for APRM signals. These calibration errors must be accounted for while determining the setpoints for any detect and suppress long term methodology. The calibration values for the different long-term solutions are specified in the associated sections of this SE, discussing the stability methodology.

19. Void-Quality Correlation 1 (Section 7.2.7)

For applications involving PANCEA/ODYN/ISCOR/TASC for operation at EPU and MELLLA+, an additional 0.01 will be added to the OLMCPR, until such time that GE expands the experimental database supporting the Findlay-Dix void-quality correlation to demonstrate the accuracy and performance of the void-quality correlation based on experimental data representative of the current fuel designs and operating conditions during steady-state, transient, and accident conditions.

20. Void-Quality Correlation 2 (Section 7.2.8)

The NRC staff is currently reviewing Supplement 3 to NEDE-32906P, "Migration to TRACG04/PANAC11 from TRACG02/PANAC10," dated May 2006 (Reference 40). The adequacy of the TRACG interfacial shear model qualification for application to EPU and MELLLA+ will be addressed under this review. Any conclusions specified in the NRC staff SE approving Supplement 3 to LTR NEDC-32906P (Reference 40) will be applicable as approved.

21. Mixed Core Method 1 (Section 8.2):

Plants implementing EPU or MELLLA+ with mixed fuel vendor cores will provide plant-specific justification for extension of GE's analytical methods or codes. The content of the plant-specific application will cover the topics addressed in this SE as well as subjects relevant to application of GE's methods to legacy fuel. Alternatively, GE may supplement or revise LTR NEDC-33173P (Reference 1) for mixed core application.

22. Mixed Core Method 2 (Section 8.2):

For any plant-specific applications of TGBLA06 with fuel type characteristics not covered in this review, GE needs to provide assessment data similar to that provided for the GE fuels. The Interim Methods review is applicable to all GE lattices up to GE14. Fuel lattice designs, other than GE lattices up to GE14, with the following characteristics are not covered by this review:

- square internal water channels water crosses
- Gd rods simultaneously adjacent to water and vanished rods
- 11x11 lattices
- MOX fuel

The acceptability of the modified epithermal slowing down models in TGBLA06 has not been demonstrated for application to these or other geometries for expanded operating domains.

Significant changes in the Gd rod optical thickness will require an evaluation of the TGBLA06 radial flux and Gd depletion modeling before being applied. Increases in the lattice Gd loading

that result in nodal reactivity biases beyond those previously established will require review before the GE methods may be applied.

#### 23. MELLLA+ Eigenvalue Tracking (Section 8.3)

In the first plant-specific implementation of MELLLA+, the cycle-specific eigenvalue tracking data will be evaluated and submitted to NRC to establish the performance of nuclear methods under the operation in the new operating domain. The following data will be analyzed:

- Hot critical eigenvalue,
- Cold critical eigenvalue,
- Nodal power distribution (measured and calculated TIP comparison),
- bundle power distribution (measured and calculated TIP comparison),
- Thermal margin,
- Core flow and pressure drop uncertainties, and
- The MIP Criterion (e.g., determine if core and fuel design selected is expected to produce a plant response outside the prior experience base).

Provision of evaluation of the core-tracking data will provide the NRC staff with bases to establish if operation at the expanded operating domain indicates: (1) changes in the performance of nuclear methods outside the EPU experience base; (2) changes in the available thermal margins; (3) need for changes in the uncertainties and NRC-approved criterion used in the SLMCPR methodology; or (4) any anomaly that may require corrective actions.

#### 24. Plant-Specific Application (Section 8.5)

The plant-specific applications will provide prediction of key parameters for cycle exposures for operation at EPU (and MELLLA+ for MELLLA+ applications). The plant-specific prediction of these key parameters will be plotted against the EPU Reference Plant experience base and MELLLA+ operating experience, if available. For evaluation of the margins available in the fuel design limits, plant-specific applications will also provide quarter core map (assuming core symmetry) showing bundle power, bundle operating LHGR, and MCPR for BOC, MOC, and EOC. Since the minimum margins to specific limits may occur at exposures other than the traditional BOC, MOC, and EOC, the data will be provided at these exposures.

### 10.0 CONCLUSION

The NRC staff reviewed the application of GE analytical methods and codes to operation at EPU and expanded operating domains. The NRC staff reviewed: (1) if the analytical methods were being applied within the NRC-approved applicability; (2) the adequacy of the uncertainties applied to the safety analyses; (3) the conservatism in the analytical methods; (4) the margins available; and (5) the adequacy of the available qualifications data. Additional margins were implemented where the NRC staff found the extension of the methods to EPU and MELLLA+ operation merits additional benchmarking data. The review of the interim methods includes number of commitments by GE to obtain experimental data that in the long term will provide additional confidence in the extension of the methods to EPU and expanded operating domain operation.

Based on the review performed, the information provided in the RAI responses, the insights from the NRC staff confirmatory analyses, and the additional margins included in the methods, the NRC staff finds that the application of GE methods to EPU and the expanded operating domains is acceptable with the limitations and conditions stipulated in Section 9.0 of this SE.

## 11.0 REFERENCES

1. GE Letter (MFN 06-056), L. M. Quintana to NRC, GE Licensing Topical Report NEDC-33173P, Applicability of GE Methods to Expanded Operating Domains, February 10, 2006. (ADAMS Package Accession No. ML060450677).
2. GE Letter (MFN 05-141), L. M. Quintana to NRC, NEDC-33006P, Revision 2 "General Electric Boiling Water Reactor Maximum Extended Load Line Limit Analysis Plus," November 28, 2005. (ADAMS Accession No. ML053360526).
3. GE Letter (MFN 05-022), G. B. Stramback to NRC, Responses to RAIs 2-6, 3-1, 21-2, and 28, March 31, 2005. (ADAMS Package Accession No. ML051020023).
4. GE Letter (MFN 05-005), G. B. Stramback to NRC, "Methods Interim Process, Enclosures 1, 2, and 3," March 25, 2005. (ADAMS Package Accession No. ML051010013).
5. GE Letter (MFN 04-026), G. B. Stramback to NRC, Completion of Responses to MELLLA Plus AOO RAIs (TAC No. MB6157), March 4, 2004. (ADAMS Accession No. ML040700161).
6. GE Letter (MFN 05-053), L. M. Quintana to NRC, "Revised Response to RAI 28-2 - Methods Interim Process (TAC No. MC5780)," June 20, 2005. (ADAMS Accession No. ML051750570).
7. GE Letter (MFN 06-424), R. E. Brown to NRC, Update of NEDC-32950P, November 2, 2006. (ADAMS Accession No. ML063110060).
8. GE Letter (MFN 06-434), R. E. Brown to NRC, Updated Response to RAI 28-2 - NEDC-33173P, November 22, 2006. (ADAMS Accession No. ML063350054).
9. GE Letter (MFN-06-207), L. M. Quintana to NRC, Responses to Methods RAIs 1 and 5 - Interim Methods LTR, June 29, 2006.
10. GE Letter (MFN 06-195), L. M. Quintana to NRC, "Responses to Methods RAIs Interim Methods LTR," June 23, 2006. (ADAMS Package Accession No. ML061860283).
11. GE Letter (MFN 05-029), G. B. Stramback to NRC, Responses to RAIs Methods Interim Process (TAC No. MC5780), Response to RAIs 5, 25, 26, 27, and 29, April 8, 2005. (ADAMS Accession No. ML051050023).
12. GE Letter (MFN 04-020), G. B. Stramback to NRC, Response to MELLLA Plus AOO RAIs, February 27, 2004. (ADAMS Accession No. ML040630823).
13. GE Letter (MFN 04-048) to NRC, Request for Additional Information - MELLLA+ LTR RAI 6, March 24, 2004.
14. GE Letter (MFN 06-435), R. E. Brown to NRC, Commitment to Update GE's Void Fraction Data, November 03, 2006. (ADAMS Accession No. ML063350054).
15. GE Letter (MFN 05-045) NRC, Response to RAIs 4-6, 12, and 17 - Methods Interim Process, May 26, 2006.
16. GE Letter (MFN 04-061), G. B. Stramback to NRC, Revision Letter - Supporting Lattice Information - MELLLA RAI AOO 6, July 26, 2004. (ADAMS Accession No. ML042110355).
17. GE Letter (MFN 04-067), G. B. Stramback to NRC, MELLLA Plus RAI AOO 6, TGBLA Lattice Physics Data, July 01, 2004. (ADAMS Accession No. ML041910361).

18. GE Letter (MFN 05-032), G. B. Stramback to NRC, Request for Additional Information - MELLLA+ LTR Rev 1, April 21, 2005. (ADAMS Accession No. ML051170313).
19. GE Letter (MFN 05-038), L. M. Quintana to NRC, Responses to RAIs 1, 13, 14-1, 18, and 22, Mary 03, 2005. (ADAMS Accession No. ML051260402).
20. GE Letter (MFN 05-048), G. B. Stramback to NRC, Responses to RAIs 11 and 16 - Methods Interim Process, May 27, 2005. (ADAMS Accession No. ML051570355).
21. GE Letter (MFN 05-049), L. M. Quintana to NRC, Status of RAI Responses - Methods Interim Process, May 31, 2005. (ADAMS Accession No. ML051570122).
22. GE Letter (MFN 05-082) to NRC, Part 21 Notification Power Distribution Uncertainty Reassessment, August 18, 2005.
23. GE Letter (MFN 06-209) to NRC, Remaining Responses to Methods RAIs - Interim Methods LTR, June 30, 2006.
24. GE Letter (MFN 06-211), R. E. Brown to NRC, Compilation of Responses to Methods RAIs - Interim Methods LTR, July 18, 2006. (ADAMS Accession No. ML062270612).
25. GE Letter (MFN 06-481), R. E. Brown to NRC, Responses to RAIs 7, 8, 9, 10, and 11 - NEDC-33173P, December 5, 2006. (ADAMS Package Accession No. ML063450449).
26. Safety Evaluation for Vermont Yankee Nuclear Power Station Constant Pressure Power Uprate, dated October 21, 2005. (ADAMS Accession No. ML052910264).
27. Entergy letter (BVY 05-072) to NRC dated August 1, 2005, "Vermont Yankee Nuclear Power Station, Technical Specification Proposed Change No. 263, Supplement No. 30, Extended Power Uprate - Response to Request for Additional Information."
28. Entergy letter (BVY 05-083) to NRC dated September 10, 2005, "Vermont Yankee Nuclear Power Station, Technical Specification Proposed Change No. 263, Supplement No. 32, Extended Power Uprate - Additional Information."
29. Entergy letter (BVY 05-086) to NRC dated September 18, 2005, "Vermont Yankee Nuclear Power Station, Technical Specification Proposed Change No. 263, Supplement No. 34, Extended Power Uprate - Additional Information."
30. Entergy letter (BVY 05-088) to NRC dated September 28, 2005, "Vermont Yankee Nuclear Power Station, Technical Specification Proposed Change No. 263, Supplement No. 35, Extended Power Uprate - Response to Request for Additional Information."
31. GE Presentation Slides, "Power Distribution Uncertainties: Gamma Scans Benchmarking," October 2005. (ADAMS Accession No. ML070540474).
32. Steady-State Nuclear Methods, NEDE-30130-P-A and NEDO-30130-A, April 1985, and for TGBLA Version 06 and PANACEA Version 11, Letter from S. A. Richards (NRC) to G. A. Watford (GE) Subject: "Amendment 26 to GE Licensing Topical Report NEDE Attachment 24011-P-A, GESTAR II Implementing Improved GE Steady-State Methods," (TAC NO. MA6481), November 10, 1999.
33. LTR NEDC-32601P-A, "Methodology and Uncertainties for Safety Limit MCPR Evaluation", August 1999.
34. LTR NEDC-32694P-A, "Power Distribution Uncertainties for Safety Limit MCPR Evaluations", August 1999.
35. Standard Review Plan for the Review of Safety Analysis Reports for Nuclear Power Plants (NUREG-0800).

36. TVA letter to NRC, "Browns Ferry Nuclear Plant (BFN) - Units 1, 2, and 3 - Technical Specifications (TS) Changes TS-431 and TS-418 - Extended Power Uprate (EPU) – Response to Round 8 Requests for Additional Information (TAC Nos. MC3812, MC3743, and MC3744). (ADAMS Accession No. ML062360361).
37. LTR NEDC-32505, Revision 1, "R-Factor Calculation Method for GE11, GE12 and GE13 Fuel," June 1997.
38. GESTAR II, Revision 5, Appendix B (RAI responses).
39. LTR NEDE-32906P, "TRACG Application for Anticipated Operational Occurrences Transient Analysis."
40. LTR NEDE-32906P, Supplement 3, "Migration to TRACG04/PANAC11 from TRACG02/PANAC10," May 2006.
41. GE Nuclear Energy, "The GESTR-LOCA and SAFER Models for the Evaluation of the Loss-Of-Coolant Accident, Volume III, SAFER/GESTR Application Methodology," NEDE-23785-1-PA Rev. 1, October 1984.
42. LTR NEDC-32950P, "Compilation of Improvements to GENE's SAFER ECCS-LOCA Evaluation Model," January 2000.
43. NRC letter, S. A. Richards to GE (J. F. Klapproth), General Electric Nuclear Energy (GEH) Topical Reports GENE-32950P and GENE-32084P Acceptability Review, May 24, 2000 (ADAMS Accession No. ML003717617).
44. GE14 Compliance with Amendment 22 of NEDE-24011-P-A (GESTAR II), NEDC-32868P, Revision 1, September 2000.
45. GEH Letter (MFN 170-84), J.S. Charnley to NRC (R. Lobel), "Fuel Property and Performance Model Revisions."
46. GEH Letter (MFN 027-086), J.S. Charnley to NRC (R. Lobel), "Fuel Property and Performance Model Revisions," April 7, 1986.
47. LTR NEDE-24011PA, "General Electric Standard Application for Reactor Fuel," September 2005.
48. NRC letter, Alan Wang to GE (Louis Quintana), Request For Additional Information – Licensing Topical Report NEDC-33006P, Revision 1, "General Electric Boiling Water Reactor Maximum Extended Load Line Limit Analysis Plus (MELLLA+)" (TAC No. MB6157), April 11, 2005. (ADAMS Accession No. ML050980187).
49. TVA Letter to NRC, " Browns Ferry Nuclear Plant (BFN)-Unit 1 - Technical Specification (TS) Change TS-431 - Extended Power Uprate (EPU) – Supplement Response to NRC Round 6 Request For Additional Information (RAI) SBWB -26 and SBWB-30 and Partial Response to Round 8 on Fuel Analysis Methods (TAC No. MC3812)," August 16, 2006. (ADAMS Accession No. ML062330041).
50. LTR NEDC-33075P, Revision 5, "General Electric Boiling Water Reactor Detect and Suppress Solution – Confirmation Density" November 2005.
51. Final Safety Evaluation For General Electric Nuclear Energy (GEH) Licensing Topical Report (LTR) NEDC-33075P, Revision 5, "General Electric Boiling Water Reactor Detect And Suppress Solution - Confirmation Density" (TAC No. MC1737), dated November 27, 2006. (ADAMS Accession No. ML062640346).

52. LTR NEDE-21565, J. A. Findlay and G. E. Dix, BWR Void Fraction and Data, January 1977.
53. [http://www.cmla.enscachan.fr/Utilisateurs/perfortmans/Cargese00/Cargese00\\_pro/coddi ngton\\_Macian.pdf](http://www.cmla.enscachan.fr/Utilisateurs/perfortmans/Cargese00/Cargese00_pro/coddi ngton_Macian.pdf).
54. Collier, J. G., Convective Boiling and Condensation, McGraw-Hill, New York, (second edition), pp 71.
55. NEDE-32177PA, "Licensing Topical Report, TRACG Qualification."
56. NRC letter, H. K. Nieh to GE (R. E. Brown), Final Safety Evaluation for GE Hitachi Nuclear Energy Americas, LLS (GEH) Topical Report (TR) NEDC-33006P, "Maximum Extended Load Line Limit Analysis Plus," (TAC No. MB6157), September 17, 2007. (ADAMS Accession No. ML072190207).
57. GE Letter (MFN 07-040), J. Post to NRC, "Part 21 Notification: Adequacy of GE Thermal-Mechanical Methodology, GESTR-M," January 21, 2007. (ADAMS Package Accession No. ML072290203).
58. GNF Letter (FLN-2007-001), A. A. Lingenfelter to NRC, The PRIME Model for Analysis of Fuel Rod Thermal-Mechanical Performance, January 19, 2007. (ADAMS Package Accession No. ML070250414).

Principal Contributors: Z. Abdullahi  
Dr. Timothy Collins  
Paul Clifford

ORNL principal contributors: Dr. Jose March-Leuba  
Dr. Grady Yoder  
Dr. Jess Gehin

Date: July 21, 2009

## APPENDIX A – RAI EVALUATIONS

### Evaluation of NRC RAIs Section 1 - Linear Heat Generation Rate (LHGR)

#### RAI 1.1

*Different pins peak at different exposures and in some lattices exhibit high power-peaking later in life. Therefore, it is important to assess the overall operating LHGR in these pins relative to the LHGR limit and to understand the available margins such pins have in terms of internal rod pressures. In addition, operating plants data indicates that peak rods could be operating at the limit. Provide internal rod pressure calculations for rods that are operating at the limit for different exposures, including late in the fuel life. Use representative bundles that have lower Gd loading (e.g., 6 percent or lower).*

- (a) *Provide a Minimum LHGR (MLHGR) scatter plots for extended power uprate (EPU) plant.*
- (b) *Select most limiting MLHGR at different exposures, including late in the fuel life.*
- (c) *Calculate the internal pressure (P) based history for once, twice, and thrice burned fuel near LHR limit and placed on limit for reasonable duration. Compare and discuss the results and exposures.*

#### **Evaluation of RAI 1.1**

Figure 1.1-1 provided EPU actual LHGR operating history for a core containing GE13 and GE14 fuel designs. The data shows that the plant operated with a margin to the LHGR exposure dependent limit. The RAI response provided sensitivity analysis to demonstrate that [

nodes [ ] operating at the limit are closer to the reference envelop than nodes operating at the limit later in the fuel life. Table 1.1-1 provides the results of the sensitivity analyses.

#### RAI 1.2

*For Gadolinia (Gd) bearing rod (6 percent) near beginning-of-life (0 to 5.392 gigawattdays per short ton (GWd/ST)), the LHGR limit increased from 5.392 GWd/STU when the Gd concentration is high to 12.55 GWd/ST at 5 GWd/ST. The Gd rods will be operating at lower powers and the limit is low when the Gd concentration is high. However, it appears that the plant monitoring systems are based on 12.55 GWd/ST. Explain the discrepancies. State why the limit is reduced at low exposures for the Gd loaded pins, when the Gd concentration is high. Discuss under transient conditions if the Gd pin margin to the melting temperature will be much lower?*

#### **Evaluation of RAI 1.2**

The RAI response provided operating history of Gd-bearing rods. As expected, for the specific plant, the Gd-bearing rods operated within the exposure dependent LHGR limit since at early life the Gd rods operate at low powers. Although the Gd rod early life power is low and thus non-limiting, however the uncertainty in the prediction of the LHGR for the Gd rod before the gadolinium isotopes transmuted may be higher. The RAI response investigated whether the higher early life uncertainties of the Gd rod affect the rod thermal mechanical performance later in life. The conclusions of the results are that while there is some affect, it was not significant. This assessment provides sufficient bases to accept the current practice of monitoring the Gd rods early life at the higher LHGR limit instead of the actual Gd rod LHGR limit.

RAI 1.3

*Fuel failure due to fuel duty is precluded by limiting the initial steady-state operating kilowatt per foot (kW/ft) through the LHGR limit. Show that thermal-mechanical fuel duty benchmark data is applicable to EPU conditions.*

RAI 1.4

*Describe the internal rod pressure validation data that are currently available for both GE fuel designs and legacy fuels.*

**Evaluation of RAI 1.3 and 1.4**

The RAI provided the qualification database supporting the thermal-mechanical methodology. The response also discussed the wide range of the supporting data and its adequacy to the current fuel designs and operating conditions. The NRC staff reviewed the qualification data presented in Table 1.3-1.

As can be seen by Table 4.6 of the NRC staff SE, the data supporting the fuel temperature and the internal rod pressures are not well supported in terms of the fuel length and the exposures ranges that data is available. Both the internal rod pressures and the fuel temperature calculations are important to the thermal-mechanical performance of the fuel. In addition, both parameters change with exposure as the fuel depletes. Therefore, the NRC staff finds the lack of supporting data for the current rod designs and licensed exposures are relevant in the qualification database supporting application to EPU and MELLLA+.

In RAI 28 to MFN-06 or 05-022 (Reference 48) and in the December 2005 gamma scan presentation to the NRC staff, GE stated that the gamma scans will include plenum fission gas and rod exposure scans. In addition, GENE states that it intends to submit PRIME which will provide updated thermal mechanical performance methodology. Since the current Methodology is based on Refs. 30 and 31, the NRC staff finds updating of the licensing methodology important. Therefore, the NRC staff accepts the qualification database and the justifications presented in RAI 1.3 and 1.4 acceptable based on the additional gamma scans and the updating of the licensing thermal mechanical methodology.

Evaluation of NRC RAIs Section 2 - Shutdown Margin (SDM)

RAI 2.1

*The demonstration of the shutdown margin is dependent on the cold critical measurement performed at the plant and the eigenvalue for the core with all rods inserted, but with the strongest rod out (Ksro). The code critical measurements are performed after each outage and can be used to demonstrate the adequacy of the neutronics methods for this "distributed" criticality. However, the Ksro value requires experiments to be performed with single rods out, which represent "local" criticality experiments. These local experiments are not performed very frequently, yet the prediction of the SDM relies on the accurate calculation of the Ksro value. The data provided does not distinguish between local cold critical and in-sequence cold critical measurements.*

- (a) *Local cold critical measurements are a more physical demonstration of the stuck rod out (SRO) condition enforced by the 0.0038  $\Delta k/k$  technical specification limit. Please separate out this data and provide an assessment of the methods accuracy for prediction of the local critical states demonstrating that the bias and uncertainties that are currently applied are adequate for MELLLA+.*



- (b) *As in Figure 2-5, provide the predicted (e.g., design basis) and measured eigenvalues. Compare the performance versus the distributed cold critical measurements and discuss any other biases or uncertainties that are applied to the Ksro values in the SDM demonstration.*

### **Evaluation of RAI 2.1(a)**

The RAI response provided a table of data for a particular plant (Plant C) that contains both distributed and local critical data. The table of data provided the demonstrated cold critical eigenvalue and the Nuclear Design Basis (NDB) reference eigenvalue from which the cold shutdown margin can be determined. The data provided was reviewed and the applicability of Plant C, which is a small BWR/4 with 240 bundles (see Table 2.4 of NEDC-33173P (Reference 1)) was assessed. Plant C has a high power density core and provided that the information desired is for local criticality the data is applicable to the current plants being considered for EPU and MELLLA+. The current U.S. fleet of plants do not perform local critical calculations and therefore, this database of information is essential for the assessment of the prediction of the shutdown margin. The data provided by GE for this RAI is acceptable.

### **Evaluation of RAI 2.1(b)**

The tables provided in response to RAI 2.1(a) contain a comparison of the calculated critical state to the nuclear design basis eigenvalue. The comparison of these two numbers provides an indication of the accuracy of the nuclear methods to predict the local criticality. The standard deviation of all differences for the local critical demonstrations is [ ], which is similar to that of the distributed criticals. The RAI response also indicates that a [

]. The RAI response provides the requested results and comparisons and the discussion of biases and uncertainties related to prediction of Ksro.

### **RAI 2.2**

*NEDC-33173P (Reference 1) states that the same SDM Technical Specification value used for non-EPU core designs is adequate for EPU and expanded operating domain conditions. Provide the basis as to why cold SDM is not a strong function of the current operating strategies by comparing cold critical data before and after EPU. Include in the discussion the impact of core designs necessary to achieve EPU and maintain extended cycle lengths (e.g., larger batch fractions, higher bundle enrichments and different core loading patterns).*

### **Evaluation of RAI 2.2**

The RAI response provides a discussion of the computational nature of the shutdown margin calculation along with the demonstration cold critical measurement that is performed at beginning of cycle. The application of the non-EPU core TS shutdown margin, which is typically 0.38 percent  $\Delta k/k$  to EPU cores requires an assessment of the appropriateness of the biases and uncertainties for EPU operation in comparison to non-EPU operation. The EPU and MELLLA+ cores have larger batch fraction than non-EPU cores. The response indicates that GE has current experience with a wide range of batch fractions for non-EPU cores. The response for RAI 2.1(b) indicates that the local critical data prediction is not significantly affected by EPU operation. Results were provided in the RAI response for a BWR/4 that has undergone a 120 percent EPU that shows no change in the prediction of the cold critical eigenvalue (distributed eigenvalue). The other components of the bias and uncertainties such as fuel enrichment, manufacturing tolerances, gadolinium enrichments are not affected by EPU operation as long as the fuel designs are similar to those of the non-EPU fuel and core designs

and the cold critical demonstration provides an indication of the impact of these other parameters. The current GNF methodology provides a SDM design criteria of 1 percent  $\Delta k/k$  to allow additional margin. The response provided is acceptable.

### RAI 2.3

*An equation is provided in Section 2.3.2 stating what the technical specification for cold shutdown requires in terms of  $k_{sro}$  and  $k_{demo}$ . Explain the basis for this equation and describe its relationship to the equation relating the SDM calculation to  $k_{crit}$ ,  $k_{sro}$ , and the period and temperature corrections (e.g., startup CR withdrawal sequence).*

### **Evaluation of RAI 2.3**

The RAI response provides a derivation that relates the two definitions of shutdown margin. The relevant detail is that the equation in terms of  $k_{crit}$ ,  $k_{sro}$ , is normalized to a demonstration ( $k_{demo}$ ) value of unity. With this additional requirement the two equations are identical. The RAI response is acceptable.

Evaluation of NRC RAIs Section 3 - Bypass Voiding

### RAI 3.1, Neutronic Methods

- (a) *Provide a short description of the methodology used to account for the bypass thermal-hydraulic conditions for transient and stability calculations.*
- (b) *Discuss the accuracy of the assumption that the lattice physics parameters can be characterized as a function of the lattice average moderator density. Discuss the impact of bypass and water rod voiding on lattice depletion. Discuss what impact the presence of bypass voiding (e.g., during RPT) not accounted for in the neutronic methods will have on the core thermal-hydraulic conditions (e.g., power distribution). Discuss the effects of bypass and water rod voiding on lattice power distribution for the exposed fuel.*

### **Evaluation of RAI 3.1**

A short description of the methodology was provided for RAI 3.1(a). The RAI response states that "Thus, by the use of the lattice average water density parameter, potential changes in the bypass and water rod voiding (water density) are **accurately** modeled in the core steady-state and transient simulators." While the NRC staff agrees that the potential changes in bypass and water density are taken into account by the homogenized nodal density, this is just an approximation whose **accuracy** needs to be demonstrated. This is the essence of RAI question 3.1(b).

The RAI response presents Figure A-1 to justify the use of interpolation and extrapolation between the 0 percent, 40 percent, and 70 percent void fraction levels used in the lattice calculations with 0 percent bypass and water rod fractions. A TGBLA06 case with 55 percent in-channel void and 0 percent bypass and water rod void was calculated, and the  $k$ -infinity value is plotted against the interpolated polynomial. The agreement between the TGBLA06 value and the interpolated polynomial value is better than [ ]. In addition, a TGBLA06 case with 90 percent in-channel void and 0 percent bypass and water rod void was calculated and compared against the polynomial fit. The error is less than [ ]. This indicates that the interpolation and extrapolation models using values at 0 percent, 40 percent, and 70 percent results in acceptable errors up to a void fraction of 90 percent with zero bypass and water rod voids.

The issue of the presence of voids in the bypass and its effect on the calculated values was addressed using the results of a TGBLA06 calculation with 85 percent in-channel voids, 10

percent bypass voids, and 25 percent water rod voids. This case results in a lattice-average void fraction similar to an in-channel void case of 90 percent. Comparison of both cases agrees well with the polynomial fit and has an error smaller than [ ]. This indicates that the lattice-averaging procedure for effective lattice water density is acceptable within a [ ].

The NRC staff agrees with the conclusion that "Since the nominal operating core does not experience bypass and water rod voiding and that the core conditions with bypass and water rod voiding are transitory in nature, there will be no significant impact on core depletion simulation."

The NRC staff concludes that both high in-channel void fraction and bypass and water-rod void conditions introduce an error in the neutronic methodology. Based on the data presented in this RAI, the NRC staff estimates that operation at high void fractions results in an error of the order of [ ] in the calculated power distributions.

For BWRs operating under current licensed domains, the occurrence of bypass voiding is restricted to operation in the high-power, low flow region; therefore, it is limited to transients, and, for most events, operation at bypass-voiding conditions is short lived due to scram. The data available for this evaluation suggests that bypass and water rod voiding results on an error in neutronic methods of the order of [ ].

**Conclusion:** The above two methodology errors are a contributing factor to the 0.02 SLMCPR penalty imposed for high-void-fraction operation. The addition to the 0.02 SLMCPR penalty is equivalent to increasing the OLMCPR by 0.02, which provides additional margin for this type of transients.

### RAI 3.2, Stability Protection (Instrumentation Reliability)

#### RAI 3.2(a)

*Quantify the bypass voiding for rated power operation and power levels associated with EPU and MELLLA+.*

- (i) Describe the methodologies used by GE to calculate bypass voiding.*
- (ii) Quantify the best-estimate bypass void fraction (BP VF) for the worst point in the operating map (NC + MELLLA+, MELLLA, OLTP) that could be used for stability calculations.*
- (iii) Quantify the best-estimate BP VF for the expected conditions where ODYSY stability methodology is used for LTS.*

#### RAI 3.2(b)

*Describe the method for the determination of the impact of BP VF on stability analysis.*

#### RAI 3.2(c)

*Section 2.6.2.1 concludes that the effect of BP VF on APRM calibration is less than 1 percent. Section 2.6.2.3 concludes that the effect of BP VF on OPRM calibration is less than 3 percent. Please describe the methodology used for these analyses and quantify the BP VF levels used.*

### **Evaluation of RAI 3.2(a)(i)**

A description was provided in Table A-1 for the methodologies of the different codes used by GENE: ISCOR, PANACEA, ODYSY, and TRACG. Each code has a different set of

assumptions and models and, in general, results from different codes will not be directly comparable.

### **Evaluation of RAI 3.2(a)(ii)**

For a high-power density core operating at natural circulation the most limiting MELLLA+ rod line, the following bypass void fractions are calculated at the TAF:

As stated above, the differences between the values calculated by the different codes are a function of the code assumptions. For example, the difference between the core-average TRACG and ISCOR values are caused by [

]. The ISCOR four-channel bypass edit estimate is a very conservative bounding calculation which [

]. The actual value of the hot channel bypass void fraction is somewhere between the estimates for core-average, [

].

Table A-1 provides a comparison of bypass boiling levels for OLTP, MELLLA, and MELLLA+. The increase in bypass boiling between OLTP and MELLLA+ is not significant [ using the ISCOR average channel methodology). Therefore the impact of bypass boiling on the methodology affects OLTP reactors and not only the MELLLA+ domain.

### **Evaluation of RAI 3.2(a)(iii)**

ISCOR calculations for Vermont Yankee at the boundaries of the exclusion region show that no bypass boiling occurs at the interception with the high-flow control line. However, at the intersection with the natural circulation line, ISCOR predicts a void fraction of [ ]. ODYSY uses a bypass boiling model and input similar to ISCOR; therefore, it would predict similar values. These values have are the basis for the conclusions of the evaluation of RAI 3.2(b) below.

### **Evaluation of RAI 3.2(b)**

GENE has not performed a detailed evaluation of the effect of bypass boiling on ODYSY stability calculations; however, we note that:

1. ODYSY models the bypass channel with [ ] and feeds back to the core reactivity its effects; therefore, at least to first order, ODYSY models the effect on stability of bypass boiling.
2. On the response for RAI 4.1d, Table A-2 shows a benchmark between DRs measured at Vermont Yankee at high power-to-flow ratio conditions and those calculated by ODYSY. On this table, point 9P corresponds approximately to the interception of the exclusion region with the natural circulation line, where ISCOR calculates an [ ] bypass void (note that Table A-2 is based on OLTP, and the ISCOR calculation is based on EPU powers). Points 8P and 7N have higher power, so they should have some degree of bypass boiling. The agreement between the measured and the ODYSY DRs is acceptable, indicating that any errors associated with bypass voiding in the ODYSY DR calculation are absorbed or compensated by conservatism on the modeling assumptions

The RAI states that “however, both the regional and core-wide DIVOM analyses are based on the hot channels, which are away from the periphery of the core where bypass voiding is highest”. While it is true that when reverse flow is established on the periphery bypass region high void fraction (up to 80 percent) may be present at the bypass exit because it draws voids from the upper plenum, all the evaluations of bypass voiding presented in this RAI correspond

to the center regions of the bypass where the voiding is caused by core heating. Thus, bypass voiding (excluding the reverse flow effect) is highest on the hot channels where the DIVOM correlation is evaluated, and the NRC staff does not agree with the RAI statement.

Nevertheless, the NRC staff concludes that both ODYSY and TRACG provide a reasonable model of bypass voiding. For both codes, a first-order estimate of the bypass void level is calculated by the code, and these bypass voids are used by the code using the lattice-average moderator density methodology. Both TRACG and ODYSY use a core-average bypass region, which is sufficient to provide the dynamic feedback effect of bypass boiling during transients. TRACG models the bypass regions [

]. While the TRACG axial nodalization is not as accurate as the ODYSY or ISCOR nodalizations, [ ] is typically sufficient to provide the necessary reactivity feedback during transient analysis because bypass voiding is only expected in the top half of the core and the void fraction levels are relatively small [ ]].

The NRC staff also concurs with GENE's evaluation of the impact of bypass voids on ODYSY stability calculations for Long Term Stability Solutions (LTSS). This evaluation indicates that the bypass void fraction is very low or zero along the calculated LTSS exclusion regions.

### **Evaluation of RAI 3.2(c)**

The apparent discrepancies in the values cited in the RAI were caused by using different codes and assumptions for each separate evaluation (see RAI 3.2(a)(i)). The response to this RAI clarifies the situation. The APRM error was based on a bypass void fraction level estimated from the core-average ISCOR model, while the OPRM error was based on the hot-channel ISCOR model. The difference on the assumed ISCOR models (average vs. hot-channel) account for the reported differences.

Evaluation of RAIs Section 4 - Use of 40 percent Void Fraction History Depletion Assumption for Instantaneous Void Fraction Changes.

### **RAI 4.0 Use of 40 percent Void Fraction History Depletion Assumption for Instantaneous Void Fraction Changes.**

*The neutronics methods perform void history calculations at 0 percent, 40 percent, and 70 percent void fractions, but the instantaneous branch cases are performed only for the 40 percent void history case. As a result, the impact of instantaneous changes in the void fraction for all void histories is assumed to be that of the 40 percent void history case. The impact of this assumption results in errors in the prediction of the void reactivity effect for void fraction histories lower and higher than 40 percent and can be evaluated by examining the void coefficient of reactivity. In order to assess the impact of the 40 percent void fraction history assumption:*

#### **RAI 4.1 Void Coefficient and Stability**

##### **RAI 4.1(a)**

*Provide an evaluation of the error created by the 40 percent void fraction history assumption on the local void coefficient.*

##### **RAI 4.1(b)**

*Provide an estimate of the error in the global void coefficient introduced by the 40 percent void fraction history assumption.*

##### **RAI 4.1(c)**

*Provide TRACG stability calculations with and without the void history correction for void coefficient.*

RAI 4.1(d)

*Provide and include the cited instability benchmarking that demonstrates the accuracy of ODYSY and TRACG in the TR. Provide some assessment of the similarities of core thermal-hydraulic conditions between the benchmark plants and the EPU plants.*

RAI 4.1(e)

*What is the impact on stability of void fraction histories less than 40%?*

#### **Evaluation of RAI 4.1(a)**

An estimate of the error induced by the 40 percent depletion assumption was provided in the form of Figure A-2. This figure shows that for high exposure conditions, the local void coefficient error can be as high [ ].

The RAI states that "[

]."

This statement is based on a comparison of these results with a previous series of Vermont Yankee calculations. No evidence is provided for the differences; therefore, the NRC staff concludes that the statement is not supported by any data presented in this or previous RAIs, and it is an unsupported over simplification.

#### **Evaluation of RAI 4.1(b)**

A special version of TRACG was modified to include the void coefficient error associated with the 40 percent void fraction history as defined in Figure 4.1a-1. Using a series of TRACG calculations, the RAI demonstrates that an error [ ] on global void coefficient is equivalent to the error introduced by the 40 percent void fraction history assumption. Even though for some high-burnup nodes the local void coefficient error can be as high [ ], most high power nodes operate at lower exposure values. The NRC staff concludes that, when the effective core-average effect of the error is computed, its effect is essentially negligible.

#### **Evaluation of RAI 4.1(c)**

Figure 4.1c-1 shows comparisons of a TRACG –computed instability with and without the 40 percent void history correction. Note that this evaluation uses the data of Figure 4.1a-1, which only includes the errors for void fractions greater than 40 percent and not for lower void fractions (see RAI 4.1(e)). The NRC staff concurs that the differences are negligible. Therefore, the overall effect on stability of the 40 percent void history error is negligible.

#### **Evaluation of RAI 4.1(d)**

The requested benchmark data was provided. The benchmark database includes the recent Nine Mile Point 2 and Perry events. In both cases, the stability criteria (core DR > 0.8) is met, but barely. These benchmarks show the importance of maintaining the 0.2 uncertainty criteria for stability calculations.

#### **Evaluation of RAI 4.1(e)**

Figure 4.1a-1 presents the effect on void coefficient of void histories greater than 40%. This RAI asks the effect of lower void histories. As result of this RAI, GE has not performed new calculations to evaluate the impact. Instead, GE makes an argument that [

]. The NRC staff concludes that this statement is unsupported by the evidence

presented, and the effect of void fractions lower than 40 percent is not known accurately at the time.

Nevertheless, in view of the response to RAI 4.1(a) and (b), the NRC staff concludes that the possible error introduced by void fractions lower than 40 percent should be of similar magnitude [ ]. Given the sensitivities calculated on the previous RAI responses, the NRC staff concludes that the impact on stability of this error should also be negligible.

#### RAI 4.2 ATWS

*Address the impact of the 40 percent depletion assumption on the ATWS response.*

#### **Evaluation of RAI 4.2**

For an isolation ATWS event, closing the Main Steam Isolation Valve (MSIV) causes a rapid increase in reactor vessel pressure, which results in core void reduction and an associated power increase. A Recirculation Pump Trip (RPT) is initiated on high pressure and the core flow begins to decrease. When the steam production decreases to the point at which the S/RV capacity is sufficient to relieve all of the steam generation, the pressure and core power begin to fall. To further reduce the core power, the vessel water level is lowered, which uncovers the feedwater spargers and reduces the subcooling. Boron injection through the SLCS is initiated if the suppression pool begins to heat up or oscillations are developed.

Typically, the limiting criteria for ATWS events are: (1) the early pressure rise must not result in pressures higher than the ASME Level C criteria for the weakest link in the primary (typically 1500 psi), and (2) the suppression pool temperature must remain low enough to prevent over-pressurization of the containment to the point where it may fail. Criterion (1) is challenged in the early phase of the transient (less than one minute) and criterion (2) is challenged at the end of the transient (20 to 30 minutes after initiation for stand-pipe BWRs).

The neutronic methodology errors will affect an ATWS transient through the void reactivity coefficient. An increase of void coefficient magnitude has two competing effects:

The initial pressure increase after MSIV closure will result in a larger power response, which in turn will increase the pressure further.

The flow reduction after the RPT results in a larger reduction of core power

Thus, in principle, an error in void reactivity coefficient could change the transient in either a conservative or non-conservative direction.

To evaluate the effect of errors in void reactivity coefficient, GE presents a number of sensitivity studies with TRACG and ODYN. The TRACG analysis results show that the peak pressure results are [

]. Two ODYN analyses were performed; the case at BOC conditions resulted in [ ]. Both pressure changes were small [ ].

A large sensitivity analysis to 27 ODYN input parameters identified in a PIRT analysis is presented in Figure A-3. This analysis shows that the largest sensitivity is to core interfacial shear. The sensitivity to void coefficient is essentially zero.

Based on the data presented in this RAI, the NRC staff concurs with GE's evaluation that the effect of neutronic methodology errors on ATWS performance is small when compared to the uncertainty to other modeling parameters and assumptions.

## Evaluation of RAIs Section 5 - Void-Quality Correlation

### RAI 5-1

*Figure 2-2 of NEDC-33173P (Reference 1) shows a plot of the typical void-quality relation at high power-to-flow ratio. Evaluate the database supporting the void fraction correlation and plot the supporting validation measurement data on Figure 2-2. Identify the type of validation data on the plot, including the supporting tests types and the associated thermal-hydraulic conditions.*

### **Evaluation of RAI 5-1**

Figure 5-1 of RAI 5-1 shows both void fraction predictions using the Findlay-Dix correlation, and selected data taken from the database upon which it is based. The correlation predictions were actually performed for a 10X10 rod bundle operating at a Reynolds number of  $1.1e5$ , while the void fraction data presented on Figure 5-1 were taken in 8X8 rod bundle geometry using local gamma densitometry measurements. As noted in the response, "Comparing this calculation to the void fraction data used in the development of the Findlay-Dix correlation is not perfectly meaningful as the bundle geometry and test conditions are not identical." However, the figure does indicate the correlation trends are consistent with the data presented.

Unfortunately, none of the database upon which the Findlay-Dix correlation was developed included 10X10 bundle geometry, or bundles with partial length rods. Using the correlation to predict behavior in the 10X10 bundle requires extrapolating the correlation to a smaller hydraulic diameter [

], and to different bundle geometry (the 10X10 bundle has both a fully rodged region and a partially rodged region). Additional discussion of this extrapolation is presented in RAI 5-2.

### RAI 5-2

*The void fraction calculation affects both the accuracy of the physics and the thermal-hydraulic calculations used to perform the design bases safety analyses. The objective is to confirm the void-quality correlation applicability ranges and assess any changes in the uncertainty of the correlation and its impact on the OLMCPR. Justify why the void-quality correlation and the assumed uncertainty in the correlation are applicable for modern fuel (e.g., part-length rods, mixing vanes) and high energy operating conditions.*

### **Evaluation of RAI 5-2**

GE responds that "the database for the void correlation covers all fuel products including 10X10 fuel and all operating ranges including EPU conditions. GE notes a hydraulic diameter range of the database of [ ] hydraulic diameter data was developed from rectangular tube experiments, taken from the "simple geometry" portion of the database presented in NEDE-21565 (Reference 35), which was not included in the uncertainty evaluation presented in Table 5-2 (RAI 5-2), nor in the development of the Findlay-Dix correlation. There is also no partial length rod bundle data used in development of the correlation nor in development of the uncertainty values. GE presents figures taken from Japanese void fraction experimentation using bundles with partial length rods, and concludes that "8X8 data taken at normal operating pressure shows a small increase, on the order of [



- A-11 -

]." The figures shown support this statement.

However, there was no quantitative comparison of the Findlay-Dix correlation with this data, and the [ ] is, in fact, larger than the quoted uncertainty in the correlation.

### RAI 5-3

NEDC-33173P (Reference 1) references relevant plots and information provided in the Vermont Yankee (VY) RAIs. Include the relevant discussion and plots in this LTR.

The response to this RAI was combined with that of RAI 5-2.

### RAI 5-4

*Provide a summary of how the void-quality correlation uncertainties are accounted for in the model uncertainties for the codes and the analytical methodologies used to perform the licensing bases safety analyses*

### **Evaluation of RAI 5-2**

The void fraction in the core impacts two major core characteristics: the core power (through void feedback), and the core flow (by influencing pressure drop).

GE notes that uncertainties for core power are generated for SLMCPR, LHGR, LOCA related limits are in general taken from in core power measurements in operating plants. These are developed by comparing code predictions to TIP response in operating plants. For OLMCPR, LHGR, and Stability limits power uncertainties are determined using overall uncertainties in the transient models that are generally developed from comparison to plant transients. Thus the uncertainty in these limits is not dependent directly on the uncertainty in the void prediction, but rather relies on uncertainties developed directly from power measurements or from overall transient prediction uncertainties. The NRC staff finds that void uncertainty levels therefore do not directly impact core power predictions for these cases. GE notes that the TRACG includes explicit void uncertainty in its statistical model, however TRACG does not use the Findlay-Dix correlation for void prediction.

The experimental void fraction database (NEDE-21565 (Reference 35)) was also used to optimize the two-phase pressure drop correlation. Based on the newly developed void fraction correlation, GE effectively re-optimized their pressure drop correlation using the new void calculation technique. The document (NEDE-21565 (Reference 35) 5) reports an improvement in pressure drop calculation, with standard deviations (for pressure drop) ranging from [ ] depending on the data set to which it is compared.

GE reports (BVY-05-083) that comparisons have been made to pressure drop data taken in the ATLAS test facility using full-scale test assemblies for all fuel products including the current 10X10 GE14 fuel. This testing covers a wide range of conditions including EPU conditions. For GE14 the bundle pressure drop was predicted with a mean error of [ ].

Since the void correlation is incorporated into the pressure drop calculation, and pressure drop measurements are taken for all new bundle geometries, the uncertainties in the void-quality relationship are accounted for in the overall pressure drop uncertainty. The void influence should be covered by the pressure drop uncertainties, as long as the pressure drop database covers the appropriate data ranges. Therefore, the NRC staff finds that the void-quality uncertainty need not be explicitly incorporated in the pressure drop calculation.

## Evaluation of RAIs Section 6 – Process

### RAI 6.1

*NEDC-33173P (Reference 1) summarizes the content of the VY RAIs. However, this eliminates relevant figures and evaluations. For the void fraction correlation, void reactivity coefficient, and Option 1D include the relevant figures and discussions so that the supporting information is integrated in this LTR.*

### **Evaluation of RAI 6.1**

The relevant figures, tables, and discussion from the VY RAIs have been incorporated into the body of NEDC-33173P (Reference 1). Appropriate references have also been included.

### RAI 6.2

*Appendix A contains many RAIs not related to the methods review. All EPU SRXB-A RAIs were cited in Appendix A. Many of these RAIs, did not address nor are they relevant to the Methods review. This array of RAIs hampers efficient use of the reference material. Delete the SRXB-A RAIs that were not part of the methods review.*

### **Evaluation of RAI 6.2**

The table in Appendix A was reduced to include only the VY RAIs that were related to the methods review.

### RAI 6.3

*Vermont Yankee SRXB-A Figures 6-1 thru 6-6 show the maximum bundle operating conditions of high density and EPU plants. Each plant specific application should, include the plant-specific data in the plots containing the high density and EPU plants maximum bundle operating conditions (Attachment 3, BVY 05-024)*

- (a) *Therefore, include in the EPU applications the following bundle operating conditions with exposure in the EPU maximum bundle operating condition plots: maximum bundle power, maximum bundle power-to-flow ratio, exit void fraction of maximum power bundle, maximum channel exit void fraction, peak linear heat generation rate and peak end-of-cycle nodal exposure*
- (b) *Provide quarter core map (assuming core symmetry) showing the bundle operating linear heat generation (MLHGR) and the minimum CPR (MCPR) for beginning-of cycle (BOC), middle-of-cycle (MOC) and end-of-cycle (EOC). Similarly, show the associated bundle powers.*

### **Evaluation of RAI 6.3**

Section 4.3 of NEDC-33173P (Reference 1) was modified, to specify that the requested core operating information be included with plant specific applications of NEDC-33173P.

### RAI 9

*As part of the ESBWR design certification review, the NRC staff discovered a discrepancy in the GSTRM thermal-mechanical calculations, supporting the GE14 fuel designs. Specifically, the GSTRM UO<sub>2</sub> under-predicted the fuel temperature calculations in comparison to both FRAPCON-3 and PRIME calculations. It is possible that the observed differences are primarily due to GSTRM UO<sub>2</sub> fuel thermal conductivity model, which does not model exposure dependency compared to the other two codes. The potential non-conservatisms in GSTRM could be applicable to thermal-mechanical*

- A-13 -

*performance calculations for operating reactors as well the calculation of the associated limits.*

*a. Provide an assessment of the impact of the non-conservatism in GSTRM UO2 fuel temperature calculation regarding the adequacy of the fuel rod thermal-mechanical performance for the GE13 and G14 fuel designs.*

*b. Evaluate the impact of the GSTRM UO2 under-predictions on the fuel temperature, internal rod pressure, and TOP/MOP calculation during anticipated operational occurrences (AOOs).*

*c. Assess the impact of the GSTRM UO2 non-conservatism (e.g., thermal conductivity model) on peak cladding temperature (PCT) for both the limiting small and large break loss of coolant accidents (LOCAs) at EPU conditions. This assessment should also include the most limiting axial power profile.*

*d. In MFN 06-207, RAI 1 contains thermal-mechanical performance results for along the linear heat generation rate (LHGR) envelope (e.g., internal rod pressures, fuel temperature, and cladding circumferential strain) for the UO2 and the UGdO2 rods. Discuss if the potential non-conservatisms will change the results for operation on the LHGR envelope or the related sensitivity analysis in RAI 1.*

#### **Evaluation of RAI 9**

In addition to the GE response to the above RAI, the NRC staff evaluated GE's GSTRM T-M methodology in "NRC staff Evaluation of General Electric GSTRM Thermal-Mechanical Methodology Part 21 Report (MFN 07-040)," dated September 4, 2007 (ADAMS Accession No. ML072480672). This evaluation was performed in response to a GE Part 21 evaluation on the GSTRM T-M methodology. Section 3.2.6.5.8 of the SE for NEDC-33173 provides further information on the GE Part 21 Evaluation and corresponding NRC staff evaluation.

The NRC staff evaluation concluded that although the GSTRM best estimate calculation under-predicts the fuel centerline temperature, the conservative uncertainty treatment compensates for the under-prediction, resulting in bounding 95/95 fuel centerline temperatures. The NRC staff concludes that the GSTRM fuel temperature calculation with the 95% uncertainty treatment is acceptable.

The NRC staff also evaluated the adequacy of GSTRM methodology and its qualification database to determine the licensing rod internal pressures. Regarding the rod internal pressure calculation, the NRC staff concludes that the adequacy of the GSTRM uncertainty treatment needs to be confirmed through measurement qualification data and corrected for licensing applications. Therefore the NRC staff position as provided in "NRC staff Evaluation of General Electric GSTRM Thermal-Mechanical Methodology Part 21 Report (MFN 07-040)," is applicable for GSTRM rod internal pressure calculations.

**Table A-1 Bypass and in-channel void fractions calculated by different codes**

[

]

**Table A-2 Summary of ODYSY Results for Vermont Yankee High DR Tests**

<b>Test Point</b>	<b>Power/Flow (% rated)</b>	<b>Test Data</b>		<b>ODYSY Results</b>	
		<b>DR</b>	<b>Frequency</b>	<b>DR</b>	<b>Frequency</b>
6P	57.2/38.5	0.74	0.44	0.67	0.39
7N	51.2/32.6	1.00	0.43	0.99	0.38
8P	50.9/32.6	0.96	0.43	0.97	0.37
9P	48.1/32.4	0.81	0.42	0.86	0.36
10P	49.8/33.0	0.90	0.42	0.97	0.37
11P	67.1/38.5	0.85	0.47	0.85	0.42
12P	63.1/38.5	0.78	0.47	0.75	0.42

[

**Figure A-1 Fit Uncertainty for TGBLA06 Reactivity**

]

[

**Figure A-2 Void Coefficient Ratio MNCP / TGBLA06**

]

[

Figure A-3 Hot Channel Power and Growth Rate with (V33) and without (NV) Void History  
Correction for Void Coefficient ]

## APPENDIX B CONFIRMATORY LATTICE PHYSICS DATA COMPARISONS

### TGBLA/MCNP Comparisons

#### Overview

Comparisons of TGBLA06 and MCNP were performed by GNF in response to MELLLA+ RAIs (Reference 13, RAI 6, Enclosure 6) for five lattices that are representative of lattices that would be used in high-energy fuel cycles. MCNP is a continuous-energy neutron transport code developed by LANL that is commonly used as a reference code for comparison of methods incorporating more approximate methods. The code provides for a detailed representation of lattice geometry, accurate treatment of the neutron transport, and detailed representation of the energy dependence of neutrons. The methods employed in MCNP are independent of those used by the TGBLA06 lattice physics code. The comparisons between the results of the two codes is intended to provide a measure of the error resulting from the more approximate methods used in the TGBLA06 lattice physics code.

In the Licensing Topical Report a discussion is provided on the use of MCNP for the method uncertainty in the local pin power error in the discussion of the treatment of fuel parameter uncertainties on SLMCPR. The method uncertainty for the pin power error was evaluated with comparisons between TGLBA06 and MCNP version 4A.

#### Comparison Results

The information presented in Enclosure 3 of the above referenced document was used to address the accuracy of TGBLA for high-void (approximately 90 percent void fraction) lattices and incorporating the cross section fitting used in GNF methodology. MCNP was used as an independent code for comparison purposes and because the accuracy of TGBLA06 at high void fractions was in question. Several plots were provided to demonstrate the accuracy of the cross section fitting process with results from both MCNP and TGBLA. The results indicate that the fitting process is generally accurate for  $k_{inf}$  and three-group cross sections, with the exception being the migration area and flux ratios at high void fractions, which have fitting errors of 5-10 percent at 90 percent void fraction. These parameters are utilized in the core simulator, PANACEA, and the impact of these fitting errors must be assessed at the core level with the impact on the nodal powers. However, the impact of these errors at the core level was not directly assessed.

Comparisons of cross sections and lattice physics parameters and pin powers were performed for instantaneous changes in water density, which is equivalent to change in the coolant void fraction, for depletion with a constant 40 percent void fraction. Comparisons were performed for the cross sections, lattice physics parameters, and pin powers as a function of exposure and void fraction. These results represent an absolute comparison of the cross sections and lattice physics parameters between the two codes. Figure B-1 through Figure B-3 show the average error of the lattice comparisons and the spread of the data for the  $k_{inf}$  values,  $\nu\Sigma_3$ , and pin powers. Values are provided with TGLBA06 calculations at 90 percent void fraction as well as the extrapolation to 90%. A comparison of the errors for the "90" and "Fit at 90" provides an indication of the accuracy of the fitting process. The variation in the  $k_{inf}$  error with void fraction is small for the controlled state, but a trend does occur with the controlled conditions. Some of the macroscopic cross sections also exhibit an increasing error trend with void fraction; an example is given for  $\nu\Sigma_3$ , which represents the neutron production cross section for the thermal group. This parameter is related to the nodal power generation. The RMS and Max pin powers,

- B-2 -

presented in Figure B-3, also exhibit increasing errors with void fraction. Additional comparisons of MCNP results demonstrating the accuracy of the cross section and lattice parameter fitting process is provided in Figure B-5 through Figure B-12.

A comparison of the pin powers computed with TGBLA06 and MCNP at 90 percent void fraction as a function of exposure is shown in Figure B-4. The results do not show a trend with exposure, but as noted above the depletion calculation was performed with TGBLA06. This does not, therefore, provide an indication of the error in these historical results (depletion calculation). In addition, the impact of depletion at different void fractions cannot be assessed with these TGBLA06/MCNP comparisons. The RMS pin power error at 90 percent void fraction shown in Figure B-4 [ ] should be compared to the value currently being used by GNF [ ] in the determination of their SLMCPR.

### Assessment

The MCNP code is routinely used as a reference calculational method and based on its use of the continuous energy MCNP method is widely recognized as being one of the most rigorous neutronics available. Comparisons between TGBLA06 and MCNP provide an indication of the level of error in the TGBLA06 neutron transport methods and resonance processing and multi-group neutron energy treatment.

There are sources of error in TGBLA that cannot be assessed by comparisons with MCNP. The nuclear data libraries used in the MCNP calculations are based on the ENDF/B-VI nuclear data files, which also correspond to the same data source as TGLBA06. Errors in cross sections, lattice physics parameters, and pin powers resulting from deficiencies in nuclear data cannot be assessed. In addition, since MCNP is a steady-state code, comparisons provided at different exposure conditions utilized isotopic compositions computed with the TGBLA06 code, and the results, therefore, cannot be considered as a code-to-code validation of historical effects that occur during depletion. The impact of depletion at high void fractions is not addressed with these TGBLA06/MCNP comparisons.

Comparisons with MCNP, therefore, are a useful part of assessing the accuracy of TGBLA06, but the results do not provide all possible sources of error that must be included to obtain an indicated of the overall level of accuracy, namely nuclear data errors and depletion errors. Direct measurement based on core operating history, in-core measurements, bundle and pin gamma-scan measurements, and critical experiments are additional sources of data that must also be considered to fully address the validation of a lattice-physics code such as TGBLA06.

The TGBLA06 and MCNP comparisons were used to demonstrate the accuracy of the cross section fitting and extrapolation process and demonstrated that sizeable errors result in the extrapolation of the migration area and flux ratios. The impact of these errors was not fully assessed at the core level. The comparisons of some key cross section and lattice physics parameters indicate an increasing error trend with increasing void fraction. This includes an increasing error trend in the pin power with increasing void fraction. The GNF methodology to assess pin power errors relies on comparisons between TGBLA06 and MCNP to provide the RMS error in pin power used in the LHGR and SLMCRP limit determination. This trend indicates the need for a reassessment of the pin power errors for operating domains with increases in void fraction.

### TGBLA06/HELIOS Comparisons

Assessment by code-to-code benchmarking of TGBLA06 with other independent codes for lattices and operating conditions typical of EPU conditions can reasonably ensure the



- B-3 -

consistency of the results from the GE lattice physics methods. Code-to-code comparisons are included in Reference 69, Enclosure 3, comparing TGBLA to MCNP for particular lattices. Given that depletion cannot be performed with MCNP, additional results were obtained with the HELIOS lattice physics code. Additional code-to-code comparisons were also included in the VYPNS RAI SRXB-66 response (Reference27) comparing CASMO and TGBLA.

As indicated above, code-to-code comparisons are useful for confirming consistency of results, evaluating numerical and method approximations used in the codes, and identifying code errors. In most cases, it is unknown which code is more accurate, and the code with the higher fidelity methods is typically taken as the reference. However, unless the codes are carefully assessed with measured data, the absolute accuracy, in terms of bias and uncertainty, of the codes cannot be established because the codes may use common fundamental data (e.g., ENDF/B-VI) and methods that may lead to better agreement than would be observed with comparisons with measurements. Also, without measurement data, the overall applicability of the data and methods to expanding ranges of operating conditions cannot be established.

For this evaluation, comparisons were performed for representative lattices and comparisons of  $K_{inf}$ , peak pin power, plutonium isotopic inventory, and cross-sections and lattice physics parameters. Example results will be presented based on the confirmatory analysis performed with HELIOS for a lattice configuration (enrichment and gadolinium loading) typical of EPU designs. The specific lattice (5168) is for the upper region of the fuel bundle in which the void impacts are the largest. The results for the lower region of the fuel bundle (5166) provide similar results. The lattice contains nine pins with Gadolina loadings of 6 and 7 wt. percent and a average enrichment of 4.5 wt. %. The assessments performed are limited to lattice results computed with lattice physics codes. An assessment of axial and radial power distributions within the core was not performed. Therefore, the comparisons cannot evaluate the GE tools for prediction radial and axial power profiles within the core.

### Kinf Comparisons

Comparing lattice  $K_{inf}$  values allow evaluation of the lattice physics methods and data for predicting lattice reactivity vs exposure. This information, along with additional cross-section parameters, is used in the full-core analysis to predict the core eigenvalue and global power distribution. Lattice  $k_{inf}$  values were compared for typical designs as a function of exposure based on calculations with HELIOS and TGBLA06. Figure B-13 provides an example of the level of agreement in the lattice infinite multiplication factor,  $k_{inf}$ , and depletion at various void fractions. The overall level of agreement is excellent with the  $k_{inf}$  values agreeing very well at high exposures. The differences are larger in the 0 – 20 GWd/ST burnup range, which is when the gadolinium is burning out. The burnout of Gd, particularly at high void fractions, results in differences between TGBLA06 and HELIOS. The differences are smaller for void fractions of 40 percent and 70%, which represent the average void-fraction value for a core. The differences for the high-void-fraction depletion case (90 percent void fraction) occur at the maximum bundle  $k_{inf}$  point at about 20 GWd/ST and improve to excellent agreement at higher exposures. Note that the GE methodology does not directly use the 90 percent depletion cases, but rather relies on extrapolation of values from 0%, 40%, and 70 percent void-fraction depletions. The error in  $k_{inf}$  introduced in this extrapolation process has been demonstrated to be small; therefore, a comparison of directly calculated values at 90 percent void fraction is appropriate. Overall, there is excellent agreement in  $k_{inf}$ , with a larger difference for higher void fractions. The level of agreement is not expected to result in any major differences in predicting core eigenvalue and the global bundle- power densities.

### Power Distribution Comparisons

The pin-fission densities computed with TGBLA06 and HELIOS were compared and the RMS difference and peak pin-fission rates were calculated. The pin-fission densities are related to the pin power distribution used in calculating the LHGR and R-factors for the SLMCPR limits. Figure B-14 and Figure B-15 show an example of the typical results obtained for the RMS differences and peak relative fission rate, respectively. The RMS differences are largest for fresh fuel, when the highest peaking occurs, and for the high void-fraction cases; the differences decrease with fuel exposure as the peak locations are depleted. Pin-by-pin comparisons for lattice 5166 as a function of exposure at a void fraction of 40 percent and for lattice 5168 as a function of exposure at a void fraction 90 percent are shown in Figure B-17 through Figure B-22. These figures show the percent difference in the fission rates calculated with TGBLA06 and HELIOS1.6. The largest differences occur at zero exposure and the peaks decrease as the exposure increases. The largest differences, on a percent basis tend to occur in corner pins and Gd pins.

The RMS error is applied to the SLMCPR. Previous analysis comparing TGBLA06 and MCNP has shown that for a variety of lattices and exposures that the RMS difference is [ ] percent. However, in these comparisons, the isotopic concentrations were taken from TGBLA and used in MCNP; therefore, errors in depletion were not included. This figure shows that on a code-to-code basis that, for the lower void fractions, the RMS difference at low exposures and at high void fraction exceeds the [ ] percent RMS value, with maximum differences of about [ ] percent. For the fuel exposures above the gadolinium burnout and for lower void fractions, the differences are consistent with the [ ] percent value. Note that the results for the 90 percent void fraction in the code-to-code comparisons do not include potential errors caused by the quadratic fit and extrapolation used in GE's neutronic methods. Similar results were obtained for other lattices and with comparisons between TGBLA06 and CASMO-4 provided in (Reference27). Note, however, that the lattices considered in these comparisons resulted in significantly higher peaking at high void fractions and exposures, as shown in Figure B-16, which provides a comparison of the peak fission rate calculated with TGBLA06 and HELIOS 1.6 for lattice 7007. This lattice differs from 5168 in that it has more gadolinium pins. Note that in comparison of the peak fission rate for lattices 5168 (Figure B-15) and 7007(Figure B-16) that the later has a value at high void fraction at high exposure approaching that of the fresh fuel. Based on these code-to-code results, the RMS power distribution differences indicate that the RMS differences may exceed the [ ] percent value determined previously. Therefore, this supports the need for increasing the pin power-peaking uncertainty to [ ] percent as was done for the SLMCPR.

The comparison of the peak pin-fission rates is applicable to the assessment of the LHGR accuracy, and the example provided Figure B-15 is typical of the comparisons observed and shows good agreement between the two codes. However, it should be noted that the overall LHGR is a product of the local pin relative-power and the bundle power. A complete assessment of the differences in LHGR also requires an assessment of the bundle power accuracy, which may be larger for high void fractions given the larger differences in the lattice kinf values indicated above. This analysis requires the use of core-level simulation and was not performed for this evaluation.

Pin fission rates for the controlled condition (control blade inserted) were also calculated with HELIOS1.6 to investigate the gradient in the power distribution from the controlled side to the uncontrolled side of the bundle. The relative power distribution (shown as a difference from a bundle-averaged value of 1) is presented in Figure B-23. These results show that the relative fission rate changes by from -50 percent to +50 percent of the average across the bundle. This

- B-5 -

generally is not a concern given that controlled assemblies may not have significant power, but is an effect that should be investigated in terms of accuracy of burnup and prediction of isotopics over the course of extended periods of controlled operation for this bundle. In addition, the insertion of a strong absorber and the corresponding gradients can be a challenge for lattice physics codes, such as TGLBA06 and HELIOS1.6 to model. Additional calculations were performed with MCNP for the same bundles and conditions as for the HELIOS1.6 results presented. A comparison of the HELIOS1.6 and MCNP pin-fission rates is presented in Figure B-24. The level of agreement between the two codes is good, with the largest difference occurring in the high-powered pins. These results provide some confidence that standard lattice physics tools can predict these controlled configurations. Comparisons with TGBLA06 were not performed and therefore, the accuracy of TGBLA06 for the controlled configurations has not been assessed.

An additional area not assessed is the impact on axial power distribution upon withdrawal of a control blade. During operation with the control blade inserted the fuel depletion is significantly lower and the neutron spectrum is harder in the controlled section of the bundle. The harder spectrum results in enhanced plutonium production and combined with the limited depletion of the  $^{235}\text{U}$  in the fuel, creates an axial variation in fissile content such that when the control blade is withdrawn there is a peak in the axial power profile in these locations. The core conditions in expanded operating domains, such as a higher exit void fraction, may enhance this axial power-peaking. The two-dimensional lattice physics codes discussed in this section cannot be used to analyze the axial power shapes as analysis for the axial dimension is required. Such an analysis was not performed as part of the confirmatory analysis and therefore, the impact of axial power-peaking resulting from control blade movement was not evaluated. This represents a topic for further assessment.

### Isotopic Comparisons

Isotopic comparisons were performed for key actinides (uranium and plutonium), which are computed using the lattice physics tools. Of particular interest is the comparison of the plutonium compositions as an indication of the prediction of the neutron spectrum and to further investigate potential impacts on the void reactivity coefficient and SDM. The neutron spectrum is highly dependent upon the local void fraction, which has an impact on the neutron moderation. In addition, BWRs can be operated to enhance the plutonium production in the upper part of the core by using a bottom-peaked power distribution with higher void fractions in the core's upper regions. This spectral shift operation results in more energy generation as power distribution becomes more top-peaked near end of cycle in which the generated plutonium is used. As a result, the prediction of isotopic compositions can have a substantial impact on the axial power distribution as well. The comparison of the Pu-239, Pu-240, and Pu-241 isotopic composition, as presented in Figure B-27, Figure B-28, and Figure B-29, show very good agreement, particularly at the lower void fractions. Notably, Pu-239, the primary fissile plutonium species present, has very close agreement between the two codes. It should be noted that the results included in the comparisons are based on a version of TGBLA06 that employs a correction of the Pu-240 resonance at high exposures for lattices. An assessment of this correction is provided in RAI SRXB-A-67e of Reference 27, indicating that this error resulted in a [ ] percent  $\Delta k$  difference on the lattice level and has a small impact on the core eigenvalue predictions.

### Cross-Sections and Lattice Physics Parameters

The cross-sections and lattice physics parameters computed by TGBLA06 are used in the PANAC11 core simulator and other codes used for safety analyses. The impact of the accuracy of the extrapolation errors on cross-sections and lattice physics parameters has been assessed, but it is difficult to directly compare cross-sections because of differing energy group boundaries and definitions. Based on the lattices modeled with HELIOS and TGBLA06, a comparison of the key macroscopic cross-sections was performed for the absorption and fission cross-sections. Figure B-25 and Figure B-26 provide a comparison for a particular lattice for the thermal (group 3) cross sections. The level of agreement is good and the differences can be attributed to differences in prediction of isotopic compositions, as previously discussed, in addition to the fundamental cross-section data (both HELIOS and TGBLA06 use ENDF/B-VI data). The primary lattice parameter considered is  $k_{inf}$ , which was discussed above. In addition, lattice parameters such as the migration area, diffusion coefficient, and flux ratios are also of interest, but cannot be directly compared because of differing definitions used in the computer codes.

### Conclusions

The NRC staff concludes that the code-to-code comparisons provide reasonable assurance that the TGBLA06 neutronic methods are acceptable for analyzing the lattices and conditions for EPU and MELLLA+. The differences in the pin-fission rates observed indicate the need for additional measured data to confirm the accuracy of the lattice physics and core simulator prediction. The code-to-code comparisons are insufficient for assessing the uncertainties in the code predictions because of potential commonalities in fundamental data and methods employed as well as general applicability to EPU conditions of interest. GE plans to perform gamma scan measurements to confirm that the assumptions used in the neutronic methods for current GE fuel designs are still appropriate.

[

Figure B-1. Comparison of  $k_{inf}$  between TGBLA06 and MCNP as a function of void fraction ]

[

Figure B-2. Comparison of  $v\Sigma_3$  between TGBLA06 and MCNP as a function of void fraction ]

[

Figure B-3. Comparison of pin powers between TGBLA06 and MCNP as a function of void fraction ]

[

Figure B-4. Comparison of pin powers between TGBLA06 and MCNP as a function of exposure at a void fraction of 90% ]

[

Figure B-5. Error in fit of RMS, peak pin, and max error as a function of exposure at a void fraction of 90%

[

Figure B-6. Error in fit of thermal absorption cross section as a function of exposure at a void fraction of 90%

[

Figure B-7. Error in fit of thermal nu x fission cross section as a function of exposure at a void fraction of 90%

[

Figure B-8. Error in fit of group 1 to 2 slowing down cross section as a function of exposure at a void fraction of 90%.

]



[

Figure B-9. Error in fit of group 2 to 3 slowing down cross section as a function of exposure at a void fraction of 90%.

[

Figure B-10. Error in fit of fast removal cross section as a function of exposure at a void fraction of 90%.

]

[

Figure B-11. Error in fit of fast flux ratio as a function of exposure at a void fraction of 90%. ]

[

Figure B-12 Error in fit of the epi-thermal flux ratio as a function of exposure at a void fraction of 90% ]

[

Figure B-13 Comparison of TGBLA06 and HELIOS lattice k-infinity values as a function of fuel exposure.

[

Figure B-14. RMS difference between TGBLA06 and HELIOS pin-fission densities.

]

[

**Figure B-15. TGBLA06 and HELIOS peak pin relative fission rate comparison.**

]

[

**Figure B-16. TGBLA06 and HELIOS peak pin relative fission rate comparison for lattice 7007.**

]

[

**Figure B-17. Comparison (in percent difference) of the TGBLA06 and HELIOS Pin Fission Rate Distribution for Lattice 5168 at an Exposure of 0 GWd/ST and a void fraction of 40%.**

[

**Figure B-18. Comparison (in percent difference) of the TGBLA06 and HELIOS Pin Fission Rate Distribution for Lattice 5168 at an Exposure of 15 GWd/ST and a void fraction of 40%.**

[

**Figure B-19. Comparison (in percent difference) of the TGBLA06 and HELIOS Pin Fission Rate Distribution for Lattice 5166 at an Exposure of 60 GWd/ST and a void fraction of 40%.**

[

**Figure B-20. Comparison (in percent difference) of the TGBLA06 and HELIOS Pin Fission Rate Distribution for Lattice 5168 at an Exposure of 0 GWd/ST and a void fraction of 90%.**

[

**Figure B-21. Comparison (in percent difference) of the TGBLA06 and HELIOS Pin Fission Rate Distribution for Lattice 5168 at an Exposure of 15 GWd/ST and a void fraction of 90%.**

[

**Figure B-22. Comparison (in percent difference) of the TGBLA06 and HELIOS Pin Fission Rate Distribution for Lattice 5168 at an Exposure of 60 GWd/ST and a void fraction of 90%.**

[

Figure B-23. Pin Fission Rate Distribution for Lattice 5166 at an Exposure of 0 GWd/ST and a void fraction of 0 percent for the controlled configuration. ]

[

Figure B-24. Comparison of HELIOS1.6 and MCNP Pin Fission Rate Distribution for Lattice 5166 at an Exposure of 0 GWd/ST and a void fraction of 0 percent for the controlled configuration. ]



[

Figure B-25. Comparison of the TGBLA06 and HELIOS group 3 absorption cross section as a function of historical void fraction and fuel exposure.

[

Figure B-26. Comparison of the TGBLA06 and HELIOS group 3 fission cross section as a function of historical void fraction and fuel exposure.

[

Figure B-27. Comparison of the TGBLA06 and HELIOS Pu-239 isotopic compositions for Lattice 5168.

[

Figure B-28. Comparison of the TGBLA06 and HELIOS Pu-240 isotopic compositions for Lattice 5168.

[

Figure B-29. Comparison of the TGBLA06 and HELIOS Pu-241 isotopic compositions for Lattice 5168. ]

## APPENDIX C TRANSIENT LHGR LIMIT CONFIRMATORY ANALYSIS

### Objective

Use FRAPCON-3 to perform a limiting fuel thermal-mechanical design study of the GE14 Fuel Rod Thermal-Mechanical Design to support the Browns Ferry extended power uprate (EPU).

### Inputs and Assumptions

1. GE14 fuel assembly and fuel rod specifications and manufacturing tolerances obtained from “GE14 Fuel Rod Thermal-Mechanical Design Report” (Reference 50) and “GE Fuel Bundle Designs.” (Reference 51)
2. Browns Ferry COLR Thermal-Mechanical Operating Limit (TMOL) as follows:

	<u>Nodal Burnup</u> (GWd/MTU)	<u>Nodal Power</u> (kW/ft)	
		<u>UO2</u>	<u>UGdO2</u>
[			
]			

3. Average U235 enrichment of [.....].
4. Gadolinium enrichment of [ ].

### Results

Table C-1 lists the results from the FRAPCON-3 cases. Examination of the FRAPCON results leads to the following conclusions.

#### **Rod Internal Pressure:** [

].

Manufacturing tolerances were selected to minimize plenum volume and maximize fission gas release. Based upon the results, the UO2 fuel rod is more limiting than the UGdO2 fuel rod due to (1) less plenum volume and (2) higher rod power. Even though the Gd rods exhibit significantly higher operating fuel temperatures [

], is able to accommodate the higher fission gas release.

The FRAPCON-3 algorithms are tuned to produce best-estimate predictions. Even though manufacturing tolerances are set at worst case, the modeling uncertainty (which represents the spread in the empirical database) needs to be accounted for. Operating a single rod on the TMOL peak nodal power for its entire lifetime is extremely conservative (as the peak node would migrate to many different fuel rods). This scenario coupled with a [ ] is judged to be more than adequate to accommodate any modeling uncertainty.

Examination of the Table 1 results reveals that the worst rod internal pressure experienced is [

].

-C-2-

**Fuel Temperature (TOP):** The design criteria is that fuel centerline temperature remains below incipient melting conditions. Note that UO<sub>2</sub> melting temperature is calculated as follows:

$$\text{UO}_2 \text{ Tmelt} = 5080^\circ\text{F} - 58^\circ\text{F per 10 GWd/MTU.}$$

$$\text{UGdO}_2 \text{ Tmelt} = 5080^\circ\text{F} - 60^\circ\text{F (8 percent Gd)} - 58^\circ\text{F per 10 GWd/MTU.}$$

Manufacturing tolerances were selected to maximize fuel temperature (e.g., maximum clad thickness, maximum crud/oxide). Based upon the results, the UGdO<sub>2</sub> fuel rod is more limiting than the UO<sub>2</sub> fuel rod due to lower fuel thermal conductivity.

Examination of the Table 1 results reveals that the UO<sub>2</sub> fuel rod is able to accommodate [ ]].

The FRAPCON-3 algorithms are tuned to produce best-estimate predictions. Even though manufacturing tolerances are set at worst case, the modeling uncertainty (which represents the spread in the empirical database) needs to be accounted for. The modeling uncertainty related to predicted fuel temperature increases significantly with burnup. [ ]].

**Clad Strain (MOP):** The design criteria is that cladding strain be limited to 1 percent plastic strain during normal operation and AOOs.

Manufacturing tolerances were selected to maximize fuel thermal expansion and clad stress (e.g., minimum clad thickness, maximum fuel pellet diameter, maximum crud/oxide). Based upon comparable strain at lower power levels, the UGdO<sub>2</sub> fuel rod is slightly more limiting than the UO<sub>2</sub> fuel rod.

Examination of the Table 1 results reveals that the UO<sub>2</sub> fuel rod is able to accommodate [ ]].

The FRAPCON-3 algorithms are tuned to produce best-estimate predictions. Even though manufacturing tolerances are set at worst case, the modeling uncertainty (which represents the spread in the empirical database) needs to be accounted for. The modeling uncertainty related to predicted fuel swelling and cladding strain is high, especially as burnup increases. The spread in empirical data for power ramp tests may exceed 50%. As a result, an uncertainty on the best-estimate FRAPCON cladding strain calculations should be approximately 50%. Based upon the calculated strains and a 50 percent uncertainty in the model accuracy, [ ]].

**Table C-1 FRAPCON-3 GE14 Fuel Rod Design Stud**

[

]

APPENDIX D CORE TRACKING DATA TABLE

**Plant A – Cycle 18**

Cycle Expo.	Core Power	Core Flow	Bundle RMS	Axial RMS	Nodal RMS	Avg.Core Exit Void Fract.	Max Chan. Exit Void Fract.	MFLCPR	MFLPD	MAPRAT
GWd/ST	%OLTP	% Rated	%	%	%					
2.34	104	93.6	[			0.74	0.84	[		
3.37	103.4	94.2				0.73	0.84			
4.18	112.2	94.4			]	0.75	0.86			]

**Plant A – Cycle 19**

0.24	112.4	94.8	[			0.76	0.83	[		
1.17	112.5	92.8				0.76	0.83			
2.13	112.4	94.3				0.76	0.84			
2.5	112.3	95.4				0.75	0.85			
3.16	112.3	96.9				0.75	0.85			
4.19	112.5	93.6				0.76	0.86			
4.51	112.2	97.6				0.75	0.84			
5.18	112.5	97.9				0.75	0.84			
6.26	112.3	94.4				0.76	0.85			
7.22	112.4	94.4				0.75	0.86			
8.13	112.6	94.3				0.75	0.86			
9.02	112.6	96			]	0.75	0.86			]

**Plant B – Cycle 9**

0.26	104.8	99.4	[			0.74	0.83	[		
0.54	104.9	90.6				0.76	0.84			
0.79	104.9	91.1				0.76	0.84			
1.42	104.8	96.9				0.74	0.83			
1.61	105	94.9				0.75	0.84			
2.2	104.6	89.7				0.76	0.85			
2.5	104.9	89.7				0.76	0.86			
3.41	104.6	85.7				0.76	0.87			
3.87	104.6	85				0.76	0.87			
4.39	105	92.1				0.75	0.86			
5.92	104.7	87.6				0.76	0.86			
6.92	105.1	86.4				0.76	0.87			
7.2	105	98				0.74	0.86			

NEDO-33173-A, Revision 1  
 Non-Proprietary Information

D-2

7.76	104.9	95.5		0.74	0.86	
8.49	105	92.9		0.75	0.87	
9.2	105	91		0.75	0.87	
9.58	96.8	103.9		0.7	0.82	
10.06	105.1	100.6		0.73	0.85	
10.34	104.8	99.6		0.73	0.85	
11.12	105.1	99.5		0.73	0.85	
12	101.1	103.3		0.71	0.85	
13.21	104.6	101.3		0.72	0.85	
13.71	104.8	93.1		0.74	0.87	
14.24	104.9	97.2		0.73	0.86	
14.49	104.1	102.9		0.72	0.84	
14.76	104.6	102.1		0.72	0.85	
15.21	102.8	104.1		0.71	0.84	
15.63	88.1	103.5		0.67	0.81	
15.99	89.2	103.6	]	0.67	0.81	]

**Plant B – Cycle 10**

0.19	94.1	102.7	[	0.7	0.8	[
0.27	104.5	102.1		0.73	0.83	
0.8	105	98.1		0.74	0.84	
1.64	104.9	96.9		0.74	0.84	
2.45	105	96.7		0.74	0.85	
4.1	104.9	92.3		0.75	0.85	
4.18	105	92.6		0.75	0.85	
4.46	104.9	95.6		0.74	0.85	
5.01	104.9	95.5		0.74	0.86	
5.77	104.9	94		0.74	0.86	
6.61	104.9	93		0.74	0.87	
7.08	104.8	97.4		0.73	0.86	
7.92	104.9	95.4		0.74	0.87	
8.2	105.1	95.4		0.74	0.87	
8.68	105	92.3	]	0.74	0.88	]

**Plant C – Cycle 30**

0.43	110	98.2	[	0.71	0.88	[
1.13	109.8	97.7		0.71	0.87	
1.85	109.8	94.7		0.71	0.88	
2.25	109.5	93.8		0.72	0.89	
2.53	109.8	93.4		0.72	0.89	
3.33	109.7	94.5		0.72	0.87	
3.84	109.9	88.6		0.73	0.9	
4.01	109.9	90.2		0.73	0.9	
4.71	109.5	98.9		0.71	0.88	



NEDO-33173-A, Revision 1  
 Non-Proprietary Information

D-3

5.34	106.7	87		0.72	0.9
6.25	109.5	105.7		0.68	0.87
6.48	94.3	88.5		0.68	0.87
6.91	105.1	109.8	]	0.65	0.85

**Plant C – Cycle 31**

0.5	103.7	87.7	[	0.72	0.88	[
0.98	110.2	97.8		0.72	0.87	
1.68	110	93.7		0.72	0.87	
2.45	109.9	92.3		0.72	0.87	
3.1	109.7	93		0.72	0.87	
3.92	109.9	94.8		0.72	0.87	
4.61	109.6	90.9		0.72	0.88	
5.38	109.6	99.1		0.71	0.87	
5.86	109.7	90.1		0.72	0.9	
6.72	109.5	107.8		0.68	0.86	
7.28	109.3	109.2	]	0.66	0.85	]

**Plant E – Cycle 9**

0.25	111.1	92.6	[	0.75	0.87	[
0.51	111.2	98.2		0.74	0.86	
3.72	111.7	94		0.76	0.86	
3.77	111.6	94.7		0.75	0.86	
4.78	109.8	92.5		0.75	0.86	
5.69	109.5	90.9		0.76	0.87	
7.54	109.3	90.8		0.76	0.87	
9.31	109.5	92.5		0.76	0.87	
10.2	111.5	93.7		0.76	0.87	
11.03	112	94.6		0.76	0.87	
11.98	112.2	95		0.76	0.86	
12.91	109	94		0.75	0.86	
14.62	106	103.2		0.73	0.82	
15.4	100.8	104.3	]	0.7	0.8	]

**Plant E – Cycle 10**

0.14	111.7	95.4	[	0.76	0.84	[
0.79	111	93.9		0.76	0.84	
1.71	113.5	95.6		0.77	0.85	
2.47	114.6	96.6		0.76	0.85	
3.58	114.2	96.2		0.77	0.86	
5.73	113.8	97.5		0.76	0.85	

NEDO-33173-A, Revision 1  
Non-Proprietary Information

D-4

6.58	113.3	96.6		0.76	0.85	
7.38	113.9	95.9		0.77	0.86	
8.45	110.8	95.8	]	0.76	0.86	]

APPENDIX E PROPAGATION OF VOID FRACTION ERRORS TO VOID REACTIVITY COEFFICIENT

This appendix performs a simple calculation of the impact of void-fraction errors on the value of the void reactivity coefficient. Note, the terms void reactivity coefficient (VRC) and density reactivity coefficient (DRC) are used to represent the change in core eigenvalue when the moderator density changes. As the moderator density changes, the slowing down of the high-energy fission neutrons changes; thus changing the core eigenvalue. The moderator density can change because of a number of different effects. One of them is a change of void fraction; thus, the terms void- and moderator-coefficient are often treated as interchangeable.

For this sample evaluation, we have used one particular example, which has been extracted from a LAPUR code input deck. This particular deck corresponds to the Cofrentes instability event in 1992. The cross sections and the LAPUR deck were developed by the Spanish Consejo de Seguridad Nuclear (CSN) based on plant data.

LAPUR input deck cards number 20 & 21 contain the density reactivity coefficient in units of %dK/K per g/cm<sup>3</sup>. The moderator density is relative to the liquid density at 1000 psi.

**Table E-1. Density reactivity coefficient versus relative moderator density**

Relative Moderator Density	0	0.2	0.4	0.6	0.8	1	1.2
DRC	43.97	32.71	24.15	18.28	15.10	14.62	16.83

Using the density of liquid and steam at 1000 psi, we can convert this table as function of the void fraction.

**Table E-2. Density reactivity coefficient versus void fraction at 1000 psi**

Void Fraction	0	0.2	0.4	0.6	0.8	1	1.2
DRC	43.97	32.71	24.15	18.28	15.10	14.62	16.83

Figure E-1 shows these data graphically, with an approximation given by the equation:

$$\frac{\Delta K/K}{g/cm^3} = 14.62 + 25.41 \times \alpha^2$$

Using the above equation, we have derived the error expected in the DRC given an error in void fraction ( $\alpha$ ). The results are shown graphically in Figure E-2. As observed in this figure, the DRC error is a function of the void fraction, but it levels to an approximate value of 1.25 percent for void fractions greater than 60%, which is the range of interest. Therefore, we conclude that a DRC error of 1.25 percent is a reasonable approximation of the error induced by a change in actual void fraction of 1%. For example, if the predicted void fraction is 70%, but the actual void fraction is 71%, the actual DRC is 1.25 percent higher than predicted.

Note that the numbers used in this report are representative of a BWR6, but DRC values change with core loading, exposure, operating condition, etc.; therefore, the 1.25 percent error should be consider as an indication for order of magnitude calculation. It is definitely not a bounding number.

E-2

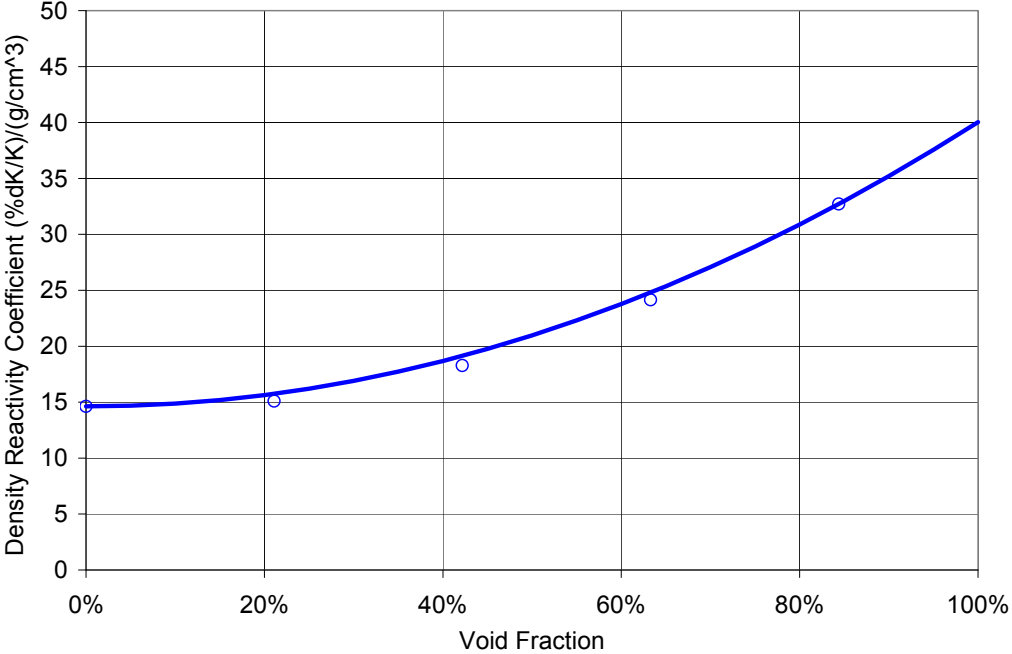


Figure E-1. Density reactivity coefficient as function of void fraction (1000 psi)

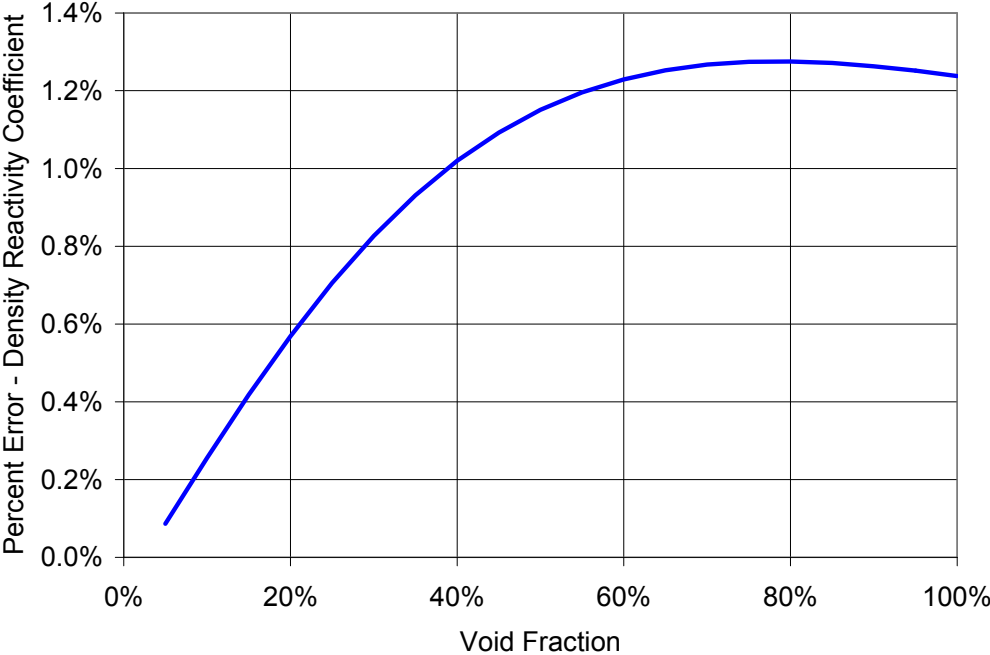


Figure E-2. Percent change in DRC per 1 percent absolute change in void fraction

## APPENDIX F – PART 21 EVALUATION

### Evaluation of GHNE Part 21 Notification: Adequacy of GE thermal-Mechanical Methodology, GSTRM

#### 1.0 BACKGROUND

During the design certification review for the Economic Simplified Boiling Water Reactor (ESBWR), the NRC staff discovered an issue in the GSTRM thermal-mechanical (T-M) calculations, supporting the GE14 fuel designs. Specifically, the NRC staff discovered that the GSTRM under-predicted the UO<sub>2</sub> fuel temperature calculations in comparison to both FRAPCON-3 and PRIME calculations for high exposures. PRIME is a new T-M code (currently under NRC review), which GHNE used for sensitivity analysis in response to ESBWR requests for additional information (RAIs). From the review of the ESBWR, the NRC staff attributed the observed differences primarily to the GSTRM UO<sub>2</sub> fuel thermal conductivity model, which does not model the exposure dependency as compared to the other two codes.

In the NRC staff safety evaluation (SE) of GHNE licensing topical report (LTR) NEDC-33173P, Revision 1 (Reference 1), the NRC staff evaluated the conservatism in the GSTRM T-M methodology. Specifically, the confirmatory analyses performed in this review and the data provided in the RAI responses revealed that GSTRM appeared to under-predict the internal rod pressure calculation. During the review of the GSTRM T-M methodology in NEDC-33173P, the NRC staff established that additional GSTRM benchmarking data was needed for the current fuel designs as operated in the current core designs and operating strategies. GHNE had committed to perform fission gas release (internal rod pressure) and exposure gamma scans. However, the NRC staff needs additional information regarding the status and schedule of the gamma scans. Attached are RAIs which address the additional benchmarking data status needed.

The NRC staff requested that GHNE initiate an evaluation under Title 10 of the *Code of Federal Regulations* (10 CFR) Part 21 in order to demonstrate the adequacy of the GSTRM T-M methodology, regarding the observed GSTRM under-predictions in fuel temperature and internal rod pressure, including its impact on the T-M fuel performance. In a letter dated January 21, 2007, GE submitted the Part 21 Notification (Reference 2) that evaluated the GSTRM T-M methodology.

The SE of LTR NEDC-33173P contains limitations and conditions that pertain to the performance of the T-M methodology. Specifically, Limitation 14 in Section 9.0 of the SE, states that the conclusions of the NRC staff assessment of information provided in the GSTRM Part 21 Notification will be applicable to the use of GE GSTRM T-M methodology.

This appendix provides the NRC staff assessment of the content of GE's GSTRM Part 21 Notification (Reference 2) and the associated RAI 9 responses (Reference 3). The conclusions of this assessment applies to Limitation 14 of the NRC staff SE of NEDC-33173P, until such time that the NRC staff receives T-M submittal that addresses the issues raised in the attached RAIs and any follow-on staff audits.

## 2.0 STAFF ASSESSMENT

The NRC staff evaluated the Part 21 Notification and the data provided in the T-M RAI responses and found that it was inadequate for verifying the adequacy of GSTRM calculated fuel rod temperatures and rod pressures.

### Fuel Temperatures

In the Part 21 Notification, GHNE suggested that [ ]. However, this assessment was based on old data obtained and used to validate GSTRM before 1984. Based on comparisons to NRC code FRAPCON 3.3, the GSTRM best estimate fuel temperatures appear to be under-predicted, even at relatively low burnups.

However, examination of the uncertainties applied to GSTRM fuel temperature calculations provided in the RAI 9 response (Reference 3) shows that although the GSTRM best estimate calculation underestimates the fuel centerline temperature, the conservative uncertainty treatment compensates for the under-prediction, resulting in bounding 95/95 fuel centerline temperatures. Therefore, the NRC staff concludes that the GSTRM fuel temperatures calculation with the 95 percent uncertainty treatment is acceptable. This judgment is based on the uncertainties applied in the RAI 9 (Reference 3) fuel temperature calculation, which is based on NRC-approved uncertainty treatment methodology.

### Rod Pressure

The analysis of rod pressure,  $P_{rod}$  (term used here for clarity and not by GHNE), [

]. GSTRM calculation of rod pressures relies on two internal models: the fission gas release and the internal rod void volume model. The fidelity of the internal rod pressure calculation depends on the accuracy of these two models. [

].

GSTRM also appears to under-predict fission gas release and fuel rod pressures at the current end-of-life high burnup levels. In the Part 21 Notification, GHNE states that the dated database covered the range of current operating conditions. However, considering the database available at the time of the GSTRM approval suggests that the linear heat generation rate (LHGR) range may have been above the LHGR limits for current fuel designs only at low burnup levels and may be significantly below current LHGR limits at high burnup levels characteristic of current fuel designs. At high burnup levels, the LHGRs for which GHNE used to validate GSTRM were most likely very low (much lower than current LHGR limits for the current fuel designs at high burnup) and the uncertainties in fission gas release were also very high. Thus, the corresponding rod pressure uncertainties were also high.

F-3

The most recent industry fission gas release data at high burnups are either near or above the GHNE LHGR limit and would be expected to provide a much better benchmarking database than the GSTRM 1984 verification data. In addition, [ ], while currently available data from Halden exceeds 80 GWD/MTU.

[ ]. The NRC staff FRAPCON 3.3 confirmatory calculation shows that GSTRM under-predicts the internal rod pressure by 600 psi both for the nominal and the 95 percent confidence level. The lower prediction demonstrates that although the internal rod pressure prediction meets the acceptance criteria in terms of the  $P_{critical}$ , the adequacy of the GSTRM uncertainty treatment needs to be confirmed through measurement qualification data and corrected for licensing applications.

[

].

The NRC staff FRAPCON 3.3 confirmatory calculation determined a  $P_{critical}$  value of 3200 psi rod pressure limit (best estimate). This pressure limit ( $P_{critical}$ ) is used to determine the maximum rod pressure where cladding creep equals fuel swelling consistent with the GE criterion for rod pressure. [

].

Therefore, the GSTRM code needs to be verified against fission gas release data typical of current fuel design, at LHGRs near the GE LHGR limit at rod average burnups between 40 and 62 GWd/MTU. The fission gas release data used for verification needs to be provided in order to demonstrate that it is near or bound their LHGR limits at high burnup based on current fuel designs as operated.

Recently, a separate NRC staff audit performed for the ESBWR followed up on the GE's GSTRM T-M methodology. The NRC staff reviewing the ESBWR design revised FRAPCON-3.3 confirmatory analyses and removed small differences in the input (e.g., stack densification and void volumes). The new FRAPCON confirmatory analyses comparisons to the GSTRM rod pressure calculation demonstrated that the GSTRM under-prediction may be less than the 500 -

F-4

600 psi under-prediction established in the earlier FRAPCON confirmatory calculations (Reference 3). Therefore, the NRC staff finds that a decrease in the  $P_{critical}$  margin from 500 to 350 psi is warranted considering the results of the corrected FRAPCON calculation. This shows the difficulty of relying on code-to-code comparisons in validating the accuracy of calculational methodology and code. The best approach to establishing the degree of GSTRM under-prediction and uncertainties is by direct comparison of GSTRM internal rod pressure calculations against measurement data (fission gas release and void volume) comparable to design and maximum operating conditions for commercial fuel designs. The attached RAIs request that such comparison be provided, using the dated GE11 and GE13 rod punctured test data.

During this ESBWR audit GE also indicated that accounting for the “operating history” assumption in the derivation of the LHGR and the calculation of the internal rod pressures compensates for some of the non-conservatisms in the GSTRM internal rod pressure calculation, with exposure. The assumption that the rod operates with bottom-, mid-, and top-peaked power shapes through out the rod resident time in the core such that it places a node of the rod at the LHGR limit is sometimes referred to as the “operating history” assumption. This assumption increases the fission gas release, thus adding conservatism to the internal rod pressure calculations. However, the internal rod pressure calculations provided in the RAI 9 response (Reference 3) were based on consistent GSTRM/FRAPCON comparison in which both codes utilized the same operating history assumption. The NRC staff acknowledges that GHNE needs to submit additional follow-up information in order to conclude the adequacy of GSTRM calculations in the long-term. The attached RAIs provide guidance of the information and validation data that needs to be provided in the future GSTRM submittal. Beyond responses to NRC staff audit findings, GHNE had not submitted or updated GSTRM since the initial approval in the 1980s and an updated submittal is needed in order resolve the NRC staff findings based on RAI response reviews, without a submittal. In the short-term, the NRC staff concludes the observed GSTRM internal rod pressure calculations necessitates additional margin to compensate for the internal rod pressure under-predictions.

### Conclusion

The NRC staff determined that until such time that GE benchmarks the GSTRM methodology, the  $P_{critical}$  acceptance criteria will be reduced by 350 psi. This adjusted  $P_{critical}$  must be used to verify that the LHGR limit for the current fuel designs remains applicable with burnup.

Responses to the attached RAIs are needed in order to demonstrate the adequacy of GSTRM for use in licensing applications.

### 3.0 REFERENCES

1. NRC staff Draft Safety Evaluation for GE Topical Report, “Applicability of GE Methods to Expanded Operating Domain,” NEDC-33173P, March 14, 2007. (Accession No. ML070390406)



F-5

2. Letter from Jason S. Post (GE) to NRC, "Part 21 Notification: Adequacy of GE thermal-Mechanical Methodology, GSTRM," MFN 07-40, January 21, 2007. (ADAMS Package Accession No. ML072290203)
3. GE Letter (MFN 06-481), R. E. Brown to NRC, Responses to RAIs 7, 8, 9, 10, and 11 - NEDC-33173P, December 05, 2006. (ADAMS Package Accession No. ML063450449).

ATTACHMENT TO  
APPENDIX F OF NRC STAFF SAFETY EVALUATION OF NEDC-33173P

REQUEST FOR ADDITIONAL INFORMATION RELATING TO  
PART 21 NOTIFICATION: ADEQUACY OF GE THERMAL-MECHANICAL METHODOLOGY,  
GSTRM

- 1.0 GESTR-M Internal Rod Pressure Calculation Benchmarking (Kr-85 Plenum Gamma Scan)
- a. Provide PRIME and GESTR-M rod internal pressure comparisons up to high burnup at EOL.
  - b. For the GE11 and GE13 fission gas release data used in the Part 21 Notification (Reference 1), demonstrate that the operating LHGR rate for these data are near the GE14 LHGR limit at high exposure. Correct for the geometric differences when translated to measured GE14 internal rod pressures.
  - c. Compare fission gas data for GE11 and GE13 to corresponding GSTRM calculations to demonstrate the deviations between measured and predicted. Include in your discussion how the GE11 and GE13 standard deviation and bias from GSTRM predictions is obtained and compare to the GSTRM (original) assumed standard deviations and 95 percent confidence level.
- 2.0 Fuel Swelling and Creep Models Benchmarking

The Part 21 Notification (Reference 1) states that the 100 psi under-prediction at the 95 percent uncertainty level in the GESTRM rod internal pressure analysis is acceptable, because the critical pressure calculation was conservative. GE attributes the stated conservatism to the large conservatism in the fuel swelling model. The Part 21 Notification also shows that the uncertainty in fuel swelling model was reduced by approximately a factor of 2.3 such that the  $P_{critical}$  value is increased. However, originally, the large conservatism was added in the fuel swelling model to compensate for lack of conservatisms and uncertainties in the cladding creep model. Therefore, it must be demonstrated that the conservative uncertainties in the GSTRM fuel swelling and cladding creep models used to calculate  $P_{critical}$  compensates for the GSTRM under-prediction in rod pressure at the 95percent confidence level.

- a. The following RAIs address the validation and benchmarking of the fuel swelling and creep models.
  - i) Using available fuel swelling data such as the Halden data, demonstrate that the conservatisms in the GSTRM fuel swelling model. Quantify both the uncertainties and any biases.
  - ii) Quantify the cladding creep uncertainties based on post-irradiation diameter measurements.

- 2 -

- b. Compare the critical pressure determined using the GSTRM current licensing bases against the critical pressures based on the newly derived biases and uncertainties for cladding creep and fuel swelling.

### 3.0 Process

As interim, the NRC concludes that non-conservatism in GSTRM internal rod pressure calculations needs to be corrected for the licensing bases application of GSTRM. [

]. The NRC staff FRAPCON confirmatory calculations have shown that GSTRM under-predicts the internal rod pressure by 350 to 500 psi both for the nominal and the 95percent level. The lower prediction demonstrates that although the internal rod pressure prediction meets the acceptance criteria in terms of the  $P_{critical}$ , the adequacy of the GSTRM uncertainty treatment needs to be confirmed through measurement qualification data and corrected for licensing applications.

Therefore, the NRC staff determined that until such time that GE benchmarks the GSTRM methodology or demonstrates that  $P_{critical}$  bounds the non-conservatism in GSTRM, the  $P_{critical}$  acceptance criteria will be reduced by 350 psi. This  $P_{critical}$  adjusted must be used to verify that LHGR limit for the current fuel designs remains applicable with burnup. The current T-M licensing basis specifies the calculational methodology.

For the long-term resolution of the adequacy of the use of GSTRM to licensing application, provide an update and status of the fission gas and exposure gamma scans committed to in Reference 1.

- a. Provide an assessment of the GSTRM benchmarking. Determine if current GSTRM licensing methodology covers the uncertainties and any biases established through the benchmarking requested in 1 and 2 above.
- b. Submit the results of the requested validation and analyses. Provide any proposed modification to the GSTRM methodology established through the requested benchmarking data.

NEDO-33173-A, Revision 1  
Non-Proprietary Information

#	Location in Draft SE	Draft SE Text	GHNE Comment	GHNE Comment Basis	NRC Staff Resolution
1	<p>Page 132 Section 9.1</p> <p>Comment also applies to: Section 3.1.5.2</p>	<p>The neutronic methods used to simulate the reactor core response and that feed into the downstream safety analyses supporting operation at EPU/MELLLA+ will apply TGBLA06/PANAC11 or other NRC-approved neutronic method.</p>	<p><a href="#">For future license applications</a>, the neutronic methods used to simulate the <a href="#">actual</a> reactor core response and that feed into the downstream safety analyses supporting operation at EPU/MELLLA+ will apply TGBLA06/PANAC11 or other NRC-approved neutronic method.</p>	<p>Representative core analysis in license applications issued after this SE is issued may be based on TGBLA04/PANAC10, but the actual core analysis performed for the actual EPU or MELLLA+ core will be based on TGBLA06/PANAC11.</p> <p>As written, the Limitation seems to allow the use of TGBLA04/PANAC10 since they are NRC approved.</p>	<p>Comment not incorporated. Section revised as: The neutronic methods used to simulate the reactor core response and that feed into the downstream safety analyses supporting operation at EPU/MELLLA+ will apply TGBLA06/PANAC11 or later NRC-approved version of neutronic method.</p>
2	<p>Page 132 Section 9.3</p> <p>Comment also applies to: Sections 3.1.4.2, 3.1.5.1 multiple locations, and 3.1.5.2.</p>	<p>Plant-specific EPU and expanded operating domain applications will confirm that the power-to-flow ratio will not exceed 50 MWt/Mlbm/hr at any statepoint in the allowed operating domain. For plants that exceed the power-to-flow value of 50 MWt/Mlbm/hr, the application will provide power distribution assessment to establish that neutronic methods axial and nodal power distribution uncertainties have not increased.</p>	<p>Plant-specific EPU and expanded operating domain applications will confirm that the <a href="#">core thermal power to total core flow</a> ratio will not exceed 50 MWt/Mlbm/hr at any statepoint in the allowed operating domain. For plants that exceed the power-to-flow value of 50 MWt/Mlbm/hr, the application will provide power distribution assessment to establish that neutronic methods axial and nodal power distribution uncertainties have not increased.</p>	<p>Clarification</p>	<p>Comment accepted for Section 9.3.</p>

#	Location in Draft SE	Draft SE Text	GHNE Comment	GHNE Comment Basis	NRC Staff Resolution
3	Page 132 Section 9.7	For applications requesting implementation of EPU or MELLLA+, the small and large break ECCS-LOCA analysis will include top-peaked and mid-peaked power shape in establishing the MAPLHGR and determining the PCT. This limitation is applicable for both the licensing bases PCT and the upper bound PCT.	For applications requesting implementation of EPU or MELLLA+, the small and large break ECCS-LOCA analysis will include top-peaked and mid-peaked power shape in establishing the MAPLHGR and determining the PCT. <del>This limitation is applicable for both the licensing bases PCT and the upper bound PCT.</del> The plant specific EPU or MELLLA+ application will report the limiting large break and small break nominal and Appendix K PCT.	During discussions regarding the NRC review of NEDC-33006P, GE concurred with a verbal discussion of a similar limitation regarding ECCS-LOCA. The limitations in NEDC-33006P and 33173P should be consistent, or, preferably, listed in a single SE.	Part of comment accepted. Section 9.7 revised as follows: For applications requesting implementation of EPU or MELLLA+, the small and large break ECCS-LOCA analysis will include top-peaked and mid-peaked power shape in establishing the MAPLHGR and determining the PCT. This limitation is applicable for both the licensing bases PCT and the upper bound PCT. <u>The plant-specific applications will report the limiting small and large break licensing basis and upper bound PCTs.</u>

#	Location in Draft SE	Draft SE Text	GHNE Comment	GHNE Comment Basis	NRC Staff Resolution
4	Page 133 Section 9.8	<p>The ECCS-LOCA will be performed for all the statepoints in the upper boundaries of the expanded operating domains (e.g., MELLLA+ 80 percent and 55 percent core flow statepoint). The plant-specific application will report the limiting ECCS-LOCA results as well as the rated power and flow results. The SRLR will include both the limiting statepoint ECCS-LOCA results and the rated conditions ECCS-LOCA results.</p>	<p>Replace limitation wording with: <a href="#">Plant-specific MELLLA+ application will include calculations for the Appendix K and Nominal PCT at rated power/rated core flow, rated power/MELLLA+ boundary and the low flow point on the MELLLA+ boundary at which the off-rated flow dependent LHGR or MAPLHGR setdown begins to apply. This point will be at or between the 55% core flow MELLLA+ boundary point and the rated power/MELLLA+ boundary. If the small break PCT is within 50°F of limiting, the MELLLA+ plant submittals will include report of calculations for the limiting small break at rated power/rated core flow and rated power/MELLLA+ boundary. The Licensing Basis PCT, considering all calculated statepoint and power shapes, will be reported in the plant-specific EPU or MELLLA+ application and the Supplemental Reload Licensing Report</a></p>	<p>During discussions regarding the NRC review of NEDC-33006P, GE concurred with a verbal discussion of a similar limitation regarding ECCS-LOCA. The limitations in NEDC-33006p and 33173P should be consistent, or, preferably, listed in a single SE.</p>	<p>Comment not incorporated. Section 9.8 reworded as follows: The ECCS-LOCA will be performed for all statepoints in the upper boundary of the expanded operating domain, including the minimum core flow statepoints, the transition statepoint as defined in Reference 2 and the 55 percent core flow statepoint. The plant-specific application will report the limiting ECCS-LOCA results as well as the rated power and flow results. The SRLR will include both the limiting statepoint ECCS-LOCA results and the rated conditions ECCS-LOCA results.</p>

#	Location in Draft SE	Draft SE Text	GHNE Comment	GHNE Comment Basis	NRC Staff Resolution
5	Page 133 Section 9.10  Comment also applies to: Page 48 Section 3.2.6.5.1	Each EPU and MELLLA+ fuel reload will document in the SRLR the calculation results of the analyses demonstrating compliance to transient T-M acceptance criteria.	Delete	The SRLR is not provided to the NRC. However, the EPU and MELLLA+ license applications, which are submitted for NRC review, will report the calculations results  Alternative, GE could provide a supplemental data sheet to the SRLR for each reload.	Section 9.10 reworded as follows: Each EPU and MELLLA+ fuel reload will document the calculation results of the analyses demonstrating compliance to transient T-M acceptance criteria. The plant T-M response will be provided with the SRLR or COLR, or it will be reported directly to the NRC as an attachment to the SRLR or COLR

#	Location in Draft SE	Draft SE Text	GHNE Comment	GHNE Comment Basis	NRC Staff Resolution
6	<p>Page 133 Section 9.11</p> <p>Comment also applies to:</p>	<p>Unlike TRACG, nodal void reactivity bias with exposure cannot be incorporated into the ODYN 1D transient modal. To account for the impact of the void history bias, plant-specific EPU and MELLLA+ applications will demonstrate an equivalent to 10 percent margin to the fuel centerline melt and that the 1 percent cladding circumferential plastic strain acceptance criteria due to pellet-cladding mechanical interaction for all of limiting AOO transient events, including equipment out-of-service. Limiting transients in this case, refers to transients that will result in higher TOP and MOP. If the void history bias is incorporated into the transient model within the code, then the additional 10 percent TOP and MOP margin is no longer required. This holds for TRACG, which has the capability to incorporate void reactivity bias in the 3D nodal void reactivity response surface.</p>	<p><del>Unlike TRACG, nodal void reactivity bias with exposure cannot be incorporated into the ODYN 1D transient modal.</del> To account for the impact of the void history bias, plant-specific EPU and MELLLA+ applications will demonstrate an equivalent to 10 percent margin to the fuel centerline melt and that the 1 percent cladding circumferential plastic strain acceptance criteria due to pellet-cladding mechanical interaction for all of limiting AOO transient events, including equipment out-of-service. Limiting transients in this case, refers to <a href="#">limiting pressurization</a> transients that will result in higher TOP and MOP. If the void history bias is incorporated into the transient model within the code, then the additional 10 percent <a href="#">margin to the fuel centerline melt and that the 1 percent cladding circumferential plastic strain</a> is no longer required. <del>This holds for TRACG, which has the capability to incorporate void reactivity bias in the 3D nodal void reactivity response surface.</del></p>	<p>The uncertainties for ODYN may be increased to address the void bias and the Limitation should not exclude that potential.</p> <p>Clarification. The 10% margin is applied to the margin to the fuel centerline melt and that the 1 percent cladding circumferential plastic strain, not to the TOP and MOP.</p> <p>Clarifying that the context in all of this is for limiting pressurization transients</p>	<p>Comment incorporated. Section 9.11 reworded as follows: To account for the impact of the void history bias, plant-specific EPU and MELLLA+ applications using either TRACG or ODYN will demonstrate an equivalent to 10 percent margin to the fuel centerline melt and that the 1 percent cladding circumferential plastic strain acceptance criteria due to pellet-cladding mechanical interaction for all of limiting AOO transient events, including equipment out-of-service. Limiting transients in this case, refers to transients where the void reactivity coefficient plays a significant role (such as pressurization events). If the void history bias is incorporated into the transient model within the code, then the additional 10 percent margin to the fuel centerline melt and the 1 percent cladding circumferential plastic strain is no longer required.</p>



#	Location in Draft SE	Draft SE Text	GHNE Comment	GHNE Comment Basis	NRC Staff Resolution
7	Page 134 Section 9.13	GENE will include the GSTR-M Part 21 report as an Appendix in the "-A" version of LTR NEDC-33173P.	Delete	This is not a restriction on the use of GE's analytical methods. GE will treat MFN 07-040 like an RAI response and include the letter in the '-A' version of NEDC-33173P	Comment incorporated. Section 9.13 deleted.
8	Page 134 Section 9.14	Any conclusions drawn from the NRC staff evaluation of the GENE's Part 21 report will be applicable to the GSTR-M thermal-mechanical assessment of this SE. GENE submitted the T-M Part 21 evaluation, which is currently under NRC staff review. Upon completion of its review, NRC staff will inform GENE of its conclusions.	Any conclusions drawn from the NRC staff evaluation of the GENE's Part 21 report will be applicable to the GSTR-M thermal-mechanical assessment of this SE <a href="#">for future license application</a> . GENE submitted the T-M Part 21 evaluation, which is currently under NRC staff review. Upon completion of its review, NRC staff will inform GENE of its conclusions.	This Limitation is an unknown. Preferably, the Limitation should be deleted. The NRC can decide any additional action when its review of the report is completed. At a minimum, the Limitation should be clarified as indicated.	Any conclusions drawn from the NRC staff evaluation of the GE's Part 21 report will be applicable to the GSTRM T-M assessment of this SE for future license application. GE submitted the T M Part 21 evaluation, which is currently under NRC staff review. Upon completion of its review, NRC staff will inform GE of its conclusions.

#	Location in Draft SE	Draft SE Text	GHNE Comment	GHNE Comment Basis	NRC Staff Resolution
9	Page 134 Section 9.15	The conclusions of the plenum fission gas and fuel exposure gamma scans have been submitted for NRC staff review and approval, and revisions to the T-M methods will be included in the T-M licensing process. This revision will be accomplished through Amendment to GESTAR II or in T-M LTR review. Once the T-M LTR and its application are approved, future license applications for EPU and MELLLA+ referencing LTR NEDC-33173P must utilize these revised T-M methods.	Deletion	The Limitation is an unknown. The NRC review of the T-M methods is ongoing and the NRC should incorporate the required limitations applicable to EPU and M+ in the SE for the T-M methods.	<p>Comment not incorporated. Renumbered as Section 9.12 and reworded as follows:</p> <p>In MFN 06-481, GE committed to submit plenum fission gas and fuel exposure gamma scans as part of the revision to the T-M licensing process. The conclusions of the plenum fission gas and fuel exposure gamma scans of GE 10x10 fuel designs as operated will be submitted for NRC staff review and approval. This revision will be accomplished through Amendment to GESTAR II or in a T-M licensing LTR. PRIME (a newly developed T-M code) has been submitted to the NRC staff for review (Reference 58). Once the PRIME LTR and its application are approved, future license applications for EPU and MELLLA+ referencing LTR NEDC-33173P must utilize the PRIME T-M methods.</p>

#	Location in Draft SE	Draft SE Text	GHNE Comment	GHNE Comment Basis	NRC Staff Resolution
10	<p>Page 134 Section 9.17</p> <p>Comment also applies to: Page 129 Last paragraph of Section 8.4</p>	<p>A supplement to TRACG /PANAC11 for AOO is under NRC staff review (Reference 40). TRACG internally models the response surface for the void coefficient biases and uncertainties for known dependencies due to the relative moderator density and exposure on nodal basis. Therefore, the void history bias determined through the methods review can be incorporated into the response surface "known" bias or through changes in lattice physics/core simulator methods for establishing the instantaneous cross-sections. Including the bias in the calculations negates the need for ensuring that plant-specific applications showing sufficient margin. For application of TRACG to EPU and MELLLA+ applications, the TRACG methodology must incorporate the void history bias. The manner in which this void history bias is accounted for will be established by the NRC staff SE approving NEDE-32906P, Supplement 3, "Migration to TRACG04/PANAC11 from TRACG02/PANAC10," May 2006 (Reference 40). This limitation applies until the new TRACG/PANAC methodology is approved by the NRC staff.</p>	Delete	<p>This Limitation is an unknown. The NRC review of TRACG /PANAC11 for AOO is under NRC staff review (Reference 40) is ongoing and the NRC should incorporate the required limitations applicable to EPU and M+ in the SE for the TRACG /PANAC11 for AOO is under NRC staff review (Reference 40).</p>	<p>Comment not incorporated. Renumbered as Section 9.16.</p> <p>A supplement to TRACG /PANAC11 for AOO is under NRC staff review (Reference 40). TRACG internally models the response surface for the void coefficient biases and uncertainties for known dependencies due to the relative moderator density and exposure on nodal basis. Therefore, the void history bias determined through the methods review can be incorporated into the response surface "known" bias or through changes in lattice physics/core simulator methods for establishing the instantaneous cross-sections. Including the bias in the calculations negates the need for ensuring that plant-specific applications show sufficient margin (see limitation 11). For application of TRACG to EPU and MELLLA+ applications, the TRACG methodology must incorporate the void history bias. The manner in which this void history bias is accounted for will be established by the NRC staff SE approving NEDE-32906P, Supplement 3, "Migration to TRACG04/PANAC11 from TRACG02/PANAC10," May 2006 (Reference 40). This limitation applies until the new TRACG/PANAC methodology is approved by the NRC staff.</p>

#	Location in Draft SE	Draft SE Text	GHNE Comment	GHNE Comment Basis	NRC Staff Resolution
11	Page 134 Section 9.18	For EPU and MELLLA+, the bypass voiding will be evaluated on a cycle-specific basis to guarantee that the void fraction remains below 5 percent at all LPRM levels when operating at steady-state conditions. The highest calculated bypass void will be included in the plant-specific SRLR.	For EPU and MELLLA+, the bypass voiding will be evaluated on a cycle-specific basis to guarantee that the void fraction remains below 5 percent at all LPRM levels when operating at steady-state <a href="#">rated power</a> conditions. The highest calculated bypass void will be included in the plant-specific SRLR.	Clarification	Comment not incorporated. Section 9.18 reworded as follows: The NRC staff concludes that the presence bypass voiding at the low-flow conditions where instabilities are likely can result in calibration errors of less than 5 percent for OPRM cells and less than 2 percent for APRM signals. These calibration errors must be accounted for while determining the setpoints for any detect and suppress long term methodology. The calibration values for the different long-term solutions are specified in the associated sections of this SE, discussing the stability methodology.
12	Page 135 Section 9.20	For applications involving PANCEA/ODYN/ISCOR/TASC for operation at EPU and MELLLA+, an additional 0.01 will be added to the OLMCPR, until such time that GE expands the experimental database supporting the Findlay-Dix void-quality correlation to demonstrate the accuracy and performance of the void-quality correlation based on experimental data representative of the current fuel designs and operating conditions during steady-state, transient, and accident conditions.	For applications involving PANCEA/ODYN/ISCOR/TASC for operation at EPU and MELLLA+, an additional 0.01 will be added to the OLMCPR, until such time that GE expands the experimental database supporting the Findlay-Dix void-quality correlation to demonstrate the accuracy and performance of the void-quality correlation based on experimental data representative of the current fuel designs and operating conditions during steady-state, transient, <del>and accident</del> conditions.	Clarification. In MFN 06-435, GE provided the commitment to resolve the Limitation	Renumbered as Section 9.19.  Comment not incorporated.  <u>Staff comment:</u> The countercurrent flow model of the void quality correlation needs to be addressed. This model relates to the LOCA, which is an accident. The staff had issued RAIs related to this model in the follow-up guidance for the VQ.

#	Location in Draft SE	Draft SE Text	GHNE Comment	GHNE Comment Basis	NRC Staff Resolution
13	Page 136 Section 9.21	The NRC staff is currently reviewing Supplement 3 to NEDE-32906P, "Migration to TRACG04/PANAC11 from TRACG02/PANAC10," dated May 2006 (Reference 40). The adequacy of the TRACG interfacial shear model qualification for application to EPU and MELLA+ will be addressed under this review. Any conclusions specified in the NRC staff SE approving Supplement 3 to LTR NEDC-32906P (Reference 40) will be applicable as approved.	Delete	This Limitation is an unknown. The NRC review of Supplement 3 to NEDE-32906P is under NRC staff review. The NRC should incorporate the required limitations applicable to EPU and M+ in the SE for the Supplement 3 to NEDE-32906P.	Comment not incorporated. Renumbered as Section 9.20.

#	Location in Draft SE	Draft SE Text	GHNE Comment	GHNE Comment Basis	NRC Staff Resolution
14	Page 136 Section 9.24	<p>The fuel lattice geometry cannot deviate significantly from GE lattices; particularly the performance of TGBLA06 for expanded operating domains has not been demonstrated for fuel assemblies with water crosses, square internal water channels, Gd rods simultaneously adjacent to water and vanished rods, or 11x11 lattices. The acceptability of the modified epithermal slowing down models in TGBLA06 have not been demonstrated for application to these or other geometries for expanded operating domains. Significant changes in the Gd rod optical thickness will require an evaluation of the TGBLA06 radial flux and Gd depletion modeling before being applied. Increases in the lattice Gd loading that result in nodal reactivity biases beyond those previously established will require review before the GE methods may be applied. The NRC staff did not assess the TGBLA06 upgrade for use with 11x11 and higher lattices, water crosses, water boxes, or MOX fuels at EPU conditions. For any plant-specific applications of TGBLA06 with the above fuel types, or changes as described above, GENE needs to provide assessment data similar to that provided for the GE fuels.</p>	<p>The fuel lattice geometry cannot deviate significantly from GE lattices; particularly the performance of TGBLA06 for expanded operating domains has not been demonstrated for fuel assemblies with water crosses, square internal water channels, <del>Gd rods simultaneously adjacent to water and vanished rods</del>, or 11x11 lattices. <del>The acceptability of the modified epithermal slowing down models in TGBLA06 have not been demonstrated for application to these or other geometries for expanded operating domains. Significant changes in the Gd rod optical thickness will require an evaluation of the TGBLA06 radial flux and Gd depletion modeling before being applied. Increases in the lattice Gd loading that result in nodal reactivity biases beyond those previously established will require review before the GE methods may be applied.</del> The NRC staff did not assess the TGBLA06 upgrade for use with 11x11 and higher lattices, water crosses, water boxes, or MOX fuels at EPU conditions. For any plant-specific applications of TGBLA06 with the above fuel types, or changes as described above, GENE needs to provide assessment data similar to that provided for the GE fuels.</p>	<p>Corrections. The second, third and fourth sentences do not bear on mixed vendor cores.</p>	<p>Comment not incorporated. Renumbered as to Section 9.22 and reworded as follows:</p> <p>For any plant-specific applications of TGBLA06 with fuel type characteristics not covered in this review, GE needs to provide assessment data similar to that provided for the GE fuels. The Interim Methods review is applicable to all GE lattices up to GE14. Fuel lattice designs, other than GE lattices up to GE14, with the following characteristics are not covered by this review:</p> <ul style="list-style-type: none"> <li>• square internal water channels</li> <li>• water crosses</li> <li>• Gd rods simultaneously adjacent to water and vanished rods</li> <li>• 11x11 lattices</li> <li>• MOX fuel</li> </ul> <p>The acceptability of the modified epithermal slowing down models in TGBLA06 has not been demonstrated for application to these or other geometries for expanded operating domains.</p> <p>Significant changes in the Gd rod optical thickness will require an evaluation of the TGBLA06 radial flux and Gd depletion modeling before being applied. Increases in the lattice Gd loading that result in nodal reactivity biases beyond those previously established will require review before the GE methods may be applied.</p>

#	Location in Draft SE	Draft SE Text	GHNE Comment	GHNE Comment Basis	NRC Staff Resolution
15	<p>Page 136 Section 9.25</p> <p>Comment also applies to:</p> <p>Page 129 Section 8.5, second paragraph</p>	<p>Provision of evaluation of the core-tracking data will provide the NRC staff with bases to establish if operation at the expanded operating domain indicates: (1) changes in the performance of nuclear methods outside the EPU experience base; (2) changes in the available thermal margins; (3) need for changes in the uncertainties and NRC-approved criterion used in the SLMCPR methodology; or (4) any anomaly that may require corrective actions.</p>	<p>Provision of evaluation of the core-tracking data will provide the NRC staff with bases to establish if operation at the expanded operating domain indicates: (1) changes in the performance of nuclear methods <del>outside the EPU experience base</del>; (2) changes in the available thermal margins; (3) need for changes in the uncertainties and NRC-approved criterion used in the SLMCPR methodology; or (4) any anomaly that may require corrective actions.</p>	<p>Clarification. GE will provide the similar No assessment of the comparisons is planned.</p>	<p>Renumbered as Section 9.23.</p> <p>Comment not incorporated.</p> <p><u>Staff Comments:</u> The staff will assess whether the data is outside the EPU experience base.</p> <p>The objective of the limitation is to compare the already compiled EPU database for all future EPU plants. Staff will use the comparisons in its plant-specific review.</p>
16	<p>Page 136 Section 9.26</p> <p>Comment also applies to:</p> <p>Page 129 Section 8.5, second paragraph</p>	<p>The plant-specific applications will provide prediction of key parameters for cycle exposures for operation at EPU and MELLLA+. The plant-specific prediction of these key parameters will be compared against the EPU experience base and MELLLA+ operating experience, if available. For evaluation of the margins available in the fuel design limits, plant-specific applications will also provide quarter core map (assuming core symmetry) showing bundle power, bundle operating LHGR, and MCPR for BOC, MOC, and EOC. Since the minimum margins to specific limits may occur at exposures other than the traditional BOC, MOC, and EOC, the data will be provided at these exposures.</p>	<p>The plant-specific applications will provide prediction of key parameters for cycle exposures for operation at EPU and MELLLA+. <del>The plant-specific prediction of these key parameters will be compared against the EPU experience base and MELLLA+ operating experience, if available.</del> For evaluation of the margins available in the fuel design limits, plant-specific applications will also provide quarter core map (assuming core symmetry) showing bundle power, bundle operating LHGR, and MCPR for BOC, MOC, and EOC. Since the minimum margins to specific limits may occur at exposures other than the traditional BOC, MOC, and EOC, the data will be provided at these exposures.</p>	<p>Clarification. No assessment of the comparisons is planned.</p>	<p>Renumbered as Section 9.24.</p> <p>Comment not incorporated.</p>

#	Location in Draft SE	Draft SE Text	GHNE Comment	GHNE Comment Basis	NRC Staff Resolution
17	Page 25 Section 3.1.9 1 <sup>st</sup> paragraph	<p>In RAI 28 of MFN 05-053 (Reference 6), GENE committed to perform gamma scan measurements to confirm that the assumptions used in the neutronic method are still appropriate. GENE also presented plans for gamma and plenum fission gas scans (Reference 31). The planned measurement data includes:</p> <ol style="list-style-type: none"> <li>1. fission gas benchmarks for T-M models,</li> <li>2. rod exposure benchmarks for lifetime integrated rod power,</li> <li>3. rod-by-rod power-peaking benchmarks,</li> <li>4. bundle power allocation benchmarks around instrument positions, and</li> <li>5. core octant bundle-by-bundle nodal power benchmarks.</li> </ol>	<p><a href="#">In response to RAI 9 in MFN 06-481, GE committed to submit plenum fission gas and fuel exposure gamma scans for NRC review as part of the T-M licensing review.</a></p>	<p>GE is committed to provide the required plenum fission gas and fuel exposure gammas to support the T-M licensing review. The development of scans specifics and submittal dates is expected to involve the cooperation of a utility partner.</p> <p>Reference 31 was present to the NRC for information only and did not contain GE commitments. Further, Reference 31 was not presented for the purposes of supporting the review of NEDC-33173P and should not be referenced by this SE.</p>	<p>Comment not incorporated.</p> <p><u>Staff comment:</u> Reference 31 [Dec 2005 presentation] describes the benchmarking plan where RAI 9 does not describe any measurement plan. The revised RAI 28-1 excluded the fission gas and rod exposure benchmarking. Reference 31 [Dec 2005 presentation] is docketed and supports the SE.</p>
18	Page 59 Section 3.2.6.5.9 Item 6  Comment also applies to: Page 50 Section 3.2.6.5.5 1st	<p>Preliminary review of the T-M qualification data indicates that the current database does not extend to the current fuel designs and the currently licensed exposures. The experimental qualification database will be expanded to the current fuel designs and exposures as proposed in the December 2005 presentation (Reference 31) and the initial RAI 28 response (MFN-</p>	<p>Preliminary review of the T-M qualification data indicates that the current database does not extend to the current fuel designs and the currently licensed exposures. <a href="#">In response to RAI 9 in MFN 06-481, GE committed to submit plenum fission gas and fuel exposure gamma scans for NRC review as part of the T-M licensing review.</a> <del>MFN-05-022 also states that "GE already</del></p>	<p>Reference 31 was present to the NRC for information only and did not contain GE commitments. Further, Reference 31 was not presented for the purposes of supporting the review of NEDC-33173P and should not be referenced by this SE</p>	<p>Comment not incorporated, see resolution to comment #17.</p> <p>Item 6 was reworded as follows:</p> <p>NRC staff evaluation of the T-M qualification data indicates that the current database does not extend to the current fuel designs and need to be expanded to the current fuel designs and exposures. GE intends to perform additional scans as presented to the</p>



#	Location in Draft SE	Draft SE Text	GHNE Comment	GHNE Comment Basis	NRC Staff Resolution
	<p>paragraph</p> <p>Section 8.4 Page 129, 2<sup>nd</sup> paragraph</p>	<p>05-022, Reference 3). GE states that additional target spectral lines from other isotopes may be used for determination of plenum fission gas (85Kr) or fuel exposure (137Cs/144Pr). MFN-05-022 also states that "GE already intends to perform plenum fission gas gamma scan measurements to provide needed input to T-M methodology qualification and determination of fuel high exposure fuel designs. Additionally, GE will continue to perform hot-cell gamma scan (and pellet mass spectrometry) measurements on rod exposure for a limited number of rods." The NRC staff agreed with this proposal and the NRC staff approval of LTR NEDC-33173P (Reference 1) relies on the confirmations of the internal rod pressures and the exposure for the GE14 fuel up to the licensed exposure. The confirmation will also include extension of the fuel temperature to the current licensed exposures; and</p>	<p><del>intends to perform plenum fission gas gamma scan measurements to provide needed input to T-M methodology qualification and determination of fuel high exposure fuel designs. Additionally, GE will continue to perform hot-cell gamma scan (and pellet mass spectrometry) measurements on rod exposure for a limited number of rods.</del></p> <p>The NRC staff agreed with this proposal and the NRC staff approval of LTR NEDC-33173P (Reference 1) relies on the confirmations of the internal rod pressures and the exposure for the GE14 fuel up to the licensed exposure. The confirmation will also include extension of the fuel temperature to the current licensed exposures; and</p>	<p>Further, the quotes from MFN 05-022 are taken out of context. Please note that MFN 05-022 further states, "GE cannot <i>a priori</i> commit to any gamma scan program without utility partners. Instead, the interim process proposes a conservative treatment of SLMCPR uncertainties." Based on subsequent discussions with the NRC, GE modified the response to RAI 28-2 in MFN 05-053. In that letter, GE stated efforts were underway to develop a gamma scan system and to obtain utility partner(s) for a gamma scan program. Specifics of a program were not provided at that time. MFN 06-434 defines the specific scans required to support removal of the added SLMCRP margins.</p> <p>Regarding scans to support the T-M licensing reviews, as stated in MFN 06-481,</p>	<p>NRC staff (Reference 31), as stated in the initial RAI 28-1 response (Reference 3) and as committed to in RAI 9 response (Reference 25). The NRC staff agreed with this proposal and the NRC staff approval of LTR NEDC-33173P (Reference 1) relies in the long-term on the confirmations of the internal rod pressures and the exposure for the GE14 fuel up to the licensed exposure. The confirmation will also include extension of the fuel temperature data to the current licensed exposures.</p>

#	Location in Draft SE	Draft SE Text	GHNE Comment	GHNE Comment Basis	NRC Staff Resolution
				GE is committed to provide the required plenum fission gas and fuel exposure gammas. The development of scans specifics and submittal dates is expected to involve the cooperation of a utility partner.	
19	Page 58 Section 3.2.6.5.9 Item 1	The higher bundle powers during steady-state operation reduce the margins to the LHGR limit. In addition, the higher plant response during transients increases the fuel pellet overpower response.	Delete	LHGR limit is already an active constraint for regular cores. The plant is not operating with higher bundle power at EPU/M+.	Comment is no longer applicable in the Final SE.
20	Page 44 Section 3.2.6 1 <sup>st</sup> paragraph on, 3 <sup>rd</sup> sentence	The ratio of the steady-state operating peak nodal kW/ft over the steady-state LHGR limit is referred to as MLHGR.	The ratio of the steady-state operating peak nodal kW/ft over the steady-state LHGR limit is referred to as <del>MLHGR</del> MFLPD (Maximum Fraction of Linear Power Density)	Clarification	Comment incorporated.

#	Location in Draft SE	Draft SE Text	GHNE Comment	GHNE Comment Basis	NRC Staff Resolution
21	<p>Page 46            3.2.6.5            3<sup>rd</sup> sentence</p> <p>Comment also applies to:            Page 47            Section 3.2.6.5.1</p> <p>4th paragraph            4th sentence</p>	<p>Therefore, the TOP and MOP responses during limiting AOO events are expected to be higher for operation at EPU and MELLLA+.</p>	Delete	TOP and MOP responses during limiting AOO events are NOT expected to be higher for operation at EPU and MELLLA+	<p>Comment not incorporated.  <u>Staff comment:</u> GHNE comment is not supported by data showing that using same methods and codes the TOP and MOP response will not increase for EPU and MELLLA+ operation relative to pre-EPU conditions. Note that GE does not include plant-specific T-M over-power response in the SRLR or the COLR. Therefore, any assessment of pre- and post-EPU/MELLLA+ data cannot be performed by the NRC staff.</p> <p>Phenomenological assessments indicate that increases in the T-M over-power response are highly likely because the void coefficient is higher at the higher core-average void fractions expected at MELLLA+.</p> <p>Several GHNE comments in this document relate to this topic. The current limitations in the NRC staff SE require reporting of the T-M over-power response. Therefore, in the future, the staff will be able to assess changes in T-M over-power response.</p> <p>The SE was updated to clarify this topic.</p>

#	Location in Draft SE	Draft SE Text	GHNE Comment	GHNE Comment Basis	NRC Staff Resolution
22	Page 47 3.2.6.5.1 4 <sup>th</sup> paragraph 1 <sup>st</sup> sentence	Although the transient LHGR limit is a SAFDL that ensures the fuel integrity limit will be met during an AOO, the current licensing process does not include the TOP and MOP screening criteria or the demonstration that the T-M fuel design limits will be met during an AOO on cycle-specific bases.	<a href="#">The LHGR limit is a way to ensure that SAFDL limit will be met during an AOO. The 1% strain and centerline melt are SAFDLs and these are confirmed for each fuel reload through the use of the MOP/TOP screening criteria or more detailed calculations.</a>	LHGR is not SAFDL (see Table 1-1 of NEDC-33173P, and the SE for GESTAR, Amendment 10)	GHNE comment is no longer applicable in the Final SE.
23	3.2.6.5.4 3 <sup>rd</sup> paragraph	In addition, it appears that GENE's licensed T-M methodology qualification data is limited to MFN-170-84 (Reference 45) and MFN-027-086 (Reference 46), which were approved in 1984 and 1986 respectively.	In addition, <del>it appears that</del> GENE's licensed T-M methodology qualification data is <a href="#">provided in</a> MFN-170-84 (Reference 45) and MFN-027-086 (Reference 46), which were approved in 1984 and 1986 respectively. <a href="#">GENE has revised GSTRM material properties and performance models since its initial approval through following. MFN-036-85, MFN-082-85, MFN-056-87, MFN-037-98, MFN-031-99</a>	MFNs provide the additional information.	Comment not incorporated.  <u>Staff comment:</u> GHNE has not specified the NRC approved licensing document associated with the listed MFNs. These documents were not part of the review and cannot be approved by this SE. Paragraph revised to clarify issue.

#	Location in Draft SE	Draft SE Text	GHNE Comment	GHNE Comment Basis	NRC Staff Resolution
24	<p>Section 3.2.6.5.5 5th paragraph last sentence</p> <p>Comment also applies to:            Page 52, Section 3.2.6.5.6 6<sup>th</sup> paragraph First two sentences</p> <p>Page 52, Section 3.2.6.5.6 5<sup>th</sup> paragraph First two sentence</p>	<p>This scenario coupled with a 10 percent power penalty is judged to be more than adequate to accommodate any modeling uncertainty.</p>	<p>This scenario coupled with a <a href="#">10 percent margin to the fuel centerline melt and that the 1 percent cladding circumferential plastic strain acceptance criteria</a> is judged to be more than adequate to accommodate any modeling uncertainty.</p>	<p>Clarification of statement</p>	<p>Comment incorporated.</p>
25	<p>Page 51 Section 3.2.6.5.5 FRAPCON-GSTRM Internal Rod Pressure Comparison 4<sup>th</sup> paragraph last sentence</p>	<p>As an interim measure, the NRC staff accepts the current licensing bases as providing reasonable assurances in the short-term. The NRC staff agreed with GENE's proposal in MFN 05-022 (Reference 3). However subsequent revision of RAI 28 response (MFN 05-053, Reference 6) did not include the proposals to perform fission gas and exposure gamma scans. Moreover as of date, GENE had not submitted specific schedule outlining when the additional internal rod pressure and exposure accounting qualification</p>	<p>As an interim measure, the NRC staff accepts the current licensing bases as providing reasonable assurances in the short-term. The NRC staff agreed with GENE's proposal in MFN <del>06-481 (Reference 25) 05-022 (Reference 3). However subsequent revision of RAI 28 response (MFN 05-053, Reference 6) did not include the proposals to perform fission gas and exposure gamma scans. Moreover as of date, GENE had not submitted specific schedule outlining when the additional internal rod pressure and</del></p>	<p>IN MFN 06-481, GE agreed to address the need for scans as part of PRIME LTR licensing review (FLN 2007-001).</p>	<p>GHNE comment is no longer applicable in the Final SE.</p>

#	Location in Draft SE	Draft SE Text	GHNE Comment	GHNE Comment Basis	NRC Staff Resolution
		<p>data will be submitted to the Commission. Therefore, GENE's commitment is documented in this SE as limitation.</p> <p>The conclusions of the plenum fission gas and fuel exposure gamma scans will be submitted for NRC staff review and approval and inclusions in the T-M licensing process. This can be accomplished by submitting one of the following for review: a supplement to LTR NEDC-33173P (Reference 1), an Amendment to GESTAR II, or a separate T-M LTR. If neither of the commitments is fulfilled, the NRC staff has the option to increase the modeling uncertainties from 6 percent to 10 percent for the internal rod pressures.</p>	<p><del>exposure accounting qualification data will be submitted to the Commission. Therefore, GENE's commitment is documented in this SE as limitation.</del></p> <p><del>The conclusions of the plenum fission gas and fuel exposure gamma scans will be submitted for NRC staff review and approval and inclusions in the T-M licensing process. This can be accomplished by submitting one of the following for review: a supplement to LTR NEDC-33173P (Reference 1), an Amendment to GESTAR II, or a separate T-M LTR. If neither of the commitments is fulfilled, the NRC staff has the option to increase the modeling uncertainties from 6 percent to 10 percent for the internal rod pressures.</del></p>		
26	<p>Page 27 Section 3.2.2</p> <p>Comment also applies to: Page 25 Section 3.2</p> <p>Page 28 Section 3.2.2.2, 5th paragraph</p>	<p>Section 2.2.1 of MFN 05-005 (Reference 4) evaluates the SLMCPR calculational methodology and the impacts of potential increases in the power distribution uncertainties.</p>	<p>Section 2.2.1 of MFN 05-005 (Reference 4) evaluates the SLMCPR calculational methodology and the impacts of potential increases in the power distribution uncertainties. NEDC-33173P superseded MFN 05-005 and is the subject of the review of this SE</p>	<p>MFN 05-005 is superseded by NEDC-33173P</p>	<p>GHNE comment is no longer applicable in the Final SE.</p>

#	Location in Draft SE	Draft SE Text	GHNE Comment	GHNE Comment Basis	NRC Staff Resolution
27	Page 37 Section 3.2.4.3 3 <sup>rd</sup> paragraph  Comment also applies to: Page 37 Section 3.2.4.3 3 <sup>rd</sup> paragraph	It is feasible that the bases for the 40 percent depletion assumption could stem from the core average 40 percent void fraction for the historical operating strategies (OLTP at the 100 percent rod line). However, for the current operating strategies including EPU's and high density BWR/6 plants, the core averaged void fraction is 70 percent or greater.	It is feasible that the bases for the 40 percent depletion assumption could stem from the core average 40 percent void fraction for the historical operating strategies (OLTP at the 100 percent rod line). However, for the current operating strategies including EPU's and high density BWR/6 plants, the core averaged void fraction is <u>50 percent</u> <del>or greater</del> .	Inconsistent comparison. Core average exit voids are > 70% not the general core average.	Comment incorporated.
28	Page 38 Section 3.2.4.4 item 1 2 <sup>nd</sup> paragraph last sentence	However, plant-specific application should confirm that the peak ASME overpressure vessel and TS dome pressures have adequate margin of at least 5 psig.	Delete	The conclusions of the NRC review in this regard were not discussed. GE has not had the opportunity to assess this conclusion. All codes have some uncertainties. Please clarify if this additional margin is applicable to all vendor's ASME calculations. What is the remedy to remove this additional margin. Is this penalty required for the application only or for each reload?	Comment not incorporated.  <u>Staff comment:</u> There are no specific limitations in this SE that require any action related to the 5 psig ASME over-pressure margin. However, it is within the NRC staff's prerogative to state in this SE that if only 5 psig margin is available, the key input parameters and assumptions should be scrutinized in greater detail by the NRC staff reviewers.

#	Location in Draft SE	Draft SE Text	GHNE Comment	GHNE Comment Basis	NRC Staff Resolution
29	Page 60 Section 3.2.7 2 <sup>nd</sup> paragraph	GENE had committed in the initial RAI 28 response (Reference 3) to perform both fission gas and exposure benchmarking. The NRC staff considers this benchmarking important, because a hot rod can accumulate higher exposure early in its core resident life and remain in the core. The NRC staff will track the RAI 28 commitment to ensure that the qualification data is submitted for NRC staff review and approval. The NRC staff requests that GE present this as an agenda item at their annual fuel design meeting.	<del>GENE had committed in the initial RAI 28 response (Reference 3) to perform both fission gas and exposure benchmarking. GE committed to provide benchmarking scans in MFN 06-481 as part of the review of the T-M LTR</del> The NRC staff considers this benchmarking important, because a hot rod can accumulate higher exposure early in its core resident life and remain in the core. <del>The NRC staff will track the RAI 28 commitment to ensure that the qualification data is submitted for NRC staff review and approval. The NRC staff requests that GE present this as an agenda item at their annual fuel design meeting.</del>	See comment 19.  The statement to track the submittal of the scans is unnecessary since the NRC review of the T-M licensing is underway.  Further, requests for information at annual GE presentations is inappropriate in an SE.	Comment not incorporated.  <u>Staff comment:</u> It is within the staff prerogative to provide guidance to the reviewers in a SE. There is no limitation or actions associated with this topic that requires GE actions.



#	Location in Draft SE	Draft SE Text	GHNE Comment	GHNE Comment Basis	NRC Staff Resolution
30	Page 62 Section 3.2.8.1 2nd paragraph	The accuracy in the prediction of the SDM, therefore, depends on the accuracy of the neutronics methods to predict the distributed criticality (corresponding to $k_{B_{demo}}$ ) and local criticality (corresponding to $k_{B_{sroB}}$ ). The distributed critical configuration is that with a uniform control blade insertion consistent with the all-rods-in configuration and is well represented by the in-sequence cold critical measurement. The local criticality consists of a configuration in which the core becomes critical with all-rods-in and adjacent control blades are removed. The local cold critical provides a demonstration of ability to predict the worth of the strongest-rod-out configuration.	The accuracy in the prediction of the SDM, therefore, depends on the accuracy of the neutronics methods to predict the distributed criticality (corresponding to $k_{B_{demoB}}$ ) and local criticality (corresponding to $k_{B_{sroB}}$ ). <del>The A</del> distributed critical configuration is <u>represented by the in-sequence cold critical measurement, where control rods are pulled in a relatively uniform manner in all regions of the core. A local critical configuration is represented by a configuration in which the core becomes critical with a relatively small number of adjacent control blades removed.</u> The local cold critical provides a better demonstration of ability to predict the worth of the strongest-rod-out configuration.	Clarification	Comment incorporated.
31	Page 126 Section 8, , 2 <sup>nd</sup> paragraph, 1 <sup>st</sup> sentence	NEDC-33173P (Reference 1) is applicable for operation at EPU and MELLA+.	NEDC-33173P (Reference 1) is applicable <del>for operation at EPU and MELLA+.</del> <u>to expanded operating domains, greater than OLTP up to and including 120% OLTP with MELLA+.</u>	NEDC-33173P Expanded operating domains includes all domains greater than OLTP up to and including EPU and M+.	GHNE comment is no longer applicable in the Final SE.

#	Location in Draft SE	Draft SE Text	GHNE Comment	GHNE Comment Basis	NRC Staff Resolution
32	Section 8.4 1 <sup>st</sup> and 2 <sup>nd</sup> paragraph on page 129	The NRC staff compared the performance of TGBLA06AE4 against HELIOS with lattices with and without vanished rods, and Gd content from 6 percent to 7 percent. From the code-to-code comparisons, as well as the TGBLA06-CASMO4 comparisons provided, the NRC staff finds that the TGBLA06AE4 modifications, including the above Pu-240 modifications, are acceptable for production.	The NRC staff compared the performance of <del>TGBLA06AE4</del> TGBLA06AE5 against HELIOS with lattices with and without vanished rods, and Gd content from 6 percent to 7 percent. From the code-to-code comparisons, as well as the TGBLA06-CASMO4 comparisons provided, the NRC staff finds that the <del>TGBLA06AE4 modifications</del> TGBLA06AE5, including the above Pu-240 modifications, are acceptable for production.	Clarification	Comment incorporated.
33	Table 8-1	Uncertainties Not Assessed for Legacy Fuel	Remove Table 8-1	The P4B, TIP, PAL, Channel Bow, Gradient, & manufacturing uncertainties are all based on legacy fuel. The only thing not conducted was the analysis to support infinite lattice uncertainties with the procedure identified here.	Comment incorporated.

#	Location in Draft SE	Draft SE Text	GHNE Comment	GHNE Comment Basis	NRC Staff Resolution
34	Page 40 3.2.5.1 Item 6	6. The full spectrum base ECCS-LOCA analysis is performed during initial implementation of SAFER methodology, new fuel introduction, transition to GENE methodology and fuel, or if new operating conditions are implemented (e.g., MELLLA+).	6. The full spectrum base ECCS-LOCA analysis is performed during initial implementation of SAFER methodology, <del>new fuel introduction, or</del> transition to GENE methodology and fuel, <del>or if new operating conditions are implemented (e.g., MELLLA+).</del> For new fuel introduction or if new operating conditions are implemented (e.g., MELLLA+), the limiting areas of the full spectrum base ECCS-LOCA analysis are reanalyzed to assure continued compliance with the 10CFR50.46 acceptance criteria for the new fuel or operating conditions.	The full spectrum base ECCS-LOA analysis is not repeated for new fuel introduction or operating condition changes.	Comment incorporated.

#	Location in Draft SE	Draft SE Text	GHNE Comment	GHNE Comment Basis	NRC Staff Resolution
35	<p>Page 41            3.2.5.1.1            1st            paragraph,            3rd sentence</p> <p>Comment            also applies            to:</p> <p>Section            3.2.5.1.2            p. 42            2<sup>nd</sup>            paragraph</p>	<p>[</p> <p style="text-align: center;">]</p>	<p><del>For small breaks, recent sensitivity analyses based on the current fuel design shows that early dryout penetrates to the high power nodes for mid-peaked and toppeaked axial shapes. The top peaked power shape can have a higher PCT than mid-peaked power shape for the limiting small.</del></p> <p>For small breaks, fuel typically remains in nucleate boiling until the time it is uncovered. Peak cladding temperature is driven by fuel heatup for the duration that the node is uncovered, until vessel level from ECCS actuation recovers the node elevation. Recent sensitivity analyses based on the current fuel design shows that the top-peaked power shapes can <i>result in</i> a higher PCT <i>for small breaks</i> than <i>comparable calculations assuming a</i> mid-peaked axial shape, <i>given that the nodes higher in the core remain uncovered longer.</i></p>	<p>There is no early dryout or boiling transition for small break LOCAs. Nucleate boiling is maintained until the node uncovers.</p>	<p>Comment incorporated.</p> <p>[</p> <p style="text-align: center;">]</p>

#	Location in Draft SE	Draft SE Text	GHNE Comment	GHNE Comment Basis	NRC Staff Resolution
36	Page 41 3.2.5.1.1 1st paragraph	[ ]	[ ]	[ ]	Comment incorporated.

#	Location in Draft SE	Draft SE Text	GHNE Comment	GHNE Comment Basis	NRC Staff Resolution
37	Section 3.2.5.1.2 1 <sup>st</sup> paragraph	For EPU and MELLLA+ application, the NRC staff will review the plant-specific ECCS-LOCA response and the available margins to the key parameters in the ECCS-LOCA requirements (e.g., PCT limit of 2200° F). The licensing application will include comparisons of the key parameters for each application against the experience (see Section 4.3 of NEDC-33173P (Reference X1X), "Plants Specific Application Process.") For those applications, in which the key parameters are outside the experience base in terms of the conditions of the high powered bundles and/or in those cases in which the margins to the PCT are deemed to have low margins, the NRC staff will audit and review the specific input parameters applied in the ECCS-LOCA analysis. In these cases, the NRC staff can request additional sensitivity analyses in order to obtain additional assurances that ECCS-LOCA assumptions and methodology are acceptable.	For EPU and MELLLA+ application, the NRC staff will review the plant-specific ECCS-LOCA response and the available margins to the key parameters in the ECCS-LOCA requirements (e.g., PCT limit of 2200° F). <del>The licensing application will include comparisons of the key parameters for each application against the experience (see Section 4.3 of NEDC-33173P (Reference X1X), "Plants Specific Application Process.") For those applications, in which the key parameters are outside the experience base in terms of the conditions of the high powered bundles and/or in</del> In those cases in which the margins to the PCT are deemed to have low margins, the NRC staff will audit and review the specific input parameters applied in the ECCS-LOCA analysis. In these cases, the NRC staff can request additional sensitivity analyses in order to obtain additional assurances that ECCS-LOCA assumptions and methodology are acceptable.	Section 4.3 of NEDC-33173P states "Each plant seeking to apply the Methods LTR must provide information supporting the application that demonstrates that the plant parameters are within the applicability definition in Section 4.2."  Section 4.2 basically commits to staying within each GE technology code's associated "application statement" defining the application range. The application of these codes complies with the limitations, restrictions and conditions specified in the approving NRC SER for each code.  Section 4.2 commits to "The plant specific application process will confirm that operations proposed by the plant specific license amendment meet the Applicability of GE	Comment not incorporated.

#	Location in Draft SE	Draft SE Text	GHNE Comment	GHNE Comment Basis	NRC Staff Resolution
				<p>Methods to Expanded Operating Domains LTR applicability envelope requirements.”</p> <p>Further, the basis of the request for the comparison is that maximum powered bundle increase relative to the pre-EPU conditions. Please see comment 30, 40, and 60.</p>	
38	Page viii SE Summary Section 1.0 7 <sup>th</sup> sentence	In addition, in some EPU core designs the power levels of the maximum powered bundle increase relative to the pre-EPU conditions.	<del>In addition, in some EPU core designs the power levels of the maximum powered bundle increase relative to the pre-EPU conditions.</del>	Misleading statement. As worded, this sentence implies that the power increase was directly caused by the change to EPU. However, the same increase in peak power could have been designed into a non-EPU reload core.	GHNE comment is no longer applicable in the Final SE.

#	Location in Draft SE	Draft SE Text	GHNE Comment	GHNE Comment Basis	NRC Staff Resolution
39	Page 2 Section 1 5 <sup>th</sup> paragraph of Section 1	The NRC staff concludes that implementation of MELLLA+ will result in operation outside the current experience base. Specifically, for some applications, the hot bundle conditions may be outside the current operating experience base in terms of key parameters such as bundle power-to-flow ratio, exit void fractions, and bundle powers.	The NRC staff concludes that implementation of MELLLA+ will result in operation outside the current experience base. <del>Specifically, for some applications, the hot bundle conditions may be outside the current operating experience base in terms of key parameters such as bundle power-to-flow ratio, exit void fractions, and bundle powers.</del>	Statement is incorrect since bundle power is limited by CPR constraint and it does not change with EPU or MELLLA+.	Comment not incorporated.
40	Page ix SE Summary Impact of Operation at High Void Conditions	4. Extension of the qualification data for the thermal-mechanical methodology to high exposures	Delete	Voids do not have impact on T-M methodology	Comment not incorporated.  <u>Staff comment:</u> Bullet 4 does not refer to void fraction levels, but rather biases associated with the 40% depletion assumption at high exposures. However, the staff agrees that the SE section heading needs to be changed. Section heading changed to: "Impact on Methods Qualification Databases" First paragraph revised as follows: "The high void conditions and other characteristics of EPU and MELLLA+ conditions could affect the key assumptions in the analytical methods that impact the safety analyses supporting EPU and MELLLA+ operations or safety features. The methods review evaluates these effects and the adequacy of the qualification database supporting the analytical methods. The topics of review are as follows:"



#	Location in Draft SE	Draft SE Text	GHNE Comment	GHNE Comment Basis	NRC Staff Resolution
41	Page xi SE Summary Section 3.0 Item 4a	The transient LHGR limit, although a specified acceptable fuel design limit (SAFDL), is ...	The transient LHGR limit, <del>although a specified acceptable fuel design limit (SAFDL), is ...</del>	LHGR is not SAFDL (See Table 1-1 of NEDC-33173P)	Comment incorporated.
42	Page xi SE Summary Section 3.0 Item 4b	EPU and MELLLA+ operation will result in a higher overpower response during pressurization transients due to the higher initial steam flow (24 percent) for the fixed safety relief valve (SRV) capacity and the higher reactivity associated-with the core design. Plant-specific EPU and MELLLA+ applications will include discussion of the plant-specific thermal and mechanical overpower response.	<del>EPU and MELLLA+ operation will result in a higher overpower response during pressurization transients due to the higher initial steam flow (24 percent) for the fixed safety relief valve (SRV) capacity and the higher reactivity associated with the core design.</del> Plant-specific <del>EPU and MELLLA+ applications</del> reload applications will include <del>discussion of the a</del> plant-specific thermal and mechanical overpower response.	Higher overpower response during pressurization transients is not cause by fixed SRV capacity.	GHNE comment is no longer applicable in the Final SE.
43	Page 3 Section 2.1 2 <sup>nd</sup> paragraph First three sentences	There are no specific limits on the operating bundle powers, bundle operating power-to-flow ratio, or void fractions. Instead, the core design and the operating strategy employed are constrained by the thermal limits. The maximum powered bundles must meet the thermal limits during steady-state, transient, and accident conditions.	There are no <del>direct specific</del> limits on the operating bundle powers, bundle operating <del>core thermal</del> power-to- <del>total core</del> flow ratio, or void fractions. Instead, the core design and the operating strategy employed are constrained by the thermal limits. The maximum powered bundles must meet <del>the</del> <u>respective</u> thermal limits during steady-state operation <u>so that tech spec safety limits or other absolute limits are not violated during transient or accident conditions.</u>	Thermal limits are derived such that operation at steady-state will be protected in the event of a transient or accident. Thermal limits are expected to be exceeded in both transients and accidents though the SAFDLs (safety limits, PCT, or Tech. Spec limits are satisfied.	Comment not incorporated.
44	Page 17 Section 3.1.4.2. 4 <sup>th</sup> paragraph 3 <sup>rd</sup> sentence	The increased cycle energy was achieved by increasing the GE14 reload batch fraction from 188 to 128 and by increasing the average enrichment from 3.53 to 3.89 weight percent.	The increased cycle energy was achieved by increasing the GE14 reload batch fraction from 188 to <u>268</u> and by increasing the average enrichment from 3.53 to 3.89 weight percent.	Correction.	Comment incorporated.

#	Location in Draft SE	Draft SE Text	GHNE Comment	GHNE Comment Basis	NRC Staff Resolution
45	Section 3.1.5.2. Last two sentences on page 21	For future EPU/MELLLA+ application for plants with thermal TIPs, the NRC staff should evaluate the plant-specific TIP core-tracking data against compiled EPU Reference Plant core-tracking data. The objective is to determine if the power distribution uncertainties need to be increased for cores with thermal TIPs installed.	Delete	Neutron (thermal) TIPs do perform with wider variability, but this is an instrumentation accuracy limitation rather than methods problem.	Comment not incorporated.
46	Section 3.2.3	Figure 3-10 shows that both the SLMCPR value and the corresponding RIP value increase early in the bundle exposures and also increase after approximately 15 GWd/ST. Note that for the current Gd concentrations, the poison burnups after the first cycle (15 GWd/ST or once burned fuel). However, the increase is relatively modest compared to beginning of the bundle life whereby the increase could be as high as 0.008, which would round up to 0.01 significance threshold.	Delete	In regards to RIP, Figure 3-10 shows that the impact on RIP for the higher void profile is negative after 5 GWd/ST of bundle exposure and remains negative until 40 GWd/ST, well past the point where the bundles cease to contribute in the SL calculation. From this figure it is concluded that the RIPs and the resultant SL are not impacted by the R-factor differences seen for the 70% void profile - at least for the bundle shown in this figure	GHNE comment is no longer applicable in the Final SE.

#	Location in Draft SE	Draft SE Text	GHNE Comment	GHNE Comment Basis	NRC Staff Resolution
47	Page 32 Section 3.2.4, 1 <sup>st</sup> paragraph	(2) the OLMCPR is established by combining the change in the MCPR due to the transient overpower to the initial steady-state MCPR such that rod operating power is limited to preclude transition boiling.	(2) the OLMCPR is established <del>by combining the change in the MCPR due to the transient overpower to the initial steady-state MCPR</del> such that rod operating power is limited to preclude transition boiling	The current sentence implies some combining with the initial steady state MCPR, which is not true. Suggested wording is more accurate for ODYN and TRACG.	Comment not incorporated.
48	3.2.4.1, second paragraph	In terms of power distributions, top-peaked core power profile will reduce the scram reactivity early in the transient and the delayed scram time will increase the transient MCPR change.	In terms of power distributions, top-peaked core power profile will reduce the scram reactivity early in the transient and the <u>reduced</u> scram <u>reactivity may</u> increase the transient MCPR change.	The scram is not delayed but the scram reactivity rate is reduced.	Comment incorporated.
49	Page 33 Section 3.2.4.2, 2 <sup>nd</sup> paragraph 3 <sup>rd</sup> sentence	[  ]	[  ]	Control blade history is more commonly known for its affect on local bundle power distribution, not in the context of the axial average power shape.	Comment not incorporated.
50	Page 33 Section 3.2.4.2, 5 <sup>th</sup> paragraph	[  ]	[  ]	[  ]	Comment incorporated.

#	Location in Draft SE	Draft SE Text	GHNE Comment	GHNE Comment Basis	NRC Staff Resolution
51	Page 36 Section 3.2.4.2.4 1 <sup>st</sup> paragraph 2 <sup>nd</sup> sentence	For operation at EPU and MELLLA+ conditions, where the CPR response will potentially be higher due to the fixed safety relief valve (SRV) relief capacity relative to the increase in the pressurization response, TRACG, which has the capability to simulate 3D core conditions, is expected to be more attractive to licensees.	For operation at EPU and MELLLA+ conditions, where additional CPR <del>margin will be needed</del> , TRACG... <del>where the CPR response will potentially be higher due to the fixed safety relief valve (SRV) relief capacity relative to the increase in the pressurization response, TRACG,</del> which has the capability to simulate 3D core conditions, is expected to be more attractive to licensees.	Delete the use of SRVs in this context. The SRV capacity is not a factor in the CPR calculation.	GHNE comment is no longer applicable in the Final SE.
52	1 <sup>st</sup> sentence on page 54	Most importantly, the 10 percent Gd rod fuel temperature shows that fuel centerline temperature may not be avoided with 10 percent Gd content. The 10 percent Gd calculation is based on non-barrier fuel and GENE states that the 10 percent Gd data was available only for non-barrier fuel.	Most importantly, the 10 percent Gd rod fuel temperature shows that fuel centerline <del>melting</del> temperature may not be avoided with 10 percent Gd content. The 10 percent Gd calculation is based on non-barrier fuel <del>and is more conservative. GENE states that the 10 percent Gd data was available only for non-barrier fuel.</del>	Non barrier fuel is more conservative.	GHNE comment is no longer applicable in the Final SE.
53	Section 3.2.6.5.9 Staff Conclusion #1	The higher bundle powers during steady-state operation reduce the margins to the LHGR limit.		LHGR limit was already an active constraint for regular cores. The plant is not operating with higher bundle power at EPU/M+	GHNE comment is no longer applicable in the Final SE.
54	Section 5.0 4 <sup>th</sup> paragraph 1 <sup>st</sup> sentence	Table 5-1 shows the void fractions calculated using the different models (and their standard assumptions) for a high-power-density plant	Recommend adding the core thermal power (MWth) and core flow (Mlb/hr) assumed in the development of Table 5-1 since it appears to be an offrated case.	This result may look out of line if reader assumes it is at rated conditions.	Comment not incorporated.

#	Location in Draft SE	Draft SE Text	GHNE Comment	GHNE Comment Basis	NRC Staff Resolution
55	Section 5.4 3 <sup>rd</sup> paragraph 3 <sup>rd</sup> sentence page 87	In addition, the R-factor methodology is limited to GE12 fuel designs and do not include the current fuel designs and operating conditions.	In addition, the R-factor methodology is <del>limited to GE12</del> applicable to GE9x9 and 10x10 fuel designs. and do not include the current fuel designs and operating conditions.	Clarification. See FLN 2001-016	GHNE comment is no longer applicable in the Final SE.
56	Section 7.2.2 2 <sup>nd</sup> paragraph page 102	GE has correlated this parameter to the GE database as a function of Reynolds number, fluid properties (pressure), and void fraction (the solution to the GE drift flux model is therefore iterative).	GE has correlated this parameter to the GE database as a function of Reynolds number, fluid properties (pressure), and void fraction <del>(the solution to the GE drift flux model is therefore iterative).</del>	Correction.	Comment incorporated.
57	Page 108 Section 7.2.4, 2 <sup>nd</sup> paragraph	As shown in Table 7-1, the individual data ranges cover the expected parameter ranges reasonably well; however, some of the 10X10 bundle parameters are outside of the range of the database	As shown in Table 7-1, the individual data ranges cover the expected parameter ranges reasonably well; <del>however, some of the 10X10 bundle parameters are outside of the range of the database.</del>	Table 7-1 in the discussion has 2 of the 10x10 parameters outside the data ranges (Mass flux and axial power shape). The mass flux entry is discussed in the next item (Comment 67). The APS is understood to vary in the reactor and is not a practical constraint – if it were, no vendor could have a correlation.	Comment not incorporated.

#	Location in Draft SE	Draft SE Text	GHNE Comment	GHNE Comment Basis	NRC Staff Resolution
58	Page 114, Section 7.2.7 4th paragraph (or 2 <sup>nd</sup> paragraph on page 114)	The NRC staff also finds that since the void fractions can be higher than [ ] at steady-state for the proposed MELLLA+, extrapolation of the void-quality correlation is not "momentary" during transients as characterized in NEDC-33173P (Reference 1).	Remove item.	Steady-state void fractions cannot be [ ]	Comment not incorporated.
59	Section 7.2.7 5th paragraph	The NRC staff also finds that for most of GE's analytical methods and codes, uncertainties are not applied to the void-quality correlation prediction, with the exception of ODYN. Implicitly, the safety analyses assume that the void-quality correlation is supported by applicable benchmarking data and that the uncertainties associated with it are small. Historically, the NRC staff had also never directly reviewed or approved the correlation and its supporting database.	The NRC staff also finds that for <del>most of</del> GE's analytical methods and codes, uncertainties are not applied to the void-quality correlation prediction, <del>with the exception of ODYN.</del>	The ODYN uncertainty analysis (referred to here) included void fraction. However, this was a <u>supporting analysis</u> and not the basis for setting margins. NRC reviewed as part of GE Amendment 11 and TACS LTR NEDC-32084P-A	Comment incorporated.

NEDO-33173-A, Revision 1  
 Non-Proprietary Information  
 - 36 -

#	Location in Draft SE	Draft SE Text	GHNE Comment	GHNE Comment Basis	NRC Staff Resolution
60	Table 7-1 Page 119	Mass flux for a 10x10 BWR bundle = 4,001,350 kg/m <sup>2</sup> /s	Mass flux for a 10x10 BWR bundle = <del>4,001,350 kg/m<sup>2</sup>/s</del> [                    ]	The given mass flux translates [          ]	Comment incorporated.

## TABLE OF CONTENTS

	<b>Page</b>
Executive Summary .....	vii
Revisions.....	viii
Acronyms and Abbreviations .....	ix
1.0 Introduction .....	1-1
1.1 Background.....	1-1
1.2 Purpose.....	1-1
1.3 Analysis Process .....	1-2
1.4 Overview.....	1-2
2.0 Safety Parameters Influenced by Uncertainties .....	2-1
2.1 Introduction.....	2-1
2.2 Critical Power .....	2-2
2.2.1 Safety Limit Critical Power Ratio (SLMCPR) .....	2-2
2.2.2 Operating Limit Critical Power Ratio (OLMCPR).....	2-17
2.3 Shutdown Margin (SDM) .....	2-24
2.3.1 Fuel Parameters That Affect SDM .....	2-24
2.3.2 Treatment of Fuel Parameter Uncertainties .....	2-25
2.3.3 Adequacy of Existing Treatment and Alternate Approach.....	2-29
2.4 Fuel Rod Thermal-Mechanical Performance.....	2-29
2.4.1 Fuel Parameters That Affect Thermal-Mechanical Limits .....	2-29
2.4.2 Treatment of Fuel Parameter Uncertainties .....	2-29
2.4.3 Adequacy of Existing Treatment and Alternate Approach.....	2-33
2.5 LOCA Related Nodal Power Limits.....	2-34
2.5.1 Fuel Parameters That Affect LOCA Related Nodal Power Limits.....	2-34
2.5.2 Treatment of Fuel Parameter Uncertainties .....	2-34
2.5.3 Adequacy of Existing Treatment and Alternate Approach.....	2-36
2.6 Stability.....	2-36
2.6.1 Fuel Parameters That Affect Stability.....	2-37
2.6.2 Treatment of Fuel Parameter Uncertainties .....	2-37
2.6.3 Adequacy of Existing Treatment and Alternate Approach.....	2-52
2.7 Licensed Exposure.....	2-52
2.7.1 Fuel Parameters That Affect Pellet Exposure.....	2-52
2.7.2 Treatment of Fuel Parameter Uncertainties .....	2-52
2.7.3 Adequacy of Existing Treatment and Alternate Approach.....	2-53
3.0 Extension of Safety Parameter Bases to the MELLLA+ Operating Domain .....	3-1
3.1 Introduction.....	3-1



3.2	Critical Power .....	3-1
3.2.1	Safety Limit Critical Power Ratio (SLMCPR) .....	3-1
3.2.2	Operating Limit Critical Power Ratio (OLMCPR).....	3-2
3.3	Shutdown Margin .....	3-2
3.4	Fuel Rod Thermal Mechanical Performance .....	3-2
3.5	LOCA Related Nodal Power Limits .....	3-3
3.6	Stability .....	3-3
3.7	Licensed Exposure .....	3-6
4.0	Licensing Application .....	4-7
4.1	Overview.....	4-7
4.2	Applicability .....	4-7
4.3	Plant Specific Application Process .....	4-8
5.0	Summary and Conclusion .....	5-1
6.0	References .....	6-1
Appendix A	Vermont Yankee Reactor Systems Branch Questions	
Appendix B	Not Used	
Appendix C	GEH Responses to NRC RAIs	

## LIST OF TABLES

<b>Table</b>	<b>Title</b>	<b>Page</b>
Table 1-1	Fuel Design Limits & Associated Methods.....	1-4
Table 2-1	Summary of SLMCPR Uncertainties.....	2-3
Table 2-2	Summary of Bundle Power Uncertainties.....	2-4
Table 2-3	Summary of Pin Power Uncertainty Subjects.....	2-5
Table 2-4	Summary of TGBLA-MCNP Pin Power Comparisons.....	2-5
Table 2-5	Summary of High Power Density Plant Tracking Results.....	2-7
Table 2-6	Summary of Four Bundle Power Subjects.....	2-8
Table 2-7	Bundle Power Subject.....	2-10
Table 2-8	Comparison Between Void Correlation and Database.....	2-15
Table 2-9	Thermal-Hydraulic Subjects.....	2-16
Table 2-10	TRACG Impact of High Exposure Void Coefficient Bias.....	2-21
Table 2-11	Void Coefficient Comparison between TGBLA06 and MNCP.....	2-22
Table 2-12	OLMCPR Subjects.....	2-24
Table 2-13	Summary of Same Core Critical Experiments.....	2-27
Table 2-14	Summary of Uncertainty Components for LHGR Evaluations.....	2-32
Table 2-15	Fuel Performance Related Subjects.....	2-33
Table 2-16	LOCA/ECCS Related Subjects.....	2-36

## LIST OF FIGURES

<b>Figure</b>	<b>Title</b>	<b>Page</b>
Figure 2-1	GEXL14 Application Range.....	2-11
Figure 2-2	8X8 Void fraction Data – Sensitivity to PLR for Low Flow .....	2-13
Figure 2-3	8X8 Void fraction Data – Sensitivity to PLR for High Flow .....	2-13
Figure 2-4	Typical Void-Quality Relation at High Power/Flow Ratio .....	2-14
Figure 2-5	Reactivity Change for a Small Quality Perturbation ( $\Delta X = 0.001$ ) as a Function of Void Fraction.....	2-18
Figure 2-6	Reference Plants Cold Critical Eigenvalues .....	2-26
Figure 2-7	Difference Between Measured and Predicted Cold Critical Eigenvalues .....	2-28

## **EXECUTIVE SUMMARY**

In the NRC review of GE's generic Maximum Extended Load Line Limit Analysis Plus (MELLLA+) submittal [Reference 1] and the Vermont Yankee Nuclear Power Station (VYNPS) Constant Pressure Power Uprate submittal [Reference 2], the NRC requested additional information (RAI) related to the uncertainties and biases utilized in GE's bundle lattice and core simulation methodologies and the potential effect on safety parameters influenced by such uncertainties and biases. The VYNPS responses to the NRC proposed an additional margin to the safety limit minimum critical power ratio (SLMCPR) and provided bases for the conclusion that other safety parameters did not require additional margin. [References 3 through 7]

This LTR is consistent with and based on the approach used for the VYNPS extended power uprate review. It is intended to be referenced by near-term license applications for Extended Power Uprate, Constant Pressure Power Update, and the MELLLA+ operating domain expansion. A temporary additional SLMCPR margin of 0.02 is proposed, consistent with that accepted for VYNPS, without the provision for decreasing the additional margin for a specific plant application. The range of applicability includes any expanded operating range up to 120% of Original Licensed Thermal Power and including the MELLLA+ operating domain expansion. The approach in the enclosed LTR is to be implemented on a temporary basis pending the resolution of the NRC's RAIs regarding GE methods. GE is committed to the activities necessary to demonstrate the adequacy of GE's methods.

The treatment of the uncertainties in the safety limit development is discussed and the additional SLMCPR margin is supported. The effect on six safety parameters is addressed: critical power (safety and operating limit), shutdown margin, fuel rod thermal-mechanical performance, LOCA-related nodal power limits, stability, and licensed pellet exposure.

## REVISIONS

NEDC-33173P-A, Revision 1 replaces Revision 0 in its entirety. Revision bars in the right margin delineate the changes to Revision 1. The following table summarizes the key changes.

<b>Revision</b>	<b>Changes</b>
0	Initial Issue
Revision 1	Created the '-A' version  Added the NRC's SE and the GEH responses to the NRC Requests for Additional Information (See Appendix C)  Added Revision History table  Response to RAI 6  6.1 – Added information from VY RAIs to make a more complete and self sufficient document  6.2 – Removed all Non-Methods RAIs from Appendix A and Deleted Appendix B and all document references to Appendix B.  6.3 – Added requested core design information to Section 4.3 for plant specific applications

## ACRONYMS AND ABBREVIATIONS

<b>Term</b>	<b>Definition</b>
AOO	Anticipated Operational Occurrence
APRM	Average Power Range Monitor
ATWS	Anticipated Transient Without Scram
BOC	Beginning Of Cycle
BT	Boiling Transition
BWR	Boiling Water Reactor
BWROG	BWR Owners Group
CDA	Confirmation Density Algorithm
CPPU	Constant Pressure Power Uprate
CPR	Critical Power Ratio
DIVOM	Delta over Initial MCPR Versus Oscillation Magnitude
DSS-CD	Detect and Suppression Solution – Confirmation Density
$\Delta$ CPR	Delta Critical Power Ratio
ECCS	Emergency Core Coolant System
EOC	End Of Cycle
EOP	Emergency Operating Procedure
EPU	Extended Power Uprate
FMCP	Final Minimum Critical Power Ratio
FWCF	Feedwater Controller Failure Event
FWHOOS	Feedwater Heating Out-of-Service
FSAR	Final Safety Analysis Report
GE	General Electric Company
GESTAR	General Electric Standard Application for Reload Fuel
GEXL	GE Boiling Transition Correlation
GSTRM	GESTR Mechanical
HBB	Hard Bottom Burn
HCOM	Hot Channel Oscillation Magnitude
ICPR	Initial Critical Power Ratio
IV	Instantaneous Void
LHGR	Linear Heat Generation Rate
LOCA	Loss Of Coolant Accident
LTR	Licensing Topical Report
LPRM	Local Power Range Monitor
MAPLHGR	Maximum Average Planar Linear Heat Generation Rate
MCPR	Minimum Critical Power Ratio
MELLLA+, M+	Maximum Extended Load Line Limit Analysis Plus

NEDO-33173-A, Revision 1  
Non-Proprietary Information

<b>Term</b>	<b>Definition</b>
Methods LTR	Applicability of GE Methods to Expanded Operating Domains Licensing Topical Report
MNCP	A General Monte Carlo N-Particle Transport Code
NRC	Nuclear Regulatory Commission
ODYN	1-D Transient Model
ODYSY	GE Best-Estimate Frequency Domain Stability Code
OLMCPR	Operating Limit MCPR
OLTP	Original Licensed Thermal Power
OPRM	Oscillation Power Range Monitor
Option II	Stability Detect and Suppress LTS for BWR/2
Option III	Stability OPRM-Based Detect and Suppress LTS
PANACEA	Current GE BWR Core Simulator
PCT	Peak Cladding Temperature
PHE	Peak-Hot Excess
PLR	Part Length Rod
PU	Power Uprate
RAI	Request for Additional Information
RPS	Reactor Protection System
SAFDLs	Specified Acceptable Fuel Design Limits
SDM	Shutdown Margin
SE, SER	Safety Evaluation Report
SLMCPR	Safety Limit MCPR
SLO	Single Loop Operation
TGBLA	Current GE BWR lattice physics code
TIP	Traversing In-Core Probes
TRACG	Transient Reactor Analysis Code (GE proprietary version)
UB	Under Burn
UTL	Upper Tolerance Limit
VH	Void History
1-D	One Dimensional
3-D	Three Dimensional

## **1.0 INTRODUCTION**

### **1.1 BACKGROUND**

Based on previous NRC-approved licensing topical reports and associated NRC Safety Evaluations (SE) for GE's methods, GE has evaluated the accuracy of its methodologies as it has introduced new fuel designs and operating strategies. In the review of the Maximum Extended Load Line Limit Analysis Plus (MELLLA+) submittal [Reference 1] and the Vermont Yankee Nuclear Power Station (VYNPS) Constant Pressure Power Uprate submittal [Reference 2], the NRC requested additional information related to the standard uncertainties and biases utilized in GE's bundle lattice and core simulation methodologies and the potential effect on safety parameters influenced by such uncertainties and biases. The VYNPS RAI responses accepted by the NRC proposed an additional margin to the safety limit minimum critical power ratio (SLMCPR) of 0.02 and provided the bases for the conclusion that other safety parameters did not require additional margin. [References 3 through 7]

### **1.2 PURPOSE**

The purpose of the Applicability of GE Methods to Expanded Operating Domains Licensing Topical Report (Methods LTR) is to provide a licensing basis that allows the NRC to issue SEs for expanded operating domains including Constant Pressure or Extended Power Uprate applications and the MELLLA+ LTR. The SE for the Applicability of GE Methods to Expanded Operating Domains LTR would approve the use of GE's methods, including the use of a temporary additional SLMCPR margin of 0.02 as described in the Methods LTR, for expanded operating domains bounded by EPU or CPPU power uprates and MELLLA+ until final resolution of the NRC RAIs regarding GE's analytical methods [References 8 and 9].

Upon approval of the Methods LTR, each licensee's application for an expanded operating range (CPPU or EPU) may refer to the Methods LTR as a basis for the license change request regarding the applicability of GE's methods to the requested changes. The Methods LTR is a required part of the implementation of the MELLLA+ LTR [Reference 1]. Approval of the Methods LTR would eliminate repetitive RAIs, improve the NRC review schedule, and minimize the resources expended on these reviews by NRC, GE, and the licensees.



### **1.3 ANALYSIS PROCESS**

The approach applied to CPPU, EPU, and MELLLA+ evaluations is discussed in each of the applicable LTRs [References 1, 10, 11, and 12]. An equilibrium cycle core design is the generic approach applied in each of these methods for reactor core and fuel performance related evaluations supporting license change requests. Following the licensing of the proposed changes, the core design for the operating cycle, in which implementation will take place, is evaluated and documented per GESTAR II requirements [Reference 13]. The GESTAR based evaluations effectively set the operating limits for the core. A summary of the applicable limits and the associated methods are given in Table 1-1.

Most licensed core designs typically involve mixed cores (cores containing more than one fuel design or geometry). A licensee may have utilized more than one fuel vendor, in which case there will be legacy fuel bundle designs resident in the current cycle that were not originally designed with GE methods. In these cases, GE complies with the requirements of GESTAR by working with the licensee and vendor to put a proprietary agreement in place. Under this (restrictive and limited) proprietary agreement, sufficient data (e.g., cladding thickness and material type, pellet diameter and density, etc.) is obtained to model the other vendor's fuel design using GE's standard, approved methods. The fuel vendor's original limits are used directly or, as in the case for critical power, an equivalent GE correlation is developed from supplied data. In either case, considerations for uncertainties are taken, and if necessary, additional margin for the legacy fuel uncertainty is incorporated into the applicable limits. This approach is consistent with GE's current approved application methodology.

### **1.4 OVERVIEW**

The subsequent sections of the Methods LTR provide a review of GE methodologies, uncertainties, and biases for acceptability to license applications for expanded operating domains (e.g., CPPU, EPU, and MELLLA+). The uncertainty parameters of interest are identified and their treatment discussed in the context of applications to CPPU, EPU, and MELLLA+ operations. The key safety parameters potentially influenced by increased uncertainties are

established and the effect of the increase is evaluated. The adequacy of the existing margin, and, as applicable, augmented margin for each of these safety parameters is provided.

Section 2 focuses on the evaluation of the effect of uncertainties in the determination of safety parameters for CPPU and EPU applications. Section 3 extends the Section 2 basis to the MELLLA+ operating domain.

Section 4 presents the licensing application framework for the Methods LTR including the applicability range in terms product line, power uprate, and operating domain parameters. The plant specific application process is also included in Section 4. Section 5 summarizes the evaluation of each safety parameter and, if necessary, the resulting margin adjustments.

**Table 1-1 Fuel Design Limits & Associated Methods**

Limit	Primary Technology	Description	Evaluation Frequency & Notes
SLMCPR	SLMCPR, PANACEA	The SLMCPR is a MCPR value at which 99.9% of the fuel rods in the core are expected to avoid BT. This value considers the core power distribution and uncertainties.	The limit is evaluated on a plant/cycle specific basis (i.e., each core design).
OLMCPR	ODYN, TRACG, PANACEA	The OLMCPR is additional margin above the SLMCPR to account for the MCPR change due to AOOs. Adherence to the limit assures that in the event of an AOO, 99.9% of the fuel rods are expected to avoid BT.	The limit is evaluated on a plant/cycle specific basis. The FSAR transients that are limiting or potentially limiting with respect to pressure and fuel thermal limits are analyzed for each reload. Transients are confirmed to be within the LHGR basis.
SDM	PANACEA	SDM is maintained regardless of the core design (the value of the limit does not vary with core characteristics like SLMCPR or OLMCPR). The shutdown margin requirement assures that the reactor can be brought and held subcritical with the control system alone. Most BWRs have a TS value of 0.38%. The "working definition" of SDM is the quantity of reactivity needed to reach criticality in a xenon free core with the strongest worth control rod fully withdrawn and all other control rods inserted.	Each core is designed to conform to this limit. SDM margin is demonstrated on a plant/cycle specific basis.
LHGR	GSTRM (GESTR-Mechanical)	LHGR Operating Limits represent an envelope of acceptable linear heat generation rates, as a function of exposure, designed to maintain fuel integrity during normal operation, including Anticipated Operational Occurrences. The LHGR limits reflect the application of SAFDLs on the following fuel performance parameters: <ul style="list-style-type: none"> <li>• Fuel temperature</li> <li>• Cladding stress</li> <li>• Cladding strain</li> <li>• Cladding fatigue usage</li> <li>• Fuel rod internal pressure</li> <li>• Cladding creep</li> </ul>	LHGR Operating Limits are developed generically for each fuel product line (e.g., GE14). They are determined from thermal-mechanical considerations and independent of any particular core design.
MAPLHGR	SAFER	MAPLHGR is a an average planar linear heat generation rate limit that is a product of the plant ECCS-LOCA evaluation performed to demonstrate compliance with 10CFR50.46 acceptance criteria.	ECCS-LOCA evaluations are performed as plant specific, cycle independent analyses. These analyses are typically performed for each initial introduction of new fuel product lines. The analysis output is a Licensing Basis PCT and a set of parameters that are confirmed every cycle to ensure applicability of the analysis.
Stability	ODYSY TRACG	There are several accepted stability solutions, each designed to protect the SLMCPR. The solutions include prevention and detect and suppress strategies, as well as combinations of both elements.	The stability methodologies are applied and/or confirmed for every reload (every cycle).
Exposure	GSTRM (GESTR-Mechanical)	The licensed exposure limit is a result of the LHGR evaluation methodology discussed above.	The exposure limit is developed generically for each fuel product line from thermal-mechanical considerations. It is independent of the core design.

## 2.0 SAFETY PARAMETERS INFLUENCED BY UNCERTAINTIES

### 2.1 INTRODUCTION

GE has reviewed its methodologies to determine the uncertainties and biases that were confirmed by earlier gamma scan test data or measurements of irradiated fuel isotopics. The purpose of this review was to confirm that the existing uncertainties included in GE's NRC-approved treatment of uncertainties and biases address the NRC staff questions regarding the absence of recent confirmatory test data.

The associated fuel parameters related to such test data and measurements that are not otherwise measurable directly or indirectly by existing operating plant instrumentation, e.g., local power range monitors (LPRMs) and traversing in-core probes (TIPs), are:

1. Local fuel pin power and exposure (depletion) vs. axial position,
2. Relative local fuel pin power and exposure (local in-bundle peaking),
3. Void reactivity coefficient, and
4. [[ ]]

The fuel parameter uncertainties of interest are thus related to relative local and pin power peaking, void reactivity coefficient, and [[ ]]. Other nodal fuel and bundle parameters, e.g., lattice reactivity, bundle power, and bundle axial power shape, are satisfactorily and adequately confirmed by comparisons to operating plant data or tests, e.g., TIP data and shutdown margin demonstrations.

The safety parameters potentially influenced by local and relative local pin power uncertainties and the [[ ]] uncertainty are:

1. Critical power (controlled by the SLMCPR and OLMCPR),
2. Shutdown margin (controlled with a technical specification limit of 0.38%  $\Delta k/k$ ),
3. Fuel rod thermal-mechanical performance (controlled by limits on linear heat generation rate, LHGR),
4. LOCA-related nodal power limits (controlled via the maximum average planar linear heat generation rate, MAPLHGR),
5. Stability (protected by the SLMCPR, OLMCPR, and stability solutions), and
6. Licensed pellet exposure (e.g., 70 GWd/MT for GE14 fuel)

Each of the uncertainties in question is currently included and addressed in the treatment of uncertainties and biases in GE's NRC-approved methodologies to determine these safety parameters. GE believes it is appropriate to continue to utilize the NRC-approved GE treatment of uncertainties and biases. If consideration of larger uncertainties is deemed appropriate, such uncertainties can be utilized in the existing treatments of propagation and combination of uncertainties. Direct application of biases into best estimate codes in an attempt to address potential uncertainty concerns is not appropriate because such introduction of unqualified biases can lead to potential non-conservatism in resulting applications. Therefore, the fidelity of GE's codes and methods is best maintained by not artificially adding biases. Conservative limits on safety parameters, developed with consideration for such uncertainties, provide adequate and reasonable assurance of safety.

A discussion of the adequacy of the margin existing in, and, as applicable, augmented margin for each of these safety parameters is provided below.

## **2.2 CRITICAL POWER**

Fuel bundle critical power is controlled through two analytical limits, the Safety Limit Minimum Critical Power Ratio (SLMCPR) and the Operating Limit Minimum Critical Power Ratio (OLMCPR). The GE treatment of these limits considers uncertainties and biases contained in the methods used to evaluate MCPR.

### **2.2.1 Safety Limit Critical Power Ratio (SLMCPR)**

The SLMCPR is determined as a MCPR value at which 99.9% of the fuel rods in the core are expected to avoid Boiling Transition (BT). The development of the SLMCPR considers uncertainties associated with the determination of total core thermal power from plant instrumentation, as well as the predicted power and flow distribution within the core. The methods and uncertainties used to evaluate the SLMCPR have been approved by the NRC and are documented in NEDC-32601P-A and NEDC-32694P-A [References 14 and 15]. NEDC-32601P-A contains the SLMCPR methodology and uncertainties related to the thermal-hydraulic, pin power peaking and plant instrumentation. NEDC-32694P-A contains uncertainties related to the plant process computer's evaluation of the bundle power distribution.

### 2.2.1.1 Fuel Parameters That Affect SLMCPR

Table 2-1 and Table 2-2 contain a summary of the uncertainties relevant to the evaluation the SLMCPR.

**Table 2-1 Summary of SLMCPR Uncertainties**

Uncertainty Parameter	Uncertainty $\sigma$ (%)	Evaluation Basis
Feedwater Flow System Overall Flow Uncertainty	[[	Section 2.2 of NEDE-32601P-A
Feedwater Temperature Measurement		Section 2.3 of NEDE-32601P-A
Reactor Pressure Measurement		Section 2.4 of NEDE-32601P-A
Core Inlet Temperature		Section 2.5 of NEDE-32601P-A
Total Core Flow Measurement		Section 2.6 of NEDE-32601P-A
TIP Reading and Bundle Power		Table 2-2 Below
TIP Reading Random Uncertainty		Section 2.1 of NEDE-32601P-A
Channel Flow Area Variation		Section 2.7 of NEDE-32601P-A
Friction Factor Multiplier Uncertainty		Section 2.8 of NEDE-32601P-A
Channel Friction Factor Multiplier		Section 2.9 of NEDE-32601P-A
R-factor Uncertainty	]]	Section 3 & Appendix C of NEDE-32601P-A
Critical Power Uncertainty	Different for Each Fuel Type	Evaluated for each fuel product Line Using full-scale critical power test data

The measurement uncertainty items in Table 2-1 (e.g., feedwater temperature) are related to the determination of core thermal power through a heat balance. The total core flow, friction factor, and flow area uncertainties relate to the determination channel flows. The TIP and R-factor uncertainties are relevant to the prediction of bundle and local power. The critical power uncertainty is associated with the GEXL correlation's accuracy for MCPR prediction.

The R-factor is an input to the GEXL critical power correlation that captures the local peaking (pin powers and lattice location) influence on the predicted onset of BT. The R-factor uncertainty is related to the uncertainty associated with nuclear methods in determining the fuel pin power peaking. In addition, the (total) R-factor uncertainty includes terms for manufacturing and channel bow uncertainties.

Uncertainties in bundle power are derived from the parameters shown in Table 2-2, which lists the parameters at the time of the approval of NEDE-32694P-A and their evaluation basis. The parameters are generally based on TIP comparisons from operating plants, [[  
 ]] from gamma scan measurements.

**Table 2-2 Summary of Bundle Power Uncertainties**

Uncertainty Parameter	Uncertainty $\sigma$ (%)	Evaluation Basis
[[		
		]]

The local pin power peaking (axial and in-bundle) and [[  
 ]] uncertainties are factors which affect SLMCPR. The SLMCPR is not affected by void reactivity coefficient uncertainties.

**2.2.1.2 Treatment of Fuel Parameter Uncertainties**

GE's NRC-approved process for determining the SLMCPR incorporates the applicable uncertainties in the lattice and core physics parameters, and the method of determining SLMCPR assures that fuel is adequately protected from BT when such uncertainties are incorporated. Uncertainties in local pin power peaking, [[  
 ]] are explicitly included in the SLMCPR determination and considered separately, then cumulatively below.

**Pin Power Peaking**

A key method related uncertainty is the local (pin) peaking factor uncertainty. This value is primarily associated with the lattice code TGBLA [Reference 18]. The  $1\sigma$  uncertainty was

evaluated to be [[ ]] in NEDE 32601P-A, based on comparisons with MCNP Monte Carlo evaluations. The overall pin peaking uncertainty, including operational, flux gradient, and manufacturing effects was confirmed by comparison to pin gamma scan measurements performed in an 8x8 lead use assembly. Additional detail regarding the accuracy of the TGBLA code for the evaluation of pin power peaking can be found in the accepted VYNPS RAI responses summarized in Table 2-3.

**Table 2-3 Summary of Pin Power Uncertainty Subjects**

Related Technology	Subject	RAI
TGBLA, MCNP	Explanation provided to justify acceptability of basing assessment of pin power accuracy on BOL conditions	SRXB-A-37
TGBLA, MCNP	Explanation provided for use of different uncertainties for GE14 and later designs. Refer to response to SRXB-6	SRXB-A-38
TGBLA, MCNP	Explanation provided regarding Cross Sections for High void operation. Refer to generic EPU and MELLLA+ studies.	SRXB-A-46
PANACEA, ISCOR	Justify acceptability of basing assessment of pin power accuracy on code-to-code comparisons. Alternate approach and SLMCPR procedures proposed in response to SRXB-6	SRXB-A-34

The data presented in NEDE-32601P and in the RAI responses above were for the most part based on GE designs. TGBLA-MCNP [Reference 19] comparisons carried out on other vendor's fuel designs show results consistent with those obtained with the GE designs. Table 2-4 is a summary of standard deviation between TGBLA and MCNP pin powers for GE11, GE14, and several Non-GE fuel designs. These results show the overall TGBLA pin power accuracy to be similar for the Non-GE designs and the GE 9x9 and 10x10 designs.

**Table 2-4 Summary of TGBLA-MCNP Pin Power Comparisons**

Product	Standard Deviation Range 0% Voids	Standard Deviation Range 40% Voids	Standard Deviation Range 70% Voids
[[ ]]			
			]]



The potential effect of larger pin power uncertainty on the SLMCPR has been considered. First, in lieu of an arbitrary increase in the uncertainty, a review of [[

]] In the determination of SLMCPR, the use of additional pin power uncertainty so derived, i.e., [[  
]], providing real additional critical power margin relative to GE's standard methodology and addressing local peaking uncertainty concerns.

#### **Four Bundle Power**

GE has continued to provide the NRC with BWR fleet information on the consistency of integral TIP comparisons on periodic basis, e.g., in fuel technology updates. These comparisons provide the basis for the [[  
]] in Table 2-2. In 2005, GE provided a large amount of data for uprated plants loaded primarily with 10x10 fuel in methods related RAI responses on the MELLLA+ docket [Reference 20]. The results of plant tracking studies performed with the current methods are summarized in Table 2-5, which yield an overall [[  
]]. Examination of these data confirms the applicability and conservatism of the original [[  
]] uncertainty documented in GE's approved topical reports [References 14, NEDC-32601P-A and 15, NEDC-32694P-A] describing the SLMCPR methodology, for uprated power densities as high as 62 KW/liter.

**Table 2-5 Summary of High Power Density Plant Tracking Results**

Plant	GE BWR Type	Number of Bundles	Original Licensed Thermal Power (OLTP) MWt	Rated Flow (Flow at OLTP) Mlbm/hr	Licensed Power Uprate (PU) % OLTP	Licensed Core Flow Range at PU % Rated Flow	Power Density at Licensed PU kW/l	Cycle	Number of TIP sets	Radial RMS	Nodal RMS
[[											
]]											

1 -- Plant E is a thermal TIP Plant. All the others have Gamma TIPs

Additional detail for the core tracking and four bundle power subjects can be found in the accepted VYNPS RAI responses summarized below in Table 2-6.

**Table 2-6 Summary of Four Bundle Power Subjects**

<b>Related Technology</b>	<b>Subject</b>	<b>RAI</b>
PANACEA, ISCOR	Information provided for maximum bundle power and power density before and after EPU	SRXB-A-64
PANACEA, ISCOR	Explanation provided for increase in nodal uncertainties with elevation	SRXB-A-25
PANACEA, ISCOR	Information and discussion supplied regarding criteria for axial and nodal uncertainties	SRXB-A-27
PANACEA, ISCOR	Information and discussion of SLMCPR evaluation and monitoring accounting for axial and nodal uncertainties	SRXB-A-28
PANACEA, ISCOR	Application of nodal uncertainties and increases with exposure. Refer to SRXB-6 and SRXB-31.	SRXB-A-32
PANACEA, ISCOR	Core Follow Data Supplied	SRXB-A-35
PANACEA, ISCOR	Explanation of effect on pin power due to neighboring bundles provided with explicit results for 10x10 lattices	SRXB-A-39
PANACEA, ISCOR	Discussion of bypass voiding on instrumentation provided	SRXB-A-44
PANACEA, ISCOR	Refer to SRXB-A-19 for Representative Core definition	SRXB-A-9
PANACEA, ISCOR	Reasons for differences between PCTIP and axial power distributions provided	SRXB-A-36
PANACEA, ISCOR, ODYN	Explanation of inclusion of axial and nodal uncertainties in transient and accident evaluations provided	SRXB-A-29

**Bundle Power**

[[ ]] is a component of the total bundle power uncertainty. The total bundle power uncertainty for application within GE’s approved SLMCPR determination process consists of the component uncertainties in Table 2-2, which is from Table 4.2, page 4-2 in NEDC-32694P-A. The basis of the SLMCPR uncertainties is embodied in the 3D Simulator PANACEA and the SLMCPR methods. [[ ]]

]]

BWRs have always operated at void fractions higher than 70% with some of the earlier gamma scan data from fuel exceeding 80% void fractions so that the effect of void fraction is included in confirmation of local and bundle power peaking uncertainty and, thus, not a significant concern. Instead, the largest differences in bundle power are the result of depletion and are not the result of differing product lines, composition, or core power. This key aspect is already addressed in the current NRC approved value [[

]] Therefore, the procedure of using the original gamma scan data to determine a conservative bound on the uncertainty is adequate and reasonable.

Additional detail regarding the bundle power subject can be found in the accepted VYNPS RAI responses shown in Table 2-7 below.

**Table 2-7 Bundle Power Subject**

Related Technology	Subject	RAI
PANACEA, ISCOR	Explanation supplied for the uncertainties applied to LHGR. Refer to SRXB-A-68	SRXB-A-24
PANACEA, ISCOR	Explanation provided for increase in nodal uncertainties with elevation	SRXB-A-25
PANACEA, ISCOR	Information and discussion supplied regarding criteria for axial and nodal uncertainties	SRXB-A-27
PANACEA, ISCOR	Information and discussion of SLMCPR evaluation and monitoring supplied for axial and nodal uncertainties in safety limit analyses	SRXB-A-28

[[

]] This additional critical power margin provides adequate additional assurance of safety and is developed consistent with current NRC-approved bundle power uncertainty methodology.

The effects of [[ ]] in Table 2-2 on the bundle power uncertainty for SLMCPR determination [[

]]

### **Critical Power Correlation**

In addition to power distribution uncertainties, thermal-hydraulic parameters are also included in the SLMCPR evaluation. The GEXL correlation uncertainty is used to establish the probability of boiling transition. The application range of the GEXL correlation is illustrated in Figure 2-1.

The critical power correlation is developed from full-scale critical power test data for each fuel product line. The critical power data are obtained for bundle mass fluxes ranging from [[

]], inlet subcooling [[

]] and pressures from [[ ]]. These

data cover flow ranges from less than natural circulation to well beyond rated flow and include the flow ranges for EPU and MELLLA+ applications. These data cover bundle power levels up

to the actual critical power for each set of conditions, which is in the range of [[ ]] for 10x10 fuel. These fluid parameter ranges also cover the expected ranges for LOCA and transient events. The development of GEXL correlation coefficients and constants for a fuel assembly follows the NRC approved process described in GESTAR II [Reference 13]. Figure 2-1 shows the GE14 application range together with the expected range for typical operational transients. The box representing the correlation application range encloses the expected ranges for transients. For LOCA application, the GEXL correlation is used for the calculation of the early boiling transition during the flow coast down immediately following the break. This typically occurs when the flow has dropped to 30-50% of the initial value. This is well within the application range for the GEXL correlation. The range of bundle powers and hydraulic conditions for the GEXL correlation covers those expected in MELLLA+ and EPU operation.

**Figure 2-1 GEXL14 Application Range**

[[

]]

### **Void Fraction**

Steam void fraction uncertainty does not appear explicitly in Table 2-1, but is incorporated into the SLMCPR evaluation through the other flow related uncertainties. The void correlation is based on void fraction data up to approximately [[ ]], which covers the void fraction range expected for normal steady state operation and the abnormal operational occurrences that set the

operating limit minimum critical power ratio (OLMCPR). Attachment A, “BWR Fuel Void Fraction,” of Appendix A to NEDC-32601P-A [Reference 14], contains an extensive discussion of the void correlation, fuel design evolution, and sensitivities (e.g., nuclear performance).

As discussed in Attachment A to NEDC-32601P-A, the part length rod (PLR) is the major new feature in current fuel products. The impact of PLRs has been experimentally investigated for a 4X4 bundle for a pressure of 145 psia and more recently for an 8X8 bundle at rated BWR pressure of 1044 psia. A small increase, approximately [[ ]], was observed in void fraction downstream of the PLRs compared to the case with no PLR for the low-pressure 4X4 data. More recent representative 8X8 data taken at normal operating pressure shows a small increase, on the order of [[ ]]

]].

A void fraction of [[ ]] is relatively high and typical of the conditions where boiling transition will occur in a BWR fuel bundle. Also, since the OLMCPR is determined such that boiling transition will not occur, it is highly unlikely that a void fraction of [[ ]] will be exceeded (e.g., perhaps momentarily during a transient) by any significant amount. Some aspects of void fraction and bundle power warrant a brief discussion. For illustrative purposes, consider a one-dimensional, steady state energy balance for a BWR fuel channel. It can be shown that the flow quality is

$$X(z) = \frac{h_{in} - h_f}{h_{fg}} + \frac{1}{\dot{m}h_{fg}} \int_0^z \dot{q}'(\xi) d\xi,$$

where the definition of flow quality is given by  $X = \frac{\dot{m}_g}{\dot{m}_f + \dot{m}_g}$

The flow quality is a function of pressure (fluid properties), inlet flow rate and subcooling, and the heat addition rate. For the case of “z” equal to the exit elevation, the integral term essentially represents the channel power. The steady state exit quality is directly proportional to the integrated channel power.

**Figure 2-2 8X8 Void fraction Data – Sensitivity to PLR for Low Flow**

[[

]]

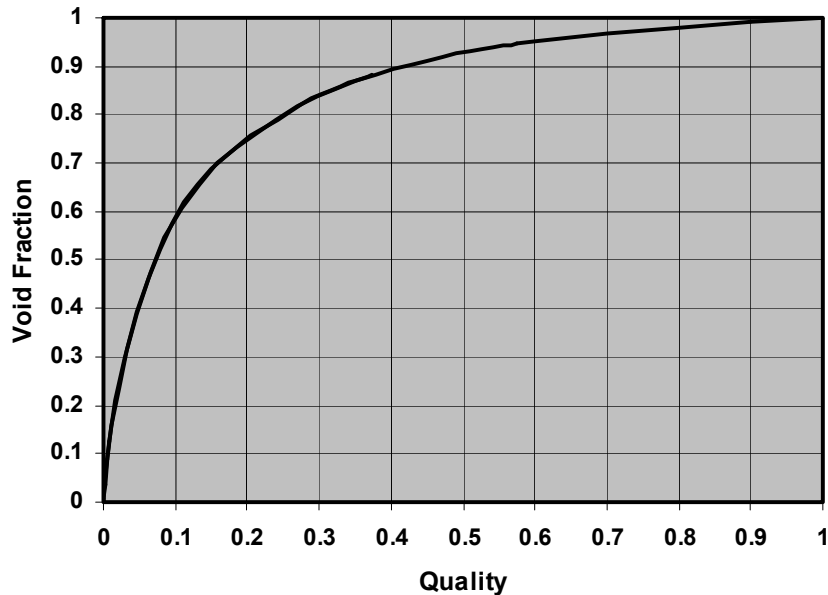
[[

**Figure 2-3 8X8 Void fraction Data – Sensitivity to PLR for High Flow**

]]



**Figure 2-4 Typical Void-Quality Relation at High Power/Flow Ratio**



It should be recognized that a BWR fuel bundle is designed and operated such that boiling transition will not occur during steady-state or abnormal operational occurrences, and, therefore, high void fractions, i.e., higher than [[ ]], will not occur. Figure 2-4 illustrates this point, noting that less than half of the quality range ( $X < 0.5$ ) covers up to 90% void fraction. A significant power increase (or a factor of 2 change in quality) is required to drive the void fraction from 90 to 100%. It would require a bundle power of approximately [[ ]] for a bundle at rated flow to reach a void fraction of [[ ]], while in reality a high power fuel bundle operates at approximately [[ ]].

The void quality correlation is based on sound physical principles, particularly for high void fractions, and extrapolates the measured data to a void fraction of 1.0. Using the Zuber-Findlay expression [Reference 16] for two-phase flow, the void fraction  $\alpha$  can be expressed as

$$\alpha = \frac{j_g}{C_0 j + \overline{V}_{gj}}$$

Where:

- $C_0$  = distribution parameter
- $\overline{V}_{gj}$  = drift velocity
- $j_g$  = volumetric flux of steam vapor
- $j$  = volumetric flux of the mixture

The drift velocity is the difference in velocity between the vapor and liquid phase. Generally the vapor phase velocity is greater because of buoyant forces. At high quality, the annular flow regime predominates. In the annular flow regime the liquid phase surrounds the fuel rods and channel. As the void fraction increases, the drift velocity decreases, as the buoyant forces become less important. In the GE void correlation, the drift velocity is characterized as

$$\overline{V}_{gj} \propto (1 - \alpha)$$

This characterization is applied over the entire annular flow region, or for void fractions greater than about 0.4. For high void fractions and small values of  $\overline{V}_{gj}$ , the void fraction is dominated by the ratio of vapor mass flux to total mass flux, determined by a simple mass and energy balance for each node. The outstanding agreement with the data demonstrated by Table 2-8 and the trends shown in Figure 2-2 and Figure 2-3 over the entire range validates this simple model for the drift flux.

**Table 2-8 Comparison Between Void Correlation and Database**

Data Source	Data Points (N)	Average Error $\overline{\Delta\alpha} = \overline{\alpha_m} - \alpha_c$	Standard Deviation $S_{\Delta\alpha}$
[[			
			]]
(References 14 and 17)			

An extrapolation based on this model to void fractions all the way to pure steam flow is justified. In summary, the GE void correlation is based on test data and covers a broad range of conditions. The correlation supports the full range of conditions expected during BWR operation, including CPPU, EPU and MELLLA+ conditions. The correlation uncertainty is appropriately accounted for in the SLMCPR. It is not necessary to incorporate additional margin for void fraction uncertainty.

Additional detail regarding the thermal-hydraulic subjects can be found in the accepted VYNPS RAI responses shown in Table 2-9 below.

**Table 2-9 Thermal-Hydraulic Subjects**

<b>Related Technology</b>	<b>Subject</b>	<b>RAI</b>
Void and pressure drop correlations	Pressure Drop data base information provided, reference made to generic MELLLA+ report	SRXB-A-52
Void and pressure drop correlations	Void fraction measurement data made through Safety Limit Document reference	SRXB-A-53
Void and pressure drop correlations	Are void fraction uncertainties included in water density? Explanation provided	SRXB-A-54
Void and pressure drop correlations	Explanation and information provided regarding Void fraction uncertainties	SRXB-A-69
Void and pressure drop correlations	Explanation provided regarding acceptable to exceed correlations range. Refer to SRXB-A-55	SRXB-A-70

**2.2.1.3 Adequacy of Existing Treatment and Alternate Approach**

The use of alternative, more conservative, values for uncertainties in the local peaking factor [[ ]] results in an increase in the SLMCPR relative to that calculated with current GE standard methodology. [[ ]]

[[ ]] 0.02 ΔCPR effect on SLMCPR based on the conservatively increased local peaking [[ ]] uncertainties. The approach for the SLMCPR evaluation applied to updated operating conditions involves a two-step process. First, the SLMCPR is evaluated following the standard (cycle specific) process. Second, this evaluation is repeated with the increased uncertainties discussed in Section 2.2.1.2. The final SLMCPR is determined as the greater of the standard evaluation with an additional 0.02 ΔCPR (added to the safety limit), or the SLMCPR calculated with normal approved GE methods and the increased uncertainties. This approach accounts for any potential unique situations or designs and provides additional reasonable assurance of safety with respect to SLMCPR. No other uncertainties warrant an increase in the SLMCPR margins or considerations in the evaluation process.

## 2.2.2 Operating Limit Critical Power Ratio (OLMCPR)

The analysis of anticipated operational occurrences (AOOs) examines the change in critical power ratio relative to the starting initial conditions and determines the most limiting event.

### 2.2.2.1 Fuel Parameters That Affect OLMCPR

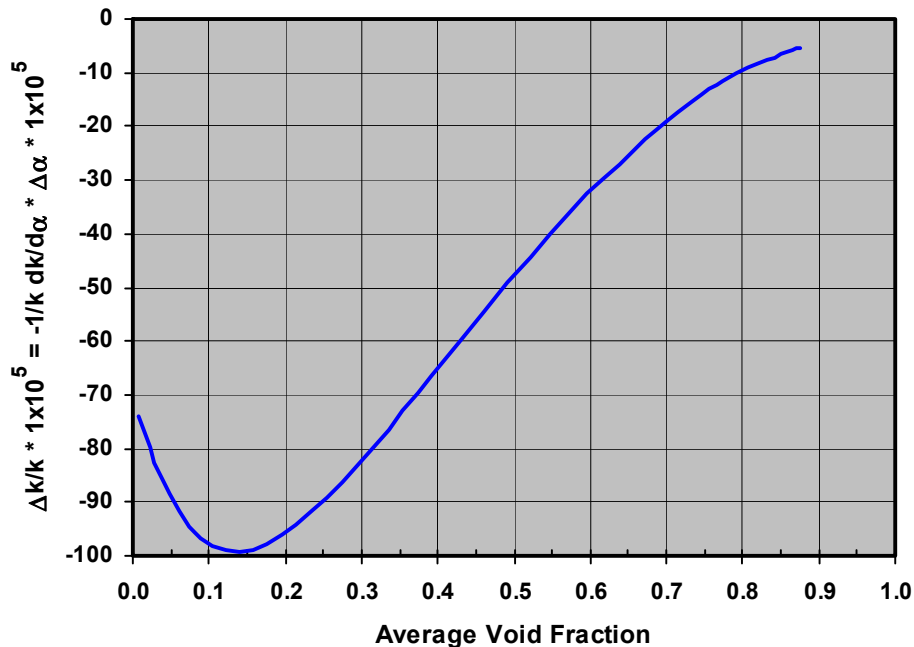
The fuel parameters identified previously, i.e., the local pin power peaking, void reactivity coefficient, and three dimensional power distribution are factors in the evaluation of limiting AOOs. The typical AOO response (e.g., pressurization event) is mainly affected by the reactivity void coefficient and the axial power distribution at the beginning of the event. Power distributions peaked to the top of the core will reduce the scram reactivity early in the transient and most of the time will increase the transient MCPR change. The transient response also depends on the void and Doppler coefficients of reactivity. An increase in fuel temperature increases the resonance absorption in the fuel isotopes and reduces the reactivity during a pressurization transient. The overall Doppler effect is, however, quite small in BWRs and uncertainties in Doppler reactivity have a negligible effect on transient behavior. The transient behavior is more sensitive to the void reactivity coefficient. A larger void coefficient can increase the initial flux increase during a pressurization transient such as a turbine trip, but will also act to aid in shutdown once the increase in power results in revoiding the core.

Figure 2-4 shows a typical plot of the void-quality relationship for a flow typical of a high power/flow ratio fuel bundle for the entire range from zero to one. Recognizing the relationship between quality and energy input (channel power), the figure has two interesting points relevant to discussions of the void coefficient and void feedback. First, Figure 2-4 shows that the lower end of the quality range has a relatively steep slope. Small power changes in this lower quality range correspond to a relatively large void fraction change. This behavior has implications relative to the impact of the void coefficient. In general, the void coefficient becomes more negative with increasing (average) void fraction. However, the net power effect considering the void-quality behavior is that in general, core power response is more strongly influenced by regions of the core with low void fraction. In other words, the quantity  $\Delta\alpha \cong \left(\frac{\partial\alpha}{\partial X}\right)\Delta X$  tends

to be larger at low void fraction, so that the effective feedback  $\Delta k/k \cong 1/k (\partial k/\partial \alpha) \Delta \alpha$  tends to be larger. Second, the higher quality (or power) range is relatively flat with respect to void fraction. Changes in power at high quality result in relatively small void fraction changes. In terms of core power response, effective void feedback tends to be milder at higher void fractions.

Void coefficient uncertainties and biases have a lower effective worth (in terms of reactivity feedback) at high void conditions than at lower void conditions. This relative difference is depicted in Figure 2-5, which was derived from the void and quality values shown in Figure 2-4 combined with a simple expression for the derivative  $\partial \alpha/\partial X = f(X)$  based on a homogeneous flow model. Figure 2-5 shows the reactivity effect of a small quality perturbation ( $\Delta X = 0.001$ ) using a representative void coefficient over a range of void fraction values.

**Figure 2-5 Reactivity Change for a Small Quality Perturbation ( $\Delta X = 0.001$ ) as a Function of Void Fraction**



Accommodation for uncertainties in local pin power peaking and [[ ]] (and bundle power), i.e., consideration of bundle and nodal powers higher (or lower) than expectations, is directly incorporated in the licensing methodology. Thus, there is no effect on

$\Delta$ CPR due to the NRC staff questions regarding the local pin power peaking and [[  
]] uncertainties.

### **2.2.2.2 Treatment of Fuel Parameter Uncertainties**

As stated above, the core axial power shape can influence the transient response. Uncertainties in the axial power shape are not directly included in the transient response uncertainty. Rather the input conditions for the transient are developed in a way that ensures that the axial shape is conservative. [[

]] This assures that the analysis is both realistic but conservative.

Both the ODYN and TRACG transient methodologies [References 21, 22, and 23] have established application ranges for void coefficient uncertainty. The approval of and GE confidence in the basis for these methodologies are based upon comparison of calculations for a wide variety of plant transients in which the nominal void coefficient is used. The acceptable performance of these codes relative to the data justifies that no large errors in void coefficient exist. The response to VYNPS questions related to void coefficients are SRXB-A-51 and SRXB-A-68 included in References 4 and 7.

The TGBLA06 methodology is applied in core design, transient analysis, stability analysis, and monitoring. TGBLA06 and MCNP have been utilized to generate void coefficient data and for 5 representative 10x10 lattices for the full range of instantaneous void (called IV) conditions. The calculations are based on a 40% void history (called VH) depletion followed by branch calculations at 0, 40, and 70% IV. The results are extrapolated above 70% IV. The average bias

over the full exposure range is approximately [[ ]] at 70% IV. The average bias at 40% IV is approximately [[ ]]. Over this IV range, the magnitude of the bias is considered [[ ]]. The average uncertainty at 70% IV is [[ ]]. This uncertainty is representative of the 40% void fraction range (also [[ ]]). The value assumed in the Revised Supplementary Information Regarding Amendment 11 to GESTAR [Reference 24] is [[ ]]

Additional analyses have been performed in which MCNP calculations have been performed from 40% void history, 70% void history, and 90% void history. MCNP branch cases have been performed to instantaneous voids of 70%, 80% and 90%. These analyses were performed for lattice exposures of [[ ]]

]] Table 2-10 provides the TRACG results.

**Table 2-10 TRACG Impact of High Exposure Void Coefficient Bias**

Parameter (*)	Base	High Exposure Biased	** % Difference
[[			
			]]
<p>* LRNBP is Generator Load Rejection without Bypass, MSIVF is MSIV Closure with Flux Scram            ** % Difference is defined as (High Exp Biased – Base)/ (High Exp Biased) X 100</p> <p>[[</p> <p style="text-align: right;">]]</p>			



[[

]]

In summary, for applications that utilize TGBLA06 based modeling (PANAC11, ODYN, TRACG, and ODYSY) the evaluation discussed above for [[ ]] void fraction and summarized in Table 2-11 is applicable to the consideration of both the TGBLA06 cross section extrapolation process and the TGBLA06 void history assumption.

**Table 2-11 Void Coefficient Comparison between TGBLA06 and MCNP**

Exposure (GWd/ST)	Void Coef TGBLA06 (dk/dα)/k	Void Coef MCNP (dk/dα)/k	% Difference	Standard Deviation for 5 lattices
[[				
				]]

An assumption of [[ ]] bias and a 2σ uncertainty of [[ ]] is justified.

The key transients analyzed were pressurization events in which the void fraction decreases due to increasing core pressure and then later increases due to higher heat flux. These conclusions can also be applied to cold water events. The transient response to cold-water events initiated by lower feedwater temperature is generally less severe than the pressurization events initiated from full power. For example,

- The feedwater controller event (FWCF) triggers a rise in reactor power, which in turn initiates a turbine trip. Hence sensitivities developed for other pressurization events apply to the FWCF transient.
- The loss of feedwater heating (LOFW) event initiates a slow rise in power to a level just below the APRM scram set point. This event is analyzed by the PANACEA steady-state simulator. The initial and final core void fractions for this event are nearly the same, because the effect of the reduced inlet temperature is offset by the increased reactor power. The sensitivity of this event to variations in void coefficient is negligibly small as discussed in Section 8.4.1.5 of NEDE-32906P-A. [Reference 23]
- Transients initiated from operation with feedwater heating out of service (FWHOOS) are less severe, because they start from a lower power and result in a lower pressurization rate. Sensitivities developed for other transients initiated from full power can be applied to one initiated from FWHOOS conditions.

The ODYN model uncertainty is based on comparisons to the benchmark Peach Bottom turbine trip tests. [[

]]

Because inputs to the OLMCPR analysis are conservative, and the pressurization transients that typically establish the limiting  $\Delta$ CPRs are conservatively analyzed by TRACG or ODYN, the conservatism in the process of determining OLMCPRs address NRC questions related to gamma scans and fuel isotopics as they relate to OLMCPR.

Additional detail regarding the OLMCPR subjects can be found in the accepted VYNPS RAI responses shown in Table 2-12 below.

**Table 2-12 OLMCPR Subjects**

<b>Related Technology</b>	<b>Subject</b>	<b>RAI</b>
ODYN	NRC staff approved evaluation model identified for ATWS and discussion provided on EOP's	SRXB-A-22
ODYN	Explanation of uncertainties in power during transients	SRXB-A-58
ODYN	Over pressure protection analysis code was identified	SRXB-A-7
TGBLA, MCNP	Explanation of Cross Sections for High void operation provided. Refer to generic EPU and MELLLA+ studies	SRXB-A-46
TGBLA, MCNP	Plots of isotopic concentrations provided	SRXB-A-47
TGBLA, MCNP	Information on the isotopic influence on void coefficient	SRXB-A-48
TGBLA, MCNP	Discussion provided on Void reactivity coefficients for transients and accidents, including ATWS and SBO.	SRXB-A-51
TGBLA, MCNP	Explanation provided on the effect of EPU on spent fuel storage Refer to SRXB-A-11	SRXB-A-61
TGBLA, MCNP	Describe transients used to determine MCPR	SRXB-A-63
TGBLA, MCNP	CASMO/TGBLA code comparisons	SRXB-A-66
TGBLA, MCNP	Void reactivity coefficients -- provided more information than response to SRXB-A-51	SRXB-A-68
TGBLA, MCNP	Clarification and detail on response to SRXB-A-57	SRXB-A-71

### **2.2.2.3 Adequacy of Existing Treatment and Alternate Approach**

The standard GE methodologies utilized to establish the OLMCPR conservatively address uncertainty issues and provide reasonable assurance of safety for CPPU and EPU applications including MELLLA+.

## **2.3 SHUTDOWN MARGIN (SDM)**

The Technical Specification for Shutdown Margin requires that the core be designed so that it can be shut down at any time in life while in the most reactive condition (usually cold, 20°C) with the most reactive control blade removed. This condition is verified by experiment at cycle startup and is often repeated later in the operating cycle.

### **2.3.1 Fuel Parameters That Affect SDM**

The analysis of SDM considers whether core reactivity can be safely controlled. The fuel parameters identified previously, i.e., the local pin power peaking and [[

]], are secondary factors in the evaluation of SDM since uncertainties in those parameters may ultimately influence prediction of fuel depletion and, thus, fuel reactivity. Void reactivity coefficient is not a contributor since essentially zero voiding is present at hot or cold shutdown conditions. The GE bundle lattice and core simulation methodologies are best estimate predictions so that validation of operating benchmark data, core follow, and core licensing can proceed using consistent methodology. Comparisons to actual plant cold critical states are an important part of this validation because errors in bundle or nodal power (or exposure) would tend to degrade the ability of the core simulator to establish a stable bias (in eigenvalue), which is a measure of the ability of the model to reliably predict core hot and cold critical conditions. Conversely, the establishment of a stable eigenvalue bias for hot and cold critical conditions is indicative of adequate fidelity of the model to predict bundle and nodal power and exposure.

### **2.3.2 Treatment of Fuel Parameter Uncertainties**

A shutdown margin demonstration experiment is performed at the beginning of each operating cycle. This demonstration is performed in the cold, or most reactive criticality condition. The demonstration configuration attempts to simulate the most reactive rod out condition. In order to obtain a critical condition, other rods are also withdrawn. The 3D simulator [Reference 18] is used to calculate the demonstration condition. Let  $k_{\text{demo}}$  be the calculated critical eigenvalue for the demonstration condition. The cold shutdown technical specification requires that

$$k_{\text{sro}} \leq k_{\text{demo}}(1. - 0.0038)$$

where  $k_{\text{sro}}$  is the calculated criticality for the strongest rod withdrawn condition and 0.0038 is the required shutdown margin. This required shutdown margin is meant to account for possible differences in critical eigenvalue between the demonstration condition and the technical specification condition. The value was originally determined to account three uncertainties on the critical configuration: the impact of manufacturing tolerances, variations in predictive capability within the same core and variations in exposure on the critical configuration. The 0.0038 magnitude represents the 2 sigma value of the RMS combinations of the aforementioned uncertainties. The current validity of the 0.0038 requirement can be determined by comparing

critical eigenvalue demonstrations, all of which are carried out on the same core. Figure 2-6 below is a reproduction of one shown in the response to [Reference 20] and is a summary of the cold critical analyses carried out on the five reference plants.

**Figure 2-6 Reference Plants Cold Critical Eigenvalues**

[[

]]

Of the 39 critical experiments shown in Figure 2-6, there were five cores, summarized in Table 2-13, for which multiple cold critical experiments were performed on the same core. The standard deviation of the critical eigenvalues for the cores in Table 2-13 relative to the average obtained for the same core is [[                      ]]. This standard deviation can be compared to the Technical Specification allowance of 0.38%  $\Delta k/k$ ., indicating that for application to high power density cores, the data supports the continued use of the current Technical Specification limit.

**Table 2-13 Summary of Same Core Critical Experiments**

Plant	Cycle	Cycle Exposure (GWD/ST)	Number of Critical Experiments	Standard Deviation of $k_{demo}$
[[				
				]]

While the Technical Specification for SDM is 0.38%  $\Delta k/k$  reactivity (for an in-sequence check only), normal GE design procedure is to provide design cold shutdown margins of 1% or more depending on customer request and GE procedure. The standard design SDM is 1.0%  $\Delta k/k$  to provide additional flexibility in cycle length and operations, although each plant is free to require more design margin if deemed appropriate. The uncertainty in cold critical predictive capability is considered and included in this choice of SDM requirement. The ability to meet the projected margin has also been evaluated for the data presented in Figure 2-7. Before cycle startup, a cold critical eigenvalue is projected for the cycle. This critical eigenvalue is based on previous cycle experience and is the result of a well-defined design procedure. The difference between the projected and measured eigenvalue is plotted in Figure 2-7 as a function of cycle exposure. The standard deviation of the differences is [[                      ]]. The behavior shown in Figure 2-7 shows that the nuclear methods together with procedures for projecting critical eigenvalues for the next cycle accurately predict design margins.

**Figure 2-7 Difference Between Measured and Predicted Cold Critical Eigenvalues**

[[

]]

A failure to meet the Technical Specification SDM requirement is severe in that a redesign of the core loading and/or fuel design would be required to restart the plant. A design margin of 1% SDM has been used by GE for many years to ensure that  $\geq 0.38\% \Delta k/k$  is always satisfied. The additional margin between the Technical Specification SDM and 1% allows for the following factors to impact the prediction capability of the simulator:

1. Operation of the plant different than that projected
2. Fuel manufacturing tolerances
3. Control rod worth reduction due to depletion of control rod absorber material
4. Methodology approximations
5. Inexact tracking of actual plant parameters
6. Other unidentified factors

Of these factors, the most significant is allowance for operation different from that projected. Each core design must maintain sufficient operational flexibility to protect the core and fuel while meeting economic objectives. Factors affecting the GE application methodology are quantified through the uncertainty in cold critical eigenvalue and deviation from expectations.

### **2.3.3 Adequacy of Existing Treatment and Alternate Approach**

The current design process and Technical Specification SDM, in combination with the existing plant verification of SDM and trending of hot eigenvalues, provide reasonable assurance of adequate SDM. The GE procedure of designing for 1% SDM provides substantial additional assurance of adequate SDM.

## **2.4 FUEL ROD THERMAL-MECHANICAL PERFORMANCE**

For each GE/GNF fuel design, thermal-mechanical based linear heat generation rate limits (LHGR Operating Limits) are specified for each fuel rod type (for both UO<sub>2</sub> and gadolinia-bearing rods) such that, if each rod type is operated within its LHGR limit, all thermal-mechanical design and licensing criteria, including those which address response to anticipated operational occurrences (AOOs), are explicitly satisfied and fuel rod integrity is maintained.

### **2.4.1 Fuel Parameters That Affect Thermal-Mechanical Limits**

The fuel parameters identified previously, i.e., the local pin power peaking, void reactivity coefficient, [[ ]], are factors, to differing extents, in the development of LHGR Operating Limits. These fuel parameters ultimately determine the local power, which is explicitly addressed by the LHGR Operating Limit.

### **2.4.2 Treatment of Fuel Parameter Uncertainties**

A number of fuel rod thermal-mechanical analyses are performed to evaluate fuel performance relative to Specified Acceptable Fuel Design Limits (SAFDLs). The SAFDLs include considerations such as the fuel rod internal pressure developed during normal steady-state operation, and the maximum fuel temperature and cladding strain experienced during Anticipated Operational Occurrences (AOOs). An output from these analyses is the specification



of an LHGR Operating Limit, in conjunction with a [[ ]] exposure limit. LHGR Operating Limits are determined and specified in the form of allowable [[ ]] LHGR as a function of [[ ]] exposure. These fuel rod thermal-mechanical performance based operating limits are specified for each fuel rod type (UO<sub>2</sub> or (U,Gd)O<sub>2</sub> for various gadolinia concentrations) so that if each fuel rod type is operated within its respective exposure-dependent LHGR limit, all thermal-mechanical design and licensing criteria (SAFDLs), including those which address response to AOOs, are explicitly satisfied.

The exposure-dependent LHGR Operating Limits are determined through the performance of a number of fuel rod thermal-mechanical analyses. An important assumption with these analyses is [[

]]. This assumption represents a significant conservatism; [[

]]

With this conservative [[ ]] assumption, the thermal-mechanical analyses are performed either on a worst tolerance basis or statistically. For those analyses performed statistically, such as the fuel rod internal pressure analysis, the uncertainty in each fuel rod fabrication parameter is determined and specifically addressed. The fuel rod thermal-mechanical model prediction uncertainty is also determined and addressed. [[

]]

For the GE14 fuel rod thermal-mechanical design and licensing analyses, the values of the preceding component uncertainties are: [[

]]

The LHGR Operating Limit is derived for an individual fuel design using the following basic procedure.

[[

]]

[[

]]

**Table 2-14 Summary of Uncertainty Components for LHGR Evaluations**

Component	NEDE-32601	Revised
[[		
		]]

[[

]]

Additional detail regarding the LHGR Operating Limit subjects can be found in the accepted VYNPS RAI responses shown in Table 2-15 below. The relationship between the methods uncertainties and LHGR criteria is summarized in the response to SRXB-A-65.

**Table 2-15 Fuel Performance Related Subjects**

<b>Related Technology</b>	<b>Subject</b>	<b>RAI</b>
GSTRM (GESTR-Mechanical)	Uncertainties in LHGR limit evaluations	SRXB-A-65
PANACEA, ISCOR	Uncertainties applied to LHGR	SRXB-A-24
PANACEA, ISCOR	Application of nodal uncertainties to nodal exposure to MAPLHGR and LHGR values	SRXB-A-30
PANACEA, ISCOR	Does LHGR limit in 3D simulator include decrease with exposure	SRXB-A-31
PANACEA, ISCOR	Application of nodal uncertainties and increases with exposure	SRXB-A-32
PANACEA, ISCOR	Describe how core monitoring system calculate pin wise power parameters	SRXB-A-33
PANACEA, ISCOR	Effect on pin power due to neighboring bundles	SRXB-A-39

### 2.4.3 Adequacy of Existing Treatment and Alternate Approach

The standard GE methodology for determining LHGR limits includes conservative consideration for, and provides reasonable assurance of adequate margin to address, the power and void reactivity uncertainties in question.

## 2.5 LOCA RELATED NODAL POWER LIMITS

The purpose of the maximum average planar linear heat generation rate (MAPLHGR) limits is to assure adequate protection of the fuel during a postulated loss-of-coolant accident (LOCA) with the defined operation of the emergency core cooling system (ECCS).

### 2.5.1 Fuel Parameters That Affect LOCA Related Nodal Power Limits

The fuel parameters identified previously, i.e., the local pin power peaking and [[  
]], are factors, to differing extents, in the development of LHGR limits. The fuel parameters ultimately determine the local power, which is the subject of the MAPLHGR, a local limit. The void reactivity coefficient is not a factor in the ECCS-LOCA analysis.

### 2.5.2 Treatment of Fuel Parameter Uncertainties

The ECCS-LOCA analysis follows the NRC-approved SAFER/GESTR application methodology documented in Volume III of NEDE-23785-1-PA [Reference 25]. The analytical models used to perform ECCS-LOCA analyses are documented in Volume II of NEDE-23785-1-PA [Reference 26] together with NEDE-30996P-A [Reference 27] and NEDC-32950P [Reference 28].

When SAFER/GESTR methodology is applied, the hot bundle is initialized with a [[  
]] In addition, a [[

]] In order to ensure that the SAFER analysis is bounding for all exposures, the hot rod of the hot bundle is placed at the exposure corresponding to the [[  
]] In addition to these analytical conservatisms, margin to the MAPLHGR limits is maintained during plant operations.

Total bundle power is also important to the severity of the ECCS-LOCA analysis. [[

]] Furthermore, the ECCS-LOCA basis target MCPR is

set lower than the OLMCPR so that the OLMCPR is not set by the ECCS-LOCA analysis (i.e., it is set by the AOO analysis).

Pin power peaking for the hot rod is set to a [[  
]] to further ensure that the ECCS-LOCA results are bounding.

Lastly, the axial power profile [[

]]

The above considerations indicate that significant conservatisms related to initial local pin and bundle powers exist in the GE SAFER/GESTR ECCS-LOCA methodology.

In addition to the above conservatisms, the Licensing Basis peak cladding temperature (PCT) determined by the methodology described above must be greater than the Upper Bound PCT. The Licensing Basis PCT includes application of Appendix K modeling assumptions and plant variables uncertainties. The Upper Bound PCT in the SAFER/GESTR methodology adjusts the nominal PCT to account for modeling and plant variable uncertainties (at 95% probability). The 95% probability PCT includes an uncertainty of [[  
]] on the LHGR.

Additional detail regarding the LOCA/ECCS analyses can be found in the accepted VYNPS RAI response shown in Table 2-16 below.

**Table 2-16 LOCA/ECCS Related Subjects**

<b>Related Technology</b>	<b>Subject</b>	<b>RAI</b>
SAFER	Information supplied regarding PCT difference in VYNPS LBLOCA analysis	SRXB-A-10

The SAFER/GESTR methodology assumes a bounding post-LOCA core power decay and, thus, core kinetics are not modeled. The average and hot bundle void profile is determined by SAFER at the limiting initial conditions described above as well as at the post-LOCA conditions. Uncertainties in predictions of void reactivity have no impact in the SAFER/GESTR methodology. The overall SAFER/GESTR methodology is designed to maximize the PCT.

### **2.5.3 Adequacy of Existing Treatment and Alternate Approach**

The conservatism of the present ECCS-LOCA methodology used to determine MAPLGHR limits adequately considers the effects of the uncertainties in local and bundle power and provides adequate and reasonable assurance that those limits provide adequate margin to protect the fuel.

## **2.6 STABILITY**

Thermal-hydraulic stability analyses are performed to assure that the SLMCPR is protected in the event of a thermal-hydraulic instability event. Specific analyses are associated with each of the long-term stability solutions that have been licensed and implemented in the U.S. These long-term solutions include Option I-D, Option II, Option III, and Enhanced Option I-A.

10CFR50, Appendix A, General Design Criterion (GDC) 10 requires that the reactor core and associated coolant, control, and protection systems shall be designed with appropriate margin to assure that specified acceptable fuel design limits are not exceeded during any condition of normal operation, including the effects of anticipated operational occurrences.

10CFR50, Appendix A, GDC 12 requires that the reactor core and associated coolant, control, and protection systems shall be designed to assure that power oscillations which can result in conditions exceeding specified acceptable fuel design limits are not possible or can be reliably and readily detected and suppressed.

### **2.6.1 Fuel Parameters That Affect Stability**

The fuel parameters identified previously, i.e., the local pin power peaking, void reactivity coefficient, and [[ ]], affect stability performance to differing extents.

### **2.6.2 Treatment of Fuel Parameter Uncertainties**

The treatment of the fuel parameter uncertainties for each of the long-term stability solutions listed above is provided in the following discussion.

#### **2.6.2.1 Option I-D**

Option I-D has (1) “prevention” elements and (2) a “detect & suppress” element. The prevention portion of the solution includes separate administratively controlled exclusion and buffer regions, which are evaluated for every reload. The detect-and-suppress portion of the solution is a flow-biased APRM flux scram trip that prevents oscillations of significant magnitude. This scram ensures the Fuel Cladding Integrity SLMCPR is protected for the dominant core wide mode of coupled thermal-hydraulic/neutronic reactor instability.

Stability analyses for both the EPU and fuel cycle specific conditions are performed to define the exclusion and buffer regions as well as to confirm that the scram setpoints meet the design basis. With respect to power distribution uncertainties of the nuclear simulator data, the results pertaining to the exclusion region may be slightly affected, but this is not considered to have any safety significance for reasons described below. The power distribution uncertainties of the nuclear simulator data are considered in the determination of the limiting bundle conditions and therefore have insignificant impact on the flow-biased APRM flux scram trip setpoint and the SLMCPR protection. An increase to the void reactivity used in the GE stability analysis models (the frequency domain code ODYSY and the time-domain code TRACG) may also affect the predicted results. However, the current stability models have been used to model actual instability events, and the decay ratio acceptance criteria have been established consistent with the uncertainty as documented in the approved licensing reports. Furthermore, recent instability events at two domestic BWRs have also been evaluated with the stability models and shown to



meet the previously established criteria. This provides high confidence that the GE methodology is adequately simulating recent fuel designs and fuel power densities. Therefore, no adjustment to stability models or analysis is necessary due to potential void reactivity uncertainties.

### ***Exclusion Region Calculation***

The NRC-approved ODYSY methodology (NEDC-32992P-A) is used in the exclusion region calculation for every reload [Reference 29]. The calculation of the exclusion region boundary is based on a very conservative core wide decay ratio ([[ ]]) that may be influenced by the core wide axial power distribution calculation. [[

]] An additional protection feature includes a cycle-specific buffer region, which is 5% in rated core power or 5% in rated core flow, beyond the exclusion region. Manual monitoring of the decay ratio is required while operating in the buffer region.

The decay ratio calculation includes a cycle-specific confirmation that core wide oscillation is the predominant reactor instability mode and that regional mode instability is not probable. The dominance of the core-wide mode oscillation is confirmed for every reload at the most limiting state point on the EPU power/flow map. The calculation to confirm that the regional mode of instability is not likely to be affected by uncertainties in power distribution because it considers the limiting bundle power. [[

]] Therefore, reasonable potential local or bundle power distribution uncertainties do not affect the confirmation that regional oscillations are not likely for plants with the Option I-D stability solution.

### ***Detect and Suppress Calculation***

The detect and suppress evaluation for Option I-D plants is performed under the approved LTR basis (NEDO-32465-A) [Reference 30]. The flow-biased APRM scram setpoints are initially established with conservative margin such that they are found applicable to future fuel cycles during reload confirmation calculations. The calculation of the scram setpoints is based on the limiting fuel bundle being at the Operating Limit MCPR (OLMCPR) and the SLMCPR not being exceeded during the instability oscillation.

The detect and suppress calculation requires the use of the DIVOM (which is defined as the Delta CPR over Initial MCPR Versus the Oscillation Magnitude) curve. Per the BWROG Guideline, Plant-Specific Core-Wide Mode DIVOM Procedure Guideline, [Reference 31] a plant and cycle-specific DIVOM evaluation is used to establish the plant specific relationship between the Hot Channel Oscillation Magnitude (HCOM) and the relative change in MCPR such that the initial MCPR value corresponds to the OLMCPR and the limiting MCPR value remains above the SLMCPR. [[

]]

[[

]] The scram setpoint analytical limit is established such that the hot channel power is maintained below acceptable values.

### ***Bypass Voiding***

The following discussion provides an assessment of the impact of bypass voiding on the effectiveness of the flow-biased APRM scram to provide SLMCPR protection for Option I-D. The primary effect of voiding in the bypass region on the neutron detectors (LPRMs and TIPs) is to reduce the detector response, assuming the same power in the adjacent fuel. This reduction is due to a decrease in the moderation caused by the presence of voids, which decreases the thermal neutron flux incident on the detectors for the same neutron flux generated in the adjacent fuel.

There is also the potential for some additional noise in the neutron flux signal, but that has a minor impact on steady state operation. These impacts are greatest for the highest elevation LPRM (D level) where the highest bypass voiding occurs.

For the Option I-D stability solution, the APRM flow-biased scram is used to mitigate stability transients. The analytical limit for the scram setpoint is based on assuring that the scram occurs before power oscillations become large enough to cause the MCPR to approach the SLMCPR. High bypass voids can potentially reduce the APRM reading, and so the margin to scram would increase and this could be non-conservative from the stability mitigation point of view since it would take higher amplitude oscillations to initiate an APRM scram.

The worst-case impact is at natural circulation (following a two recirculation pump trip) when the bypass voids are highest. An evaluation was performed at this condition for the Vermont Yankee plant (49.4% power and 31.3% core flow). [[

]]

The flow-biased APRM scram setpoint analytical limits are initially established with conservative margin such that they are found applicable to future fuel cycles during reload confirmation calculations. The calculation of the scram setpoint analytical limits is based on the limiting fuel bundle being at the OLMCPR and the SLMCPR not being exceeded during the power oscillation. The detect and suppress evaluation for Vermont Yankee Cycle 24 under EPU conditions was reevaluated to assess the impact of bypass voiding on the safety margins. The detect and suppress calculation assumes a flow runback along the rated licensing rodline to natural circulation flow. The flow-biased APRM trip analytical limit at natural circulation is 53.7% of rated power. [[

]] Hence, the SLMCPR is fully protected for Option 1-D plants, including the effects of bypass voiding.

The increased voiding in the bypass region could potentially affect (increase) the LPRM noise because of the steam bubbles going by the LPRM instrument assembly in the water gap. The increase in noise depends upon the bubble dynamics as described below. Note that the discussion in this section refers only to the extra noise caused by the bubbles in the bypass region, and not the normal noise (~2% for APRM) that is present because of the flow induced

vibration of the LPRM assembly in the water gap and because of other thermal-hydraulic phenomena inside the fuel channels. Note that there is an additional LPRM detector noise component due to the random nature of the process that produces neutron flux, which is proportional to the square-root of the neutron flux and is the source of the signal used for the IRM detectors. However the magnitude of that noise for LPRMs is small in the low frequency range of interest in this measurement, and does not need to be considered for this evaluation.

[[

]]

The noise due to bypass voids slightly increases the overall APRM neutron noise at off-rated conditions where the voids may be significant. However, the impact of this noise on the APRM scram setpoint is negligible because the setpoint (derived from the analytical limit by considering noise and other instrument errors) is based on the normal (no void) noise at rated conditions (~2% of rated power), and this bounds the increased noise at off-rated conditions because the decrease in normal noise at off-rated conditions is more than the increase due to bypass voiding.

An assessment of the impact of the 40% void depletion history assumption on stability can be summarized as follows. As stated in Section 2.2.2.2, [[

]]

A similar assessment can be made for the axial and radial power distributions. Therefore, based on these assessments and those provided above, no adjustment to stability models or analysis is necessary due to potential void coefficient or power distribution uncertainties.

An assessment of the impact of extrapolating beyond 70% voids on stability can be summarized as follows. As stated in Section 2.2.2.2, [[

]] Therefore, no adjustment to stability models or analysis is necessary due to potential void coefficient uncertainties.

There may be differences in bypass voiding between GE and non-GE fuel due to their geometric and lattice differences, however the impact on stability is insignificant because of the need for thermal-hydraulic compatibility of the fuel types in the core.

### **2.6.2.2 Option II**

Option II has (1) a “prevention” element and (2) a “detect & suppress” element. The prevention portion of the solution includes an administratively controlled exclusion region, which is evaluated for every reload. The detect-and-suppress portion of the solution is a quadrant-based flow-biased APRM flux scram trip that prevents oscillations of significant magnitude. This scram ensures the Fuel Cladding Integrity SLMCPR is protected for both the core wide and regional modes of coupled thermal-hydraulic/neutronic reactor instability. Option II differs from Option I-D in that it has no buffer region and the quadrant-based APRM is able to detect both regional and core-wide mode oscillations.

Stability analyses for both the EPU and fuel cycle specific conditions are performed to define the exclusion region as well as to confirm that the scram setpoints meet the design basis. With respect to power distribution uncertainties of the nuclear simulator data, the results pertaining to the exclusion region may be slightly affected, but this is not considered to have any safety significance for reasons described below. The power distribution uncertainties of the nuclear simulator data are considered in the determination of the limiting bundle conditions and therefore have insignificant impact on the flow-biased APRM flux scram trip setpoint and the SLMCPR protection. An increase to the void reactivity used in the GE stability analysis models (the frequency domain code ODYSY and the time-domain code TRACG) may also affect the predicted results. However, the current stability models have been used to model actual instability events, and the decay ratio acceptance criteria have been established consistent with the uncertainty as documented in the approved licensing reports. Furthermore, recent instability events at two domestic BWRs have also been evaluated with the stability models and shown to meet the previously established criteria. This provides high confidence that the GE methodology is adequately simulating recent fuel designs and fuel power densities. Therefore, no adjustment to stability models or analysis is necessary due to potential void reactivity uncertainties.

#### ***Exclusion Region Calculation***

The NRC-approved ODYSY methodology [Reference 29] is used in the exclusion region calculation for every reload. The calculation of the exclusion region boundary is based on a very

conservative core wide decay ratio ([[ ]]) that may be influenced by the core wide axial power distribution calculation. [[

]]

### ***Detect and Suppress Calculation***

The detect and suppress evaluation for Option II plants is performed under the approved LTR basis [Reference 30]. The flow-biased APRM scram setpoints are initially established with conservative margin such that they are found applicable to future fuel cycles during reload confirmation calculations. The calculation of the scram setpoints is based on the limiting fuel bundle being at the OLMCPR and the SLMCPR not being exceeded during the instability oscillation.

The detect and suppress calculation requires the use of the DIVOM curve. Per the BWROG Guideline, “Plant-Specific Regional Mode DIVOM Procedure Guideline” [Reference 32], a plant- and cycle-specific DIVOM evaluation is used to establish the plant specific relationship between the HCOM and the relative change in MCPR such that the initial MCPR value corresponds to the OLMCPR and the limiting MCPR value remains above the SLMCPR. [[

]]

[[

]] The scram setpoint analytical limit is established such that the hot channel power is maintained below acceptable values.



### ***Bypass Voiding***

The bypass voiding discussion provided in Section 2.6.2.1 for Option I-D is fully applicable to Option II because both stability solutions use the flow-biased APRM scram to provide SLMCPR protection.

#### **2.6.2.3 Option III**

Option III is a “detect & suppress” solution that combines closely spaced Local Power Range Monitor (LPRM) detectors into Oscillation Power Range Monitor (OPRM) “cells” to detect either core-wide or regional (local) modes of reactor instability. The detect and suppress evaluation for Option III plants is performed under the approved LTR basis [Reference 30]. The OPRM scram setpoints are established such that the SLMCPR is not exceeded during the instability oscillation.

The examination of core and fuel stability behavior begins with fuel assumed to be at the OLMCPR and terminates once power oscillations cause fuel critical power to reach the SLMCPR. Therefore, if any uncertainties are increased and applied to the SLMCPR, they are directly incorporated into the stability methodology. As discussed before in relation to nodal and core reactivity, uncertainties or biases in depletion isotopics at high exposure and void conditions from prediction, which might have a postulated effect on the void reactivity coefficient, would manifest themselves in separately observable differences in local and core power and reactivity. The variation of void reactivity coefficient across the GE BWR fleet encompasses significant variations in bundle and core exposures and void fraction and is well behaved. The effect of the void reactivity coefficient on instability events is well understood via existing code qualification parametric studies. Large unknown uncertainties in the void reactivity coefficient would be noticeable and be manifest as an inability to reasonably model instability events. The existing GE thermal-hydraulic stability models reasonably and adequately model the magnitude and period of industry thermal-hydraulic instability events. Both the GE stability codes (frequency domain code ODYSY and time-domain code TRACG) model past events relatively well, including the recent thermal-hydraulic instability events at two domestic BWRs. This demonstrates the accuracy of the void model in the GE methodology and provides high

confidence in the simulation of recent fuel designs and fuel power densities. Because the transient analysis results (delta/initial) are not affected and the difference between OLMCPR and SLMCPR remains unchanged, the stability envelope will not be affected.

Key inputs to the stability-based OLMCPR analysis are the DIVOM slope and HCOM. These inputs would not be affected by an increase in the OLMCPR or the SLMCPR. Key HCOM inputs are LPRM to OPRM assignments, total scram delay time, RPS trip logic, and averaging/conditioning filter cutoff frequencies. A new HCOM is required only if one of these key (but unrelated to OLMCPR or SLMCPR) parameters changes. If the current SLMCPR is increased by 0.02, the overall effect on the stability based OLMCPRs (note these values are determined at OPRM amplitude setpoints from 1.05 to 1.15 or 1.20) would be that they would increase by the ratio of the new SLMCPR to the old SLMCPR. But the acceptance criteria for selecting the appropriate OPRM setpoint, i.e., the transient OLMCPR, would also increase. Consequently, the OPRM setpoint would remain essentially unchanged if there were a change in SLMCPR and OLMCPR.

Further, a 5-10% uncertainty in radial peaking factor is applied in this analysis, primarily to address variations in bundle peaking from initial rod pattern selection. This relatively large radial peaking factor reasonably encompasses the small (<~1%) increase in bundle power uncertainty (described above) for the SLMCPR determination, in particular because the stability analysis is otherwise conservative for plant specific conditions or settings.

Per the BWROG Guideline, “Plant-Specific Regional Mode DIVOM Procedure Guideline” [Reference 32], a plant- and cycle-specific DIVOM evaluation is used to establish the plant specific relationship between HCOM and the relative change in MCPR such that the initial MCPR value corresponds to the OLMCPR and the limiting MCPR value remains above the SLMCPR. [[

]]

[[

]] The scram setpoint analytical limit is established such that the hot channel power is maintained below acceptable values.

### ***Bypass Voiding***

The following discussion provides an assessment of the impact of bypass voiding on the effectiveness of the OPRM scram to provide SLMCPR protection for Option III. The primary effect of voiding in the bypass region on the neutron detectors (LPRMs and TIPs) is to reduce the detector response, assuming the same power in the adjacent fuel. This reduction is due to a decrease in the moderation caused by the presence of voids, which decreases the thermal neutron flux incident on the detectors for the same neutron flux generated in the adjacent fuel. There is also the potential for some additional noise in the neutron flux signal, but that has a minor impact on steady state operation. These impacts are greatest for the highest elevation LPRM (D level) where the highest bypass voiding occurs.

For the Option III stability solution, the OPRM scram is used to mitigate stability transients. The scram setpoint is based on assuring that the scram occurs before power oscillations become large enough to cause the MCPR to approach the SLMCPR. High bypass voids can potentially reduce the OPRM reading, and so the margin to scram would increase and this could be non-conservative from the stability mitigation point of view since it would take higher amplitude oscillations to initiate an OPRM scram.

The worst-case impact is at natural circulation (following a two recirculation pump trip) when the bypass voids are highest. An evaluation was performed at 49.4% power and 31.3% core flow for a BWR/4 with 764 fuel assemblies at 120% OLTP MELLLA operation. [[

]]

The D and C level LPRM detectors may also indicate additional noise due to the void bubbles in the bypass region. The frequency of this noise is inversely related to the bubble transit time across the LPRM detector (~ 2 inches). For a typical bypass flow velocity at natural circulation of 0.4 ft/sec, the noise frequency is ~2.4 Hz. This noise due to bypass voids has a negligible impact on the ability of the Option III detection algorithms to detect instability oscillations because the noise is high frequency (~2.4 Hz) and is effectively filtered out by the double pole Butterworth “cut-off” filter (~1 Hz) in the OPRM equipment.

An assessment of the impact of the 40% void depletion history assumption on stability can be summarized as follows. As stated in Section 2.2.2.2, [[

]]

A similar assessment can be made for the axial and radial power distributions. Therefore, based on these assessments and those provided above, no adjustment to stability models or analysis is necessary due to potential void coefficient or power distribution uncertainties.

An assessment of the impact of extrapolating beyond 70% voids on stability can be summarized as follows. As stated in Section 2.2.2.2, [[

]] Therefore, no

adjustment to stability models or analysis is necessary due to potential void coefficient uncertainties.

There may be differences in bypass voiding between GE and non-GE fuel due to their geometric and lattice differences, however the impact on stability is insignificant because of the need for thermal-hydraulic compatibility of the fuel types in the core.

#### **2.6.2.4 Enhanced Option I-A**

Enhanced Option I-A (EIA) is a “prevention” solution that automatically prevents reactor operations within an Exclusion Region by modifying the flow-biased APRM flux scram function to contain this region. This scram ensures the Fuel Cladding Integrity SLMCPR is protected for both the core wide and regional modes of coupled thermal-hydraulic/neutronic reactor instability. Reactor operations within a Restricted Region are automatically restricted by modifying the flow-biased APRM control rod block function to contain this region. An administratively controlled Monitored Region provides additional protection outside of the Restricted Region.

Stability analyses for both the EPU and fuel cycle specific conditions are performed to define the stability region boundaries as well as to confirm that the scram setpoints meet the design basis. With respect to power distribution uncertainties of the nuclear simulator data, the results pertaining to the region boundaries may be slightly affected, but this is not considered to have

any safety significance for reasons described below. The power distribution uncertainties of the nuclear simulator data are considered in the determination of the limiting bundle conditions and therefore have insignificant impact on the flow-biased APRM flux scram trip setpoint and the SLMCPR protection. An increase to the void reactivity used in the GE stability analysis model (the frequency domain code ODYSY) may also affect the predicted results. However, the current stability model has been used to model actual instability events, and the decay ratio acceptance criteria have been established consistent with the uncertainty as documented in the approved licensing reports. Furthermore, recent instability events at two domestic BWRs have also been evaluated with the stability model and shown to meet the previously established criteria. This provides high confidence that the GE methodology is adequately simulating recent fuel designs and fuel power densities. Therefore, no adjustment to stability models or analysis is necessary due to potential void reactivity uncertainties.

### ***Region Boundary Calculations***

The NRC-approved ODYSY methodology [Reference 33] is used in the region boundary calculations for every reload. The calculation of the region boundaries is based on conservative decay ratio criteria that may be influenced by the core wide axial power distribution calculation.

[[

]]

### ***Bypass Voiding***

The bypass voiding discussion provided in Section 2.6.2.1 for Option I-D is fully applicable to EIA because both stability solutions use the flow-biased APRM scram to provide SLMCPR protection. In addition, the EIA solution makes use of a 40% flow clamp such that a scram is initiated if core flow falls below 40% of rated. There is less bypass voiding at 40% flow than at natural circulation, so bypass voiding is less significant for EIA than for Option I-D.

### 2.6.3 Adequacy of Existing Treatment and Alternate Approach

The uncertainties in power distribution calculation and void reactivity do not significantly affect the safety margin in the stability analysis.

## 2.7 LICENSED EXPOSURE

GE fuel designs are licensed to a [[ ]] exposure limit (i.e., 70 GWd/MTU for GE14). [Reference 34] This is equivalent to a GE14 rod average exposure of [[ ]], although an explicit rod average exposure limit is not specified for GE14 or other GE fuel designs. This exposure limit is specified and applied in the process computer to assure that fuel is not operated beyond its analyzed basis. In this application, the best estimate value of the [[ ]] exposure condition is monitored against the specified exposure limit.

### 2.7.1 Fuel Parameters That Affect Pellet Exposure

The fuel parameters and associated uncertainties identified previously (i.e., the local pin power peaking, void reactivity coefficient, [[ ]]) are included in the development of the LHGR Operating Limits, and the fuel exposure limit. These fuel parameters ultimately determine both the local power and local exposure.

### 2.7.2 Treatment of Fuel Parameter Uncertainties

The fuel rod thermal-mechanical performance consideration of greatest interest at exposures near the [[ ]] exposure limit is the fuel rod internal pressure. [[ ]]

] therefore, no additional conservatism in local exposure monitoring is required to maintain fuel integrity.

### **2.7.3 Adequacy of Existing Treatment and Alternate Approach**

In summary, the GE standard fuel thermal-mechanical analysis basis considers and provides adequate margin for uncertainties in local and bundle power and exposure.



## **3.0 EXTENSION OF SAFETY PARAMETER BASES TO THE MELLLA+ OPERATING DOMAIN**

### **3.1 INTRODUCTION**

Since the early 1980s, the BWR fleet has commonly used an operating strategy known as spectral shift operation. Spectral shift refers to promoting Pu-239 buildup early in the cycle by favoring a “harder” neutron energy spectrum (i.e., increasing voids). This is achieved by overemphasizing the bottom peak in the core axial power shape. The overemphasized bottom peak is attained through reduced core flow, or control rod patterns, or through the enrichment and burnable poison distributions designed into the fuel, or through combinations of all these tactics. Reducing flow to promote spectral shift is generally favored over tactics such as power shaping with control rods.

MELLLA+ operation allows the reactor to be at full power down to 80% of core rated flow [Reference 1]. Like Extended Power Uprate, (EPU), these conditions increase the amount of steam voids in the core. The void amount is a direct function of the power to flow ratio. Raising the average bundle power (EPU) or lowering the flow (MELLLA+) have the same affect, and for the most part raise similar technical issues. This section addresses those technical issues unique to MELLLA+ operation.

### **3.2 CRITICAL POWER**

#### **3.2.1 Safety Limit Critical Power Ratio (SLMCPR)**

The approach for the SLMCPR evaluation applied to MELLLA+ operating conditions is the same (with respect to the process) as described under Section 2.2.1. This process was modified in 2004 as part of the resolution to a Part 21 on SLMCPR [Reference 35]. The MELLLA+ operating domain has an additional high power state point that is considered in the evaluation. The current design process for determining the cycle-specific SLMCPR considers the highest licensed power level at two flow points, rated flow and the lowest licensed flow at 100% power (e.g., ~80% flow for MELLLA+ operation). These power/flow state points are considered at (minimum) three exposure points in the cycle, for a total of 6 evaluation points. The SLMCPR

determined using this approach is appropriately conservative to cover the MELLLA+ power/flow operating conditions [Reference 36].

### **3.2.2 Operating Limit Critical Power Ratio (OLMCPR)**

MELLLA+ evaluation procedures require consideration of OLMCPR values for each limiting corner of the power flow map. If changes are required to account for OLMCPR at different flow points, this change is reflected in the process computer algorithm for MFLCPR (Ratio of bundle critical power to OLMCPR) for each bundle. The same conservatisms apply for the nuclear inputs to the transient evaluations. The sensitivities remain the same as those evaluated at the full power conditions.

### **3.3 SHUTDOWN MARGIN**

It should be noted that the data in Section 2.3 supports a  $2\sigma$  demonstration margin criteria of 0.38%  $\Delta k/k$ . This is done by showing that the same core  $1\sigma$  spread for the [[ ]] cores is [[ ]]. The cores comprising this dataset are all high energy, modern fuel, spectral shift operation. Relative to steady state methods, MELLLA+ operation is a method of spectral shift operation. The [[ ]] from the spectral shift, high energy cores is less than the [[ ]] from early cores reported in Reference 22 for earlier versions of PANACEA and essentially the same as the [[ ]] for the current version of PANACEA reported in [Reference 37] for a broader, fleet-wide statistical assessment of cold eigenvalues for plants covering a range of operating conditions, but without a large representation of high energy density cores (such cores were not prevalent at that time). The similarity in the cold eigenvalue variation for the various populations indicates that the methods have maintained fidelity in cold eigenvalue prediction, even as core and fuel advances have been made.

### **3.4 FUEL ROD THERMAL MECHANICAL PERFORMANCE**

One of the benefits of MELLLA+ operation is that it supports spectral shift operation, wherein the flow is reduced early in the cycle to promote a bottom peaked axial power shape. Spectral shift operation has the potential to increase axial peaking lower in the core at BOC, then in the upper portion of the core near EOC. The fuel rod thermal-mechanical analyses explicitly address

the variation in the axial power distribution that may occur as a result of spectral shift operation, and therefore the specified LHGR Operating Limits and exposure limit are directly applicable to MELLLA+ operation.

### **3.5 LOCA RELATED NODAL POWER LIMITS**

There are no differences in the ECCS-LOCA methodology between EPU and MELLLA+ except that for MELLLA+ the ECCS-LOCA analyses are performed for at least two additional state points. MELLLA+ ECCS-LOCA analyses will include calculations for the rated power/MELLLA+ boundary point and the low flow point on the MELLLA+ boundary at which the off-rated flow dependent LHGR or MAPLHGR setdown begins to apply. The Licensing Basis PCT is based on the analyzed state point with the highest PCT using Appendix K assumptions.

### **3.6 STABILITY**

The GE BWR Detect and Suppress Solution – Confirmation Density (DSS-CD) (NEDC-33075P, Revision 5) is the only licensed (SER pending) stability solution for operation in the MELLLA+ domain [Reference 38]. DSS-CD is a “detect & suppress” solution and represents an evolutionary step from Stability Solution Option III (see Section 2.6.2.3). DSS-CD introduces an enhanced detection algorithm, the Confirmation Density Algorithm (CDA), which reliably detects the inception of power oscillations and generates an early power suppression trip signal prior to any significant oscillation amplitude growth and MCPR degradation.

TRACG analysis is performed to demonstrate significant margin to the SLMCPR for the generic OPRM CDA setpoints. Conservative multipliers are applied to the TRACG results in the assessment of the CPR margin for limiting instability scenarios. These multipliers accommodate the uncertainties in power distribution and void reactivity. The DSS-CD LTR defines a generic applicability envelope for MCPR margin such that a similar increase in the SLMCPR and the OLMCPR will not affect the applicability of DSS-CD.

In summary, the DSS-CD has been designed for the MELLLA+ domain and uncertainties in power distribution calculation and void reactivity are accounted for in the significant safety margin in the stability analysis.

### ***Bypass Voiding***

The following discussion provides an assessment of the impact of bypass voiding on the effectiveness of the OPRM scram to provide SLMCPR protection for DSS-CD. The primary effect of voiding in the bypass region on the neutron detectors (LPRMs and TIPS) is to reduce the detector response, assuming the same power in the adjacent fuel. This reduction is due to a decrease in the moderation caused by the presence of voids, which decreases the thermal neutron flux incident on the detectors for the same neutron flux generated in the adjacent fuel. There is also the potential for some additional noise in the neutron flux signal, but that has a minor impact on steady state operation. These impacts are greatest for the highest elevation LPRM (D level) where the highest bypass voiding occurs.

For the DSS-CD stability solution, the OPRM scram is used to mitigate stability transients. The scram setpoint is based on assuring that the scram occurs before power oscillations become large enough to cause the MCPR to approach the SLMCPR. High bypass voids can potentially reduce the OPRM reading, and so the margin to scram would increase and this could be non-conservative from the stability mitigation point of view since it would take higher amplitude oscillations to initiate an OPRM scram.

The worst-case impact is at natural circulation (following a two recirculation pump trip) when the bypass voids are highest. An evaluation was performed at this condition for the highest power density BWR type (~60% power and ~30% core flow) with 120% uprated MELLLA+ operation. [[

]]

The D and C level LPRM detectors may also indicate additional noise due to the void bubbles in the bypass region. The frequency of this noise is inversely related to the bubble transit time across the LPRM detector (~ 2 inches). For a typical bypass flow velocity at natural circulation of 0.4 ft/sec, the noise frequency is ~2.4 Hz. This noise due to bypass voids has a negligible impact on the ability of the DSS-CD detection algorithm to detect instability oscillations because the noise is high frequency (~2.4 Hz) and is effectively filtered out by the double pole Butterworth “cut-off” filter (~1 Hz) in the OPRM equipment.

An assessment of the impact of the 40% void depletion history assumption on stability can be summarized as follows. As stated in Section 2.2.2.2, [[

]]

A similar assessment can be made for the axial and radial power distributions. Therefore, based on these assessments and those provided above, no adjustment to stability models or analysis is necessary due to potential void coefficient or power distribution uncertainties.

An assessment of the impact of extrapolating beyond 70% voids on stability can be summarized as follows. As stated in Section 2.2.2.2, [[

]] Therefore, no

adjustment to stability models or analysis is necessary due to potential void coefficient uncertainties.

There may be differences in bypass voiding between GE and non-GE fuel due to their geometric and lattice differences, however the impact on stability is insignificant because of the need for thermal-hydraulic compatibility of the fuel types in the core.

### **3.7 LICENSED EXPOSURE**

As noted in Section 3.4, spectral shift operation has the potential to increase axial peaking lower in the core at BOC, then in the upper portion of the core near EOC. The fuel rod thermal-mechanical analyses explicitly address the variation in the axial power distribution that may occur as a result of spectral shift operation, and therefore the specified LHGR Operating Limits and exposure limit derived from the fuel rod thermal-mechanical analyses are directly applicable to MELLLA+ operation.

## **4.0 LICENSING APPLICATION**

### **4.1 OVERVIEW**

The purpose of the Applicability of GE Methods to Expanded Operating Domains Licensing Topical Report (LTR) is to provide a licensing basis that allows the NRC to issue Safety Evaluations (SEs) for Constant Pressure and Extended Power Uprate (CPPU, EPU) applications and the MELLLA+ LTR. The SE for the Applicability of GE Methods to Expanded Operating Domains LTR would approve the use of GE's methods for extended power uprates (EPU or CPPU) and MELLLA+ operating domain expansion until final resolution of the Methods RAIs.

The Applicability of GE Methods to Expanded Operating Domains LTR is for temporary application and it is expected that it would be necessary for only a limited number of utility license applications until the NRC's review of the Methods RAIs is complete. GE anticipates that a limited number of future license applications, associated with extended power uprate and MELLLA+, will reference the Applicability of GE Methods to Expanded Operating Domains LTR. GE intends to resolve the Methods RAIs as soon as practical and thereby eliminate the need for referencing the Applicability of GE Methods to Expanded Operating Domains LTR in the long term.

### **4.2 APPLICABILITY**

The Applicability of GE Methods to Expanded Operating Domains LTR basis is applicable to current GE BWR product lines licensed with GE nuclear and safety analysis methods. The Methods LTR is applicable to plants that include current GE and non-GE legacy fuel designs. The Methods LTR is applicable to plants seeking NRC approval for CPPU and EPU power uprates, and MELLLA+ operating domain expansion, including currently licensed operating domains and operational flexibility features. The Methods LTR is applicable to plants applying licensed GE Stability Solutions.

Each GE technology code has an associated “application statement” defining the application range. The application of these codes complies with the limitations, restrictions and conditions specified in the approving NRC SER for each code.

The parameters establishing the Applicability of GE Methods to Expanded Operating Domains applicability envelope are:

<b>Parameter</b>	<b>Generic Value</b>
BWR Product Line	BWR/2-6
Fuel Product Line	GE and non-GE fuel designs using square arrays of fuel rods, including 7x7, 8x8, 9x9, and 10x10 designs
Licensing Methodology	GE Nuclear and Safety Analysis Methods
Operating Domain	CPPU, EPU, with MELLLA+ including currently licensed operating domains (e.g., ELLA, MELLLA) and operational flexibility features
Maximum Rated Power Level	120% OLTP
Stability Solution	GE Stability Solutions

The evaluations documented in this report, demonstrating the acceptability of the margins associated with the Applicability of GE Methods to Expanded Operating Domains, encompass the above applicability envelope parameters. The plant specific application process will confirm that operations proposed by the plant specific license amendment meet the Applicability of GE Methods to Expanded Operating Domains LTR applicability envelope requirements.

### **4.3 PLANT SPECIFIC APPLICATION PROCESS**

Each plant seeking to apply the Methods LTR must provide information supporting the application that demonstrates that the plant parameters are within the applicability definition in Section 4.2.

In addition, each plant seeking to apply the Methods LTR must provide plots of the following bundle operating conditions as a function of exposure:

- Maximum bundle power,
- Maximum bundle power/flow ratio,
- Exit void fraction of maximum power bundle,
- Maximum channel exit void fraction,
- Core average exit void fraction, and
- Peak linear heat generation rate.



The peak end-of-cycle nodal exposure should also be provided in the plant specific application of the Methods LTR.

A quarter core map (assuming core symmetry) showing bundle power, bundle operating linear heat generation rate, and minimum critical power ratio for beginning, middle, and end-of-cycle must also be provided in the plant specific application of the Methods LTR.

## 5.0 SUMMARY AND CONCLUSION

The evaluations presented in Sections 2 and 3 demonstrate that for CPPU, EPU, or MELLLA+ license amendment requests, an operational restriction in bundle critical power ratio via an increase in the SLMCPR of 0.02  $\Delta$ CPR is sufficient to provide additional and reasonable assurance of safety. No additional operational restrictions are required for CPPU or EPU applications and no other operational restrictions are required for MELLLA+ applications.

### **Safety Limit Critical Power Ratio (SLMCPR)**

An adjustment to the SLMCPR of 0.02  $\Delta$ CPR is proposed to provide additional and reasonable assurance of safety for CPPU or EPU including MELLLA+ conditions. The standard, cycle specific evaluation (but with increased uncertainties) will be performed to assure that the adjustment is adequate. The adjustment to SLMCPR accounts for potential increases in the power distribution uncertainties, pending the acquisition of confirmatory gamma-scan data for 10x10 fuel designs. The adjustment will be removed and standard  $1\sigma$  uncertainties applied considering updated data as it becomes available. This adjustment is also applicable to non-GE fuel designs in CPPU or EPU and MELLLA+ applications.

### **Operating Limit Critical Power Ratio (OLMCPR)**

Adequate conservatism in the analyses that establish the OLMCPR is demonstrated. Therefore, no additional margin to the OLMCPR is required.

### **Shutdown Margin (SDM)**

The Technical Specification (TS) limit for the SDM of 0.38 %  $\Delta$ k/k is not increased for CPPU or EPU and MELLLA+ applications. The uncertainty does not increase to a degree that warrants an increase in the TS limit. GE normally provides 1% SDM in the core design.

### **Fuel Rod Thermal-Mechanical Performance**

Consistent with the SLMCPR treatment of uncertainties, increases in the assumed pin and bundle power distribution uncertainties are applicable to the power distribution aspects of the thermal-mechanical calculations. However, adequate overall modeling uncertainties are included within

the current design basis for generation of the LHGR Operating Limits and exposure limit. Therefore, no changes are required in the LHGR Operating Limits and exposure limit.

### **LOCA Related Nodal Power Limits**

The conservatisms applied in the calculation of the limit in the ECCS-LOCA calculations provide justify the adequacy of current methodology for application in CPPU or EPU and MELLLA+ applications. Therefore, no additional margin is applied to the MAPLHGR limit.

### **Stability**

The additional SLMCPR margin noted above and conservatisms in detect and suppress methodologies for the GE stability options justify that no additional margin is necessary. The effectiveness of the neutron monitoring systems and detect and suppress methodologies is not significantly affected by postulated increases in bypass voiding for CPPU or EPU applications including MELLLA+.

### **Licensed Exposure**

As discussed regarding LHGR, increases in the assumed pin and bundle power distribution uncertainties are also applicable to the power distribution aspects included in the thermal-mechanical calculations. However, adequate overall modeling uncertainties are included within the current design basis for generation of the LHGR Operating Limits and exposure limit. Therefore, no changes are required in the LHGR Operating Limits and exposure limit.

## 6.0 REFERENCES

1. Letter from George Stramback (GE) to NRC, Submittal of GE Proprietary Licensing Topical Report NEDC-33006P, Revision 1, General Electric Boiling Water Reactor Maximum Extended Load Line Limit Analysis Plus, August 2002, MFN 02-050, August 23, 2002.
2. Entergy letter to U.S. Nuclear Regulatory Commission, Vermont Yankee Nuclear Power Station, License No. DPR-28 (Docket No. 50-271), Technical Specification Proposed Change No. 263, Extended Power Uprate " BVY 03-80, September 10, 2003.
3. Entergy letter to U.S. Nuclear Regulatory Commission, "Vermont Yankee Nuclear Power Station, License No. DPR-28 (Docket No. 50-271), Technical Specification Proposed Change No. 263 - Supplement No. 24, Extended Power Uprate - Response to Request for Additional Information," BVY 05-024, March 10,2005.
4. Entergy letter to U.S. Nuclear Regulatory Commission, "Vermont Yankee Nuclear Power Station, License No. DPR-28 (Docket No. 50-271), Technical Specification Proposed Change No. 263 - Supplement No. 30, Extended Power Uprate - Response to Request for Additional Information," BVY 05-072, August 1,2005.
5. Entergy letter to U.S. Nuclear Regulatory Commission, "Vermont Yankee Nuclear Power Station, License No. DPR-28 (Docket No. 50-271), Technical Specification Proposed Change No. 263 - Supplement No. 32, Extended Power Uprate - Response to Request for Additional Information," BVY 05-083, September 10,2005.
6. Entergy letter to U.S. Nuclear Regulatory Commission, "Vermont Yankee Nuclear Power Station, License No. DPR-28 (Docket No. 50-271), Technical Specification Proposed Change No. 263 - Supplement No. 34, Extended Power Uprate - Response to Request for Additional Information," BVY 05-086, September 18,2005.
7. Entergy letter to U.S. Nuclear Regulatory Commission, "Vermont Yankee Nuclear Power Station, License No. DPR-28 (Docket No. 50-271), Technical Specification Proposed Change No. 263 - Supplement No. 35, Extended Power Uprate - Response to Request for Additional Information," BVY 05-088, September 28,2005.

8. Letter from Alan Wang (NRC) to James Klapproth (GE), Request For Additional Information – Licensing Topical Report NEDC-33006P, Revision 1, "General Electric Boiling Water Reactor Maximum Extended Load Line Limit Analysis Plus (MELLLA+)" (TAC No. MB6157), MFN 04-111, October 1, 2004.
9. Letter from Alan Wang (NRC) to Louis Quintana (GE), Request For Additional Information – Licensing Topical Report NEDC-33006P, Revision 1, "General Electric Boiling Water Reactor Maximum Extended Load Line Limit Analysis Plus (MELLLA+)" (TAC No. MB6157), MFN 05-031, April 11, 2005.
10. GE Nuclear Energy, "Constant Pressure Power Uprate Licensing Topical Report," NEDC-33004P-A, Revision 4, July 2003.
11. GE Nuclear Energy, "Generic Guidelines for General Electric Boiling Water Reactor Extended Power Uprate", NEDC-32424P-A, February 1999.
12. GE Nuclear Energy, "Generic Evaluations of General Electric Boiling Water Reactor Extended Power Uprate", NEDC-32523P-A, February 2000, Supplement 1, Volume I, February 1999, and Supplement 1, Volume II, April, 1999.
13. GE Nuclear Energy, "General Electric Standard Application for Reactor Fuel", NEDE-24011-P-A and NEDE-24011-P-A-US, (latest approved revision).
14. NEDC-32601P-A, "Methodology and Uncertainties for Safety Limit MCPR Evaluation", August 1999.
15. NEDC-32694P-A, "Power Distribution Uncertainties for Safety Limit MCPR Evaluations", August 1999.
16. NEDE-21565, J. A. Findlay and G. E. Dix, BWR Void Fraction and Data, January 1977.
17. Letter, G. Stramback (GE) to NRC, Completion of Responses to MELLLA Plus AOO RAIs (TAC No. MB6157), MFN 04-026, March 4, 2004.
18. Steady-State Nuclear Methods, NEDE-30130-P-A and NEDO-30130-A, April 1985, and for TGBLA Version 06 and PANACEA Version 11, Letter from S.A. Richards (NRC) to G.A. Watford (GE) Subject: "Amendment 26 to GE Licensing Topical Report

- NEDE-24011-P-A, GESTAR II Implementing Improved GE Steady-State Methods," (TAC NO. MA6481), November 10, 1999
19. J. F. Briesmeister, "MCNP - A General Monte Carlo N-Particle Transport Code, Version 4A," LA-12625-M Manual, Los Alamos National Laboratory, (1993).
  20. Letter from George Stramback (GE) to Herbert Berkow (NRC), Responses to RAIs - Methods Interim Process (TAC No. MC5780), Response to RAIs 5, 25, 26, 27, and 29, MFN 05-029, April 8, 2005.
  21. NEDO-24154P-A, Volume III, "Qualification of the One-Dimensional Core Transient Model for Boiling Water Reactors", October 1978.
  22. GE Nuclear Energy, "Qualification of the One-Dimensional Core Transient Model (ODYN) for Boiling Water Reactors (Supplement 1 - Volume 4)," Licensing Topical Report NEDC-24154P-A, Revision 1, Supplement 1, Class III, February 2000.
  23. NEDE-32906P-A, Rev. 1, TRACG Application for Anticipated Operational Occurrences (AOO) Transient Analyses, April 2003.
  24. Letter J. S. Charnley (GE) to H. N. Berkow (NRC), Revised Supplementary Information Regarding Amendment 11 to GE Licensing Topical Report NEDE-24011-P-A," MFN-003-86, January 16, 1986.
  25. GE Nuclear Energy, "The GESTR-LOCA and SAFER Models for the Evaluation of the Loss-Of-Coolant Accident, Volume III, SAFER/GESTR Application Methodology," NEDE-23785-1-PA Rev. 1, October 1984.
  26. GE Nuclear Energy, "The GESTR-LOCA and SAFER Models for the Evaluation of the Loss-Of-Coolant Accident, Volume II, SAFER – Long Term Inventory Model for BWR Loss-of-Coolant Analysis," NEDE-23785-1-PA Rev. 1, October 1984.
  27. GE Nuclear Energy, "SAFER Model for Evaluation of Loss-of-Coolant Accidents for Jet Pump and Non-jet Pump Plants, Volume I, SAFER – Long Term Inventory Model for BWR Loss-of-Coolant Analysis," NEDE-30996P-A, October 1987.
  28. GE Nuclear Energy, "Compilation of Improvements to GENE's SAFER ECCS-LOCA Evaluation Model," NEDC-32950P, January 2000.

29. NEDC-32992P-A, "ODYSY Application for Stability Licensing Calculation", July 2001.
30. NEDO-32465-A, BWR Owners' Group Reactor Stability Detect and Suppress Solutions Licensing Basis Methodology for Reload Applications, August 1996.
31. GE-NE-0000-0031-6498-R0, "Plant-Specific Core-Wide Mode DIVOM Procedure Guideline," June 2005.
32. GE-NE-0000-0028-9714-R1, "Plant-Specific Regional Mode DIVOM Procedure Guideline," June 2005.
33. "Reactor Stability Long-Term Solution: Enhanced Option I-A, ODYSY Application to E1A", NEDC-32339P-A, Supplement 1, December 1996.
34. GE14 Compliance With Amendment 22 of NEDE-24011-P-A (GESTAR II), NEDC-32868P, Revision 1, September 2000.
35. Letter J. S. Post (GE) to Chief, Information Management Branch (NRC), Subject: Part 21 Final Report: Non-conservative SLMCPR, MFN 04-108, September 29, 2004.
36. Letter from George Stramback (GE) to NRC, Revised Responses to MELLLA+ RAIs - (TAC No. MC6157), MFN 05-081, August 16, 2005.
37. Letter from G. A. Watford (GNF) to R. M. Pulsifer (NRC) Subject: Proprietary Presentation Material from GE/NRC Meeting of November 10, 1999, FLN-1999-012, November 12, 1999.
38. GE Nuclear Energy, "Detect And Suppress Solution–Confirmation Density Licensing Topical Report," NEDC-33075P, Revision 5, November 2005.

## APPENDIX A VERMONT YANKEE REACTOR SYSTEMS BRANCH QUESTIONS

Appendix A includes a profile of the questions from the NRC Reactor Systems Branch that were recently addressed on the VYNPS EPU docket. Some of the RAIs are not related to GE methods and some are questions seeking specific VYNPS information. The following table presents the VYNPS reference letters and associated RAI responses.

Entergy letter to U.S. Nuclear Regulatory Commission, "Vermont Yankee Nuclear Power Station, License No. DPR-28 (Docket No. 50-271), Technical Specification Proposed Change No. 263 - Supplement No. 24, Extended Power Uprate - Response to Request for Additional Information," BVY 05-024, March 10,2005.	Attachment 3 – SRXB-A-6
Entergy letter to U.S. Nuclear Regulatory Commission, "Vermont Yankee Nuclear Power Station, License No. DPR-28 (Docket No. 50-271), Technical Specification Proposed Change No. 263 - Supplement No. 30, Extended Power Uprate - Response to Request for Additional Information," BVY 05-072, August 1,2005.	Attachment 1 – Revised SRXB-A-6  Attachment 9 – SRXB-A-7 thru SRXB-A-58
Entergy letter to U.S. Nuclear Regulatory Commission, "Vermont Yankee Nuclear Power Station, License No. DPR-28 (Docket No. 50-271), Technical Specification Proposed Change No. 263 - Supplement No. 32, Extended Power Uprate - Response to Request for Additional Information," BVY 05-083, September 10,2005.	Attachment 4 – Revised SRXB-A-17  Attachment 5 – SRXB-A-59, 60, 61, 62, 63, 64, 66, 69, and 70
Entergy letter to U.S. Nuclear Regulatory Commission, "Vermont Yankee Nuclear Power Station, License No. DPR-28 (Docket No. 50-271), Technical Specification Proposed Change No. 263 - Supplement No. 34, Extended Power Uprate - Response to Request for Additional Information," BVY 05-086, September 18,2005.	Attachment 2 – SRXB-A-66 Data CD  Attachment 3 – Supplement to SRXB-A-64  Attachment 4 – SRXB-A-65 and 67  Attachment 6 – SRXB-A-71
Entergy letter to U.S. Nuclear Regulatory Commission, "Vermont Yankee Nuclear Power Station, License No. DPR-28 (Docket No. 50-271), Technical Specification Proposed Change No. 263 - Supplement No. 35, Extended Power Uprate - Response to Request for Additional Information," BVY 05-088, September 28,2005.	Attachment 1 – SRXB-A-68

The RAIs are presented in the following table. The subject column provides the subject and a few words regarding the response and resolution.



NEDO-33173-A, Revision 1  
 Non-Proprietary Information

Related Technology	Subject	RAI
Steady state and transient nuclear, Steady state and transient thermal hydraulic, fuel rod mechanical	Strategy for Application of Methods to design and addition SLMCPR margin to account for lack of experimental data	SRXB-A-06
PANACEA, ISCOR	Explanation supplied for the uncertainties applied to LHGR. Refer to SRXB-A-68	SRXB-A-24
PANACEA, ISCOR	Explanation provided for increase in nodal uncertainties with elevation	SRXB-A-25
PANACEA, ISCOR	Information and discussion supplied regarding criteria for axial and nodal uncertainties	SRXB-A-27
PANACEA, ISCOR	Information and discussion of SLMCPR evaluation and monitoring supplied for axial and nodal uncertainties in safety limit analyses	SRXB-A-28
PANACEA, ISCOR, ODYN, SAFER	Explanation provided for inclusion of axial and nodal uncertainties in transient and accident evaluations	SRXB-A-29
PANACEA, ISCOR	Application of nodal uncertainties to nodal exposure to MAPLHGR and LHGR values	SRXB-A-30
PANACEA, ISCOR	Does LHGR limit in 3D simulator include decrease with exposure	SRXB-A-31
PANACEA, ISCOR	Application of nodal uncertainties and increases with exposure. Refer to SRXB-6 and SRXB-31.	SRXB-A-32
PANACEA, ISCOR	Describe how core monitoring system calculate pin wise power parameters	SRXB-A-33
PANACEA, ISCOR	Justify acceptability of basing assessment of pin power accuracy on code-to-code comparisons. Alternate approach and SLMCPR procedures proposed in response to SRXB-6	SRXB-A-34
PANACEA, ISCOR	Core Follow Data Supplied	SRXB-A-35
PANACEA, ISCOR	Reasons for differences between PCTIP and axial power distributions provided	SRXB-A-36
TGBLA, MCNP	Explanation provided to justify acceptability of basing assessment of pin power accuracy on BOL conditions	SRXB-A-37
TGBLA, MCNP	Explanation provided for use of different uncertainties for GE14 and later designs. Refer to response to SRXB-6	SRXB-A-38
PANACEA, ISCOR	Explanation of effect on pin power due to neighboring bundles provided with explicit results for 10x10 lattices	SRXB-A-39
SLMCPR	Provided confirmation that current channel bow uncertainties are included in SLMCPR evaluations	SRXB-A-40
SLMCPR	Provide uncertainty analysis for 3D MONICORE	SRXB-A-41
SLMCPR	Provided explanation of R-factor uncertainty procedures	SRXB-A-42

NEDO-33173-A, Revision 1  
 Non-Proprietary Information

Related Technology	Subject	RAI
SLMCPR	Justification of Inlet Sub cooling Uncertainties provided	SRXB-A-43
PANACEA, ISCOR	Discussion of bypass voiding on instrumentation provided	SRXB-A-44
SLMCPR	Explanation provided regarding why axial TIP not included in SLMCPR	SRXB-A-45
TGBLA, MCNP	Explanation provided regarding Cross Sections for High void operation. Refer to generic EPU and MELLLA+ studies.	SRXB-A-46
TGBLA, MCNP	Plots of isotopic concentrations provided	SRXB-A-47
TGBLA, MCNP	Information provided on the isotopic influence on void coefficient	SRXB-A-48
GEXL	Double Hump Power distributions for GEXL accounted for in SLMCPR calculations	SRXB-A-49
GEXL	Power flow ranges for GEXL shown to be adequate	SRXB-A-50
TGBLA, MCNP	Discussion provided on Void reactivity coefficients for transients and accidents, including ATWS and SBO. Refer to SRXB-A-6	SRXB-A-51
Void and pressure drop correlations	Pressure Drop data base information provided, reference made to generic MELLLA+ report	SRXB-A-52
Void and pressure drop correlations	Void fraction measurement data made through Safety Limit Document reference	SRXB-A-53
Void and pressure drop correlations	Are void fraction uncertainties included in water density? Explanation provided	SRXB-A-54
Instrument effects	Effect high void fractions on instrument response during transients. Effects of bypass voids on instrument response explained	SRXB-A-55
Instrument effects	Explanation provided for impact of instrument random noise during plant maneuvers	SRXB-A-56
ODYN	Explanation of uncertainties in power during transients	SRXB-A-58
GSTRM (GESTR-Mechanical)	Uncertainties in LHGR limit evaluations	SRXB-A-65
TGBLA, MCNP	CASMO/TGBLA code comparisons	SRXB-A-66
PANACEA, ISCOR	Shutdown margin verification and qualification Data and procedure provided	SRXB-A-67
TGBLA, MCNP	Void reactivity coefficients -- provide more information than response to SRXB-A-51	SRXB-A-68
Void and pressure drop correlations	Explanation and information provided regarding Void fraction uncertainties	SRXB-A-69
Void and pressure drop correlations	Explanation provided regarding acceptable to exceed correlations range. Refer to SRXB-A-55	SRXB-A-70
TGBLA, MCNP	Clarification and more detail on response to SRXB-A-57	SRXB-A-71

**APPENDIX B NOT USED**



**APPENDIX C      GEH RESPONSES TO NRC RAIS**



## Appendix C – Request for Additional Information

### Table of Contents

#### AOO RAIs [MFN 04-026]

<u>RAI</u>	<u>PAGE</u>
1. Time Varying Axial Power Shapes (TVAPS).....	C-2
2. TVAPS Effect for Brunswick.....	C-5
3. Effect of Lumping Water Rod Flow into the Bypass Region.....	C-12
4. Effects of Bypass Voiding.....	C-16
5. Bypass Voiding for Brunswick and Clinton.....	C-18
6. Void Fraction Greater than 90 Percent.....	C-20
7. Brunswick and Clinton - Effect of Void Fractions Greater than 90 Percent.....	C-27
8. Increased Core Flow.....	C-28
9. Hot Channel Void Fraction.....	C-29
10. ISCOR/ODYN/TASC Application.....	C-31
11. Plutonium Buildup.....	C-36
12. Spectrum Hardening.....	C-37
13. Thermal Margins.....	C-38
14. Rod Withdrawal Error.....	C-39
15. Axial Power Profiles.....	C-41
16. Reload Analyses.....	C-42
17. Thermal Limits Assessment.....	C-44
18. GEXL-Plus Correlation.....	C-58
19. Using ATWS-Recirculation Pump Trip (RPT) for AOO.....	C-59
20. Mechanical Overpower (MOP) and Thermal Overpower (TOP).....	C-60
21. Brunswick AOO.....	C-61
22. Brunswick AOO Data Request.....	C-67
23. Separate Effects, Mixed Vendor Cores and Related Staff Restrictions.....	C-68
24. Reactor Safety Performance Evaluations.....	C-70
25. Large Break ECCS-LOCA.....	C-72
26. Small Break ECCS-LOCA Response.....	C-75
27. Small Break Containment Response.....	C-77
28. Assumed Axial Power Profile for ECCS-LOCA.....	C-79
29. Power/Flow Map - Linear Upper Boundary.....	C-82
30. Power/Flow Map - Minimum Statepoint.....	C-83

**Methods RAIs [MFN 06-211]**

<b><u>RAI</u></b>	<b><u>PAGE</u></b>
1.0 Linear Heat Generation Rate (LHGR).....	C-86
1.1.....	C-86
1.2.....	C-92
1.3.....	C-99
1.4.....	C-107
2.0 Shutdown Margin (SDM).....	C-116
2.1.....	C-116
2.2.....	C-119
2.3.....	C-122
3.0 Bypass Voiding.....	C-124
3.1.....	C-124
3.2.....	C-140
3.2(a).....	C-140
3.2(b).....	C-148
3.2(c).....	C-149
4.0 Use of 40 % Void Fraction History Depletion Assumption for Instantaneous Void Fraction Changes .....	C-151
4.1.....	C-151
4.1(a).....	C-151
4.1(b).....	C-153
4.1(c).....	C-156
4.1(d).....	C-158
4.1(e).....	C-176
4.2.....	C-177
5.0.....	C-183
5.1.....	C-183
5.2.....	C-185
5.3.....	C-193
5.4.....	C-194
6.0.....	C-197
6.1.....	C-197
6.2.....	C-198
6.3.....	C-199
31 R-Factor .....	C-200
31-1 .....	C-207

NEDO-33173-A, Revision 1  
Non-Proprietary Information

**Other RAIs  
RAI**

<b>RAI</b>	<b>Page</b>
MFN 04-020 Response to MELLLA Plus AOO RAIs .....	C-209
MFN 04-033 TRACG Analyses for MELLLA Plus AOO RAI 22 .....	C-210
MFN 04-048 Request for Additional Information - MELLLA+ LTR RAI 6 .....	C-211
MFN 04-060 Revised Response to MELLLA Plus ATWS RAIs .....	C-212
MFN 04-061 Supporting Lattice Information - MELLLA+ RAI AOO 6 .....	C-213
MFN 04-067 MELLLA Plus AOO 6, TGBLA Lattice Physics Data .....	C-214
MFN 04-074 Off-Rated Conditions - MELLLA+ RAI AOO 22 .....	C-215
MFN 05-022 Responses to RAIs - Methods Interim Process 2-6, 3-1, 21-2, and 28.....	C-216
MFN 05-029 Responses to RAIs - Methods Interim Process 5, 25, 26, 27, and 29 .....	C-231
MFN 05-038 Responses to RAIs 1, 13, 14-1, 18 and 22 - Methods Interim Process .....	C-441
MFN 05-045 Response to RAIs 4-6, 12, and 17 - Methods Interim Process .....	C-470
MFN 05-048 Responses to RAIs 11 and 16 - Methods Interim Process .....	C-474
MFN 05-053 Revised Response to RAI 28-2 - Methods Interim Process .....	C-478
MFN 05-081 Revised Responses to MELLLA+ RAIs.....	C-479
MFN 06-195 Responses to Methods RAIs - Interim Methods LTR .....	C-480
MFN 06-207 Responses to Methods RAIs 1 and 5- Interim Methods LTR.....	C-481
MFN 06-209 Remaining Responses to Methods RAIs - Interim Methods LTR ..	C-482
MFN 06-434 Updated Response to RAI 28-2 .....	C-483
MFN 06-481 Responses to RAIs 7, 8, 9, 10, and 11 - NEDC-33173P .....	C-484
MFN 07-041 MELLA Plus LTR NEDC-33006P, Revised Response to RAIs AOO 3, 9, 10, and 17 .....	C-496
 REFERENCES .....	 C-497

**MFN 04-026**

**AOO RAIs**



**NRC RAI 1, Time Varying Axial Power Shapes (TVAPS)**

a. [[

]]

b. (Based on the audit). Provide a background discussion on why the fuel channels experience axial power shape changes during pressurization transients.

[[

]]

c. What are the principle factors that control the severity of  $\Delta$ CPR response to TVAPS. Does the severity of the CPR change with TVAPS increase for the EPU/MELLLA operating condition? Explain the impact of the EPU/MELLLA+ condition on the factors that control the severity of the CPR change due to TVAPS effect. Would the effect of TVAPS on the  $\Delta$ CPR be more severe for 55% CF, 80% CF, 100% CF along the MELLLA+ upper boundary or the EPU/ICF as an initial condition. Does the severity of the TVAPS effect on the CPR differ for different pressurization transient?

d. Amendment 27 to GESTAR II (submitted for staff review) states that "NRC-agreed upon methodology for evaluating GE11 and later fuel uses time varying axial power shape (TVAPS), thereby changing the need for assuring this check. See GENE-666-03-0393 and NRC staff agreement at meeting on April 14, 1993." Explain this statement and state if the NRC reviewed and approved the method used to check or account for the effect of TVAPS on the CPR change during pressurization transients.

e. If the method used to evaluate the effect of TVAPS during a pressurization transient was not reviewed by the staff in the supplement to Amendment 27, provide sufficient information, including sensitivity results so that the staff can review the method and the effects of TVAPS on the transient response for plants operating with the EPU/MELLLA+ core design.

**Response**

a. [[

]] This is described in GESTAR, Section 4.3.1.2.1.

b. Channels experience TVAPS primarily due to the reactor scram that occurs coincident with the power increase that occurs during a pressurization transient. This

effect is described in GENE-666-03-0393. The  $\Delta$ CPR result is a function of both the trend in the ODYN integral power or heat flux and TVAPS. [[

]] The dominant effect will dictate the  $\Delta$ CPR.

c. [[

]] The sequence of events and resulting affect on steam quality is shown in GENE-666-03-0393.

[[

]]

d. Initially the NRC did not formally review and approve the method used to check or account for the effect of TVAPS on the CPR change, during pressurization transients.

NEDO-33173-A, Revision 1  
Non-Proprietary Information

The NRC was first informed of the changes to the transient analysis procedure during a meeting on September 11, 1991. GE to US-NRC Letter MFN-140-91, "Pressurization Transient Analysis Procedures For GE11" [1], November 5, 1991 documents the meeting and provides a summary of the change to the analysis procedure. Subsequent to the GE11 Audit in March 1992, GENE-666-03-0393 [2,3] was provided to the NRC for information. The inclusion of the TVAPS effect in the analysis increases the conservatism in the analysis, which is an allowable change without NRC review per 10CFR50.59.

The use of TVAPS in the transient analysis is described the section 1 of the TASC Licensing Topical Report [4] and is also described in 4.3.1.2.1 of GESTAR II [5]. Since these documents are NRC approved, the use of TVAPS in the transient analysis process is considered NRC approved.

- e. TVAPS is considered NRC approved (see the response to RAI 1.4). The effect of TVAPS is described in Reference 3 and the impact of operating conditions is discussed in the response to RAI 1.3.

#### References

1. J. S. Charnley (GE) to R. C. Jones (NRC), Pressurization transient Analyses procedures for GE11, MFN-91-038, November 5, 1991.
2. J. F. Klapproth (GE) to USNRC, Time Varying Axial Power Shape for pressurization Transients, MFN-069-93, May 3, 1993.
3. Impact of Time Varying Axial Power Shape on Pressurization Transients, GENE-666-03-0393, March 1993.
4. TASC-03A, A Computer program for Transient Analysis of a Single Channel, NEDC-32084P-A, Revision 2, July 200.
5. General Electric Standard Application for Reactor Fuel, GESTAR II, NEDE-24011-P-A-14, June 2000.

**NRC RAI 2, TVAPS Effect for Brunswick**

For the Brunswick EPU/MELLLA+ analyses, explain what method will be used to calculate TVAPS. According to the proposed Amendment 27 changes to Section 4.3.1.2.1 of GESTAR, the time varying axial power shape for GE 11 fuel and later products is calculated using ODYN. The staff has been informed that Progress Energy is using TRACG to perform the EPU/MELLLA+ reload analysis. As such, how does ODYN interface with TRACG? Based on the Brunswick EPU/MELLLA+ core, provide a description of how the TVAP effect on the CPR was accounted for and calculated. Provide plots of the results.

**GE Response [Updated by MFN 05-081]**

The Brunswick-1 TRACG model includes a hot channel. Section 8.1 of NEDC-32906P-A, Revision 1, *TRACG Application for Anticipated Operational Occurrences (AOO) Transient Analysis*, describes the channel grouping process. Since the hot channel is intricate to the TRACG 3D-Kinetic method, the hot channel includes all same boundary conditions that are used in the ODYN/TASC method (although the TRACG hot channel flow is driven from the plenum-to-plenum pressure drop). The TVAPS is obtained from the 3D prediction of the hot channel power. Figures AOO-2-1, AOO-2-4, AOO-2-5 and AOO-2-6 provides the same time histories as provided in Figure 8-3 through 8-6 in NEDC-32906P-A but for Brunswick-1 Cycle 15 at MELLLA+ conditions. Figures AOO-2-2 and AOO-2-3 provide additional results for key TVAPS phenomena.

[[

]]

Figure AOO-2-1. TRACG M+ Power and Flow Response for TTNB Event

[[

]]

Figure AOO-2-2. TRACG M+ CPR Response for TTNB Event

[[

Figure AOO-2-3. TRACG M+ Channel Inlet Mass Flow Rate for TTNB Event ]]

[[

Figure AOO-2-4. TRACG M+ CPR Response for TTNB Event

]]



[[

Figure AOO-2-5. TRACG M+ Pressure and Relief Valve Response for TTNB Event ]]

[[

Figure AOO-2-6. TRACG M+ Vessel Inlet and Exit Flow for TTNB Event ]]

**NRC RAI 3, ]]**

]]

- i the performance and accuracy of the results obtained from the codes used to perform core response, during steady state, transients, and accidents (e.g., TRACG, ODYN/ISCOR/PANCEA),
- ii the CPR response for all events,
- iii the calculation of the moisture carryover and carryunder, and
- iv bundle level.

c. [[

]] Explain how this modeling technique affects the accuracy of the corresponding results. State whether the effect [[

]]

d. [[ detect and suppress instability response and the ATWS instability response. [[ ]]

]] please reanalyze all supporting cases.

e. [[

]] the ATWS instability, the detect and suppress instability, and the anticipated operational occurrence (AOO) analyses. For each event type, discuss what impact the water rod flow would have on the plant's response in terms of the parameters that are important in each phenomenon of interest. [[

]]

**GE Response [updated by MFN 07-041]**

Response to part a

[[

]]

Response to part b

The impact of [[

]] The response to RAI #5 has shown that bypass voiding is not significant for the MELLLA+ region of operation. [[

]] Therefore, the water rod modeling assumptions are not challenged for steady-state and transient calculations, CPR response, and bundle level. The accuracy of moisture carryover and carryunder are related to steam separator performance and not directly related to bypass and water rod flow modeling.

However, the following information is provided to clarify the water rod and out channel flows modeling assumptions:

- [[

]] The effects of MELLLA+ on bypass voids as simulated by ISCOR is provided in the response to RAI 5b.

[[

]]

- TRACG has a large degree of modeling flexibility. In particular, [[

]] In particular, the TRACG analysis for  
the Brunswick MELLLA+ evaluations model [[  
]]

Response to part c

See the response to RAI 3b.

Response to part d

Detect and Suppress Instability

The Detect and Suppress instability analysis using TRACG [[  
]] (e.g. TRACG analysis documented in NEDC-33075P Rev 3,  
January 2004).

ATWS Instability

TRACG analysis was performed to address [[

]] The event was initiated at 120% OLTP and 70% rated core flow  
statepoint. For the evaluated plant, this rated core power to flow ratio is 52.5 MW/Mlb/hr  
in absolute units, which is bounding of all plants expected to implement MELLLA+.

[[

]]

Response to part e  
TRACG ATWS:  
||

||

**NRC RAI 4, Effects of Bypass Voiding**

The operation at higher power at reduced core flow, the flatter power profile, and the over 24 percent higher steam flow during EPU/MELLLA+ operation may result in increased voiding in the upper bypass region, which affects both the low power range monitor (LPRM) and the traversing in-core probe (TIP) detector response. The effect of bypass voiding on the instrumentation is not random (and therefore cannot be combined with random uncertainties to determine an increase in uncertainty), but rather is a systematic effect which can bias the detector response. Therefore, the effect of bypass voiding on the core performance code systems (e.g., MONICORE - minimum critical power ratio (MCPR), linear heat generation rate (LHGR) and safety systems (e.g., average power range monitor, rod block monitor) which receive input from this instrumentation should be evaluated.

- a. Provide an evaluation of the potential for bypass voiding for the EPU and EPU/MELLLA+ operation. Describe how the bypass voiding affects the accuracy of the core monitoring instrumentation.
- b. Explain the bases for the [[ ]]
- c. Identify the codes and the corresponding models that would be affected by [[ ]]. Explain the impact of bypass voiding on the accuracy and the assumptions of the codes and the corresponding models used to simulate the boiling water reactor (BWR) response during steady state, transient, or accident conditions.
- d. [[ ]]  
[[ ]] but would not be predicted by the core simulator. Evaluate the effect of potential errors introduced by [[ ]]  
[[ ]]
- e. Supplement the MELLLA+ application to evaluate the potential and effects of bypass voiding. The supplement should provide sufficient justification and supporting sensitivity analyses to conclude that bypass voiding for the EPU and EPU/MELLLA+ will remain within an acceptable limit.

**GE Response**

- 4a. Please see the response to RAI 3a and RAI 5b for the magnitude of impact of MELLLA+ on bypass voiding. The impacts of bypass voiding on core monitoring uncertainties are covered in the Response to RAI 6e.

NEDO-33173-A, Revision 1  
Non-Proprietary Information

- 4b. LPRM uncertainty increases with increasing void. LPRM specifications limit the presence of void to [[                      ]]
- 4c. See the response to RAI 6e.
- 4d. The validity of assumptions regarding [[                      ]]  
    ]] is discussed in the response to RAI 3b.
- 4e. For additional information on the sensitivity of bypass voiding on analyses for MELLLA+ are discussed in the response to RAI 6e.



**NRC RAI 5, Bypass Voiding for Brunswick and Clinton**

- a. State whether Brunswick and Clinton are gamma tip plants. Gamma tip LPRMs are sensitive to bypass voiding.
- b. Based on the MELLLA+ core design and the most limiting core power profile and hot bundle power condition, determine whether Brunswick and Clinton would experience bypass voiding. [[  
 ]] Perform the evaluation at the different statepoints on the EPU/MELLLA+ upper boundary. Specifically, demonstrate that the bypass voiding would remain below [[  
 ]] for operation at the 55 percent CF and the 85 percent core flow statepoints.
- c. [[  
 ]] justify why the predicted bypass voiding is accurate. Provide similar justifications for the TRACG analyses.
- d. If the predicted bypass voiding is within the acceptable range, [[  
 ]] Suggest procedures or methods for checking this parameter during the reload. This is particularly important [[  
 ]] which could invalidate some of the analytical methods and affect the accuracy of the monitoring instrumentation.

**GE Response**

- 5a. Both Brunswick units (BWR/4) use gamma sensitive TIPs while Clinton (BWR/6) use thermal neutron TIPs.
- 5b The following are bounding (based on 4 bundle average power) ISCOR results for Brunswick and Clinton at the two points:

[[		
		]]

The predicted bypass voids are within [[  
 ]].

- 5c. As demonstrated in the response to RAI 5(b), the assessment of bypass voiding at the MELLLA+ condition has been performed using ISCOR, [[  
 ]] This assessment has shown that any

NEDO-33173-A, Revision 1  
Non-Proprietary Information

- significant bypass voiding will not occur in the MELLLA+ condition. Therefore, the validity of the [[ ]] models for PANACEA or TRACG application is not challenged. For more information, please see the responses to RAI 3(b) and RAI6(e).
- 5d. The plant specific applications performed thus far indicate that bypass voiding exceeding [[ ]] will not occur at the MELLLA+ boundary. For safety and licensing analysis verification, a check on bypass voiding will be implemented. However, as indicated in the response to RAI 6(e), methods adequacy will be confirmed following plant application of MELLLA+.

**NRC RAI 6, Void Fractions Greater than 90 Percent**

The Brown Ferry steady state TRACG analysis shows that the hot channel exit void fraction is greater than 90 percent. This could potentially affect the validity of the exit conditions assumed in the computational models used to perform the safety analyses. The audit documents indicates that GENE had evaluated the effect of the high exit void fraction on the analytical models, techniques and methods. However, the evaluations and the bases of the conclusions were not discussed in the MELLLA+ LTR or submitted for NRC review as an amendment to GESTAR II. The following RAIs address the effect of the high exit void fraction and quality on the EPU/MELLLA operation.

- a. Provide an evaluation of the analytical methods that are affected by the hot channel high exit void fraction (>90 percent) and channel exit quality. Discuss the impact the active channel exit void fraction would have on:
  - i. the steady-state nuclear methods (e.g., PANAC/ISCOR),
  - ii. the transient analyses methods (e.g., ODYN/TASC/ODSYS),
  - iii. the GEXL correlation, and
  - iv. the plant instrumentation and monitoring.
- b. Evaluate whether the higher channel void fraction would affect any benchmarking or separate effects testing performed to assess specific thermal-hydraulic and/or neutronic phenomena.
- c. Include in your evaluation, the effect of the high void fractions on the accuracy and assessment of models used in all licensing codes that interface with and/or are used to simulate the response of BWRs, during steady state, transient, and accident conditions.
- d. Submit an amendment to the appropriate NRC-approved codes (e.g., TRACG for AOO, ODYN/ISCOR/TASC, SAFER/GESTR/TASC, ODSYS) that updates and evaluates the impact of the EPU/MELLLA+ operating conditions such as the high exit void fraction on the computational modeling techniques and the applicability range.
- e. Submit a supplement to the MELLLA+ LTR that addresses the impact of the EPU/MELLLA+ core operating conditions, including high exit void fraction, on the applicability of the currently approved licensing methods.

**GE Response [updated with MFNs 04-061, 04-067, and 04-048]**

In addition to the responses below, the NRC requested lattice information to support confirmatory calculations. Some of the information provided by GEH letter MFN 04-061 is based on the Perry Plant. Please understand that Perry Plant has not undergone an extended power uprate and that the studies, which generated the enclosed information, are not representative of the Perry Plant's current operations. Further TGBLA lattice

NEDO-33173-A, Revision 1  
Non-Proprietary Information

physics data information was provided at the NRC's request in GE letter, MFN 04-067, dated July 1, 2004.

In both cases, the requested information in MFNs 04-061 and 04-067 is extensive, was provided on a compact disk to the NRC, and is not repeated herein.

Additionally, a presentation regarding GEH's response to NRC RAI AOO 6 was made to the NRC on March 17, 2004. Resulting from the discussions, some additional clarification has been added to the original presentation. The clarification is intended both to document the discussion during the NRC meeting and to provide the additional information requested. At the NRC's request, the final presentation was transmitted in GEH letter dated March 24, 2004 (MFN 04-048) and is provided in Enclosure A herein.

Response to Part 6 a, b, c

Please see the documentation associated with the response to RAI 6e.

Response to Part 6d

Licensing topical reports for NRC approved methodologies such as ODYSY (NEDC-32992P-A, July 2001) were submitted as generic methods reports and remain correct as written. MELLLA+ is an expansion of the range of application of these methodologies. Therefore, the methods were examined and documented collectively, not individually, per common practice for new applications. Evidence of this examination is provided in the response to RAI 6e.

Response to Part 6e

Enclosure 3 [see Enclosure B herein], Applicability of NRC Approved Methodologies to MELLLA+, has been provided which supplies technical evaluation of key technical models used within the NRC licensed methodologies as well as summary statements on the NRC licensed methodologies themselves. This information has been provided to demonstrate the applicability of the GE methodology to the MELLLA+ operating range.

Tables 6-1 and 6-2 summarize the evaluations performed and the conclusions reached. The "Steady-State Nuclear Methods" items are fundamental models, which may affect all methods employed by GE. The other items are more specific in their scope to transient analysis, GEXL, and SLMCPR.

NEDO-33173-A, Revision 1  
Non-Proprietary Information

<b>Table 6-1</b>		
<b>Enclosure Section</b>	<b>Item</b>	<b>Assessment</b>
	<b>Steady-State Nuclear Methods</b>	
2.1	Extrapolation of lattice parameters to in-channel 90% Void Fraction	<p>The technique of fitting the lattice physics data [[  ]] There is no substantial change of this assumption for MELLLA+ operating strategies. [[  ]] For these reasons, confirmation of eigenvalue tracking will be executed for the plants operating with MELLLA+ per standard procedure. Confirmation of thermal limits uncertainties (e.g., power distribution) will be executed for initial implementation of MELLLA+ strategy. See item 2.5 for disposition of derivative parameters.</p>
2.2	Void-Quality Correlation	<p>The use of the GE standard model is adequate for modeling pressure drop for the MELLLA+. The database supporting the void correlation in use by the ECPs sufficiently covers the MELLLA+ operating range.</p>
2.3	Flow Distribution Models	<p>The upper plenum pressure is nearly uniform at MELLLA+ such that steady-state bundle flow will not be impacted. The database supporting the pressure drop in use by the ECPs sufficiently covers the MELLLA+ operating range.</p>
2.4	Diffusion Theory	<p>The method is adequate. Confirmation of eigenvalue tracking will be executed for the plants operating with MELLLA+ per standard procedure. Confirmation of thermal limits uncertainties (e.g., power distribution) will be executed for initial implementation of MELLLA+ strategy.</p>

NEDO-33173-A, Revision 1  
Non-Proprietary Information

<b>Table 6-1</b>		
<b>Enclosure Section</b>	<b>Item</b>	<b>Assessment</b>
2.5	1 ½ Group Assumption	<p>The method is adequate. There is no substantial change of this assumption in going from MELLLA to MELLLA+ operating strategies.</p> <p>[[</p> <p style="text-align: center;">]] Confirmation of eigenvalue tracking will be executed for the plants operating with MELLLA+ per standard procedure. Confirmation of thermal limits uncertainties (e.g., power distribution) will be executed for initial implementation of MELLLA+ strategy.</p>
2.6	Spectral History Impacts of Extended High Void Operation	<p>The method is adequate. The dominant spectral effect in MELLLA+ of physical void history is included in PANACEA. The use spectral history model of PANAC11 is an additional improvement since it makes a correction to the nuclear library lookup process to account for effects due to hardened spectrum separate from void history.</p>
2.7	Direct Moderator Heating Model	<p>The method is adequate. MCNP calculations show that [[</p> <p style="text-align: center;">]] Additionally, the [[</p> <p style="text-align: center;">]] of the current model is confirmed at the higher void fractions associated with MELLLA+.</p>
2.8	Bypass Void Models	<p>The method is adequate for MELLLA+ application. Even if [[</p> <p style="text-align: center;">]] were to occur at the D level LPRM, the resulting nodal power error is about [[</p> <p style="text-align: center;">]] and the impact on bundle power is negligible. Confirmation of eigenvalue tracking will be executed for the plants operating with MELLLA+ per standard procedure. Confirmation of thermal limits uncertainties (e.g., power distribution) will be executed for initial implementation of MELLLA+ strategy.</p>



NEDO-33173-A, Revision 1  
Non-Proprietary Information

<b>Table 6-1</b>		
<b>Enclosure Section</b>	<b>Item</b>	<b>Assessment</b>
5.2	Review GETAB and Reduced SLMCPR Uncertainties	The method is adequate for licensing. Confirmation of thermal limits uncertainties (e.g., power distribution) will be executed for initial implementation of MELLLA+ strategy.



NEDO-33173-A, Revision 1  
Non-Proprietary Information

For additional clarification, the following table provides a cross reference of applicable NRC approved methodologies (Reference 1) and the areas of concern for MELLLA+ operation.

IMPACT AREA\ METHODOLOGY	TGBLA	PANACEA	ISCOR	ODYN	TASC	ODYSY	SAFER	TRACG	SLMCPR
<b>Steady State Nuclear Methods</b>	[[								
Extrapolation of XS to 90% Void									
Void Quality Correlation									
Flow Distribution Models – Pressure Drop									
Diffusion Theory									
1.5 Group Assumption									
Spectral History Impacts									
Direct Moderator Heating Model									
Bypass Void Models									
[[									
TIP/LPRM Correlations									
<b>Transient Analysis Methods</b>									
Steam Separator Model									
High Power/Low Flow Ratio									
Time/Depth of Early BT									
<b>GEXL Correlation</b>									
Database over 90% Void									
Off-rated Conditions									
<b>Plant Instrumentation &amp; Monitoring</b>									
D LPRM Level Void Uncertainty									
SLMCPR Uncertainties									]]

The final technical conclusion is that GE has systematically examined its NRC approved methodologies with regard to operation in the MELLLA+ domain. GE has found that these methods are adequate.

However, GE believes that methodology performance within the MELLLA+ operating domain be examined carefully once a significant set of plant data is available. [[

]] In addition, while no licensing issues have been determined to be outstanding regarding the methods and their application ranges, a recommendation that the thermal limits uncertainties be confirmed for the initial implementation of the MELLLA+ strategy applies to the technology areas. This confirmation should include [[

in NEDC-32694P-A. Also at the time of implementation, the [[ ]]] will be reviewed as per the NRC instruction in NEDC-32601P-A.

**NRC RAI 7, Brunswick and Clinton - Effect of Void Fractions Greater than 90 Percent**

- a. Explain how the core averaged void fraction reported in the heat balance table is computed. For example, the Brunswick MELLLA+ application reports core averaged void fractions in the range of 0.51 to 0.54 for different statepoints.
- b. For the EPU/MELLLA+ core design, what is the hot channel exit void fraction for the steady state operation at the EPU 120 percent power/99 percent CF, EPU/MELLLA+ 120 percent power/85 percent CF and the EPU/MELLLA+ 77.6 percent power/55 percent CF statepoints? Use bounding conditions.

**GE Response**

- a. This value is the active coolant average void fraction. The bypass and unheated regions are not included in this average.

$$\langle VF \rangle = \frac{\sum_{i=1}^{\# \text{ each type}} n_i \frac{\sum_{k=1}^{24} VF_k FlowArea_k}{24 \langle FlowArea \rangle}}{\text{Total \# of Bundles}}$$

, where i is the ISCOR channel types and k is the axial nodes.

- b. The following are results for Brunswick 1, Cycle 15 at the MOC transient point.

[[		
		]]

Note, values at 120% / 104.5% are provided instead of 120% / 99% to provide the full range of void fractions with licensed core flow.

**NRC RAI 8, ICF**

Are the shutdown margin, standby liquid control system shutdown capability and mislocated fuel bundle analyses performed at the rated conditions (100 percent EPU power/100 percent CF). If so, justify why these calculations are not performed for the nonrated conditions such as the ICF condition. Provide supporting sensitivity analysis results for your conclusions or update the GESTAR II licensing methodology, stating that these calculations would be performed at the ICF statepoint.

**GE Response**

These analyses are performed for each reload core design to confirm that the acceptance criteria documented in GESTAR-II is met.

**a. SDM and SLCS**

These analyses confirm that acceptable reactivity margins exist in the core throughout the cycle. [[

are not performed at rated conditions. ]]

**b. Mislocated Bundle**

This analysis confirms that the fuel thermal margins for the worst postulated fuel load mislocation are within those acceptable for AOOs. [[

analysis is not performed at rated conditions. ]]

**NRC RAI 9, Hot Channel Void Fraction**

The hot channel void fraction increases with decreasing flow along the MELLLA+ upper boundary. Therefore, the void fraction at the 55 percent CF and the 80 percent CF statepoints are higher than the void fraction at 99 percent CF. Consequently, it is feasible that the initial conditions of the hot channels could be higher at the minimum core flow statepoints or at the offrated conditions.

- a. Justify why the steady-state initial critical power ratio (ICPR) is assumed in determining the offrated AOO response, instead of the ICPR calculated from offrated conditions.
- b. For the most bounding conditions, compare the steady-state ICPR calculated based on the actual conditions at the state points (rated, 80 percent CF, and 55 percent CF or offrated lower power and flow conditions).

**GE Response [updated by MFN 07-041]**

a. [[

]]

b. The ICPR associated with the results in Table 9-2 of the M+ LTR is as follows:

[[		

NEDO-33173-A, Revision 1  
Non-Proprietary Information

[[		
		]]

The offrated ICPR at 55% core flow is as follows:

[[		
		]]

[[

]]

**NRC RAI 10, ISCOR/ODYN/TASC Application**

The transient CPR and the peak cladding temperature (PCT) calculations are performed using the ODYN/ISCOR/TASC combination. The staff understands that ISCOR calculates the initial steady-state thermal-hydraulic core calculations. ODYN (1-D code) provides the reactor power, heat flux, core flow conditions, and the axial power shapes of the hot bundle during the transient. [[

]] The ISCOR/TASC combination is also used to calculate the PCT for ECCS-LOCA and Appendix R calculations. In addition, ISCOR/TGBLA/PANAC code combinations are also used in core and fuel performance calculations.

- a. ISCOR is widely used in many of the safety analyses, but the code was never reviewed by the NRC. The use of a non-NRC-approved code in a combined code system applications is problematic. Therefore, submit the ISCOR code for NRC review.
- b. Although ISCOR is not an NRC-approved code, our audit review did not reveal specific shortcomings. [[

]]  
Therefore, include in the ISCOR submittal a description and evaluation of the ISCOR/ODYN or ISCOR/TGBLA/PANAC code combination discussed above. Provide sufficient information in the submittal, including sensitivity analyses, to allow the staff to assess the adequacy of these combined applications.

- c. During the MELLLA+ audit , the staff discovered that GENE had internally evaluated a potential non-conservatism that may result from the use of the flow-driven ISOR/ODYN/TASC combination to calculate the transient  $\Delta$ CPR. [[

]]

**GE Response [updated by MFN 07-041]**

Response to part a.

ISCOR calculates the flow distribution between the fuel channels and the bypass region for a given total core flow. The calculation of the flow distribution is based on a balancing of the pressure drop between the different channels; the flow is distributed such that all channels all have the same pressure drop. The thermal hydraulic model for the

pressure drop is described in Section 4.2 of GESTAR II (Reference 1) and further details are contained in the response to request for additional information on Section 4 – Steady State Hydraulic Analyses in Appendix B of GESTAT II US Supplement (Reference 2). The response to the RAI describes the process for the calculation of the hot bundle flow. Further details on the model are provided in Section 4 of reference 3. All of these documents are NRC approved documents.

The hot channel response is calculated by TASC (Reference 4), which is an NRC approved report and describes the use of ISCOR to calculate the hot channel flow for TASC (see Figure 1-1 in Reference 4).

This methodology of using ISCOR in the transient methodology to provide input for the single channel analysis from the core average response has been used in both the GENESIS as well as the GEMINI methodologies. References 5-7 contain the qualification of the combined process starting with the calculation of the system response and ending with the calculation of the hot channel transient CPR response. References 5-7 are NRC approved documents.

GE considers the ODYN/ISCOR/TASC methodology approved based on references 1-7. There is therefore no need to submit ISCOR for NRC review.

Response to part b.

See the response to 10.a and 10.c, part iii.

Response to part c.

i. Describe the issues identified in the PRC

The PRC 91-01 issue was identified as follows:

“For some of the GE performed transient analyses, output of the system response code ODYN is used as input to the GETAB/TASC codes to calculate the transient change in MCPR for the hot bundle. This result is then combined with the Safety Limit MCPR and may be used to determine the operating limit MCPR. Currently, the ODYN calculated core flow is used as an input; a GETAB/TASC (ISCOR) determines the flow/pressure drop and transient Critical Power Ratio (CPR) for the hot bundle. Another approach is to assume that the ODYN calculated core pressure drop is the same for all fuel bundles, and have GETAB/TASC calculate the flow and CPR change for the hot bundle. Apparently, previous studies indicated that there was little difference in the results of the two approaches. However, some recent scoping studies have indicated that for some plants, some transients, and some critical power correlations, the latter approach results in higher calculated transient CPR changes that could result in calculationally exceeding the Safety Limit MCPR”

ii. Explain if an alternative approach was proposed in the PRC

The design basis NRC approved method is the ODYN flow driven method. The alternative approach is the ODYN pressure drop driven method. When GE

reviewed the complete ODYN/TASC process, it was evident that the ODYN prediction of pressure drop had a strong influence on the result and there was a concern that the flow driven method may not be adequately conservative.

iii. Explain why it was concluded that the alternative approach was not technically acceptable

The conclusion was that the existing NRC approved ODYN flow driven method is technically acceptable. The alternate ODYN pressure driven method is more conservative, but since the existing approved method is acceptable, it is not necessary to change to the ODYN pressure driven method. Since TRACG is the most complete model, it was utilized to determine the overall accuracy of the approved ODYN/GETAB/TASC (ISCOR) flow driven method. The resulting design transient  $\Delta$ CPR was found to be conservative relative to TRACG. [[

]] The ODYN/GETAB/TASC (ISCOR) flow driven method was (and still is) considered the NRC approved method. Had the TRACG analysis not shown that the approved ODYN flow driven method was adequate, GE would have informed the NRC of their desire to change to the more conservative ODYN pressure driven method.

iv. Explain the bases for closing the PRC

The PRC 91-01 evaluation determined that the current flow driven method is acceptable. Best estimate calculations for limiting transients showed that the  $\Delta$ CPR using the current NRC approved analysis procedure provides acceptably conservative results. Therefore, it was concluded that this issue did not represent a Reportable Condition under of 10CFR Part 21.

v. Justify why the NRC was not informed, considering that a non-NRC approved codes were being used to both evaluate the identified non-conservatism (TRACG) and correct the ODYN 1-D hot bundle flow deficiencies (ISCOR)

The NRC is informed when there is a reportable condition, 60 Day Interim Notification, or when a GENE PRC evaluation relates to an industry identified issue. The NRC is not normally informed of issues evaluated by GENE when it is concluded that it is not reportable or a Part 21 Transfer of Information is issued because GENE does not have the necessary information to complete the evaluation. In some cases, GENE may use more realistic, though still



conservative methods to perform a PRC evaluation. For this case, that included using a non-NRC approved code to examine the adequacy of the simpler ODYN method to assess a potential non-conservative aspect of the approved procedure. Use of more realistic methods in a GENE internal PRC evaluation does not change the criteria by which an issue is reported to the NRC, i.e., it is reported only when it has been determined to be a reportable condition, the evaluation cannot be completed in 60 days, or it relates to an industry identified issue.

#### References

1. General Electric Standard Application for Reactor Fuel, GESTAR II, NEDE-24011-P-A-14, June 2000.
2. General Electric Standard Application for Reactor Fuel (Supplement for United States), NEDE-24011-P-A-14-US, June 2000.
3. Steady State Nuclear Methods, NEDE-30130-P-A, April 1985.
4. TASC-03A Computer Program for Transient Analysis of a Single Channel, NEDC-32084P-A, July, 2002.
5. Qualification of the One-Dimensional Core Transient Model for Boiling Water Reactors. NEDO-24154-A, Volume I, August 1986.
6. Qualification of the One-Dimensional Core Transient Model for Boiling Water Reactors. NEDO-24154-A, Volume II, August 1986
7. Qualification of the One-Dimensional Core Transient Model for Boiling Water Reactors. NEDE-24154-P-A, Volume III, August 1988

[[

]]

**NRC RAI 11, Plutonium Buildup**

It is expected that a EPU/MELLLA+ core would produce more Pu(239). What are the consequences of this increase from a neutronic and thermal-hydraulic standpoint during steady-state, transient, and accident conditions?

**GE Response**

The core simulator will properly capture any resulting increase of plutonium from high void operation. Additionally, the cycle specific transient analyses consider variation on the burn strategy and Pu production by varying the degree at which the bottom of the core is burned early in the cycle. Therefore, any changes in isotopic inventory because of MELLLA+ operation will be explicitly modeled for the purposes of determining cycle specific analyses including selection of rod patterns, safety evaluations (SDM), transient evaluations, as well as others.

**NRC RAI 12, Spectrum Hardening**

How does the harder spectrum from the increased Pu affect surrounding core components such as the shroud, vessel, and steam dryer?

**GE Response**

The hardening of neutron spectrum from the increased Pu mainly affects the thermal and epi-thermal energy regions and has insignificant effect on fast neutrons with energy greater than 1 MeV. Since the damage effect of neutron irradiation on the surrounding core components such as the shroud, vessel, and steam dryer is based on fast neutron ( $E > 1$  MeV) fluence, the increased Pu does not have significant effect on the surrounding core components. [[

]] The increased void fraction does affect the flux distribution near the top of the core and beyond. The extent of impact could vary from plant to plant and requires plant specific evaluation. [[

]]

NRC RAI 13, Thermal Margins

How do the thermal margins change as a function of flow and transients for a EPU/MELLLA+ cores?

**GE Response**

The only EPU/MELLLA+ core is Brunswick-1 Cycle 15. The  $\Delta\text{CPR}/\text{ICPR}$  is determined with TRACG. The following table provides  $\Delta\text{CPR}/\text{ICPR}$  as a function of power and flow.

[[			
			]]

**NRC RAI 14, Rod Withdrawal Error**

Demonstrate that the rod withdraw error (RWE) for the EPU/MELLLA+ domain is less limiting than the non-MELLLA+ domain throughout the cycle.

**GE Response [Updated with MFN 05-081]**

The analysis procedure varies depending on the type of rod block monitoring (RBM) system. Plants crediting the flow biased RBM system utilize the Plant/Cycle Specific Analysis procedure described in GESTAR II Section S.2.2.1.5. [[

]] The results of the analysis are used as the plant/cycle specific limit.

[[

]] The plant/cycle analysis procedure for this type basis also requires a conservative initial rod pattern assumption. [[

]] The results of the analysis are compared to the generic statistical limit for each applicable setpoint. If the plant/cycle analysis results exceed the generic limit, the plant/cycle results are applied; otherwise, the generic limits are applied.

[[

]] The following are the results of this study:

[[		
		]]

The following is a similar study for Brunswick-1 Cycle 15 at MELLLA+:

[[		
		]]

NEDO-33173-A, Revision 1  
Non-Proprietary Information

[[ ]] A comparison of the RWE  $\Delta$ CPR/ICPR response comparing rated core flow to the EPU/MELLLA+ domain will be provided in the plant-specific EPU/MELLLA+ application.

**NRC RAI 15, Axial Power Profiles**

If the axial power profile is expected to be more pronounced (more limiting) for a EPU/MELLLA+ core, demonstrate and provide a quantitative and qualitative technical justification of the effects of these more pronounced profiles on the normal and transient behavior of the core.

**GE Response**

[[

]]



**NRC RAI 16, Reload Analyses**

Since the startup and intermediate rod patterns are developed by the licensees and subject to change during plant maneuvers, explain how you ensure that the core and fuel assessment analyses performed during the reload are still applicable. For example, if the safety limit for minimum critical power (SLMCPR) is performed at different burnup conditions during the cycle, how do you ensure that the plant's operating history does not invalidate the reload assumptions? How are the corrections or adjustments made to the plant's core and fuel performance analyses to ensure the parameters and conditions assumed during the reload analyses remain applicable during the operation. The staff's concern stems from the additional challenges that EPU/MELLLA+ pose in terms of core and fuel performance.

**GE Response [Updated with MFN 05-081]**

The reload licensing analysis is based on a reference core loading which is documented in the Supplemental Reload Licensing Report (SRLR) for the plant and cycle being licensed. Deviations to this licensed reference core loading are allowed under the criteria defined in Section 3.4 of GESTAR II. Any variations in the core loading outside of these allowable deviations must undergo a re-examination as spelled out in that same section of GESTAR II. This re-examination can result in up to a complete relicensing analysis if necessary.

The reload license analysis is also based on an assumed operational trajectory or set of design rod patterns. These design rod patterns represent a relatively detailed simulation of core operation at rated power using an operational philosophy that incorporates any utility instructions (regarding how they intend to operate), that optimizes core performance in regards to energy capability, thermal margins, operational simplicity and that meets all design and licensing requirements. The key nuclear reactivity assessments for reload licensing [strong-rod-out (SRO) shutdown margin and standby liquid control system (SLCS) shutdown margin as specified in Section 3.2 of GESTAR II] are analyzed both at beginning of cycle (BOC) and at selected exposure points through the cycle in enough detail to assure the maximum reactivity point during the cycle has been determined and that it meets the specified licensing criteria. To assure that the analysis will cover operational uncertainties in the previous cycle shutdown, these reactivity analyses are performed assuming a minimum energy accumulation scenario for the previous cycle. This previous cycle minimum energy requirement is also documented in the SRLR. Typically this previous cycle energy assumption has a stronger effect on the cold reactivity calculations (because it results in the carryover of additional reactivity on all of the exposed fuel) than variation in operational rod patterns. This is especially true for the SLCS analysis which is a core-wide reactivity event, not particularly sensitive to changes in local reactivity, and which most often exhibits minimum margin at BOC. For the SRO shutdown margin analysis a BOC demonstration is required of the plant and this demonstration is performed on the actual as-loaded core conditions.

The end of cycle (EOC) pressurization transients from which the core delta critical power ratio ( $\Delta$ CPR) and ultimately the core minimum critical power ratio operating limit

(OLMCPR) are derived based on [[

]]

The statistical limit minimum critical power ratio (SLMCPR) analysis is performed under procedures and criteria approved by the NRC. In the SLMCPR analysis limiting rod patterns are established at multiple exposure points during the cycle so as to adequately characterize the core behavior. The limiting rod pattern criteria is constructed to achieve a core state at each of the exposure points that represents a limiting condition for establishing the SLMCPR. The object of the limiting rod pattern is to place a substantial fraction of the high power, interior bundles near the MCPR limit and then perform statistical analysis to determine the SLMCPR value at which 0.1% of the fuel rods would become susceptible to boiling transition. The object of achieving a relatively flat, near-limits core condition with the limiting rod pattern is to place a higher percentage of fuel bundles (and thus fuel rods) closer to this boiling transition threshold; enabling the 0.1% criteria to be reached at a higher SLMCPR. The statistical analysis for determining the SLMCPR is performed at all exposure points and the most limiting of these values is used to establish the SLMCPR for the plant/cycle.

**NRC AOO RAI 17, Thermal Limits Assessment**

- a. SLMCPR. It is possible that the impact on the critical heat flux (CHF) phenomena may be higher at the off rated or minimum core flow state points. Is the SLMCPR value provided in the SLMCPR amendment requests and reported in the TS based on the rated conditions? If so, justify why the SLMCPR is not calculated for state points other than the rated conditions. Quantitatively demonstrate that the SLMCPR calculated at the minimum 80 percent and 55 percent state points would be lower than the SLMCPR calculated at the rated conditions. Use power profiles and core designs that are representative of the EPU/MELLLA+ conditions. Discuss the assumptions made. Include the Brunswick EPU/MELLLA+ application in your sensitivity analyses.
- b. SLMCPR at EPU/MELLLA+ Upper Boundary. The SLMCPR at the non-rated conditions (EPU power/80 percent CF) could be potentially higher than the SLMCPR at rated conditions, explain how "state point-dependent" SLMCPR would be developed and implemented for operation at the EPU/MELLLA+ condition. Use the Brunswick EPU/MELLLA+ application to demonstrate the implementation of "state point-dependent" SLMCPR.
- c. Exposure-Dependent SLMCPR. Discuss the development of the exposure-dependent SLMCPR calculation. State whether this is an NRC-approved method and refer to the applicable GESTAR II amendment request.

**GE Response [updated by MFN 07-041, which replaced 05-081]**

Response to Part a and b

Summary

The 10CFR21 evaluation documented in MFN 04-108 determined that a lower flow condition at rated power could have a more limiting SLMCPR than the rated flow condition. As a result, the SLMCPR process requires analysis at rated core power and both rated core flow and the minimum licensed core flow. The SLMCPR at off-rated power conditions (including the 55% flow point on the MELLLA+ rod line) will not differ significantly (bounded or less than 0.005 higher) from the rated core power result. The Technical Specification SLMCPR is set to the resulting value or a conservative value.

The Technical Specification SLMCPR is applied to all operating conditions. In other words, state point dependency is not approved.

A comparison of the 55% flow point on the MELLLA+ rod line SLMCPR with rated core power SLMCPR results will be provided in the plant-specific EPU/MELLLA+ application.

SLMCPR Process Background

The calculated SLMCPR was previously based on the highest rated licensed power and flow conditions. This approach had been shown in NEDC-32601P-A to produce

SLMCPR values that are slightly conservative compared to off-rated flow conditions (note in particular Figure II.4-1 on page B-5). However, recently it was determined that a rated power / reduced flow condition may result in a higher SLMCPR value due to changes in limiting control rod patterns to compensate for lower reactivity at reduced flow, as was discussed in MFN 04-108. All current SLMCPR evaluations account for this condition by determining the SLMCPR at both rated and lowest licensed flow corresponding to the rated power conditions, and then using the highest calculated SLMCPR value for the cycle specific licensing evaluation. The following discussion extends the evaluation to off-rated power / flow operating conditions, including the MELLLA+ region, and concludes that the cycle specific SLMCPR value calculated as discussed above is conservative to cover off-rated power / flow operating conditions. The two key phenomena at off-rated conditions that affect the SLMCPR are addressed here, first is the off-rated power distribution and second are the off-rated power and flow uncertainties. As discussed herein, the power distribution and, consequently, the CPR distribution tend to have a slightly less limiting effect at reduced power. Additionally, both the power and flow uncertainties are relatively constant at the higher power and flow range, and bounded by the values applied in the design analysis, and become larger at non-limiting low power and flow conditions.

#### Impact of MELLLA+ Operation on SLMCPR

Whereas CPRs are sensitive to flow and CPR decreases as the flow decreases, the SLMCPR is sensitive to the relative distribution of the CPRs, not their absolute values. The relative distribution of CPRs in the core does not change appreciably with flow changes in the operating domains where the power is high enough for CPRs to be a concern. Rather, the SLMCPR is dominated by the uncertainty in CPRs as a result of the uncertainties in the two dominant inputs: power and flow.

Due to a slight flattening of the relationship between critical power and flow at the higher flows, the CPR distributions in the core tend to be slightly flatter at the higher flows so the calculated SLMCPR increases very slightly for the higher flows (as shown in Figure II.4-1 on page B-5 of NEDC-32601P-A).

The bundle designs and core loading configuration strongly influence the SLMCPR. Both of these are accounted for by performing cycle-specific analyses utilizing the actual bundle designs and the reference core loading. The bundles must be designed and the core loaded to support MELLLA+ operation. From the perspective of CPR performance this generally means that the bundles must have a very flat critical power response over a wide range of flows. MELLLA+ operations that use reduced flow to harden the neutron spectrum in order to build-in plutonium and extend cycle operation have two competing effects on bundle design. (1) Rod peaking factors must be maintained low enough that CPR performance can still be achieved at high powers and lower flows, e.g., the bundle designs need to be flattened. (2) Rod enrichments need to be high enough to achieve the desired cycle exposures and maintain sufficient reactivity to offset the negative impact of higher core voiding at the reduced flows, e.g., the bundle peakings are increased to accommodate more enrichment and the associated increases in gadolinium loaded to control the reactivity. All these effects are accounted for in the present cycle-specific

SLMCPR methodology that evaluates the actual bundle designs to be loaded. Generally speaking, bundle designs for MELLLA+ operations tend to go in the same direction as for extended power uprates (EPU) and longer-exposure cycles, namely in the direction of being slightly more peaked which means that calculated SLMCPRs continue to trend downward.

Higher core power levels require lower radial peaking factors to maintain adequate margin to the operating limit MCPR (OLMCPR). Consequently, each bundle must be closer in power to the average bundle power so that either the average power per bundle can increase as is the case for EPU or the flow can be reduced for the same bundle power, as is the case for MELLLA+. Both scenarios result in a flatter MCPR distribution in the as-loaded core. If this were the only effect, one would expect that calculated SLMCPR values would be increasing whereas, in fact, they are not. This is because higher core powers also require higher fresh reload fuel batch fractions. These fresh fuel batches must consist of mixed streams of different bundle designs in order to control reactivity during the cycle and minimize enrichment costs. Thus, the number and distribution of MCPRs for the highest power bundles in the design that set the SLMCPR for the core remain approximately constant. The absolute power needed to drive the MCPR in these bundles down to the SLMCPR during a postulated AOO event remains unchanged since this power depends only on the critical power capability of the bundle. The fact that these limiting bundles may start at a lower MCPR because of reduced flow (or higher power) is relevant for the assessment of the OLMCPR, but is not relevant for the SLMCPR that depends only on the relative distributions of these bundle MCPRs.

Both the SLMCPR and the OLMCPRs for different scenarios are determined on a cycle-specific basis considering the actual bundle designs, the reference loading pattern, and the use of CPR distribution limiting control blade patterns. Again the key point with respect to the SLMCPR is that these considerations are no different from those that are already considered as part of the cycle-specific SLMCPR evaluations.

#### Off-Rated SLMCPR Sensitivity Demonstration

The Brunswick 1 Cycle 15 core design was selected to illustrate the effects of off-rated power and flow conditions on the SLMCPR calculation for EPU/MELLLA+ applications. The proposed MELLLA+ power / flow map for the Brunswick nuclear units is shown in Figure 17-1. SLMCPR values were determined for three power / flow state points along the upper boundary of the map and for the rated power / lowest flow point being considered for generic MELLLA+ operation (100%P / 80%F), as defined in Table 17-1.

Case (1) was the rated condition (state point “E” in Figure 17-1) SLMCPR evaluation that was used in the Reload Licensing Analysis for Brunswick 1 Cycle 15. Case (2) determined the SLMCPR for the rated power / lowest licensed flow condition (state point “N” in Figure 17-1). Case (3) determined the SLMCPR for rated power / lowest flow for the generic MELLLA+ application, for comparison purposes. Case (4) determined the SLMCPR for the highest off-rated power / lowest off-rated flow statepoint along the Brunswick 1 MELLLA+ upper boundary (point “M” in Figure 17-1).

Cases (1) and (2) addressed the Part 21 reportable condition (MFN 04-108) for the Brunswick 1 MELLLA+ extended operating domain. As discussed above, the SLMCPR for the cycle specific application is the most limiting of these two cases.

Cases (2) and (4) correspond to points N and M, respectively, on the MELLLA+ boundary, as seen in Figure 17-1. The SLMCPR calculations for these two cases used a fixed set of control rod patterns for a given exposure point calculation, as shown in Figure 17-2. This was done to illustrate the impact to SLMCPR when moving between state points M and N along or near the MELLLA+ boundary line without the effects of changing the limiting control rod configuration, which is typical of plant operation following control blade maneuvers which are performed at off-rated conditions.

The SLMCPR calculations for all cases (1) through (4) used uncertainties that have been previously reviewed and approved by the NRC as listed in Table 17-2 and described in NEDC-32601P-A, except for the R-factor uncertainty, which was slightly increased to conservatively account for effects of potential increased channel bow.

It was determined that it is appropriate to use the feedwater and core flow uncertainties currently used for SLMCPR evaluation at rated conditions for the off-rated SLMCPR evaluations. Figure 17-3 provides the change in the feedwater and core flow uncertainties as the core flow decreases, as calculated for various BWR design types. Figure 17-4 provides the sensitivity of the calculated SLMCPR value to changes in the four most significant uncertainties. Figure 17-4 shows that the feedwater flow rate uncertainty has the strongest impact on SLMCPR, followed by the core flow uncertainty. In SLMCPR evaluations a feedwater flow uncertainty of  $\pm 1\%$  is used for rated conditions, which Figure 17-3 shows is valid down to approximately  $\pm 1\%$  rated feedwater core flow, covering all off-rated cases of interest. Similarly for core flow, an uncertainty of  $\pm 1\%$  is used for rated conditions and is valid down to approximately  $\pm 1\%$  rated core flow. This directly covers the off-rated conditions for cases (2) and (3). Case (4) uses only  $\pm 1\%$  lower core flow (55% rated core flow), and Figure 17-3 shows that the core flow uncertainty for this case is approximately  $\pm 1\%$ . Using the SLMCPR / core flow uncertainty relationship from Figure 17-4, the impact of the corresponding uncertainty increase from  $\pm 1\%$  would be about +0.0012, a negligible effect compared to the inherent 1 sigma uncertainty ( $>0.005$ ) of the Monte Carlo SLMCPR calculation methodology. Therefore, the rated condition uncertainties in Table 17-2 are appropriate to use for the SLMCPR calculations at off-rated conditions.

Tables 17-3 and 4 summarize the results of the SLMCPR evaluations for Brunswick 1 Cycle 15. For each case, three distinct cycle exposure points were analyzed: beginning-of-cycle (BOC, 181 MWd/ST), peak-hot-excess (PHE, 9072 MWd/ST), and near the end-of-cycle (EOC, 14440 to 14940 MWd/ST). The last column in Table 17-4 shows, for each case, the most limiting SLMCPR result for the entire cycle exposure range. Each column labeled BOC, PHE, EOC, and SLMCPR, is further divided into two sub-columns, the first displaying the SLMCPR results, and the second showing the difference between the two adjacent cases. The last row of Table 17-4 shows the total change in

NEDO-33173-A, Revision 1  
Non-Proprietary Information

SLMCPR as we follow the path on the power-flow map from the rated point E to the lower MELLLA+ boundary point M (see Figure 17-1). For each exposure point, the total impact in SLMCPR as power and flow vary from the most limiting of the rated case (1) and the low flow case (2) to the lower MELLLA+ boundary case (4) is between -0.01 to -0.00.

A change in SLMCPR by more than 0.005 is considered a significant change. This threshold was chosen to correspond to the inherent variability in the Monte Carlo process for determining the safety limit. It is also consistent with the accepted practice of rounding and reporting SLMCPR values to two places past the decimal point. By definition, a change in a statepoint condition that goes into the evaluation of a SLMCPR is not significant unless it results in an increase in the calculated SLMCPR by +0.005. From the results shown in Tables 17-3 and 4, the changes in power and flow expected with EPU/MELLLA+ operation would not result in any significant changes compared to SLMCPR at the rated power condition.

Consequently, a SLMCPR evaluated for rated power MELLLA+ conditions is also valid for MELLLA+ off-rated power / flow conditions.

Response to Part c

SLMCPR analyses are performed for multiple exposure points throughout the cycle. Exposure interval end points are then selected such as to be equal to an SLMCPR analysis exposure point. The maximum SLMCPR analysis value within that exposure interval (including end points) is selected to be the exposure dependent SLMCPR value for that exposure interval. The following tables present an arbitrary example where five SLMCPR analyses are performed to create two exposure dependent SLMCPR intervals (Note: In this example four unique exposure dependent SLMCPR intervals are possible, but they were collapsed into the use of only two exposure dependent SLMCPR intervals).

NRC approval of GESTAR II Rev. 14 (NEDE-24011-P-A-14) specifically allows the SLMCPR values to be stipulated as a function of exposure. The exposure-dependent SLMCPR values were introduced in Amendment 25 to GESTAR II that was submitted for NRC review and approval in December 1996. The NRC SER approving this approach was issued March 11, 1999. This approval was reflected in section 1.1.5.B.vii of GESTAR II Rev. 14.

SLMCPR Analysis Results

Exposure (GWd/ST)	BOC	5.0	10.0	15.0	EOC
SLMCPR	1.11	1.10	1.09	1.08	1.10

NEDO-33173-A, Revision 1  
Non-Proprietary Information

Exposure dependent SLMCPR

Exposure Range (GWd/ST)	SLMCPR
BOC to 10.0	1.11
10.0 to EOC	1.10



**Table 17-1. Brunswick 1 Cycle 15 SLMCPR Evaluation Case Description**

Evaluation Case Number	Case Description
Case (1)	100%P / 100%F – rated EPU case (state point E in Figure 17-1)
Case (2)	100%P / 85%F – upper BSEP MELLLA+ Power-Flow map case (NEDC-33063P) (state point N in Figure 17-1)
Case (3)	100%P / 80%F – upper generic MELLLA+ Power-Flow map case (NEDC-33006P)
Case (4)	77.6%P / 55%F – lower BSEP MELLLA+ Power-Flow map case (NEDC-33063P) (state point M in Figure 17-1)

**Table 17-2. Uncertainties Used for Brunswick 1 Cycle 15 SLMCPR Evaluation Cases**

<b>Description</b>	<b>Brunswick 1 Cycle 15</b>
<b>Standard Non-power Distribution Uncertainties</b>	Revised NEDC-32601P-A
Core flow rate (derived from pressure drop)	2.5 (Two Loop)
Individual channel flow area	[[ ]]
Individual channel friction factor	5.0
Friction factor multiplier	[[ ]]
Reactor pressure	[[ ]]
Core inlet temperature	0.2
Feedwater temperature	[[ ]]
Feedwater flow rate	[[ ]]
<b>Standard Power Distribution Uncertainties</b>	Revised NEDC-32601P-A
GEXL R-factor	[[ ]]
Random effective TIP reading	1.2 (Two Loop)
Systematic effective TIP reading	[[ ]]
Integrated effective TIP reading	[[ ]]
Bundle power	[[ ]]
Effective total bundle power uncertainty	[[ ]]
<b>Exceptions to the Standard Uncertainties</b>	
GEXL R-factor	[[ ]]

**Table 17-3. Summary of SLMCPR Results for Brunswick 1 Cycle 15**

II												
												II

**Table 17-4. SLMCPR Sensitivity Results for Brunswick 1 Cycle 15**

II									
									II

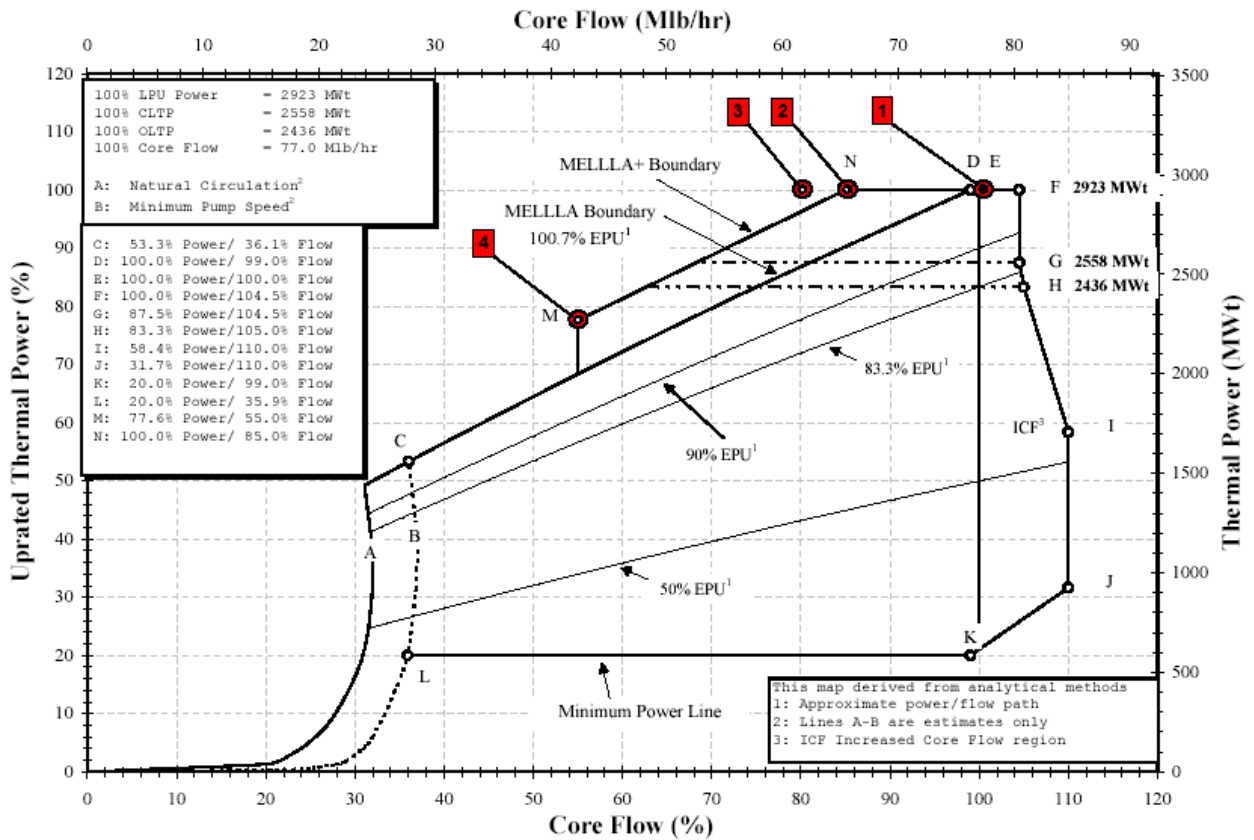


**Figure 17-1 BSEP 1 and 2 MELLLA+ Operating Range Power-Flow Map (NEDC-33063P)**

[[

**Figure 17-2 Limiting Rod Patterns Used in Cases 100P/85F and 77.6P/55F**

]]

[[

**Figure 17-3 Total Core Flow and Feedwater Flow Uncertainties for BWRs 4/5/6**

]]

[[

**Figure 17-4 Four Dominant SLMCPR Sensitivities for a Factor Change in the Generic GETAB Uncertainty Value**

]]



**NRC RAI 18, GEXL-PLUS Correlation**

Confirm that the GEXL-PLUS correlation is still valid over the range of power and flow conditions of the EPU/MELLLA+ operations.

**GE Response**

See the response to RAI 6(e) for justification of adequacy of the GEXL+ correlation for MELLLA+ conditions.

**NRC RAI 19, Using ATWS-Recirculation Pump Trip (RPT) for AOOs**

GENE licensing methodology allows using anticipatory ATWS-RPT in some AOO transients to decrease the power and pressure response. Therefore, the anticipatory RPT is used in some plants to minimize the impact of the pressurization transient on the  $\Delta$ CPR response. For the EPU MELLLA+ operation, RPT may subject the plant to instability. Evaluate the runbacks associated with the AOOs and demonstrate that the scram and the RPT timings would not lead to an AOO transient resulting in an instability.

**GE Response**

[[

]]

**NRC RAI 20, Mechanical Overpower (MOP) and Thermal Overpower (TOP)**

Are the fuel-specific mechanical and thermal overpower limits determined based on the generic fuel design or for each plant-specific bundle lattice design? How is it confirmed that the generic MOP and TOP limits for GE14 fuel bounds the plant-specific GE14 lattice designs intended to meet the cycle energy needs at the EPU/MELLLA+ conditions?

**GE Response**

[[

]]

**NRC RAI 21, Brunswick AOO**

The Brunswick Units 1 and 2 are the first plants to apply TRACG for performing the reload analyses.

- a. Compare the Brunswick EPU and the EPU/MELLLA+ core designs and performance.
- b. State what is the benefit of using TRACG instead of ODYN for the EPU/MELLLA+ reload analyses.
- c. Provide a comparison of the TRACG and ODYN AOO analyses results based on the EPU/MELLLA+ core design.

**GE Response**

a. [[

]]

b. [[

]]

c. Figures AOO-21-1 through AOO-21-5 provides the comparison

[[

]]

Figure AOO-21-1. TRACG vs ODYN Neutron Flux TTNB Event at M+

[[

]]

Figure AOO-21-2. TRACG vs ODYN Core Flow TTNB Event at M+

[[

]]

Figure AOO-21-3. TRACG vs ODYN Vessel Stream Flow TTNB Event at M+

[[

]]

Figure AOO-21-4. TRACG vs ODYN Vessel Pressure TTNB Event at M+



[[

]]

Figure AOO-21-5. TRACG vs ODYN SRV Flow TTNB Event at M+

**NRC RAI 22, Brunswick AOO Data Request**

Submit the following data on compact disc for the Brunswick EPU/MELLLA+ core and fuel performance analyses.

- a. TRACG input file including the PANCEA wrap file for a limiting transient initiated from different statepoints along the EPU/MELLLA+ boundary, if available. Include the corresponding output file in ASCII form.
- b. ODYN output file (ASCII) for the same transients and statepoints.

**GE Response [Updated with MFN 04-033, 04-074]**

The data at rated conditions was provided in GE letter MFN 04-020, G. Stramback (GE) to NRC, February 27, 2004, *Responses to MELLLA Plus AOO RAIs (TAC No. MB6157)*. Subsequent conversations with the NRC indicated that additional analyses were required, which was provided on a compact disk in GEH letter dated March 23, 2004 (MFN 04-033).

Further data was requested and also provided on a compact disk in GEH letter dated August 5, 2004 (MFN 04-074). The TRACG02 related MELLLA+ analysis files are contained in the file "melllap\_cases.sav". This is a SAVE SET created on an ALPHA AXP architecture machine running the OpenVMS 7.3 operating system with the DCL BACKUP command.

To run the TRACG cases:

- (1) Transfer the SAVE SET to your OpenVMS ALPHA machine using binary FTP.
- (2) Change the file attributes on the OpenVMS platform using the following command:  
SET FILE/ATTRIB=(RFM=FIX,LRL=32256) MELLLAP\_CASES.SAV
- (3) Extract the files with the following command (will extract to the current directory):  
BACKUP MELLLAP\_CASES.SAV/SAVE\_SET \*.\*
- (4) Modify the DCL command files as necessary for your directory names and TRACG02 executable name.

The requested information is extensive, was provided on a compact disk to the NRC, and is not repeated herein.

**NRC RAI 23, Separate Effects, Mixed Vendor Cores and Related Staff Restrictions**

Separate effects: revise Section 1.0, "Introduction," of the MELLLA+ LTR and remove the list of "separate effects" changes. The MELLLA+ LTR lists plant-specific operating condition changes that could be implemented concurrently with the EPU/MELLLA+, but would be evaluated in a separate submittal. All of these lists of changes would affect the safety analyses that demonstrate the impact of EPU/MELLLA+ on the plant's response during steady-state, transients, accidents, and special events. The plant-specific EPU/MELLLA+ application must demonstrate how the plant would be operated during the implementation of MELLLA+. In addition, the EPU/MELLLA+ reduces the available plant margins. Therefore, the staff cannot make its safety finding based on assumed plant operating conditions that are neither bounding nor conservative relative to the actual plant operating conditions. Revise the MELLLA+ LTR and delete the paragraphs that propose evaluating additional operating condition changes in a separate submittal while the EPU/MELLLA+ application assumes that these changes would not be implemented.

Add the following statements in the MELLLA+ LTR to address staff restrictions including: (1) the implementation of additional changes concurrent with EPU/MELLLA+, (2) the applicability of the generic analyses supporting the EPU/MELLLA+ operation, and (3) the approach used to support new fuel designs or mixed vendor cores.

- a. The plant-specific analyses supporting the EPU/MELLLA+ operation will include all planned operating condition changes that would be implemented at the plant. Operating condition changes include but are not limited to increase in the dome pressure, maximum core flow, increase in the fuel cycle length, or any changes in the currently licensed operation enhancements. For example, with increase in the dome pressure, the ATWS analysis, the American Society of Mechanical Engineers (ASME) overpressure analyses, the transient analyses, and the ECCS-LOCA analysis must be reanalyzed based on the increased dome pressure. Any changes to the safety system settings or actuation setpoint changes necessary to operate with the increased dome pressure should be included in the evaluations (e.g., safety relief valve setpoints).
- b. For all of the principal topics that are reduced in scope or generically dispositioned in the MELLLA+ LTR, the plant-specific application will provide supporting analyses and evaluations that demonstrate the cumulative effect of EPU/MELLLA+ and any additional changes planned to be implemented at the plant. For example, if the dome pressure would be increased, the ECCS performance needs to be evaluated on a plant-specific basis.
- c. Any generic sensitivity analyses provide in the MELLLA+ LTR will be evaluated to ensure that the key input parameters and assumptions used are still applicable and bounding. If the additional operating condition changes affects these generic sensitivity analyses, a bounding generic sensitivity analyses will be provided. For example, with increase in the dome pressure, the TRACG ATWS sensitivity analyses

that model the operator actions (e.g., depressurization if the heat capacity temperature limit is reached) needs to be reanalyzed, using the bounding dome pressure condition.

- d. If a new GE fuel or another vendor's fuel is loaded at the plant, the generic sensitivity analyses supporting the EPU/MELLLA+ condition will be reanalyzed. For example, the ATWS instability analyses supporting the EPU/MELLLA+ condition are based on the GE14 fuel response. New analyses that demonstrate the ATWS stability performance of the new GE fuel or legacy fuel for the EPU/MELLLA+ operation needs to be provided. The new ATWS instability analyses can be provided as supplement to the MLTR or as an Appendix to the plant-specific application.
- e. If a new GE fuel or another vendor's fuel is loaded at the plant, analyses supporting the EPU/MELLLA+ application will be based on core specific configuration or bounding core conditions. In addition, any principle topics that are generically dispositioned or reduced in scope will be demonstrated to be applicable or new analyses based on the transition core conditions or bounding conditions would be provided.
- f. If a new GE fuel or another vendor's fuel is loaded at the plant, the plant-specific application will reference the fuel-specific stability detect and suppress method supporting the EPU/MELLLA+ operation. The plant-specific application will demonstrate that the analyses and evaluation supporting the stability detect and suppress method are applicable to the fuel loaded in the core.
- g. For EPU/MELLLA+ operation, instability is possible in the event of transient or plant maneuvers that place the reactor at high power/low flow condition. Therefore, plants operating at the EPU/MELLLA+ condition must have an NRC reviewed and approved instability detect and suppress method operable. In the event the stability protection method is inoperable, the applicant must employ NRC reviewed and approved backup stability method or must operate the reactor at a condition in which instability is not possible in the event of transient. The licensee will provide technical specification changes that specify the instability method operability requirements for EPU/MELLLA+ operation.

**GE Response [Updated by MFN 07-241]**

Per the RAI request, Section 1 of the MELLLA+ LTR were be modified in NEDC-33006P-A, Revision 3. Portions of the suggested content of the RAI have been changed to provide consistency with the MELLLA+ LTR and implementation process. For example, each instance of EPU/MELLLA+ contained in the suggested content of the RAI has been changed to MELLLA+. The MELLLA+ LTR is supported by analyses at power levels up to 120% OLTP. However, the LTR is based on the premise that there is no change in power level with the MELLLA+ application. Therefore, the power level for a plant specific application will be the plant's CLTP, which may not be at the 120% OLTP (EPU) power level.

**NRC RAI 24, Reactor Safety Performance Evaluations**

From the AOO audit, the staff determined that (1) GENE did not provide statistically adequate sensitivity studies that demonstrate the impact of EPU/MELLLA+ operation, [[

]] (3) the generic anticipatory reactor trip system (ARTS) response may not be applicable for all BWR applications, and (4) the EPU/MELLLA+ impact was not insignificant. The staff also finds that it is not acceptable to make safety findings on two major changes (20 percent uprate based on the CPPU approach and MELLLA+) without reviewing the plant-specific results. [[

]] EPU/MELLLA+ applications must provide plant-specific fuel thermal margin and AOO evaluations and results. The following discussion summarizes the staff's bases for concluding that the plant-specific EPU/MELLLA+ application must provide a plant-specific thermal limits assessment and plant-specific transient analyses results.

- a. EPU/MELLLA+ Core Design. Operation in the MELLLA+ domain will require significant changes to the BWR core design. Expected changes include (1) adjustments to the pin-wise enrichment distribution to flatten the local power distribution, reduce the r-factor, and increase CPR margin; (2) increased gadolinium (Gd) loading in the bottom of the fuel bundle to reduce the axial power peaking resulting from increased coolant voiding, and (3) changes in the core depletion due to the sequential rod withdrawal/flow increase maneuvers expected during operation in the MELLLA+ flow window. [[

]] However, the model used for these AOO calculations is not based on a MELLLA+ core, which has been designed for reduced flow at uprated power. Therefore, none of the sensitivity analyses supporting MELLLA+ operation have been performed for a core which includes the unique features of a MELLLA+ core design. Consequently, the effect of MELLLA+ on AOO  $\Delta$ CPR has not been adequately quantified.

- b. Reload-Specific Evaluation of the AOO Fuel Thermal Margin. [[

]] The available data is also limited.

- c. Offrated Limits. The staff determined that the offrated limits (including along the MELLLA+ upper boundary)  $\Delta$ CPR response may be more limiting than transients initiated from rated conditions. Therefore, AOO results from EPU applications

cannot be used as sufficient bases to justify not providing the core and fuel performance results for the plant-specific MELLLA+ applications. Moreover, it has not been demonstrated that the generic ARTS limits are applicable and will bound the plant and core-specific offrated transient response for all of the BWR fleet. Therefore, offrated transient analyses must be performed to demonstrate the plant's  $\Delta$ CPR response.

- d. Mixed Core. Many of the BWRs seeking to implement the EPU/MELLLA+ operating domain may have mixed vendor cores. GENE's limited (MELLLA+) sensitivity analyses were based on GE14 fuel response of two BWR plants. Additional supporting analyses and a larger MELLLA+ operating experience database will be required before generic conclusions can be reached about the impact of MELLLA+ on core and fuel performance. Specifically, there is no operating experience or corresponding database available for assessing the performance of mixed vendor cores designed for EPU/MELLLA+ operation. As such, plant-specific fuel and core performance results must be submitted until a sufficient operating experience and analyses data base is available. In addition, new fuel designs in the future may change the core and fuel performance for the operation at the EPU/MELLLA+ operation. Therefore, the staff's EPU/MELLLA+ safety finding must be based on plant-specific core and fuel performance.
- e. For the CPPU applications, the core and fuel performance assessments are deferred to the reload. Therefore, MELLLA+ LTR proposes that the staff approve an EPU/MELLLA+ application without reviewing the plant's response for two major operating condition changes. This approach would not meet the agency's safety goals.

**GE Response**

The plant-specific EPU/MELLLA+ application will provide plant-specific thermal limits assessment and transient analyses results.

**NRC RAI 25, Large Break ECCS-LOCA**

- a. Mixed Core. For a plant-specific EPU/MELLLA+ application, state if equilibrium ECCS-LOCA analyses of each type would be performed or core configuration specific ECCS-LOCA analyses would be performed. If a core configuration specific ECCS-LOCA analyses will be performed, state which NRC-approved codes or methods would be used.
- b. Reporting Limiting ECCS-LOCA Results. The MELLLA+ audit indicated that the rated ECCS-LOCA results are reported although it may not be for the most limiting results. For the EPU/MELLLA+ operation, the most limiting ECCS-LOCA result is at the MELLLA+ statepoint of 55 percent CF. Revise the MELLLA+ LTR to state that the ECCS-LOCA result at rated condition, minimum core flow at EPU power level and at the 55 percent CF statepoint will be reported. In addition, revise the applicable documents that specify the GENE licensing methods to state that the ECCS-LOCA result corresponding to the rated and the most limiting statepoint will be provided. Report in the supplemental reload licensing report (SRLR), the ECCS-LOCA results at the rated and the most limiting statepoints. Confirm that the steady-state initial conditions (e.g., operating limit maximum critical power ratio [OLMCPR]) assumed in the ECCS-LOCA analyses will be reported in the SRLR.
- c. Adder Approach. Was the licensing bases PCT calculated by incorporating a delta PCT adder to the Appendix K PCT? If this is the method used, please justify why the 10 CFR 50.44 insignificant change criteria is acceptable.

**GE Response [Parts a and c updated with MFN 04-060; part b updated with MFN 05-081]**

Response to Part a.

The ECCS-LOCA analysis for EPU/MELLLA+ follows the approved SAFER/GESTR application methodology documented in NEDE-23785-1-PA Rev. 1, "The GESTR-LOCA and SAFER Models for the Evaluation of the Loss-Of-Coolant Accident Volume III, SAFER/GESTR Application Methodology," October 1984. [[

]] The analytical models used to perform ECCS-LOCA analyses are also documented in NEDE-23785-1-PA together with NEDE-30996P-A, "SAFER Model for Evaluation of Loss-of-Coolant Accidents for Jet Pump and Non-jet Pump Plants, Volume I, SAFER – Long Term Inventory Model for BWR Loss-of-Coolant Analysis," October 1987, and NEDC-32950P, "Compilation of Improvements to GENE's SAFER ECCS-LOCA Evaluation Model," January 2000.

Response to Part b

The MELLLA+ LTR (NEDC-33006P-A, Revision 3) was revised to state that the MELLLA+ plant submittals will include calculations for the Appendix K and Nominal PCT at rated power/rated core flow, rated power/MELLLA+ boundary (point D of Figure 1-1), and the low flow point on the MELLLA+ boundary at which the off-rated flow

dependent LHGR or MAPLHGR setdown begins to apply. This point will be at or above 55% core flow and between points D and E on Figure 1-1 (call point E’).

The analyses at points D and E’ will be initialized at the rated power LHGR and MAPLHGR limits. The initial MCPR at point E’ will include application of the power dependent MCPR multiplier to the rated power assumed MCPR. Note that the MCPR assumption has no reliance on the safety limit MCPR since the hot channel is assumed to dry out at a MCPR of 1.0 in accident analyses.

When SAFER/GESTR methodology is applied, the hot bundle is initialized with a hot rod at the LHGR limit and the average rod at the MAPLHGR limit. The dryout times are determined with the TASC code assuming the hot bundle starts at the ECCS basis Initial MCPR. These initial conditions are designed to maximize the PCT. Further discussion on the impact of axial power shape on the PCT is contained in the response to RAI 28.

Since credit is taken for these off-rated limits, the plant will be required to apply these limits during core monitoring.

The Licensing Basis PCT, considering all calculated statepoint as described, will be reported in the plant-specific MELLLA+ Safety Analysis Report.

GE agrees to change future SAFER/GESTR analyses and SRLRs as follows:

1. The SAFER/GESTR report will provide the Licensing Basis PCT considering all calculated statepoints. The Licensing Basis PCT will be calculated either using the previous Licensing Basis PCT plant variable uncertainty (e.g., NEDE-23875-1-PA, Section 3.1.3) or with a plant variable uncertainty specific to the calculated statepoint with the highest Appendix K PCT. Only one Licensing Basis PCT will be reported because it is the single PCT which considers all required licensing conservatism.
2. Only SRLRs, for both MELLLA+ plants and non-MELLLA+ plants, which report these future SAFER/GESTR analyses will report the Licensing Basis PCT considering all calculated statepoints as described above. No change will be made in SRLR reporting of previous SAFER/GESTR analyses.
3. Section 6 of NEDC-32950P will be revised to include determining the Licensing Basis PCT considering all calculated statepoints as described above. No other documents that specify the GENE licensing methods will be revised.

The Initial MCPR assumed in the ECCS/LOCA analyses is reported in the SRLR.

#### Response to Part c

The 10 CFR 50.46 (a)(3)(i) change criterion does not apply to the MELLLA+ evaluation because the MELLLA plus evaluation is not a change to an acceptable evaluation model or error. The MELLLA+ ECCS performance evaluation demonstrates that plant operation in the MELLLA+ power/flow region meet the 10CFR50.46 acceptance criteria



NEDO-33173-A, Revision 1  
Non-Proprietary Information

and is in compliance with NRC requirements for the SAFER/GESTR application methodology. These results are reported to the NRC in the plant-specific MELLLA+ licensing submittal.

**NRC RAI 26, Small Break ECCS-LOCA Response**

[[

]] assuming high pressure coolant injection (HPCI) failure and automatic depressurization system depressurization. At the 55 percent CF statepoint (Point M), the hot bundle may be at a more limiting initial condition in terms of initial void content and the ADS would depressurize the reactor leading to core uncover as well. Provide a sensitivity ECCS-LOCA analysis, using the bounding initial condition. Provide a small break LOCA analysis at point M (77.6 percent Power/55 percent CF), based on the bounding initial condition, worst case small break scenario and placing the hot bundle at the most limiting conditions (peaking factors). Use initial SLMCPR and OLMCPR condition that is bounding for operation at 80 percent CF or 55 percent CF statepoint.

**GE Response [Updated with MFN 05-081]**

[[

]]

[[

]] If the small break PCT is at or near limiting, the MELLLA+ plant submittals will include calculations for the limiting small break at rated power/rated core flow and rated power/MELLLA+ boundary (point D of Figure 1-1). The following is a comparison of the small break PCT impact to the large (DBA) break (Appendix K assumptions) along the MELLLA+ boundary.

NEDO-33173-A, Revision 1  
Non-Proprietary Information

[[



]] Based on these result and the aforementioned expectations, near limiting is defined as within [[            ]] of the limiting Appendix K PCT.

**NRC RAI 27, Small Break Containment Response**

Using the most limiting small break LOCA, in terms of containment response (possibly at rated condition if limiting), demonstrate whether the suppression pool temperature response to a design basis accident is limiting. Wouldn't a small break LOCA (e.g., assuming HPCI failure and depressurization of the reactor) be more limiting in terms of suppression pool response? Base your evaluations on the Brunswick and Clinton applications.

**GE Response**

The peak suppression pool temperature for the small break accident (SBA) with vessel depressurization is not expected to exceed the peak suppression pool temperature for the DBA-LOCA. The key energy sources that affect the peak suppression pool temperature are the vessel decay energy and the initial vessel sensible energy.

The decay energy is determined by the decay power time-history and the initial power level. These parameters are the same for both events.

For a DBA-LOCA, the initial vessel sensible liquid energy is rapidly transferred to the suppression pool during the initial vessel blowdown period. The liquid break flow from the vessel during the blowdown period partially flashes in the drywell, resulting in a homogeneous mixture of steam and liquid in the drywell. This mixture is forced rapidly from the drywell, through the vent system, to the suppression pool. The vessel is depressurized to the ambient drywell pressure within a few minutes of the start of the event. This effectively transfers the initial vessel liquid sensible energy to the pool within minutes of the start of the event. [[

]] After the vessel blowdown period, relatively cold ECCS liquid from the suppression pool enters the vessel. The ECCS flow floods the vessel to the break elevation and delivers a stream of liquid from the vessel to the drywell. [[

]] After vessel

depressurization is completed for the SBA, decay energy continues to produce steam in the vessel. This decay energy is transferred to the suppression pool via intermittent SRV discharges to the suppression pool, which maintains the vessel at low pressure. This process produces a slow heat up of the suppression pool. As with the DBA-LOCA, the peak pool temperature occurs when the energy removal rate by the RHR system equals the energy addition rate to the suppression pool.

[[

]]

#### Analysis Confirmation

To confirm the discussion provided above, the results of SBA containment analyses were compared to the results of DBA-LOCA containment analyses. Sensitivity analyses of the SBA event were performed for Brunswick with EPU conditions. SBA containment analyses were not available for the Clinton EPU application. However, the results of SBA analyses performed with EPU conditions for another, non-US, BWR/6-218 plant with a Mark III containment (similar to Clinton) were reviewed for the evaluation.

The Brunswick EPU SBA sensitivity analyses assumed HPCI failure and vessel depressurization. The analyses included cases where vessel depressurization with ADS was modeled and cases where manually controlled vessel depressurization was modeled. The peak suppression pool temperature obtained for the analysis with ADS modeled was 204.4°F. The peak suppression pool temperature with controlled vessel depressurization modeled was 206.9°F. In both cases the peak suppression pool temperatures were similar to but not higher than the peak suppression pool temperature obtained from the DBA-LOCA value of 207.7°F.

The SBA analysis performed for the BWR/6-218 plant assumed manually controlled vessel depressurization. The peak suppression pool temperature obtained from the SBA analysis was slightly higher than the peak DBA-LOCA suppression pool temperature but only by 0.8°F.

These results confirm that the SBA event does not produce more limiting conditions with respect to peak suppression pool temperature.

**NRC RAI 28, Assumed Axial Power Profile for ECCS-LOCA**

[[

]] Base your discussion on the predicted response in terms of dryout times. In addition, explain what the axial power peaking would be if the fuel is placed at the LHGR limit at rated conditions, 80 percent CF and 55 percent CF condition. If the axial power peaking would be higher for the non-rated flow conditions, state what axial power peaking were used in the ECCS-LOCA sensitivity analyses reported in MELLLA+ LTR for the 80 percent and 55 percent CF statepoints.

**GE Response**

[[

]] The table below shows the effect of the power / flow (P/F) and power profile on the dryout times of the peak power node of the hot bundle.

Dryout Times of Peak Power Node for Various P/F Conditions and Power Shape

	[[	
		]]

[[

]]

The axial peaking factors (APFs) in the table below are the factors needed to place the hot bundle on the PLHGR target when the bundle power places the bundle on the MCPR target. These APFs are much larger than would be expected to occur during plant operation. It is also unlikely that a top peak shape would be on the PLHGR target and MCPR target at the same time.

Axial Peaking Factors for Various P/F Conditions and Power Shape

	[[	
		]]

The effect of the power profile on the PCT is shown in the table below. The effect of the power profile on the PCT is small. The impact of the power profile is larger on 1<sup>st</sup> Peak PCT than on the limiting 2<sup>nd</sup> Peak PCTs. [[

]]

**Appendix K PCTs for Various P/F Conditions and Power Shape**

	[[			
				]]

The following table provides the axial peaking factors used in the analyses supporting the MELLLA+ LTR. The analyses supporting the LTR used a slightly different approach than the above analyses in setting the hot bundle on the MCPR target. In the above analyses, the limiting R-factor based on the specific fuel bundle type (GE14) is used and the bundle power is varied to place the bundle on the MCPR limits; this results in different radial and axial peaking factors for each case. Using a fixed limiting R-factor gives more representative trends.

In the analyses supporting the LTR, the bundle power is fixed at a value higher than expected during operation and the R-factor is varied to place the bundle on the MCPR target as long as it remains above a minimum value. If the minimum is reached, the bundle power is reduced to obtain the MCPR target. This approach results in the same peaking factors except at low core flow.

**Axial Peaking Factors Used in the Analyses Supporting the LTR**

[[	
	]]

In conclusion, the dryout times of the peak power node for the mid-peaked profile are about the same or earlier than those of the top-peaked profile. [[

]]



**NRC RAI 29, Power/Flow Map**

The MELLLA+ LTR states that the slope of the linear upper boundary was derived primarily from reactor operating data. Expand on this statement. Explain what operating data was used. Were all plant types represented? Was the line developed as a bounding line or as a fit to the referred reactor operating data?

**GE Response**

One of the goals for the MELLLA+ project was to incorporate utility input as to the characteristics of the region to be used for the analyses. The general utility input was that the MELLLA+ upper boundary should be more representative of plant performance, in contrast to the MELLLA upper boundary bias toward a steep load line. Recent operating plant data from 4 BWRs with newer fuel designs was extrapolated to higher load lines to derive the analytical upper boundary for the MELLLA+ operating region. While a specific load line is influenced by some plant specific factors, such as feedwater temperature and core size, the variation of load line due to changing core characteristic factors, such as reactivity coefficients and power distribution, indicates that a few typical plants with different core characteristics will be representative. The resulting MELLLA+ upper boundary represents a nominal power to flow load line. The MELLLA+ upper boundary line represents the analyzed operating region and it is therefore a requirement for normal operation. The evaluations performed to justify operation in the MELLLA+ region assure that all operating condition within the MELLLA+ upper boundary are acceptable.

**NRC RAI 30, Power/Flow Map**

The MELLLA+ minimum statepoint for rated EPU power was limited to 80 percent CF. Explain what the limitations were in establishing the minimum core flow statepoint. Similarly, discuss the limitations considered in establishing the 55 percent core statepoint. Discuss why the feedwater heater out-of-service and single loop operation is also not allowed for the EPU/MELLLA+ operation.

**GE Response**

Both the minimum core flow of 80% of rated for 100% power and the minimum core flow of 55% of rated for the low boundary represent the practical limitations of normal BWR operation. [[

was selected. [[

]] Thus the 80% of rated core flow

]]

- (a) FWHOOS; The establishment of the MELLLA+ region included considerations of practical application, as well as limiting adverse consequences in plant safety analyses. [[

]] However, this feedwater temperature reduction would need to be evaluated on a plant specific basis and is not part of the standard MELLLA+ evaluation. Finally, it should also be noted that operation in FWHOOS is considered only a contingency option, for temporary feedwater heater equipment deficiency therefore, this limitation is not expected to impose a significant limitation to plant availability.

- (b) SLO; The core flow attainable with a single recirculation pump is typically 50% of rated, and not expected to be higher than 60% of rated. Then it follows that since the MELLLA+ region is limited to a minimum flow of 55% of rated, it would be extremely difficult for a BWR to maneuver into the high power condition corresponding to the MELLLA+ region, where little flow margin for

NEDO-33173-A, Revision 1  
Non-Proprietary Information

operation exists. Therefore, there is no incentive to operate in SLO at higher power in MELLA+.

**MFN 06-211**

**Methods RAIs**

NRC RAI 1.0 Linear Heat Generation Rate (LHGR)

NRC RAI 1.1

Different pins peak at different exposures and in some lattices exhibit high power peaking later in life. Therefore, it is important to assess the overall operating LHGR in these pins relative to the LHGR limit and to understand the available margins such pins have in terms of internal rod pressures. In addition, operating plants data indicates that peak rods could be operating at the limit. Provide internal rod pressure calculations for rods that are operating at the limit for different exposures, including late in the fuel life. Use representative bundles that have lower Gd loading (e.g., 6% or lower).

1. Provide a Minimum LHGR (MLHGR) scatter plots for extended power uprate (EPU) plant.
2. Select most limiting MLHGR at different exposures, including late in the fuel life.
3. Calculate the internal pressure (P) based history for once, twice, and thrice burned fuel near LHR limit and placed on limit for reasonable duration. Compare and discuss the results and exposures.

Response

[[

]]

To respond to RAI 1.1, Brunswick 1 uprated Cycle 15 has been evaluated in detail. The bundles analyzed represent the actual GE14 bundles operated during Brunswick 1 Cycle 15 and reflect six different bundle types; [[

]]

The red diamonds shown in Figure 1.1-2 are the specific cases selected for fuel rod internal pressure evaluation. [[

]]

**Table 1.1-1 Fuel Rod Internal Pressure Comparison**

[[



]]



[[

]]

**Figure 1.1-1 Comparison of Pre-EPU and EPU MLHGR Operating Conditions**

[[

]]

**Figure 1.1-2 Brunswick 1 Uprated Cycle 15 MLHGR Characterization**

**NRC RAI 1.2**

For Gadolinia (Gd) bearing rod (6 percent) near beginning-of-life (0 to 5.392 gigawatt-days per short ton (GWD/ST)), the LHGR limit increased from 5.392 GWd/STU when the Gd concentration is high to 12.55 GWd/ST at 5 GWD/ST. The Gd rods will be operating at lower powers and the limit is low when the Gd concentration is high. However, it appears that the plant monitoring systems are based on 12.55 GWD/ST. Explain the discrepancies. State why the limit is reduced at low exposures for the Gd loaded pins, when the Gd concentration is high. Discuss under transient conditions if the Gd pin margin to the melting temperature will be much lower?

**GE Response**

Figure 1.2-1 presents the standard design and licensing analysis basis GE14 6 w/o Gd<sub>2</sub>O<sub>3</sub>-UO<sub>2</sub> fuel rod peak pellet LHGR vs. exposure power history as compared to the corresponding LHGR operating limit applied in the plant monitoring system. [[

]]

At low exposures, the presence of the high neutron absorption cross-section gadolinium isotopes causes significant neutron flux suppression and a correspondingly low gadolinia fuel rod linear heat generation rate (LHGR). With continued irradiation, the high neutron absorption cross-section gadolinium isotopes progressively transmute to lower neutron absorption cross-section isotopes thereby resulting in a progressive increase in gadolinia fuel rod LHGR. [[





**Table 1.2-1 Effect of Early Life LHGR Variation GE14 6 w/o Gd<sub>2</sub>O<sub>3</sub>-UO<sub>2</sub>**

[[



]]

[[

Figure 1.2-1 GE14 6 w/o  $Gd_2O_3$ - $UO_2$  LHGR Operating Limit and Analysis Basis ]]

[[

]]

**Figure 1.2-2 Comparison of Analyzed and Predicted 6 w/o Gd<sub>2</sub>O<sub>3</sub>-UO<sub>2</sub> Power Ascension**



[[

]]

**Figure 1.2-3 GE14 6 w/o Gd<sub>2</sub>O<sub>3</sub>-UO<sub>2</sub> LHGR Operating Limit and Biased History**

**NRC RAI 1.3**

Fuel failure due to fuel duty is precluded by limiting the initial steady state operating kilowatt per foot (kw/ft) through the LHGR limit. Show that thermal-mechanical fuel duty benchmark data is applicable to EPU conditions.

**GE Response**

[[

]]

Qualification of the GNF fuel rod thermal-mechanical performance model (GESTR-Mechanical) was performed in a manner to challenge the prediction capability over a wide range of not only duty conditions, but also dimensional conditions and fabrication parameters, to confirm the robustness of the embodied fundamental physical process and mechanism representations. [[

]]

The results of the GESTR-Mechanical experimental qualification have been previously provided to the USNRC (e.g., Reference 1.3-1 and 1.3-2). [[

]]

Regardless, the GNF fuel rod thermal-mechanical performance model (GESTR-Mechanical) has been extensively qualified to pertinent available fuel rod thermal and mechanical performance measurements that extend well beyond extended power uprate conditions, as shown in Table 1.3-1. On this basis, it is concluded that GESTR-Mechanical remains equally applicable to extended power uprate conditions.

References

- 1.3-1 J. S. Charnley, letter to R. Lobel, "Fuel Property and Performance Model Revisions", MFN-170-84, December 14, 1984.
- 1.3-2 J. S. Charnley, letter to G. C. Lainas, "Fuel Property and Performance Model Revisions", MFN-027-086, April 7, 1986.

**Table 1.3-1 GSTR-Mechanical Qualification Database**

[[

]]

[[

]]

**Figure 1.3-1 GESTR-Mechanical Fuel Temperature Qualification**

[[

]]

**Figure 1.3-2 Predicted/Measured Fuel Temperature as a Function of Exposure**

[[

]]

**Figure 1.3-3 GESTR-Mechanical Cladding Diametral Deformation Qualification**



[[

]]

**Figure 1.3-4 Predicted – Measured Cladding Diametral Deformation vs. Exposure**

**NRC RAI 1.4**

Describe the internal rod pressure validation data that are currently available for both GE fuel designs and legacy fuels.

GE Response

The fuel rod internal pressure is given by

$$P = \frac{nRT}{V}$$

where P = fuel rod internal pressure (psia)  
n = gas content occupying the fuel rod void space (gm-moles)  
R = universal gas constant  
T = temperature of the gases occupying the fuel rod void volume (°R)  
V = fuel rod void volume (in<sup>3</sup>)

The gas constituents are comprised of the fuel rod initial helium fill gas and released fission gases. [[

]]

Qualification of the prediction capability for the [[  
fission gas release component (isotopes of krypton and xenon) has been performed by  
comparison of predictions to fission gas release measurements [[

]]

[[

]]

The GE14 fuel rod thermal-mechanical analyses, including the fuel rod internal pressure calculation, has been performed with the GESTR-Mechanical model and associated

application methodology. These analyses represent the design and licensing basis for GE14. [[

]]

[[

]]

**Figure 1.4-1 GESTR-Mechanical Helium Release Comparison**

[[

]]

**Figure 1.4-2 GESTR-Mechanical Fission Gas Release Qualification**

[[

]]

**Figure 1.4-3 Predicted – Measured FGR vs. Exposure (Measured FGR < 5%)**

[[

]]

**Figure 1.4-4 Predicted/Measured FGR vs. Exposure (Measured FGR > 5%)**



[[

]]

**Figure 1.4-5 GESTR-Mechanical Fuel Rod Internal Pressure Qualification**

[[

]]

**Figure 1.4-6 Predicted – Measured Fuel Rod Internal Pressure vs. Exposure**

**NRC RAI 2.0 Shutdown Margin (SDM)**

Section 2.3 addresses the adequacy of the 0.0038  $\Delta k/k$  in the calculation of SDM.

**NRC RAI 2.1**

The demonstration of the shutdown margin is dependent on the cold critical measurement performed at the plant and the eigenvalue for the core with all rods inserted, but with the strongest rod out (Ksro). The code critical measurements are performed after each outage and can be used to demonstrate the adequacy of the neutronics methods for this "distributed" criticality. However, the Ksro value requires experiments to be performed with single rods out, which represent "local" criticality experiments. These local experiments are not performed very frequently, yet the prediction of the SDM relies on the accurate calculation of the Ksro value. The data provided does not distinguish between local cold critical and in-sequence cold critical measurements.

- (a) Local cold critical measurements are a more physical demonstration of the stuck rod out (SRO) condition enforced by the 0.0038  $\Delta k/k$  technical specification limit. Please separate out this data and provide an assessment of the methods accuracy for prediction of the local critical states demonstrating that the bias and uncertainties that are currently applied are adequate for expanded operating domains.
- (b) As in Figure 2-5, provide the predicted (e.g., design basis) and measured eigenvalues. Compare the performance versus the distributed cold critical measurements and discuss any other biases or uncertainties that are applied to the Ksro values in the SDM demonstration.

**GE Response:**

Of the plant data provided in Figure 2-5 of Reference 2-1, plant C contains both in-sequence (distributed) and local cold critical demonstrations. The following Table 2.1-1 includes the local critical data of the figures, plus additional information from prior cycles for plant C. Table 2.1-1 includes both the demonstrated cold critical eigenvalue and the Nuclear Design Basis (NDB) reference eigenvalue for cold shutdown margin and local critical experiments.

The design basis eigenvalue includes [[

]] By comparison with the data reported in Reference 2-1 which indicates that

the standard deviation of all differences (both local and distributed) is [[ ]], one may conclude that the predictive performance for local criticals is essentially the same. Additionally, the procedure to [[ ]] is effective. This performance again supports the margin discussion contained in Reference 2-1.

Finally, one must note that this database of local critical data for plant C is applicable to other plants primarily because the localized nature of the experiment, which consists of only a small number of withdrawn or partially withdrawn control blades, isolates the event to a very small portion of the core. So, the predictive accuracy for a local critical experiment in any core is readily transferable to other plants and cycles. Additional discussion on the insensitivity of cold critical data to power rating or operational strategy is provided in the response to RAI 2.2.

**Table 2.1-1 Plant C Local Critical Eigenvalue Performance**

Plant C	Cycle	Test Data	NDB	Delta
Local 1	[[			
Local 2				
Local 3				
Local 1				
Local 2				
Local 3				
Local 4				
Local 1				
Local 2				
Local 3				
Local 1				
Local 2				
Local 1				
Local 2				
Local 3				
Local 4				
Local 5				
Local 6				
Local 7				
Local 8				
Local 1				
Local 2				
Local 3				
Local 1				
Local 2				
Local 3				]]

### **NRC RAI 2.2**

The LTR states that the same SDM Technical Specification value used for non-EPU core designs is adequate for EPU and expanded operating domain conditions. Provide the basis as to why cold SDM is not a strong function of the current operating strategies by comparing cold critical data before and after EPU. Include in the discussion the impact of core designs necessary to achieve EPU and maintain extended cycle lengths (e.g., larger batch fractions, higher bundle enrichments and different core loading patterns).

### **GE Response:**

Cold shutdown margin (SDM) calculations by their nature are not directly evaluated at EPU conditions. Being a calculation (and a subsequent demonstration) performed at the most reactive core conditions, it is evaluated in a cold, unvoided, xenon-free state; not at the rated power/flow conditions. However, as noted, changes in core and fuel designs resulting from design requirements needed to support EPU could potentially impact the calculational accuracy of the SDM analysis. Provided below is a brief discussion of the purpose and limitations of the SDM demonstration itself, followed by a brief discussion of the impact of EPU related design changes on SDM calculations.

During the design and licensing of a reload core, SDM is calculated to provide assurance that the reactor can remain subcritical in the most reactive condition with the highest worth control rod fully withdrawn. The plant Technical Specifications (Tech Specs) further require that a SDM demonstration be performed prior to startup after any core reconfiguration (i.e., at the start of a new cycle) to demonstrate that the plant does indeed remain subcritical with the calculated strongest worth control rod fully withdrawn.

Tech Specs typically require a SDM value of 0.38%  $\Delta k/k$  be demonstrated. This demonstration requirement has been put in place so that predictive calculations are not the sole basis of this Tech Spec. By doing so, the bulk of the uncertainties associated with the modeling of SDM are minimized. The Tech Spec requirement has been established because the SDM demonstration itself is subject to variations regarding the core and fuel that cannot be reasonably eliminated. Among these are fuel manufacturing tolerances in  $^{235}\text{U}$  enrichment, gadolinia enrichment and component dimensionalities; and control blade reactivity uncertainties due to manufacturing tolerances and control blade burnup variations. These demonstration uncertainties are not dependent primarily on calculational methods or rated power level (i.e., EPU versus non-EPU), but on manufacturing and operational variations.

In performing SDM licensing calculations, a design criterion considerably greater than the Tech Spec requirement is imposed so that there will be a high assurance of success when the demonstration is actually performed. This high assurance of success is desirable from both a safety and a commercial standpoint. At GNF, a SDM design criterion of 1%  $\Delta k/k$  has always been required.

Given that a demonstration is always required, the inaccuracies associated with the analytical determination of SDM will always have a built-in confirmation; however, the

potential impact of EPU designs on SDM calculations is nevertheless expected to be minimal. The primary influence of EPU designs is the consequence that a higher operating power level (at a similar capacity factor) will require that the core produce more energy for a given cycle length. This higher energy requirement necessitates the loading of fuel of higher enrichment and/or a higher batch fraction of fresh fuel. As for batch fraction, there continues to be a variety of cycle lengths supported by GNF as utilities continue to request designs for annual, eighteen month, and two year cycles, with accompanying variations in batch size. This has allowed GNF to gain considerable experience with both small, intermediate and large batch sizes for both high and low power density cores. The cold critical information previously provided demonstrates that the cold critical calculational accuracy of GNF methods has not suffered a degradation with increasing batch size.

As for enrichment (and discharge exposure), discharge exposure is currently constrained to a maximum value of 70 GWd/MT peak pellet exposure. Many of GNF's non-EPU designs already approach this licensing limit. Thus the ability for EPU fuel designs to increase enrichment and discharge exposure is limited by the constraints already imposed on peak exposure (as well as peak pellet  $^{235}\text{U}$  enrichment). Given this, bundle designs for EPU applications are expected to be very similar in enrichment and gadolinia content to non-EPU designs. Batch fractions, however, are proportionally greater than pre-EPU designs. Since somewhat larger batch fraction designs do not result in fuel of higher discharge exposure or significantly different isotopic content, these proportionally larger fresh fuel batch fractions are not viewed as increasing the cold reactivity calculational uncertainties. The validity of this conclusion will be confirmed in the beginning-of-cycle SDM demonstration for EPU cores prior to startup of the initial cycle. Further confirmation will occur as subsequent cycles are operated.

As a final demonstration of these concepts, the trending of the cold eigenvalues for a BWR/4 through a 120% EPU transition is provided in Figure 2.2-1. The scale of the data is consistent with that given in Figure 2-4 of NEDC-33173P. There is no identifiable aberration with the trend because of EPU.

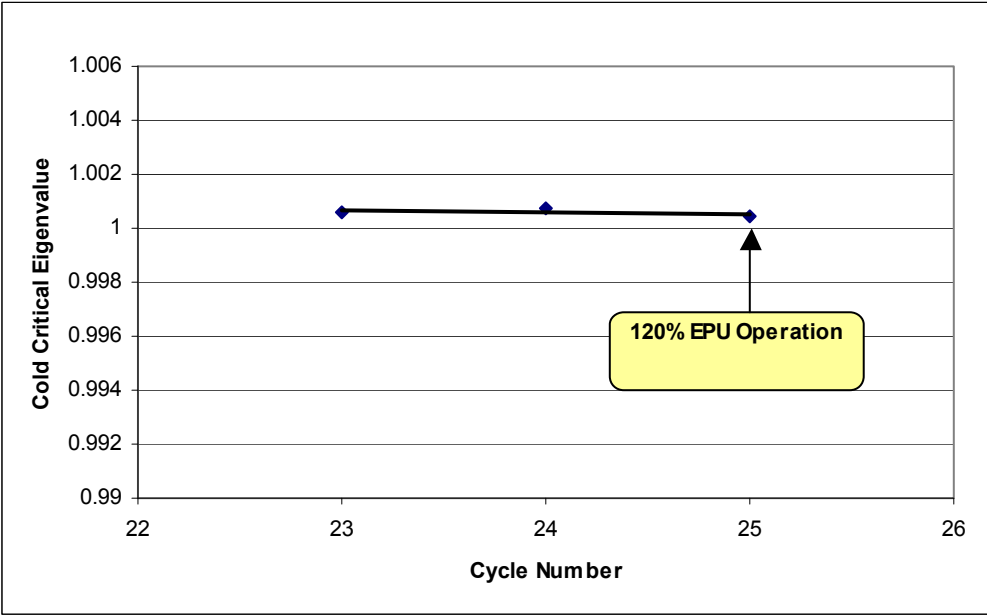


**Figure 2.2-1 Sensitivity of Cold Critical Eigenvalue to EPU Operation**



**NRC RAI 2.3**

An equation is provided in Section 2.3.2 stating what the technical specification for cold shutdown requires in terms of  $k_{sro}$  and  $k_{demo}$ . Explain the basis for this equation and describe its relationship to the equation relating the SDM calculation to  $k_{crit}$ ,  $k_{sro}$ , and the period and temperature corrections (e.g., startup control rod withdrawal sequence).

**GE Response**

The text of interest from Reference 2-1 states the following:

The cold shutdown technical specification requires that

$$k_{sro} \leq k_{demo}(1. - 0.0038)$$

where  $k_{sro}$  is the calculated criticality for the strongest rod withdrawn condition and 0.0038 is the required shutdown margin.

The derivation is different than that provided previously.

$$SDM = k_{crit} - k_{sro} - R + \Delta k_{temp} - \Delta k_{per}$$

Where:

$k_{crit}$  is the multiplication factor for the critical rod pattern;  
 $k_{sro}$  is the multiplication factor for the strongest rod out;  
 R is the maximum decrease in SDM throughout the cycle ;  
 $\Delta k_{temp}$  is the temperature correction; and  
 $\Delta k_{per}$  is the period correction.

The relationship between the two components may be established. SDM at the point in the cycle where the demonstration is performed is

$$SDM = k_{crit} - k_{sro} - R + \Delta k_{temp} - \Delta k_{per},$$

and the demonstration of plant criticality is

$$k_{demo} = k_{crit} - R + \Delta k_{temp} - \Delta k_{per}.$$

Then,

$$SDM = k_{demo} - k_{sro}$$

$$\frac{SDM}{k_{demo}} = 1 - \frac{k_{sro}}{k_{demo}}$$

Interpreting the SDM requirement as  $\frac{\Delta k}{k} \geq 0.0038$ , the following must be true:

$$\frac{SDM}{k_{demo}} \geq 0.0038$$

Equating the last two relationships results in the original equation.

NEDO-33173-A, Revision 1  
Non-Proprietary Information

$$\frac{\text{SDM}}{k_{demo}} = 1 - \frac{k_{sro}}{k_{demo}} \geq 0.0038$$
$$k_{demo} - k_{sro} \geq 0.0038k_{demo}$$
$$k_{sro} \leq k_{demo} (1 - 0.0038)$$

Considering that  $k_{demo} \cong 1$ , either interpretation of the SDM requirement is that the strongest rod out is more than 0.38% subcritical.

Reference

2-1 NEDC-33173P “Applicability of GE Methods to Expanded Operating Domains”  
February 2006.

### **NRC RAI 3.0 Bypass Voiding**

The evaluation of the bypass voiding and its impact on the: (1) neutronic method, (2) effectiveness of the instability protection instrumentation and (3) in-channel thermal-hydraulic conditions are not interim measure in lieu of additional benchmarking data. Instead, the objective of this review is to establish if bypass voiding will yield nonconservative results in the safety analyses and seeks conclusive resolution.

### **NRC RAI 3.1**

- (a) Provide a short description of the methodology used to account for the bypass thermal-hydraulic conditions for transient and stability calculations.
  
- (b) Discuss the accuracy of the assumption that the lattice physics parameters can be characterized as a function of the lattice average moderator density. Discuss the impact of bypass and water rod voiding on lattice depletion. Discuss what impact the presence of bypass voiding (E.g., during RPT) not accounted for in the neutronic methods will have on the core thermal-hydraulic conditions (e.g. power distribution). Discuss the effects of bypass and water rod voiding on lattice power distribution for the exposed fuel.

### **GE Response**

#### **Response to Part (a)**

The regular cross section generation process creates homogenized cross sections at many depleted and instantaneous conditions. The effects of reduced moderation due to voiding are calculated by performing lattice physic statepoint analysis of different in-channel void conditions. During this process, the out-channel water and water rod are assumed to have the density of saturated water for hot conditions ( $>100^{\circ}C$ ) and the density of solid sub-cooled water for temperatures  $<100^{\circ}C$ .

To accommodate changes in the water rod and bypass water density, the cross sections are then parameterized as a function of node-average relative water density.

$$U = \left( \frac{A_f}{A_f + A_{byp} + A_{wr}} \right) \frac{\rho_f}{\rho_o} + \left( \frac{A_{byp} + A_{wr}}{A_f + A_{byp} + A_{wr}} \right) \frac{\rho_{byp}}{\rho_o}$$

where

$\rho_f$  is the in-channel density with radial (bundle or channel) and axial dependence,

$\rho_{byp}$  is the axially dependent bypass density,

$\rho_o$  is a standard base density,

$A_f$  is the in-channel flow area

$A_{byp}$  is the out-channel (bypass) flow area

$A_{wr}$  is the water rod flow area

and

the subscripts of  $f$ ,  $byp$  and  $wr$  indicate the in-channel, bypass, and water rod regions of the lattice.

During the steady-state or kinetics simulator application, the calculated conditions in the bypass, water rod, and active region are combined to calculate the observed node average relative water density and inquire appropriate cross sections.

$$U_{ijk} = \left( \frac{A_f}{A_f + A_{byp} + A_{wr}} \right) \frac{\rho_{ijk}}{\rho_o} + \left( \frac{A_{byp}}{A_f + A_{byp} + A_{wr}} \right) \frac{\rho_{byp,k}}{\rho_o} + \left( \frac{A_{wr}}{A_f + A_{byp} + A_{wr}} \right) \frac{\rho_{wr,k}}{\rho_o}$$

where

$\rho_{f,ijk}$  is the in-channel density with radial (bundle or channel) and axial dependence,

$\rho_{byp,k}$  is the axially dependent bypass density,

$\rho_{wr,k}$  is the axially dependent water rod density for each bundle modeled.

and

$A_f$  is the in-channel flow area

$A_{byp}$  is the out-channel (bypass) flow area

$A_{wr}$  is the water rod flow area

In the 3D simulator PANACEA, the bypass regions and the water rod regions are combined into a single axial nodalized channel for purposes of modeling moderator density. The in-channel, bypass and water rod regions are then combined as described in the equation above to form the nodal average lattice moderator density.

In the plant transient simulator TRACG, the bypass and water rod regions are treated separately and are nodalized in the axial direction as specified by application. The in-channel, bypass and water rod regions are then combined as described in the equation above to form the nodal average lattice moderator density.

Thus, by the use of the lattice average water density parameter, potential changes in the bypass and water rod voiding (water density) are accurately modeled in the core steady-state and transient simulators.

#### Response to Part (b)

The presence of bypass and water rod voiding is accounted for in the neutronic methods through the process discussed in the response to RAI 3.1(a). The accuracy of the nodal, axial and radial power distribution is directly related to the ability of the 3D simulators to model the nodal reactivity accurately. In the following discussion, it is shown that the

nominal impacts for bypass and water rod voids on the axial power distribution are accurately accounted for in the 3-dimensional steady state and transient methods.

In MFN 05-31 RAI 1.4, the adequacy of the polynomial fitting process under high in-channel voids with and without bypass and water rod voiding was addressed using MCNP. The review in MFN 05-31, RAI 1.4 covered the ability to extrapolate to either the 90% in-channel void without water rod and bypass void state or to the 85% in-channel void with 25% water rod and 10% bypass void state. In this RAI, the error in the reactivity ( $k$ -infinity) fit extrapolation from the 0, 40, and 70% void fraction base data to the 90% void fraction level was shown to be less than 0.7% for the lattice evaluated. The error associated with the presence of bypass and water rod voiding is less than 0.5% and will not contribute to a significant decrease in the ability of the 3D simulators to predict the axial power distributions. Figure 3.1-1 is taken from MFN 05-31, RAI 1.4 for completeness.

Additional evaluations of the accuracy of this assumption for the components of  $k$ -infinity are provided to support the accuracy of the lattice average moderator assumption. The component cross sections evaluated are macroscopic thermal absorption (capture + fission), macroscopic thermal fission, macroscopic fast to epi-thermal scattering cross section and the epi-thermal to thermal scattering cross section. The calculated flux ratios are also presented to demonstrate the overall effectiveness of this assumption.

To perform this evaluation, a lattice depletion at a 40% void fraction was performed to create the base data for the instantaneous void evaluation using TGBLA. Using the isotopics generated by the base depletion case, the state points identified in Table 3.1-1, Instantaneous Void Evaluation Conditions were evaluated with MCNP. The instantaneous void data is fit as a function of lattice average moderator density at several exposure points from beginning of lattice life to assumed end of lattice life (65 Gwd/st). The base fits are performed by use of the 0, 40, and 70% void fraction data and these fits are then evaluated at lattice average moderator density values equivalent from a 0% in-channel state to a 90% in-channel without bypass or water rod voiding state to provide the fitted data representation in Figure 3.1-2 through Figure 3.1-7. Two explicit MCNP calculations for high voids with and without bypass voiding at each of the 4 exposure points were then performed to provide the basis for the comparison.

From Figure 3.1-2 through Figure 3.1-7, it can be seen that these significant nodal parameters can be fit and extrapolated with a high degree of accuracy and that the presence of bypass and water rod voiding can be parameterized as overall lattice average moderator density with a high degree of accuracy. No noticeable degradation in the nodal evaluations can be attributed to the presence of bypass and water rod void.

Since the nominal operating core does not experience bypass and water rod voiding and that the core conditions with bypass and water rod voiding are transitory in nature, there will be no significant impact on core depletion simulation.

The lattice physic state point analysis assumes non-voided bypass regions and water rods; therefore, the local pin power distributions do not account for the voided bypass and water rod effects. Evaluations for the impact of the non-voided bypass and water rod assumption show that the uncertainty in the local pin power distribution is small and that the subsequent impact on the R-factor process is small.

In the reactor core, the probability that a node experiencing bypass and water rod voiding is a maximum powered node is extremely small. However, to review the impact of bypass and water rod voiding, a comparison was made between a lattice at 90% in-channel voids without bypass and water rod voiding and a lattice at 85% in-channel voids with 10% bypass voids and 25% water rod voids. This combination of in-channel, bypass and water rod voids produces essentially identical average moderator density. To perform this comparison, an upper zone lattice from a bundle designed for MELLLA+ operation was chosen and the isotopics are based on a 70% in-channel void fraction without water rod and bypass void depletion case.

In Figure 3.1-8 and Figure 3.1-9, the impact on local pin fission density is presented. In Figure 3.1-8, the normalized fission density peaking is presented for the lattice at 90% in-channel void fraction without water rod and bypass voiding and for the lattice at 85% in-channel void fraction with 25% water rod and 10% bypass voiding. Figure 3.1-9 contains the delta normalized fission density for four (4) fuel pins for which at some point in the lattice lifetime are the peak powered rod. The contiguous rod peaking is plotted to demonstrate the impact as the peak powered rod changes location as a function of lattice exposure.

[[

]] This impact will not impact the accuracy of the LHGR evaluation in the neutronic methods.

From MFN 05-31 RAI 18, the Figure 3.1-10 below shows that the impact of the voiding of the bypass and water rods has a minimal impact on the value of the R-factor. A bundle that was designed for use in a MELLLA+ core design was used for this evaluation. This comparison is made by using the standard “production” three void points (0, 40, and 70%) without bypass and water rod voiding as the base case for the R-factor generation process. The 90VF\_axial-4VP model is generated by using four void points at 0, 40, 70, and 90VF without bypass and water rod voiding. The 90VF\_20BP-4VF was generated by using 0, 40, and 70 VF without bypass and water rod voiding and a 90 in-channel void with 20% bypass and water rod voiding case for the fourth data point for the R-factor generation process.

As can be seen below, the magnitude of the perturbed R-factor can vary both positive and negative relative to the base “production” R-factor and hence the modeling of bypass and water rod voiding in the R-factor generation process is neither conservative nor non-conservative.

**Table 3.1-1 Instantaneous Void Evaluation Conditions**

Lattice State	Lattice Exposure (Gwd/st)	In-channel Void (%)	Bypass Void (%)	Water Rod Void (%)
1	0.2,13,65	0	0	0
2	0.2,13,65	40	0	0
3	0.2,13,65	70	0	0
[[				
				]]



[[

]]

**Figure 3.1-1 Fit Uncertainty for TGBLA06 Reactivity**

[[

]]

**Figure 3.1-2 Macroscopic Group 3 (thermal) Sigma Absorption**

[[

]]

**Figure 3.1-3 Macroscopic Group 3 (thermal) Sigma Fission**

[[

]]  
**Figure 3.1-4 Macroscopic Sigma Slowing Group 1 (Fast) to Group 2 (Epi-thermal)**

||

||

**Figure 3.1-5 Macroscopic Sigma Slowing Group 2 (Epi-thermal) to Group 3 (thermal)**

[[

]]

**Figure 3.1-6 Group 1 (Fast) to Group 3 (thermal) Flux Ratio**

[[

]]

**Figure 3.1-7 Group 2 (Epi-thermal) to Group 3 (thermal) Flux Ratio**

[[

]]

**Figure 3.1-8 Peak Rod Fission Density Impact for Bypass and Water Rod Voiding**



[[

]]

**Figure 3.1-9 Peak Rod Delta Fission Density for Bypass and Water Rod Voids**

[[

]]

**Figure 3.1-10 R-factor Response for 20% Bypass/Water Rod Void Fraction  
(from MFN 05-133 RAI 18)**

**NRC RAI 3.2**

**NRC RAI 3.2(a)**

Quantify the bypass voiding for rated power operation and power levels associated with EPU and MELLLA+.

- (i) Describe the methodologies used by GE to calculate bypass voiding.
- (ii) Quantify the best estimate bypass void fraction (BP VF) for the worst point in the operating map (NC + MELLLA+, MELLLA, OLTP) that could be used for stability calculations.
- (iii) Quantify the best estimate BP VF for the expected conditions where ODYSY stability methodology is used for LTS.

**GE Response:**

**Response to Part 3.2(a)(i)**

The core bypass region modeling used in the various GE codes (ISCOR, PANACEA, ODYSY and TRACG) is described below. A summary comparison table is provided at the end.

**ISCOR**

ISCOR employs a core-averaged bypass model. [[

]]

**PANACEA**

PANACEA utilizes a core-averaged bypass model that is consistent with the ISCOR model described above. [[

]] The PANACEA bypass model considers the same sources of heating as the ISCOR model. The core-averaged bypass region uses the same axial nodalization as the PANACEA active channel model. Pressure drop and void correlations used in PANACEA are consistent with the ISCOR correlations.

**ODYSY**

ODYSY utilizes a core-averaged bypass model that is consistent with the ISCOR model described above. The ISCOR calculated bypass and water rod flow is used as input for the ODYSY calculations. [[

]] The core-averaged bypass region uses the same axial nodalization as the ODYSY active channel model. Pressure drop and void correlations used in ODYSY are consistent with the ISCOR correlations.

**TRACG**

In TRACG, the bypass region is modeled as [[

]] The two ring nodalization is shown in Figure 3.2(a)-1.

[[

]]

**SUMMARY**

Table 3.2-1 below summarizes the key elements of the bypass modeling for the various GE codes.

Response to Part 3.2(a)(ii)

TRACG is used to compute the best estimate bypass void fraction for the worst point in the power/flow operating map, i.e. at the intersection of the natural circulation line and the MELLLA+ boundary. [[

]] This is a best estimate value of the bypass voids and the TRACG bypass voiding methodology is described in the response to RAI 3.2a(i).

ISCOR is used to compute bounding values of the bypass void fraction for the worst point in the power/flow operating map, i.e. at the intersection of the natural circulation line and the MELLLA+ boundary, for comparison to the values calculated by TRACG. ISCOR calculations are also performed at the intersection of the natural circulation line and the MELLLA boundary and at the intersection of the natural circulation line and the original licensed thermal power (OLTP) rated rod line to show the sensitivity of bypass voids to power level. ISCOR core average and hot channel bypass voids are shown in Table 3.2-2 and the ISCOR bypass voiding methodology is described in the response to 3.2a(i). ISCOR in-channel voids are also provided in Table 3.2-2 for reference. [[

]]

Therefore, because TRACG computes best estimate bypass voiding and the calculation for the worst point on the power/flow map of [[

]], which has a negligible effect on the effectiveness of the instability protection instrumentation.

Response to Part 3.2(a)(iii)

ODYSY is used to calculate the stability exclusion region for BWROG Long-Term Solution Options I-D and II. The Vermont Yankee Cycle 25 Option I-D exclusion region analysis was reviewed to determine the bypass void fractions computed by ISCOR for the endpoints of the exclusion region boundary. [[

Therefore, bypass voiding has no effect on the ODYSY exclusion region methodology (e.g., application to Options I-D and II). ]]

**Table 3.2-1**

	<b>ISCOR</b>	<b>PANACEA</b>	<b>ODYSY</b>	<b>TRACG</b>
[[				
				]]

Reference

3.2(a)-1 NEDE-32176P, Revision 3, "TRACG Model Description Licensing Topical Report," April 2006.

**Table 3.2-2**

[[					

]]



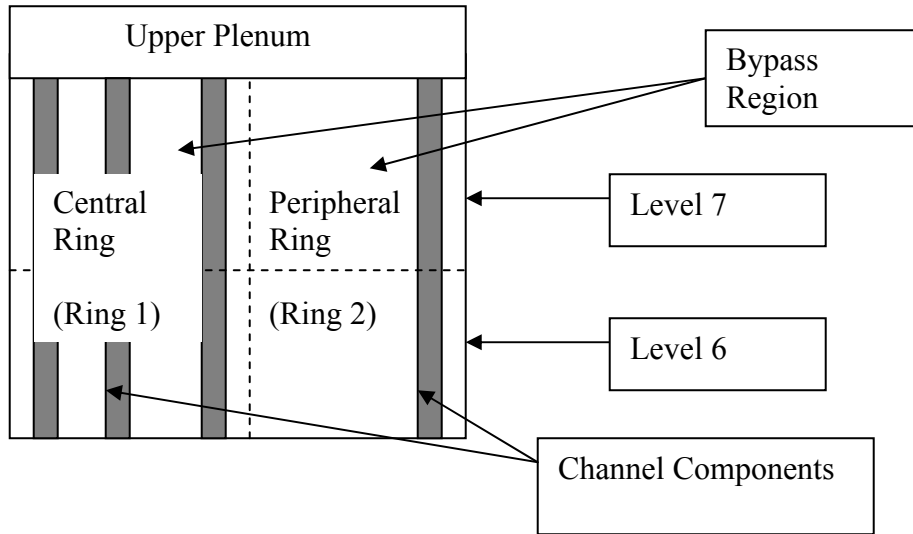
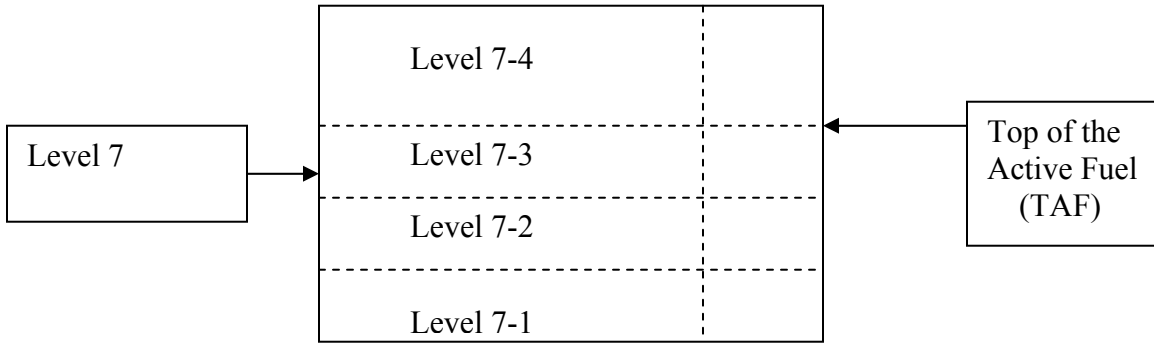


Figure 3.2(a)-1



**Figure 3.2(a)-2**

**NRC RAI 3.2(b)**

Describe the method for the determination of the impact of BP VF on stability analysis.

**GE Response**

Two different approaches are used in GE stability analysis – the frequency-domain code ODYSY and the time-domain code TRACG.

ODYSY employs the conservative estimates for direct moderator heating from ISCOR.

[[

]] Therefore, the ODYSY model provides a reasonably bounding value of bypass voiding.

[[

]] Both the regional and core-wide DIVOM analyses are performed at a reasonably limiting power/flow point where bypass voiding tends to be the worst. (The core-wide DIVOM analysis is performed at the rated rod line and the natural circulation line, while the regional DIVOM analysis is performed on the highest flow boundary and natural circulation flow). However, both the regional and core-wide DIVOM analyses are based on the hot channels, which are away from the periphery of the core where bypass voiding is highest. This mitigates the bypass voiding impact on the DIVOM evaluation.

**Reference**

3.2(b)-1 NEDE-32906P-A, Revision 2, “TRACG Application for Anticipated Operational Occurrences Transient Analyses,” February 2006.

**NRC RAI 3.2(c)**

Section 2.6.2.1 concludes that the effect of BP VF on APRM calibration is [[  
]] Section 2.6.2.3 concludes that the effect of BP VF on OPRM calibration is  
[[  
]] Please describe the methodology used for these analyses and  
quantify the BP VF levels used.

**GE Response**

The APRM evaluation in Section 2.6.2.1 makes use of the core average bypass voids computed by the ISCOR thermal-hydraulics model. This is appropriate because the APRM is a core average response. The OPRM evaluation in Section 2.6.2.3 makes use of the hot channel bypass voids computed by ISCOR. This is appropriate because the OPRM is a localized response. [[

]] The bypass voids used in the analyses and the corresponding in-channel voids are provided in Table 3.2(c)-1. The APRM evaluation data is from Vermont Yankee under EPU/MELLLA conditions. The OPRM evaluation data is from another BWR/4 under EPU/MELLLA conditions.

**Table 3.2-1**

[[				

]]

**NRC RAI 4.0 Use of 40 % Void Fraction History Depletion Assumption for Instantaneous Void Fraction Changes**

The neutronics methods perform void history calculations a 0%, 40%, and 70% void fractions, but the instantaneous branch cases are performed only for the 40% void history case. As a result, the impact of instantaneous changes in the void fraction for all void histories is assumed to be that of the 40% void history case. The impact of this assumption results in errors in the prediction of the void reactivity effect for void fraction histories lower and higher than 40% and can be evaluated by examining the void coefficient of reactivity. In order to assess the impact of the 40% void fraction history assumption:

**NRC RAI 4.1**

**NRC RAI 4.1(a)**

Provide an evaluation of the error created by the 40% void fraction history assumption on the local void coefficient.

**GE Response**

**Response to 4.1(a)**

As described in Reference 4.1(a)-1 Section 2.2.2.2, the local void coefficient error created by the [[

]]

**References**

- 4.1(a)-1 Licensing Topical Report, "Applicability of GE Methods to Expanded Operating Domains," NEDC-33173P, February 2006.
- 4.1(a)-2 Entergy letter to U.S. Nuclear Regulatory Commission, "Vermont Yankee Nuclear Power Station, License No. DPR-28 (Docket No. 50-271), Technical Specification Proposed Change No. 263 - Supplement No. 35, Extended Power Uprate - Response to Request for Additional Information," BVY 05-088, September 28, 2005.

[[

**Figure 4.1a-1 Void Coefficient Ratio MNCP / TGBLA06**

]]

**NRC RAI 4.1(b)**

Provide an estimate of the error in the global void coefficient introduced by the [[  
]] assumption.

**GE Response**

TRACG was used to estimate the error in the global void coefficient introduced by the [[  
]] assumption. Analysis was performed for a high power density BWR/6 at natural circulation and a high rod line. A TRACG base case was run with the void coefficient correction included. The hot channel power response for this case is shown in Figure 4.1b-1. To estimate the error in the global void coefficient due to the [[  
]] assumption, a second TRACG case was run using an input variable to increase the global void coefficient. It was determined that [[  
]] in the global void coefficient yields results that closely match the results with the void coefficient correction included. The hot channel power response for the second case is shown in Figure 4.1b-2. Therefore, the error in the global void coefficient introduced by the [[  
]] assumption is [[  
]].

[[

]]

**Reference**

- 4.1(b)-1 Licensing Topical Report, "ODYSY Application for Stability Licensing Calculations," NEDC-32992P-A, July 2001.
- 4.1(b)-2 Licensing Topical Report, "Reactor Stability Detect and Suppress Solutions Licensing Basis Methodology for Reload Applications," NEDO-32465-A, August 1996.



[[

]]

**Figure 4.1b-1 Hot Channel Power Response with Void Coefficient Correction**

[[

**Figure 4.1b-2 Hot Channel Power Response with [[ Coefficient ]]**  
**]] Increase in Global Void**

**NRC RAI 4.1(c)**

Provide TRACG stability calculations with and without the void history correction for void coefficient.

**GE Response**

TRACG analysis was performed for a high power density BWR/6 at natural circulation and a high rod line. Figure 4.1c-1 shows the hot channel power and growth rate with and without the void history correction for the void coefficient. The data with the correction is labeled “V33” and the data without the correction is labeled “NV”. As can be seen in Figure 4.1(c)-1, the correction produces [[

]].

[[

Figure 4.1c-1 Hot Channel Power and Growth Rate with (V33) and without (NV)  
Void History Correction for Void Coefficient

**NRC RAI 4.1(d)**

Provide and include the cited instability benchmarking that demonstrates the accuracy of ODYSY and TRACG in the TR. Provide some assessment of the similarities of core thermal-hydraulic conditions between the benchmark plants and the EPU plants.

**GE Response:**

**ODYSY**

ODYSY stability benchmarking is provided in References 4.1(d)-1 and 2. Reference 4.1(d)-1 provides a comparison of ODYSY calculated decay ratios to plant data for core-wide mode oscillations from Vermont Yankee high decay ratio tests and the 1988 LaSalle instability event. These data are shown in Tables 4.1d-1 and 4.1d-2, respectively. It can be seen from the data that the ODYSY calculated decay ratios are in good agreement with the test data. The ODYSY predicted frequency is slightly lower than the test data.

Reference 4.1(d)-1 also provides ODYSY predicted core and limiting channel decay ratios for regional mode oscillations from tests at Leibstadt and KRB-C and the 1991 Cofrentes instability event. The ODYSY results are compared to the ODYSY stability criteria map in Figure 4.1d-1. Regional mode oscillations are possible when the limiting channel decay ratio exceeds the curved line that begins at 0.56. As can be seen in Figure 4.1d-1, the ODYSY predicted core and limiting channel decay ratios for the tests and instability event exceed the stability criteria. Therefore, the combination of the ODYSY calculated decay ratios and the ODYSY stability criteria map provide a good prediction for regional mode oscillations.

Also provided in Reference 4.1(d)-1 is a comparison of ODYSY predicted channel decay ratio versus TRACG predicted channel decay ratio for selected channels from Leibstadt and LaSalle. This comparison is shown in Figure 4.1d-2. As can be seen in Figure 4.1d-2, the ODYSY calculated channel decay ratios are in good agreement with the TRACG calculated channel decay ratios.

Reference 4.1(d)-2 provides a qualification study of the 1995 Laguna Verde instability event. The ODYSY calculated core and limiting channel decay ratios at instability inception for different power and xenon assumptions are provided in Table 4.1d-3. Condition 3c is believed to be the most accurate calculation. The actual event produced a limit cycle oscillation, so the actual core decay ratio was exactly 1.0 when the oscillation was fully developed. The ODYSY predicted core decay ratio is in good agreement with the actual decay ratio.

The ODYSY predicted core and limiting channel decay ratios for the 2003 Nine Mile Point 2 (NMP-2) instability event versus the ODYSY stability criteria are shown in Figure 4.1d-3. Two conditions were analyzed. The first calculation was performed at the Average Power Range Monitor (APRM) measured power of 44.9%, a measured core flow of 28%, and a measured feedwater temperature of 360 °F. The second calculation was performed at a predicted power of 47.1%, the measured core flow of 28%, and the measured feedwater temperature of 360 °F. The 47.1% power was based on a GE 3D

BWR core simulator prediction for the measured core flow, feedwater temperature, and rated power and flow eigenvalue. It is believed that the predicted core power of 47.1% is more accurate for the event. As can be seen in Figure 4.1d-3, the ODYSY prediction for the 47.1% power case is greater than the ODYSY stability criteria, indicating that core-wide mode oscillations are possible.

The ODYSY predicted core and limiting channel decay ratios for the 2005 Perry instability event versus the ODYSY stability criteria are shown in Figure 4.1d-4. Four conditions were analyzed corresponding to the progression of the feedwater temperature from the rated condition to the equilibrium condition. It is believed that the case with the equilibrium feedwater temperature of 372 °F is believed to be the most accurate calculation. As can be seen in Figure 4.1d-4, the ODYSY prediction for the 372 °F feedwater temperature case is greater than the ODYSY stability criteria, indicating that core-wide mode oscillations are possible.

ODYSY has been qualified to a very broad range of conditions and events. The ODYSY predicted results have universally shown good agreement to plant data and ODYSY is believed to be a very good tool for predicting and evaluating core and channel decay ratios for both core-wide and regional mode oscillations.

#### TRACG

TRACG stability benchmarking is provided in the TRACG qualification report (NEDE-32177P, Reference 4.1(d)-3). Simulations of the instability events at LaSalle and Cofrentes and the stability tests at Leibstadt and Forsmark are presented.

The 1988 LaSalle event provides an assessment of the prediction of core-wide mode oscillations. TRACG successfully calculated the core-wide oscillations observed during the event. The characteristics of the oscillations and sensitivity to the feedwater flow fluctuations were well predicted. The prediction of the reactor transient response following the pump trip was also well predicted. Figures 4.1d-9 and 10 (Figures 7.4-10 and 7.4-11 from Reference 4.1(d)-3) are included below.

The 1991 Cofrentes event provides an assessment of the regional oscillation mode predictive capability of TRACG. Reasonable agreement between TRACG and the event data for APRM frequency and magnitude was obtained. The TRACG analysis of the event demonstrates that the oscillations were out-of-phase and that operator action reduced the effect of the out-of-phase oscillation. Figures 4.1.d-11 and 12 (Figures 7.7-7 and 7.7-8 from Reference 4.1(d)-3) are included below.

The Leibstadt stability tests provide data to assess the prediction of regional oscillation characteristics. TRACG successfully calculated the limit cycle regional oscillations observed during the tests. The characteristics of the oscillations and sensitivity to changes in test conditions were well predicted. Tables 4.1d-7 and 8 (Tables 7.5-1 and 7.5-2 from Reference 4.1(d)-3) are included below.

The Forsmark stability tests provide data for the assessment of TRACG to calculate core decay ratios for an internal pump plant. The TRACG model of Forsmark Unit 1 was validated against plant data. The TRACG calculated and measured decay ratios correspond well for the five tests considered. At the limit cycle condition, TRACG predicts the limit cycle oscillation. Tables 4.1d-6 and 7 (Figures 7.6-1 and 7.6-3 from Reference 4.1(d)-3) are included below.

A TRACG benchmark calculation was performed for the recent NMP-2 instability event and the result is shown in Figure 4.1d-5. The figure presents a comparison of the TRACG calculated Oscillation Power Range Monitor (OPRM) cell signal to the plant OPRM cell signal just prior to the reactor scram. It can be seen from the figure that the oscillation frequency and growth rate are well predicted.

Analysis was performed relative to the NMP-2 Instability TRACG benchmark to show the sensitivity of the oscillation response to core flow, power and feedwater temperature. The flow sensitivity is shown in Figure 4.1d-6. It can be seen from the figure that the oscillation growth rate is very sensitive to the core flow, while the frequency has a small sensitivity. The power sensitivity is shown in Figure 4.1d-7. It can be seen from the figure that the oscillation growth rate is not as sensitive to power as core flow. The frequency is not affected. The feedwater temperature sensitivity is shown in Figure 4.1d-8. It can be seen from the figure that the oscillation growth rate is very sensitive to the feedwater temperature, while the frequency has a small sensitivity.

#### Core Thermal-Hydraulic Conditions

The ISCOR core average and hot channel in-channel voids for the benchmark NMP-2 and Perry instability events and the VY and Hope Creek EPU/MELLLA conditions are provided in the Table 4.1d-4. The NMP-2 and Perry instability events occurred very near natural circulation at a high rodline. The VY and Hope Creek data is shown for natural circulation at the MELLLA rodline. It can be seen from the data that the in-channel voids for the benchmark plants are very close to the in-channel voids for the EPU plants. Therefore, it can be concluded that the validation database adequately covers the EPU plants.

#### References

- 4.1d-1 NEDC-32339P-A, "Reactor Stability Long-Term Solution: Enhanced Option I-A, ODYSY Application to E1A," December 1996.
- 4.1d-2 NEDC-32992P-A, "ODYSY Application for Stability Licensing Calculations," July 2001.
- 4.1d-3 NEDE-32177P, Rev. 2, "TRACG Qualification," January 2000.

**Table 4.1d-1 Summary of ODYSY Results for Vermont Yankee High Decay Ratio Tests**

Test Point	POWER/FLOW (% rated)	Test Data		ODYSY Results	
		Decay Ratio	Frequency	Decay Ratio	Frequency
6P	57.2/38.5	0.74	0.44	0.67	0.39
7N	51.2/32.6	1.00	0.43	0.99	0.38
8P	50.9/32.6	0.96	0.43	0.97	0.37
9P	48.1/32.4	0.81	0.42	0.86	0.36
10P	49.8/33.0	0.90	0.42	0.97	0.37
11P	67.1/38.5	0.85	0.47	0.85	0.42
12P	63.1/38.5	0.78	0.47	0.75	0.42

**Table 4.1d-2 Summary of ODYSY Results for LaSalle Event**

Condition	Power/Flow (% rated)	Event Data		ODYSY Results	
		Decay Ratio	Frequency	Decay Ratio	Frequency
17:35 Threshold	42/28	1.00	0.45	1.00	0.40
17:37 At Scram	45/28	Unstable >1.00	0.45	1.18	0.44

**Table 4.1d-3 Summary of ODYSY Results for Laguna Verde Event**

Condition	Description	Xenon Assumption	Core Decay Ratio	Channel Decay Ratio
3a	After flow control valve closure at initiation of reactor instability, 31.8% power, 32% core flow	Constant xenon at 16% power	0.89	0.48
3b	Repeat of Case 3a with transient xenon model	Transient xenon model	0.94	0.50
3c	Repeat of Case 3a with transient xenon model and at 33.1% power	Transient xenon model	1.04	0.54



**Table 4.1d-4 ISCOR In-Channel Voids for Selected Events and Conditions**

Event/Condition	ISCOR Core Average In-Channel Voids (Top of Active Fuel)	ISCOR Hot Channel In-Channel Voids (Top of Active Fuel)
NMP-2 Instability Event	73%	81%
Perry Instability Event	75%	86%
VY EPU/MELLLA	76%	85%
Hope Creek EPU/MELLLA	76%	86%

**Table 4.1d-5 (NEDE-32177P Rev 2 Table 7.5-1) Leibstadt Test Conditions**

Test	Power (MW)	Flow (kg/s)	Dome Pressure (MPa)	Feedwater Temperature (K)
4	1646	3434	6.736	448
4A	1599	3211	6.736	448
5	1528	3434	6.698	434
5A	1392	3234	6.698	434

**Table 4.1d-6 (NEDE-32177P Rev 2 Table 7.5-2) Leibstadt Test Data TRACG Comparison Summary**

Test	LPRM (%)*		APRM (%)*		Freq (Hz)	
	Data	TRACG	Data	TRACG	Data	TRACG
4	14	20	4	2	0.45	0.41
4A	66	26	8	3	0.45	0.39
5	12	19	4	2	0.45	0.41
5A	12	13	4	2	0.45	0.39

\* (P – P)/A

**Table 4.1d-7 (NEDE-32177P Rev 2 Table 7.6-1) Forsmark Test Conditions**

<b>Test</b>	<b>5</b>	<b>7</b>	<b>8</b>	<b>15</b>
Power (% of 2800 MW)	62.7	73.4	70.0	103.5
Flow (kg/s)	4205	4797	4530	10166.
CR Position (-10000 notches)	128	272	324	634
Xe (t/cm)	870	809	833	1311

**Table 4.1d-8 (NEDE-32177P Rev 2 Table 7.6-3) Forsmark Decay Ratio Comparison**

<b>Test</b>	<b>5</b>	<b>7</b>	<b>8</b>	<b>15</b>
DR Data	0.84	0.86	0.96	0.05
Freq (Hz)	0.51	0.55	0.54	
DR TRACG	0.77	0.97	1.03	<0.20
Freq (Hz)	0.55	0.61	0.60	

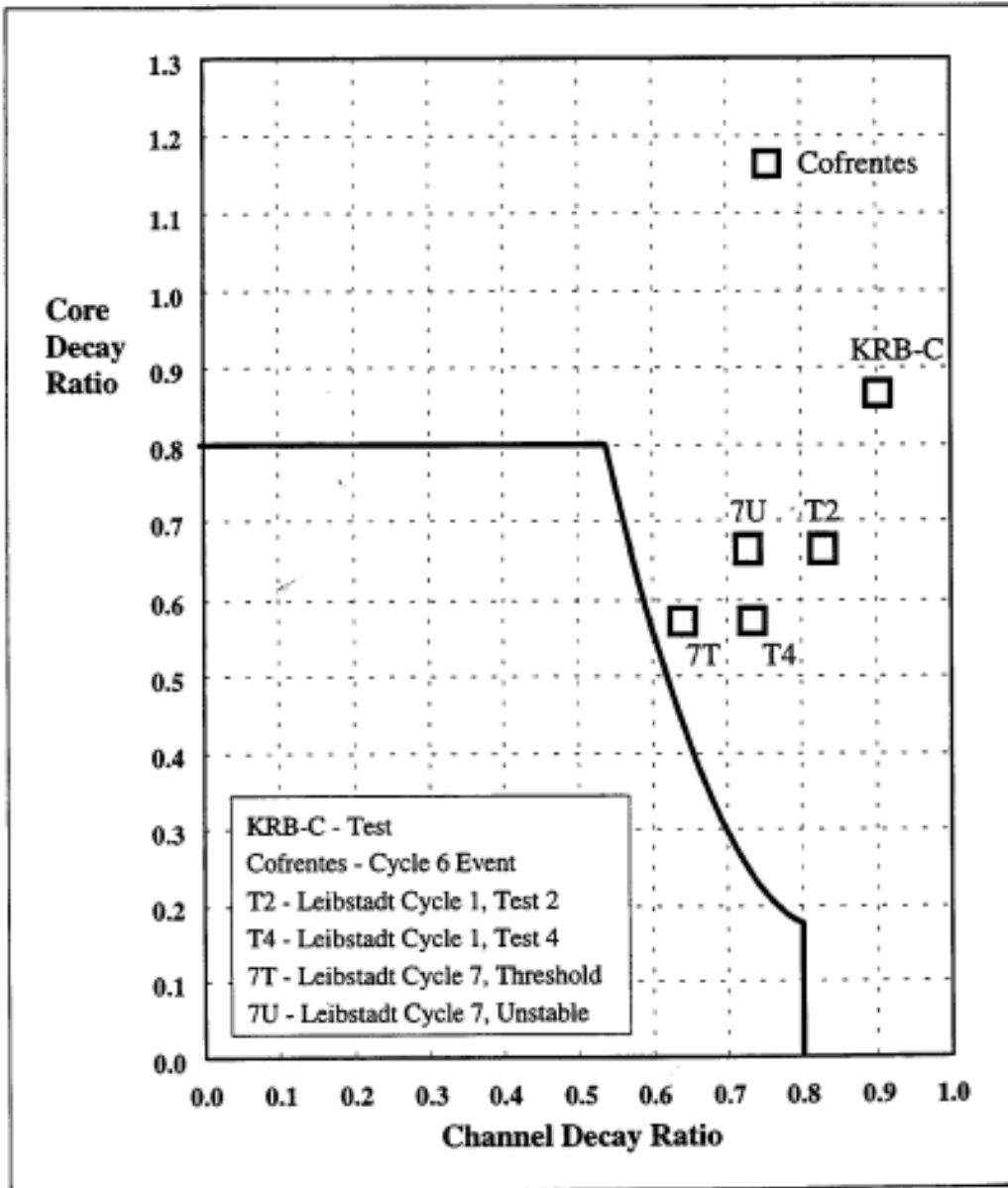


Figure 4.1d-1 Regional Mode Instability Event and Test Decay Ratios:  
ODYSY Results vs. ODYSY Stability Criteria Map

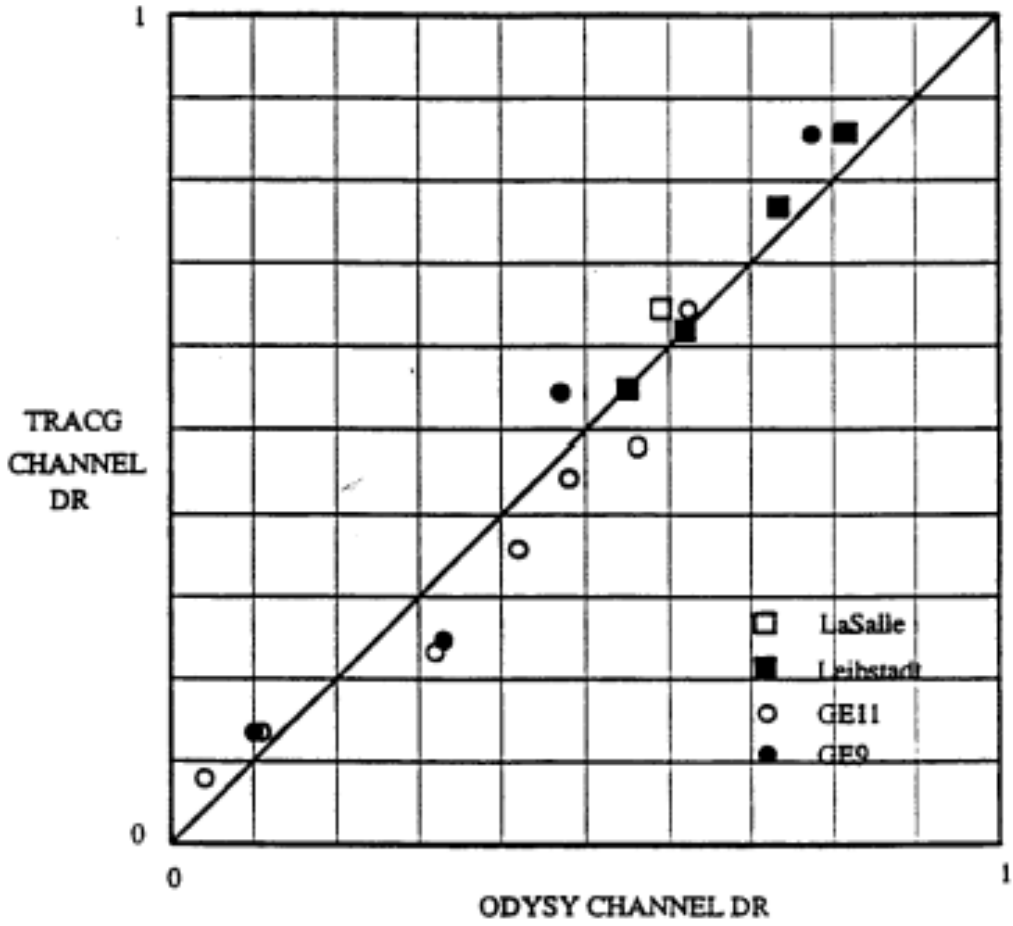
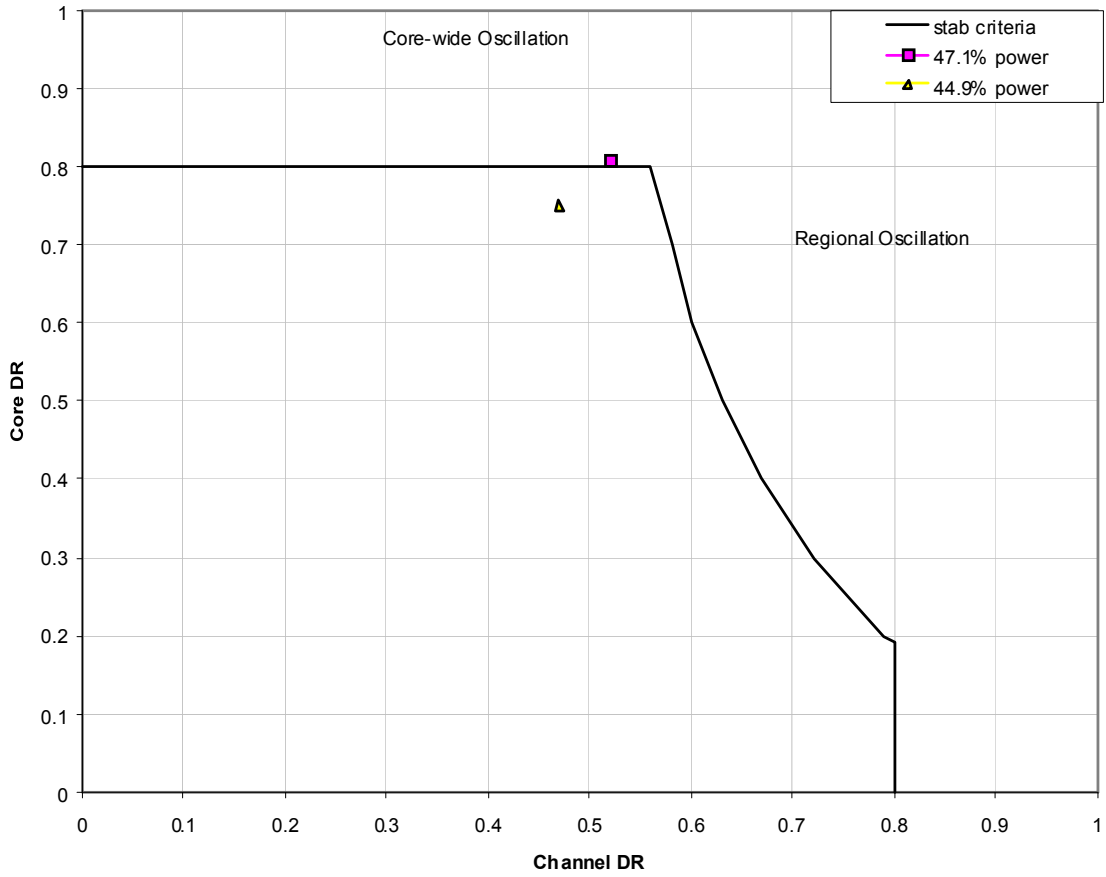
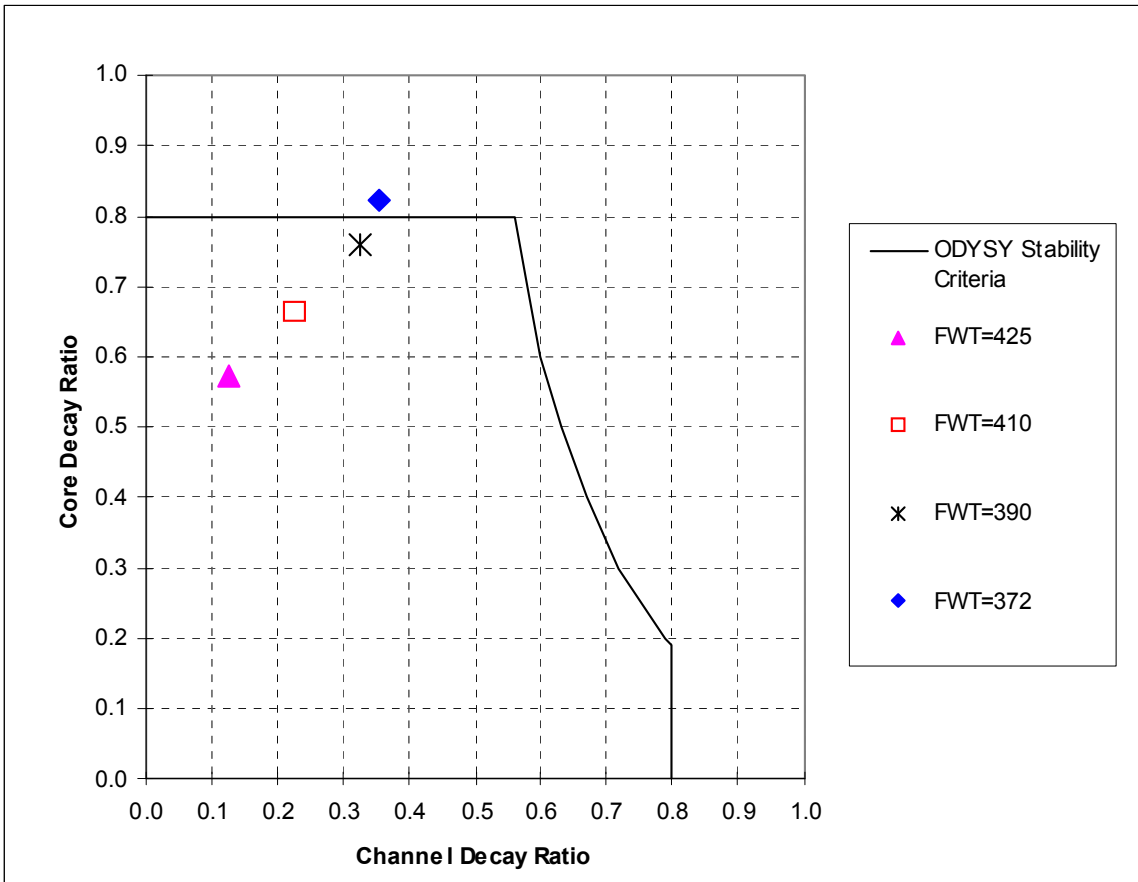


Figure 4.1d-2 TRACG Channel Decay Ratio vs. ODYSY Channel Decay Ratio



**Figure 4.1d-3 NMP-2 Instability Event ODYSY Benchmark**



**Figure 4.1d-4 Perry Instability Event ODYSY Benchmark: 425°F @ 47.4% power;  
410°F @ 49.8% power; 390°F @ 52.2% power; 372°F @ 54.2% power**

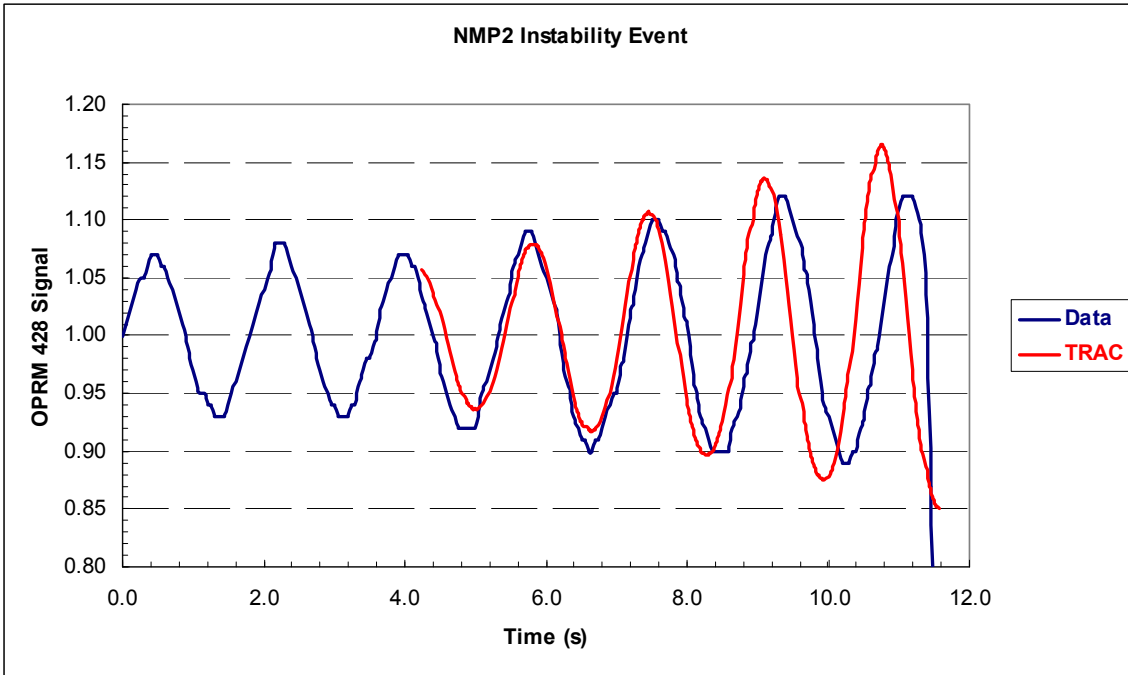


Figure 4.1d-5 NMP-2 Instability Event TRACG Benchmark

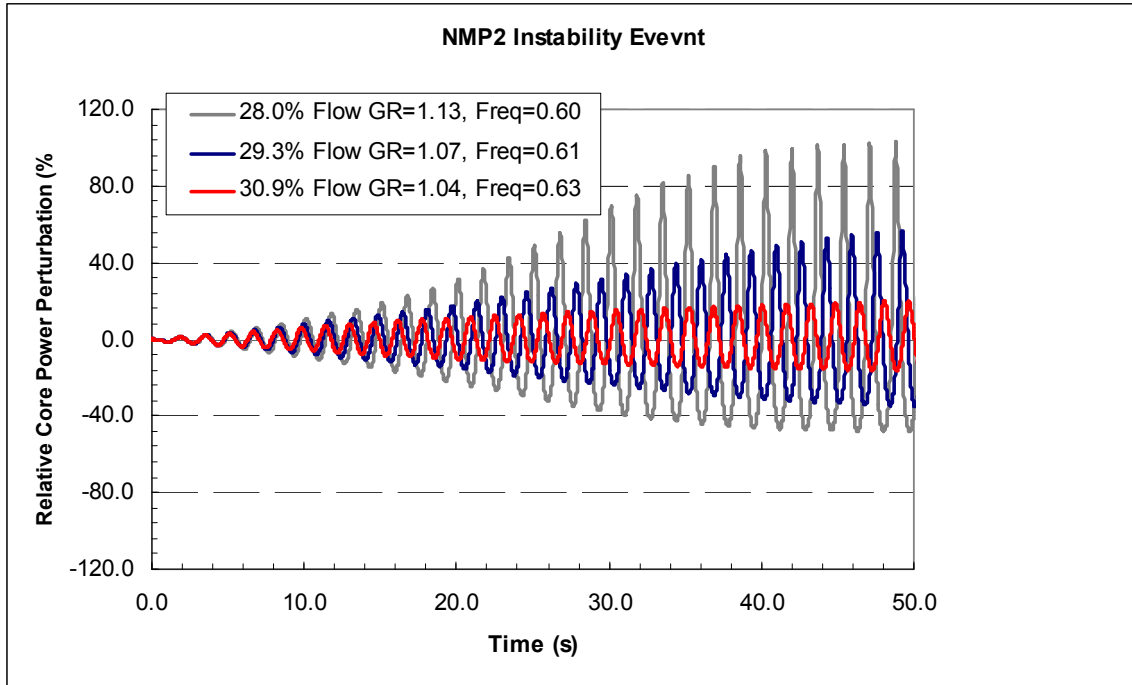


Figure 4.1d-6 NMP-2 Instability Event TRACG Flow Sensitivity



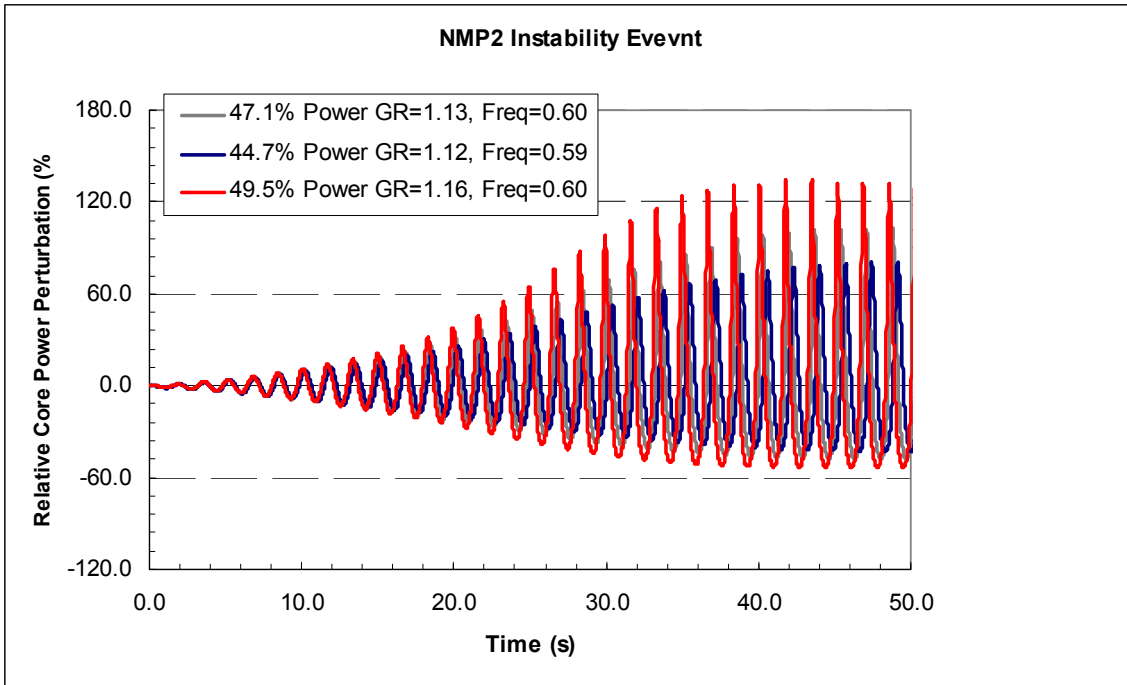


Figure 4.1d-7 NMP-2 Instability Event TRACG Power Sensitivity

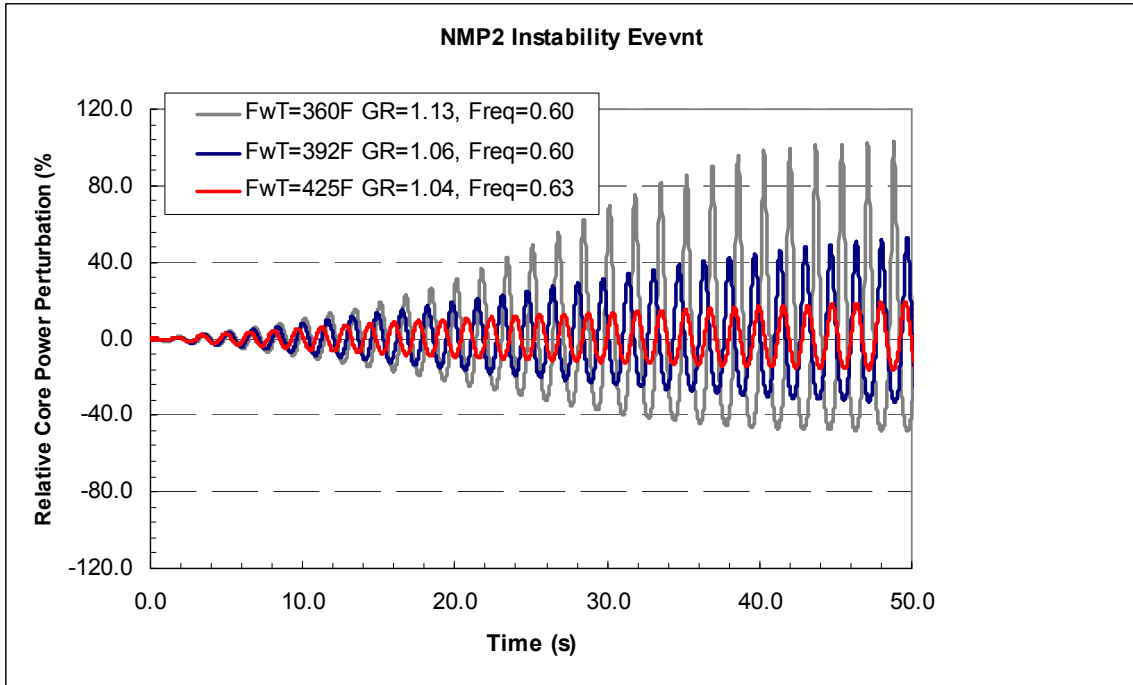
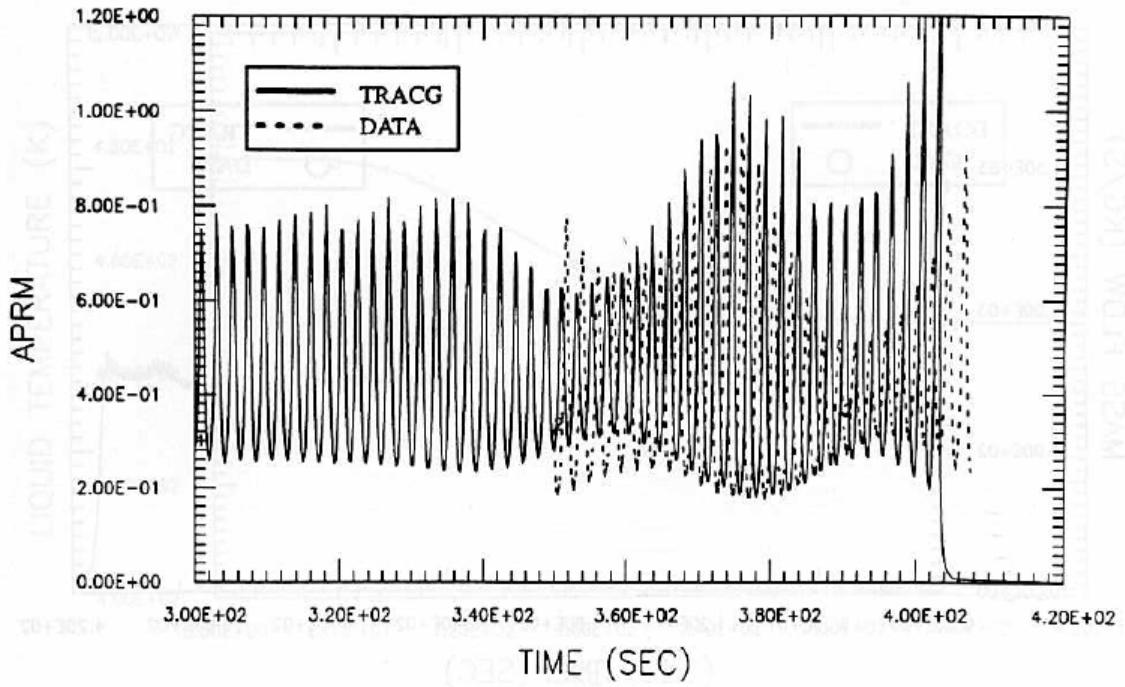


Figure 4.1d-8 NMP-2 Instability Event TRACG Feedwater Temperature Sensitivity



**Figure 4.1d-9 (NEDE-32177P Rev 2 Figure 7.4-10) LaSalle Event Detailed APRM Comparison**

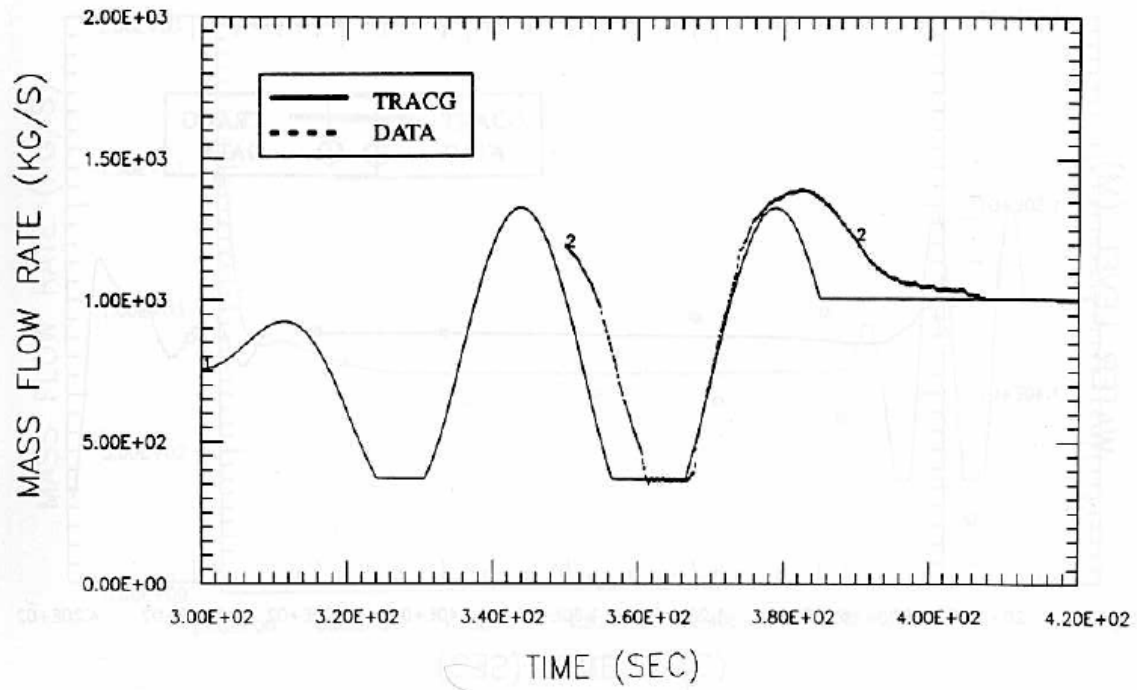
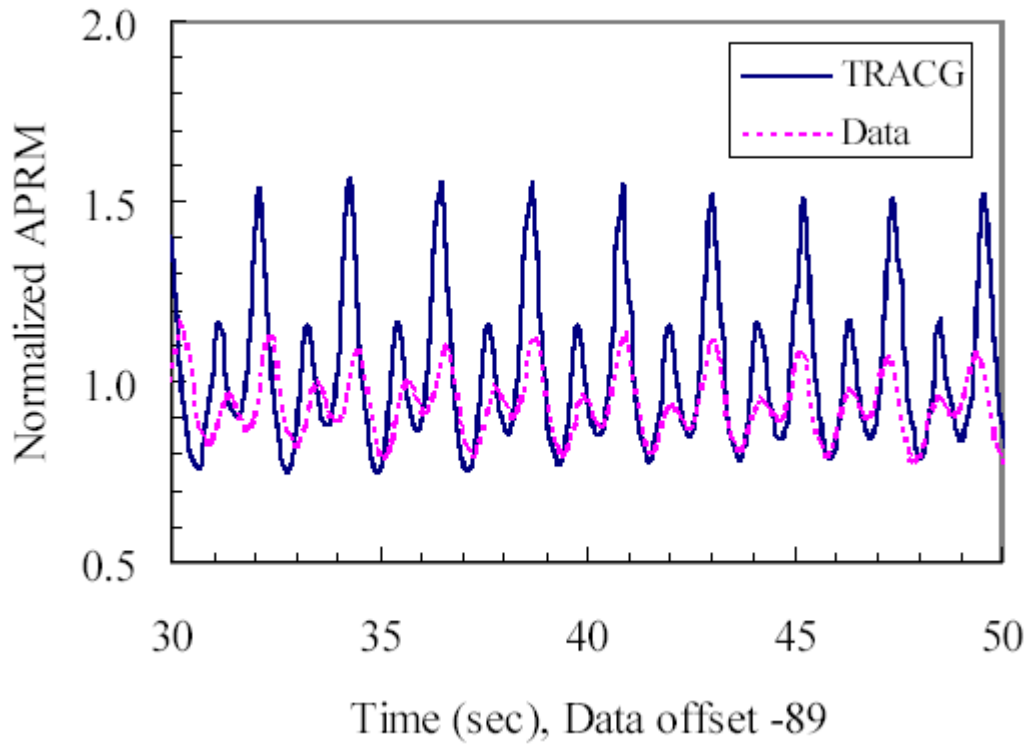
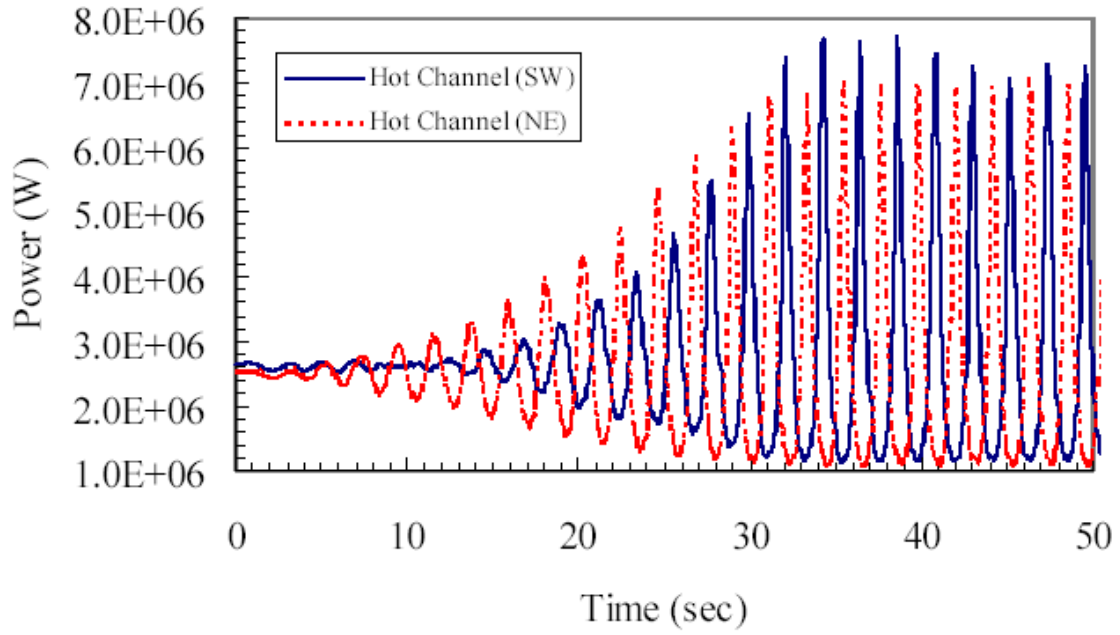


Figure 4.1d-10 (NEDE-32177P Rev 2 Figure 7.4-11) LaSalle Event Detailed Feedwater Flow Comparison



**Figure 4.1d-11 (NEDE-32177P Rev 2 Figure 7.7-7) Cofrentes Event Detailed APRM Comparison**



**Figure 4.1d-12 (NEDE-32177P Rev 2 Figure 7.7-8) Cofrentes Event Channel Power Response**

**NRC RAI 4.1(e)**

What is the impact on stability of void fraction histories less than 40%?

**GE Response**

[[

]]

**NRC RAI 4.2**

Address the impact of the 40 percent depletion assumption on the ATWS response.

**GE Response**

The 40% void depletion assumption can affect the void coefficient. The effect of void coefficient uncertainty has been addressed in previous studies. With respect to ATWS Overpressure results, uncertainty screening was performed in NEDE-32906P Supplement 1-A (MFN 03-148, November 26, 2003). The initial conditions for this study were for a plant at 113% of original rated power and 73% core flow, which are MELLLA+ type of conditions.

For an ATWS event, the steam line isolation causes a rapid increase in reactor vessel pressure, which results in core void reduction. Consequently, power increases with positive void reactivity insertion. For ATWS simulation purposes, the expected MSIV position and high flux scrams do not occur. The power excursion is initially mitigated by void production from the increased core heat flux, as well as negative doppler reactivity from increasing fuel temperature. Soon after the time the MSIVs are fully closed, Recirculation Pump Trip (RPT) is initiated on high pressure, such that core flow begins to decrease. At about this same time, the Safety/Relief Valves (S/RVs) open, reducing the rate of pressure increase. As core flow continues to decrease, core voiding increases, causing the power to decrease in parallel. Finally, the steam production decreases to the point at which the S/RV capacity is sufficient to relieve all of the steam generation, and the pressure begins to fall. Figures 4.2a and 4.2b show the response of key parameters for this event. These figures also contain the results for the void coefficient perturbation.

Analyses have been performed at +/- 1 $\sigma$  level for each of the model uncertainties. The results of the screening are shown in Figure 4.2c.

The analysis results show that the peak pressure results are [[

]]

Analyses have also been performed for another EPU plant with ODYN with a core-wide [[ ]] increase in ODYN void coefficient magnitude. The results are presented in Table 4.2a for BOC and EOC conditions. [[



]]

In addition, the effect on the peak pool temperature response is also addressed. Sensitivity studies have been performed with a core-wide [[ ]] increase in the ODYN void coefficient magnitude. A sensitivity study was performed for a limiting Pressure Regulator Failure – Open (PRFO) at both BOC and EOC exposure conditions. The results shown in Table 4.2b below show that the peak pool temperature is [[ ]].

**Table 4.2a ODYN Peak Vessel Pressure Void Coefficient Study**

Event and Description	Exposure	Peak Vessel Pressure (psig)
PRFO Base Case	BOC	[[
PRFO with 10% void coefficient increase	BOC	
PRFO Base Case	EOC	
PRFO with 10% void coefficient increase	EOC	]]

**Table 4.2b Suppression Pool Peak Temperature Void Coefficient Study**

Event and Description	Exposure	Peak Suppression Pool Temperature (°F)
PRFO Base Case	BOC	[[
PRFO with 10% void coefficient increase	BOC	
PRFO Base Case	EOC	
PRFO with 10% void coefficient increase	EOC	]]

[[

]]

**Figure 4.2a TRACG Power and Flow Response for MSIVC Event**

[[

**Figure 4.2b TRACG Pressure and Relief Valve Response for MSIVC Event**

]]

[[

]]

**Figure 4.2c MSIVC ATWS Peak Vessel Pressure Sensitivity to Individual Uncertainties  
(P<sub>case</sub>-P<sub>nominal</sub> [kPa])**

**NRC RAI 5.0 Void-Quality Correlation**

**NRC RAI 5-1**

Figure 2-2 of NEDC-33173P shows a plot of the typical void quality relation at high power/flow ratio. Evaluate the database supporting the void fraction correlation and plot the supporting validation measurement data on Figure 2-2. Identify the type of validation data on the plot, including the supporting tests types and the associated thermal-hydraulic conditions.

**GE Response**

The database for the Findlay Dix Correlation is described in the response to VY RAI 69 and further details are contained in the Reference 5-1 and in Attachment A to Reference 5-7.

As described in NEDE-21565, the 713 series of data were primarily used in the development of the correlation while other test series such as the 813 series were used for validation. The void-quality relation shown in Figure 2-2 is based on a calculation for a typical modern fuel bundle with a mass flux of 0.8 Mlb/ft<sup>2</sup>-hr. This mass flux corresponds to a Reynolds number of approximately 1.1E5 in the fully rodded region of the bundle. Comparing this calculation to the void fraction data used in the development of the Findlay-Dix correlation is not perfectly meaningful as the bundle geometry and test conditions are not identical. However, the Findlay-Dix correlation is primarily a function of the Reynolds number, quality and fluid properties, and data were obtained for a Reynolds number of approximately 1.1E5 for both the 713 and 813 series. These data have been added to Figure 5-1 and are shown below. This Figure allows a qualitative assessment of the correlation. Detailed quantitative comparisons of the Findlay-Dix correlation to the test data are contained in Reference 5-1.

There are no significant trend differences between the comparisons to the development and validation data.

[[

**Figure 5-1 Void Fraction versus Quality - Data and Calculation.** ]]

### **NRC RAI 5-2**

The void fraction calculation affects both the accuracy of the physics and the thermal-hydraulic calculations used to perform the design bases safety analyses. The objective is to confirm the void-quality correlation applicability ranges and assess any changes in the uncertainty of the correlation and its impact on the operating limit MCPR. Justify why the void quality correlation and the assumed uncertainty in the correlation are applicable for modern fuel (e.g., part-length rods, mixing vanes) and high energy operating conditions.

### **GE Response**

The void correlation is correlated as a function of Reynolds number, quality and fluid properties. Since the Reynolds number is a function of mass flux, hydraulic diameter and fluid properties, and the fluid properties are a function of pressure, the void correlation can also be correlated as a function of hydraulic diameter, mass flux, quality and pressure. The parameter ranges for the void fraction data used to develop the void fraction correlation are given in Table 5-1. It is seen from this table that the parameter ranges cover all GE fuel products and operating ranges.

- The range in hydraulic diameters in the data is [[ ]], which is much larger than the range of hydraulic diameters in the fuel designs. The hydraulic diameter in recent GE fuel products range from [[ ]] for 8X8 fuel to [[ ]] in the fully rodded region of 10X10 fuel. In the region above the part length rods, the hydraulic diameters range from [[ ]] for 10X10 fuel to [[ ]] for 9X9 fuel.
- The pressure range covers atmospheric pressure to twice normal operating pressure for a BWR.
- The mass flux in a BWR ranges from approximately 400 kg/m<sup>2</sup>-sec at natural circulation to approximately 1350 kg/m<sup>2</sup>-sec at rated core flow, and it is seen that the mass flux range in the data far exceeds this range.
- The void fraction range in the data is from [[ ]] for simple geometry data and from [[ ]] for rod bundle data, while a typical exit void fraction in BWR fuel ranges from [[ ]], for the average bundle, to approximately [[ ]] for a high power 10X10 fuel bundle such as GE14 under EPU conditions.

In summary, the database for the void correlation covers all fuel products including 10X10 fuel and all operating ranges including EPU conditions.

The GE void fraction correlation is described in detail in the approved Reference 5-3. The qualification documented in the approved Reference 5-4, where the void correlation was compared to [[ ]] data points from the most representative full-scale bundles, yielded a standard deviation of [[ ]] in the void fraction, while the qualification against the wider set of [[ ]] data points as documented in Reference 5-1, 5-5 and the approved Reference 5-7 yielded a standard deviation or [[ ]] in the void fraction (See Table 5-2).



A void fraction of  $[\quad]$ , a limiting estimate of a void fraction observed in a transient under MELLA+ and EPU conditions, is relatively high and typical of the conditions where boiling transition will occur in a BWR fuel bundle. Also, since the OLMCPR is determined such that boiling transition will not occur, it is highly unlikely that a void fraction of  $[\quad]$  will be exceeded (e.g., perhaps momentarily during a transient) by any significant amount. Some aspects of void fraction and bundle power warrant a brief discussion. For illustrative purposes, consider a one-dimensional, steady state energy balance for a BWR fuel channel. It can be shown that the flow quality is

$$x(z) = \frac{h_m - h_f}{h_{fg}} + \frac{1}{\dot{m}h_{fg}} \int_0^z \dot{q}'(\xi) d\xi,$$

where the definition of flow quality is given by

$$x = \frac{\dot{m}_g}{\dot{m}_f + \dot{m}_g}$$

The flow quality is a function of pressure (fluid properties), inlet flow rate and subcooling, and the heat addition rate. For the case of “z” equal to the exit elevation, the integral term essentially represents the channel power. The steady state exit quality is directly proportional to the integrated channel power.

Figure 5-1 shows a typical plot of the void-quality relationship for a flow typical of a high power/flow ratio fuel bundle for the entire range from zero to one. Recognizing the relationship between quality and channel power, the figure has two interesting points. First, the lower end of the quality range has a relatively steep slope. Small power changes in this lower quality range correspond to a relatively large void fraction change. This behavior has implications relative to the impact of the void coefficient. In general, the void coefficient becomes more negative with increasing (average) void fraction. However, the net power effect considering the void-quality behavior is that in general, core power response is more strongly influenced by regions of the core with lower void fraction. In other words, the quantity  $\Delta\alpha \square \left(\frac{\partial\alpha}{\partial P}\right) \Delta P$  (P is power) tends

to be larger at low void fraction, so that the feedback  $\frac{\Delta k}{k} \square \frac{1}{k} \left(\frac{\partial k}{\partial \alpha}\right) \Delta\alpha$  tends to be larger.

Second, the higher quality (or power range) is relatively flat with respect to void fraction. Changes in power at high power result in relatively small void fraction changes. Also, in terms of core power response, net void feedback tends to be milder at higher void fractions.

It should be recognized that a BWR fuel bundle is designed and operated such that boiling transition will not occur during steady-state or abnormal operational occurrences, and, therefore, high void fractions, i.e., higher than  $[\quad]$ , will not occur. Figure 5-1 illustrates this point, noting that less than half of the quality range ( $X < 0.5$ ) covers up to 90% void fraction. A significant power increase (or a factor of 2 change in quality) is required to drive the void fraction from 90 to 100%. It would require a bundle power of approximately  $[\quad]$  for a bundle at rated flow to reach a void fraction of  $[\quad]$ , while in reality a high power fuel bundle operates at approximately  $[\quad]$ .

For high void fractions, the void quality correlation is based on sound physical principles, and accurately extrapolates the measured data to a void fraction of 1.0. Using the Zuber-Findlay expression for two-phase flow, the void fraction  $\alpha$  can be expressed as

$$\alpha = \frac{j_g}{C_0 j + v_{gj}}$$

Where:

$C_0$	=	distribution parameter
$v_{gj}$	=	drift velocity
$j_g$	=	volumetric flux of steam vapor
$j$	=	volumetric flux of the mixture

The drift velocity is the difference in velocity between the vapor and the mixture volumetric flux. Generally the vapor phase velocity is greater because of buoyant forces. At high quality, the annular flow regime predominates. In the annular flow regime the liquid phase surrounds the fuel rods and channel. Locally  $v_g = j + v_{gj}$ . When substituting  $j = \alpha v_g + (1 - \alpha)v_\ell$  into this equation one get  $v_{gj} = (1 - \alpha)v_R$ , where  $v_R$  is the local relative velocity. From this expression, it follows that  $\overline{v_{gj}}$  must approach 0.0 at the limit of  $\alpha = 1.0$ . It can similarly be shown that  $C_0$  must approach 1.0 at the limit of  $\alpha = 1.0$ . In the GE void correlation, the drift velocity is characterized as:

$$\overline{v_{gj}} \propto (1 - \alpha)$$

This characterization is applied over the entire annular flow regime, or for void fractions greater than about 0.7. For high void fractions and small values of  $\overline{v_{gj}}$ , the void fraction is dominated by the ratio of vapor mass flux to total mass flux, determined by a simple mass and energy balance for each node. The outstanding agreement over the entire range shown in the qualification [5-1] and illustrated in the response to RAI 5-1 validates this simple model for the drift flux. An extrapolation based on this model to void fractions all the way from 0.98 (the upper end of the data base) to pure steam flow is therefore justified. In summary, the GE void correlation is based on test data and covers a broad range of conditions. The correlation supports the full range of conditions expected during BWR operation, including CPPU, EPU and MELLLA+ conditions.

The part length rod (PLR) is the major new feature in current fuel products. The impact of PLRs has been investigated for a 4X4 bundle for a pressure of 1 MPa and more recently for an 8X8 bundle at rated BWR pressure of 7.2 MPa [5-7]. A small increase, approximately [[ ]], was observed in void fraction downstream of the PLRs compared to the case with no PLR (See Figure 5-2) for the low-pressure 4X4 data. The recent more representative 8X8 data taken at normal operating pressure shows a small increase, on the order of [[

]].

The void correlation has been implemented into the GE design codes such as PANACEA/ODYN/ISCOR/TASC and the correct implementation of the void correlation has been tested by functional testing. Therefore, the qualification of the void correlation applies for all design codes except TRACG. TRACG [5-6] has been separately compared to a set of the same data discussed above and yielded a standard deviation of [[            ]] in the void fraction.

**Table 5-1 Void Fraction Correlation Database.**

Data Source	Geometry	Hydraulic Diameter (m)	Pressure (MPa)	Mass Flux (kg/m <sup>2</sup> -sec)	Inlet subcooling (K)	Exit quality (Max.)	Max void fraction
Simple Geometry	Tube or Annulus	[[					
CISE	[[						
ASEA-513							
GE							
ASEA-713							
ASEA-813	]]						]]

**Table 5-2 Comparison Between Void Correlation and Database (Taken from References 5-5 and 5-7)**

Data Source	Data Points (N)	Average Error $\overline{\Delta\alpha} = \overline{\alpha_m - \alpha_c}$	Standard Deviation $\sigma_{\Delta\alpha}$
CISE	[[ ]]	[[ ]]	[[ ]]
GE	[ ]]	[[ ]]	[[ ]]
ASEA-713	[[ ]]	[[ ]]	[[ ]]
Subtotal	[[ ]]	[[ ]]	[[ ]]
ASEA-813	[[ ]]	[[ ]]	[[ ]]
ASEA-513	[[ ]]	[[ ]]	[[ ]]
TOTAL	[[ ]]	[[ ]]	[[ ]]

[[

**Figure 5-2 4X4 Void fraction Data – Sensitivity to PLR**

]]

[[

**Figure 5-3 8x8 Void Fraction Data – Sensitivity to PLR for Low Flow**

]]

[[

**Figure 5-4 8x8 Void Fraction Data Sensitivity to PLR for High Flow**

]]

**NRC RAI 5-3**

The LTR references relevant plots and information provided in the Vermont Yankee (VY) RAIs. Include the relevant discussion and plots in this LTR.

**GE Response**

Please see the Response to RAI 6.1, which was issued in GE Letter MFN 06-195, dated June 23, 2006.



**NRC RAI 5-4**

Provide a summary of how the void-quality correlation uncertainties are accounted for in the model uncertainties for the codes and the analytical methodologies used to perform the licensing bases safety analyses

**GE Response**

The impact of Void Fraction Uncertainties is summarized below for each of the major methods categories:

SLMCPR The MCPR Safety Limit is governed by uncertainties in quantities that influence the boiling transition process, namely thermal hydraulic and power distribution conditions. The SLMCPR is based on uncertainties in the Core Monitoring System. The monitoring system is based on a best estimate calculation with PANACEA and is used to monitor that the design limits, such as the OLMCPR, are not exceeded. The PANACEA power distribution uncertainties are based on a coupled nuclear thermal hydraulic evaluation. The nodal and radial power distribution uncertainties are determined directly from comparisons of PANACEA and TIP response from operating plants. Gamma scan data are also used to establish the power distribution accuracy directly. The result is a power distribution uncertainty that includes any void fraction uncertainty together with nuclear model uncertainties. The SLMCPR also includes uncertainties in the R-factor, which is a function of local pin power peaking. The sensitivity of R-factor to channel void fraction is discussed in detail in the response to RAIs 31 and 31-1 of Reference 5-11. This response (see RAIs 31 and 31-1 in MFN 06-211) shows a net OLMCPR change of less than 1% for a change of 20% in bundle void fraction. Thermal hydraulic conditions such as pressure drop can also be influenced by void fraction. The pressure drop correlations are developed under prototypical conditions along with the critical power correlation. Since the void fraction is included in the comparisons with pressure drop data, the void fraction effect is included in the pressure drop uncertainties. The SLMCPR model includes thermal hydraulic model uncertainties as described in Reference 5-7.

OLMCPR The effect of void fraction uncertainty on the transient  $\Delta$ CPR and the OLMCPR is included in the transient model uncertainty. The model uncertainty is traditionally determined from comparisons plant transient tests and verified by model perturbations. The details of the transient model uncertainties are documented in References 5-4, 5-5 and 5-6. The TRACG uncertainty includes an explicit void coefficient component in its statistical uncertainty model.

Fuel Rod thermal Mechanical (LHGR) Similar to the SLMCPR, the majority of the power distribution uncertainty is determined by direct power distribution measurements and therefore includes void fraction uncertainties. However the local pin peaking uncertainty is determined from model calculations and therefore has a void coefficient component. The peak pin power in a typical fuel bundle is a weak function of void fraction, changing about 3% over a span from 0% void to 40% void and another 4% from 40% void to 70% void. Assuming a 3% uncertainty in void fraction at any one axial height, the void fraction contributes about 0.3% to the overall peak pin power uncertainty. This void uncertainty, when statistically combined with the other pin peaking uncertainties results in a negligibly small component of the overall peaking uncertainty.

Cold Shutdown Margin (SDM) The cold shutdown model does not directly depend on the void fraction model since it is analyzed at 0% voids. It indirectly depends on the void model because the exposure distribution depends on the void model used while the reactor is at power. Like the power distribution uncertainty, the shutdown margin uncertainty is determined directly by measurement and therefore includes any void model uncertainty in the PANACEA 3-D simulator.

LOCA Related Nodal Power Limits Nodal power limits and associated uncertainties are based on direct nodal power measurements taken from TIP and LPRM responses, which include any void distribution effects. The uncertainties are included in the determination of the upper bound peak cladding temperature (PCT). The conservatism of the licensing basis PCT is guaranteed by the conservative inputs required by 10 CFR 50 Appendix K. The licensing basis PCT has been shown to be more conservative than the upper bound PCT [Reference 5-10].

Stability In addition to other transient and steady state uncertainties discussed above, the void fraction influences the total steam volume and feedback under low flow conditions. The void fraction uncertainties are reflected in the overall transient model uncertainties, similar to those employed for determination of the OLMCPR uncertainties. For plants using an exclusion region, the void fraction uncertainty is included through the use of conservative inputs and the 0.2 margin that is applied to the decay ratio. For plants using a detect and suppress methodology, the set points are determined such the SLMCPR will not be violated, and the void fraction uncertainty are covered by the power distribution uncertainties included in the SLMCPR determination.

## References

- 5-1 J. A. Findlay and G. E. Dix, BWR Void Fraction and Data, NEDE-21565, January 1977. General Electric Proprietary Information.
- 5-2 N. Zuber and J. A. Findlay, Average Volumetric Concentration in Two-Phase Flow Systems, ASME J. Heat Transfer, November 1965.
- 5-3 TASC-03A, A Computer Program for Transient Analysis of a Single Channel, NEDC-32084P-A, Revision 2, July 2002.
- 5-4 Letter, J. S. Charnley (GE) to H. N. Berkow (NRC), Revised Supplementary Information Regarding Amendment 11 to GE Licensing Topical Report NEDE-24011-P-A, MFN-003-086, January 16, 1986.
- 5-5 Letter, G. Stramback (GE) to NRC, Completion of Responses to MELLLA Plus AOO RAIs (TAC No. MB6157), MFN 04-026, March 4, 2004.
- 5-6 TRACG Application for Anticipated Operational Occurrences (AOO) transient Analyses, NEDE-32906P-A, Revision 1, April 2003.
- 5-7 Methodology and Uncertainties for Safety Limit MCPR Evaluations, NEDC-32601P-A, August 1999.

NEDO-33173-A, Revision 1  
Non-Proprietary Information

- 5-8 Power Distribution Uncertainties for Safety Limit MCPR Evaluation, NEDC-32694P-A, August 1999.
- 5-9 Applicability of GE Methods to Expanded Operating Domain, NEDC-33173P, February 2006.
- 5-10 GESTR-LOCA and SAFER Models for Evaluation of Loss-of-Coolant Accident, Volume III, Supplement 1, Additional Information for Upper Bound PCT Calculation, NEDE-23785P-A, Supplement 1, Revision 1, March 2002.
- 5-11 MFN-05-031, Letter to Louis Quintana, “REQUEST FOR ADDITIONAL INFORMATION – LICENSING TOPICAL REPORT NEDC-33006P, REVISION 1 “GENERAL ELECTRIC BOILING WATER REACTOR MAXIMUM EXTENDED LOAD LINE LIMIT ANALYSIS PLUS (MELLA+)” (TAC NO. MB6157)” April 11, 2005

**NRC RAI 6.0 Process**

**GE Response**

The changes to the LTR proposed by the RAI 6 responses are reflected in Enclosure 3 [Changes incorporated into NEDO-33173-A herein] and shown by revisions bars. The LTR will be formally issued, reflecting these and other required changes, approximately 2 weeks after the closure of the methods related RAIs supporting the review of Tennessee's Valley Authority's license change request for an extended power uprate.

**NRC RAI 6.1**

The LTR summarizes the content of the VY RAIs. However, this eliminates relevant figures and evaluations. For the void fraction correlation, void reactivity coefficient, and Option 1D include the relevant figures and discussions so that the supporting information is integrated in this LTR.

**GE Response**

The relevant figures, tables, and discussion from the VY RAIs have been incorporated into the body of the LTR. Appropriate references have also been included.

**NRC RAI 6.2**

Appendix A contains many RAIs not related to the methods review. All EPU SRXB-A RAIs were cited in Appendix A. Many of these RAIs, did not address nor are they relevant to the Methods review. This array of RAIs hampers efficient use of the reference material. Delete the SRXB-A RAIs that were not part of the methods review.

**GE Response**

The table in Appendix A will be reduced to include only the VY RAIs that are related to the methods review.

In addition, because the VY RAIs in Appendix B are grouped and formatted according to the VY Supplemental submittals, the removal of individual RAIs would result in the section being fragmented and difficult to follow. GE believes that Appendix B is no longer an essential part of the Interim Methods LTR and, therefore, proposes its removal.

See Revision 1 of NEDC-33173P for the revised Appendix A.

**NRC RAI 6.3**

Vermont Yankee SRXB-A Figures 6-1 thru 6-6 show the maximum bundle operating conditions of high density and EPU plants. Each plant specific application should, include the plant-specific data in the plots containing the high density and EPU plants maximum bundle operating conditions (Attachment 3, BVY 05-024)

- (a) Therefore, include in the EPU applications the following bundle operating conditions with exposure in the EPU maximum bundle operating condition plots:
  - maximum bundle power,
  - maximum bundle power/flow ratio,
  - exit void fraction of maximum power bundle,
  - maximum channel exit void fraction,
  - peak linear heat generation rate and
  - peak end-of-cycle nodal exposure
  
- (b) Provide quarter core map (assuming core symmetry) showing the bundle operating linear heat generation (MLHGR) and the minimum critical power ratio (MCPR) for beginning-of-cycle (BOC), middle-of-cycle (MOC) and end-of-cycle (EOC). Similarly, show the associated bundle powers.

**GE Response**

Revision 1 of NEDC-33173P-A, Section 4.3 was modified, to specify that the requested core operating information be included with plant specific applications of the Methods LTR.

**NRC RAI 31, R-Factor**

The R-factor methodology is described in NEDC-32505P, “An R-Factor Calculation Method for GE11, GE12, and GE13 Fuel,” dated July 1999. Evaluate the R-factor methodology to ensure that the key assumptions in the R-factor methodology remain applicable to the EPU/MELLLA+ conditions. Also evaluate the pin peaking factors used in the R-factor calculation for operation at high-void conditions. Amend the topical report accordingly, and amend the RAI responses for operation at the EPU/MELLLA+ conditions. RAIs 31-1 through 31-4 pertain to several features of the R-factor calculation, specifically the effects of the axial power shape, peaking distribution, exposure, and void fraction on the pin power peaking factor.

**GE Response**

The R-factor is an input to the GEXL correlations which accounts for the effects of the fuel rod power distributions and the fuel assembly and channel geometry on the fuel assembly critical power. [[





NEDO-33173-A, Revision 1  
Non-Proprietary Information

]]

References

- 31-1 NEDC-32851P Rev.2,"GEXL14 Correlation for GE14 Fuel", Sept. 2001.
- 31-2 NEDC-32601P, "Methodology and Uncertainties for Safety Limit MCPR Evaluations",Dec.1996.



[[

]]

||

||

[[

]]

**NRC RAI 31-1**

RAI 5 (Attachment B) and RAI 4 (Attachment D) of NEDC-32505P-A address the methods used to calculate the R-factor in terms of the axial power shape, peaking factors, local exposure, and void fraction. Provide updated responses to these RAIs. Explain the statement that the lattice peaking factors are weak functions of exposure and void and the relative rod power peaking factors  $r_i$  are weak functions of the axial power shape,  $P(z)$ .

**GE Response**

Response to Part 1

The R-factor calculation method for GE14 is essentially identical as the method described in NEDC-32050P-A for the GE12 product. The updated weighting parameters for GE14 have been provided in Reference 31-1. The change in the length of the PLRs is the only significant change in the generation of GE14 R-factors relative to the GE11, GE12, and GE13 process. The R-factor methodology for GE14 is given in Section 8 of Reference 31-1. The axial weighting shapes are defined and examples of the R-factor weighting process are given in Sections 8.2 through 8.5.

Response to Part 2

In NEDC-32505P-A, [[

]].

**OTHER RAIs**

**MFN 04-020 Response to MELLA Plus AOO RAIs**

See MFN 04-026 for updated responses.



**MFN 04-033 TRACG Analyses for MELLLA Plus AOO RAI 22**

The response to RAI 22 included a compact disk containing TRACG analyses files. Subsequent conversations with the NRC indicates that additional analyses are required. The requested information is extensive, was provided on a compact disk to the NRC, and is not repeated herein..

**MFN 04-048 MELLLA+ RAI 6**

MFN 04-048 transmits presentation information requested during an NRC review at the NRC offices on March 17, 2004. Mr. Frank Akstulewicz of the NRC staff requested that GNF-A provide this information to facilitate the staff's review of Licensing Topical Report (LTR) NEDC-33006P, Revision 1, *General Electric Boiling Water Reactor Maximum Extended Load Line Limit Analysis Plus*. Specifically, this presentation was in support of GEH's response to RAI 6 regarding NEDC-33006P.

Resulting from the discussions on March 17, some additional clarification has been added to the presentation. This clarification is intended both to document the discussion and to provide the additional requested information. Some reordering of the material from the original presentation was necessary and the changes are as follows:

- Page 43 provides a description of the valid 10x10 cycles for the TIP uncertainty as discussed in FLN-2001-004.
- Page 44 provides a summary, with description of the figure shown on page 42 of the original material. The figure is now on page 45. Conclusions also have been added.
- Page 48 explains the planned GNF actions relative to data comparisons between actual operation of the first MELLLA+ cycle and the predicted behavior.
- Also, minor additional explanatory detail was added to the SLMCPR evaluation process flowchart presented in Pages 7-23.

The presentation as transmitted in MFN 04-048 is provided in Enclosure A herein.

**MFN 04-060 Revised Response to MELLLA Plus ATWS RAIs**  
See updated RAI 25 in MFN 04-026.

**MFN 04-061 - NRC RAI AOO 6**

By MFN 04-026, GEH provided responses to NRC requests for additional information (RAI) to support review of the Licensing Topical Report (LTR) NEDC-33006P, Revision 1, *General Electric Boiling Water Reactor Maximum Extended Load Line Limit Analysis Plus*. Susequently, the NRC requested lattice information to support confirmatory calculations. The requested information is extensive, was provided on a compact disk to the NRC and is not repeated herein.

**MFN 04-067 MELLLA Plus AOO 6, TGBLA Lattice Physics Data**

By MFN 04-061, GEH provided the NRC with lattice data to support confirmatory calculations. During an audit, the NRC requested GEH to provide additional TGBLA lattice physics data information.

The requested information is extensive, was provided on a compact disk to the NRC, and is not repeated herein.

**MFN 04-074 Off-Rated Conditions - MELLLA+ RAI AOO 22**

See the response to RAI 22 in MFN 04-026.

**MFN 05-022 NRC RAI 2-6, Error Acceptance Criteria**

For each fuel design change, GNF-A assesses the sensitivity of the lattice physics parameters. Provide a discussion on GNF-A’s current method for establishing what is an acceptable error criteria for the lattice physics parameters. Explain which lattice parameters are these error acceptable criteria defined. For the current review, define the acceptance criteria associated with the cross sections and lattice parameters and resolve or justify the high errors.

**GE Response**

As new fuel designs and plant operating strategies evolve, it is highly desirable that the nuclear method systems provide a response that is consistent with past performance in terms of trends, biases, and uncertainties. In keeping with this desire, a “Range of Usage” assessment must be done for each nuclear method system (TGBLA, PANACEA, etc.). Maintaining consistent trends, biases, and uncertainties enables a “seamless” use of the nuclear methods in the currently allowed and the extended usage range.

Assessment of the viability of the nuclear parameters in the GE lattice physics methods is performed with a series of reviews. Reviews are conducted to assess the ability of the TGBLA nuclear geometric models to adequately represent the requested usage range extension. Reviews are conducted to assess the adequacy of any approximations that are required to accommodate the requested usage range extension. For the lattice physics system (TGBLA), comparisons to MCNP results are used to establish that the response of TGBLA in the extended usage range is consistent with responses observed in the previously defined usage range. Consistent trends and biases in the lattice physics results between the defined usage range and the extended usage range provide the basis for the allowance of the extended usage range.

The parameters in the lattice physics assessment are the lattice k-infinity and the rod-wise fission densities. These parameters are used as assessment parameters because of their global characteristics and/or due to their potential impact on the safety limit evaluations.

The definition of k-infinity in 3 groups is as follows

$$k_{\infty} = \frac{\left( \nu_1 \Sigma_{f_1} + \nu_2 \Sigma_{f_2} \frac{\phi_2}{\phi_1} + \nu_3 \Sigma_{f_3} \frac{\phi_3}{\phi_1} \right)}{\left( \Sigma_{a_1} + \Sigma_{s_{12}} + \Sigma_{s_{13}} \right)}$$

where,

- $\nu_g$  = number of neutrons per fission in energy group g
- $\Sigma_{fg}$  = macroscopic fission cross section in energy group g
- $\phi_g$  = neutron flux in energy group g
- $\Sigma_{a1}$  = macroscopic absorption cross section in energy group 1
- $\Sigma_{s1g}$  = macroscopic slowing down cross section from energy group 1 to g

By use of k-infinity as an assessment parameter, a review of all significant cross sections and fluxes may be made.

The state-points analyzed for the lattice physics usage range assessment are generally beginning of life and selected state-points with exposed fuel isotopic concentrations. The isotopic content used by MCNP for exposed conditions is [[ ]]. Both hot and cold conditions are included as well as controlled and borated conditions.

To extend the usage range, acceptance criteria are defined to provide an initial review of the system performance. A failure to meet the acceptance criteria dictates that a more detailed review should be performed. The lattice k-infinity including a bias is expected to be within [[ ]] for all analyzed state points. A bias trend is expected for gadolinium bearing lattices of [[ ]] at beginning of life increasing to [[ ]] prior to the point of maximum reactivity and returning to [[ ]] for exposures greater than the point of maximum reactivity. The nominal bias trend for non-gadolinium lattices is [[ ]].

The rod-wise fission densities are defined as

$$F_r = V_r \sum_{g=1}^G \sum_i \Sigma_{f_r}^{g,i} \phi_r^g$$

where

$V_r$  is the volume of fuel rod r

$\Sigma_{f_r}^{g,i}$  is the macroscopic fission cross section for group g, isotope i and rod r

$\phi_r^g$  is the flux for group g and rod r

The normalized array for the rod-wise fission density is generated as follows:

$$\tilde{F}_r = F_r / \left( \frac{1}{N} \sum_{r=1}^N F_r \right)$$

The use of the fission density parameter allows an assessment of the uncertainty of the fuel rod fluxes. This provides an assurance that the fluxes used for fuel rod isotopic depletion are reasonable and that the uncertainty of the fuel rod flux distribution is consistent with expectations.

The state-points used for the fission density assessment are the same as the state-points used for the reactivity assessment except that only the hot uncontrolled conditions are utilized in the global weighted average assessment. The fission density uncertainty assessment is based on an average of the hot uncontrolled 0, 40, and 70% void lattice pin-wise fission density results obtained from the MCNP tallies and compared to the TGBLA results. The Hot Uncontrolled 0, 40, and 70% void state-point results are compared and the RMS of the resulting rod-wise differences is obtained. The fission density RMS comparison for individual lattices is



anticipated to be less than [[ ]]. As in the k-infinity assessment, exceeding the fission density assessment criteria indicates a need for more detailed study.

Ultimately for safety limit analysis, these comparisons are performed for a representative number of lattice designs over the range of usage for TGBLA and a global weighted average over the range of 0, 40, and 70% voids is obtained and compared to the [[ ]] value used for current fuel designs in subsequent safety limit analysis (see for instance NEDE-32601P-A). This value of [[ ]] is deemed to be the minimum approved value but is subject to increase as fuel designs and other considerations evolve to maintain the desired level of conservatism in the safety limit analysis.

Closure of the “range of usage extension” study can potentially result in several different conclusions. The conclusions can be as follows:

1. The “range of usage” request is generically allowed and the stated usage range for the method is modified to include the requested usage extension.
2. The “range of usage” request is not generically allowed and system modification must be made before generic allowance is granted. The system usage remains restricted until the required modifications are completed and all required reviews are completed.
3. The “range of usage” request is not generically allowed but specific project allowance is given for use. Any future use of the system must again request the “range of usage extension” review.
4. The “range of usage” request is not allowed and a conclusion is reached that system modifications cannot be made to support this request at this time.

**MFN 05-022 NRC RAI 3-1**

In the conclusion provided in Section 2.1.2 it is stated that [[  
]] and in Section 2.1.4 it is stated  
that [[  
]]

- a Provide an explanation of the reasons for these difficulties with TGBLA.
- b New assemblies have a large number of Gd pins and therefore any inaccuracies in the Gd depletion are likely to have a larger impact on the results obtained for the higher Gd-loaded bundles. Since the previous benchmarking data was based on lower Gd loading, can these benchmarking results be applied to the current more heavily Gd loaded assemblies? Provide justification for the use of TGBLA/PANAC under the hard spectral conditions typical of the EPU/MELLLA+ operation for cores loaded with heavily Gd loaded assemblies.

**GE Response**

Response 3-1a:

The document in which this statement originally appeared is an “internal review report” of the status of PANACEA and TGBLA in support of the MELLLA+ plant operation. The Methods Enclosure included this statement directly from the design review documentation. The internal document expresses the individual opinions and concerns of all parties represented in the design review. The statement in Section 2.1.2 is a statement of opinion from the design review. The statement should read "[[  
]]”.

The statement in Section 2.1.4 of the enclosure is also a statement of opinion from members of the review team, and it is correct in that TGBLA [[  
]] for Gd pellets. The other isotopes in the Gd pellets (e.g., Uranium, Plutonium, fission products, etc.) are treated [[  
]], the same as is done in the non-gadolinia bearing pellets. However, the inference that this leads to significant deficiencies is not valid. The effect of [[  
]]

]] generated lattice average cross sections.

However, since the use of TGBLA at 90% void fractions is not required in the standard production process for generating lattice nuclear constants, usage of TGBLA has not been validated for void fractions above 70%. In response to the request for additional analyses of the PANACEA cross section fitting interpolation/extrapolation process, a “usage range extension” study has been performed to allow examination of 90% void depletion uncertainties. [[

As the impact on the 0, 40, and 70% void data is minimal, this weakness does not significantly impact the fitting errors for extrapolation to void fractions higher than 70%. ]]

Response 3-1a:

The results presented in Section 2 of the Methods Enclosure include a lattice with [ ] gadolinium bearing rods [ ]. This design represents one of the highest number of gadolinium bearing rod designs in current use. This design is also for the upper zone of the fuel bundle, which generally has the highest ratio of gadolinium atoms to uranium atoms due to the presence of vanished rods (regions over part length fuel rods). This type of design generally produces the highest expected sensitivity to gadolinium depletion and as such is representative of a worst case study for depletion methods.

The plant tracking data obtained over numerous cycles of operation has not indicated any correlation with increasing gadolinium concentration or number of gadolinium bearing rods. The response to RAI 25 contains data to confirm this conclusion.

As gadolinium concentrations have increased, “range of usage” studies have been performed to assess the capability of TGBLA to perform under these conditions. These studies have currently concluded that TGBLA is capable of modeling gadolinium concentrations [ ]. Studies to extend the range of TGBLA to greater than [ ] have not been performed and; therefore, the current system is limited to usage of [ ] pellet concentrations.

**MFN 05-022 NRC RAI 21-2, SLMCPR:**

21-2 Explain the differences between the nodal TIP RMS, bundle TIP RMS, the axial TIP RMS, and the nodal RMS.

**GE Response**

Three-dimensional power shape information as recorded by the TIP instrument readings can be compared to calculated instrument readings from the simulator to determine its ability to calculate power distributions. Strings of either thermal neutron sensitive detectors (often referred to as thermal TIPs) or gamma-ray sensitive detectors (referred to as gamma TIPs) may be used to assess the normalized axial power shape along almost the entire length of the bundles within a four-bundle cell. The integrated signals may be combined to evaluate the radial power distribution within the core.

The 3D simulator models the response of the instrument to the appropriate particle species at the detector location to produce a simulated signal. For TIP comparisons, this simulated detector response is compared to the relative strength of the measured signal. TIP distributions take time to accumulate and hence are obtained periodically throughout an operating cycle. The most common interval between TIP measurements is several weeks. During the time between TIP measurements the Local Power Range Monitors are used to monitor the core power distribution. For a given TIP string, the measurement is a response to the integrated influence of the surrounding bundles. This signal strength from the fuel is primarily due to the cumulative power production of fuel rods in the four bundles surrounding the string.

The process for the TIP comparison basis is described below. The definitions of the quantities used in the calculations are:

$$P(k, j) = PCTIP(k, j)$$

$$C(k, j) = CALTIP(k, j)$$

$$I(j) = IFTIP(j)$$

$$S_j \Leftarrow j \in (I(j) = 0)$$

$$J = \# \text{ of elements in } S_j$$

$$K = K_{up} - K_{low} + 1$$

$K_{low}, K_{up}$  = Node limits for axial comparison, usually 2 and 23

where

$PCTIP(k, j)$  = the measured six inch average TIP reading in axial segment k of TIP string j

$CALTIP(k, j)$  = the calculated six inch average TIP reading in axial segment k of TIP string j

$IFTIP(j)$  = an indicator of when TIP readings are failed by the process computer, manually failed by the operator, or rejected by the core monitor for statistically poor performance

The measured and calculated TIP strings are normalized, respectively, as follows:

$$\sum_{j \in S_j} \sum_{k=Klow}^{Kup} P(k, j) = J \cdot K$$

$$\sum_{j \in S_j} \sum_{k=Klow}^{Kup} C(k, j) = J \cdot K$$

Nodal Statistic

The nodal RMS assesses all the predicted to measured instrument signals (for valid strings). Encompassing both radial peaking and axial structure, it is an global indicator of power shape efficacy across the core for a given statepoint.

$$R_{nod} = \sqrt{\frac{\sum_{j \in S_j} \sum_{k=Klow}^{Kup} (P(k, j) - C(k, j))^2}{J \cdot K}}$$

The nodal statistic may also be reported for a given string.

$$\Delta_{j,nod} = \sqrt{\frac{\sum_{k=Klow}^{Kup} (P(k, j) - C(k, j))^2}{K}}$$

With this form, the nodal RMS becomes the following form.

$$R_{nod} = \sqrt{\frac{\sum_{j \in S_j} \Delta_{j,nod}^2}{J}}$$

Radial Statistic

The radial (or bundle) RMS assesses the string average predicted to measured instrument signals. In this way, the ability to predict the four bundle average peaking as applied in the SLMCPR process is measured.

$$R_{rad} = \sqrt{\frac{\sum_{j \in S_j} \left( \left( \frac{\sum_{k=Klow}^{Kup} P(k, j)}{K} \right) - \left( \frac{\sum_{k=Klow}^{Kup} C(k, j)}{K} \right) \right)^2}{J}}$$

The bundle statistic may be reported for a given string and may be positive or negative.

$$\Delta_{j,rad} = \left( \frac{\sum_{k=Klow}^{Kup} C(k,j)}{K} \right) - \left( \frac{\sum_{k=Klow}^{Kup} P(k,j)}{K} \right)$$

With this form, the bundle RMS may be written in the following form.

$$R_{rad} = \sqrt{\frac{\sum_{j \in S_j} (\Delta_{j,rad})^2}{J}}$$

### Axial Statistic

The axial RMS assesses only the axial shape component of the predicted to measured instrument signals. The radial peaking between strings is normalized out for this measurement. Thus, it is a good indicator of the axial power shape performance for the core state.

$$R_{axial} = \sqrt{\frac{\sum_{k=Klow}^{Kup} \left( \left( \frac{\sum_{j \in S_j} P(k,j)}{J} \right) - \left( \frac{\sum_{j \in S_j} C(k,j)}{J} \right) \right)^2}{K}}$$

The axial statistic may be reported for a given string if the string is first normalized unto itself.

$$P'(k,j) = \frac{\sum_{k=Klow}^{Kup} P(k,j)}{K}$$

$$C'(k,j) = \frac{\sum_{k=Klow}^{Kup} C(k,j)}{K}$$

$$\Delta_{j,axial} = \sqrt{\frac{\sum_{k=Klow}^{Kup} (P'(k,j) - C'(k,j))^2}{K}}$$

Combining Multiple TIP Sets

For collapsing the uncertainties for two different plants or multiple TIP sets from a single plant, a weighted averaging method is used. This method is defined in NEDC-32694P-A. If there are a total of N TIP comparison sets, and the total number of TIP strings in each plant is  $M_i$ , the method of combining the multiple TIP sets to obtain a weighted uncertainty  $R_{weighted}$  is:

$$R_{weighted} = \sqrt{\frac{\sum_{i=1}^N (M_i - 1)R_i^2}{(\sum_{i=1}^N M_i - N)}}$$

**MFN 05-022 NRC RAI 28, Gamma Scan Benchmarking**

The standard industry practice is to do bundlewise and pinwise gamma scans for new fuel designs to benchmark the analytical methods used to predict the bundle and pin power peaking and distribution. GNF-A's SLMCPR methodology requires that the power allocation uncertainty,  $\sigma$  PAL<sub>j</sub>, for each bundle in a four-bundle core cell be determined through gamma scans.

- 28-1 Provide statistically significant gamma scan data to benchmark the bundle and pin power distribution. The objective is evaluate the accuracy of the TGBLA and PANAC codes in predicting the bundle and pin peaking and power distribution for depletion at high-void conditions. Select bundles that are once burned, twice burned, and, if necessary, thrice burned. Gamma scans should also be used to benchmark the codes' accuracy in predicting the axial power distribution and to determine whether GNF-A's code systems need any changes for depletion at high-void conditions. Your gamma scan data should therefore include high-powered bundles that have high Gd loadings and operate at high-void conditions. Most important, the gamma scan data and the corresponding calculational analysis should provide additional validation for the statement in Section 2.1.4 of the methods enclosure (see RAI 3-1).
- 28-2 If gamma scan data is not available, make a commitment to do the gamma scans. Your commitment should include an action plan and a timetable for doing the gamma scans for the GE14 fuel design. Also describe your proposed future approach you incorporate new fuel designs into your licensing methodology. The proposed approach should be similar to the approach used for core follow benchmarking. Interim actions are covered in RAIs 30-7, 30-8, and 35 below.

**GE Response [Response to 28-2 updated to reflect MFN 06-434, which superseded the update of MFNs 05-022 and 05-053]**

**Background**

Gamma scanning is a non-destructive method to determine the relative fission product inventory in nuclear fuel. Gamma scan programs vary by specification of the physical locality of the measurement, time of performing the measurement, measuring time, and number of measurements.

For example, the technique for measurements of "power" employs measurement of the 1.6 Mev gamma which accompanies beta decay of <sup>140</sup>La with a half-life of 40.2 hours. <sup>140</sup>La accumulates in fuel mainly from the beta decay of the fission product <sup>140</sup>Ba which has a half-life of 12.8 days. After about 10 days or so following reactor shutdown, <sup>140</sup>La is proportional to the <sup>140</sup>Ba atom density and decays with the <sup>140</sup>Ba half-life. The <sup>140</sup>Ba distribution in fuel is characteristic of the fission distribution or integrated power history over the last 5 half-lives or so (approximately 60 days) of reactor operation. Thus the scan results can be used to determine "recent" core power distribution. The 12.8 day half life of <sup>140</sup>Ba makes it imperative that the Gamma Scan data be collected as soon as possible after core shutdown, and has the possibility of interrupting refueling operations. A follow-on comparison of the measured <sup>140</sup>Ba distribution with predictions using the analytical tools of GE (i.e. TGBLA/PANACEA) constitute a benchmark of methods which may



be used for methods licensing or determination of other licensing uncertainties. Additional target spectral lines from other isotopes may be used for determination of plenum fission gas ( $^{85}\text{Kr}$ ) or fuel exposure ( $^{137}\text{Cs}/^{144}\text{Pr}$ ).

The procedure of comparing GE steady-state analytical methods to gamma scan measurements was last formally documented in Reference 28-1 (TGBLA/PANAC LTR). It was then used in Reference 28-2 (NEDC-32694P-A, Power Distribution Uncertainties) in support of the revised SLMCPR uncertainties (NEDC-32601P-A, Reference 28-3). Technically, gamma scans have only been used by GE to determine [[  
]]indicated on pages 3-2 and 3-4 of NEDC-32694P-A.

[[

]]

When the SER on the revised SLMCPR process was issued, subsequent discussions with the NRC clarified the requirements of the SER on the SLMCPR uncertainties as documented by letter in Reference 28-5. GE complied with the intent and direction of the SER for the GE14 product line as documented in 2001 through References 28-6, 28-7, and 28-8.

#### Response 28-1

GE has continued to use gamma scans for technical validation of its methods. The performance of steady-state core simulator predictions to high exposure have recently been validated. The comparison between PANAC10, PANAC11,  $^{137}\text{Cs}$  gamma scan, and more accurate  $^{148}\text{Nd}$  point measurements for a full length  $\text{UO}_2$  rod are shown in Figure 28-1. With peak exposures exceeding [[  
]], predicted pin exposures for both codes agree very well with both measurements while agreement between PANAC11 UPINEX (reconstructed pin exposures) and the sensitive  $^{148}\text{Nd}$  point measurements is extremely favorable. Figure 28-2 shows the excellent agreement for a part length rod approaching [[  
]]. The exposure prediction capability does not degrade for part length rods. Since exposure accumulation is just the integration of the power history, these measurements serve to validate the applicability of the TGBLA06/PANAC11 methodology to high burnup application as well as imply accurate power prediction throughout the life of the fuel bundle. This information partially satisfies Methods Audit RAI 24.

Response 28-2

GE intends to engage in an ongoing qualification program to confirm the continued applicability of the pin power and assembly power uncertainties and to confirm on a continuing basis the acceptability of power distribution predictions. Performing gamma scans requires a utility partner or partners who will allow GE access to their fuel during an outage. Outage durations and availability of appropriate bundles are some of the constraints in defining a desired schedule for gamma scans with a partner. The schedules and scope of future gamma scan data acquisitions will be established as opportunities are available and as is technically necessary.

In order to address NRC RAIs regarding NEDC-33173P, Methods LTR, GE is committed to provide the necessary data, including gamma scans data, to provide additional support for the existing technical validation of its methods based on Monte Carlo and plant monitoring data. Specifically, during a meeting with the NRC at GE's Wilmington offices in January 2005, GE stated that efforts were underway to develop a gamma scan system and to obtain utility partner(s) for a gamma scan program.

GE has completed the development of a gamma scan system and has successfully used the system to obtain additional scan data. GE has also obtained gamma scan data from an additional plant. A summary of the fuel types and scans for the new data are presented in Table 28-1.

A future revision of Methods LTR will document the analysis of the new gamma scan data and sufficient reanalysis of existing data currently summarized in NEDC-32694P-A. GE anticipates additional data will be obtained by December 2006 and a revision of NEDC-33173P would be issued by December 2007.

GE considers the available gamma scan data summarized in Table 28-1 as sufficient to provide the basis for the verification of GE's methods in expanded operating domains. GE anticipates that the revised Methods LTR will justify the use of GE's analytical methods for expanded operating domains, up to and including MELLLA+, without the use of the temporary adders currently included in the Methods LTR.

**Table 28-1 Active GE Gamma Scan Validation Programs**

FUEL	SCAN TYPE	LICENSED POWER LEVEL	SCOPE	BURNUP	PLANT
GE12 – 10x10 GE11 – 9x9 Other – 10x10	In-pool 4-bundle corner <sup>140</sup> Ba at multiple axial elevations	Stretch Power Uprate	50 bundles	15-40 GWd/STU (bundle average)	Cofrentes
GE14 – 10x10 GE12 – 10x10 Other – 10x10	In-pool 4-bundle corner <sup>140</sup> Ba at multiple axial elevations	Extended Power Uprate	50 bundles	15-40 GWd/STU (bundle average)	Cofrentes
GE14 – 10x10	Rod pin <sup>140</sup> Ba at multiple axial elevations	Stretch Power Uprate	~58 rods	21 GWd/STU (bundle average)	Fitzpatrick
GE14 – 10x10	Rod pin <sup>140</sup> Ba at multiple axial elevations	Stretch Power Uprate	~58 rods	38 GWd/STU (bundle average)	Fitzpatrick

[[

**Figure 28-1 Predicted versus measured exposure profiles for a full length UO<sub>2</sub> rod**

**Figure 28-2 Predicted versus measured exposure profile for a part length UO<sub>2</sub> rod**

]]

NEDO-33173-A, Revision 1  
Non-Proprietary Information

RAI 28 References

- 28-1 NEDE-30130-P-A, Steady State Nuclear Methods, April 1, 1985.
- 28-2 NEDC-32694-P-A, Power Distribution Uncertainties for Safety Limit MCPR Evaluations, August 1999.
- 28-3 NEDC-32601P-A, Methodology and Uncertainties for Safety Limit MCPR Evaluations, April 1999.
- 28-4 Letter from G.A. Watford (GE) to R. M. Pulsifer (NRC), FLN-1999-012, "Proprietary Presentation Material from GE/NRC Meeting of November 10, 1999", November 12, 1999.
- 28-5 Letter, Glen A. Watford (GE) to U. S. Nuclear Regulatory Commission Document Control Desk with attention to J. Donoghue (NRC), "Additional Information Associated with SLMCPR Methodology and Uncertainty Topical Reports NEDC-32601P and NEDC-32694P", MFN-002-99, March 1, 1999.
- 28-6 Letter from G.A. Watford (GE) to R. M. Pulsifer (NRC), FLN-2001-004, "Request for Additional Information – GE14 Review – Power Distribution Uncertainties and GEXL Correlation Development Procedure", March 27, 2001.
- 28-7 Letter, Glen A. Watford (GE) to U. S. Nuclear Regulatory Commission Document Control Desk with attention to R. Pulsifer (NRC), "Confirmation of 10x10 Fuel Design Applicability to Improved SLMCPR, Power Distribution and R-Factor Methodologies", FLN-2001-016, September 24, 2001.
- 28-8 Letter, Glen A. Watford (GE) to U. S. Nuclear Regulatory Commission Document Control Desk with attention to J. Donoghue (NRC), "Confirmation of the Applicability of the GEXL14 Correlation and Associated R-Factor Methodology for Calculating SLMCPR Values in Cores Containing GE14 Fuel", FLN-2001-017, October 1, 2001

**MFN 05-029 NRC RAI RAI 5**

Plant Data, PANAC comparisons, and Applicability to MELLLA+ Conditions. Several conclusions in the Methods Enclosure 3 [see Enclosure B herein] state that the methods are adequate and that eigenvalue tracking per standard procedures will be used. Although, there are no EPU/MELLLA+ operational data, the adequacy of the GNF-A neutronic method must be substantiated through benchmark data or through data that is as close to the EPU/MELLLA+ conditions (e.g., high in channel void conditions 90% or greater). However, there is substantial data based on historical and current operation that are of interest. The following RAIs address benchmarking data needed to demonstrate the adequacy of the GNF-A method for the MELLLA+ conditions.

5-1 Section 2.1.2 states, [[

]]

5-2 Confirmation of Eigenvalues During MELLLA+ Implementation. In several sections, the conclusion states that "confirmation of thermal limits uncertainties (e.g., power distribution) should be executed for initial implementation of MELLLA+ strategy. Explain what is meant by this statement and how this confirmation is performed. As proposed, the eigenvalue tracking results and conclusions would be obtained during MELLLA+ operation after the staff's approval of plant-specific EPU/MELLLA+ application. State what process would be available to the staff for review or assessments of the eigenvalue benchmarking data after the approval of the plant-specific application. What process will this benchmarking data and the corresponding conclusions of the confirmation of the thermal limits uncertainties be provided to the staff for review and assessment?

5-3 Provide plant data and PANAC calculation results for core operating conditions that are as close to MELLLA+ operating conditions (120% power, 80% flow) as available. In this data provide:

- a. Calculated radial and axial void fraction distributions. Provide plots and tabular data for comparisons with MELLLA+ conditions.
- b. Measured TIP profiles and corresponding PANAC TIP predictions. Provide both plots and tabulation of the individual TIP readings and PANAC predictions and compute RMS deviations. The tabulation provides a better means to show the difference between the individual four bundle TIP reading and the associated PANAC results.

5-4 Provide the PANAC calculated data for the same parameters as requested in RAI 5-3 for a core with MELLLA+ conditions for comparison with existing plant data and corresponding PANAC predictions. Provide in plots and tabular form to be consistent with results provided in the response to RAI 5-3.

- 5-5 Provide a discussion of how the core follow data is used to benchmark the GNF-A analytical methods. Explain the important plant instrumentation readings that are obtained from the licensees to simulate the core response using "offline" PANAC calculations. Discuss how the data is compared to the core monitoring system predictions. Provide tabulated data (shown during the audit), comparing the PANAC calculations and the plant's core monitoring system calculational results (e.g., core thermal power, exposure, core flow, thermal limits calculations) for the given cycle data points. Use Brunswick Units 1 and 2 core follow data and a high density BWR plant operating with the highest core void conditions. Include core follow data for operation in the high power/low flow offrated conditions for a high density plant. This is of interest in order to assess the GNF-A code system's accuracy under high void offrated conditions as close to the EPU/MELLLA+ condition.

**GE Response**

Response to RAI 5-1

[[

]]

Response to RAI 5-2

Once a core has operated within the MELLLA+ domain, the following are to be evaluated:

- Hot critical eigenvalue
- Cold critical eigenvalue
- Nodal power distribution
- Bundle power distribution
- Rod-to-rod power distribution
- The core flow and pressure drop uncertainty
- The MIP criterion.

For the evaluation of eigenvalue behavior, see Response 25. The evaluation of nodal and bundle power distributions are conducted via comparison between measured and calculated TIP readings. Rod-to-rod power distributions can be evaluated by comparison between TGBLA and MCNP for the lattice designs present. The plant uncertainties are confirmed using plant data. The MIP criterion is evaluated during the SLMCPR generation process to determine if the core & fuel design selected for operation is expected to produce a plant response substantially outside of prior experience.

When this operational data has been analyzed, a revision to the Methods LTR will be provided to the staff for further review. Additionally, much of this same information will be provided when Licensed Topical Reports for GE approved methodologies are revised per the staff's request.

Response to RAI 5-3

The information regarding operational data for high power/flow ratio situations is provided in both graphical and tabular form in responses to RAIs 27 and 29. Additionally, the responses to RAIs 25 and 26 are pertinent to the data requested.

Response to RAI 5-4

The Methods Interim Process (Reference 5-1) definition includes [[

]] Therefore, this type of information would be submitted on a plant specific application for those plants that elected to utilize the Methods Interim Process.

Response to RAI 5-5

Plant core follow data is used to benchmark GNF-A methods as demonstrated in NEDC-30130P-A which includes evaluation of hot eigenvalues, cold eigenvalues, and TIPs. For this MELLLA+ analysis, a comprehensive evaluation of the same spirit is included as a part of RAI 25.

Additionally, comparison of core monitoring thermal limits and core follow thermal limits is available in Tables 5-2 through 5-10. The statistical summary is shown in Table 5-1. For each cycle, the thermal limits of the official core follow calculations are compared with the core monitoring output. It should be noted that for Plant B Cycle 9 and Plant E Cycle 9, the core monitor and off-line core following are performed with PANAC10. Additionally, the thermal-mechanical limits for these cycles are protected using composite MAPLHGR limits as defined Amendment 19 of GESTAR-II. Therefore, the MFLPD for these cycles is not relevant and is omitted from the tables for these cycles, as well as the statistical rollup for MFLPD.

For Plant D, the off-line core following is PANAC10 while the core monitor is a non-GE core monitoring system.

As demonstrated in Figures 5-1, 5-2, and 5-3, the data shows no significant trending versus core power/flow ratio, defined as core power (MWt) divided by total core flow (Mlbm/hr). [This indicator is also used in the response to RAI 25 in order to capture changes in the operating domain or region of the core power/flow map.] The overall average and standard deviation are consistent with methods requirements for nuclear design. Any specific trending is minor. Specific differences for a given cycle are procedurally reviewed prior to each new cycle of operation.

A similar review was conducted by GE in 2002 and presented to the NRC. This information, where PANAC10 and PANAC11 were specifically separated, was formally transmitted to the NRC as a part of Reference 5-2. They are repeated here in Figure 5-4 for additional information. Comparison of this historical analysis to the present indicates that the results are very similar and end up with statistical behavior between the PANAC10 and PANAC11 specific distributions, as expected.



NEDO-33173-A, Revision 1  
Non-Proprietary Information

**Table 5-1 Statistical Summary of Thermal Margin Prediction  
(Offline – Core Monitoring)**

	<b>DELTA MFLPD</b>	<b>DELTA MAPRAT</b>	<b>DELTA MFLCPR</b>
<b>AVG</b>	[[		]]
<b>STDEV</b>			

NEDO-33173-A, Revision 1  
Non-Proprietary Information

**Table 5-2 Plant A, Cycle 18 Thermal Limits Comparison**

N	CYCEXP	RP	WCT	PANAC	PANAC	PANAC	CM	CM	CM
				MFLPD	MAPRAT	MFLCPR	MFLPD	MAPRAT	MFLCPR
1	19.07	544.00	27.08	[[					
2	32.26	969.00	27.30						
3	169.47	1241.00	38.81						
4	205.11	1317.00	31.13						
5	341.75	1660.00	48.07						
6	366.13	768.00	28.33						
7	383.82	1333.00	32.15						
8	406.48	1658.00	47.53						
9	723.83	1657.00	47.49						
10	753.10	880.00	28.15						
11	775.72	1658.00	46.51						
12	1049.26	1656.00	46.67						
13	1163.30	1655.00	45.67						
14	1207.88	1655.00	45.75						
15	1246.74	1417.00	35.37						
16	1260.82	804.00	27.56						
17	1283.49	1652.00	47.90						
18	1443.08	1655.00	47.07						
19	1610.91	1658.00	46.33						
20	1637.19	1384.00	34.87						
21	1659.87	1655.00	47.92						
22	1910.73	1657.00	46.67						
23	2138.76	1658.00	46.29						
24	2344.02	1657.00	45.64						
25	2663.26	1658.00	45.86						
26	2731.68	1657.00	45.31						
27	3044.61	1657.00	45.71						
28	3057.86	751.00	37.54						
29	3071.82	797.00	33.50						
30	3094.32	1581.00	41.94						
31	3208.21	1654.00	47.13						
32	3367.70	1658.00	46.99						
33	3411.50	1654.00	46.83						
34	3427.40	1157.00	36.15						
35	3447.35	1501.00	36.82						
36	3469.08	1599.00	42.02						
37	3512.75	1656.00	45.28						
38	3548.56	1562.00	39.84						
39	3571.44	1656.00	45.00						
40	3595.21	1717.00	46.27						
41	3692.02	1760.00	46.84						

NEDO-33173-A, Revision 1  
Non-Proprietary Information

**Table 5-2 Plant A, Cycle 18 Thermal Limits Comparison**

N	CYCEXP	RP	WCT	PANAC	PANAC	PANAC	CM	CM	CM
				MFLPD	MAPRAT	MFLCPR	MFLPD	MAPRAT	MFLCPR
42	3962.59	1789.00	47.02						
43	4184.18	1790.00	46.17						
44	4504.30	1780.00	46.32						
45	4627.43	1791.00	46.83						
46	4644.69	955.00	30.03						
47	4667.83	1786.00	47.96						
48	4959.86	1769.00	48.29						
49	5252.02	1770.00	47.34						
50	5264.14	846.00	24.40						
51	5281.94	1497.00	35.67						
52	5306.17	1769.00	45.68						
53	5573.94	1768.00	46.77						
54	5768.73	1768.00	46.10						
55	5939.16	1770.00	45.60						
56	6129.19	1768.00	47.23						
57	6148.73	1420.00	39.47						
58	6172.36	1731.00	43.40						
59	6369.31	1788.00	46.61						
60	6566.21	1788.00	46.26						
61	6910.95	1788.00	47.31						
62	7156.70	1789.00	46.42						
63	7178.40	1789.00	46.33						
64	7399.96	1792.00	47.33						
65	7621.56	1789.00	46.48						
66	7818.53	1790.00	45.95						
67	7847.05	1791.00	47.33						
68	7875.36	1214.00	31.79						
69	7898.28	1768.00	44.17						
70	7922.88	1789.00	46.98						
71	8144.47	1788.00	46.18						
72	8415.33	1791.00	45.91						
73	8636.51	1786.00	47.13						
74	8858.10	1789.00	46.86						
75	9103.54	1791.00	46.35						
76	9125.01	1772.00	48.14						
77	9149.58	1787.00	47.38						
78	9420.38	1789.00	46.68						
79	9678.82	1792.00	46.69						
80	9692.61	753.00	29.59						
81	9716.17	1749.00	44.67						
82	9740.74	1788.00	46.64						
83	10060.79	1788.00	46.03						
84	10089.00	1739.00	46.36						

NEDO-33173-A, Revision 1  
Non-Proprietary Information

**Table 5-2 Plant A, Cycle 18 Thermal Limits Comparison**

N	CYCEXP	RP	WCT	PANAC	PANAC	PANAC	CM	CM	CM
				MFLPD	MAPRAT	MFLCPR	MFLPD	MAPRAT	MFLCPR
85	10111.74	1064.00	31.87						
86	10129.10	1255.00	44.04						
87	10180.09	1240.00	29.17						
88	10198.26	1281.00	34.84						
89	10222.65	1790.00	46.12						
90	10345.66	1789.00	47.67						
91	10616.45	1788.00	47.04						
92	10788.76	1788.00	46.12						
93	11010.26	1789.00	46.74						
94	11025.84	1074.00	33.58						
95	11042.68	1230.00	33.26						
96	11066.76	1748.00	44.04						
97	11263.69	1792.00	47.56						
98	11485.27	1788.00	46.06						
99	11706.87	1789.00	47.17						
100	11903.80	1791.00	46.12						
101	12125.40	1789.00	47.45						
102	12346.90	1789.00	45.90						
103	12568.50	1790.00	47.56						
104	12691.60	1791.00	47.05						
105	12912.70	1790.00	47.54						
106	13232.70	1792.00	47.04						
107	13251.50	1347.00	36.18						
108	13276.00	1792.00	46.30						
109	13374.50	1791.00	47.87						
110	13575.20	1792.00	46.89						
111	13592.19	1135.00	26.28						
112	13615.56	1665.00	48.59						
113	13639.88	1787.00	47.87						
114	13886.01	1789.00	45.76						
115	13984.48	1789.00	47.42						
116	14082.94	1786.00	47.47						
117	14156.79	1791.00	48.09						
118	14230.63	1789.00	48.08						
119	14304.47	1790.00	48.34						
120	14353.71	1788.00	48.16						
121	14445.74	1789.00	48.18						

]]

NEDO-33173-A, Revision 1  
Non-Proprietary Information

**Table 5-3 Plant A, Cycle 19 Thermal Limits Comparison**

N	CYCEXP	RP	WCT	PANAC	PANAC	PANAC	CM	CM	CM
				MFLPD	MAPRAT	MFLCPR	MFLPD	MAPRAT	MFLCPR
1	19.18	997.00	31.93	[[					
2	43.04	1737.00	43.49						
3	67.57	1787.00	47.39						
4	190.47	1789.00	47.28						
5	239.64	1790.00	46.48						
6	510.12	1790.00	47.18						
7	854.37	1791.00	46.69						
8	1100.25	1790.00	45.72						
9	1173.95	1791.00	45.27						
10	1468.88	1791.00	46.35						
11	1763.87	1786.00	45.58						
12	2058.89	1790.00	46.44						
13	2132.66	1790.00	46.22						
14	2378.23	1789.00	46.02						
15	2400.54	1783.00	46.79						
16	2425.09	1789.00	47.75						
17	2498.84	1789.00	46.68						
18	2720.14	1789.00	46.43						
19	3035.95	1788.00	45.76						
20	3060.38	1787.00	45.67						
21	3158.71	1792.00	47.40						
22	3379.98	1790.00	47.24						
23	3724.21	1787.00	46.74						
24	4043.84	1792.00	46.12						
25	4191.37	1791.00	45.75						
26	4363.48	1789.00	45.51						
27	4434.32	1789.00	47.32						
28	4505.56	1792.00	47.94						
29	4801.28	1789.00	47.60						
30	4869.83	508.00	25.57						
31	5184.95	1792.00	47.89						
32	5406.20	1790.00	48.09						
33	5524.65	1788.00	46.29						
34	5793.33	1788.00	47.31						
35	6014.63	1793.00	47.06						
36	6260.54	1789.00	46.23						
37	6506.52	1789.00	45.76						
38	6727.89	1790.00	45.12						
39	6949.30	1791.00	46.74						
40	6969.49	1478.00	48.56						
41	6993.99	1791.00	46.05						

NEDO-33173-A, Revision 1  
Non-Proprietary Information

**Table 5-3 Plant A, Cycle 19 Thermal Limits Comparison**

N	CYCEXP	RP	WCT	PANAC	PANAC	PANAC	CM	CM	CM
				MFLPD	MAPRAT	MFLCPR	MFLPD	MAPRAT	MFLCPR
42	7215.37	1791.00	46.18						
43	7387.54	1792.00	46.00						
44	7608.93	1792.00	45.28						
45	7953.29	1791.00	47.06						
46	8125.50	1791.00	46.13						
47	8174.70	1791.00	45.97						
48	8193.89	1544.00	46.60						
49	8210.90	1023.00	26.39						
50	8235.36	1787.00	47.72						
51	8259.94	1789.00	47.58						
52	8278.03	944.00	26.69						
53	8302.29	1781.00	45.02						
54	8572.82	1787.00	47.40						
55	8843.39	1786.00	47.37						
56	9015.59	1790.00	46.98						
57	9138.58	1791.00	46.85						
58	9261.12	1790.00	46.72						
59	9307.89	1790.00	47.65						
60	9578.25	1794.00	45.88						
61	9824.20	1791.00	45.61						
62	10045.57	1788.00	45.63						
63	10340.72	1794.00	45.43						
64	10635.89	1794.00	45.51						
65	10931.02	1791.00	45.67						
66	11176.97	1793.00	45.98						
67	11422.89	1786.00	45.95						
68	11668.51	1788.00	46.89						
69	11763.69	1789.00	47.72						
70	11911.22	1788.00	46.95						
71	12009.56	1791.00	47.43						
72	12378.42	1792.00	47.09						
73	12525.93	1790.00	46.05						
74	12718.90	1791.00	47.15						
75	12756.90	1472.00	44.29						
76	12821.59	1490.00	39.31						
77	12842.13	1498.80	39.73						
78	12856.49	905.00	29.45						
79	12879.40	1545.00	36.13						
80	12903.92	1791.00	47.84						
81	12928.49	1789.00	47.46						
82	13248.08	1792.00	47.12						
83	13592.33	1794.00	47.00						
84	13764.33	1787.00	46.70						

NEDO-33173-A, Revision 1  
 Non-Proprietary Information

**Table 5-3 Plant A, Cycle 19 Thermal Limits Comparison**

N	CYCEXP	RP	WCT	PANAC	PANAC	PANAC	CM	CM	CM
				MFLPD	MAPRAT	MFLCPR	MFLPD	MAPRAT	MFLCPR
85	13810.41	1792.00	48.26						
86	13859.58	1790.00	46.82						
87	14007.10	1795.00	47.81						
88	14277.63	1792.00	47.04						
89	14474.27	1784.00	46.81						
90	14621.80	1792.00	47.61						
91	14720.15	1789.00	47.72						
92	14769.31	1789.00	48.02						
93	14941.42	1788.00	47.27						
94	15088.61	1789.00	47.80						
95	15260.71	1791.00	47.33						
96	15482.01	1788.00	47.23						
97	15693.58	1768.00	48.83						]]

NEDO-33173-A, Revision 1  
Non-Proprietary Information

**Table 5-4 Plant B, Cycle 9 Thermal Limits Comparison**

N	CYCEXP	RP	WCT	PANAC	PANAC	CM	CM
				MAPRAT	MFLCPR	MAPRAT	MFLCPR
1	261.69	3760.00	103.97	[[			
2	392.69	3751.00	102.99				
3	540.80	3755.00	94.70				
4	792.08	3756.00	94.45				
5	930.11	2770.00	107.51				
6	1163.98	3755.00	100.26				
7	1416.58	3761.00	100.90				
8	1614.65	3753.00	98.22				
9	1891.15	3757.00	97.32				
10	2195.62	3756.00	93.97				
11	2499.26	3749.00	93.04				
12	2803.19	3761.00	91.99				
13	3107.13	3759.00	90.85				
14	3410.34	3749.00	88.24				
15	3486.24	3750.00	87.88				
16	3688.63	3757.00	89.57				
17	3865.74	3753.00	88.19				
18	4118.83	3754.00	88.56				
19	4393.85	3763.00	95.40				
20	4672.42	3758.00	94.00				
21	4976.32	3752.00	92.43				
22	5223.99	3754.00	92.36				
23	5348.47	3755.00	91.33				
24	5471.67	3195.00	95.05				
25	5688.96	3752.00	91.29				
26	5916.87	3758.00	91.43				
27	6059.69	3758.00	90.61				
28	6231.34	3748.00	100.78				
29	6356.54	3753.00	90.85				
30	6634.90	3756.00	90.64				
31	6919.06	3748.00	89.32				
32	7203.31	3752.00	101.37				
33	7481.62	3746.00	99.88				
34	7760.08	3759.00	98.90				
35	8037.19	3751.00	96.01				
36	8314.94	3762.00	93.49				
37	8491.94	3757.00	95.99				
38	8744.65	3755.00	97.36				
39	8972.33	3752.00	96.12				
40	9200.13	3755.00	94.12				
41	9326.39	3755.00	99.64				



NEDO-33173-A, Revision 1  
Non-Proprietary Information

**Table 5-4 Plant B, Cycle 9 Thermal Limits Comparison**

N	CYCEXP	RP	WCT	PANAC	PANAC	CM	CM
				MAPRAT	MFLCPR	MAPRAT	MFLCPR
42	9377.92	3748.00	102.32				
43	9583.04	3757.00	104.59				
44	9785.23	3747.00	103.53				
45	10057.69	3754.00	104.70				
46	10335.91	3759.00	104.38				
47	10563.46	3764.00	104.00				
48	10841.69	3763.00	103.31				
49	11120.07	3759.00	103.24				
50	11398.25	3761.00	103.64				
51	11695.55	3760.00	104.04				
52	11861.01	3752.00	99.46				
53	11998.08	3621.00	107.57				
54	12198.06	3726.00	107.78				
55	12372.59	3694.00	108.04				
56	12648.98	3760.00	99.93				
57	12927.22	3758.00	104.03				
58	13205.09	3752.00	106.38				
59	13255.55	3741.00	107.67				
60	13454.96	3756.00	94.50				
61	13708.11	3760.00	98.26				
62	13961.24	3730.00	101.01				
63	14237.24	3746.00	101.77				
64	14489.93	3739.00	107.47				
65	14763.69	3756.00	107.15				
66	14863.66	3714.00	107.95				
67	15034.43	3741.00	108.10				
68	15207.85	3655.00	108.67				
69	15342.44	3617.00	109.15				
70	15500.17	3166.00	108.68				
71	15627.24	3132.00	108.50				
72	15840.25	3193.00	103.76				
73	15990.45	3188.00	108.36				
74	16193.23	3117.00	109.21				

]]

NEDO-33173-A, Revision 1  
Non-Proprietary Information

**Table 5-5 Plant B, Cycle 10 Thermal Limits Comparison**

N	CYCEXP	RP	WCT	PANAC	PANAC	PANAC	CM	CM	CM
				MFLPD	MAPRAT	MFLCPR	MFLPD	MAPRAT	MFLCPR
1	191.01	3752.00	104.86	[[					
2	267.23	3756.00	106.57						
3	444.96	3744.00	104.25						
4	521.16	3745.00	105.59						
5	800.48	3749.00	102.74						
6	1079.95	3749.00	102.57						
7	1359.42	3749.00	102.30						
8	1638.20	3758.00	101.14						
9	1883.99	3759.00	100.59						
10	2101.25	3757.00	100.36						
11	2253.07	3754.00	101.24						
12	2451.32	3750.00	99.51						
13	2515.04	3143.00	109.15						
14	2713.55	3751.00	95.89						
15	2822.36	3733.00	108.40						
16	3071.29	3750.00	97.00						
17	3322.81	3756.00	97.01						
18	3576.46	3758.00	97.09						
19	3829.77	3759.00	96.01						
20	4098.37	3757.00	96.43						
21	4178.58	3755.00	103.88						
22	4455.24	3754.00	98.81						
23	4733.80	3754.00	99.80						
24	5013.16	3753.00	98.31						
25	5156.27	3751.00	98.30						
26	5220.20	3595.00	108.21						
27	5495.19	3753.00	98.37						
28	5774.08	3751.00	97.89						
29	6053.51	3757.00	97.46						
30	6332.70	3760.00	97.01						
31	6612.04	3757.00	96.57						
32	6739.09	3758.00	94.91						
33	6804.45	3528.00	108.65						
34	7079.33	3754.00	100.81						
35	7358.64	3754.00	100.03						
36	7637.04	3756.00	99.08						
37	7915.93	3759.00	99.08						
38	8195.32	3751.00	97.79						
39	8449.34	3754.00	96.36						
40	8680.67	3759.00	95.96						
41	8953.97	3760.00	98.45						

NEDO-33173-A, Revision 1  
Non-Proprietary Information

**Table 5-5 Plant B, Cycle 10 Thermal Limits Comparison**

N	CYCEXP	RP	WCT	PANAC	PANAC	PANAC	CM	CM	CM
				MFLPD	MAPRAT	MFLCPR	MFLPD	MAPRAT	MFLCPR
42	9233.34	3752.00	98.67						
43	9512.33	3757.00	98.85						
44	9791.72	3758.00	98.62						
45	10071.07	3763.00	98.24						
46	10299.58	3760.00	97.56						
47	10528.19	3752.00	98.26						
48	10756.80	3757.00	98.61						
49	11010.32	3748.00	102.41						
50	11238.74	3755.00	103.54						
51	11467.28	3747.00	103.92						
52	11530.77	3748.00	99.10						
53	11630.58	3754.00	94.81						
54	11800.43	3750.00	99.53						
55	12079.80	3750.00	100.87						
56	12308.21	3748.00	103.13						
57	12512.36	3756.00	104.19						
58	12715.46	3756.00	107.50						
59	12992.27	3747.00	100.06						
60	13271.55	3741.00	103.76						
61	13576.18	3724.00	107.57						
62	13725.07	3751.00	103.37						
63	13923.32	3750.00	104.38						
64	14163.43	3568.00	108.46						
65	14391.74	3494.00	108.15						]]

NEDO-33173-A, Revision 1  
Non-Proprietary Information

**Table 5-6 Plant C, Cycle 30 Thermal Limits Comparison**

N	CYCEXP	RP	WCT	PANAC	PANAC	PANAC	CM	CM	CM
				MFLPD	MAPRAT	MFLCPR	MFLPD	MAPRAT	MFLCPR
1	28.22	553.00	22.80	[[					
2	51.25	1085.00	28.87						
3	121.68	1092.00	31.82						
4	285.84	1092.00	28.47						
5	426.66	1095.00	29.15						
6	682.10	1094.00	29.31						
7	940.49	1094.00	29.29						
8	1128.41	1092.00	28.96						
9	1434.20	1093.00	28.70						
10	1739.62	1094.00	28.54						
11	1853.68	1094.00	28.03						
12	2135.52	1094.00	27.89						
13	2252.96	1095.00	27.82						
14	2417.35	1094.00	27.85						
15	2534.80	1094.00	27.78						
16	2792.80	1095.00	27.71						
17	3050.94	1091.00	27.70						
18	3237.72	1096.00	27.90						
19	3331.62	1093.00	28.11						
20	3589.86	1097.00	28.32						
21	3715.89	1094.00	28.73						
22	3726.46	602.00	23.45						
23	3749.43	1091.00	32.36						
24	3771.81	1090.00	27.27						
25	3842.19	1094.00	26.29						
26	4006.37	1093.00	26.85						
27	4217.56	1093.00	27.16						
28	4381.54	1093.00	27.78						
29	4545.85	1093.00	28.44						
30	4710.15	1094.00	29.49						
31	4874.44	1095.00	29.88						
32	5037.76	1096.00	30.71						
33	5177.59	1096.00	31.49						
34	5338.56	1064.00	25.93						
35	5498.18	1057.00	25.92						
36	5638.93	1094.00	28.65						
37	5850.10	1093.00	30.02						
38	6061.20	1086.00	31.39						
39	6248.86	1094.00	31.39						
40	6344.99	1094.00	31.29						
41	6368.13	1088.00	28.86						

NEDO-33173-A, Revision 1  
 Non-Proprietary Information

**Table 5-6 Plant C, Cycle 30 Thermal Limits Comparison**

N	CYCEXP	RP	WCT	PANAC	PANAC	PANAC	CM	CM	CM
				MFLPD	MAPRAT	MFLCPR	MFLPD	MAPRAT	MFLCPR
42	6390.56	985.00	28.87						
43	6412.42	1046.00	31.64						
44	6434.06	1058.00	32.02						
45	6454.85	849.00	23.16						
46	6475.04	932.00	25.89						
47	6558.57	949.00	27.22						
48	6693.98	1050.00	31.64						
49	6787.36	859.00	24.33						
50	6848.84	975.00	31.46						
51	6914.54	1048.00	32.64						
52	7068.27	1031.00	32.85						
53	7238.79	874.00	28.08						
54	7307.74	805.00	24.65						
55	7382.15	878.00	29.83						
56	7481.68	916.00	32.70						
57	7535.50	869.00	31.42						
58	7604.86	732.00	22.75						]]

NEDO-33173-A, Revision 1  
Non-Proprietary Information

**Table 5-7 Plant C**

<b>N</b>	<b>CYCEXP</b>	<b>RP</b>	<b>WCT</b>	<b>PANAC MFLPD</b>	<b>PANAC MAPRAT</b>	<b>PANAC MFLCPR</b>	<b>CM MFLPD</b>	<b>CM MAPRAT</b>	<b>CM MFLCPR</b>
1	11.80	483.00	19.40	[[					
2	22.49	537.00	22.80						
3	36.81	663.00	19.31						
4	58.64	1092.00	26.40						
5	127.99	1093.00	27.90						
6	267.29	1096.00	28.51						
7	383.64	1095.00	28.78						
8	496.46	1031.00	26.00						
9	659.08	1097.00	29.09						
10	821.87	1096.00	29.09						
11	984.89	1093.00	29.02						
12	1147.89	1094.00	28.84						
13	1311.95	1097.00	28.84						
14	1474.95	1096.00	28.77						
15	1684.09	1095.00	27.86						
16	1893.66	1095.00	27.71						
17	2103.14	1096.00	27.56						
18	2311.05	1094.00	27.38						
19	2450.80	1095.00	27.31						
20	2613.86	1098.00	27.29						
21	2776.73	1094.00	27.13						
22	2939.64	1093.00	27.09						
23	3102.01	1092.00	27.60						
24	3264.96	1095.00	27.59						
25	3427.83	1095.00	27.60						
26	3590.68	1096.00	27.68						
27	3753.32	1095.00	27.86						
28	3916.13	1098.00	28.19						
29	4102.17	1094.00	28.32						
30	4286.02	1090.00	28.66						
31	4472.08	1095.00	28.98						
32	4611.41	1093.00	27.05						
33	4774.23	1093.00	27.22						
34	4935.85	1094.00	27.66						
35	5098.68	1095.00	28.16						
36	5261.19	1094.00	28.65						
37	5377.46	1094.00	29.46						
38	5585.81	1092.00	29.98						
39	5702.12	1096.00	30.79						
40	5864.37	1092.00	26.77						
41	6073.73	1092.00	27.39						
42	6281.43	1094.00	28.44						

NEDO-33173-A, Revision 1  
 Non-Proprietary Information

**Table 5-7 Plant C**

<b>N</b>	<b>CYCEXP</b>	<b>RP</b>	<b>WCT</b>	<b>PANAC MFLPD</b>	<b>PANAC MAPRAT</b>	<b>PANAC MFLCPR</b>	<b>CM MFLPD</b>	<b>CM MAPRAT</b>	<b>CM MFLCPR</b>
43	6490.72	1095.00	29.71						
44	6606.96	1095.00	30.87						
45	6723.22	1093.00	32.13						
46	6955.70	1094.00	31.94						
47	7160.47	1096.00	32.31						
48	7276.69	1089.90	32.43						
49	7391.51	1078.60	32.52						
50	7579.33	966.90	30.91						
51	7667.27	1035.50	32.65						
52	7825.45	900.70	28.73						

]]

NEDO-33173-A, Revision 1  
 Non-Proprietary Information

**Table 5-8 Plant D**

<b>N</b>	<b>CYCEXP</b>	<b>RP</b>	<b>WCT</b>	<b>PANAC MFLPD</b>	<b>PANAC MAPRAT</b>	<b>PANAC MFLCPR</b>	<b>CM MFLPD</b>	<b>CM MAPRAT</b>	<b>CM MFLCPR</b>
1	349.87	2921.40	79.44	[[					
2	615.16	2920.50	79.40						
3	880.48	2924.60	78.06						
4	1145.81	2922.50	78.00						
5	1409.16	2927.60	80.17						
6	1727.54	2922.10	78.25						
7	1873.02	2923.70	79.91						
8	2111.79	2921.70	78.15						
9	2376.93	2918.40	76.69						
10	2642.03	2916.60	76.93						
11	2827.54	2921.30	78.67						
12	2969.29	2922.50	79.54						
13	3234.52	2914.50	78.60						
14	3403.00	2921.10	78.18						
15	3593.05	2920.40	79.33						
16	3858.26	2923.60	79.29						
17	4123.51	2917.70	78.27						
18	4388.74	2920.10	77.87						
19	4654.04	2926.20	76.92						
20	4849.98	2925.90	77.82						
21	5115.19	2922.20	78.38						
22	5247.85	2918.50	77.41						
23	5377.00	2920.50	78.60						
24	5642.28	2916.70	77.73						
25	5907.49	2924.60	79.48						
26	6172.76	2924.30	79.31						
27	6437.89	2919.80	78.06						
28	6728.40	2923.20	79.31						
29	6993.61	2925.70	78.63						]]



NEDO-33173-A, Revision 1  
Non-Proprietary Information

**Table 5-9 Plant E, Cycle 9 Thermal Limits Comparison**

N	CYCEXP	RP	WCT	PANAC	PANAC	CM	CM
				MAPRAT	MFLCPR	MAPRAT	MFLCPR
1	281.27	3215.00	78.19	[[			
2	579.35	3211.00	82.63				
3	888.96	3221.00	82.72				
4	1158.62	3279.00	82.97				
5	1378.09	3292.00	82.88				
6	1637.54	3282.00	79.16				
7	1851.06	3288.00	79.19				
8	2064.50	3282.00	80.97				
9	2331.60	3284.00	80.41				
10	2598.33	3286.00	80.13				
11	2891.95	3278.00	81.16				
12	3076.91	3261.00	78.66				
13	3336.79	3260.00	79.03				
14	3599.85	3232.00	78.25				
15	3914.44	3228.00	79.41				
16	4228.39	3214.00	78.25				
17	4540.20	3178.00	76.88				
18	4822.55	3169.00	77.97				
19	5106.23	3176.00	77.09				
20	5260.84	3168.00	76.56				
21	5415.38	3170.00	76.19				
22	5656.71	3170.00	76.97				
23	5955.78	3171.00	75.91				
24	6135.83	3167.00	77.09				
25	6315.89	3171.00	75.66				
26	6593.41	3163.00	80.56				
27	6850.99	3164.00	79.03				
28	7056.56	3163.00	77.81				
29	7236.61	3168.00	77.16				
30	7389.51	3172.00	78.06				
31	7543.78	3164.00	77.47				
32	7697.97	3165.00	76.16				
33	7903.42	3166.00	78.13				
34	8108.81	3157.00	76.41				
35	8339.86	3161.00	76.59				
36	8468.29	3162.00	77.44				
37	8621.00	3159.00	77.09				
38	8757.27	3156.00	78.66				
39	8936.77	3158.00	78.47				
40	9013.73	3159.00	78.56				
41	9142.13	3166.00	78.56				

NEDO-33173-A, Revision 1  
Non-Proprietary Information

**Table 5-9 Plant E, Cycle 9 Thermal Limits Comparison**

N	CYCEXP	RP	WCT	PANAC	PANAC	CM	CM
				MAPRAT	MFLCPR	MAPRAT	MFLCPR
42	9296.28	3173.00	77.91				
43	9476.57	3172.00	77.63				
44	9624.08	3171.00	78.72				
45	9833.08	3230.00	79.16				
46	10016.09	3214.00	78.75				
47	10199.38	3226.00	79.16				
48	10278.04	3236.00	80.16				
49	10540.82	3239.00	80.53				
50	10777.66	3228.00	80.41				
51	10935.93	3245.00	81.94				
52	11120.22	3242.00	80.31				
53	11304.63	3237.00	80.56				
54	11489.20	3252.00	80.09				
55	11621.02	3245.00	78.94				
56	11699.95	3244.00	81.44				
57	11858.13	3246.00	80.44				
58	12069.42	3254.00	80.16				
59	12227.88	3252.00	82.06				
60	12306.81	3235.00	78.84				
61	12438.02	3231.00	81.38				
62	12485.24	3157.00	81.88				
63	12768.11	3170.00	79.41				
64	12947.69	3164.00	78.66				
65	13126.98	3152.00	78.13				
66	13306.22	3151.00	78.22				
67	13485.89	3153.00	80.50				
68	13743.26	3155.00	79.94				
69	13831.22	3225.00	83.78				
70	14144.82	3226.00	83.44				
71	14426.98	3182.00	86.72				
72	14620.81	3102.00	87.06				
73	14836.51	3041.00	87.41				
74	14934.45	2994.00	87.72				
75	15204.23	3042.00	87.81				
76	15485.38	2926.00	86.97				
77	15761.77	2827.00	88.75				
78	15981.40	2712.00	89.25				

]]

NEDO-33173-A, Revision 1  
Non-Proprietary Information

**Table 5-10 Plant E, Cycle 10 Thermal Limits Comparison**

N	CYCEXP	RP	WCT	PANAC MFLPD	PANAC MAPRAT	PANAC MFLCPR	CM MFLPD	CM MAPRAT	CM MFLCPR
1	174.07	3215.30	80.66	[[					
2	357.79	3227.50	84.91						
3	541.67	3225.60	83.00						
4	614.91	3225.40	82.75						
5	907.12	3218.30	80.78						
6	1194.86	3219.80	80.31						
7	1486.05	3279.30	82.53						
8	1779.71	3288.20	82.16						
9	1837.28	1668.70	63.34						
10	2078.90	3300.90	80.22						
11	2319.92	3293.60	80.94						
12	2561.44	3311.00	81.34						
13	2830.29	3300.30	79.41						
14	2910.81	3303.00	79.81						
15	3125.56	3303.30	79.53						
16	3340.80	3308.80	80.03						
17	3385.63	3314.50	82.03						
18	3648.16	3309.70	81.44						
19	3917.25	3309.20	82.03						
20	4185.95	3313.00	81.59						
21	4454.79	3314.70	80.88						
22	4562.31	3309.40	81.09						
23	4589.14	3298.70	82.41						
24	4640.39	3311.80	83.81						
25	4855.56	3301.80	82.66						
26	4909.24	3316.10	81.97						
27	5204.28	3308.30	83.41						
28	5472.07	3291.90	81.69						
29	5766.70	3297.90	82.38						
30	5819.00	3283.90	85.16						
31	6139.27	3282.30	82.91						
32	6460.36	3273.80	80.78						
33	6780.44	3292.60	81.13						
34	7100.63	3283.30	80.38						
35	7339.21	3288.50	81.50						
36	7579.67	3288.80	81.44						
37	7820.09	3294.00	80.63						
38	8033.81	3301.00	81.38						
39	8266.38	3209.70	82.25						
40	8543.57	3203.80	80.34						]]

[[

]]

**Figure 5-1 Differences in MFLPD versus Core Power/Flow Ratio**

[[

]]

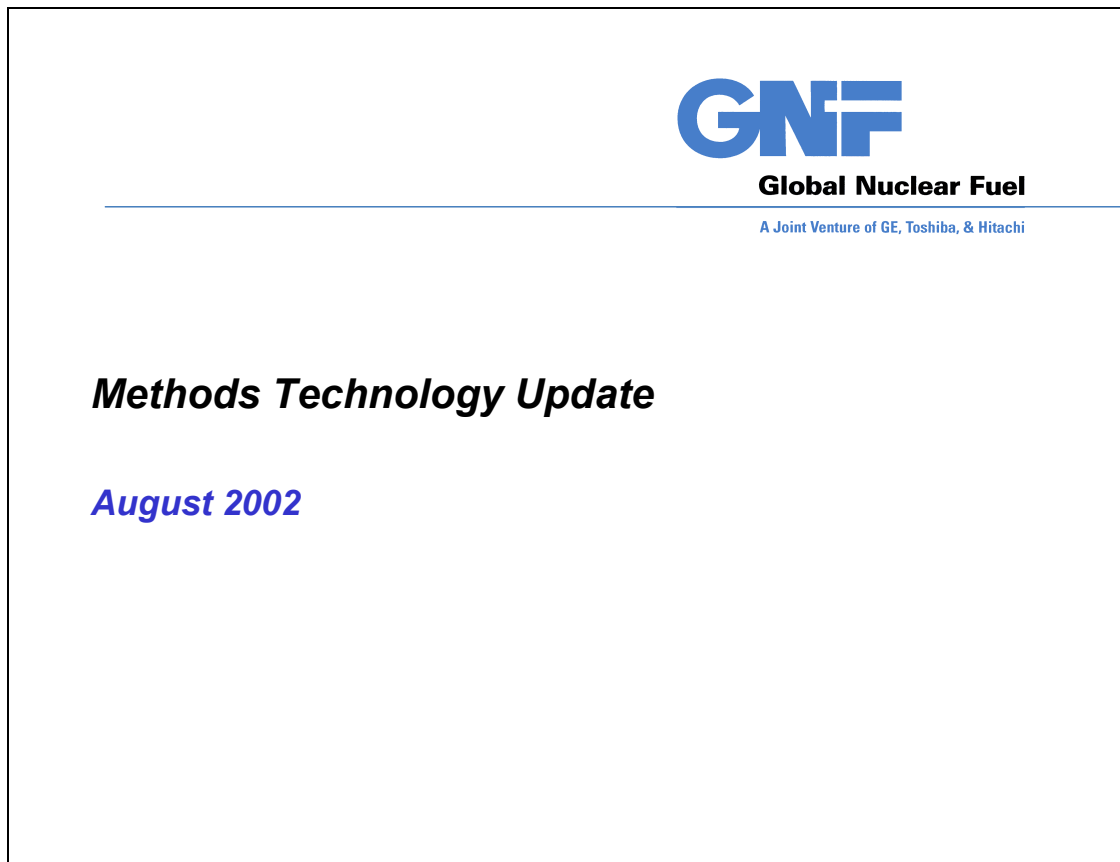
**Figure 5-2 Differences in MAPRAT versus Core Power/Flow Ratio**

[[

]]

**Figure 5-3 Differences in MFLCPR versus Core Power/Flow Ratio**

**Figure 5-4 Slides from FLN-2002-015**



### ***Selected validation database***

---

- ***PANAC10 compared with PANAC10/3DM evaluated thermal limit values***

- *8 plants for 9 cycles containing GE13 and GE14 lead fuel for a total of 468 points.*

- ***PANAC11 compared with PANAC11/3DM evaluated thermal limit values***

- *5 plants for 8 cycles containing GE12 and GE14 lead fuel for a total of 349 points.*



[[

]]

[[

]]

NEDO-33173-A, Revision 1  
Non-Proprietary Information

References:

- 5-1 MFN 05-005, Letter from George Stramback (GE) to NRC, March 25, 2005, *Methods Interim Process (TAC No. MC5780)*
- 5-2 Letter from G.A. Watford (GE) to Alan Wang (NRC), FLN-2002-015, "NRC Technology Update - Proprietary Slides - July 31 - August 1, 2002", October 21, 2002.

### **MFN 05-029 NRC RAI 25**

Core Follow Data: The objective of this review is to determine the accuracy of TGBLA and PANAC for the current operating strategies. The staff understands that GNF-A receives operating data from plants and performs offline PANAC calculations to monitor the plants' performance (i.e., eigenvalue tracking).

- 25-1 Select plants with challenging core designs (e.g., uprated plants and high-density plants with extended cycles) to benchmark the TGBLA and PANAC codes. The data from the plants should be statistically significant to current BWR operating strategies and fuel designs (GE14). The core tracking cycle exposure should extend to the number of cycles a fuel bundle may remain loaded in a core.
- 25-2 Provide plant-specific information for each set of core follow data (the plant type, whether the power level has been uprated, power density, operating domain, fuel type, cycle length, etc.). For each TIP reading, give the cycle state point, the operating power/flow state point, and the corresponding calculated thermal margin available. Evaluate the plant-specific data, including whether the core follow data indicates that the code is less accurate for higher in-channel void conditions. Explain any trends in the data in terms of operation at higher operating domain, cycle length, uprate and high high-density plants. Demonstrate that the current uncertainties and biases used in the NRC-approved analytical method (e.g. bundle power,  $\sigma$  P4B , power allocation factor,  $\sigma$  PALj, and pin power peaking etc) remain valid and applicable.

### **Proposed GE Response**

#### **Response 25-1:**

Five BWRs have been selected for this study (Plants A-E), and they will be referred to as the **Reference BWRs, or Reference Plants**. Nine operating cycles have been selected for this study (two cycles for Plants A, B, C and E; one cycle for Plant D), and these cycles will be referred to as the **studied cycles, or cycles studied**. Table 25-1 provides the key performance characteristics of each of these Reference BWRs.

These reference plants have been selected because they operate at high power density, and cover a large range of plant sizes. All but Plant C, which operates on annual cycles, are operating on nominal two-year cycles. While the power density of Plant C is not as high as that of the other reference plants, it operates at very high bundle powers because of its small core size. The high bundle powers in this plant result in high bundle (or channel) exit void fractions, which are of interest for this study. The predominant fuel type in all of these plants is high (~4.0 w/o) enriched 10x10 fuel (GE14).

Two cycles of operation have been analyzed for all plants but Plant D. Only the current operating cycle is used for Plant D, since it is operating at its licensed power uprate of 120% in the current cycle. Therefore, nine operating cycles are included in this study, which provides a statistically significant dataset for current operation at high power density in high-energy cycles.

RAI 25-1 requested that the core tracking cycle exposure extend to the number of cycles a fuel bundle may remain in the core. For two-year high-energy cycles, bundles typically remain in the core for two or three cycles. While a maximum of two cycles have been specifically analyzed in this study, the core tracking has been done for all previous cycles with the same nuclear methods (TGBLA06/PANAC11). Thus, the historical characteristics (e.g., nodal exposures and void histories) for all the fuel bundles that resided in the core in previous cycles are carried into the cycles being studied. The cycles being studied include fuel bundles that cover the entire range of exposures from fresh to highly exposed, and since all fuel characteristics are based on the nuclear methods being evaluated, the cycles being studied provide an appropriate representation of fuel at all exposures. The intent of the RAI request stated above is satisfied since all fuel in the core has been tracked using the methods being evaluated, and the fuel bundles resident in the core cover the full range of exposures in the cycles included in the study.

Response 25-2:

**Introduction**

This response will include a description of the key parameters for each cycle studied, followed by detailed data obtained from core tracking and TIP responses, and finally an analysis of this data.

Before presenting the detailed data, a brief overview of the cycles studied is provided. For Plant A, two cycles are studied, Cycles 18 and 19. Cycle 18 is of particular interest because it was uprated from 1658 MWT (104% OLTP) to 1912 MWt (120% OLTP) during this cycle. The early portion of the cycle was operated up to 104%, and then the power was increased to ~112% for the remainder of the cycle. Comparing the results of the core tracking before and after the power increase will provide insight into whether the fidelity of the core methods changes due to the increased power density and voiding in the core.

Plant B is a high power density BWR/6, but has a modest power uprate of 105%. Plant E is also a BWR/6, but it has been uprated to 120%, and has the highest power density of all the reference plants. Two cycles are studied for each of these BWR/6 plants, which coincidentally are Cycles 9 and 10 for both.

As mentioned earlier, Plant C is unique because of its small core size, which results in high bundle powers. These high bundle powers provide the opportunity to evaluate the nuclear methods for limiting high power bundles. Cycles 30 and 31 are studied for Plant C.

Plant D is a BWR/4 that began operating at its full licensed uprate power of 120% in Cycle 15. Cycle 15, the current operating cycle, is studied for this reference plant because of its high power density.

The core loading for each of the studied cycles is provided in the next section. The core loading data shows the steady progression to high-enriched GE14 fuel. It is also interesting to note that for the high-energy two-year cycles (plants A, B, D and E), the reload batch size is also increasing in most cases, with a maximum batch fraction of 50% for Plant E in Cycle 10. At the other extreme, for the annual cycles in Plant C, the reload batch size of 16.7% remains constant,

and at the low end of the BWR experience range. The increase in cycle energy for this plant is achieved with increased enrichment, rather than with a combination of increased reload batch size and enrichment.

The following sections provide details of the cycles studied for each reference plant.

### **Key Core Parameters for the Reference Plants for Each Cycle Studied**

This section summarizes the licensed operating domain, the nominal cycle length used to design the cycle, and the core loading for each of the nine cycles studied.

#### **Plant A – Cycle 18**

Licensed Thermal Power: 1912 MWt (120% of OLTP)

Flow Range at Licensed Power: 48.5 to 49.0 Mlbm/hr (99 – 100% of Rated Flow)

Nominal Cycle Length: 2 years

Core Loading:

Cycle Loaded	No. of Bundles	Fuel Type	Avg. Enrichment of Bundles Loaded
18	136	GE14 (10x10)	4.02
17	128	GE12 (10x10)	3.71
16	104	GE10 (8x8)	3.41

#### **Plant A – Cycle 19**

Licensed Thermal Power: 1912 MWt (120% of OLTP)

Flow Range at Licensed Power: 48.5 to 49.0 Mlbm/hr (99 –100% of Rated Flow)

Nominal Cycle Length: 2 years

Core Loading:

Cycle Loaded	No. of Bundles	Fuel Type	Avg. Enrichment of Bundles Loaded
19	152	GE14 (10x10)	4.11
18	136	GE14 (10x10)	4.02
17	80	GE12 (10X10)	3.71

**Plant B – Cycle 9**

Licensed Thermal Power: 3758 MWt (105% of OLTP)

Flow Range at Licensed Power: 84.2 to 109.2 Mlbm/hr (81-105% of Rated Flow)

Nominal Cycle Length: 2 years

Core Loading:

Cycle Loaded	No. of Bundles	Fuel Type	Avg. Enrichment of Bundles Loaded
9	304	GE14 (10x10)	4.16
8	278	GE12 (10x10)	3.99
7	166	GE12 (10x10)	3.69

**Plant B – Cycle 10**

Licensed Thermal Power: 3758 MWt (105% of OLTP)

Flow Range at Licensed Power: 84.2 to 109.2 Mlbm/hr (81-105% of Rated Flow)

Nominal Cycle Length: 2 years

Core Loading:

Cycle Loaded	No. of Bundles	Fuel Type	Avg. Enrichment of Bundles Loaded
10	280	GE14 (10x10)	4.13
9	304	GE14 (10x10)	4.16
8	164	GE12 (10x10)	3.99



**Plant C – Cycle 30**

Licensed Thermal Power: 1096.9 MWt (110% of OLTP)

Flow Range at Licensed Power: 25.84 to 33.0 Mlbm/hr (87 –111% of Rated Flow)

Nominal Cycle Length: 1 year

Core Loading:

Cycle Loaded	No. of Bundles	Fuel Type	Avg. Enrichment of Bundles Loaded
30	40	GE14 (10x10)	4.19
29	40	GE14 (10x10)	4.05
28	40	GE14 (10x10)	3.91
27	36 4	GE14 (10x10) GE11(9x9)	3.86
26	8 32	GE14 (10x10) GE11(9x9)	3.71
25	8	GE11(9x9)	3.60
24	17	GE11(9x9)	3.80
22	15	GE11(9x9)	3.60

**Plant C – Cycle 31**

Licensed Thermal Power: 1096.9 MWt (110% of OLTP)

Flow Range at Licensed Power: 25.84 to 33.0 Mlbm/hr (87 –111% of Rated Flow)

Nominal Cycle Length: 1 year

Core Loading:

Cycle Loaded	No. of Bundles	Fuel Type	Avg. Enrichment of Bundles Loaded
31	40	GE14 (10x10)	4.19
30	40	GE14 (10x10)	4.19
29	40	GE14 (10x10)	4.05
28	40	GE14 (10x10)	3.91
27	36 4	GE14 (10x10) GE11 (9x9)	3.86
26	8 28	GE14 (10x10) GE11 (9x9)	3.69
25	4	GE11(9x9)	3.80

**Plant D – Cycle 15**

Licensed Thermal Power: 2923 MWt (120% of OLTP)

Flow Range at Licensed Power: 76.2 to 80.5 Mlbm/hr (99 –104.5% of Rated Flow)

Nominal Cycle Length: 2 years

Core Loading:

Cycle Loaded	No. of Bundles	Fuel Type	Avg. Enrichment of Bundles Loaded
15	246	GE14 (10x10)	4.21
14	246	GE14 (10x10)	4.23
13	68	GE13 (9x9)	4.04

**Plant E – Cycle 9**

Licensed Thermal Power: 3473 MWt (120% of OLTP)

Flow Range at Licensed Power: 83.7 to 88.7 Mlbm/hr (99 –105% of Rated Flow)

Nominal Cycle Length: 2 years

Core Loading:

Cycle Loaded	No. of Bundles	Fuel Type	Avg. Enrichment of Bundles Loaded
9	268	GE14 (10x10)	3.89
8	188	GE14 (10x10)	3.53
7	168	GE10 (8x8)	3.53

**Plant E – Cycle 10**

Licensed Thermal Power: 3473 MWt (120% of OLTP)

Flow Range at Licensed Power: 83.7 to 88.7 Mlbm/hr (99 –105% of Rated Flow)

Nominal Cycle Length: 2 years

Core Loading:

Cycle Loaded	No. of Bundles	Fuel Type	Avg. Enrichment of Bundles Loaded
10	312	GE14 (10x10)	4.21
9	268	GE14 (10x10)	3.89
8	44	GE14 (10x10)	3.54

**Core Tracking Data for Each of the Cycles Studied**

The core tracking data is provided in tabular form in this section. For each of the cycles studied, the Core Power, Core Flow, Power Density, Core Average Exit Void Fraction, Maximum

Channel Exit Void Fraction, Thermal Margins, and Hot Critical Eigenvalue will be provided as a function of cycle exposure. These data are taken directly from the exposure accounting analyses, and are based solely on calculations performed by the nuclear methods. There is no adaption to the process computer data included in these results. These results are provided in Tables 25-2 through 25-10.

The thermal margins are presented for each of the three related Tech Spec limits: Critical Power, Linear Heat Generation Rate and ECCS/LOCA. These limits are referred to as the MCPR, LHGR, and MAPLHGR limits, respectively. The core tracking data provides the ratio of the most limiting value of MCPR, LHGR, and MAPLHGR in the core to its respective limit. These ratios are identified as MFLCPR, MFLPD, and MAPRAT and are checked for compliance to Tech Specs by the core monitoring system. Thus, a statepoint with a MFLPD of 0.9 indicates that the highest LHGR in the core is 10% below the LHGR limit at this statepoint. Tables 25-2 through 25-10 shows that thermal margin values greater than 1.0 are infrequently obtained for MFLPD and MAPRAT. This is not unexpected for core states that are close to the thermal limits, since there is not perfect agreement between the nuclear methods and the plant monitoring measurements as formalized in the response to RAI 5-5. A MFLPD or MAPRAT value greater than 1.0 in these tables indicates that the nuclear methods over-predict the limiting nodal power at the given statepoint.

Cold critical eigenvalue data for each of the cycles studied is provided in Table 25-11. Cold critical data is provided for each point in the cycle where a cold critical test was performed. Table 25-11 shows the cycle exposure at which the test was performed, the measured cold critical eigenvalue, and the design basis eigenvalue which was selected for design purposes prior to operation. The design basis eigenvalues are selected by the responsible design engineer and are based on the prior history of the particular plant and known trends of the nuclear methods used for design. The measured cold critical eigenvalues are obtained by running the 3D Simulator at the same exposure and with the critical rod patterns used in the test. The eigenvalue calculated by the simulator is then corrected for the positive period measured during the test. The data in Table 25-11 include both distributed control rod patterns (as would occur during normal startup or shutdown) and local criticals where control rod(s) are withdrawn in a particular core location. Note that the design basis cold eigenvalue is not provided for Plant B, Cycle 9, and Plant E, Cycle 9. The reason for this exception is that when these cycles were being designed, PANAC10 was used, but the analysis of the test was performed with PANAC11. Therefore, the actual design basis eigenvalue was based on the earlier version of the 3D Simulator, and it would not be valid to compare it to the PANAC11-based measured eigenvalue.

### **TIP Data Summary for the Cycles Studied**

Summary core-wide statistics for the TIP data taken during the cycles studied is provided in Table 25-12. (TIP analyses for local four-bundle cells are provided in the responses to RAIs 27 and 29.) This table provides the cycle exposure at which the TIP data was taken, the core power and flow, the RMS differences between the TIP data and the power distribution calculated by the 3D Simulator, the core average and maximum channel exit void fractions, and the thermal margins calculated by the 3D Simulator at each of the TIP statepoints. The RMS differences are calculated for the Bundle (Radial), Axial and Nodal quantities at each statepoint. Definitions of

these quantities, and the equations used to calculate them are provided in the response to RAI 21 2.

TIP data for Plant D, Cycle 15 are not included in Table 25-12 because they are not yet available for processing for this cycle, which is currently in operation. However, Table 25-12 contains a significant amount of data at high power density from Cycles 9 and 10 of Plant E, which were licensed to 120% power.

### **Evaluation of the Core Tracking Data and TIP Comparisons**

The purpose of this section is to analyze the plant-specific data provided above to determine whether the nuclear methods are less accurate for higher in-channel void conditions and to explain any trends observed which may result from operation higher in the operating domain at higher power/flow ratios (e.g. from power uprate and in high power density plants). In addition, to analyze any trends that may be attributed to longer cycle lengths and higher cycle energies, both of which increase the cycle exposure.

The results of these analyses will be discussed relative to the current uncertainties and biases used in the NRC-approved analytical methods. The hot and cold critical eigenvalues and TIP data comparisons will yield biases and uncertainties that can be compared to the current uncertainties. [[

]] If the TIP response continues to confirm methods adequacy, it is statistically improbable that the [[ ]] would need to be revised. RAI 28 further addresses the relationship between the gamma scans and the SLMCPR uncertainties. RAI 30 addresses pin power peaking via lattice benchmarking, and requires development of uncertainties for both pin power peaking and bundle power.

To gain an appreciation of where the Reference Plants typically operate on the core Power/Flow Map, the Power/Flow Map is provided for each plant and the operating statepoints throughout each cycle are plotted on this map. Figures 25-1 through 25-9 provide these Power/Flow Maps. From these figures, it may be seen that the plants operate over a fairly wide flow range at, or near, licensed power. Plant A operates near licensed power between 90-100% flow, Plant B from 85-105% flow, Plant C from 90-111% flow, Plant D from 99-105% flow, and Plant E from 95-100% flow.

There is a scattering of data points on these Power/Flow maps at low power/low flow conditions. Plant A, Cycle 18, has the largest number of these data points, which makes it the ideal case to study the characteristics of these off-rated conditions. Of most interest for this study is the impact of power/flow state on exit void fractions. Figure 25-10 has been constructed to answer this question.

Figure 25-10 shows the core average exit and maximum channel exit void fractions for each data point on the Power/Flow map for this cycle (Figure 25-1). The data have been divided into two regions on the Power/Flow map, those at core flows <87%, and those at core flows >87%.

Consideration of Figure 25-1 shows that for the Plant A, Cycle 18 data, 87% flow is a convenient dividing line between the high power/high flow statepoints above 100% OLTP, and those off-rated points which are not only at lower power, but are at lower flows. Essentially the same result would have been obtained by dividing the data points into two sets above and below 100% OLTP, but a few low power points at high flow (with low void fractions) would have been included in the low power off-rated data set.

Figure 25-10 shows that while some of the low power/low flow state points result in core average and maximum channel exit void fractions that are close to those at high power, their exit void fractions do not exceed those for the high power statepoints. Also, the majority of the high exit void fraction data are from the high power conditions for which the flow is near the MELLLA Limit. While it may be possible for an off-rated point very close the MELLLA limit to have higher exit void fractions, the data shows that this is not a likely operating state, and because the preponderance of the data for high void operation is at high power, the amount of exposure accumulation in such an off-rated condition would be negligible.

The data in Figure 25-10 show that the off-rated conditions are not expected to result in exit void fractions greater than those produced at high power and flow. Secondly, because the accumulation of exposure in the core is predominantly the result of high power operation, the impact of off-rated conditions on exposure accumulation in the fuel is negligible. Therefore, it is concluded that the off-rated conditions at low core powers need not be considered to study of the effect of high voiding on the nuclear methods.

However, operation at the low end of the licensed flow range near rated power does occur frequently, and does result in the highest voiding conditions in the core. The impact on methods fidelity of these statepoints is considered in both RAIs 25 and 26.

### **Analysis of Hot Critical Eigenvalues**

In plant tracking calculations, the 3D Simulator (using cross sections generated from the lattice physics model, thermal-hydraulic models, and all other model assumptions) is used to simulate the behavior of a plant during operation. The reactor power, total core flow, pressure, inlet conditions, and reactivity control inventory as a function of cycle exposure are all involved in the prediction of the critical state of the core. The actual operating reactor is critical; hence, the calculated  $k_{\text{eff}}$  is compared to 1.0. Accurate and technically well-founded simulators calculate a  $k_{\text{eff}}$  that is predictable and should not vary appreciably from cycle-to-cycle for any particular plant. Any trends in fuel exposure should be small and reproducible. Consistency of  $k_{\text{eff}}$  bias ensures that accurate cycle length estimates are obtained in future core designs.

Figure 25-11 plots the hot critical eigenvalues for all the studied cycles. The trendline for all the eigenvalue data in Figure 25-11 “Linear (Trendline for all Data),” has been added to show the trend of the data with cycle exposure. This trend is very typical for the BWR hot critical eigenvalues predicted by GE's nuclear methods. The data which are widely dispersed from the trendline, particularly for Plant A, reflects substantial deviations from steady conditions and does not affect the ability of the plant to correctly determine end of full power capability. The RMS difference between the eigenvalue data for the studied cycles and the trendline is approximately

[[ ]], which is substantially the same as reported in NEDC-30130P-A (Steady-state Nuclear Methods, 1985.)

By comparing the individual cycle data to the trendline, [[ ]] This data will be discussed in more detail below, in the section that compares the hot critical eigenvalues of Plant E for Cycles 8 and 9.

Also, Plant C is somewhat different in that its eigenvalue decreases at a steeper slope than for the other plants. This plant is unique in that it is the smallest BWR in the GE fleet, and is the only Reference Plant that operates on an annual cycle. The eigenvalues for this plant are very repeatable from cycle-to-cycle, and therefore lead to reliable predictions for design purposes.

The impact of increases in power density, Power/Flow Ratio, and void fractions will be examined by analyzing the behavior of the hot critical eigenvalues before and after significant power increases at two different plants. By using data from the same plant, it is possible to get a more direct comparison of the impact of a power increase than by trying to compare the eigenvalues from two different plants that operate at different power densities. Plants A and E will each be analyzed since they have had significant power increases since the introduction of two-year cycles and 10x10 fuel.

### **Hot Critical Eigenvalues for Plant A, Cycle 18**

To study the impact of power density, Power/Flow Ratio and exit void fraction on hot critical eigenvalues, Plant A, Cycle 18 has been selected because it operated at 104% power during the first 4 GWD/ST of the cycle, and then increased its power to 112% for the remainder of the cycle (see Table 25-2). Figure 25-12 shows how core power and flow varied during this cycle. Note that when the power increased to 112%, the core flow remained at about the same value of 95%. Therefore, there should have been essentially a step change in core Power/Flow Ratio. The values of core Power/Flow Ratio, which is simply the ratio of the total core power to the total core flow, are shown in Figure 25-13. This figure shows that the core Power/Flow data are roughly divided at a value of 37, which is expressed in units of MWt/Mlbm/hr, before and after the power increase around 4 GWD/ST. Since exit void fractions are directly related to the core Power/Flow Ratio, exit void fractions were plotted vs. core Power/Flow Ratio in Figure 25-14. This figure shows that for both the core average and maximum channel exit void fractions, a core Power/Flow value of 37 is a reasonable boundary between the exit void fraction data before and after the power increase. Below 37, the exit void fractions increase appreciably with Power/Flow Ratio, but above 37, they tend to level off.

Finally, Figure 25-15 was constructed to examine the behavior of the hot critical eigenvalue as a function of core Power/Flow Ratio (and indirectly as a function of power density and exit void fraction) for Plant A, Cycle 18. This figure divides the eigenvalue data between those values obtained from operating states with a core Power/Flow Ratio below 37 MWt/Mlbm/hr, and those for which the core Power/Flow Ratio is above 37. The trend of the eigenvalues from one core Power/Flow region to the other shows no discontinuity between the two data sets, and indicates

that there is no discernible impact of the higher core Power/Flow Ratios (or the consequential higher void fractions and power densities) on the eigenvalue trend for this cycle.

### **Hot Critical Eigenvalues for Plant E, Cycles 8 and 9**

Another comparison of hot eigenvalues before and after a significant power uprate is made by comparing Cycles 8 and 9 for Plant E. Cycle 8 was the last cycle of operation prior to the 120% power uprate in Cycle 9. The Cycle 8 exposure accounting data are provided in Table 25-13 (at the end of this section), since this was not one of the high power density cycles included in Tables 25-2 thru 25-10.

Figure 25-16 compares the power density and core Power/Flow Ratio for Cycles 8 and 9. The power density increased by ~10%, from 52.5 kW/l in Cycle 8 to an average of about 58% in Cycle 9. The core Power/Flow Ratio also increased from ~37.5 to 41-42 MWt/Mlbm/hr. Also, the cycle exposure (and cycle energy) increased significantly from 11.5 to 16.0 GWD/ST. This increase in cycle energy was achieved by increasing the reload batch size from 188 to 268 GE14 bundles, and by increasing the average enrichment of the reload bundles from 3.53 to 3.89w/o.

Figure 25-17 compares the hot critical eigenvalues for Cycles 8, 9 and 10. This figure shows very little change in the eigenvalue from Cycle 8 to Cycle 9, in spite of the significant changes in cycle energy, power density, reload batch size, and reload enrichment.

As mentioned earlier, [[

]] as shown in both Figures 25-11 and 25-17. From the Power/Flow maps shown in Figures 25-8 and 25-9, it is clear that both Cycles 9 and 10 for Plant E operated at the essentially the same power (~115%) and over the same flow range at this power level. Thus, there is no difference in power density and Power/Flow Ratio, and no significant change in exit void fractions (see Tables 25-9 and 25-10) for these two cycles. [[

]] This was the first time such a large batch size had been used, and it resulted in a loading pattern that placed high reactivity fuel on the core periphery. This loading pattern resulted in higher fast neutron leakage from the core, which could be contributing to the hot eigenvalue differences. The TIP RMS differences presented in Table 25-12 for Cycle 10 indicate that the core power distribution is being tracked reliably for this cycle. From Table 25-11, the two cold eigenvalue data points show excellent agreement between the measured and design basis cold eigenvalues for Cycle 10, [[

]] Because fast neutron leakage in a cold, unvoided core is much less than at the hot condition, this also may be an indication that fast neutron leakage may be underestimated at high power by the nuclear methods for this unique core loading. This cycle is being closely monitored and will be studied further to understand its hot eigenvalue trend.

### **Conclusions**

The hot critical eigenvalues for the studied cycles, [[

]] show the same general trends as seen in previous BWR operating cycles. Examination of the impact of power density, Power/Flow Ratio, and void fractions on the hot eigenvalues showed no apparent sensitivity to these parameters for the two plants studied (A and E). [[

]] While the noted differences exist for the hot critical eigenvalues in this latest cycle, the cold critical eigenvalues and 3D power distribution comparisons to the TIP measurements are in good agreement.

Finally, it is noted that the significant increase in cycle energy for Plant E when transitioning from Cycle 8 to Cycle 9 did not result in a change in the hot critical eigenvalue trend with cycle exposure.

### **Analysis of Cold Critical Eigenvalues**

BWRs are designed so that they can be shut down in the cold condition (68°F) with the single strongest control blade completely withdrawn. In order to qualify the 3D Simulator to accurately predict the cold shutdown margin, cold critical startup configurations are analyzed. In all cases, enough control blades were withdrawn at a given water temperature for the reactor to be critical or on a large positive period. Accurate and technically well-founded simulators calculate a  $k_{\text{eff}}$  that is predictable and should not vary appreciably from cycle-to-cycle for any particular plant. Any trends in fuel exposure should be small and reproducible. Consistency of  $k_{\text{eff}}$  bias ensures that accurate shutdown margin estimates will be obtained in future core designs.

Figure 25-18 shows cold critical eigenvalue data for all of the studied cycles. These are the same measured eigenvalues presented in Table 25-11. For convenience, the linear trend line for all this data is plotted, “Linear (Trend Line using all Data),” showing the typical reduction in eigenvalue as the core depletes. This trend is very consistent with the eigenvalue trend used in the development of the nuclear design basis in the GNF reload design process. Although the startup sequence, configurations and conditions may vary considerably between plants, the data do not show greater than expected dispersion of the critical eigenvalues. These data also contain some local critical configurations. The RMS difference between the predicted Nuclear Design Basis eigenvalue (also provided in Table 25-11) and the actual measured critical eigenvalue is [[ ]]] for the cycles studied, which is substantially the same as the [[ ]]] reported in NEDC-30130P-A (Steady-State Nuclear Methods, 1985).

To determine if there was any sensitivity to power density, the RMS difference between predicted and measured cold critical eigenvalues was calculated for the three Reference plants with the highest power density. The RMS difference was [[ ]]] for these plants; namely, Plants B, D and E. Therefore, it is concluded that the cold critical eigenvalues show no discernible trend with power density. This behavior implies that there is also no trend with historical void fraction.

Next, the RMS difference between predicted and measured cold critical eigenvalues was calculated for Plant C, the only plant operating on an annual cycle. The RMS for both cycles studied for Plant C was [[ ]]]. This value is somewhat better than the [[ ]]] obtained for all the studied cycles, but the difference between these two values does not indicate a trend in accuracy with cycle length.



In conclusion, the analysis of the cold critical eigenvalues for all of the cycles studied shows that they are well predicted by the nuclear methods, and that there are no discernible trends in accuracy of this key parameter with power density, void fraction, or cycle length.

### **Uncertainties and biases in NRC-approved methods**

In addition to the prior examination of data from operating plant experience, the TIP data from the Reference Plants may be used to determine whether the uncertainties and biases in NRC approved analytical methods remain valid. This evaluation uses the TIP RMS data tabulated in Table 25-12. This data represents the RMS differences for all operable TIP strings at each reactor statepoint at which the TIP data were obtained. RAIs 27 and 29 deal directly with a more detailed comparison of the TIP and 3D Simulator results for hot channels and limiting four-bundle cells.

To determine if there are any observable trends in RMS differences as the power density is increased and the operating domain is expanded, it is necessary to identify a meaningful correlating parameter, such as power density, core Power/Flow Ratio, or exit void fractions. Power density alone does not directly include the impact of different core flows at the same power density, and as such is not an appropriate correlating parameter. The core average exit void fraction, or the maximum channel exit void fraction would appear to be good correlating parameters, but a review of Table 25-12 shows that they do not span a very large range for the studied plants, even though there is a fairly wide range of power densities and operating flow ranges. Therefore, the core Power/Flow Ratio has been selected as the correlating parameter since there is a direct relationship between this parameter and the amount of voiding in the core. It can easily be shown to be relevant to EPU/MELLLA+ conditions, and it covers a sufficiently broad range in the cycles studied to perform trending analyses.

All of the Reference Plants have Gamma TIPs except Plant E, which has Thermal Neutron TIPS. Because of the differences in the sensitivity of these TIP systems, the RMS differences also vary. Figure 25-19 plots the core-wide Bundle (Radial), Axial and Nodal RMS differences for each of the TIP statepoints for the Gamma TIP plants. Figure 25-20 provides the same data for the Thermal TIP plant.

[[

]]

Extrapolating the trend lines for the Gamma TIP plants to 50 MWt/Mlbm/hr, the Nodal and Axial RMS values would be on the order of 6%, while the Bundle RMS would be less than 2%. A Power/Flow Ratio of 50 MWt/Mlbm/hr is expected to bound the Power/Flow Ratio for EPU/MELLLA+ operation. For example, for Plant E, which is a BWR/6, and has the highest power density of the five Reference Plants, the Power/Flow Ratio at 120% power and 85% flow is 48.4 MWt/Mlbm/hr. The maximum Power/Flow Ratio for EPU/MELLLA+ occurs at 120% power and 85% flow.

The small number of data points in Figure 25-19 for the Thermal Neutron TIP plants is insufficient to draw any definite conclusions. [[

]]

It is interesting to note that for Plant E, Cycle10, the maximum RMS values recorded in Table 25-12 throughout the entire cycle were [[ ]] for the Bundle, Axial and Nodal RMS, respectively. This indicates that the power shapes generated by the 3D Simulator are in good agreement with the TIP measurements, even though this cycle has hot eigenvalues that were higher than expected early in the cycle.

The TIP comparison results are within the results previously provided to the NRC. Furthermore, the new results compare favorably with the uncertainties compiled earlier for TGBLA06/PANAC11. The quantity to consider is the RMS difference between the calculated and measured Bundle TIP response. This RMS difference is used in part to determine the bundle power uncertainty in the Process Computer and is an input to the SLMCPR evaluation. The results are summarized below for NEDE-32694 (Power Distribution Uncertainties for Safety Limit MCPR Evaluations, 1999), which is the basis for the SLMCPR evaluations, a set of comparisons documented in 1999 (NEDE-32773-R1) for the TGBLA06/ PANAC11 model, and the results quoted for this analysis taken from the eight cycles studied. The results are shown in Table 25-14.

The data in Figures 25-19 and 25-20 demonstrate that not only is the Bundle RMS difference calculated from the eight studied cycles applicable to the range of operating experience for the high power density cycles studied in this response, but that this population of data is consistent with previous experience, as illustrated in Table 25-14.

In conclusion, the global comparison of TIP RMS differences for the eight studied cycles shows good agreement between the TIP measurements and the 3D Simulator. [[

]]

**Table 25-1. Key Core Parameters for Reference Plants**

Plant	GE BWR Type	Number of Bundles	Original Licensed Thermal Power (OLTP) MWt	Rated Flow (Flow at OLTP) Mlbm/hr	License d Power Uprate (PU) % OLTP	Licensed Core Flow Range at PU % Rated Flow	Power Density at Licensed PU kW/l
A	BWR/4	368	1593	49.0	120	99-100	58.7
B	BWR/6	748	3579	104.0	105	81-105	56.8
C	BWR/4	240	997.2	29.7	110	87-111	51.7
D	BWR/4	560	2436	77.0	120	99-105	59.0
E	BWR/6	624	2894	84.5	120	99-107	62.9

NEDO-33173-A, Revision 1  
Non-Proprietary Information

**Table 25-2: Exposure Accounting Data for Plant A, Cycle 18**

Cycle Expo.	Core Power % OLTP	Core Flow % Rated	Power Density kW/l	Avg. Core Exit Void Fract.	Max. Chan. Exit Void Fract.	MFLCPR	MFLPD	MAPRAT	Hot Critical Eigenvalue
GWD/ST									
0.02	34.1	55.3	16.7	0.54	0.66	[[			
0.03	60.8	55.7	29.7	0.70	0.77				
0.17	77.9	79.2	38.1	0.70	0.77				
0.21	82.7	63.5	40.4	0.75	0.83				
0.34	104.2	98.1	51.0	0.73	0.81				
0.37	48.2	57.8	23.6	0.63	0.71				
0.38	83.7	65.6	40.9	0.75	0.82				
0.41	104.1	97.0	50.9	0.74	0.81				
0.72	104.0	96.9	50.9	0.73	0.81				
0.75	55.2	57.4	27.0	0.67	0.74				
0.78	104.1	94.9	50.9	0.74	0.82				
1.05	104.0	95.2	50.8	0.74	0.82				
1.16	103.9	93.2	50.8	0.74	0.82				
1.21	103.9	93.4	50.8	0.74	0.82				
1.25	89.0	72.2	43.5	0.75	0.83				
1.26	50.5	56.2	24.7	0.65	0.73				
1.28	103.7	97.8	50.7	0.73	0.81				
1.44	103.9	96.1	50.8	0.74	0.81				
1.61	104.1	94.6	50.9	0.74	0.82				
1.64	86.9	71.2	42.5	0.74	0.84				
1.66	103.9	97.8	50.8	0.73	0.83				
1.91	104.0	95.2	50.9	0.73	0.84				
2.14	104.1	94.5	50.9	0.74	0.84				
2.34	104.0	93.1	50.9	0.74	0.84				
2.66	104.1	93.6	50.9	0.74	0.84				
2.73	104.0	92.5	50.9	0.74	0.84				
3.04	104.0	93.3	50.9	0.74	0.84				
3.06	47.1	76.6	23.1	0.56	0.71				
3.07	50.0	68.4	24.5	0.59	0.74				
3.09	99.2	85.6	48.5	0.74	0.85				
3.21	103.8	96.2	50.8	0.73	0.84				
3.37	104.1	95.9	50.9	0.73	0.84				
3.41	103.8	95.6	50.8	0.73	0.84				
3.43	72.6	73.8	35.5	0.69	0.79				
3.45	94.2	75.1	46.1	0.75	0.86				
3.47	100.4	85.8	49.1	0.74	0.85				
3.51	104.0	92.4	50.8	0.74	0.85				
3.55	98.1	81.3	48.0	0.75	0.86				
3.57	104.0	91.8	50.8	0.74	0.85				
3.60	107.8	94.4	52.7	0.75	0.85				
3.69	110.5	95.6	54.0	0.75	0.86				

NEDO-33173-A, Revision 1  
Non-Proprietary Information

**Table 25-2: Exposure Accounting Data for Plant A, Cycle 18**

Cycle Expo.	Core Power % OLTP	Core Flow % Rated	Power Density kW/l	Avg. Core Exit Void Fract.	Max. Chan. Exit Void Fract.	MFLCPR	MFLPD	MAPRAT	Hot Critical Eigen-value
GWD/ST									
3.96	112.3	96.0	54.9	0.75	0.86				
4.50	111.7	94.5	54.6	0.75	0.86				
4.63	112.4	95.6	55.0	0.75	0.86				
4.64	59.9	61.3	29.3	0.67	0.77				
4.67	112.1	97.9	54.8	0.75	0.86				
4.96	111.0	98.6	54.3	0.74	0.86				
5.25	111.1	96.6	54.3	0.74	0.86				
5.26	53.1	49.8	26.0	0.67	0.78				
5.28	94.0	72.8	46.0	0.76	0.85				
5.31	111.0	93.2	54.3	0.75	0.85				
5.57	111.0	95.4	54.3	0.75	0.84				
5.77	111.0	94.1	54.3	0.75	0.85				
5.94	111.1	93.1	54.3	0.75	0.85				
6.13	111.0	96.4	54.3	0.75	0.84				
6.15	89.1	80.6	43.6	0.72	0.84				
6.17	108.7	88.6	53.1	0.76	0.85				
6.37	112.2	95.1	54.9	0.75	0.85				
6.57	112.2	94.4	54.9	0.75	0.85				
6.91	112.2	96.6	54.9	0.75	0.85				
7.16	112.3	94.7	54.9	0.75	0.85				
7.18	112.3	94.6	54.9	0.75	0.86				
7.40	112.5	96.6	55.0	0.75	0.86				
7.62	112.3	94.9	54.9	0.75	0.86				
7.82	112.4	93.8	55.0	0.75	0.86				
7.85	112.4	96.6	55.0	0.75	0.86				
7.88	76.2	64.9	37.3	0.72	0.85				
7.90	111.0	90.1	54.3	0.75	0.87				
7.92	112.3	95.9	54.9	0.75	0.86				
8.14	112.2	94.2	54.9	0.75	0.86				
8.42	112.4	93.7	55.0	0.75	0.87				
8.64	112.1	96.2	54.8	0.74	0.86				
8.86	112.3	95.6	54.9	0.75	0.86				
9.10	112.4	94.6	55.0	0.75	0.87				
9.13	111.2	98.2	54.4	0.74	0.86				
9.15	112.2	96.7	54.9	0.74	0.86				
9.42	112.3	95.3	54.9	0.75	0.87				
9.68	112.5	95.3	55.0	0.75	0.87				
9.69	47.3	60.4	23.1	0.57	0.77				
9.72	109.8	91.2	53.7	0.75	0.87				
9.74	112.2	95.2	54.9	0.75	0.87				
10.06	112.2	93.9	54.9	0.75	0.87				
10.09	109.2	94.6	53.4	0.74	0.86				

NEDO-33173-A, Revision 1  
Non-Proprietary Information

**Table 25-2: Exposure Accounting Data for Plant A, Cycle 18**

Cycle Expo.	Core Power % OLTP	Core Flow % Rated	Power Density kW/l	Avg. Core Exit Void Fract.	Max. Chan. Exit Void Fract.	MFLCPR	MFLPD	MAPRAT	Hot Critical Eigenvalue
GWD/ST									
10.11	66.8	65.0	32.7	0.68	0.83				
10.13	78.8	89.9	38.5	0.66	0.82				
10.18	77.8	59.5	38.1	0.73	0.86				
10.20	80.4	71.1	39.3	0.72	0.85				
10.22	112.4	94.1	55.0	0.75	0.87				
10.35	112.3	97.3	54.9	0.74	0.86				
10.62	112.2	96.0	54.9	0.74	0.86				
10.79	112.2	94.1	54.9	0.75	0.86				
11.01	112.3	95.4	54.9	0.75	0.86				
11.03	67.4	68.5	33.0	0.67	0.80				
11.04	77.2	67.9	37.8	0.71	0.83				
11.07	109.7	89.9	53.7	0.75	0.87				
11.26	112.5	97.1	55.0	0.74	0.85				
11.49	112.2	94.0	54.9	0.75	0.86				
11.71	112.3	96.3	54.9	0.74	0.85				
11.90	112.4	94.1	55.0	0.75	0.86				
12.13	112.3	96.8	54.9	0.74	0.85				
12.35	112.3	93.7	54.9	0.75	0.85				
12.57	112.4	97.1	55.0	0.74	0.85				
12.69	112.4	96.0	55.0	0.74	0.85				
12.91	112.4	97.0	55.0	0.74	0.86				
13.23	112.5	96.0	55.0	0.74	0.86				
13.25	84.6	73.8	41.4	0.72	0.85				
13.28	112.5	94.5	55.0	0.74	0.87				
13.37	112.4	97.7	55.0	0.74	0.86				
13.58	112.5	95.7	55.0	0.74	0.86				
13.59	71.2	53.6	34.8	0.73	0.85				
13.62	104.5	99.2	51.1	0.72	0.85				
13.64	112.2	97.7	54.9	0.74	0.86				
13.89	112.3	93.4	54.9	0.74	0.87				
13.98	112.3	96.8	54.9	0.74	0.86				
14.08	112.1	96.9	54.8	0.74	0.86				
14.16	112.4	98.1	55.0	0.73	0.86				
14.23	112.3	98.1	54.9	0.73	0.86				
14.30	112.4	98.7	55.0	0.73	0.86				
14.35	112.2	98.3	54.9	0.73	0.86				
14.45	112.3	98.3	54.9	0.73	0.86				]]

NEDO-33173-A, Revision 1  
Non-Proprietary Information

**Table 25-3: Exposure Accounting Data for Plant A, Cycle 19**

Cycle Expo.	Core Power	Core Flow	Power Density	Avg. Core Exit Void Fract.	Max. Chan. Exit Void Fract.	MFLCPR	MFLPD	MAPRAT	Hot Critical Eigen-value
GWD/ST	% OLTP	% Rated	kW/l						
0.02	62.6	65.2	30.6	0.68	0.75	[[			
0.04	109.0	88.8	53.3	0.76	0.83				
0.07	112.2	96.7	54.9	0.76	0.82				
0.19	112.3	96.5	54.9	0.76	0.82				
0.24	112.4	94.9	55.0	0.76	0.83				
0.51	112.4	96.3	55.0	0.76	0.83				
0.85	112.4	95.3	55.0	0.76	0.83				
1.10	112.4	93.3	55.0	0.76	0.83				
1.17	112.4	92.4	55.0	0.76	0.83				
1.47	112.4	94.6	55.0	0.76	0.84				
1.76	112.1	93.0	54.8	0.76	0.84				
2.06	112.4	94.8	55.0	0.76	0.84				
2.13	112.4	94.3	55.0	0.76	0.84				
2.38	112.3	93.9	54.9	0.76	0.84				
2.40	111.9	95.5	54.7	0.75	0.85				
2.43	112.3	97.4	54.9	0.75	0.85				
2.50	112.3	95.3	54.9	0.76	0.85				
2.72	112.3	94.8	54.9	0.76	0.85				
3.04	112.2	93.4	54.9	0.76	0.85				
3.06	112.2	93.2	54.9	0.76	0.85				
3.16	112.5	96.7	55.0	0.75	0.85				
3.38	112.4	96.4	55.0	0.75	0.85				
3.72	112.2	95.4	54.9	0.75	0.85				
4.04	112.5	94.1	55.0	0.76	0.86				
4.19	112.4	93.4	55.0	0.76	0.86				
4.36	112.3	92.9	54.9	0.76	0.86				
4.43	112.3	96.6	54.9	0.75	0.85				
4.51	112.5	97.8	55.0	0.75	0.84				
4.80	112.3	97.1	54.9	0.75	0.84				
4.87	31.9	52.2	15.6	0.53	0.66				
5.18	112.5	97.7	55.0	0.75	0.84				
5.41	112.4	98.1	55.0	0.75	0.84				
5.52	112.2	94.5	54.9	0.76	0.85				
5.79	112.2	96.6	54.9	0.75	0.84				
6.01	112.6	96.0	55.0	0.75	0.84				
6.26	112.3	94.3	54.9	0.76	0.85				
6.51	112.3	93.4	54.9	0.76	0.85				
6.73	112.4	92.1	55.0	0.76	0.85				
6.95	112.4	95.4	55.0	0.75	0.85				
6.97	92.8	99.1	45.4	0.70	0.80				
6.99	112.4	94.0	55.0	0.76	0.86				

NEDO-33173-A, Revision 1  
Non-Proprietary Information

**Table 25-3: Exposure Accounting Data for Plant A, Cycle 19**

Cycle Expo.	Core Power	Core Flow	Power Density	Avg. Core Exit Void Fract.	Max. Chan. Exit Void Fract.	MFLCPR	MFLPD	MAPRAT	Hot Critical Eigenvalue
GWD/ST	% OLTP	% Rated	kW/l						
7.22	112.4	94.2	55.0	0.75	0.86				
7.39	112.5	93.9	55.0	0.76	0.86				
7.61	112.5	92.4	55.0	0.76	0.86				
7.95	112.4	96.0	55.0	0.75	0.85				
8.13	112.4	94.1	55.0	0.75	0.86				
8.17	112.4	93.8	55.0	0.76	0.86				
8.19	96.9	95.1	47.4	0.72	0.82				
8.21	64.2	53.9	31.4	0.70	0.81				
8.24	112.2	97.4	54.9	0.75	0.85				
8.26	112.3	97.1	54.9	0.75	0.85				
8.28	59.3	54.5	29.0	0.69	0.78				
8.30	111.8	91.9	54.7	0.76	0.86				
8.57	112.2	96.7	54.9	0.75	0.85				
8.84	112.1	96.7	54.8	0.75	0.85				
9.02	112.4	95.9	55.0	0.75	0.86				
9.14	112.4	95.6	55.0	0.75	0.86				

]]



NEDO-33173-A, Revision 1  
Non-Proprietary Information

**Table 25-4: Exposure Accounting Data for Plant B, Cycle 9**

Cycle Expo.	Core Power	Core Flow	Power Density	Avg. Core Exit Void Fract.	Max. Chan. Exit Void Fract.	MFLCPR	MFLPD	MAPRAT	Hot Critical Eigen-value
GWD/ST	% OLTP	% Rated	kW/l						
0.26	105.1	100.0	56.8	0.74	0.83	[[			
0.39	104.8	99.0	56.7	0.74	0.83				
0.54	104.9	91.1	56.8	0.76	0.84				
0.79	104.9	90.8	56.8	0.76	0.84				
0.93	77.4	103.4	41.9	0.64	0.78				
1.16	104.9	96.4	56.8	0.74	0.83				
1.42	105.1	97.0	56.8	0.74	0.83				
1.61	104.9	94.4	56.7	0.75	0.84				
1.89	105.0	93.6	56.8	0.75	0.85				
2.20	104.9	90.4	56.8	0.76	0.85				
2.50	104.7	89.5	56.7	0.76	0.86				
2.80	105.1	88.5	56.8	0.76	0.86				
3.11	105.0	87.4	56.8	0.76	0.86				
3.41	104.7	84.8	56.7	0.77	0.87				
3.49	104.8	84.5	56.7	0.77	0.87				
3.69	105.0	86.1	56.8	0.76	0.87				
3.87	104.9	84.8	56.7	0.77	0.87				
4.12	104.9	85.2	56.7	0.77	0.87				
4.39	105.1	91.7	56.9	0.75	0.86				
4.67	105.0	90.4	56.8	0.75	0.86				
4.98	104.8	88.9	56.7	0.76	0.86				
5.22	104.9	88.8	56.7	0.76	0.86				
5.35	104.9	87.8	56.8	0.76	0.87				
5.47	89.3	91.4	48.3	0.71	0.81				
5.69	104.8	87.8	56.7	0.76	0.86				
5.92	105.0	87.9	56.8	0.76	0.86				
6.06	105.0	87.1	56.8	0.76	0.86				
6.23	104.7	96.9	56.6	0.74	0.85				
6.36	104.9	87.4	56.7	0.76	0.86				
6.63	104.9	87.2	56.8	0.76	0.87				
6.92	104.7	85.9	56.6	0.76	0.87				
7.20	104.8	97.5	56.7	0.74	0.86				
7.48	104.7	96.0	56.6	0.74	0.86				
7.76	105.0	95.1	56.8	0.74	0.86				
8.04	104.8	92.3	56.7	0.75	0.87				
8.31	105.1	89.9	56.9	0.75	0.87				
8.49	105.0	92.3	56.8	0.75	0.87				
8.74	104.9	93.6	56.8	0.75	0.86				
8.97	104.8	92.4	56.7	0.75	0.87				
9.20	104.9	90.5	56.8	0.75	0.87				
9.33	104.9	95.8	56.8	0.74	0.86				

NEDO-33173-A, Revision 1  
Non-Proprietary Information

**Table 25-4: Exposure Accounting Data for Plant B, Cycle 9**

Cycle Expo.	Core Power	Core Flow	Power Density	Avg. Core Exit Void Fract.	Max. Chan. Exit Void Fract.	MFLCPR	MFLPD	MAPRAT	Hot Critical Eigen-value
GWD/ST	% OLTP	% Rated	kW/l						
9.38	104.7	98.4	56.6	0.73	0.86				
9.58	105.0	100.6	56.8	0.73	0.85				
9.79	104.7	99.5	56.6	0.73	0.85				
10.06	104.9	100.7	56.7	0.73	0.85				
10.34	105.0	100.4	56.8	0.73	0.85				
10.56	105.2	100.0	56.9	0.73	0.85				
10.84	105.1	99.3	56.9	0.73	0.86				
11.12	105.0	99.3	56.8	0.73	0.85				
11.40	105.1	99.7	56.8	0.73	0.85				
11.70	105.1	100.0	56.8	0.73	0.85				
11.86	104.8	95.6	56.7	0.74	0.86				
12.00	101.2	103.4	54.7	0.71	0.85				
12.20	104.1	103.6	56.3	0.72	0.86				
12.37	103.2	103.9	55.8	0.71	0.85				
12.65	105.1	96.1	56.8	0.73	0.87				
12.93	105.0	100.0	56.8	0.73	0.86				
13.21	104.8	102.3	56.7	0.72	0.85				
13.26	104.5	103.5	56.5	0.72	0.85				
13.45	104.9	90.9	56.8	0.75	0.87				
13.71	105.1	94.5	56.8	0.74	0.86				
13.96	104.2	97.1	56.4	0.73	0.86				
14.24	104.7	97.9	56.6	0.73	0.86				
14.49	104.5	103.3	56.5	0.72	0.84				
14.76	104.9	103.0	56.8	0.72	0.85				
14.86	103.8	103.8	56.1	0.72	0.84				
15.03	104.5	103.9	56.5	0.71	0.85				
15.21	102.1	104.5	55.2	0.71	0.84				
15.34	101.1	105.0	54.7	0.70	0.83				
15.50	88.5	104.5	47.9	0.67	0.81				
15.63	87.5	104.3	47.3	0.67	0.80				
15.84	89.2	99.8	48.3	0.68	0.82				
15.99	89.1	104.2	48.2	0.67	0.81				
16.19	87.1	105.0	47.1	0.66	0.80				

]]

NEDO-33173-A, Revision 1  
Non-Proprietary Information

**Table 25-5: Exposure Accounting Data for Plant B, Cycle 10**

Cycle Expo.	Core Power	Core Flow	Power Density	Avg. Core Exit Void Fract.	Max. Chan. Exit Void Fract.	MFLCPR	MFLPD	MAPRAT	Hot Critical Eigen-value
GWD/ST	% OLTP	% Rated	kW/l						
0.19	104.8	100.8	56.7	0.73	0.84	[[			
0.27	104.9	102.5	56.8	0.73	0.84				
0.44	104.6	100.2	56.6	0.73	0.84				
0.52	104.6	101.5	56.6	0.73	0.83				
0.80	104.7	98.8	56.7	0.74	0.84				
1.08	104.7	98.6	56.7	0.74	0.84				
1.36	104.7	98.4	56.7	0.74	0.84				
1.64	105.0	97.2	56.8	0.74	0.84				
1.88	105.0	96.7	56.8	0.74	0.84				
2.10	105.0	96.5	56.8	0.73	0.85				
2.25	104.9	97.3	56.7	0.73	0.85				
2.45	104.8	95.7	56.7	0.74	0.85				
2.52	87.8	105.0	47.5	0.68	0.79				
2.71	104.8	92.2	56.7	0.75	0.85				
2.82	104.3	104.2	56.4	0.72	0.83				
3.07	104.8	93.3	56.7	0.75	0.85				
3.32	104.9	93.3	56.8	0.75	0.85				
3.58	105.0	93.4	56.8	0.75	0.85				
3.83	105.0	92.3	56.8	0.75	0.85				
4.10	105.0	92.7	56.8	0.75	0.85				
4.18	104.9	99.9	56.8	0.73	0.84				
4.46	104.9	95.0	56.7	0.74	0.86				
4.73	104.9	96.0	56.7	0.74	0.85				
5.01	104.9	94.5	56.7	0.74	0.86				
5.16	104.8	94.5	56.7	0.74	0.86				
5.22	100.4	104.0	54.3	0.71	0.84				
5.50	104.9	94.6	56.7	0.74	0.86				
5.77	104.8	94.1	56.7	0.74	0.86				
6.05	105.0	93.7	56.8	0.74	0.86				
6.33	105.1	93.3	56.8	0.74	0.86				
6.61	105.0	92.9	56.8	0.74	0.87				
6.74	105.0	91.3	56.8	0.75	0.87				
6.80	98.6	104.5	53.3	0.70	0.85				
7.08	104.9	96.9	56.7	0.73	0.86				
7.36	104.9	96.2	56.7	0.73	0.87				
7.64	104.9	95.3	56.8	0.74	0.87				
7.92	105.0	95.3	56.8	0.74	0.87				
8.20	104.8	94.0	56.7	0.74	0.87				
8.45	104.9	92.7	56.7	0.74	0.87				
8.68	105.0	92.3	56.8	0.74	0.88				
8.95	105.1	94.7	56.8	0.73	0.87				

NEDO-33173-A, Revision 1  
Non-Proprietary Information

**Table 25-5: Exposure Accounting Data for Plant B, Cycle 10**

Cycle Expo.	Core Power	Core Flow	Power Density	Avg. Core Exit Void Fract.	Max. Chan. Exit Void Fract.	MFLCPR	MFLPD	MAPRAT	Hot Critical Eigen-value
GWD/ST	% OLTP	% Rated	kW/l						
9.23	104.8	94.9	56.7	0.73	0.87				
9.51	105.0	95.0	56.8	0.73	0.87				
9.79	105.0	94.8	56.8	0.73	0.87				
10.07	105.1	94.5	56.9	0.73	0.87				
10.30	105.1	93.8	56.8	0.74	0.87				
10.53	104.8	94.5	56.7	0.73	0.87				
10.76	105.0	94.8	56.8	0.73	0.87				
11.01	104.7	98.5	56.6	0.72	0.87				
11.24	104.9	99.6	56.8	0.72	0.86				
11.47	104.7	99.9	56.6	0.72	0.86				
11.53	104.7	95.3	56.6	0.73	0.87				
11.63	104.9	91.2	56.7	0.74	0.88				
11.80	104.8	95.7	56.7	0.73	0.87				
12.08	104.8	97.0	56.7	0.73	0.87				]]

NEDO-33173-A, Revision 1  
Non-Proprietary Information

**Table 25-6: Exposure Accounting Data for Plant C, Cycle 30**

Cycle Expo.	Core Power	Core Flow	Power Density	Avg. Core Exit Void Fract.	Max. Chan. Exit Void Fract.	MFLCPR	MFLPD	MAPRAT	Hot Critical Eigenvalue
GWD/ST	% OLTP	% Rated	kW/l						
0.03	55.5	82.6	26.1	0.58	0.75	[[			
0.05	108.8	104.6	51.1	0.71	0.88				
0.12	109.5	115.3	51.5	0.70	0.86				
0.29	109.5	103.2	51.5	0.72	0.88				
0.43	109.8	105.6	51.6	0.71	0.88				
0.68	109.7	106.2	51.6	0.71	0.87				
0.94	109.7	106.1	51.6	0.71	0.87				
1.13	109.5	104.9	51.5	0.71	0.87				
1.43	109.6	104.0	51.5	0.72	0.88				
1.74	109.7	103.4	51.6	0.72	0.88				
1.85	109.7	101.6	51.6	0.72	0.89				
2.14	109.7	101.1	51.6	0.72	0.89				
2.25	109.8	100.8	51.6	0.72	0.89				
2.42	109.7	100.9	51.6	0.72	0.89				
2.53	109.7	100.7	51.6	0.72	0.89				
2.79	109.8	100.4	51.6	0.72	0.89				
3.05	109.4	100.4	51.4	0.72	0.89				
3.24	109.9	101.1	51.7	0.72	0.89				
3.33	109.6	101.8	51.5	0.72	0.87				
3.59	110.0	102.6	51.7	0.72	0.87				
3.72	109.7	104.1	51.6	0.71	0.87				
3.73	60.4	85.0	28.4	0.59	0.77				
3.75	109.4	117.2	51.4	0.69	0.86				
3.77	109.3	98.8	51.4	0.72	0.89				
3.84	109.7	95.3	51.6	0.73	0.90				
4.01	109.6	97.3	51.5	0.72	0.90				
4.22	109.6	98.4	51.5	0.72	0.90				
4.38	109.6	100.7	51.5	0.72	0.89				
4.55	109.6	103.0	51.5	0.71	0.89				
4.71	109.7	106.8	51.6	0.71	0.88				
4.87	109.8	108.3	51.6	0.70	0.88				
5.04	109.9	111.3	51.7	0.70	0.87				
5.18	109.9	114.1	51.7	0.69	0.87				
5.34	106.7	93.9	50.1	0.72	0.90				
5.50	106.0	93.9	49.8	0.72	0.89				
5.64	109.7	103.8	51.6	0.71	0.89				
5.85	109.6	108.8	51.5	0.70	0.88				
6.06	108.9	113.7	51.2	0.69	0.87				
6.25	109.7	113.7	51.6	0.68	0.87				
6.34	109.7	113.4	51.6	0.68	0.87				
6.37	109.1	104.6	51.3	0.71	0.88				

NEDO-33173-A, Revision 1  
Non-Proprietary Information

**Table 25-6: Exposure Accounting Data for Plant C, Cycle 30**

Cycle Expo.	Core Power	Core Flow	Power Density	Avg. Core Exit Void Fract.	Max. Chan. Exit Void Fract.	MFLCPR	MFLPD	MAPRAT	Hot Critical Eigen-value
GWD/ST	% OLTP	% Rated	kW/l						
6.39	98.8	104.6	46.4	0.68	0.86				
6.41	104.9	114.6	49.3	0.68	0.86				
6.43	106.1	116.0	49.9	0.68	0.86				
6.45	85.1	83.9	40.0	0.68	0.87				
6.48	93.5	93.8	43.9	0.68	0.87				
6.56	95.2	98.6	44.7	0.68	0.86				
6.69	105.3	114.6	49.5	0.67	0.86				
6.79	86.1	88.2	40.5	0.67	0.86				
6.85	97.8	114.0	46.0	0.66	0.84				
6.91	105.1	118.3	49.4	0.65	0.85				
7.07	103.4	119.0	48.6	0.65	0.84				
7.24	87.6	101.7	41.2	0.65	0.84				
7.31	80.7	89.3	37.9	0.65	0.84				
7.38	88.0	108.1	41.4	0.64	0.83				
7.48	91.9	118.5	43.2	0.63	0.82				
7.54	87.1	113.8	41.0	0.63	0.81				
7.60	73.4	82.4	34.5	0.64	0.83				]]

NEDO-33173-A, Revision 1  
Non-Proprietary Information

**Table 25-7: Exposure Accounting Data for Plant C, Cycle 31**

Cycle Expo.	Core Power	Core Flow	Power Density	Avg. Core Exit Void Fract.	Max. Chan. Exit Void Fract.	MFLCPR	MFLPD	MAPRAT	Hot Critical Eigen-value
GWD/ST	% OLTP	% Rated	kW/l						
0.01	48.4	70.3	22.8	0.58	0.74	[[			
0.02	53.9	82.6	25.3	0.59	0.74				
0.04	66.5	70.0	31.2	0.66	0.81				
0.06	109.5	95.7	51.5	0.74	0.89				
0.13	109.6	101.1	51.5	0.72	0.88				
0.27	109.9	103.3	51.7	0.72	0.88				
0.38	109.8	104.3	51.6	0.72	0.87				
0.50	103.4	94.2	48.6	0.72	0.88				
0.66	110.0	105.4	51.7	0.72	0.87				
0.82	109.9	105.4	51.7	0.72	0.87				
0.98	109.6	105.1	51.5	0.72	0.87				
1.15	109.7	104.5	51.6	0.72	0.87				
1.31	110.0	104.5	51.7	0.72	0.87				
1.47	109.9	104.2	51.7	0.72	0.87				
1.68	109.8	100.9	51.6	0.72	0.87				
1.89	109.8	100.4	51.6	0.72	0.87				
2.10	109.9	99.9	51.7	0.72	0.87				
2.31	109.7	99.2	51.6	0.72	0.87				
2.45	109.8	98.9	51.6	0.72	0.87				
2.61	110.1	98.9	51.8	0.72	0.87				
2.78	109.7	98.3	51.6	0.72	0.87				
2.94	109.6	98.2	51.5	0.72	0.87				
3.10	109.5	100.0	51.5	0.72	0.87				
3.26	109.8	100.0	51.6	0.73	0.87				
3.43	109.8	100.0	51.6	0.73	0.87				
3.59	109.9	100.3	51.7	0.72	0.87				
3.75	109.8	100.9	51.6	0.72	0.87				
3.92	110.1	102.1	51.8	0.72	0.87				
4.10	109.7	102.6	51.6	0.72	0.86				
4.29	109.3	103.8	51.4	0.72	0.86				
4.47	109.8	105.0	51.6	0.71	0.86				
4.61	109.6	98.0	51.5	0.72	0.88				
4.77	109.6	98.6	51.5	0.72	0.88				
4.94	109.7	100.2	51.6	0.72	0.88				
5.10	109.8	102.0	51.6	0.72	0.88				
5.26	109.7	103.8	51.6	0.71	0.87				
5.38	109.7	106.7	51.6	0.71	0.87				
5.59	109.5	108.6	51.5	0.70	0.87				
5.70	109.9	111.6	51.7	0.70	0.86				

NEDO-33173-A, Revision 1  
Non-Proprietary Information

**Table 25-7: Exposure Accounting Data for Plant C, Cycle 31**

Cycle Expo.	Core Power	Core Flow	Power Density	Avg. Core Exit Void Fract.	Max. Chan. Exit Void Fract.	MFLCPR	MFLPD	MAPRAT	Hot Critical Eigen-value
GWD/ST	% OLTP	% Rated	kW/l						
5.86	109.5	97.0	51.5	0.72	0.90				
6.07	109.5	99.2	51.5	0.72	0.89				
6.28	109.7	103.0	51.6	0.71	0.89				
6.49	109.8	107.6	51.6	0.70	0.88				
6.61	109.8	111.8	51.6	0.69	0.87				
6.72	109.6	116.4	51.5	0.68	0.86				
6.96	109.7	115.7	51.6	0.68	0.86				
7.16	109.9	117.1	51.7	0.67	0.86				
7.28	109.3	117.5	51.4	0.67	0.85				
7.39	108.2	117.8	50.8	0.66	0.85				
7.58	97.0	112.0	45.6	0.66	0.84				
7.67	103.8	118.3	48.8	0.65	0.84				
7.83	90.3	104.1	42.5	0.66	0.84				]]



NEDO-33173-A, Revision 1  
Non-Proprietary Information

**Table 25-8: Exposure Accounting Data for Plant D, Cycle 15**

Cycle Expo.	Core Power	Core Flow	Power Density	Avg. Core Exit Void Fract.	Max. Chan. Exit Void Fract.	MFLCPR	MFLPD	MAPRAT	Hot Critical Eigen-value
GWD/ST	% OLTP	% Rated	kW/l						
0.35	119.9	103.2	59.0	0.75	0.84	[[			
0.62	119.9	103.1	58.9	0.75	0.84				
0.88	120.1	101.4	59.0	0.75	0.84				
1.15	120.0	101.3	59.0	0.76	0.84				
1.41	120.2	104.1	59.1	0.75	0.84				
1.73	120.0	101.6	59.0	0.76	0.84				
1.87	120.0	103.8	59.0	0.75	0.83				
2.11	119.9	101.5	59.0	0.76	0.84				
2.38	119.8	99.6	58.9	0.76	0.84				
2.64	119.7	99.9	58.9	0.76	0.84				
2.83	119.9	102.2	59.0	0.75	0.84				
2.97	120.0	103.3	59.0	0.75	0.84				
3.23	119.6	102.1	58.8	0.75	0.84				
3.40	119.9	101.5	59.0	0.76	0.84				
3.59	119.9	103.0	58.9	0.75	0.84				
3.86	120.0	103.0	59.0	0.75	0.84				
4.12	119.8	101.6	58.9	0.76	0.84				
4.39	119.9	101.1	58.9	0.76	0.84				
4.65	120.1	99.9	59.1	0.76	0.85				
4.85	120.1	101.1	59.1	0.76	0.85				
5.12	120.0	101.8	59.0	0.76	0.84				
5.25	119.8	100.5	58.9	0.76	0.85				
5.38	119.9	102.1	58.9	0.75	0.85				
5.64	119.7	100.9	58.9	0.76	0.85				
5.91	120.1	103.2	59.0	0.75	0.85				
6.17	120.0	103.0	59.0	0.75	0.85				
6.44	119.9	101.4	58.9	0.76	0.86				
6.73	120.0	103.0	59.0	0.75	0.86				
6.99	120.1	102.1	59.1	0.75	0.86				

]]

NEDO-33173-A, Revision 1  
Non-Proprietary Information

**Table 25-9: Exposure Accounting Data for Plant E, Cycle 9**

Cycle Expo.	Core Power	Core Flow	Power Density	Avg. Core Exit Void Fract.	Max. Chan. Exit Void Fract.	MFLCPR	MFLPD	MAPRAT	Hot Critical Eigen-value
GWD/ST	% OLTP	% Rated	kW/l						
0.28	111.1	92.5	58.2	0.75	0.87	[[			
0.58	111.0	97.8	58.2	0.74	0.86				
0.89	111.3	97.9	58.3	0.74	0.86				
1.16	113.3	98.2	59.4	0.75	0.86				
1.38	113.8	98.1	59.6	0.75	0.86				
1.64	113.4	93.7	59.4	0.76	0.87				
1.85	113.6	93.7	59.5	0.76	0.87				
2.06	113.4	95.8	59.4	0.75	0.86				
2.33	113.5	95.2	59.5	0.76	0.86				
2.60	113.5	94.8	59.5	0.76	0.86				
2.89	113.3	96.0	59.4	0.75	0.86				
3.08	112.7	93.1	59.1	0.76	0.87				
3.34	112.6	93.5	59.0	0.76	0.86				
3.60	111.7	92.6	58.5	0.76	0.86				
3.91	111.5	94.0	58.5	0.76	0.86				
4.23	111.1	92.6	58.2	0.76	0.86				
4.54	109.8	91.0	57.6	0.76	0.87				
4.82	109.5	92.3	57.4	0.75	0.86				
5.11	109.7	91.2	57.5	0.76	0.87				
5.26	109.5	90.6	57.4	0.76	0.87				
5.42	109.5	90.2	57.4	0.76	0.87				
5.66	109.5	91.1	57.4	0.76	0.87				
5.96	109.6	89.8	57.4	0.76	0.87				
6.14	109.4	91.2	57.4	0.76	0.87				
6.32	109.6	89.5	57.4	0.76	0.87				
6.59	109.3	95.3	57.3	0.75	0.86				
6.85	109.3	93.5	57.3	0.75	0.87				
7.06	109.3	92.1	57.3	0.76	0.87				
7.24	109.5	91.3	57.4	0.76	0.87				
7.39	109.6	92.4	57.4	0.76	0.87				
7.54	109.3	91.7	57.3	0.76	0.87				
7.70	109.4	90.1	57.3	0.76	0.87				
7.90	109.4	92.5	57.3	0.76	0.87				
8.11	109.1	90.4	57.2	0.76	0.87				
8.34	109.2	90.6	57.2	0.76	0.87				
8.47	109.3	91.6	57.3	0.76	0.87				
8.62	109.2	91.2	57.2	0.76	0.87				
8.76	109.1	93.1	57.2	0.75	0.87				
8.94	109.1	92.9	57.2	0.75	0.87				

NEDO-33173-A, Revision 1  
Non-Proprietary Information

**Table 25-9: Exposure Accounting Data for Plant E, Cycle 9**

Cycle Expo.	Core Power	Core Flow	Power Density	Avg. Core Exit Void Fract.	Max. Chan. Exit Void Fract.	MFLCPR	MFLPD	MAPRAT	Hot Critical Eigen-value
GWD/ST	% OLTP	% Rated	kW/l						
9.01	109.2	93.0	57.2	0.75	0.87				
9.14	109.4	93.0	57.3	0.75	0.87				
9.30	109.6	92.2	57.5	0.76	0.87				
9.48	109.6	91.9	57.4	0.76	0.87				
9.62	109.6	93.2	57.4	0.76	0.87				
9.83	111.6	93.7	58.5	0.76	0.87				
10.02	111.1	93.2	58.2	0.76	0.87				
10.20	111.5	93.7	58.4	0.76	0.87				
10.28	111.8	94.9	58.6	0.76	0.87				
10.54	111.9	95.3	58.7	0.76	0.86				
10.78	111.5	95.2	58.5	0.76	0.86				
10.94	112.1	97.0	58.8	0.76	0.86				
11.12	112.0	95.0	58.7	0.76	0.86				
11.30	111.9	95.3	58.6	0.76	0.86				
11.49	112.4	94.8	58.9	0.76	0.86				
11.62	112.1	93.4	58.8	0.76	0.87				
11.70	112.1	96.4	58.8	0.75	0.87				
11.86	112.2	95.2	58.8	0.76	0.86				
12.07	112.4	94.9	58.9	0.76	0.86				
12.23	112.4	97.1	58.9	0.76	0.86				
12.31	111.8	93.3	58.6	0.76	0.86				
12.44	111.6	96.3	58.5	0.76	0.86				
12.49	109.1	96.9	57.2	0.75	0.86				
12.77	109.5	94.0	57.4	0.75	0.86				
12.95	109.3	93.1	57.3	0.76	0.86				
13.13	108.9	92.5	57.1	0.76	0.86				
13.31	108.9	92.6	57.1	0.76	0.86				
13.49	108.9	95.3	57.1	0.75	0.85				
13.74	109.0	94.6	57.1	0.75	0.85				
13.83	111.4	99.1	58.4	0.75	0.85				
14.14	111.5	98.7	58.4	0.75	0.85				
14.43	110.0	102.6	57.6	0.74	0.83				
14.62	107.2	103.0	56.2	0.73	0.83				
14.84	105.1	103.4	55.1	0.73	0.82				
14.93	103.5	103.8	54.2	0.72	0.82				
15.20	105.1	103.9	55.1	0.72	0.81				
15.49	101.1	102.9	53.0	0.71	0.81				
15.76	97.7	105.0	51.2	0.70	0.79				
15.98	93.7	105.6	49.1	0.68	0.78				

]]

NEDO-33173-A, Revision 1  
Non-Proprietary Information

**Table 25-10: Exposure Accounting Data for Plant E, Cycle 10**

Cycle Expo.	Core Power	Core Flow	Power Density	Avg. Core Exit Void Fract.	Max. Chan. Exit Void Fract.	MFLCPR	MFLPD	MAPRAT	Hot Critical Eigen-value
GWD/ST	% OLTP	% Rated	kW/l						
0.17	111.1	95.5	58.2	0.76	0.84	[[			
0.36	111.5	100.5	58.5	0.75	0.83				
0.54	111.5	98.2	58.4	0.76	0.84				
0.61	111.5	97.9	58.4	0.76	0.84				
0.91	111.2	95.6	58.3	0.76	0.84				
1.19	111.3	95.0	58.3	0.76	0.84				
1.49	113.3	97.7	59.4	0.76	0.84				
1.78	113.6	97.2	59.6	0.76	0.85				
1.84	57.7	75.0	30.2	0.63	0.79				
2.08	114.1	94.9	59.8	0.77	0.85				
2.32	113.8	95.8	59.7	0.76	0.85				
2.56	114.4	96.3	60.0	0.77	0.85				
2.83	114.0	94.0	59.8	0.77	0.86				
2.91	114.1	94.4	59.8	0.77	0.85				
3.13	114.1	94.1	59.8	0.77	0.86				
3.34	114.3	94.7	59.9	0.77	0.86				
3.39	114.5	97.1	60.0	0.76	0.85				
3.65	114.4	96.4	59.9	0.77	0.86				
3.92	114.3	97.1	59.9	0.76	0.86				
4.19	114.5	96.6	60.0	0.77	0.86				
4.45	114.5	95.7	60.0	0.77	0.86				
4.56	114.4	96.0	59.9	0.77	0.86				

]]

NEDO-33173-A, Revision 1  
Non-Proprietary Information

<b>Table 25-11. Cold Critical Eigenvalues for All Studied Cycles</b>			
<b>Plant, Cycle</b>	<b>Cycle Exposure GWD/ST</b>	<b>Measured Cold Critical Eigenvalue</b>	<b>Nuclear Design Basis Cold Critical Eigenvalue</b>
Plant A, C18	0.00	[]	
	3.04		
	6.13		
	7.85		
	9.68		
	13.58		
Plant A, C19	0.00		
	4.80		
	4.87		
Plant B, C9	0.00		
	11.86		
Plant B, C10	0.00		
	0.00		
	8.68		
Plant C, C30	0.00		
	0.00		
	0.00		
	6.34		
	7.60		
	7.60		
	7.60		
	7.60		
Plant C, C31	0.00		
	0.00		
	0.00		
	0.00		
	0.00		
	0.00		
	0.00		
	0.00		
	7.83		
	7.83		
7.83			
Plant D, C15	0.00		
	3.4		
Plant E, C 9	0.00		
Plant E, C 10	0		
	3.4		[]

NOTE: PANAC10 was used to design both of these cycles, using PANAC10-based eigenvalues for the Nuclear Design Basis. The tests, however were evaluated with PANAC11, for which there were no Nuclear Design Basis eigenvalues defined.

NEDO-33173-A, Revision 1  
Non-Proprietary Information

<b>Table 25-12. TIP Comparisons for the Studied Cycles</b>										
Cycle Expo.	Core Power	Core Flow	Bundle RMS	Axial RMS	Nodal RMS	Avg. Core Exit Void Fract.	Max Chan. Exit Void Fract.	MFLCPR	MFLPD	MAPRAT
GWD/ST	%OLTP	% Rated	%	%	%					
<b>Plant A – Cycle 18</b>										
2.34	104.0	93.6	[[			0.74	0.84	[[		
3.37	103.4	94.2				0.73	0.84			
4.18	112.2	94.4			]]	0.75	0.86			]]
<b>Plant A – Cycle 19</b>										
0.24	112.4	94.8	[[			0.76	0.83	[[		
1.17	112.5	92.8				0.76	0.83			
2.13	112.4	94.3				0.76	0.84			
2.50	112.3	95.4				0.75	0.85			
3.16	112.3	96.9				0.75	0.85			
4.19	112.5	93.6				0.76	0.86			
4.51	112.2	97.6				0.75	0.84			
5.18	112.5	97.9				0.75	0.84			
6.26	112.3	94.4				0.76	0.85			
7.22	112.4	94.4				0.75	0.86			
8.13	112.6	94.3				0.75	0.86			
9.02	112.6	96.0			]]	0.75	0.86			]]
<b>Plant B – Cycle 9</b>										
0.26	104.8	99.4	[[			0.74	0.83	[[		
0.54	104.9	90.6				0.76	0.84			
0.79	104.9	91.1				0.76	0.84			
1.42	104.8	96.9				0.74	0.83			
1.61	105.0	94.9				0.75	0.84			
2.20	104.6	89.7				0.76	0.85			
2.50	104.9	89.7				0.76	0.86			
3.41	104.6	85.7				0.76	0.87			
3.87	104.6	85.0				0.76	0.87			
4.39	105.0	92.1				0.75	0.86			
5.92	104.7	87.6				0.76	0.86			
6.92	105.1	86.4				0.76	0.87			
7.20	105.0	98.0				0.74	0.86			
7.76	104.9	95.5				0.74	0.86			
8.49	105.0	92.9				0.75	0.87			
9.20	105.0	91.0				0.75	0.87			
9.58	96.8	103.9				0.70	0.82			
10.06	105.1	100.6				0.73	0.85			
10.34	104.8	99.6				0.73	0.85			
11.12	105.1	99.5				0.73	0.85			
12.00	101.1	103.3				0.71	0.85			
13.21	104.6	101.3				0.72	0.85			

NEDO-33173-A, Revision 1  
Non-Proprietary Information

<b>Table 25-12. TIP Comparisons for the Studied Cycles</b>										
Cycle Expo.	Core Power	Core Flow	Bundle RMS	Axial RMS	Nodal RMS	Avg. Core Exit Void Fract.	Max Chan. Exit Void Fract.	MFLCPR	MFLPD	MAPRAT
GWD/ST	%OLTP	% Rated	%	%	%					
13.71	104.8	93.1				0.74	0.87			
14.24	104.9	97.2				0.73	0.86			
14.49	104.1	102.9				0.72	0.84			
14.76	104.6	102.1				0.72	0.85			
15.21	102.8	104.1				0.71	0.84			
15.63	88.1	103.5				0.67	0.81			
15.99	89.2	103.6			]]	0.67	0.81			]]
<b>Plant B – Cycle 10</b>										
0.19	94.1	102.7	[[			0.70	0.80	[[		
0.27	104.5	102.1				0.73	0.83			
0.80	105.0	98.1				0.74	0.84			
1.64	104.9	96.9				0.74	0.84			
2.45	105.0	96.7				0.74	0.85			
4.10	104.9	92.3				0.75	0.85			
4.18	105.0	92.6				0.75	0.85			
4.46	104.9	95.6				0.74	0.85			
5.01	104.9	95.5				0.74	0.86			
5.77	104.9	94.0				0.74	0.86			
6.61	104.9	93.0				0.74	0.87			
7.08	104.8	97.4				0.73	0.86			
7.92	104.9	95.4				0.74	0.87			
8.20	105.1	95.4				0.74	0.87			
8.68	105.0	92.3			]]	0.74	0.88			]]
<b>Plant C – Cycle 30</b>										
0.43	110.0	98.2	[[			0.71	0.88	[[		
1.13	109.8	97.7				0.71	0.87			
1.85	109.8	94.7				0.71	0.88			
2.25	109.5	93.8				0.72	0.89			
2.53	109.8	93.4				0.72	0.89			
3.33	109.7	94.5				0.72	0.87			
3.84	109.9	88.6				0.73	0.90			
4.01	109.9	90.2				0.73	0.90			
4.71	109.5	98.9				0.71	0.88			
5.34	106.7	87.0				0.72	0.90			
6.25	109.5	105.7				0.68	0.87			
6.48	94.3	88.5				0.68	0.87			
6.91	105.1	109.8				0.65	0.85			
0.50	103.7	87.7				0.72	0.88			
0.98	110.2	97.8				0.72	0.87			
1.68	110.0	93.7				0.72	0.87			
2.45	109.9	92.3				0.72	0.87			
3.10	109.7	93.0				0.72	0.87			
3.92	109.9	94.8				0.72	0.87			

NEDO-33173-A, Revision 1  
Non-Proprietary Information

<b>Table 25-12. TIP Comparisons for the Studied Cycles</b>										
Cycle Expo.	Core Power	Core Flow	Bundle RMS	Axial RMS	Nodal RMS	Avg. Core Exit Void Fract.	Max Chan. Exit Void Fract.	MFLCPR	MFLPD	MAPRAT
GWD/ST	%OLTP	% Rated	%	%	%					
4.61	109.6	90.9				0.72	0.88			
5.38	109.6	99.1				0.71	0.87			
5.86	109.7	90.1				0.72	0.90			
6.72	109.5	107.8				0.68	0.86			
7.28	109.3	109.2			]]	0.66	0.85			]]
<b>Plant E – Cycle 9</b>										
0.25	111.1	92.6	[[			0.75	0.87	[[		
0.51	111.2	98.2				0.74	0.86			
3.72	111.7	94.0				0.76	0.86			
3.77	111.6	94.7				0.75	0.86			
4.78	109.8	92.5				0.75	0.86			
5.69	109.5	90.9				0.76	0.87			
7.54	109.3	90.8				0.76	0.87			
9.31	109.5	92.5				0.76	0.87			
10.20	111.5	93.7				0.76	0.87			
11.03	112.0	94.6				0.76	0.87			
11.98	112.2	95.0				0.76	0.86			
12.91	109.0	94.0				0.75	0.86			
14.62	106.0	103.2				0.73	0.82			
15.40	100.8	104.3			]]	0.70	0.80			]]
<b>Plant E – Cycle 10</b>										
0.14	111.7	95.4	[[			0.76	0.84	[[		
0.79	111.0	93.9				0.76	0.84			
1.71	113.5	95.6				0.77	0.85			
2.47	114.6	96.6				0.76	0.85			
3.58	114.2	96.2				0.77	0.86			
5.73	113.8	97.5				0.76	0.85			
6.58	113.3	96.6				0.76	0.85			
7.38	113.9	95.9				0.77	0.86			
8.45	110.8	95.8			]]	0.76	0.86			]]



NEDO-33173-A, Revision 1  
Non-Proprietary Information

**Table 25-13: Exposure Accounting Data for Plant E, Cycle 8**

Cycle Expo.	Core Power	Core Flow	Power Density	Power/Flow Ratio	Hot Critical Eigenvalue
GWD/ST	% OLTP	% Rated	kW/l	MWt/Mlbm/hr	
0.24	99.9	92.8	52.3	36.8	[[
0.47	100.0	96.6	52.4	35.4	
0.63	100.0	90.1	52.4	38.0	
0.84	100.0	89.9	52.4	38.1	
1.05	99.9	88.8	52.4	38.6	
1.19	100.1	90.1	52.5	38.0	
1.38	100.0	90.5	52.4	37.8	
1.57	99.9	90.9	52.4	37.7	
1.73	99.8	90.6	52.3	37.7	
1.85	99.9	91.1	52.4	37.6	
1.90	99.8	100.5	52.3	34.0	
2.08	99.7	83.7	52.3	40.8	
2.22	100.1	90.1	52.5	38.0	
2.34	100.0	95.0	52.4	36.0	
2.43	100.0	100.0	52.4	34.3	
2.77	99.9	92.6	52.4	37.0	
2.95	100.0	93.1	52.4	36.8	
3.26	100.0	93.6	52.4	36.6	
3.54	100.0	94.3	52.4	36.3	
3.75	99.9	94.7	52.4	36.1	
3.92	99.9	95.2	52.4	36.0	
4.06	99.9	94.9	52.4	36.1	
4.25	100.0	94.9	52.4	36.1	
4.39	100.0	95.0	52.4	36.1	
4.58	99.9	89.3	52.4	38.3	
4.79	100.0	89.5	52.4	38.3	
5.09	100.0	89.8	52.4	38.1	
5.40	100.0	88.7	52.4	38.6	
5.71	100.0	88.8	52.4	38.6	
5.95	100.1	87.2	52.5	39.3	
6.23	99.9	87.1	52.4	39.3	
6.51	99.9	86.6	52.4	39.5	
6.61	99.9	89.9	52.4	38.1	
6.70	99.6	91.5	52.2	37.3	
6.89	99.5	95.8	52.2	35.6	
7.10	100.0	96.0	52.4	35.6	
7.38	100.0	89.8	52.4	38.1	
7.66	99.6	89.9	52.2	37.9	
7.92	100.0	90.6	52.4	37.8	

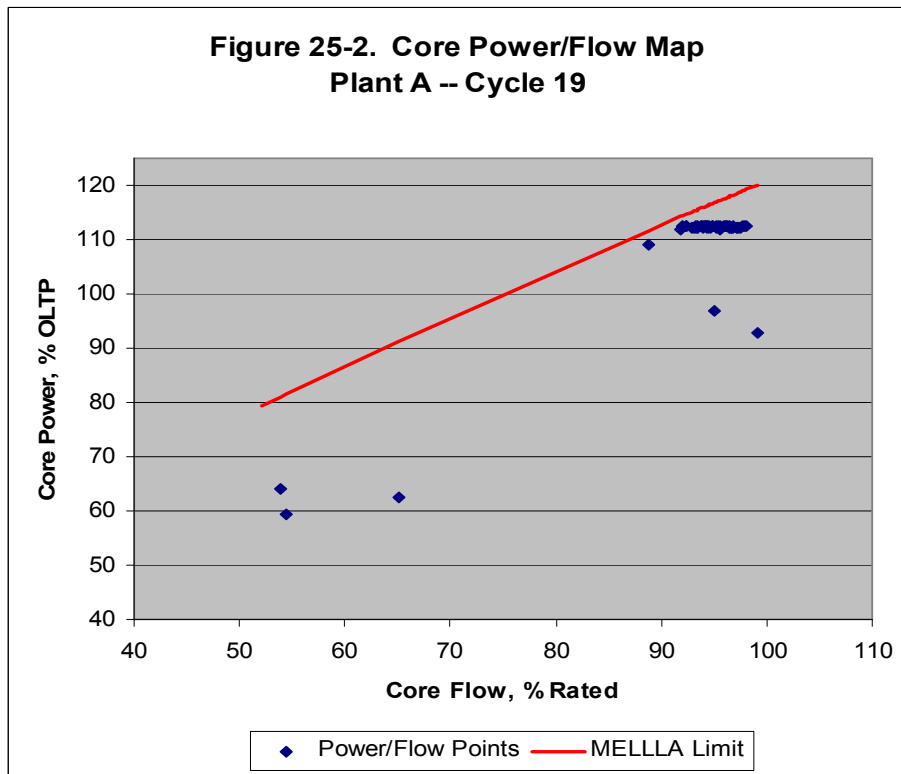
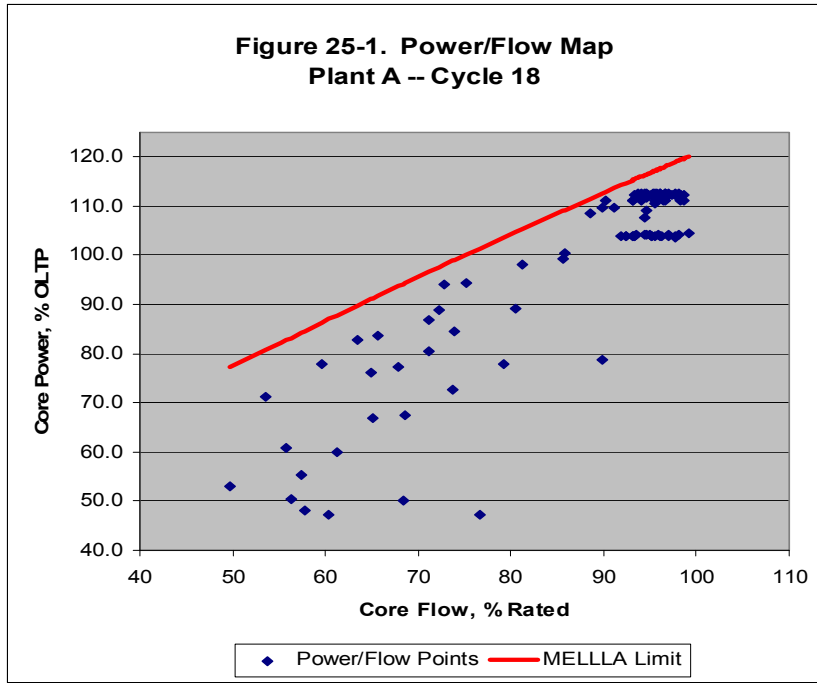
NEDO-33173-A, Revision 1  
Non-Proprietary Information

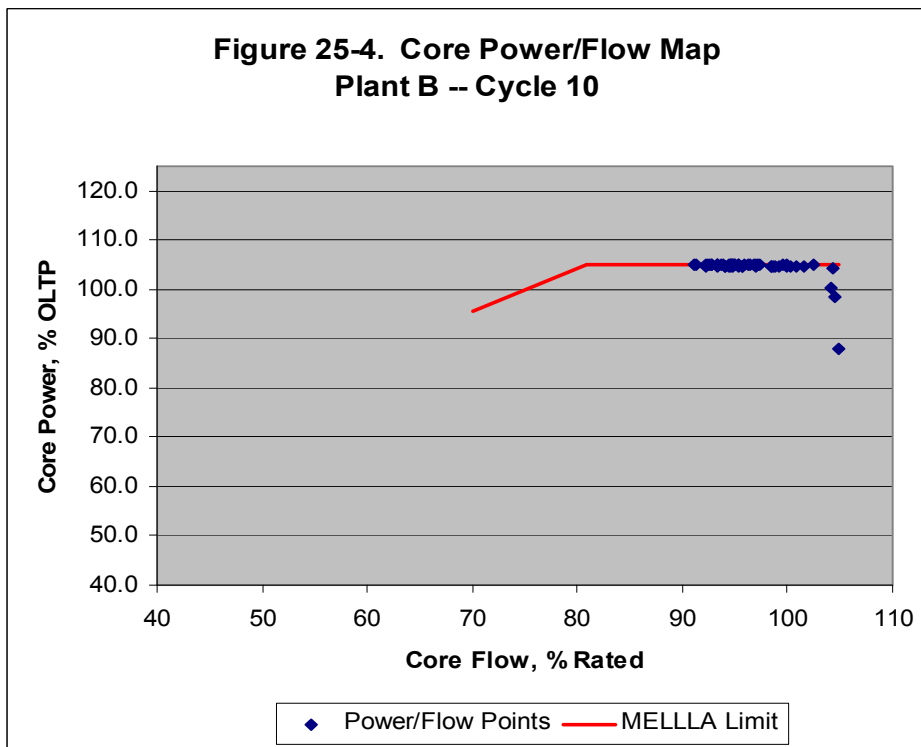
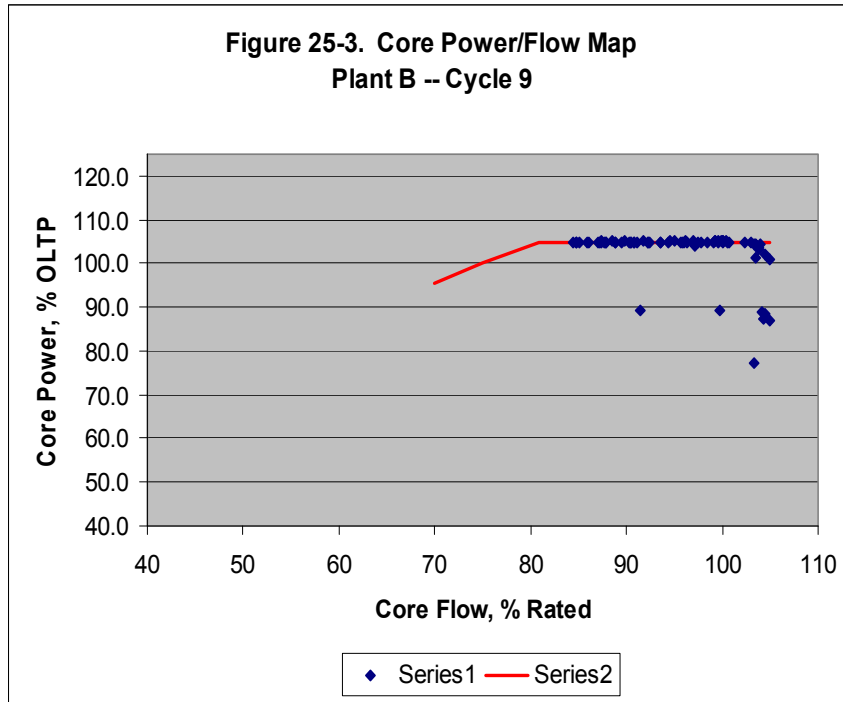
**Table 25-13: Exposure Accounting Data for Plant E, Cycle 8**

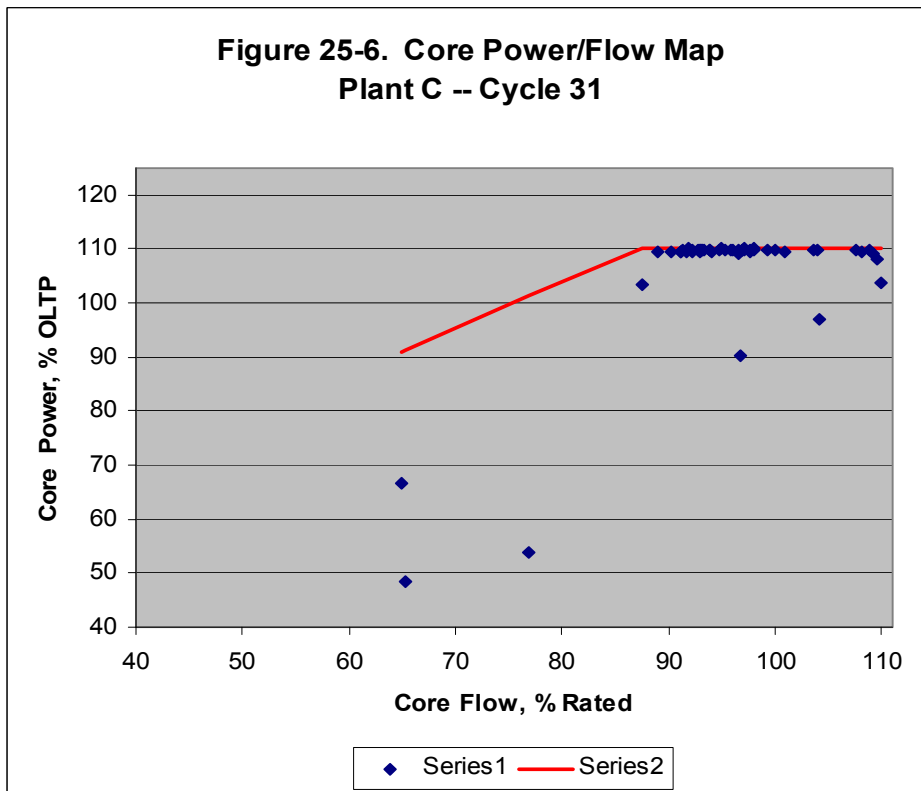
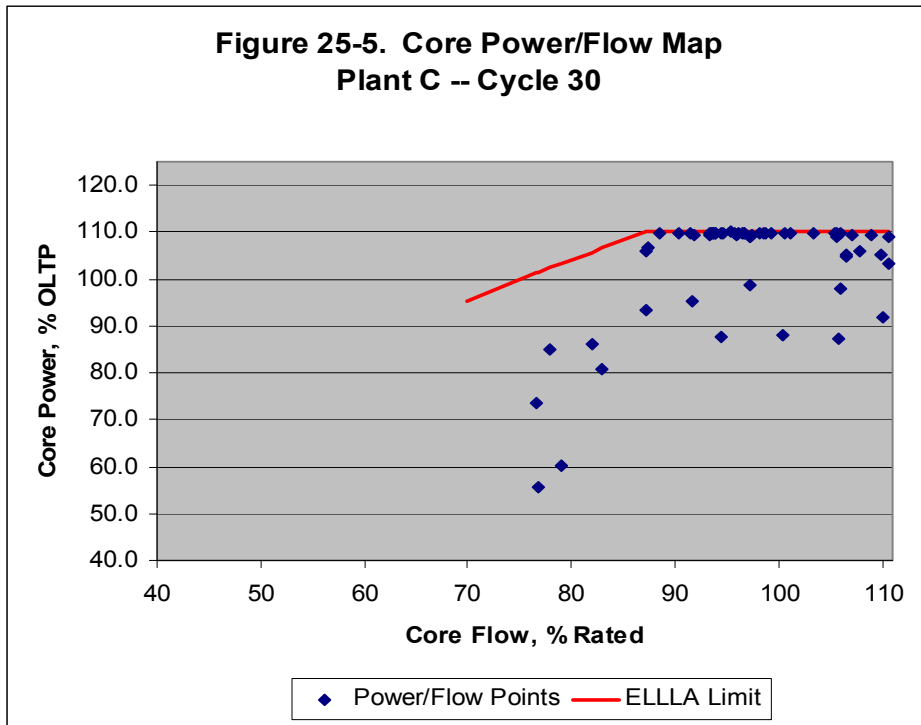
Cycle Expo.	Core Power	Core Flow	Power Density	Power/Flow Ratio	Hot Critical Eigenvalue
GWD/ST	% OLTP	% Rated	kW/l	MWt/Mlbm/hr	
8.18	100.0	90.8	52.4	37.7	
8.46	99.9	94.6	52.4	36.2	
8.65	100.0	93.0	52.4	36.8	
8.84	99.9	93.2	52.4	36.7	
9.06	99.9	93.4	52.4	36.6	
9.21	99.9	93.0	52.4	36.8	
9.35	99.9	96.3	52.4	35.6	
9.59	100.0	94.6	52.4	36.2	
9.84	100.0	95.3	52.4	36.0	
10.10	100.0	94.9	52.4	36.1	
10.33	100.0	94.6	52.4	36.2	
10.50	99.8	98.5	52.3	34.7	
10.78	99.9	89.4	52.3	38.3	
11.04	99.9	97.1	52.4	35.2	
11.13	98.9	100.2	51.8	33.8	
11.23	100.1	99.3	52.5	34.5	
11.39	98.5	100.1	51.6	33.7	
11.53	96.1	100.2	50.4	32.8	]]

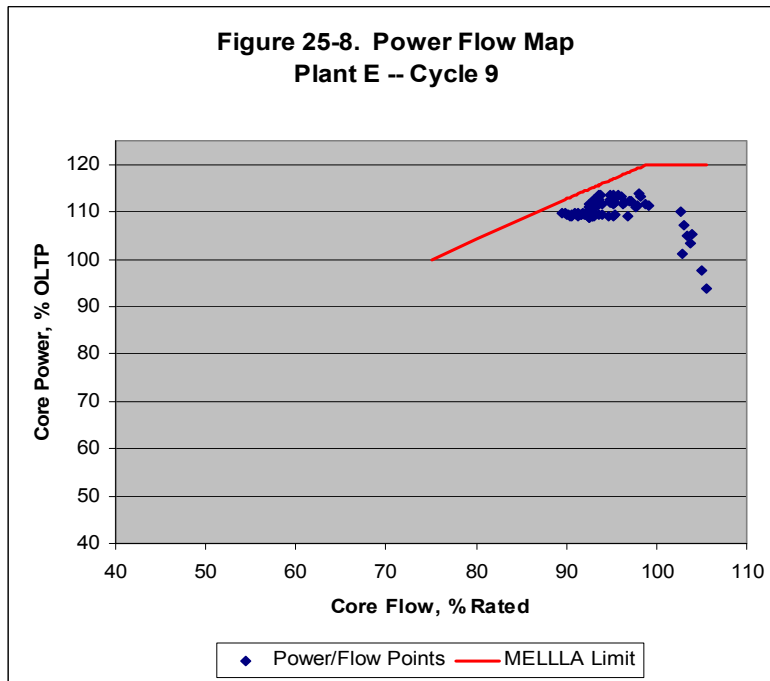
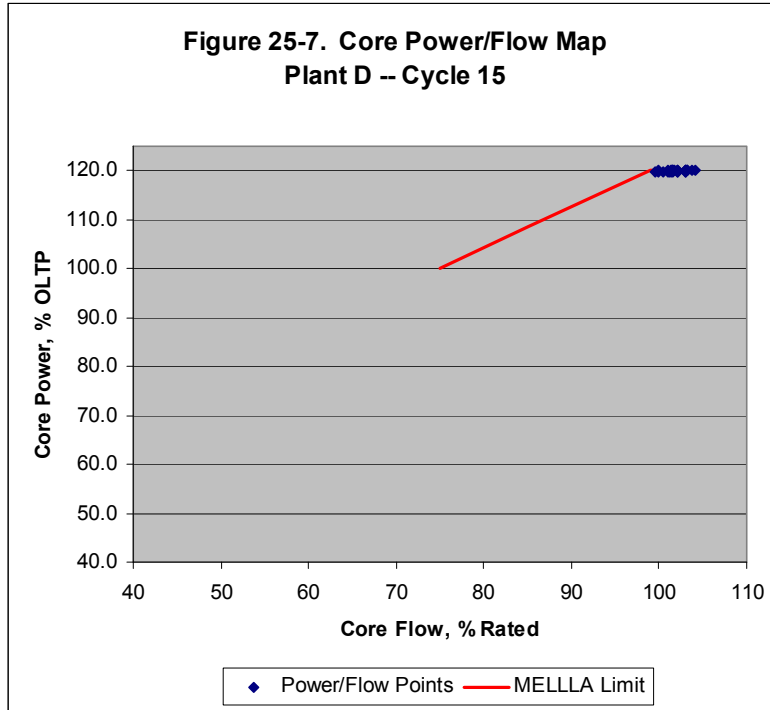
**Table 25-14. Summary of Bundle Average TIP Comparisons, Eight Cycles Studied**

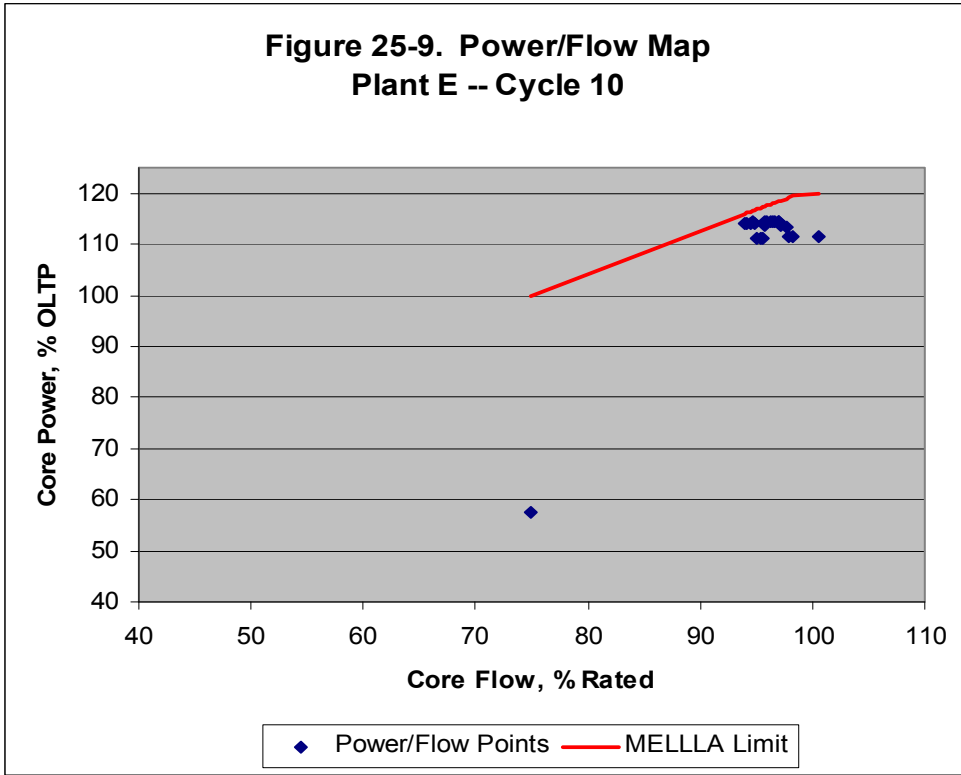
<b>Document</b>	<b>Nuclear Model</b>	<b># of TIP Sets</b>	<b>Weighted RMS Difference</b>
<b>NEDE-32694 (used in SLMCPR Analysis)</b>	<b>TGBLA04/PANAC10</b>	<b>  </b>	
<b>NEDE-32773-R1 (Jan 1999)</b>	<b>TGBLA06/PANAC11</b>		
<b>Current data from Eight Cycles Studied</b>	<b>TGBLA06/PANAC11</b>		<b>  </b>



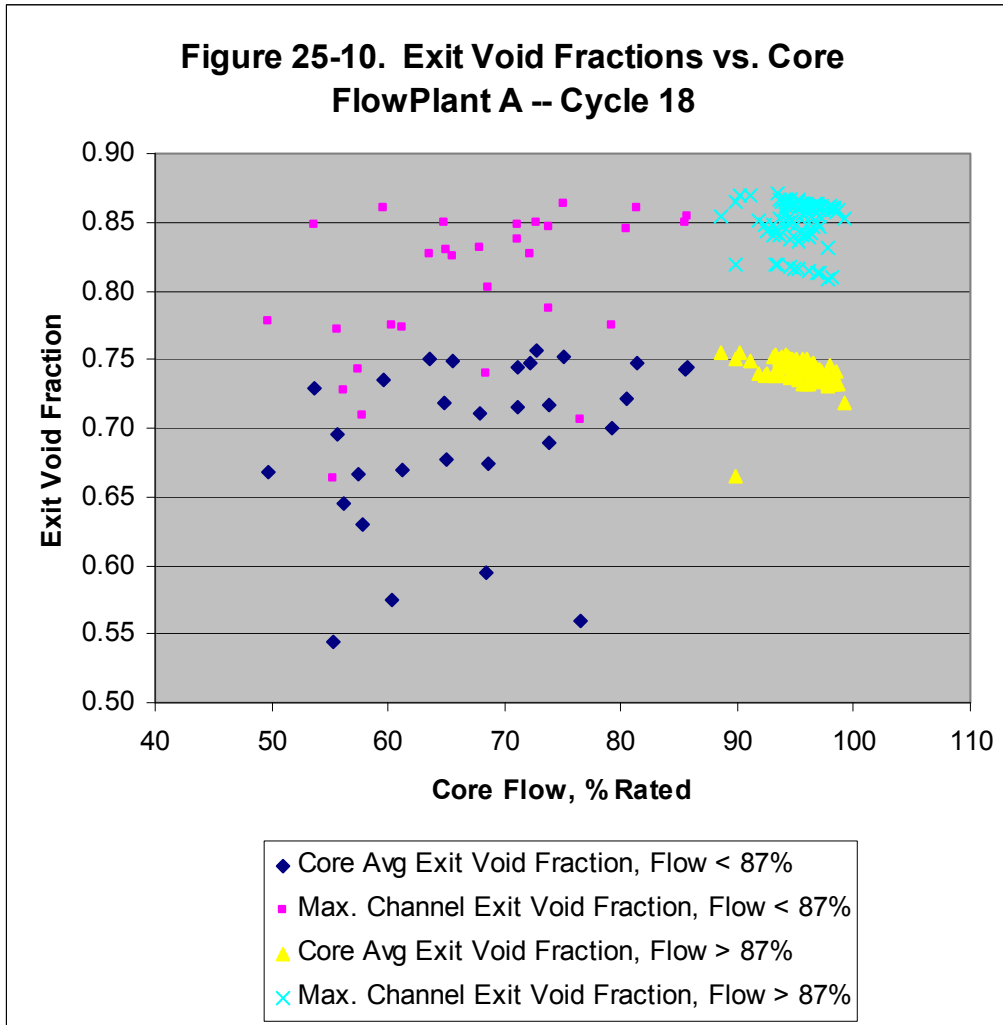








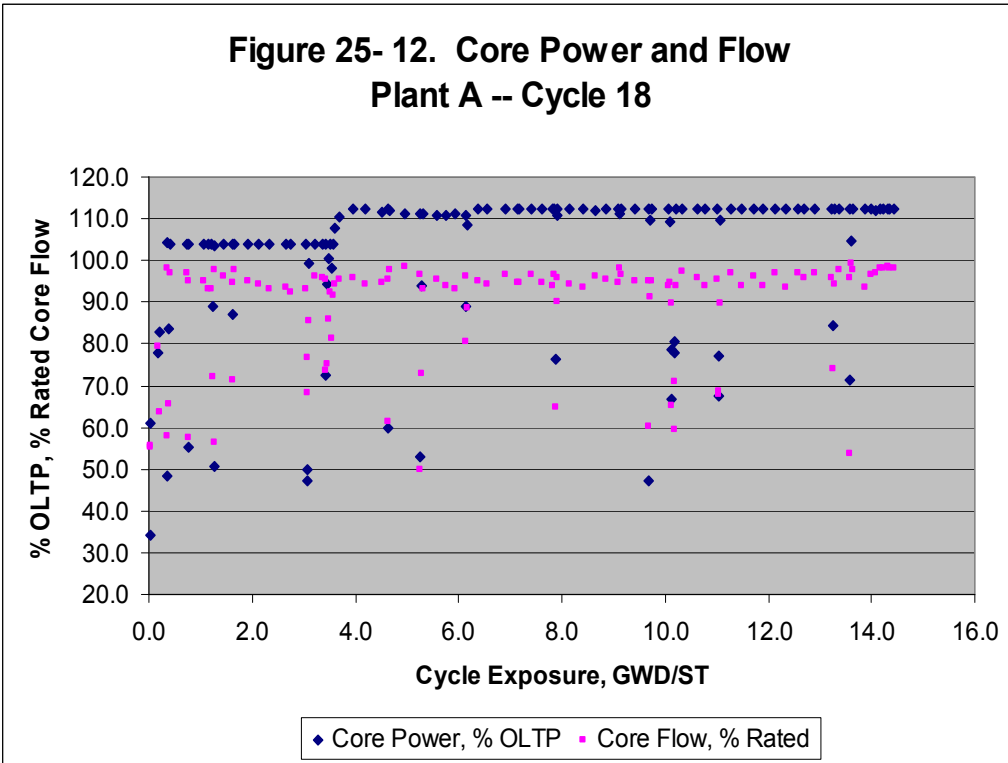




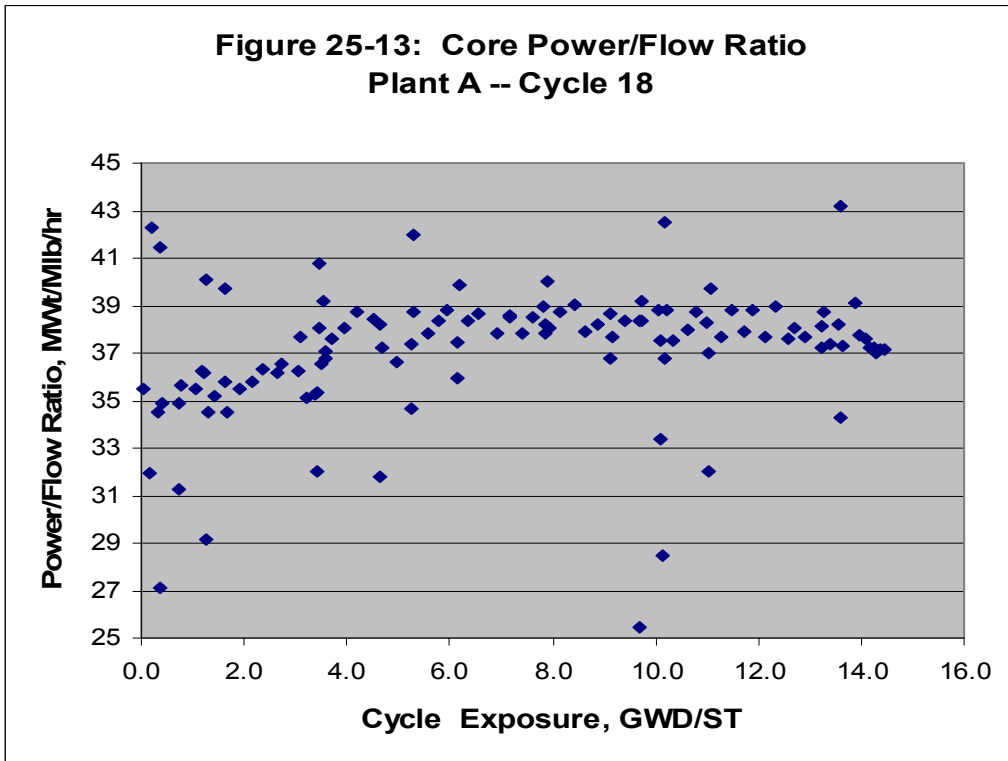
[[

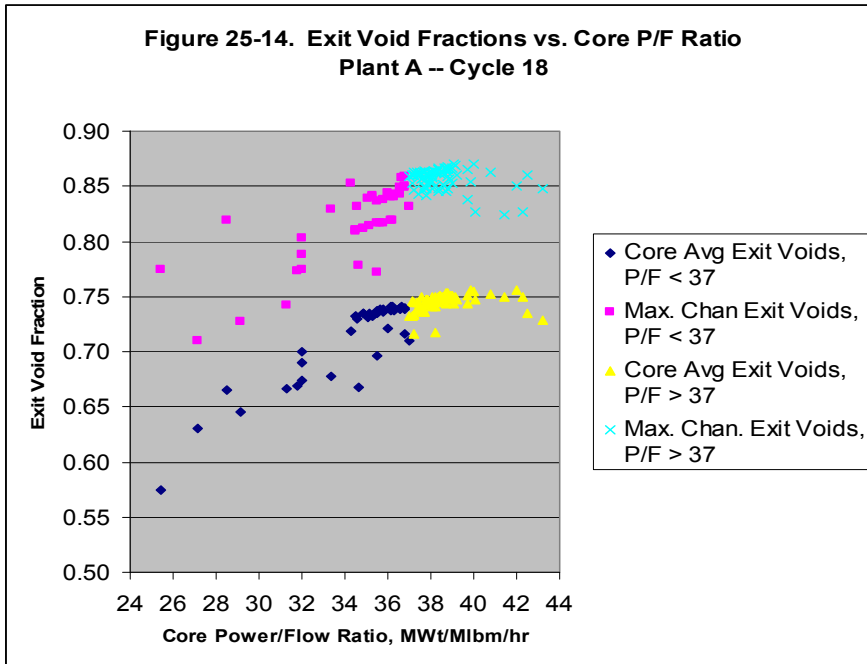
]]

**Figure 25- 12. Core Power and Flow  
Plant A -- Cycle 18**



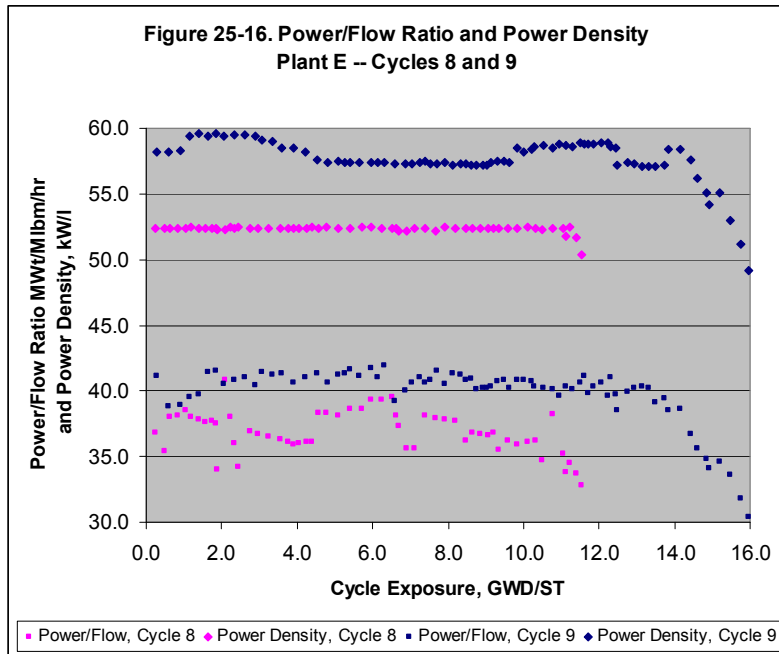
**Figure 25-13: Core Power/Flow Ratio  
Plant A -- Cycle 18**





[[

]]



[[

]]

]]

]]

[[

[[

]]

]]

**MFN 05-029 NRC RAI 26**

Low-Flow and Off-rated Conditions: BWRs currently operate with lower core flow ranges at rated power. However, the general practice is to benchmark the codes for plant operation at rated conditions on the assumption that plants do not routinely operate at the lower flow conditions. The low-flow conditions can be limiting for the thermal-hydraulic conditions (e.g., higher void conditions, axial and radial power peaking and distribution) that adversely affect the performance of the core and the fuel (critical power ratio response). As far as the available data allows, include core follow data for nonrated conditions. If core follow data during plant maneuvers (i.e., during startup, off-rated, and lower core flow at rated power operation) is not available, provide a commitment to benchmark the fidelity of your lattice physics and core simulator codes at these conditions for the EPU/MELLLA+ operation. State what actions you will take to fulfill this commitment.

**GE Response to RAI 26**

As stated in RAI 26, BWRs currently operate with lower core flow ranges at rated power. This statement is corroborated by the Power Flow Maps provided in the response to RAI 25 in Figures 25-1 through 25-9. Because the plants operate at steady state over these flow ranges at high power, these state points are included in the normal exposure accounting calculations for core tracking. Generally, off-rated conditions such as those on the plant's startup trajectory, or during control rod sequence exchanges, are not included in the core tracking because the core is not in an equilibrium state at these conditions due to transient xenon effects.

The exposure accounting data that was evaluated in the response to RAI 25 included a large number of statepoints that spanned the allowable flow range at or near rated power for all nine of the cycles studied. Therefore, the impact of operating at these lower flow conditions is included in the response to RAI 25. The three important parameters analyzed by comparison of the core tracking data to measured data; namely the hot critical eigenvalues, cold critical eigenvalues, and the TIP RMS differences, were all evaluated to see if they were sensitive the operation at high void fractions. The conclusions were that [[

]]

It was also shown in the discussion pertaining to Figure 25-10, that the exit void fractions of the low power/low flow off-rated conditions are bounded by those found at the low end of the allowable flow range at or near rated power. Also, operation at these off-rated points is generally of short duration, so the core receives very little of its total exposure accumulation at these points. Thus, the impact of higher voiding can be effectively studied by considering operation within the allowable flow range at or near rated power, which are the statepoints found in the exposure accounting. Therefore, it is concluded that the most pertinent operational data for evaluating the fidelity of the lattice physics and core simulator codes relative to EPU/MELLLA+ operation has been included in the analyses reported in RAI 25.

RAI 26 has also requested evaluation of plant maneuvers such as reactor startup. As stated in the conclusions of the previous paragraph, GE believes that the examination of operation within the



NEDO-33173-A, Revision 1  
Non-Proprietary Information

allowable flow range at or near rated power provides the pertinent operational data, and reactor startups and other off-rated maneuvers will not generate any additional insight into the methods applicability for EPU/MELLLA+, or the viability of the interim process.

**MFN 05-029 NRC RAI 27**

**Hot Channels:** The high-powered bundles are the most limiting. The core follow data is based on statistically averaged values that may not reflect how well the codes predict the conditions in the high-powered bundles. The code-to-code benchmarking using MCNP (MCNP not benchmarked with exposure and not a depletion code) may not be suitable for establishing the uncertainties and biases with depletion. In addition, the core follow TIP readings average out the four-bundle TIP readings axially within the bundle, along with all the TIP readings for a given cycle state point. In some cases, the TIP readings for different cycle points and different sets of core follow data are statistically averaged to determine the uncertainties of the core simulator codes. This approach tends to mask the accuracy of the codes in predicting hot bundle radial and axial power distribution.

Using limiting control cell loading pattern (two or three hot bundles in a control cell), benchmark the accuracy of TGBLA and PANAC in predicting the four-bundle radial and axial power distribution. Include the EPU/MELLLA+ data for the pilot plants (Brunswick Units 1 and 2 and Clinton) in your hot channel data. Provide the corresponding calculated void distribution for the hot channels.

**GE Response to RAI 27**

It is requested that the measured and calculated TIP readings surrounding limiting bundle locations be examined in more detailed so as to exclude effects of statistical averaging on the comparisons using plant instrumentation. To evaluate the available data, a consistent definition of what constitutes the limiting bundle needs to be made. The most limiting bundle in terms of assessing methods performance varies depending on the aspect of the methods being assessed. The limiting bundle within a core at any given point in the cycle may be that bundle closest to one of its thermal limits. Since operational performance of the bundle and the thermal limits are a function of exposure, the proximity of the bundle to its limit may not be for the highest power bundle, but may be, for instance, a moderately powered bundle at high exposures that is approaching the thermal mechanical limits curve. So too, the CPR of a bundle is a balance between the power, flow and local pin power peaking distribution within the bundle.

The limiting bundle may also be thought of as that bundle which is most challenging for the nuclear methods. Once again, depending on the aspect of the nuclear methods being examined, various parameters would result in different bundles being designated for more detailed study. High power, high void fractions, high axial peaking and steep flux gradients all contribute challenges to steady-state nuclear method fidelity. And simply, the highest power bundle may be thought of as the most limiting.

For the purposes of responding to this RAI, the highest power bundles that neighbor a TIP location are chosen for more detailed evaluation. This approach will often, while not necessarily always, yield the best candidates for detailed “drilling down” into the substantial amount of information that is derived from in-core instrumentation.

While this detailed comparison is not consistent with the way in which the benchmarking is used in safety limit evaluations, the investigation of potential effects that the hot channel may have on

TIP predictions relative to the core-wide performance is of interest for assessing the fidelity of the coupled set of steady-state nuclear methods. This prediction of in-core measurements can be evaluated throughout the exposure history of a bundle and without the operational restrictions necessary for adequate ex-core, post-irradiation measurement interpretation (such as gamma scans).

The following figures and tables provide the information requested which demonstrate a significant amount of experience for high void conditions and power profiles comparable to MELLLA+. These data are the off-line calculated instrument readings compared to the measured instrument readings from the plant. The power and void fraction data associated with these figures and tables are from the off-line calculations using TGBLA and PANAC.

Plants A, B, C, D, and E are typically high power density MELLLA plants or EPU/MELLLA plants (EPU/ELLLA in the case of Plant C) for which GE/GNF has extensive operational experience. These are the same plants and plant designations for which operational experience was provided in response to RAI 25. Plant F is similar to Plant D. The specific parameters are given later in this response immediately before the TIP results for this plant are presented.

For each plant cycle, the following information is provided for one or more points in each cycle.

1. For each cycle, a summary figure presents the TIP radial, axial and nodal core average RMS differences between calculated and measured TIPs. In addition, the summary figure indicates the radial difference and the axial and nodal RMS values for the TIP instrument that is adjacent to the hot channel. In this case, the “hot channel” is defined as the instrumented location with the highest power bundle of bundles surrounding instrumented locations. Cycle points where more detailed data is provided are also indicated.

The definitions of the radial, axial and nodal statistical comparisons are provided in the response to RAI 21-2. That response includes the equations, parameter description and calculational procedure for the development of the values shown in the figures and tables below.

2. For each selected cycle exposure point (noted as ‘B’ for BOC, ‘M’ for MOC, or ‘E’ for EOC), a map by TIP string of the radial and axial TIP RMS difference across the core is provided. If the TIP instrument is “Failed”, the TIP string was declared non-operational by the plant process computer and may be ignored. The failed TIP strings are identified in these maps by the use of asterisks next to the numbers for the TIP statistics. A lined border around a TIP statistic indicates the four-bundle grouping surrounding the TIP instrument that corresponds to the hot channel. The four bundle cells shaded in blue represent the TIP strings that define the line of symmetry for the instrumentation strings.
3. For each cycle exposure point selected for more detailed study, a four-bundle relative power map is provided for all four-bundle cells surrounding an instrumented location. A lined border around a four-bundle power value indicates the four-bundle grouping surrounding the TIP instrument that corresponds to the hot channel. The relative power for a single bundle is normalized such that the bundle at the average bundle power has a relative power value of 1.0. The four bundle relative power is the sum of the relative powers for the four bundles in the cell.

NEDO-33173-A, Revision 1  
Non-Proprietary Information

4. For each cycle exposure point selected for more detailed study, a plot of each measured and calculated TIP instrument reading as a function of axial height is provided. The TIP plots are arranged on a core-wide map to give the relative position of the TIP within the core.
5. For each cycle exposure point selected for more detailed study, a numerical table with the nodal powers, exposures and void fractions corresponding to the four bundles surrounding the instrument adjacent to the hot channel is provided.

These tables and figures give an overview of individual TIP string statistical results for a variety of plants, cycle exposure and operating conditions. A more detailed evaluation of individual TIP string responses, errors and trending at the nodal level is given in response to RAI 29.

**PLANT A CYCLE 18**

Figure 27 - 1 Plant A Cycle 18 TIP Comparison Data as a Function of Cycle Exposure  
[[

]]

**Figure 27- 2 Plant A Cycle 18 Four Bundle Powers and TIP String Comparisons at Cycle  
Exposure Point B**

[[

]]

**Figure 27-3 Plant A Cycle 18 TIP String Comparisons at Cycle Exposure Point B**

[[

]]

**Table 27- 1    Plant A Cycle 18 Four Bundle Nodal Power and Void Fraction Comparisons  
for Hot Channel Instrument [String 16] at Cycle Exposure Point B**

[[

]]



**Figure 27- 4 Plant A Cycle 18 Four Bundle Powers and TIP String Comparisons at Cycle  
Exposure Point M**

[[

]]

**Figure 27- 5 Plant A Cycle 18 TIP String Comparisons at Cycle Exposure Point M**

[[

]]

**Table 27- 2 Plant A Cycle 18 Four Bundle Nodal Power and Void Fraction Comparisons  
for Hot Channel Instrument [String 16] at Cycle Exposure Point M**

[[

]]

**PLANT A CYCLE 19**

Figure 27- 6 Plant A Cycle 19 TIP Comparison Data as a Function of Cycle Exposure  
[[

]]

**Figure 27- 7 Plant A Cycle 19 Four Bundle Powers and TIP String Comparisons at Cycle  
Exposure Point B**

[[

]]

**Figure 27- 8 Plant A Cycle 19 TIP String Comparisons at Cycle Exposure Point B**

[[

]]

**Table 27- 3 Plant A Cycle 19 Four Bundle Nodal Power and Void Fraction Comparisons  
for Hot Channel Instrument [String 12] at Cycle Exposure Point B**

[[

]]

**Figure 27- 9 Plant A Cycle 19 Four Bundle Powers and TIP String Comparisons at Cycle  
Exposure Point M**

[[

]]



**Figure 27- 10 Plant A Cycle 19 TIP String Comparisons at Cycle Exposure Point M**

[[

]]

**Table 27- 4    Plant A Cycle 19 Four Bundle Nodal Power and Void Fraction Comparisons  
for Hot Channel Instrument [String 8] at Cycle Exposure Point M**

[[

]]

**Figure 27- 11 Plant A Cycle 19 Four Bundle Powers and TIP String Comparisons at Cycle  
Exposure Point E**

[[

]]

**Figure 27- 12 Plant A Cycle 19 TIP String Comparisons at Cycle Exposure Point E**

[[

]]

**Table 27- 5 Plant A Cycle 19 Four Bundle Nodal Power and Void Fraction Comparisons  
for Hot Channel Instrument [String 12] at Cycle Exposure Point E**

[[

]]

**PLANT B CYCLE9**

During the middle of the cycle, a number of TIPs for Plant B Cycle 9 were failed. The failed TIPs, which were so marked by the plant process computer, included many of the hot channels. For this comparison, a cycle exposure point after these failures had been remedied is chosen for more detailed study.

**Figure 27- 13 Plant B Cycle 9 TIP Comparison Data as a Function of Cycle Exposure**

[[

]]

**Figure 27- 14 Plant B Cycle 9 Four Bundle Powers and TIP String Comparisons at Cycle  
Exposure Point B**

[[

]]

**Figure 27- 15 Plant B Cycle 9 TIP String Comparisons at Cycle Exposure Point B**

[[

]]



**Table 27- 6 Plant B Cycle 9 Four Bundle Nodal Power and Void Fraction Comparisons  
for Hot Channel Instrument [String 21] at Cycle Exposure Point B**

[[

]]

**Figure 27- 16 Plant B Cycle 9 Four Bundle Powers and TIP String Comparisons at Cycle  
Exposure Point M**

[[

]]

**Figure 27- 17 Plant B Cycle 9 TIP String Comparisons at Cycle Exposure Point M**

[[

]]

**Table 27- 7 Plant B Cycle 9 Four Bundle Nodal Power and Void Fraction Comparisons  
for Hot Channel Instrument [String 15] at Cycle Exposure Point M**

[[

]]

**Figure 27- 18 Plant B Cycle 9 Four Bundle Powers and TIP String Comparisons at Cycle  
Exposure Point E**

[[

]]

**Figure 27- 19 Plant B Cycle 9 TIP String Comparisons at Cycle Exposure Point E**

[[

]]

**Table 27- 8 Plant B Cycle 9 Four Bundle Nodal Power and Void Fraction Comparisons  
for Hot Channel Instrument [String 20] at Cycle Exposure Point E**

[[

]]

**PLANT B CYCLE 10**

**Figure 27- 20 Plant B Cycle 10 TIP Comparison Data as a Function of Cycle Exposure**

[[

]]



**Figure 27- 21 Plant B Cycle 10 Four Bundle Powers and TIP String Comparisons at Cycle  
Exposure Point B**

[[

]]

**Figure 27- 22 Plant B Cycle10 TIP String Comparisons at Cycle Exposure Point B**

[[

]]

**Table 27- 9 Plant B Cycle 10 Four Bundle Nodal Power and Void Fraction Comparisons  
for Hot Channel Instrument [String 9] at Cycle Exposure Point B**

[[

]]

**Figure 27- 23 Plant B Cycle 10 Four Bundle Powers and TIP String Comparisons at Cycle  
Exposure Point M**

[[

]]

**Figure 27- 24 Plant B Cycle10 TIP String Comparisons at Cycle Exposure Point M**

[[

]]

**Table 27- 10 Plant B Cycle 10 Four Bundle Nodal Power and Void Fraction Comparisons  
for Hot Channel Instrument [String 21] at Cycle Exposure Point M**

[[

]]

**Figure 27- 25 Plant B Cycle 10 Four Bundle Powers and TIP String Comparisons at Cycle  
Exposure Point E**

[[

]]

**Figure 27- 26 Plant B Cycle10 TIP String Comparisons at Cycle Exposure Point E**

[[

]]



**Table 27- 11 Plant B Cycle 10 Four Bundle Nodal Power and Void Fraction Comparisons  
for Hot Channel Instrument [String 24] at Cycle Exposure Point E**

[[

]]

**PLANT C CYCLE 30**

**Figure 27- 27 Plant C Cycle 30 TIP Comparison Data as a Function of Cycle Exposure**

[[

]]

**Figure 27- 28 Plant C Cycle 30 Four Bundle Powers and TIP String Comparisons at Cycle  
Exposure Point B**

[[

]]

**Figure 27- 29 Plant C Cycle 30 TIP String Comparisons at Cycle Exposure Point B**

[[

]]

**Table 27- 12 Plant C Cycle 30 Four Bundle Nodal Power and Void Fraction Comparisons  
for Hot Channel Instrument [String 9] at Cycle Exposure Point B**

[[

]]

**Figure 27- 30 Plant C Cycle 30 Four Bundle Powers and TIP String Comparisons at Cycle  
Exposure Point M**

[[

]]

**Figure 27- 31 Plant C Cycle 30 TIP String Comparisons at Cycle Exposure Point M**

[[

]]

**Table 27- 13 Plant C Cycle 30 Four Bundle Nodal Power and Void Fraction Comparisons  
for Hot Channel Instrument [String 5] at Cycle Exposure Point M**

[[

]]



**Figure 27- 32 Plant C Cycle 30 Four Bundle Powers and TIP String Comparisons at Cycle  
Exposure Point E**

[[

]]

**Figure 27- 33 Plant C Cycle 30 TIP String Comparisons at Cycle Exposure Point E**

[[

]]

**Table 27- 14 Plant C Cycle 30 Four Bundle Nodal Power and Void Fraction Comparisons  
for Hot Channel Instrument [String 8] at Cycle Exposure Point E**

[[

]]

**PLANT C CYCLE 31**

**Figure 27- 34 Plant C Cycle 31 TIP Comparison Data as a Function of Cycle Exposure**

[[

]]

**Figure 27- 35 Plant C Cycle 31 Four Bundle Powers and TIP String Comparisons at Cycle  
Exposure Point B**

[[

]]

**Figure 27- 36 Plant C Cycle 31 TIP String Comparisons at Cycle Exposure Point B**

[[

]]

**Table 27- 15 Plant C Cycle 31 Four Bundle Nodal Power and Void Fraction Comparisons  
for Hot Channel Instrument [String 9] at Cycle Exposure Point B**

[[

]]

**Figure 27- 37 Plant C Cycle 31 Four Bundle Powers and TIP String Comparisons at Cycle  
Exposure Point M**

[[

]]



**Figure 27- 38 Plant C Cycle 31 TIP String Comparisons at Cycle Exposure Point M**

[[

]]

**Table 27- 16 Plant C Cycle 31 Four Bundle Nodal Power and Void Fraction Comparisons  
for Hot Channel Instrument [String 11] at Cycle Exposure Point M**

[[

]]

**Figure 27- 39 Plant C Cycle 31 Four Bundle Powers and TIP String Comparisons at Cycle  
Exposure Point E**

[[

]]

**Figure 27- 40 Plant C Cycle 31 TIP String Comparisons at Cycle Exposure Point E**

[[

]]

**Table 27- 17 Plant C Cycle 31 Four Bundle Nodal Power and Void Fraction Comparisons  
for Hot Channel Instrument [String 8] at Cycle Exposure Point E**

[[

]]

**PLANT D CYCLE 13**

**Figure 27- 41 Plant D Cycle 13 TIP Comparison Data as a Function of Cycle Exposure**

[[

]]

**Figure 27- 42 Plant D Cycle 13 Four Bundle Powers and TIP String Comparisons at Cycle  
Exposure Point B**

[[

]]

**Figure 27- 43 Plant D Cycle 13 TIP String Comparisons at Cycle Exposure Point B**

[[

]]



**Table 27- 18 Plant C Cycle 30 Four Bundle Nodal Power and Void Fraction Comparisons  
for Hot Channel Instrument [String 24] at Cycle Exposure Point B**

[[

]]

**Figure 27- 44 Plant D Cycle 13 Four Bundle Powers and TIP String Comparisons at Cycle  
Exposure Point M**

[[

]]

**Figure 27- 45 Plant D Cycle 13 TIP String Comparisons at Cycle Exposure Point M**

[[

]]

**Table 27- 19 Plant D Cycle 13 Four Bundle Nodal Power and Void Fraction Comparisons  
for Hot Channel Instrument [String 23] at Cycle Exposure Point M**

[[

]]

**Figure 27- 46 Plant D Cycle 13 Four Bundle Powers and TIP String Comparisons at Cycle  
Exposure Point E**

[[

]]

**Figure 27- 47 Plant D Cycle 13 TIP String Comparisons at Cycle Exposure Point E**

[[

]]

**Table 27- 20 Plant D Cycle 13 Four Bundle Nodal Power and Void Fraction Comparisons  
for Hot Channel Instrument [String 25] at Cycle Exposure Point E**

[[

]]

**PLANT D CYCLE 14**

**Figure 27- 48 Plant D Cycle 14 TIP Comparison Data as a Function of Cycle Exposure**

[[

]]



**Figure 27- 49 Plant D Cycle 14 Four Bundle Powers and TIP String Comparisons at Cycle  
Exposure Point B**

[[

]]

**Figure 27- 50 Plant D Cycle 14 TIP String Comparisons at Cycle Exposure Point B**

[[

]]

**Table 27- 21 Plant D Cycle 14 Four Bundle Nodal Power and Void Fraction Comparisons  
for Hot Channel Instrument [String 11] at Cycle Exposure Point B**

[[

]]

**Figure 27- 51 Plant D Cycle 14 Four Bundle Powers and TIP String Comparisons at Cycle  
Exposure Point M**

[[

]]

**Figure 27- 52 Plant D Cycle 14 TIP String Comparisons at Cycle Exposure Point M**

[[

]]

**Table 27- 22 Plant D Cycle 14 Four Bundle Nodal Power and Void Fraction Comparisons  
for Hot Channel Instrument [String 11] at Cycle Exposure Point M**

[[

]]

**Figure 27- 53 Plant D Cycle 14 Four Bundle Powers and TIP String Comparisons at Cycle  
Exposure Point E**

[[

]]

**Figure 27- 54 Plant D Cycle 14 TIP String Comparisons at Cycle Exposure Point E**

[[

]]



**Table 27- 23 Plant D Cycle 14 Four Bundle Nodal Power and Void Fraction Comparisons  
for Hot Channel Instrument [String 14] at Cycle Exposure Point E**

[[

]]

**PLANT E CYCLE 9**

**Figure 27- 55 Plant E Cycle 9 TIP Comparison Data as a Function of Cycle Exposure**

[[

]]

**Figure 27- 56 Plant E Cycle 9 Four Bundle Powers and TIP String Comparisons at Cycle  
Exposure Point B**

[[

]]

**Figure 27- 57 Plant E Cycle 9 TIP String Comparisons at Cycle Exposure Point B**

[[

]]

**Table 27- 24 Plant E Cycle 9 Four Bundle Nodal Power and Void Fraction Comparisons  
for Hot Channel Instrument [String 19] at Cycle Exposure Point B**

[[

]]

**Figure 27- 58 Plant E Cycle 9 Four Bundle Powers and TIP String Comparisons at Cycle  
Exposure Point M**

[[

]]

**Figure 27- 59 Plant E Cycle 9 TIP String Comparisons at Cycle Exposure Point M**

[[

]]

**Table 27- 25 Plant E Cycle 9 Four Bundle Nodal Power and Void Fraction Comparisons  
for Hot Channel Instrument [String 8] at Cycle Exposure Point M**

[[

]]



**Figure 27- 60 Plant E Cycle 9 Four Bundle Powers and TIP String Comparisons at Cycle  
Exposure Point E**

[[

]]

**Figure 27- 61 Plant E Cycle 9 TIP String Comparisons at Cycle Exposure Point E**

[[

]]

**Table 27- 26 Plant E Cycle 9 Four Bundle Nodal Power and Void Fraction Comparisons  
for Hot Channel Instrument [String 9] at Cycle Exposure Point E**

[[

]]

**PLANT E CYCLE 10**

**Figure 27- 62 Plant E Cycle 10 TIP Comparison Data as a Function of Cycle Exposure**

[[

]]

**Figure 27- 63 Plant E Cycle 10 Four Bundle Powers and TIP String Comparisons at Cycle  
Exposure Point B**

[[

]]

**Figure 27- 64 Plant E Cycle 10 TIP String Comparisons at Cycle Exposure Point B**

[[

]]

**Table 27- 27 Plant E Cycle 10 Four Bundle Nodal Power and Void Fraction Comparisons  
for Hot Channel Instrument [String 12] at Cycle Exposure Point B**

[[

]]

**Figure 27- 65 Plant E Cycle 10 Four Bundle Powers and TIP String Comparisons at Cycle  
Exposure Point M**

[[

]]



**Figure 27- 66 Plant E Cycle 10 TIP String Comparisons at Cycle Exposure Point M**

[[

]]

**Table 27- 28 Plant E Cycle 10 Four Bundle Nodal Power and Void Fraction Comparisons  
for Hot Channel Instrument [String 18] at Cycle Exposure Point M**

[[

]]

**Figure 27- 67 Plant E Cycle 10 Four Bundle Powers and TIP String Comparisons at Cycle  
Exposure Point E**

[[

]]

**Figure 27- 68 Plant E Cycle 10 TIP String Comparisons at Cycle Exposure Point E**

[[

]]

**Table 27- 29 Plant E Cycle 10 Four Bundle Nodal Power and Void Fraction Comparisons  
for Hot Channel Instrument [String 13] at Cycle Exposure Point E**

[[

]]

**PLANT F CYCLE 15**

Plant F is a target plant for MELLLA+ application. GE/GNF does not routinely receive regular TIP data from this plant. However, TIP data for three exposure points in cycle 15 are available and presented below. This plant is similar to Plant D. Specific parameters for the core are:

Plant	GE BWR Type	Number of Bundles	Original Licensed Thermal Power (OLTP) MWt	Rated Flow (Flow at OLTP) Mlbm/hr	Licensed Power Uprate (PU) % OLTP	Licensed Core Flow Range at PU % Rated Flow	Power Density at Licensed PU kW/l
F	BWR/4	560	2436	77.0	120	99-105	59.0

**Figure 27- 69 Plant F Cycle 15 TIP Comparison Data as a Function of Cycle Exposure**

[[

]]

**Figure 27- 70 Plant F Cycle 15 Four Bundle Powers and TIP String Comparisons at Cycle  
Exposure Point B**

[[

]]

**Figure 27- 71 Plant F Cycle 15 TIP String Comparisons at Cycle Exposure Point B**

[[

]]



**Table 27- 30 Plant F Cycle 15 Four Bundle Nodal Power and Void Fraction Comparisons  
for Hot Channel Instrument [String 18] at Cycle Exposure Point B**

[[

]]

**Figure 27- 72 Plant F Cycle 15 Four Bundle Powers and TIP String Comparisons at Cycle  
Exposure Point E**

[[

]]

**Figure 27- 73 Plant F Cycle 15 TIP String Comparisons at Cycle Exposure Point E**

[[

]]

**Table 27- 31 Plant F Cycle 15 Four Bundle Nodal Power and Void Fraction Comparisons  
for Hot Channel Instrument [String 22] at Cycle Exposure Point E**

[[

]]

**PLANT F CYCLE 16**

For Plant F cycle 16, TIP data for only one point is available to GE/GNF. This is at a cycle exposure of 8942 MWd/st, which corresponds to a middle of cycle point. Since only one exposure point is available, no cycle summary chart throughout the cycle is presented. Instead, the data are listed in Table 27-32.

**Table 27- 32 Plant F Cycle 16 TIP Comparison Data**

<b>CYC EXP Mad/ST</b>	<b>Bundle RMS</b>	<b>Axial RMS</b>	<b>Nodal RMS</b>	<b>Max string Radial RMS</b>	<b>Max String axial RMS</b>	<b>Max String nodal RMS</b>
8492.	[[					]]

**Figure 27- 74 Plant F Cycle 16 Four Bundle Powers and TIP String Comparisons at a  
Cycle Exposure of 8942 MWd/st**

[[

]]

**Figure 27- 75 Plant F Cycle 16 TIP String Comparisons at Cycle Exposure Point B**

[[

]]

**Table 27- 33 Plant F Cycle 16 Four Bundle Nodal Power and Void Fraction Comparisons  
for Hot Channel Instrument [String 17] at Cycle Exposure Point B**

[[

]]



**MFN 05-029 NRC RAI 29**

Calculation of Nodal, Bundle, and Axial TIP Responses. RAI 29 follows up on methods RAI 21-2. The objective is to determine whether the statistical combination and normalization of the measured and the calculated TIP data comparisons show the axial and nodal differences between the calculated and the measured data for a four-bundle TIP cell.

- 29-1 Using a limiting four-bundle TIP cell (limiting number of hot bundles in a control cell, limiting enrichment, limiting cycle exposure point), tabulate the TIP calculated and measured data. Show how the axial, bundle, and nodal TIP RMS is calculated from the TIP readings.
- 29-2 For the same four-bundle TIP data, compare the absolute calculated and measured values for each TIP element reading and provide a tabulation of the corresponding bundle axial void profiles and the absolute difference in TIP data.
- 29-3 Evaluate the absolute difference in TIP readings and determine whether the fidelity of the TIP readings varies axially with void. Compare the four-bundle TIP data with core follow TIP readings for less challenging core and lattice designs and determine whether the four-bundle power uncertainties should be increased.
- 29-4 Since the four-bundle control cell can contain bundles at different exposures, explain how the accuracy of the GNF-A methods can be benchmarked for depletion under high-void conditions by using the core follow data. This issue is important because MCNP is not well-suited for benchmarking the historical effects. Use gamma scan data, if available, for bundles and peak pin at different exposures (e.g., fresh, once-burned, twice-burned). As an interim measure, select four-bundle TIP readings and cycle state points to assess the fidelity of TGBLA and PANAC for depletion at high-void conditions. State whether the accuracy of the code for the hot bundle changes with exposure at core conditions as close to EPU/MELLLA+ conditions as possible.

**GE Response**

**Response to 29-1**

To demonstrate how the bundle, axial and nodal TIP statistical values are calculated from the TIP readings, it is desirable to choose a TIP string that is limiting in the sense that it is surrounded by hot bundles with high enrichment and at a limiting point in exposure. This is necessarily a more limiting configuration than an arrangement of hot bundles in a control cell. In addition, most core configurations are not operated in control cell core configurations due to the high batch fractions.

Not all of the characteristics that result in hot bundles surrounding an instrument location are maximized at a particular exposure point in a particular cycle of a particular plant with a particular bundle arrangement at a particular TIP location, but there are a number of instances in the previously presented data where all of these parameters are at or near their maximum. In particular, TIP string 24 of Plant B cycle 10 is surrounded by two fresh and two once-burned bundles of [ ] wt% and [ ] wt% bundle average enrichment, respectively. At the end of cycle (exposure point E in the response to RAI 27), the normalized four-bundle power is

[[ ]]. For the power density of this core, that four-bundle power represents an average bundle power in the four bundles of about [[ ]]. This is the highest absolute average bundle power in any four-bundle cell in the data provided. Therefore, the hot channel TIP data from the response to RAI 27 will be used to demonstrate the TIP statistic calculations.

Table 29-1 shows the axial node of the data in the core simulator, the axial elevation in inches, the calculated TIP prediction (CALTIP), the measured TIP reading (PCTIP) and the nodal difference between the calculated TIP value and the measured TIP reading (Delta).

From the response to RAI 21-2, the radial, or bundle, statistic for a single TIP string is given by:

$$\Delta_{j,rad} = \left( \frac{\sum_{k=Klow}^{Kup} C(k,j)}{K} \right) - \left( \frac{\sum_{k=Klow}^{Kup} P(k,j)}{K} \right)$$

Each of the CALTIP and PCTIP columns is summed between the nodes of interest. As mentioned in an earlier response, instrument readings are generally of interest only in the region of nodes 2 to 23 due to end effects and instrument reading validity. Therefore, the columns are summed only over nodes 2 to 23, and the sum is divided by K, which in this case is 22. This gives a value of

$$\Delta = 1.245 - 1.263 = -0.019$$

This value results in a -1.9% radial difference. The percentage represents the difference in the axially integrated four-bundle power difference between calculated and measured expressed as a percentage of the **average** four-bundle (or TIP string) power.

From the response to RAI 21-2, the nodal RMS for the string is found by taking the square root of the sum of the squares in the “Delta” column (for nodes 2 to 23) divided by the number of values (again, in this case, 22). This gives a value of [[ ]]. Again, this represents the nodal RMS value in terms of an average node in the core.

As indicated in the response to RAI 21-2, the axial RMS value for a single string is obtained by first normalizing the CALTIP and PCTIP data for the string with itself and then performing the same operation used in calculating the nodal RMS. Again, only data between the nodes of interest are used. Table 29-2 shows the normalized data from Table 29-1.

The axial RMS is found by taking the square root of the sum of the squares of the “Delta” column in Table 29-2 divided by 22. This gives a value of [[ ]]. This is an indicator of the relative axial shape comparison between calculated and measured, without the overall radial magnitude in the comparison.

### Response 29-2

Table 29-3 repeats the data from Table 29-1. These are the absolute calculated and measured TIP element readings for the single, “hottest” TIP instrument in this particular cycle, string 24 (see response to RAI 27). The “Delta” column in Table 29-3 is the tabulation of the absolute difference at each node. Also shown is the calculated void fraction for each node for each of the four surrounding bundles. The void fraction data may also be found in the response to RAI 27.

### Response 29-3

The data from Table 29-3 are plotted in Figure 29-1. The absolute difference in TIP values shown as a function of the four bundle average void fraction reveals no correlation of the TIP difference with void fraction. The choice of average or hot channel void fraction as the abscissa does not much matter since all void fractions are roughly within 5% of one another in this particular hot channel data set. Again, the values for nodal differences are relative to the average power node in the core.

The figure does not demonstrate a correlation of TIP error with the axial variation in void fraction.

To provide context and perspective of this difference in shape, it is necessary to evaluate this TIP response relative to other TIP differences. It is instructive to look at other TIPs in the same core at the same exposure point, as well as to look at other plant cycles that have both more and less challenging conditions for TIP calculations.

Figure 29-2 shows the nodal difference between calculated and measured TIPs for Plant E Cycle 10, Exposure Point M for the instrument location that has the highest power monitored bundle. This same data may be found from the response to RAI 27.

Again, the figure does not demonstrate a correlation of TIP error with the axial variation in void fraction.

Figure 29-3 shows a similar plot for a less challenging core and lattice design. These data come from the “hottest” TIP for Plant A Cycle 18 exposure point B. Here there is a more pronounced trending with void fraction in the lower portion of the bundle, but still the majority of difference points do not have a correlation with increasing void fraction. In fact, what is being demonstrated with these graphs is that the magnitude of the nodal difference tends to follow the magnitude of the absolute nodal power, rather than the void fraction.

To compare a variety of plants, cycle exposures and operating conditions, the nodal differences for the TIP adjacent to the highest power bundle from all the data presented in response to RAI 27 are plotted together in a single graph shown in Figure 29-4. The values are the absolute TIP nodal differences plotted versus the four bundle averaged axial void fraction for the TIP with the highest power bundle for those exposure points examined in detail in RAI 27.

The relatively even data scatter about the x-axis indicates that, even considering the limiting TIP within the core and for the limiting core designs and exposure points in the cycle, the nodal

uncertainty between calculated and measured TIPs is not increasing as a result of increasing void fraction. Although the observation with axial void fraction is made using nodal differences, and the four bundle power uncertainties are defined using the RMS radial differences, it can be concluded that, lacking a void dependency on the nodal differences, the integral of those differences would also lack void dependency. Therefore, the four bundle power uncertainties do not need to be increased.

#### Response 29-4

In addressing this question, it is important to put the depletion history at high void concentrations in perspective. Plant E is an example of an aggressive application of power uprate, being a BWR/6 uprated to 120% of original rated power. In addition, Cycle 9, its most recent full cycle of operation, is a two-year cycle with an exposure of approximately 16000 MWD/ST. The operation history is summarized in Table 25-9 of RAI 25. Peak void fractions of 88% are common during its operation, leading one to believe that a significant amount of burnup is achieved at void fractions of 85% and above. In reality, bundles do not stay at the maximum power throughout their entire life, so the exposure weighted density, UH for the maximum power bundle in the core is representative of a void fraction less than the 88% maximum void fraction exhibited throughout the cycle. Nodes having high void fractions for the majority of their time in the core will also tend to have lower power density and hence lower burnup at the end of cycle. These trends are illustrated in Figure 29-5, where a plot of nodal UH (exposure weighted water density) is plotted vs. nodal exposure for all nodes in the Plant E core at the end of Cycle 9. This figure focuses on the high exposure, high void fraction part of the core (the values for UH below 0.6 are not shown for clarity). The values of UH corresponding to 80%, 83% and 86% voids are shown on the graph. The following observations can be noted from this Figure:

- No nodes have a void history greater than 86%, and those approaching 86% have a burnup around 5000 MWD/ST.
- About 4% of the nodes have a void history corresponding to greater than 83% and their maximum exposure is less than 20000 MWD/ST
- Less than 12% of the nodes have void histories greater than 80% voids and all have exposures less than 37000 MWD/MT. This 80% void fraction representing a significant fraction of depletion history is 8% less than the maximum fraction noted in the plant history tables.

The application presented here represents the highest probability for achieving high exposure at a high void fraction, i.e., a high power density plant with a high cycle exposure. A small portion of the bundles operates at very high voids and an even smaller portion of those burn to a high exposure.

Four bundle cells surrounding TIPs are comprised of bundles with various characteristics and at various exposures. Comparisons of the axial and radial TIP readings with calculations provide a benchmarking of the calculational methods in that these comparisons inherently contain the effects of depletion. These measurements are taken routinely throughout a cycle and provide

direct and immediate feedback to the core monitoring. These readings can also be used to examine the fidelity of the nuclear methods as a function of exposure. This is in contrast to gamma scans, which are discussed in the response to RAI 28.

Specifically, one can observe a single TIP string throughout the cycle. If one chooses a TIP string, around which are loaded two fresh bundles and two once-burned bundles, then the effects of high void depletion can be observed. It should be noted that, in general, high exposure bundles are not depleted under high void conditions since these bundles are naturally lower in power later in life. Figure 29-5 demonstrates this point.

Further illustration of TIP string behavior is provided in data from Plant A Cycle 19, as shown in Figure 29-6. TIP string 12 is loaded with two once burned bundles and two fresh bundles. The radial differences for TIP string 12 as the fresh bundles deplete throughout the cycle do not rise throughout the cycle. The nodal RMS values through the cycle are not significantly different than those of the core average. Figure 29-7 shows similar data for Plant B Cycle 10. TIP string 8 is loaded with two fresh bundles and two once burned bundles. Again, the radial difference of this TIP does not exhibit an increasing trend with exposure and the nodal RMS value is not significantly different than the core average nodal RMS value.

These nodal comparisons, while not directly used in evaluations of SLMCPR or other licensing parameters, have been shown to be acceptable. Both the core average RMS difference of all nodal instrument predictions to measured TIP data and the “hot” TIP string, have an average RMS nodal difference of generally less than [[      ]] for the strings depicted in Figures 29-6 and 29-7, indicating that axial power distributions are also predicted adequately. This level of agreement is generally taken to be quite good.

NEDO-33173-A, Revision 1  
 Non-Proprietary Information

**Table 29- 1 TIP Data from Plant B Cycle 10, Exposure Point E, TIP string 24**

Node	TIP Z (in)	CALTIP	PCTIP	Delta
24	141.0	[[		
23	135.0			
22	129.0			
21	123.0			
20	117.0			
19	111.0			
18	105.0			
17	99.0			
16	93.0			
15	87.0			
14	81.0			
13	75.0			
12	69.0			
11	63.0			
10	57.0			
9	51.0			
8	45.0			
7	39.0			
6	33.0			
5	27.0			
4	21.0			
3	15.0			
2	9.0			
1	3.0			]]

**Table 29- 2 Normalized TIP Data from Plant B Cycle 10, Exposure Point E, TIP string 24 for Axial Computations**

<b>Node</b>	<b>TIP Z (in)</b>	<b>CALTIP</b>	<b>PCTIP</b>	<b>Delta</b>
23	135.0	[[		
22	129.0			
21	123.0			
20	117.0			
19	111.0			
18	105.0			
17	99.0			
16	93.0			
15	87.0			
14	81.0			
13	75.0			
12	69.0			
11	63.0			
10	57.0			
9	51.0			
8	45.0			
7	39.0			
6	33.0			
5	27.0			
4	21.0			
3	15.0			
2	9.0			]]

**Table 29-3 Calculated and Measured TIP readings and Surrounding Bundle Void Fraction Profiles for Plant B Cycle 10 Exposure Point E TIP String 24**

Axial Node	BUNDLE LOCATION				CALTIP	PCTIP	Delta
	(24,14) Void	(25,14) Void	(24,15) Void	(25,15) Void			
25	[[						
24							
23							
22							
21							
20							
19							
18							
17							
16							
15							
14							
13							
12							
11							
10							
9							
8							
7							
6							
5							
4							
3							
2							
1							]]



**Figure 29-1 Difference Between Calculated and Measured TIP Readings As a Function of Surrounding Bundle Void Fraction for Plant B Cycle 10 Exposure Point E TIP String 24**

[[

]]

**Figure 29-2 Difference Between Calculated and Measured TIP Readings As a Function of Surrounding Bundle Void Fraction for Plant E Cycle 10 Exposure Point M TIP String 18**

[[

]]

**Figure 29-3 Difference Between Calculated and Measured TIP Readings As a Function of Surrounding Bundle Void Fraction for Plant A Cycle 18 Exposure Point B TIP String 16**

[[

]]

**Figure 29-4 Absolute Nodal Differences Between Calculated and Measured TIP Readings  
As a Function of Surrounding Bundle Void Fraction**

[[

]]

**Figure 29-5 Nodal Void History as a Function of End of Cycle Nodal Exposure for Plant E, Cycle 9**

[[

]]

**Figure 29-6 Nodal and Radial Differences Between Calculated and Measured TIP  
Readings for Plant A Cycle 19 TIP String 12 As a Function of Cycle Exposure**

[[

]]

**Figure 29-7 Nodal and Radial Differences Between Calculated and Measured TIP  
Readings for Plant B Cycle 10 TIP String 8 As a Function of Cycle Exposure**

[[

]]

**MFN 05-038 NRC RAI 1**

1. MCNP Generated and Extrapolated Comparison (Section 2.1.1). Figures 2-1 to 2-9 show the extrapolation errors obtained by comparing MCNP data generated data at 90% void conditions against data obtained by extrapolation to 90% void the MCNP data fit at the three void statepoints (0%, 40%, and 70% void). The following pertains to these MCNP evaluations.
  - 1-1 The MCNP extrapolation errors at 90% void are significant for some of the parameters. Evaluate the impact of these extrapolation errors on the core behavior including axial power profile and pertinent thermal limits.
    - a. Migration area (Figure 2-8) with extrapolation errors [[                    ]]
    - b. Flux ratio (Figure 2-9) with extrapolation errors [[                    ]]
  - 1-2 Exposure Dependency of MCNP Extrapolation Error. Figures 2-1 to 2-9 provide extrapolation errors as functions of lattice averaged exposure in order to illustrate any exposure dependence or isotopic dependence exist. In the evaluation of the MCNP results, the Enclosure states that the points with the worst agreement are either highly exposed conditions (65 GWd/ST) or controlled conditions or both. However, the biggest error seems to occur around 15 GWd/ST, where the plutonium content is highest. At high burnups there is less concern for large errors because the high burnup assemblies would not be at their peak reactivity. Discuss at what exposure the peak reactivity is expected to occur and identify the main contributors. Revise the Enclosure discussion and justify the peak error at 15 GWd/ST as opposed to 65 GWd/ST.
  - 1-3 Use of 40% Void TGBLA Isotopic Content. In the MCNP cases, the isotopic concentration was kept constant and the instantaneous voids changed for given exposure. For these MCNP evaluations, was the TGBLA's isotopic content at 40% void used in simulating exposed lattice? Does the depletion [[                    ]] represent the worst case for the instantaneous void extrapolation or should depletion at other void fractions, [[                    ]], also be considered with the corresponding TBGLA isotopic compositions used in additional MCNP calculations?
  - 1-4 Instantaneous Water Density Cross-section Fit Adequacy. The results discussion in Section 2.1.1 states that the fit (in instantaneous water density) is typically made in an exposure range which itself has a quadratic functional dependency assigned to it. The exception to this is the [[                    ]] or TIP detector response, which has a cubic dependence on exposure. Provide additional explanation on the above dependency statements.
  - 1-5 Figures 2-1 to 2-11 do not provide means to differentiate the data for different lattices, therefore it is difficult to determine if a high Gd lattice may show more predominant exposure dependence. In addition, the data does not indicate if the result is based on controlled or uncontrolled condition. Please include this in the update.
  - 1-6 The errors in the pin power/fission rate distribution is presented in Figures 2-21 and 2-29, which show the RMS and MAX pin power errors. Compute and include the error in the peak pin power/fission rate.



**GE Response**

**Response to RAI 1-1a**

The TGBLA-MCNP differences in migration area are not extrapolation errors, since they also exist at the lower void fractions. The differences are due to a number of factors, primarily the treatment of anisotropic scattering in the two models and the spectral weighting. The GE response to RAI 2-4 will provide further details regarding this topic.

The error propagation study performed in support of the GE response to RAI 2-7 will include any extrapolation error in the curve fit of the migration area, and diffusion coefficients, that may exist.

**Response to RAI 1-1b**

For the nodal solution in PANACEA, the infinite lattice flux fits from TGBLA output are used only in the development of the spectral history correction term and in the thermal flux instrument calculations.

The spectral history reactivity is accounted for using an "Effective Void History" model, as is normally done. This model converts the spectral history effect for each node into a historical water density during each exposure update. The underlying theory of this model is that the isotopic concentrations accumulated with exposure are not so much a function of physical water density, but rather spectral conditions. The model provides only an effective history dependent water density at which cross sections are evaluated. The instantaneous water density remains the same as that calculated by the thermal hydraulic analysis. The thermal-hydraulic historical water density (UH) continues to be accumulated in the normal fashion.

The thermal hydraulic historical water density is updated during each exposure increment as:

$$UH_{i,j,k} = \frac{1}{E_{i,j,k}} \int_0^{E_{i,j,k}} U_{i,j,k}(E) dE \quad \text{Eq (1-1)}$$

where U is the instantaneous water density as calculated by the thermal hydraulic analysis.

The spectral history corrected historical water density (UHSPH) is updated using the same expression except that the U is a calculated spectral effect not the T/H value. The relationship between spectral flux ratios and water density is fit as a function of exposure, instantaneous water density and history dependent water density. Evaluating the fit at the nodal exposure and history dependent water density and at [[ ]] water densities, a quadratic function of spectral flux ratio versus water density may be formed.

$$[[ ]] \quad \text{Eq (1-2)}$$

In order to estimate the water density that represents the same spectral flux conditions, the roots to a quadratic equation must be calculated.

[[ ]] Eq (1-3)

where  $\frac{\bar{\phi}_i}{\phi_i}$  represents the nodal flux ratio as calculated by PANACEA.

Limits are imposed on the quadratic fit of the flux ratios. If the calculated root of Eq (1-3) is beyond the bounds, the correlation between spectral index and relative water density is assumed to be suspect. Nodes that give estimates of spectral history water density outside the bounds are those that have flux ratios that differ greatly from the infinite lattice values. These nodes are generally subject to extreme nodal leakages and are generally on the periphery of the core.

The spectral history correction through the effective void history term is typically small for standard reload core designs. Figure 1-1 shows the reactivity worth of various components of the eigenvalue adjustments that are made in the core simulator. The figure shows the core average reactivity worth of various components of the core reactivity such as control blades, xenon worth, Doppler reactivity, control blade history and spectral history. Values are given as a function of exposure throughout a typical MELLLA+ introduction cycle. As seen from the figure, the spectral history is relatively constant throughout the cycle and is the smallest component of reactivity correction in the core.

The flux ratios are also used in the thermal flux instrument response calculations (i.e., LPRMs and thermal TIPS). These do not have an influence on the non-adaptive flux and power solution of the core simulator.

#### Response to RAI 1-2

It may be that RAI 1-2 arises due to a lack of clarity that exists in the language of the Enclosure 3 of MFN 04-026 [See Enclosure B herein]. This may have resulted in a misinterpretation of what was intended by the description of the exposure dependency of extrapolation errors. A restatement of this section is needed to correct any misinterpretation that may have occurred.

Section 2.1.1 of Enclosure 3 of MFN 04-026 [See Enclosure B herein] states that:

[[

]]

The phrase “worst agreement” in the second sentence above was meant to refer to “worst agreement” specifically for the fit of the slowing down cross-section from the epi-thermal group evaluated at 90% instantaneous void fraction. The slowing down from the fast group was not meant to be included in this context. From Figure 2-5 of Enclosure 3 of MFN 04-026 [See

Enclosure B herein], the intent of the statement is clearer, although the agreement at 40 GWd/sT for that parameter is also not as good as at beginning of life. Other studies (see the response to RAI-29 submitted in GE letter dated April 8, 2005, MFN 05-029) show that for void depletions above [ [ ]].

The examination of k-infinity provides a good summary of how the many components, which are individually discussed in much of Section 2 of Enclosure 3 of MFN 04-026 [see Enclosure B herein], roll up into a more macroscopic assessment of fit fidelity. The percent error in the fit of k-infinity around an exposure 15 GWd/sT is similar to that at zero exposure. The absolute magnitude of the error is, in fact, largest at this exposure since, due to the depletion of Gd isotopes in the lattice, the k-infinity itself is highest at this point. While plutonium content in the lattice is highest at the highest exposures, rather than at 15 GWd/sT, the depletion of Gd isotopes, many of which are both thermal and epi-thermal absorbers, at the medium exposure point of 15 GWd/sT accounts for the largest variance in the fit.

#### Response to RAI 1-3

For the instantaneous void comparisons, the isotopic concentrations were held constant. These isotopic concentrations are taken from TGBLA's 40% void history depletion cases. [ [

]] Changes in the isotopic concentrations are dealt with separately in the GE steady-state methods process and are included in a Sections 2.1.4 and 2.1.5 of Enclosure 3 of MFN 04-026 [see Enclosure B herein]. Consideration of other bases for the isotopic concentrations, whether better or worse for quadratic fit error estimation, would not be representative of the actual process being assessed.

#### Response 1-4:

The discussion in Section 2.1.1 of Enclosure 3 of MFN 04-026 [see Enclosure B herein] presents the method used in the prior versions of the core simulator physics. The cubic dependence on exposure for the [ [ ] ] is a process used by PANAC10 and previous versions of PANACEA. The PANAC11 process treats [ [ ] ] in the same fashion as other cross-sections. The fitting process in water density and historical water density is essentially the same between earlier and the current version of PANACEA. The discussion should be corrected to remove this error.

To better explain the dependencies, the following discussion is provided regarding the PANAC11 nuclear parameter fitting process that is currently used. All nuclear library data from the hot operational lattice physics calculations (cross section data, TIP responses, etc.) are divided into a specified number of exposure ranges. Within each exposure range, for each control state, the data are currently fit as a [ [

]]. This represents the [ [ ] ] terms needed for the [ [ ] ] fits in the [ [ ] ]

independent variables, plus an additional [[        ]] terms that capture the cross-terms between these variables. This technique is used for all cross sections, and also for other nuclear library parameters, such as fluxes, k-infinity and diffusion coefficient.

Response 1-5:

Five separate lattice nuclear designs were used to generate the data in Figures 2-1 through 2-11 of the Enclosure 3 of MFN 04-026 [see Enclosure B herein]. Four of these designs are highly enriched, with high concentrations of gadolinia. The other lattice is a top natural uranium lattice, which has vanished zones above the part length rods and the gadolinia rods. The enrichment and gadolinia characteristics of the lattices are shown below:

[[

]]

Using the above nomenclature, Figures 1-2 thru 1-9 provides updates to Figures 2-1 to 2-6 and Figures 2-9 and 2-9b of Enclosure 3 of MFN 04-026 [see Enclosure B herein] to demarcate individual lattices and control states for all points. Since calculation of the migration area and diffusion coefficient from MCNP is not appropriate (which will be addressed in a future response to RAI 2-4), Figures 2-7 and 2-8 of Enclosure 3 of MFN 04-026 [see Enclosure B herein] have not been updated, and should not be considered in the review of the Methods Interim Process.

Figures 2-10 and 2-11 of the Enclosure 3 of MFN 04-026 [see Enclosure B herein] apply explicitly to lattice 5168 in the uncontrolled state. There appear to be no clear, consistent trends in error with enrichment or gadolinia content of the lattices.

Response 1-6:

Figure 2-21 of Enclosure 3 of MFN 04-026 [see Enclosure B herein] conveys the errors for the fit of TGBLA pin power data extended to 90% in-channel void fraction relative to the MCNP calculations at 90% void fraction, sorted by control state. Figure 2-29 of Enclosure 3 of MFN 04-026 [see Enclosure B herein] conveys the fit of MCNP pin power data extended to 90% in-channel void fraction relative to the MCNP calculations at 90% void fraction, sorted by control state. Both of these figures in Enclosure 3 of MFN 04-026 [see Enclosure B herein] did not include the error on the peak pin in the lattice. The error on the peak pin is related to the actual thermal mechanical LHGR operating limit, as it is the highest peaking pin in the lattice that determines the limit in operation. Figures 1-10 and 1-11 provides an update of Figures 2-21 and 2-29 of Enclosure 3 of MFN 04-026 [see Enclosure B herein] to include this peak pin error.

Both figures show the average RMS error for a lattice comparison, the maximum error within a lattice (this generally occurs in a low power pin, and thus the percentage error appears relatively

NEDO-33173-A, Revision 1  
Non-Proprietary Information

high, but the absolute error is somewhat low) and the error on the peak pin in the lattice. Both the comparison of the fitted TGBLA data and the fitted MCNP data show excellent agreement with the calculated MCNP pin power at 90% void fraction with errors on the peak pin of [[ ]] respectively. This agreement is within Monte Carlo statistics of the calculated result.

[[

**Figure 1-1 Comparison of Core Average Reactivity Worth Components** ]]

[[

**Figure 1-2**  
**Update of Figure 2-1, Error in fit of k-infinity in U**

]]

[[

**Figure 1-3**  
**Update of Figure 2-2, Error of fit in U of Thermal Absorption Cross section**

]]



[[

**Figure 1-4**  
**Updated of Figure 2-3, Error of fit in U of  $\nu$  x fission cross section**

]]

[[

]]

**Figure 1-5**  
**Update of Figure 2-4, Error of fit in U of Group 1 to 2 Slowing Down Cross section**

[[

]]

**Figure 1-6**  
**Update of Figure 2-5, Error of fit in U of Group 2 to 3 Slowing Down Cross section**

[[

**Figure 1-7**  
**Update of Figure 2-6, Error of fit in U of Fast Removal Cross section**

]]

[[

**Figure 1-8**  
**Update of Figure 2-9a, Error of Fit in U of Fast Flux Ratio**

]]

[[

]]

**Figure 1-9**  
**Update of Figure 2-9b, Error of Fit in U of Epi-thermal Flux Ratio**

[[

]]

**Figure 1-10**  
**Update of Figure 2-21, TGBLA vs. MCNP: RMS, Peak Pin and Max Error in Pin Powers**  
**at 90% VF**

[[

]]

**Figure 1-11**  
**Update of Figure 2-29, RMS, Peak Pin and Max Error in Fit in U of Pin Fission Density Distribution**



**MFN 05-038 NRC RAI 13**

Section 2.3 - Flow Distribution Models (PANAC/ISCOR). The TRACG analysis case presented was based on 105% power and 65% CF. Provide the results for the bounding conditions of 120% power and 80% CF. Update Table 2, "TRACG Steam Separator Predictions for MELLLA+."

**GE Response**

The following is an update of Section 2.3 based on Brunswick at EPU/MELLLA+ conditions.

An analysis of the upper plenum region resulted in the conclusion that an extreme mismatch in delta-P in the upper plenum region leading to the separators is not indicated. TRACG (using a three ring upper plenum modeling) indicates a [[ ]] difference between the center ring and peripheral ring for a 100% power/ 85% core flow case (MELLLA+). A non-negligible amount of flow was calculated to move from the center and intermediate rings to the next outer ring in the plenum region. For the center ring, the total separator inlet flow was [[ ]] while the radial redistribution from the center to the intermediate ring was [[ ]] For the intermediate ring, the total separator inlet flow was [[ ]] while the radial redistribution from the center to the intermediate ring was [[ ]] of all flow entering the region. This flow indicates that a non-negligible amount of mixing does occur in the upper plenum. Study results are summarized in Table 13-1, which is an update of Table 2 of Enclosure 3 of MFN 04-026 [see Enclosure B herein].

These results can be used in determining the range of possible separator inlet qualities. Bundle exit quality is around [[ ]], but this is before mixing with the out-channel bypass. The separator inlet quality will therefore be substantially below the [[ ]] regime. The study shows that the separator inlet quality range may run from [[ ]]

**Table 13-1**

**Updated Table 2 TRACG Steam Separator Predictions for MELLLA+**

[[			
			]]

**MFN 05-038 NRC RAI 14**

Section 2.8 - Bypass Void Models (PANAC/ISCOR). AOO RAI 5 response proposes using ISCOR (4 bundle) analyses to establish if the bypass voiding remains less than 5% during steady-state. However, ISCOR is a single hot channel/average channel code and the flow distribution in the bypass flow may not be accurate.

- 14-1 Provide a confirmatory 4 bundle TRACG analyses for a MELLLA+ core (Brunswick) to establish what the bypass voiding would be during steady-state. Use limiting conditions in terms of operating conditions of the 4 bundles (e.g., cycle exposure, number of hot bundles in the control cell, and the initial OLMCPR. Perform the analysis at the EPU/MELLLA+ conditions that would lead to the most limiting in-channel and bypass voiding condition (e.g. 80% or 55% CF statepoints). Discuss the results and state if the ISCOR model would underpredict the potential for bypass voiding.

**GE Response**

The following bounding (based on 4 bundle average power) ISCOR results were provided in GE Letter dated March 4, 2004, MFN 04-026, (See GE Response to RAI. 5).

[[		
		]]

This calculation was based on a 4 bundle average radial peaking factor of 1.28.

A TRACG steady state simulation was prepared that modeled a ring of 4 bundles in the center of the core (see the TRACG Model Description LTR Section 7.8 for more details on the vessel modeling). No theta modeling is required for this simulation (i.e. R,Z only). The base nuclear condition was chosen such that the 4 bundle radial power was higher and axial power shape was more bottom peaked than the ISCOR assumption in order to maximize the bypass void fraction. The 4 bundles that were chosen were actually the 4 highest peaking bundles. These 4 bundles had an average radial peaking factor of [[

]]. The void fraction of the bypass at the “D” level was obtained from TRACG.

In order to compare the prediction of ISCOR on the same radial peaking basis, the cases from AOO RAI 5 were rerun with a 4 bundle average radial peaking factor of [[ ]].

The following are result of the bypass void fraction prediction.

[[			
			]]

The ISCOR model does not underpredict the potential for bypass voiding. ISCOR predicts a higher bypass void fraction primarily because the ISCOR direct moderator heating model [[ ]. The TRACG direct moderator heating model was determined based on detailed [[ ].

ISCOR calculation will be performed during each reload cycle to ensure that [[ ] hot channel bypass void fraction at LPRM “D” Level is not exceeded in the EPU/MELLLA+ operating domain.

**MFN 05-038 NRC RAI 18**

Section 3.3: Time and Depth of Early Boiling Transition.

- 18-1 Provide the data ranges and the expected ranges for EPU/MELLLA+ Operation.
- 18-2 Justify why the test ranges shown in Table 3 would cover the conditions expected for all BWR product line operating at EPU/MELLLA+ conditions up to GE14.
- 18-3 Explain if the experimental thermal-hydraulic data ranges are checked for all new fuel product lines or for legacy fuel.

**GE Response**

**Response to RAI 18-1**

Boiling transition is predicted for both transient and steady state conditions by the GEXL correlation, which evaluates the quality at which boiling transition occurs, depending on the pressure, characteristic mass flux, inlet enthalpy, and bundle geometry. The mass flux for the active channel portion of the fuel bundle is expressed in units of million pounds/hour-ft<sup>2</sup>. Figure 18-1 below shows the range of mass flux and inlet subcooling for various transients evaluated to demonstrate compliance with SLMCPR technical specifications. Striped areas show the transient ranges. Steady state flow ranges for interior bundles are also shown. The low end of the full power steady state flow range can extend as low as 80% of rated flow and the high end can extend to as high as 111% of rated flow. Intermediate powers cover a wider flow range. The bundles located on the edge of the core are orificed to receive less flow because of their low power. The range for edge bundles is also shown. Test points for the GEXL correlation are shown as orange squares. The major independent variables in the GEXL correlation are active channel mass flux and inlet subcooling. Since the correlation evaluates the quality at which boiling transition occurs, the major impact of system pressure is accounted for in the evaluation of quality. There is, however, an additional term in the GEXL correlation specifically devoted to system pressure. [[

]] The test matrix points for the GEXL correlation extend well beyond the steady state and transient conditions expected for BWR EPU and MELLA+ applications.

**Response to RAI 18-2**

The GEXL correlation is developed from steady state test data where the initial conditions are fixed and the bundle power is increased until boiling transition is observed. The GEXL correlation is used with the TASC code to predict boiling transition in the transient environment. The transient evaluations are qualified with special transient tests in which the input bundle power, pressure and flow are varied with time to simulate a given transient. All of the transient results shown in Figure 3 of MFN 04-026 Enclosure 3 [see Enclosure B herein] are simulations of turbine trip or load rejection transients.

In the turbine trip and load rejection transients, there is an increase in pressure and flow accompanied by an increase in surface heat flux in the channel of between 30% and 50%. Two

types of turbine trip transients are run. Many plants mitigate the severity of turbine trip and load rejection transients by tripping the recirculation pumps when the turbine trip is detected; others do not take this mitigating action. For those transients with a pump trip, the flow at the time of dryout is about 20% less than the initial flow. For those transients without a pump trip, the core flow at the time of dryout is about equal to the initial flow, which in these cases is between 1.0 and 1.1 Mlb/hr-ft<sup>2</sup>. Table 18-1 shows the transients in Table 3 of MFN 04-026 Enclosure 3 [see Enclosure B herein] and indicates which tests had a pump trip simulation and the amount of heat flux increase. Again, Figure 18-1 shows that the GEXL correlation range covers the transient range. The dryout time agreement shows that the TASC system simulates the transient behavior well.

### Response 18-3

New GEXL correlations are generated for each new product line. A new product line represents a new geometry or spacer configuration. The test range for each correlation is checked for appropriateness in the application design review for the correlation. This test matrix procedure has not changed since the introduction of the GE9 product line because it conservatively covers the thermal hydraulic operating range.

NEDO-33173-A, Revision 1  
 Non-Proprietary Information

Table 18-1 Dryout Time Comparison between ATLAS test data and TASC

Bundle	Run	ATLAS (sec)	TASC (sec)	Pump Trip	% Power Increase
[[					
					]]

[[

Figure 18-1 GEXL Test Matrix and Expected Operating Ranges

]]



**MFN 05-038 NRC RAI 22, Bypass voiding during Transient Conditions.**

TRACG analyses involving 2 RPT (ATWS and 2 RPT transient) indicating bypass voiding during the transient could reach over 30%, despite the TRACG modeling approach of lumping the 4 bundle bypass regions into rings. Evaluate other transients and confirm if bypass voiding greater than 5% would be experienced during the event. Select the transients such that would yield the most limiting conditions in terms of the potential for causing bypass voiding, including the number of hot bundles in the 4 bundle control cell and the corresponding operating limit.

**GE Response**

[[

]] Table 22-1 addresses the UFSAR categories of AOOs and the potential for bypass voiding of greater than 5% in the bypass region. The table also discusses whether the LPRM/APRM are used as part of the event mitigation. [[

]]





NEDO-33173-A, Revision 1  
Non-Proprietary Information

<b><u>Table 22-1</u></b>	
<i>Transient</i>	<i>Bypass Void Fraction Impact</i>

**MFN 05-045 NRC RAI 4-6, Instantaneous and Historical Water Density Pin Power Fit (Sections 2.1.3 and 2.1.5)**

Provide a discussion on how the lattice pin powers are fitted/interpolated to get each pin power distribution as a function of void fraction and exposure.

**GE Response**

For PANAC11, all nuclear library data from the hot operational lattice physics calculations (cross section data, TIP responses, etc.) are divided into a specified number of exposure ranges. Within each exposure range, for each control state, the data are currently fit as a [[

]]. This represents the [[ ]] terms needed for the [[ ]] fits in the [[ ]] independent variables, plus an additional [[ ]] terms that capture the cross-terms between these variables. This technique is used for all cross sections, and also for other nuclear library parameters, such as fluxes, k-infinity and diffusion coefficient.

This fitting process is also used for pin power responses on a pin-by-pin basis. That is, for every specific lattice type (geometry, composition), the local peaking response of each pin as directly calculated by the lattice physics code is preserved as a unique parameter with all of the degrees of freedom as a nuclear cross section. PANAC11 uses a pin power reconstruction technique to account for local flux gradients in addition to the correct relative peaking.

For PANAC10, the local peaking data used for predicting kW/ft is fit as a [[

]]. Each uniquely defined pin for a given geometric fuel type is modeled. PANAC10 uses a correlated gradient local peaking technique to account for local flux gradients in addition to the correct relative peaking.

In both codes (PANAC10 and PANAC11), the dependency on historical relative water density (UH) and instantaneous relative water density (U) is [[ ]]. Therefore, two separate [[ ]] polynomial forms were assumed in the error analysis performed in Sections 2.1.3 and 2.1.5. This allowed for isolation of the effects of UH and U extrapolation outside of the simulator.

**MFN 05-045 NRC RAI 12, Section 2.2 - (two phase pressure drop)**

- 12-1 Update Section 2.2 by including the test bundle pressure drops test data shown in Figure 3-1 of NEDC-328774P.
- 12-2 For Figure 2-41 (enclosure) provide an explanation of the data ranges and how ISCOR is fine tuned to using test data. Also state what is the criteria for the pressure error.

**GE Response**

**Response to RAI 12-1**

The thermal hydraulic characteristics of the GE14 fuel assembly, including critical power performance and bundle pressure drop measurements, were tested in the ATLAS facility and are documented in NEDC-32874P. Figures 3-1 and 3-2 of that document provide graphical summaries of the pressure differential for the active channel, which spans approximately the entire heated length of the bundle (but not including the bundle's simulated lower tie plate or upper tie plate). These pressure differentials are shown as a function of mass flux and bundle powers. Figure 3-2 from that document is the appropriate figure for the GE14 data (ATA784) and is provided below as Figure 12-1.

**Response 12-2:**

The referenced Figure 2-41 is contained in Enclosure 3 of MFN 04-026 [see Enclosure B herein]. This figure shows the error in predicted versus measured bundle pressure drop for a GE14 fuel bundle. The data cover a mass flux range from [[ ]], which covers flows from less than natural circulation to more than the rated flow for a BWR fuel bundle. This bounds EPU/MELLLA+ conditions, which are [[ ]] for typical operating conditions. Data were obtained for each mass flux rate in 0.1 Mlb/ft<sup>2</sup>-hr intervals at powers ranging from zero power to the critical power at the specific flow or [[ ]].

The spacer loss coefficients used in ISCOR are determined from data at [[ ]] and [[ ]], which correspond to typical average bundle conditions at rated power and flow. Figure 2-41 shows the error in the predicted versus measured pressure drop. Note that there is no error for a mass flux of [[ ]] and a power of [[ ]]. In the range of possible mass fluxes of [[ ]], the standard deviation is less than [[ ]]. This is a [[ ]] error compared to a normal total core pressure drop of approximately 20 psi. This is also a small error compared to the pressure drop uncertainties used in the calculation of the safety limit, for example the applied uncertainty for the core pressure drop range from [[ ]].

[[

{3}]

**Figure 12-1**  
**Figure 3-2 of NEDC-32874P, Test ATA784 Bundle Pressure Drop**

**MFN 05-045 NRC RAI 17. Section 3.2 ODSYS**

Provide additional data to justify the applicability of ODSYS for the MELLLA+ operation. For example, discuss the models used and give some justification for the application of ODSYS to MELLLA+ condition.

**GE Response**

GE has revised Section 3.2 of MFN 04-026, Enclosure 3 [see Enclosure B herein], to provide the discussion of the model and justification for the application of ODYSY to MELLLA+ conditions. The revised section is provided in Enclosure B herein.



**MFN 05-048 NRC RAI 11 - Section 2.2 - Void Quality Correlation**

The section discusses the applicability of the void correlations used in the GE codes for operation in the MELLLA+ conditions.

- 11-1 TRACG does not use the DIX correlation. Please provide evaluation of the applicability of the TRACG's interfacial shear model.
- 11-2 For the new DIX correlation, what are the variables and the corresponding applicability ranges? Show where the MELLLA+ operation fits within the range of applicability.

**GE Response**

**Response to RAI 11-1**

The TRACG interfacial shear model used for the calculation of the void fraction is described in the TRACG Model Description LTR, NEDE-32176P. The applicability of this model is documented in the NRC approved LTR, "TRACG Application for Anticipated Operational Occurrences (AOO) Transient Analyses", NEDE-32906P-A. The TRACG interfacial shear model is qualified for a wide range of flows including EPU/MELLLA+ conditions. TRACG predicts most void fraction data for BWR fuel bundles with a mean error of [[ ]] and a standard deviation of [[ ]].

**Response to RAI 11-2**

The Dix correlation "BWR Void Fraction Correlation and Data", NEDE-21565, is a function of Reynolds number or flow and fluid properties that can be characterized in terms of pressure and temperature. The correlation is based on data covering the ranges:

Pressure: [[ ]]  
Mass Flux: [[ ]]  
Inlet subcooling: [[ ]]

These ranges are well beyond what can be expected in an operating BWR fuel bundle and include EPU/MELLLA+ conditions.

- 16-1 The section evaluates steam separator performance of models in ODYN for operation at high void conditions. Provide similar model descriptions and evaluations for TRACG.

**MFN 05-048 NRC RAI 16, Section 3.1- Steam Separator**

16-1 The section evaluates steam separator performance of models in ODYN for operation at high void conditions. Provide similar models, descriptions and evaluations for TRACG.

16-2 Compare the TRACG modeling results against the separator performance data.

16-3 Demonstrate that the variable separator inlet qualities [[  
]] would not result in adverse impact.

16-4 [[  
  
]]. Explain the impact [[  
  
]]

**GE Response.**

Response to RAI 16-1

The TRACG separator model is described in the TRACG Model Description LTR, NEDE-32176P. The evaluation of this model is discussed in the response to RAI 16-2.

Response to RAI 16-2

The TRACG separator model qualification against data is described in the TRACG Qualification LTR, NEDE-32177P. The uncertainty in the separator performance is documented in the NRC approved LTR, "TRACG Application for Anticipated Operational Occurrences (AOO) Transient Analyses", NEDE-32906P-A. The key separator parameter that affects fuel performance is the carryunder. The uncertainty in this parameter is quantified in NEDE-32906P-A and shown to be less than [[  
]] for typical limiting conditions.

Response to RAI 16-3

Any adverse impact would not come from variable inlet qualities as TRACG uses the actual variable conditions as they occur in an operating reactor, but rather from the high inlet qualities that typically exist in the center region of the core, and which may exceed the experimental database for separator inlet qualities. The impact of exceeding the separator inlet quality database is addressed as part of the response to RAI 16-5.

Response to RAI 16-4

A sensitivity study was done to evaluate the sensitivity to the carryunder. The sensitivity study was done for a plant at EPU/MELLLA+ conditions of 100% of uprated power and 85% flow. The case chosen for the sensitivity study was the same as the case referenced in RAI 16-3, where the average separator inlet quality was [[  
]], but where the separator inlet quality varied from [[  
]] at the center of the core to [[  
]] at the periphery. Three calculations were made for a generator load rejection without bypass transient, a reference case identical to the

NEDO-33173-A, Revision 1  
Non-Proprietary Information

original calculation, a calculation where the separator carryunder was reduced by [[ ]], and a calculation where the separator carryunder was increased by [[ ]]. Note the uncertainty in the calculated separator carryunder is [[ ]] (see the response to RAI 16-2). The results of these calculations are shown on Table 16-1.

There are two main impacts of reducing the separator carryunder. First, reducing the carryunder increases the core inlet subcooling. This increased core inlet subcooling improves the initial critical power performance. From Table 16-1 it is seen that a [[ ]] reduction in carryunder improves the initial critical power ratio (ICPR) by [[ ]]. Second, reducing the carryunder reduces the amount of steam in the bulk water region. This makes the pressurization and the corresponding transient change in the critical power ratio ( $\Delta$ CPR) slightly worse. From Table 16-1 it is seen that a [[ ]] reduction in carryunder increases the transient  $\Delta$ CPR by [[ ]]. The impact on the ICPR and the  $\Delta$ CPR are in opposite directions and the net impact on the minimum critical power ratio (MCPR) is rather small; a [[ ]] reduction in carryunder reduces the MCPR by [[ ]]. From Table 16-1 it is similarly seen that a [[ ]] increase in the carryunder, increases the MCPR by [[ ]]. This is a small sensitivity compared to the total uncertainty in the transient calculation, which is approximately [[ ]] or six times larger.

The RAI states that the carryunder is underestimated for high separator inlet qualities. [[

]].

NEDO-33173-A, Revision 1  
Non-Proprietary Information

Table 16-1 Sensitivity to Separator Carryunder for EPU/MELLLA+ Conditions

[[									
									]]

**MFN 05-053 Revised Response to RAI 28-2 - Methods Interim Process**

The response was superceded by the revised response to RAI 28-2 in GEH letter, MFN 06-434.  
See the updated response to RAI 28-2 in MFN 04-026.

**MFN 05-081 Revised Responses to MELLLA+ RAIs**

See MFN 04-026 for updated responses to RAIs 2, 14, 16, 17, 25b, and 26.

**MFN 06-195 Responses to Methods RAIs**

See MFN 06-211 for responses to RAIs 2, 3, 4.2 and 6.

**MFN 06-207 Responses to Methods RAIs 1 and 5**

See MFN 06-211 for responses to RAIs 1 and 5.



**MFN 06-209 Remaining Responses to Methods RAIs**

See MFN 06-211 for responses.

**MFN 06-434 Updated Response to RAI 28-2 - NEDC-33173P**

See the updated response to RAI 28-2 as part of MFN 04-026.

### **MFN 06-481 NRC RAI 7.0, AOO Axial Power Profile**

Currently, the ODYN transient calculations assume hard bottom burn operating history from BOC to MOC, which yield top peaked power shape. From MOC to EOC, the transient analyses are performed assuming both HBB and UB. The HBB assumption from BOC to MOC yield axial power profile that is conservative in terms of the scram reactivity worth. However, for EPU and expanded operating domains, it is not apparent that the currently assumed axial power shapes with exposure (E.g., HBB from BOC to MOC and MOC to EOC and UB for MOC to EOC) will be conservative relative to the nominal or planned operating control rod and core flow strategies. Specifically, considering the impact of TVAP, the LTR did not discuss why bottom and middle peaked or double hump power profile early in the cycle will not result in higher transient response.

For ODYN, justify why the conservatism associated with the scram worth, the control rod patterns assumed in the power history envelopes and bounds the impact of axial power peaking the plant will experience at different exposure ranges. Include in your assessment the impact of TVAP that would result from the scram during power profiles other than top peaked.

### **GE Response**

Pressurization events are most limiting at EOC where control rods are full out and scram reactivity is minimized. As stated in the methods LTR (NEDC-33173P), the EOC condition is evaluated using a variation in the axial power shape at EOC through two burn strategies – a Hard Bottom Burn (HBB) and an Under Burn (UB). The main reason UB power shapes are considered is the potential effect from the Time Varying Axial Power Shape (TVAPS). The principal factors controlling the severity of the TVAPS transient CPR effect are: (a) initial axial shape, (b) initial flow, and (c) plant specific MCPR timing. Cases with a more bottom peaked initial power shape will show a more severe TVAPS effect. However, the resulting operating limit is usually insensitive to the initial power shape because of the compensating effect of the increase in scram worth. However, earlier in the cycle or when the UB is more bottom peaked, the UB will be non-limiting (or at least very similar to the HBB result) due to the increased scram reactivity. The system response becomes much more mild with the UB, and although the TVAPS effect is high, the heat flux change is mild, which limits the severity of the transient  $\Delta$ CPR.

Table 7-1 below shows a comparison of the limiting transient  $\Delta$ CPR result for the HBB and UB power shapes for several plants. In some instances the UB is a more limiting condition, but as seen from Table 7-1 below when the UB is very bottom peaked (indicated below by a higher value for the Axial Peaking at Node 4), the HBB is more limiting. In these conditions the axial power is so much more toward the bottom that the scram reactivity is improved and this more than offsets any effect of time varying axial power shapes.

Pressurization analyses covering BOC to “MOC” are actually analyzed at a condition near EOC, approximately 75% to 85% through the cycle. The “MOC” condition is at an exposure prior to EOC to assure adequate control rod density in the core such that the transient response is significantly improved with partially inserted control rods.

The analysis for “MOC” is based on the HBB with a conservative rod pattern as described below.

As described in GESTAR II (Appendix B, responses to GESTAR II, revision 5, REQUEST: Subsection 5.2.2.5 – Exposure Dependent Limits), when analyzing transient performance at exposures prior to the EOC, all-rods-out condition, it is necessary to consider the effect of the control rods on the transient parameters, because the scram reactivity and the dynamic void coefficient are sensitive to the control rod pattern. At any given exposure point, there are many control rod patterns which will render the core critical and within thermal limits. To ensure that conservative values of the important dynamic parameters are calculated, it is necessary to select special control patterns. Conservative values of both the scram reactivity and dynamic void coefficient result when “black-white” control patterns are used. A black-white control pattern is one in which control rods are either fully inserted (black), or fully withdrawn (white).

The scram reactivity is minimized with black-white patterns because:

1. the fully inserted control rods provide no contribution to the scram reactivity,
2. the fully withdrawn control rods begin their insertion in a region of zero power; thus, their impact during the early portion of the scram is minimized; and
3. there are no partially inserted control rods, which generally provide a major contribution during the early portion of the scram.

The assumption of the black-white control pattern adds significant conservatism to the results. The black-white rod pattern also results in a more bottom peaked state compared to the HBB nominal pattern, which increases the TVAPS effect for this state. Note, the HBB strategy normally produces a more bottom peaked power shape at MOC compared to the EOC exposure. Control rod configurations with rods in the core at MOC may produce double humped axial power shape. This situation is predominantly from local conditions near the partially inserted rods rather than the core average axial power distribution used with ODYN. From review of a number of cores, it was found that double humped axial power shapes occurred for conditions with partially inserted control blades. Potentially limiting double humped power shape bundles are those very near partially inserted rods where locally scram reactivity is maximized for transients. However, demonstration analyses have been performed where the partially inserted control rods are in the core and compared to the standard analysis where the “MOC” point uses the HBB with a black-white pattern. The difference in the  $\Delta$ CPR between the standard analysis method and the nominal case with partially inserted rods was about 0.06 to 0.09. This study includes new analyses from a 120% uprated power plant with GE14 fuel to demonstrate the conservatism. Therefore, the standard process of using the HBB burn strategy with the black-white is very conservative compared to the smaller difference observed in Table 7-1 when and UB shape is potentially limiting. The process of analyzing exposure dependent limits is conservative.

NEDO-33173-A, Revision 1  
 Non-Proprietary Information

Table 7-1 HBB and UB Limiting Pressurization Event Results

	HBB Node 4 Axial Peaking	HBB $\Delta$ CPR	UB Node 4 Axial Peaking	UB $\Delta$ CPR
Plant A	0.91	0.31	1.41	0.23
Plant B	0.86	0.11	1.29	0.07
Plant C	1.07	0.35	1.44	0.28
Plant D	0.85	0.30	1.22	0.28
Plant E	0.47	0.33	0.8	0.36
Plant F	0.67	0.37	1.09	0.35
Plant G	0.71	0.31	0.98	0.32
Plant H	0.64	0.30	0.89	0.30
Plant I	0.87	0.33	1.31	0.33

**MFN 06-481 NRC RAI 8.0, ECCS-LOCA**

The LTR cites the conclusions from recent sensitivity analysis in its discussion of the axial power shapes assumed in the ECCS-LOCA calculation. [[

]] For EPUs, the PCT for the small break increases. [[

]] If not, justify why this approach is acceptable for plants with high PCTs.

**GE Response**

The current GENE ECCS-LOCA methodology requires calculation of the [[

]]

**MFN 06-481 NRC RAI 9**

As part of the ESBWR design certification review, the NRC staff discovered a discrepancy in the GSTRM thermal-mechanical calculations, supporting the GE14 fuel designs. Specifically, the GSTRM UO<sub>2</sub> under-predicted the fuel temperature calculations in comparison to both FRAPCON-3 and PRIME calculations. It is possible that the observed differences are primarily due to GSTRM UO<sub>2</sub> fuel thermal conductivity model, which does not model exposure dependency compared to the other two codes. The potential non-conservatisms in GSTRM could be applicable to thermal-mechanical performance calculations for operating reactors as well the calculation of the associated limits.

- a. Provide an assessment of the impact of the non-conservatism in GSTRM UO<sub>2</sub> fuel temperature calculation regarding the adequacy of the fuel rod thermal-mechanical performance for the GE13 and G14 fuel designs.
- b. Evaluate the impact of the GSTRM UO<sub>2</sub> under-predictions on the fuel temperature, internal rod pressure, and TOP/MOP calculation during anticipated operational occurrences (AOOs).
- c. Assess the impact of the GSTRM UO<sub>2</sub> non-conservatism (e.g., thermal conductivity model) on peak cladding temperature (PCT) for both the limiting small and large break loss of coolant accidents (LOCAs) at EPU conditions. This assessment should also include the most limiting axial power profile.
- d. In MFN 06-207, RAI 1 contains thermal-mechanical performance results for along the linear heat generation rate (LHGR) envelope (e.g., internal rod pressures, fuel temperature, and cladding circumferential strain) for the UO<sub>2</sub> and the UGdO<sub>2</sub> rods. Discuss if the potential non-conservatisms will change the results for operation on the LHGR envelope or the related sensitivity analysis in RAI 1.

**Response to Part a**

Fuel rod thermal-mechanical design and licensing analyses are currently performed with the GESTR-Mechanical (GSTRM) code and its associated application methodology. The GSTRM model has been developed to provide best estimate predictions of fuel rod thermal-mechanical performance in order to provide an accurate estimate of the expected fuel performance, while also enabling a realistic assessment of design parameter performance uncertainties. The model development philosophy has been to (1) quantify and analytically describe each model component (such as fuel pellet fission product-induced swelling or cladding creep deformation) based on separate effects testing to the maximum extent possible, (2) assemble the model components, and then (3) qualify the assembled model to integral fuel performance measurements. The experimental qualification includes comparison of predictions to fuel temperatures, as obtained by placement of, and continuous measurement by, fuel thermocouples in the center of the fuel pellet column. This extensive qualification of the temperature prediction capability confirmed the GSTRM model to be a reliable best-estimate predictor of fuel rod thermal-mechanical performance while also providing quantification of the model prediction uncertainty, [[ ]]

At the time that the GSTRM experimental qualification was performed, thermal couple data existed only to ~30 GWd/MTU pellet exposure. The data was for UO<sub>2</sub> rods. [[  
]] the

GSTRM model predicted this data very well, [[  
]] Specifically, for 2 rods that were recognized by the NRC as being representative of commercial BWR rods and operated at representative BWR conditions, the GSTRM predictions were excellent, with no indication of a bias in predictive capability with exposure.

Although these 2 rods had larger diameters than the current GE14 (10x10 lattice) fuel design, the rods had cross-sections geometrically similar to the GE14 design in terms of the ratio of initial pellet-cladding gap to initial fuel pellet diameter and the ratio of initial cladding outer diameter to initial fuel pellet diameter. Also, the initial helium fill gas pressure and initial pellet density were lower and the in-reactor densification was larger for these rods than for GE14 rods. Thus the thermal performance of these rods conservatively represents the performance of GE14 rods. Additionally, the measured temperatures for the 2 rods correspond to a single axial location and are primarily a function of the linear heat generation at that point. The active fuel length has only a small impact on the measured temperatures. Thus although the 2 rods were shorter than GE14 rods (rod length was, and is, limited by the test reactor core height), the data is considered applicable to the GE14 design. Finally, it is noted that differences in rod length, as well as the other differences discussed above, between the 2 test rods and GE14 rods are explicitly addressed in the GSTRM experimental qualification and the model uncertain applied in fuel rod thermal-mechanical licensing analyses.

Recently, during review of the GE14 fuel design for ESBWR, comparison of GSTRM and FRAPCON results indicated that GSTRM predicted significantly lower temperatures than FRAPCON for UO<sub>2</sub> rods at pellet exposures of ~18 GWd/MTU. [[  
]]

An important element of the GSTRM fuel rod thermal-mechanical design and licensing analysis methodology is the development and application of an envelope of allowable operating conditions (i.e. local linear heat generation rate as a function of local exposure). All fuel rod thermal-mechanical analyses are evaluated to ensure that operation within that power-exposure envelope will conform to the fuel rod thermal-mechanical design and licensing criteria. For fuel temperature considerations, the envelope and associated overpower limits are specified to assure that fuel melting will not occur for operation on the envelope, even for anticipated operational occurrences. [[  
]]

On the basis of the discussion above, GE concludes that there is sufficient margin to the UO<sub>2</sub> overpower limits to assure adequate performance for the GE13 and GE14 fuel designs, even considering the differences in results between FRAPCON and GSTRM.



Response to Part b

As noted in the response to RAI 9a above, an important element of the GSTRM fuel rod thermal-mechanical design and licensing analysis methodology is the development and application of an envelope of allowable operating conditions (local linear heat generation rate as a function of local exposure). [[

]] Additionally, the statistical analysis methodology used for the rod internal pressure analysis directly addresses the characterized uncertainty in the GSTRM pressure predictions. [[

]] Furthermore, the difference in temperature predictions between GSTRM and FRAPCON noted for UO<sub>2</sub> rods is not observed for gadolinia rods. The GSTRM temperatures for the gadolinia rod for the comparison at 18 GWd/MTU noted above are slightly conservative relative to the FRAPCON temperatures.

Thermal Overpowers (TOP) and Mechanical Overpowers (MOP) limits were developed to provide parameters that are easily evaluated in terms of LHGR and which can be used as computational limits during design of a core. TOP and MOP limits are intended to prevent exceeding actual licensing limits (SAFDLs) such as fuel melting (TOP) or [[

]] (MOP) due to a power increase and to provide an initial screen during design of a core or an upcoming cycle to indicate when more detailed analysis is required. Violation of TOP or MOP limits does not indicate violation of actual licensing limits. GE/GNF practice is to state TOP and MOP limits on the basis of the most limiting fuel rod type, [[

]] Additionally, the TOP and MOP limits are typically stated at the most limiting exposure, which is at the knee of the LHGR limits curve. As noted above, at this exposure, the GSTRM temperature qualification results are excellent.

For these reasons, GE/GNF concludes that the possible underprediction of temperature for UO<sub>2</sub> rods has negligible impact on the GE13 and GE14 fuel designs relative to compliance with SAFDLs.

Response to Part c

As for the case of TOP and MOP limits, which are most limiting at the knee of the LHGR limits curve, LOCA response is limiting at the knee of the LHGR limits curve. At higher exposures, the reduction in LHGR and the resulting reductions in stored energy and decay heat during the LOCA event result in lower PCT. The GSTRM qualification results are excellent at these exposures, indicating that GSTRM is not non-conservative for BWR fuel at these exposures. Even if GSTRM is non-conservative, and if the non-conservatism is converted to a stored energy increase, the increase in calculated PCT due to the increase in stored energy will be relatively small.

Response to Part d

If GSTRM is shown to be non-conservative, the non-conservatism is already explicitly addressed in the response to RAI 1. The values reported in the response to RAI 1 are nominal values. The

NEDO-33173-A, Revision 1  
Non-Proprietary Information

GSTRM thermal-mechanical licensing methodology was developed to assure with at least 95% confidence that fuel rod SAFDLs are met. The impact of this requirement relative to rod internal pressure is demonstrated in Table 9-1 below. This table includes the nominal rod internal pressure results from Table 1.1-1 in the response to RAI 1 for the GE14 UO<sub>2</sub> rod operating on thermal-mechanical linear heat generation limits, but also includes the corresponding upper-95 rod internal pressure as determined by the GSTRM methodology. The impact relative to the fuel rod centerline temperature is demonstrated in Table 9-2 below. This table includes the nominal fuel centerline temperature at the knee of the thermal-mechanical linear heat generation limits for operation on the limits and the nominal and upper-95 centerline temperatures for an overpower at the knee for the GE14 UO<sub>2</sub> barrier rod and the GE14 10 w/o gadolinia non-barrier rod.

The upper-95 results in both tables are the values used to confirm compliance with rod internal pressure and fuel centerline temperature licensing requirements.

GE understands that the NRC's Safety Evaluation for the Methods LTR will contain a restriction to require the submittal of plenum fission gas and fuel exposure gamma scans for NRC review as part of the revision to the T-M licensing. GE considers the thermal-mechanical licensing process the appropriate venue to address these scans and finds the restriction acceptable.

**Table 9-1**  
 Rod Internal Pressure Results for GE14 UO2 Rod for Operation on LHGR Limits

[[		
		]]

**Table 9-2**  
 Fuel Centerline Temperature Results for GE14 UO2 and 10 w/o Gd Rod for Overpower at  
 Knee\* of LHGR Limits

Rod Type	Overpower %	Fuel Centerline Temperature at Knee °F	Fuel Centerline Temperature for Overpower °F	
		Nominal	Nominal	U95
[[				

]]

**MFN 06-481 NRC RAI 10**

Clarify if the plant-specific thermal and mechanical overpressure analysis during AOOs includes an evaluation of the performance of the UGdO<sub>2</sub> rods. Provide the GE14 TOP and MOP limits for UGdO<sub>2</sub> rods based on the compliance to Amendment 22 analysis.

**GE Response**

As noted in the response to RAI 9b, [[  
]] and are derived to assure compliance with Amendment 22 requirements. It is noted again that GSTRM results for gadolinia rods are conservative relative to FRAPCON.

**MFN 06-481 NRC RAI 11, Transient LHGR**

GESTAR II Class III NEDE-24011-P-A-14 states that GENE utilizes a number of criteria to ensure that loss of fuel rod mechanical integrity will not occur during AOOs. Two of these criteria are:

Loss of fuel rod mechanical integrity will not occur due to fuel melting.

To achieve this objective, the fuel rod is evaluated to ensure that fuel melting during normal operation and core-wide AOOs will not occur. As described in Subsection 2.2.2.5 for local AOOs such as rod withdrawal error, a small amount of calculated fuel pellet center melting may occur, but is limited by the 1% cladding circumferential plastic strain criterion.

Loss of fuel rod mechanical integrity will not occur due to pellet-cladding mechanical interaction.

To achieve this objective, the fuel rod is evaluated to ensure that the calculated cladding circumferential plastic strain due to pellet-cladding mechanical interaction does not exceed 1% during AOOs. Further discussion of this evaluation is provided in Subsection 2.2.2.7.

- a. Describe which NRC approved methods are used to evaluate these criteria.
- b. Describe which licensing document contains the result (including specific calculated values) of these evaluations.
- c. State how the plant-specific EPU and MELLA+ applications will document the demonstration that these criteria are met for these operating conditions. If the plant-specific applications will not document these results, justify why this is acceptable.

**GE Response**

**Response to Part a**

The GESTR-M code cited in Reference 11-1 and the CHT code (Reference 11-2) are used to confirm that loss of fuel rod mechanical integrity due to fuel melting or pellet-cladding mechanical interaction does not occur during normal operation or core-wide AOOs.

**Response to Part b**

GE understands that the NRC's Safety Evaluation for the Methods LTR will contain a restriction to require that each EPU and MELLA+ fuel reload will document in the Supplemental Reload Licensing Report the calculational results of the analyses to demonstrate compliance to transient thermal mechanical acceptance criteria. GE considers the SRLR an acceptable means to document the transient thermal mechanical results and accepts the restriction.

**Response to Part c**

The plant-specific EPU and M+ applications include Safety Analysis Reports (SAR), developed by GE. Future SARs that reference NEDC-33173P will document the results of the calculation results of the analyses to demonstrate compliance to transient thermal mechanical acceptance

NEDO-33173-A, Revision 1  
Non-Proprietary Information

criteria. To account for the impact of the void history bias, plant-specific EPU and MELLLA+ applications will demonstrate margin to requirements for fuel centerline melt and that the calculated cladding circumferential plastic strain due to pellet-cladding mechanical interaction does not exceed 1% for the most limiting AOO transient events, including equipment out of service.

References

- 11-1 NEDE-24011-P-A-15, "General Electric Standard Application for Reactor Fuel", September 2005.
- 11-2 NEDC-32084P-A, Rev 2, July 2002, TASC-3A, A Computer Program for Transient Analysis of a Single Channel.

**MFN 07-041 MELLA Plus LTR NEDC-33006P, Revised Response to RAIs AOO 3, 9, 10, and 17**

See MFN 04-026 for updated responses to RAIs AOO 3, 9, 10 and 17.

## REFERENCES

1. GE Letter, G. Stramback (GE) to NRC, Response to MELLLA Plus AOO RAIs, MFN 04-020, February 27, 2004
2. GE Letter, G. Stramback (GE) to NRC, Completion of Responses to MELLLA Plus AOO RAIs, MFN 04-026, March 4, 2004
3. GE Letter, G. Stramback (GE) to NRC, TRACG Analyses for MELLLA Plus AOO RAI 22, MFN 04-033, March 23, 2004
4. GNF Letter, M. Harding (GNF) to NRC, Request for Additional Information – MELLLA+ LTR RAI 6, MFN 04-048 (FLN-2004-004), March 24, 2004
5. GE Letter, G. Stramback (GE) to NRC, Revised Response to MELLLA Plus AOO & ATWS RAIs, MFN 04-060, June 6, 2004
6. GE Letter, G. Stramback (GE) to NRC, Revision letter - Supporting Lattice Information - MELLLA+ RAI AOO 6, MFN 04-061R1, July 26, 2004
7. GE Letter, G. Stramback (GE) to NRC, MELLLA Plus RAI AOO 6, TGBLA Lattice Physics Data, MFN 04-067, July 1, 2004
8. GE Letter, G. Stramback (GE) to NRC, Off-Rated Conditions - MELLLA+ RAI AOO 22, MFN 04-074, August 5, 2004
9. GE Letter, G. Stramback (GE) to NRC, Responses to RAIs - Methods Interim Process, MFN 05-022, March 31, 2005
10. GE Letter, L. Quintana (GE) to NRC, Responses to RAIs - Methods Interim Process, MFN 05-029, April 8, 2005
11. GE Letter, L. Quintana (GE) to NRC, Responses to RAIs 1, 13, 14-1, 18 and 22 - Methods Interim Process, MFN 05-038, May 3, 2005
12. GE Letter, G. Stramback (GE) to NRC, Responses to RAIs 4-6, 12 and 17- Methods Interim Process, MFN 05-045, May 26, 2005
13. GE Letter, G. Stramback (GE) to NRC, Responses to RAIs 11 and 16 - Methods Interim Process, MFN 05-048, May 27, 2005
14. GE Letter, L. Quintana (GE) to NRC, Revised Response to RAI 28-2 - Methods Interim Process, MFN 05-053, June 20, 2005
15. GE Letter, G. Stramback (GE) to NRC, Revised Responses to MELLLA+ RAIs, MFN 05-081, August 16, 2005
16. GE Letter, L. Quintana (GE) to NRC, Responses to Methods RAIs - Interim Methods LTR, MFN 06-195, June 23, 2006



NEDO-33173-A, Revision 1  
Non-Proprietary Information

17. GE Letter, L. Quintana (GE) to NRC, Responses to Methods RAIs 1 and 5- Interim Methods LTR, MFN 06-207, June 29, 2006
18. GE Letter, L. Quintana (GE) to NRC, Remaining Responses to Methods RAIs - Interim Methods LTR, MFN 06-209, June 30, 2006
19. GE Letter, R. Brown (GE) to NRC, Compilation of Responses to Methods RAIs - Interim Methods LTR, MFN 06-211, July 18, 2006
20. GE Letter, R. Brown (GE) to NRC, Updated Response to RAI 28-2 - NEDC-33173P, MFN 06-434, November 22, 2006
21. GE Letter, R. Brown (GE) to NRC, Responses to RAIs 7, 8, 9, 10, and 11 – NEDC-33173P, MFN 06-481, December 5, 2006
22. GE Letter, R. Brown (GE) to NRC, MELLLA Plus LTR NEDC-33006P, Revised Responses to RAIs AOO 3, 9, 10, and 17, MFN 07-041, January 25, 2007

NEDO-33173-A, Revision 1  
Non-Proprietary Information

Enclosure A

SLMCPR Methodology and Uncertainties Review Presentation

(GNF Letter, dated March 24, 2004, MFN 04-048 (FLN-2004-004) )

# SLMCPR Methodology and Uncertainties Review

## MELLLA+ RAI 6 Discussion

Mark Colby, Brian Moore  
March 17, 2004

Appendix C, Enclosure A-1

# Overview

## GNF SLMCPR Methodology Review

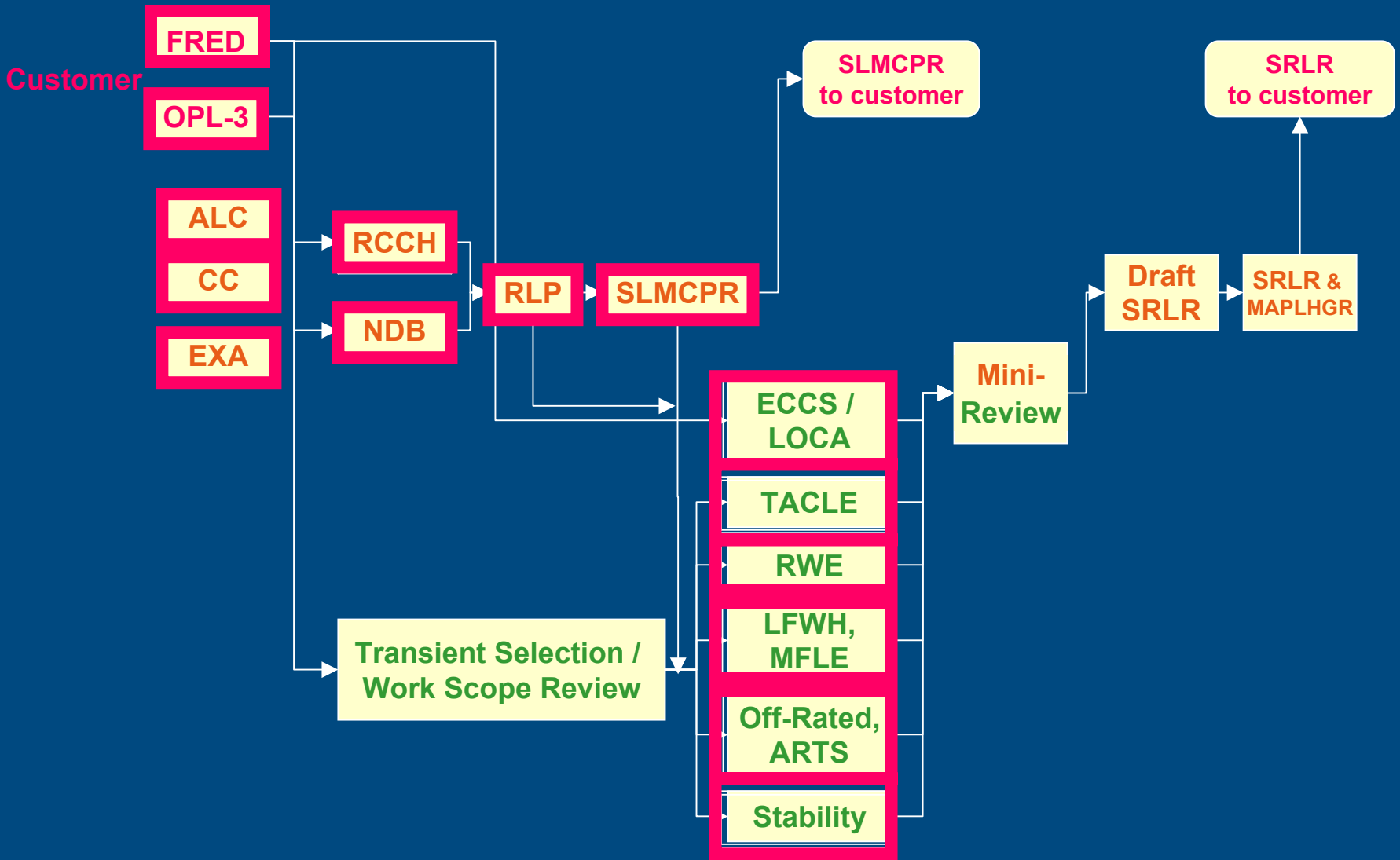
- Approved methodology

## Uncertainty Application Review

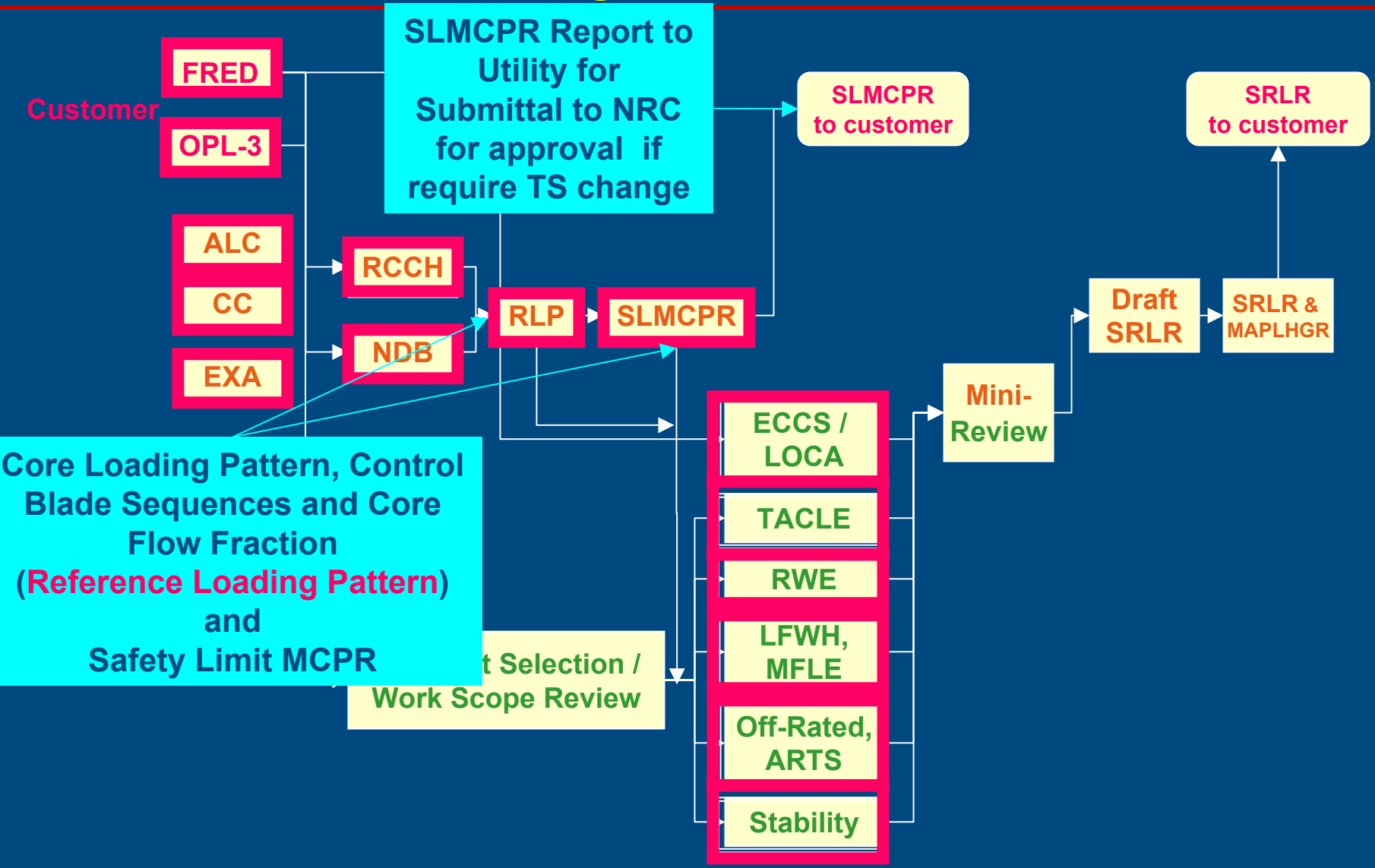
- Non-Power
- GETAB, Revised and Reduced Power
- GEXL14
- Radial TIPs
- Exit void fraction

# GNF SLMCPR Methodology Review

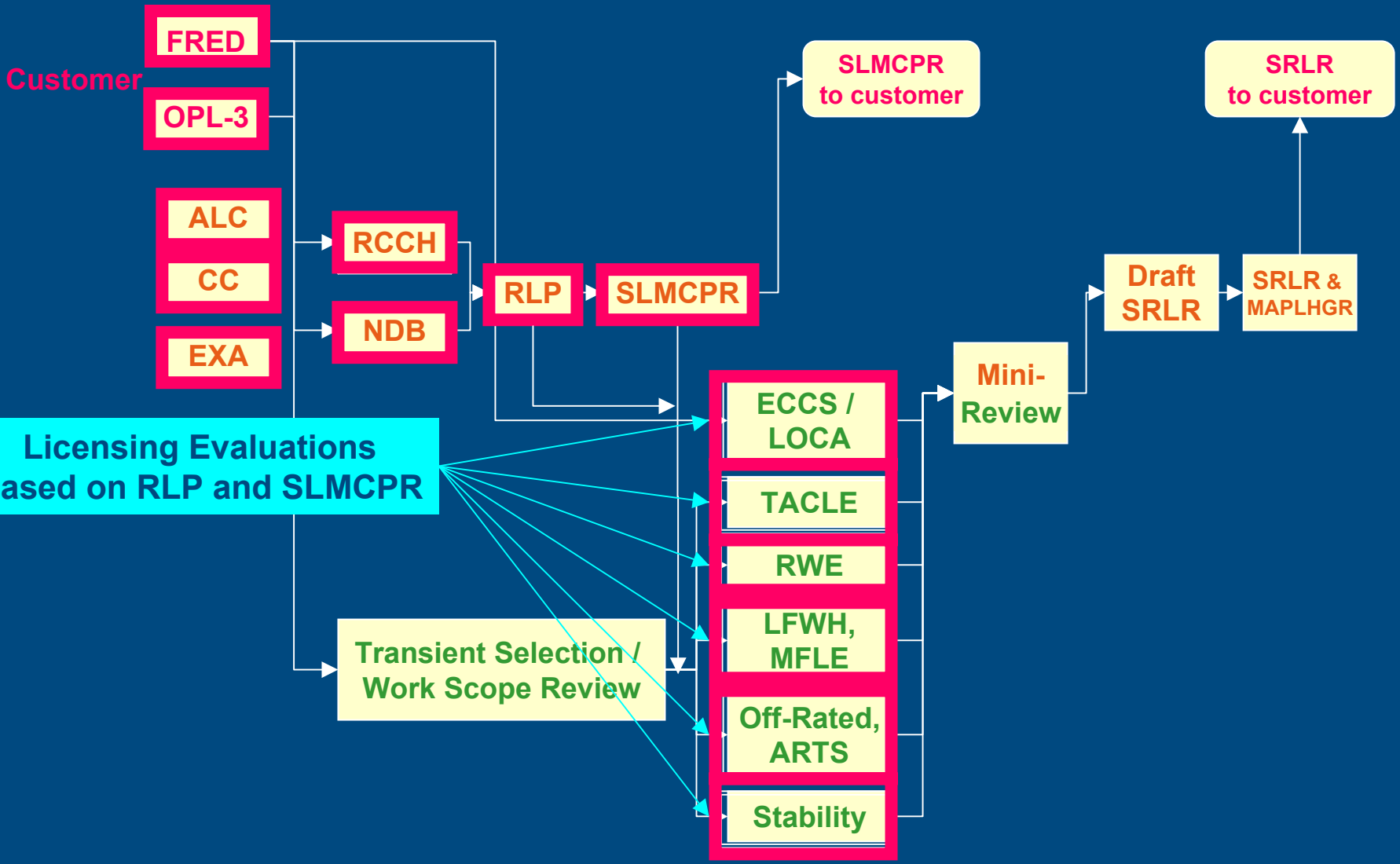
# Standard Licensing Process



# Standard Licensing Process



# Standard Licensing Process





# Determine SLMCPR – Limiting Condition



# Determine SLMCPR – Limiting Condition

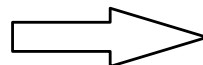
[[

]]

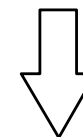


# Example Limiting Rod Patterns

	1	2	3	4	5	6	7	8	9	10	11	12	13	14	15
1									+	+	+	+			
2															
3							+	+	+	+	0				
4															
5					+	+	+	+	+	+	+	+	+	+	+
6															
7			+	+	+	+	+	0	+	+					
8															
9	+	+	+	+	+	+	+	+	+	+	+	+	+	+	+
10															
11	+	+	+	+	0	+	+	+	+	+	+	+	+	+	+
12															
13	+	+	+	+	+	+	+	+	+	+	+	+	+	+	+
14															
15	+	0	+	+	+	+	+	+	+	+	+	+	+	+	+



	1	2	3	4	5	6	7	8	9	10	11	12	13	14	15
1									+	+	+	+	+	+	+
2															
3								+	+	0	+	+			
4															
5						+	+	+	+	+	+	+	+	+	+
6															
7			+	+	0	+	+	+	+	+	+	+	+	0	+
8															
9	+	+	+	+	+	+	+	+	+	+	+	+	+	+	+
10															
11	+	0	+	+	+	+	+	+	+	+	+	+	+	+	+
12															
13	+	+	+	+	+	+	+	+	+	+	+	+	+	+	+
14															
15	+	+	+	+	0	+	+	+	+	+	+	+	+	+	+



	1	2	3	4	5	6	7	8	9	10	11	12	13	14	15
1									+	+	+	+	+	+	+
2															
3								+	+	0	+	+	0		
4															
5						+	+	+	+	+	+	+	+	+	+
6															
7			+	+	0	+	+	0	+	0	+	+	+	+	+
8															
9	+	+	+	+	+	+	+	+	+	+	+	+	+	+	+
10															
11	+	0	+	+	0	+	+	+	+	+	+	+	+	+	+
12															
13	+	+	+	+	+	+	+	+	+	+	+	+	+	+	+
14															
15	+	0	+	+	+	+	+	+	+	+	+	+	+	+	+

*Rod pattern options are consistent with core reactivity requirements*

# Determine SLMCPR – Limiting Condition

[[

]]

# Determine SLMCFR – Limiting Condition

[[

]]

# Determine SLMCFR – Limiting Condition

[[

]]

# Determine SLMCPR – Limiting Condition

]]



# Determine SLMCPR – Monte Carlo



# Determine SLMCPR – Monte Carlo

[[

]]

# Determine SLMCPR – Monte Carlo



# Determine SLMCPR – Monte Carlo



# Determine SLMCPR – Monte Carlo



# Determine SLMCPR – Monte Carlo



# Determine SLMCPR – Monte Carlo

[[

]]

# Determine SLMCPR – Monte Carlo





# Determine SLMCPR – Monte Carlo



# Uncertainty Application Review

**NEDC-32601P-A Table 2.1 Summary of SLMCPR Uncertainties**

Uncertainty Parameter	GETAB Uncertainty $\pm\sigma$ (%)	Revised Uncertainty and Procedures $\pm\sigma$ (%)	Reference
Feedwater Flow System Overall Flow Uncertainty	1.76	[[ ]]	Section 2.2
Feedwater Temperature Measurement	0.76	[[ ]]	Section 2.3
Reactor Pressure Measurement	0.50	[[ ]]	Section 2.4
Core Inlet Temperature	0.20	0.2	Section 2.5
Total Core Flow Measurement	2.5 (6.0 for Single Loop Operation)	2.5 (6.0 for Single Loop Operation)	Section 2.6
Channel Flow Area Variation	3.0	[[ ]]	Section 2.7
Friction Factor Multiplier Uncertainty	10.0	[[ ]]	Section 2.8
Channel Friction Factor Multiplier	5.0	5.0	Section 2.9

# SLMCPR Sensitivity to Non-Power related GETAB Uncertainties – Decreasing Order

Uncertain Quantity	Factor (F) to Increase SL by 0.005
feedwater total flow rate	[[ ]]
total core flow measurement	[[ ]]
channel flow area variation	[[ ]]
feedwater temperature	[[ ]]
reactor pressure measurement	[[ ]]
core inlet temperature	[[ ]]
channel friction factor multiplier	[[ ]]
friction factor multiplier	[[ ]]

NEDO-33173-A, Revision 1  
Non-Proprietary Information  
SLMCPR Change vs Factor of P Change in Uncertainty

[[

]]

**NEDC-32601P-A Table 2.1 Summary of SLMCPR Uncertainties (Cont.)**

Uncertainty Parameter	GETAB Uncertainty $\pm\sigma$ (%)	Revised Uncertainty and Procedures $\pm\sigma$ (%)	Reference
Critical Power Uncertainty	Different for Each Fuel Type	Different for Each Fuel Type	Reference 11
TIP Reading and Bundle Power	8.6 applied to quarter segment TIP reading (current procedure) 1.2 random uncertainty applied nodally	Current Uncertainties Total Bundle Integrated Power Uncertainty = [[     ]] (Applied to bundle integral)  Total TIP Integral Instrument Uncertainty = [[     ]] (applied to quarter segment)  3D MONICORE Uncertainties	Reference 1 Section 2.10  Section 2.10  Reference 10
TIP Reading Random Uncertainty	1.2 (2.85 for Single Loop Operation)	1.2 (2.85 for Single Loop Operation)	Reference 1
R-factor Uncertainty	1.5	[[     ]]	Section 3 & Appendix C

**NEDC-32601P-A Table 2.1 Summary of SLMCPR Uncertainties (Cont.)**

Uncertainty Parameter	GETAB Uncertainty $\pm\sigma$ (%)	Revised Uncertainty and Procedures $\pm\sigma$ (%)	Reference
Critical Power Uncertainty	Different for Each Fuel Type	Different for Each Fuel Type	Reference 11
TIP Reading and Bundle Power	8.6 applied to quarter segment TIP reading (current procedure) 1.2 random uncertainty applied nodally	Current Uncertainties Total Bundle Integrated Power Uncertainty = $[[ \quad ]]$ (Applied to bundle integral) Total TIP Integral Instrument Uncertainty = $[[ \quad ]]$ (applied to quarter segment) 3D MONICORE Uncertainties	Reference 1 Section 2.10  Section 2.10  Reference 10
TIP Reading Random Uncertainty	1.2 (2.85 for Single Loop Operation)	1.2 (2.85 for Single Loop Operation)	Reference 1
R-factor Uncertainty	1.5	$[[ \quad ]]$	Section 3 & Appendix C

# Bundle Power Uncertainties – Table 2.1

The total TIP uncertainty (TYP SYS) of 8.6% for a quarter TIP segment is the RMS sum of five components, i.e.,

$$\sigma_{TIP} = \sqrt{\sigma_{ran}^2 + \sigma_{geom}^2 + \sigma_{assym}^2 + \sigma_{lprm}^2 + \sigma_{mdl}^2}$$

where: [[

]]



# Bundle Power Uncertainties – Table 2.1

- > Only first two terms are related to TIP instrument response
- > Others are related to computer bundle power model
- > Revised Methodology separates the hardware (TIP) measurement and the computer power model

[[

]] **Applied to Quarter Segment**

[[

]]

# Bundle Power Uncertainties - Approved

- > NRC approved Revised Methodology is modified slightly from Table 2.1
- > Done in response to RAI III.11 (Page B –13) to recognize that distribution of 4 bundle power uncertainties surrounding a TIP is correlated
- > Best discussed by referencing Table 4.2, NEDC-32694P-A

# Bundle Power Uncertainties - Approved

**NEDC-32694P-A Table 4.2 Summary of Power Distribution Uncertainties  
 (So called Reduce Power Uncertainties)**

	Quantity	Uncertainty	Source
<b>EBPOW</b>	TIP Integral	[[ ]]	Six cycles of tracking data for 8x8 and 9x9 fuel
	Four bundle power distribution surrounding TIP location	[[ ]]	80 comparisons taken from gamma scan measurements at six operating cycles
	Contribution to bundle power uncertainty due to LPRM update	[[ ]]	Study on BWR/4 plus two cycles of detailed tracking on another BWR/4, comparing MCPR before and after TIP runs
<b><math>\sigma</math> TIP, total</b>	Contribution to bundle power due to failed TIP and LPRM	[[ ]] [[ ]]	Study carried out on BWR/4
	<b>Total Uncertainty in Calculated Bundle Power</b>	[[ ]]	<b>RMS total of first five items</b>
	Uncertainty of TIP signal nodal uncertainty	[[ ]]	Acceptance criteria for TIP asymmetry
	TIP random nodal error	[[ ]]	Instrument random error consistent with current GETAB analysis

# Bundle Power Uncertainties - Approved

- > Again, separate the hardware (TIP) measurement and the computer power model
- > Combine TIP Integral, Failed TIP, and LPRM uncertainties to get hardware component

**Failed TIP and  
LPRM uncertainty**

[[

]]

# Bundle Power Uncertainties

**GETAB Method With GETAB Uncertainties: TYP SYS = 8.6**

$$\sigma_B = \frac{TIP SYS}{\sqrt{4}} = 4.3\%$$

**Revised Method With Reduced or GETAB Uncertainties**

[[

]]

# Bundle Power Uncertainties - Summary

<u>Uncertainty Method</u>	<u>Uncertainty Basis</u>	<u>TIPSYS</u>	<u>EBPOW</u>	<u><math>\sigma</math> TIP, TOT</u>
GETAB	GETAB	8.6	0.0	4.3
Revised	GETAB	[[	]]	4.3
Revised	Reduced	[[		]]

**NEDC-32601P-A Table 2.1 Summary of SLMCPR Uncertainties (Cont.)**

Uncertainty Parameter	GETAB Uncertainty $\pm\sigma$ (%)	Revised Uncertainty and Procedures $\pm\sigma$ (%)	Reference
Critical Power Uncertainty	Different for Each Fuel Type	Different for Each Fuel Type	Reference 11
TIP Reading and Bundle Power	8.6 applied to quarter segment TIP reading (current procedure) 1.2 random uncertainty applied nodally	Current Uncertainties Total Bundle Integrated Power Uncertainty = $[[ \quad ]]$ (Applied to bundle integral) Total TIP Integral Instrument Uncertainty = $[[ \quad ]]$ (applied to quarter segment) 3D MONICORE Uncertainties	Reference 1 Section 2.10  Section 2.10  Reference 10
TIP Reading Random Uncertainty	1.2 (2.85 for Single Loop Operation)	1.2 (2.85 for Single Loop Operation)	Reference 1
R-factor Uncertainty	1.5	$[[ \quad ]]$	Section 3 & Appendix C

# GE14 CP Testing: Critical Power Range

[[

]]



# GE14 CP Testing: Inlet Mass Flux Range

[[

]]

# GE14 CP Testing: Inlet Subcooling Range

[[

]]

# GE14 CP Testing: Core Pressure Range

[[

]]

**NEDC-32601P-A Table 2.1 Summary of SLMCPR Uncertainties (Cont.)**

Uncertainty Parameter	GETAB Uncertainty $\pm\sigma$ (%)	Revised Uncertainty and Procedures $\pm\sigma$ (%)	Reference
Critical Power Uncertainty	Different for Each Fuel Type	Different for Each Fuel Type	Reference 11
TIP Reading and Bundle Power	8.6 applied to quarter segment TIP reading (current procedure) 1.2 random uncertainty applied nodally	Current Uncertainties Total Bundle Integrated Power Uncertainty = $\sqrt{\quad}$ (Applied to bundle integral) Total TIP Integral Instrument Uncertainty = $\sqrt{\quad}$ (applied to quarter segment) 3D MONICORE Uncertainties	Reference 1 Section 2.10  Section 2.10  Reference 10
TIP Reading Random Uncertainty	1.2 (2.85 for Single Loop Operation)	1.2 (2.85 for Single Loop Operation)	Reference 1
R-factor Uncertainty	1.5	$\sqrt{\quad}$ $\sqrt{\quad}$	Section 3 & Appendix C

# Uncertainties Summary & Rollup (FLN-2001-004)

10x10 TIP Comparisons are less than or equal to the approved values

[[

]]

For 2 plants, three cycles of TIP data were presented in FLN-2001-004

- > 1 cycle prior to 10x10 fuel introduction, 1<sup>st</sup> full reload of 10x10, 2<sup>nd</sup> full reload of 10x10

Note: For Plant A, a complete set of TIP data was not available for the 1<sup>st</sup> full reload of 10x10. In particular, the identification of malfunctioning (“failed”) TIP strings by the process computer and/or statistically deviating TIP strings (“rejected”) by the core monitor was not available. Therefore, this cycle of TIP data is not considered valid and not included in the statistical roll-up.

# Range of Void Fraction for TIP tracking

The TIP comparisons presented in FLN-2001-004 can be supplemented by identification of the average and exit void fractions for this data set

- > Plant A, 2<sup>nd</sup> full reload of 10x10 data
  - Peak exit void of > 87%
  - Radial TIP RMS is still < 2% which indicates no void bias
- > Plant B, all three cycles
  - Peak exit voids above 85%
  - No identifiable radial TIP RMS bias with void

# Plant A 10x10 Tip Comparisons and Void

]]

# Exit Conditions – Plant A @ 7.7 GWd/T

[[

]]



# Plant B 10x10 TIP Comparisons and Void

[[

]]

# CAR AI-7318 -- Monitoring of MELLLA+

Resulted from the design review on the Methods Assessment for MELLLA+

The following items are to be assessed following operation in the MELLLA+ domain:

- > Hot critical eigenvalue
- > Cold critical eigenvalue
- > Nodal power distribution
- > Bundle power distribution
- > Rod-to-rod power distribution
- > The core flow and pressure drop uncertainty
- > The [[     ]] criterion.

**NEDC-32601P-A Table 2.1 Summary of SLMCPR Uncertainties (Cont.)**

Uncertainty Parameter	GETAB Uncertainty $\pm\sigma$ (%)	Revised Uncertainty and Procedures $\pm\sigma$ (%)	Reference
Critical Power Uncertainty	Different for Each Fuel Type	Different for Each Fuel Type	Reference 11
TIP Reading and Bundle Power	8.6 applied to quarter segment TIP reading (current procedure) 1.2 random uncertainty applied nodally	Current Uncertainties Total Bundle Integrated Power Uncertainty = $\{ \quad \}$ (Applied to bundle integral) Total TIP Integral Instrument Uncertainty = $\{ \quad \}$ (applied to quarter segment) 3D MONICORE Uncertainties	Reference 1 Section 2.10  Section 2.10  Reference 10
TIP Reading Random Uncertainty	1.2 (2.85 for Single Loop Operation)	1.2 (2.85 for Single Loop Operation)	Reference 1
R-factor Uncertainty	1.5	$\{ \quad \}$	Section 3 & Appendix C

# Table 3.1 Uncertainty for 10x10 Fuel Only

[[

]]

Figure 2-28 □ Average Pin Power Error of TGBLA06 Data and Fit vs. MCNP data

NEDO-33173-A, Revision 1  
Non-Proprietary Information

Enclosure B

Applicability of NRC Approved Methodologies to MELLLA+

(GE Letter, dated March 4, 2004, MFN 04-026)  
[Updated with MFN 05-038 and MFN 05-045]

NEDO-33173-A, Revision 1  
Non-Proprietary Information

Enclosure B of Appendix C is completely proprietary and is included in the proprietary version of NEDC-33173P-A only.